Space Science and Engineering Center
University of Wisconsin-Madison

The Technical Proceedings of

The Fourth International TOVS Study Conference

A REPORT from the

Cooperative Institute for Meteorological Satellite Studies

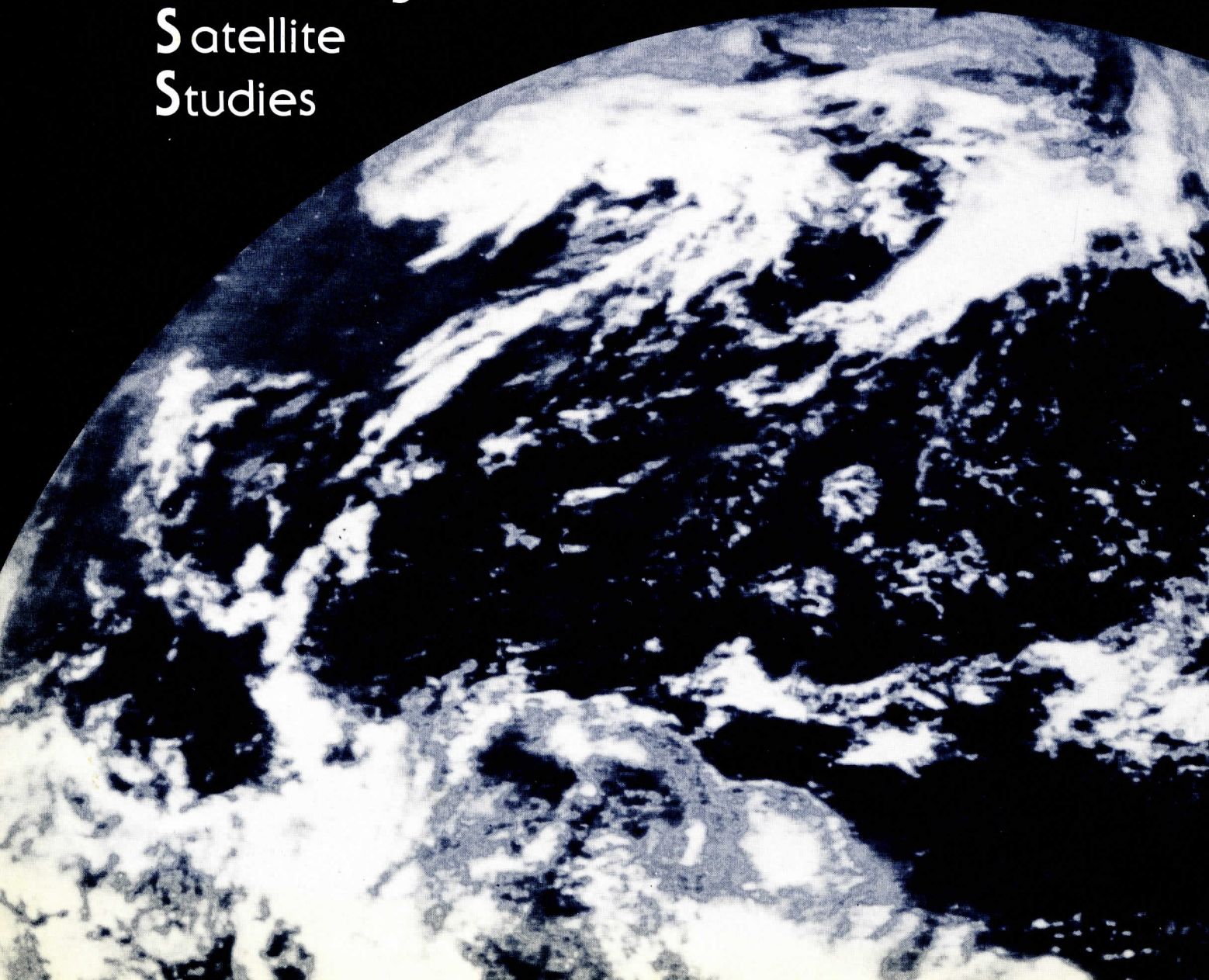

The Technical Proceedings of

The Fourth International TOVS Study Conference

Igls, Austria

March 16-22, 1988

Edited by

W. P. Menzel

Cooperative Institute for Meteorological Satellite Studies
Space Science and Engineering Center
University of Wisconsin
1225 West Dayton Street
Madison, Wisconsin 53706
(608) 262-0544

October 1988

FORWARD

These Technical Proceedings detail the scientific presentations at the Fourth International TOVS Study Conference (ITSC-IV) held in Igls, Austria from 16 to 22 March 1988. A summary of the conference recommendations and conclusions is contained in a separate document entitled "A Report on ITSC-IV" available from CIMSS at the University of Wisconsin-Madison.

The ITSC convenes the working group of the International Radiation Commission (IRC) that is studying the derivation, quality, and applicability of satellite temperature and moisture profiles retrievals for operational meteorological purposes. The ITOVS Working Group has met every eighteen months since the autumn of 1983 and has approximately 80 participants representing 20 countries.

These technical proceedings contain papers in three broad areas: the science of atmospheric sounding, the algorithms for deriving products from the satellite data, and the application of the products to numerical weather prediction. In addition, the papers detail the plans for and uses of TOVS data at the many institutes around the world that comprise the international meteorological satellite user community.

Unfortunately we were able to reproduce the figures in black and white only; if the content of the paper is unclear because of this, please contact the authors directly and they will be able to provide clarification or color copies of the relevant figures.

ACKNOWLEDGMENTS

The publication of these proceedings has been possible through the financial support from the National Oceanic and Atmospheric Administration to the Cooperative Institute for Meteorological Satellite Studies in Madison, Wisconsin.

The careful retyping of several of the edited manuscripts was done by Laura Beckett and Jan Waite-Schuster. The production and distribution was accomplished by Sue Pfefferkorn. We thank them for their efforts.

TABLE OF CONTENTS

A REGIONAL TIROS-N SERIES SOUNDING DATA OPERATIONAL PROCESSING SYSTEM

Dong Chaohua, Zhang Fengying, Luo Dongfeng,
Ran Maonong, Zheng Bo and Wu Baosuo
Satellite Meteorology Center
SMA, Beijing, PRC

ABSTRACT

In Satellite Meteorological Center (SMC) a regional data receiving and processing system of TIROS-N series launched by U.S.A. has been established. The products from the vertical sounding system involve vertical temperature and moisture structures, and total ozone amount. This paper briefly describes the system capabilities of the different aspects of the sounding project, from the reception of data to the production of atmospheric products.

1. INTRODUCTION

In 1979, the SMA proposed to establish a ground station capable of direct readout of TIROS-N type satellite signals from the High Resolution Picture Transmission (HRPT), which includes a data processing system in order to improve weather analysis and numerical weather predictions locally. During the system implementation when the data receiving was in the final stage of development, we started with developing a regional TOVS processing software package. Based on Wisconsin export package and NESDIS TOVS operational processing system, the regional TIROS-N series sounding data processing system was established during the period of 1981-1982. At present, the initial operational TOVS processing system, interfaced with the data receiving system in Beijing, can process in near real-time the TIP/HRPT data from NOAA polar-orbiting satellite on IBM 4361 computer located at the SMC/SMA, China. The system makes extensive use of disk file, both sequential and direct accesses for efficiency in I/O operations. The main program serves as a driver to perform the tasks through called subroutines or functions so that it makes easy to maintain the TOVS processing system.

2. DATA RECEPTION

The HRPT data format provides a time multiplexed output of five channels of data from the Advanced Very High Resolution Radiometer (AVHRR) and the low bit rate instrument data (e.g., TIP). The data are digital, transmitted at s-band frequencies. All information necessary to calibrate the instrument output is included in the data stream.

The Beijing receiving station is capable of receiving and processing HRPT signals transmitted in real-time from TIROS-N series satellites. The antenna is capable of tracking the satellite orbit either in an "auto-track" mode or a "program-track" mode. All data received must be processed through HP-1000 computer. TIP data is extracted from the HRPT, and recorded on CCT tape for scientific processing. The data reception block diagram in SMC is shown in Fig. 1.

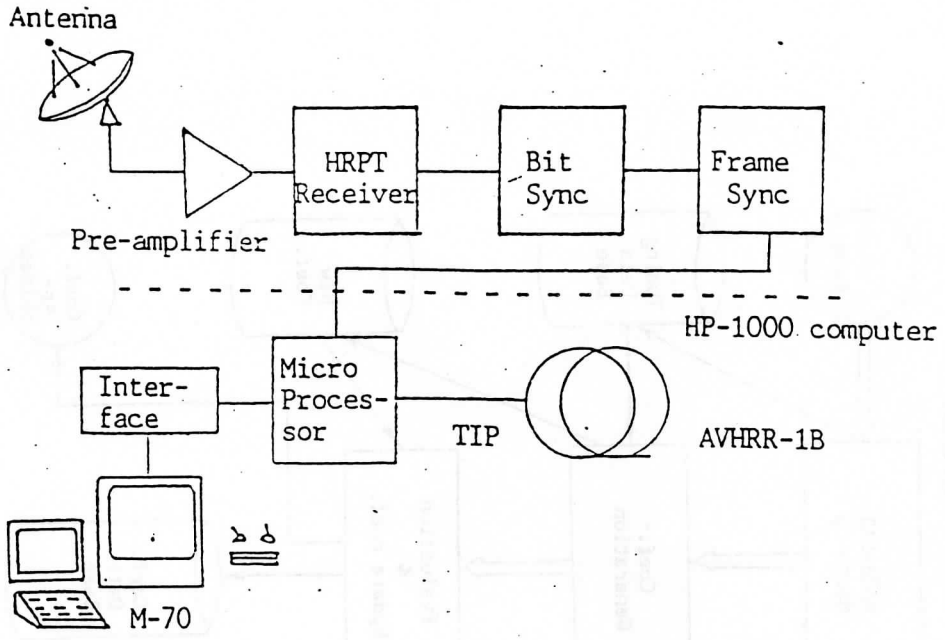

Fig. 1. HRPT/TIP data receiving system in SMC

3. TOVS PROCESSING SYSTEM

The TOVS processing system consisting of over forty main programs, including about 50,000 lines of executable code in total, is comprised of two subsystems: the operational subsystem for atmospheric sounding retrieving, and the support subsystem for generating statistical regression coefficients and monitoring products. The initial regression coefficients based upon known instrument characteristics for each spacecraft are obtained from NESDIS. The coefficients for sounding retrievals are updated at regular intervals (one week) as a function of the support subsystem to account for short and long periods atmospheric seasonal variations. The block diagram of the TOVS processing system is shown in Fig. 2.

A. Operational Subsystem

This subsystem is comprised of the following components: Data Ingestion (TIPINN, TOVS1B), SSU Mapper (TOVSING, TOVSMAP), Preprocessor (TOVSPRE), Atmospheric Parameter Retrieval Module (TOVSRET), and Output Products section. The function of each module (job) will be described briefly.

1) Data Ingestion

The raw TIP data is acquired from 1600 BPI/2400 ft magnetic tape which is done on the HP-1000 computer, and transferred to the IBM 4361 computer. The main function of the ingestion is to obtain instrument level 1B data (calibrated and earth located). It checks TIP data quality, status, parity, observation time, filter sync error, etc.; and decodes the instrument information for HIRS/2, MDU and SSU from various word lengths into standard 32-bit forms and then is manipulated to exclude unwanted information. By using the orbital elements for the relevant satellite, the data are earth-located with calibration data being extracted and applied, converting digital

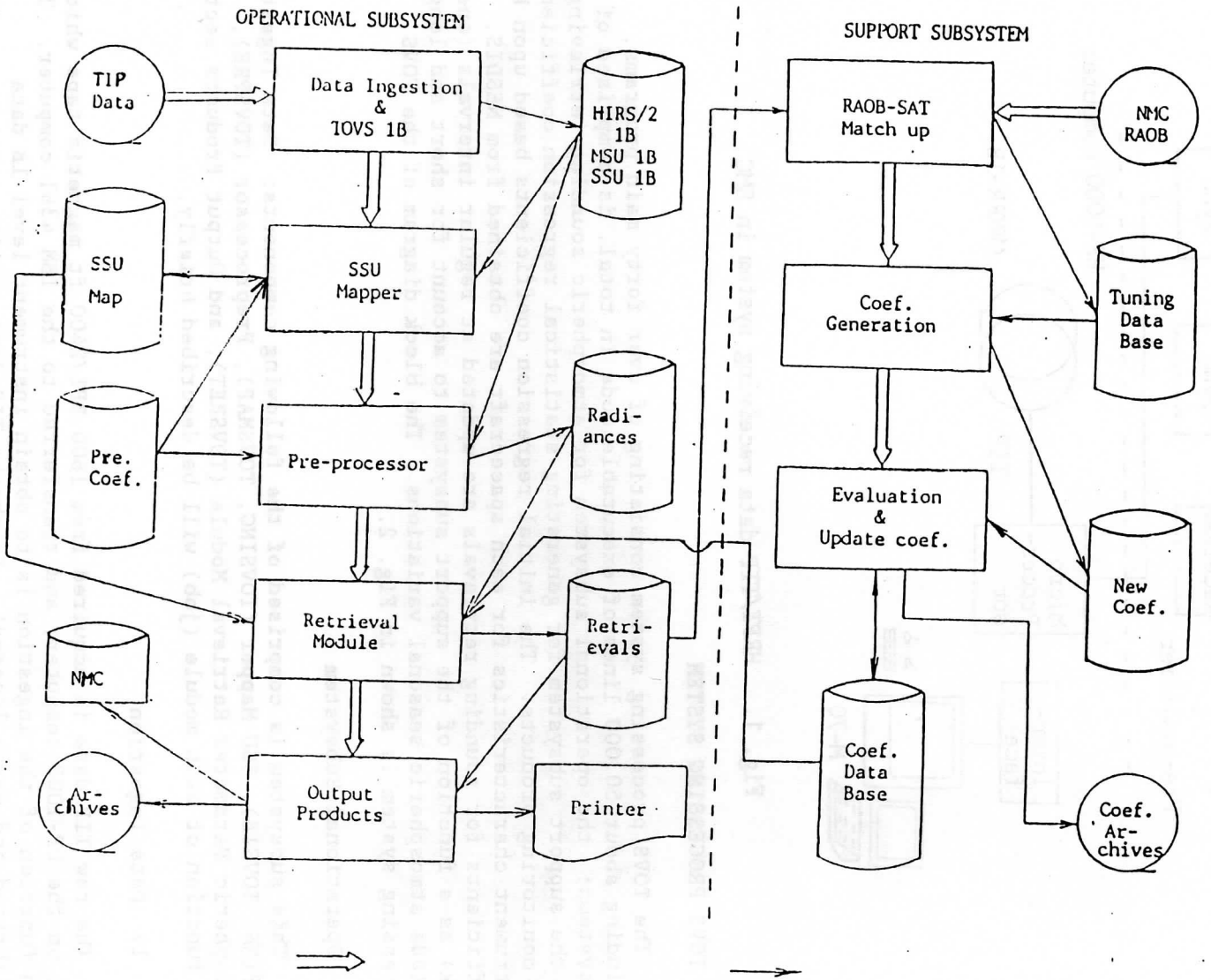

Fig. 2. TOVS DATA PROCESSING SYSTEM OF SMC

counts to radiances. After this module is finished, each instrument level 1B data is stored on disk file. The information necessary for the location of specific instrument data, its extraction from TIP, its arrangement according to instrument scanning geometry, and identification of calibration and earth view data is described in detail by Levin Lauritson et al. (1979).

2) SSU Mapper

The purpose of SSU mapper is to provide analyzed SSU (the Stratospheric Sounding Unit) data. Input to this module is HIRS/2 (The High-Resolution Infrared Sounder, Version 2) 1B and SSU11B. First, it establishes collocated array of the channels 1, 2, and 3 of HIRS/2 (Smith et al., 1979) at the position of SSU spots, and writes the combination of data of SSU & HIRS/2 on disk file. The brightness temperature observed by SSU instrument depends on the angle at which measurements are made because of the different path lengths in the atmosphere. In order to perform the type of retrieval in which we are predominantly interested (regression) without many sets of angle-dependent retrieval regression coefficients, we need to correct these measurements at different angles, so that they have the same path length as at nadir. This module applies limb regression coefficients to SSU observed radiances to produce such a correction. Finally, SSU data analyzed from the previous run (used as a first guess) are processed using "objective analysis procedures" to update the respective SSU fields during the processing of each orbit. The SSU mapped (analyzed) field (1° X 1° latitude-longitude) is used in the atmospheric parameter retrieval module (TOVSRET) to derive atmospheric temperatures above 115 mb.

3) Pre-processor

The HIRS/2 1B and MSU 1B data are acquired. The main function of the pre-processor is to provide further corrections to the calibration radiance data and store the resulting data in suitable forms for display and retrieval processing. Same as that of the SSU limb correction described above, it corrects the MSU and HIRS/2 measurements from all the channels except HIRS/2 channel 20, visible channel, for limb or slant path effects. On the infrared instrument, there are 3 channels called "window" which means the channel "sees through" (no radiation absorptions) the constant mixing ratio gases (CO_2, etc.) and ozone. They are also affected by liquid water (clouds) in which they only "see" the top of heavy clouds. So it is necessary to separate the corrections for window channel water vapor attenuation (the "effect" of water vapor) in this program. It also corrects the side lobes for the special characteristic of microwave antennas. Because the signal perceived by the MDU sensor is not the true signal from the field of view due to the fact that the antenna does not "focus" exclusively on the field of view. The module computed solar zenith angles, and corrects the certainty of the channels for fluorescence, and solar reflection in the shortwave infrared channels. After the corrections are done, the module collocates MSU to HIRS/2 locations by a distance weight interpolation scheme.

To facilitate the limb corrections, three additional files are needed: regression coefficient files for the HIRS/2 and MSU limb corrections, together with a topography file ascertaining topography type and elevation (both resolution 1° X 1° and 0.5° X 0.5° latitude-longitude). When the execution is done the two data sets are created. One, called IMAGE data set, is formatted

to facilitate the display of horizontal fields for any recorded parameter, the other, the sounder data set, is arranged to provide vertical profiles of radiance measurements for each HIRS/2 location. The retrievals will be calculated from this sounding data set.

4) Atmospheric Parameter Retrieval Module

This is the most important scientific module in the sounding data processing system. There are two functions in this module. One is to calculate "clear column radiance" measurements, the other is to derive atmospheric parameters, such as atmospheric temperature, water vapor mixing ratio, total ozone and geopotential heights using the clear column radiance.

The nominal horizontal resolution of soundings from TOVS has been set at 80 Km. Information from the Preprocessor is organized to permit the formation of "boxes" whose dimensions are 3 scan spots across the satellite track by 3 scan spots along the track.

There are in essence two approaches: either find sufficient "holes" in the clouds, form whose uncontaminated observations the desired volume estimate can be obtained or apply physical and mathematical techniques to infer clear-column radiances from the contaminated ensemble. Both methods are employed in this module.

Initially, the observations for each field of view in a box are given objective tests to determine the probable presence of clouds. Window channels are checked for consistency. The regression test is worthy of elaboration. The vertical weighting functions of several tropospheric-sensing HIRS/2 spectral intervals bracket those of the MSU channels (Smith et al., 1979). Therefore, it is physically reasonable to expect high accuracy in predicting the latter form the former in the absence of clouds. On the other hand, in the presence of clouds, the HIRS-predicted MSU radiance will be too low. Regression coefficients are generated from the data which is know to be clear. When clouds are present, the regression relationships based on clear data fail (McMillin and Dean, 1982). In the present system the difference between observed MSU channel 2 radiance and infrared-based regression estimate of the microwave brightness temperatures is calculated. A small difference implies a clear column, a large difference indicates a cloudy column. If such a "clear" spot is found, then it is used for retrieving a profile as the representative profile of the box. If the box is partly cloudy, the adjacent-pair, or N^*, technique using eigenvectors as described in Smith and Woolf (1976) is used to calculate the clear column radiances. The technique is based on two important assumptions: that the clouds in each FOV are at the same level but differ in horizontal coverage and that the temperature and moisture profiles in each FOV are identical. Again, the MSU channels are used as references for the clear column definition. If the calculated N^* clear column HIRS/2 data used to predict the MSU channel radiances give unsatisfactory results, the clear radiance for this pair is rejected, and no temperature retrieval occurs. If a clear column radiance is determined, then the eigenvector regression method is employed (Smith et al., 1976) for atmospheric parameters. The regression coefficients used for both clear radiance and retrievals are accessed from support subsystem. From this module the geopotential heights are generated based on surface pressure, moisture, and temperature. The ozone amount for a

clear box is regressed. Finally, the retrieved parameters are stored on disk file.

5) Output Products

The products from the sounding data processing system include vertical profiles of temperature for 40 pressure levels from 1000 hpa to 0.1 hpa, and water vapor mixing ratio for 40 pressure levels from 1000 hpa to 300 hpa. They also include the total ozone content in a vertical column of the atmosphere. The products are produced on average every 80 Km via the retrieval process. In addition, there is also the capability to produce geopotential height between selected standard pressure levels, and clear column radiances (in form of brightness temperature), and earth-located, calibrated radiances for 27 spectral channels of the three instruments (HIRS/2, MSU and SSU).

The product output section takes data from the intermediate data file and produces the various outputs required by users. One component of this section is to provide data to NMC (a 9600 bps line between NMC and SMC is not available now). The second is to provide a group of the software for plotting temperature, water vapor mixing ratio, etc. at a specific pressure level, as well as brightness temperature for each channel on printer. The third is to display sounding data in a special terminal to be linked with IBM 4381 computer. The fourth is to facilitate the image display of horizontal fields of window or water vapor channel brightness temperature through M-70 or laser facsimile. The fifth is to perform the archiving functions, for instance, archiving the necessary data in the magnetic tape.

B. Support Subsystem

The support subsystem has two primary functions: (a) to provide the operational subsystem with updated coefficients (for input into the atmospheric parameter retrieval module) to maintain accuracy of the sounding products, and (b) to provide evaluations twice per day of the soundings produced by the Operational Subsystem. This subsystem is comprised of two essential components - the Radiosonde Matchup Module (RAOBINF, DSD3INF, YRSM2, YXCFLTR, YCRIVIA, etc.) and the Coefficient Update Module (YPRGNU1, YPRGNU2, YPRGNU3, YPRGNU5, YPRGNU6, YCOFRET, and YCOPYCDB).

1) Radiosonde Matchup Module

Currently, the regional sounding data processing system in Beijing shows that it requires three sets of coefficients, one for each zone (70°N-60°N, 60°N-30°N, 30°N-0°N). This module reads the radiosonde data on 1600 BPI/2400 ft magnetic which is done on the HITAC M170 computer, and transfers it to IBM 4361. The program accesses the satellite temperature and moisture profiles (from the Operational Subsystem) and matches them up in space and time with radiosonde data. To adjust for time differences, radiosondes from 00Z an 12Z are interpolated to the time of the satellite sounding. This is done twice a day using radiosondes from 00Z and 12Z. Every 12 hours, a statistical evaluation is performed between the retrievals and NMC radiosondes. These error statistics are computed for each ten degree latitude band in order to monitor the accuracy of the sounding products. In every 24 hours all matchups are divided into two groups for each zone: The independent and dependent

samples are stored in a "tuning data base" which serves as input into the coefficient update module.

2) Coefficient Generation and Update Module

This module accesses the TOVS channel brightness temperature and matchups for each latitude zone from the matchup file (the tuning data base). The latitude zones rich in radiosonde data require approximately 14 days to achieve the desired sample size. The module uses eigenvector algorithms to generate eigenvalues, eigenvectors, and new coefficients for each zone on the dependent data set. The coefficients are for the retrievals of 20 lower levels (from 115 hpa to 1000 hpa) and 20 upper levels (from 0.1 hpa to 100 hpa) temperatures, and 15 lower level water vapor mixing ratios, as well as clear column radiances. These coefficients are then evaluated on the independent data. After a thorough evaluation, the new coefficients replace the old in the Operational Subsystem. The clear radiance and retrieval coefficients are updated routinely once per week.

4. COMPUTER REQUIREMENTS

The Operational Subsystem using the IBM 4361 computer requires seven minutes of cpu time, 516K of virtual storage for the processing of one orbit. The total output is approximately 300 soundings from one orbit of one spacecraft. For the support subsystem the Radiosonde Matchup Module requires two minutes of cpu time (per run). The Coefficient Update Module requires four minutes of cpu time. The maximum virtual storage for this subsystem is 1296 K.

5. RETRIEVAL ACCURACY AND PRIMARY RESULTS

The soundings from the retrieved process have been compared with the radiosonde data. Table 1 shows the differences (RMS) between matched radiosonde and satellite retrieved temperatures (except heavy cloudy area) with the coverage of the Beijing readout station (6 ten-degree latitude zones: (10°-70°N and 50°-150°E) from NOAA-10 descending orbits for 30-day period August 1987. NUM in the Table 1 means the number of match-ups. It is clear that the matchups are small in number for 10°-20° and 60°-70°N latitude zones. The low latitude results are quite good except for 1000, 200, 70, 20, and 10 hpa pressure levels. The large differences probably are caused by the poor vertical resolution problem of sounder and the poor discrimination of low clouds as well as the complicated topography. There is a trend from a small difference to a relatively large difference as latitude increases, while the results become better again in latitude zone 60°-70°N. Because of too few matchups in zone 10°-20°N, Table 2 only shows the RMS difference of temperatures for cloud-free (C) and partly cloudy (N^*) cases for zone 20°-70°N separately. The major points shown by Table 2 are the following:

- The N^* retrievals are small in number which may be caused by N^* approach.

- The temperature retrieval accuracy in cloud-free cases for 10°-40°N is much better than in partly cloudy cases, and better for the pressure levels in 50°-70°N, but for 40°-50°N the accuracy in the most pressure levels for clear cases in less accurate. Perhaps the reason is that the temperature

Table 1. The differences (RMS) between matched radiosonde and satellite Temperature from NOAA-10 for the 30-day period August 1987.

P (hpa)	10° - 20° N		20° - 30° N		30° - 40° N		40° - 50° N		50° - 60° N		60° - 70° N	
	NUM	RMS	NUM	RMS	NUM	RMS	NUM	RMS	NUM	RMS	NUM	RMS
1000	83	1.38	568	1.95	987	3.06	242	4.18	88	3.37	x	x
850	126	1.97	1252	1.81	1251	2.80	1356	3.75	1205	3.22	74	2.92
700	126	1.19	1253	1.32	1286	2.22	1392	3.03	1244	3.22	74	2.99
500	126	1.27	1256	1.42	1295	2.05	1408	2.68	1268	3.53	74	1.91
400	126	1.50	1258	1.16	1801	2.30	1414	2.42	1269	3.47	74	2.34
300	129	1.24	1264	1.46	1811	2.56	1417	3.09	1289	3.64	74	2.39
250	129	1.69	1264	1.32	1822	2.56	1432	3.67	1305	4.08	84	3.90
200	129	2.13	1265	1.62	1822	3.20	1438	4.21	1321	3.99	85	4.42
150	129	2.23	1265	1.75	1835	2.40	1475	2.51	1448	2.65	86	2.48
100	"	2.19	1268	2.06	1838	2.58	1478	2.96	1448	1.80	86	1.96
70	109	3.50	1240	2.54	1813	2.92	1401	3.16	1380	1.77	85	2.87
50	110	1.80	1241	2.02	1803	2.23	1394	2.63	1334	1.96	85	2.26
30	76	2.28	1160	2.13	1728	2.57	1361	3.57	1241	3.50	81	1.76
20	41	3.69	994	2.73	1443	2.34	1336	2.71	1330	2.86	118	2.70
10	10	4.23	134	4.12	180	4.74	334	2.99	741	2.85	106	2.80

Table 2. Same as in Table.1, but for clear (C) and partly cloud (N*) cases.

P (hpa)	20° - 30° N				30° - 40° N				40° - 50° N				50° - 60° N				60° - 70° N			
	C		N*		C		N*		C		N*		C		N*		C		N*	
	NUM	RMS	NUM	RMS	NUM	RMS	NUM	RMS	NUM	RMS	NUM	RMS	NUM	RMS	NUM	RMS	NUM	RMS	NUM	RMS
1000	474	1.89	34	4.81	941	3.02	63	3.46	235	4.21	13	3.51	96	3.33	61	4.08	x	x	x	x
850	1003	1.86	63	2.81	1644	2.80	90	2.82	1251	3.78	23	3.51	1259	3.24	154	3.55	76	2.93	5	1.53
700	1004	1.36	63	2.24	1675	2.20	90	2.28	1288	3.09	23	2.59	1291	3.27	155	4.09	76	3.06	10	1.88
500	1004	1.39	63	1.63	1682	2.00	90	3.54	1308	2.68	24	2.70	1325	3.53	156	3.24	76	2.03	10	3.83
400	1006	1.17	63	1.24	1687	2.31	90	3.71	1314	2.42	24	2.88	1333	3.52	156	3.66	76	2.34	10	2.98
300	1009	1.49	63	2.27	1702	2.57	95	3.26	1317	3.07	24	2.16	1337	3.66	160	3.60	77	2.38	10	5.47
250	1009	1.37	63	1.96	1704	2.52	98	2.93	1331	3.62	25	4.17	1383	4.13	163	4.20	88	3.97	10	5.32
200	1010	1.66	63	1.47	1704	3.18	102	3.47	1336	4.27	31	3.46	1394	4.14	171	4.92	89	4.52	10	3.99
150	1010	1.82	63	2.97	1714	2.36	102	3.32	1373	2.51	31	2.71	1531	2.71	190	4.67	91	2.63	10	3.45
100	1013	2.12	63	2.63	1711	2.44	103	3.43	1376	2.96	31	2.19	1531	1.79	191	3.60	91	2.03	10	1.79
70	995	2.48	62	3.19	1694	2.91	103	3.79	1295	3.16	31	2.18	1469	1.76	179	3.08	90	2.88	10	1.02
50	997	2.00	62	2.38	1688	2.22	104	2.52	1293	2.63	31	1.79	1417	1.91	175	1.59	90	2.26	10	1.08
30	948	2.14	60	2.25	1619	2.59	101	1.95	1271	3.57	25	2.14	1328	3.53	169	1.74	86	2.09	10	2.03
20	872	2.7	52	2.54	1344	2.36	94	2.14	1255	2.71	15	2.79	1437	2.82	147	2.96	123	2.72	10	0.90
10	96	3.51	2	6.04	169	4.86	35	4.33	337	2.99	2	3.59	804	2.89	109	3.60	118	2.89	7	2.93

gradient in low and high latitude is smaller, so the effect of cloud on the temperature retrievals is larger. For 40°-50°N, the valid cloud tests are required.

Figure 3 illustrates the retrieval analyses of 500 hpa temperature from NOAA-10 four orbits, 11 December 2312 GMT 12 December 0418 GMT.

Figure 4 presents the analyses of the conventional temperature for the corresponding location observed at 0000 GMT 12 December 1987. Comparison of the two charts shows that the good agreement found between temperature analyses of satellite and radiosonde data generally, but the retrievals are older than the radiosondes.

Figure 5 is HIRS/2 channel 8 and 11 brightness temperature pictures separately. In comparison and analysis of the brightness temperature fields between the infrared window channel image (Fig. 5a) and the channel 11 water vapour image (Fig. 5B), it is clear that the characteristics of the two low brightness temperature cloudy area in 30°-40°N and 75°-90°E is similar, however, the space system of the water vapour image is more and much clearer than the window channel image and these cloud systems is directly related to the temperature trough (Fig. 3 and 4) in the same area.

The absolute bias (divided by total water vapor mixing ratio for each pressure level) between the retrieved and radiosonde observed water vapor mixing ratio is about 30%. Figure 6 shows the comparisons of NOAA-9 TOVS retrieved and radiosonde-observed water vapor profiles for four ten-degree zones from August 22-24, 1986, and also shows the comparisons for two stations (Guangzhou and Zhangjiakou).

The accuracy of the total ozone amount is about 10% compared to values derived from Dobson measurements. Figure 7 shows the distributions of total ozone amount over China form NOAA-7 TOVS retrievals for different time in 1984.

6. FUTURE PLANS

The derivation of cloud parameters (cloud height, cloud emissivity, etc.) will be incorporated into the processing scheme. One of the areas of the retrieval process requiring further development is the specification of surface characteristics so as to identify surface effects on the outgoing radiances, especially over land. The highest mountain in the world, Qinghai-Tibet plateau, located in the west of China, plays an important role in the radiation process to significantly affect the synoptic and climatic process in this area. Improving sounding accuracy is expected over this high terrain. Accurate ground and near surface air temperature for monitoring air pollution is also expected. The high resolution sensor data, AVHRR, can be used for obtaining more accurate clear column radiances. While the present procedure uses eigenvector method, more physical methods of retrieval without any dependence on conventional data are being tested, so the improvement in accuracy is under way. The implementation and development of the Man computer Interactive Data Access System (McIDAS) is being carried out this year. It will be used particularly for the satellite data processing and display

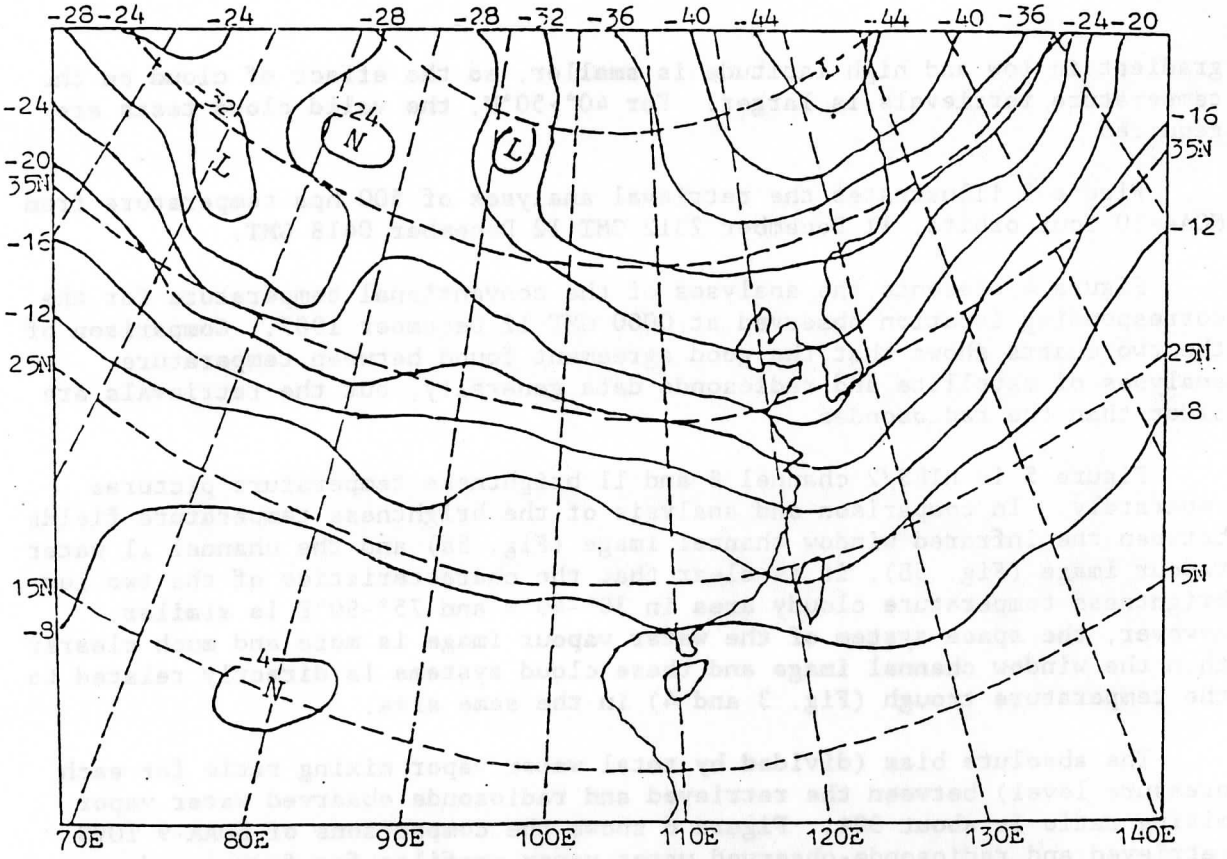

Fig. 3. Retrieval analyses of 500 hpa temperature for NOAA 10,11 December 2312 GMT 12 December 0418 GMT.

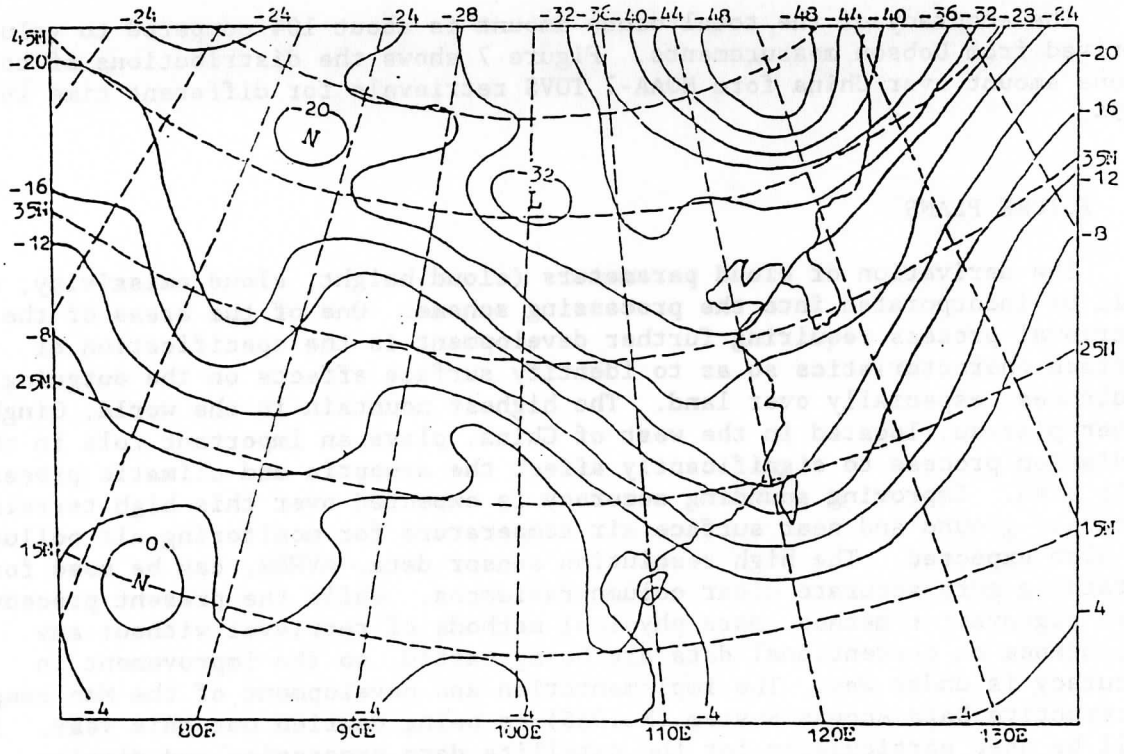

Fig. 4. Temperature analyses of 500 hpa from radiosondes 12 December 0000 GMT.

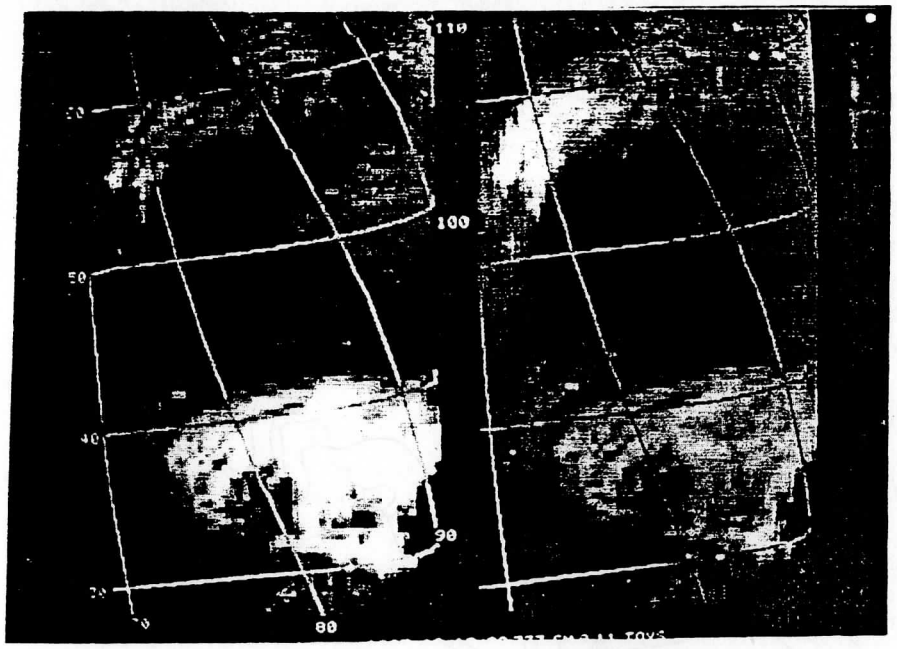

A B

Fig. 5. HIRS/2 channel 8(a) and 11 (b) pictures on 12 December 0233 GMT, NOAA-10.

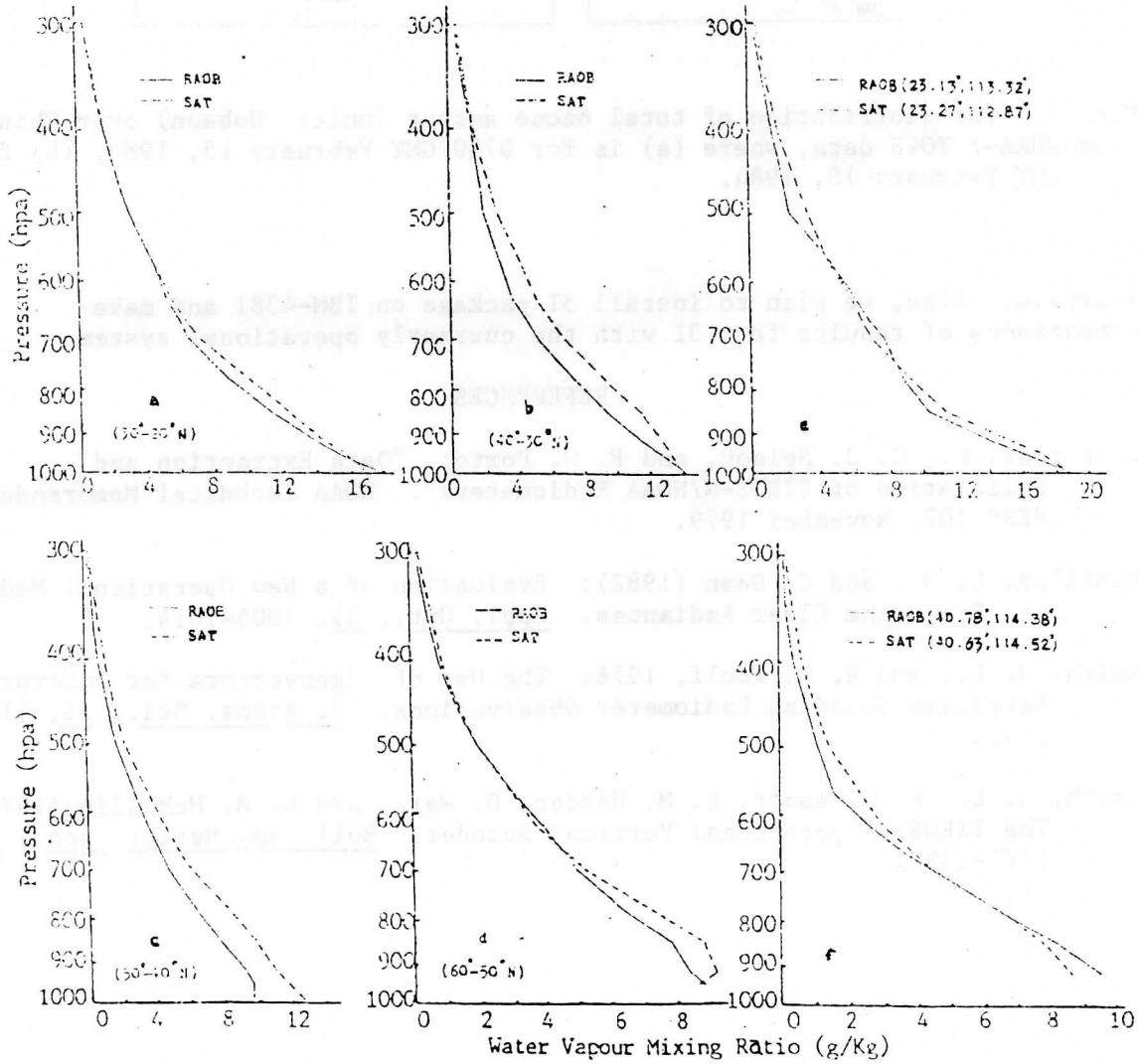

Fig. 6. Comparisons between NOAA-9 TOVS retrieved and radiosonde observed water vapor profile for four latitude zones from Aug. 22-24, 1986, and for two stations (E. Guangzhou and F. Zhangjiakou) in the morning on Aug. 24, 1986. In the end figs., solid lines indicate radiosonde observed water vapor profiles and dash lines are TOVS retrievals.

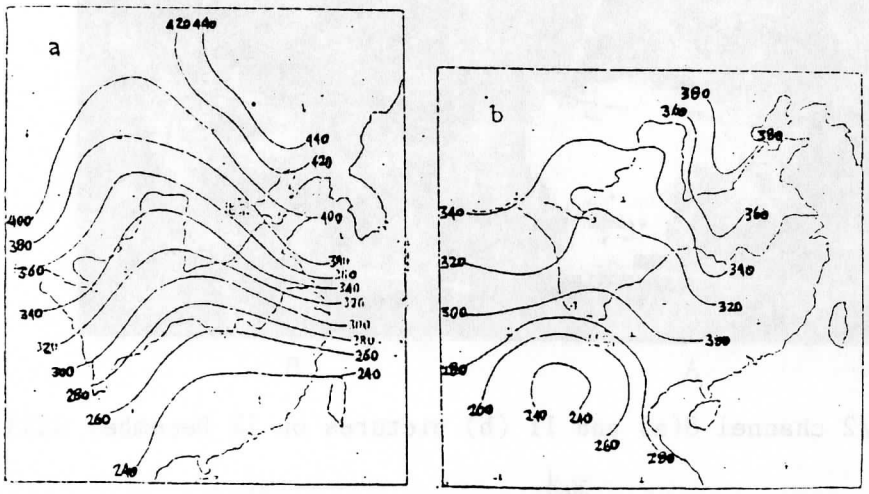

Fig. 7. The distribution of total ozone amount (unit: Dobson) over China from NOAA-7 TOVS data, where (a) is for 0730 GMT February 15, 1984, (b) for 2100 GMT February 18, 1984.

analysis. Also, we plan to install 3I package on IBM-4381 and make comparisons of results from 3I with the currently operational system.

REFERENCES

Lauritson, L., G. J. Nelson, and F. W. Porto: "Data Extraction and Calibration of TIROS-N/NOAA Radiometers". NOAA Technical Memorandum, NESS 107, November 1979.

McMillin, L. M., and C. Dean (1982): Evaluation of a New Operational Model for Producing Clear Radiances. Appl. Opt., 21, 1005-1014.

Smith, W. L., and H. M. Woolf, 1976: The Use of Eigenvectors for Interpreting Satellite Sounding Radiometer Observations. J. Atmos. Sci., 33, 1127-1140.

Smith, W. L., H. M. Woolf, C. M. Hayden, D. Wark, and L. M. McMillin (1979): The TIROS-N Operational Vertical Sounder. Bull. Am. Meteor. Soc., 60, 1177-1187.

A NEW INVERSION METHOD FOR TOVS DATA: NON-LINEAR OPTIMAL ESTIMATION APPLIED TO CLOUDY RADIANCES

J.R. Eyre

Meteorological Office Unit,
Robert Hooke Institute for Cooperative Atmospheric Research,
Clarendon Laboratory, Oxford, U.K.

1. INTRODUCTION

At present, the Meteorological Office processes TOVS data routinely in real-time using retrieval methods described in previous reports (Eyre et al. 1985, Eyre et al. 1986). Calibrated radiances undergo limb correction and other pre-processing using algorithms based on the International TOVS Processing Package (ITPP). HIRS data are then cloud-cleared using a sequential estimation scheme (Eyre and Watts 1987). Temperature and humidity profiles are retrieved simultaneously in a one-step (linear) scheme. This is a maximum probability method in which a forecast profile from a numerical weather prediction (NWP) model and its expected error covariance act as constraints on the inversion of the cloud-cleared radiances.

Recently a new method for TOVS inversion has been developed. It also uses an optimal estimation (maximum probability) approach, with a forecast profile and its error covariance as constraints. However it operates on "raw", potentially cloud-affected radiances in individual fields-of-view. The effects of clouds are to make the inverse problem highly non-linear, and an iterative algorithm is required to find the solution. Temperature and humidity profiles, surface temperature and microwave emissivity, and cloud-top pressure and cloud amount are retrieved simultaneously. The use of the forecast error covariance and the application of principles from probability theory make the retrieval method a "statistical" one. However, it is also a fully "physical" scheme, in that it involves calculations of radiances corresponding to each profile (including the effects of cloud) and also the derivatives of radiance with respect to all the profile parameters.

The theory of the new method is described fully by Eyre (1987) but is also outlined here. The method has so far been developed as an independent retrieval scheme. However, in doing so, attention has been paid to its compatibility with the assimilation procedures of an NWP scheme which might use these products. Indeed, the method could be applied as part of an NWP analysis scheme – the part which performs the analysis of satellite sounding data in the vertical, projecting radiance information on to the vertical levels of the analysis scheme, and to be followed by a horizontal analysis stage to spread the information from sounding locations to NWP model grid points. Thus, the retrievals are

no longer considered as an end in themselves but as an integral part of the NWP process; they are not treated as though they were poor quality radiosonde data, but in a manner more consistent with their true information content.

2. THEORY

The new inversion method follows the approach to the non-linear retrieval problem described by Rodgers (1976). The same method has also been proposed by Purser (1984) in the more general context of numerical analysis. Both solve a non-linear retrieval/analysis equation by Newtonian iteration.

In the context of TOVS inversion, we define a vector representing the atmospheric profile (including all variables to be retrieved simultaneously) as $\mathbf{x}$ and a vector of measured multi-channel radiances as $\mathbf{y}^m$. Using the measurements we seek the most probable value of $\mathbf{x}$, i.e. we try to maximise the conditional probability of $\mathbf{x}$ given $\mathbf{y}^m$, $P(\mathbf{x} \mid \mathbf{y}^m)$. Using Bayes' theorem we may write:

$$P(\mathbf{x} \mid \mathbf{y}^m) \; \alpha \; P(\mathbf{y}^m \mid \mathbf{x}) P(\mathbf{x}) \tag{1}$$

If the measurements have Gaussian errors of covariance $\mathbf{E}$ and the error-free measurements corresponding to profile $\mathbf{x}$ are $\mathbf{y}(\mathbf{x})$, then

$$P(\mathbf{y}^m \mid \mathbf{x}) \; \alpha \; \exp\{-\frac{1}{2}(\mathbf{y}^m - \mathbf{y}(\mathbf{x}))^T.\mathbf{E}^{-1}.(\mathbf{y}^m - \mathbf{y}(\mathbf{x}))\} \tag{2}$$

where ^{T} denotes matrix transpose and $^{-1}$ matrix inverse. The covariance of expected error in the forward model, $\mathbf{y}(\mathbf{x})$, should also be included in $\mathbf{E}$.

$P(\mathbf{x})$ represents our knowledge of $\mathbf{x}$ prior to making the radiance measurements. In the context of NWP, this is called the "background" information and is obtained from a forecast profile valid at the time of the measurement. This embodies information from previous observations and constraints imposed by equations governing the spatial and temporal variations of atmospheric fields. If the forecast profile is $\mathbf{x}^b$ with expected error covariance $\mathbf{C}$ then

$$P(\mathbf{x}) \; \alpha \; \exp\{-\frac{1}{2}(\mathbf{x} - \mathbf{x}^b)^T.\mathbf{C}^{-1}.(\mathbf{x} - \mathbf{x}^b)\} \tag{3}$$

Substituting (2) and (3) into (1) and taking the logarithm, we obtain an expression to be minimised:

$-ln\{P(\mathbf{x} \mid \mathbf{y}^m)\} + \text{constant}$

$$= \frac{1}{2}(\mathbf{y}^m - \mathbf{y}(\mathbf{x}))^T.\mathbf{E}^{-1}.(\mathbf{y}^m - \mathbf{y}(\mathbf{x})) + \frac{1}{2}(\mathbf{x} - \mathbf{x}^b)^T.\mathbf{C}^{-1}.(\mathbf{x} - \mathbf{x}^b) \tag{4}$$

This is often called the "penalty function" in numerical analysis theory. In minimising it, we obtain the profile $\mathbf{x}$ which represents the optimal simultaneous fit to the measurements and the background profile. Differentiating (4) with respect to $\mathbf{x}$ gives

$$\mathbf{C}^{-1}(\mathbf{x} - \mathbf{x}^b) - \mathbf{K}(\mathbf{x})^T.\mathbf{E}^{-1}.(\mathbf{y}^m - \mathbf{y}(\mathbf{x})) = 0 \tag{5}$$

where $\mathbf{K}(\mathbf{x}) = \mathbf{dy}(\mathbf{x})/\mathbf{dx}$.

We need to solve (5) for $\mathbf{x}$, but in general it does not have an analytic solution. This is a non-linear problem since $\mathbf{K}$ is a function of $\mathbf{x}$. This is particularly so when $\mathbf{x}$ includes cloud parameters with which the elements of $\mathbf{K}$ representing infra-red channels can vary very rapidly.

In the Newtonian iteration approach to the solution of (5), we guess a profile $\mathbf{x}_n$. In general this will not solve (5) but will lead to a residual:

$$\mathbf{R}_n = \mathbf{C}^{-1}.(\mathbf{x}_n - \mathbf{x}^b) - \mathbf{K}(\mathbf{x}_n)^T.\mathbf{E}^{-1}.(\mathbf{y}^m - \mathbf{y}(\mathbf{x}_n)) \tag{6}$$

Then the solution is approached using the iterative relation:

$$\mathbf{x}_{n+1} = \mathbf{x}_n - (\frac{d\mathbf{R}_n}{d\mathbf{x}_n})^{-1}.\mathbf{R}_n \tag{7}$$

where

$$(\frac{d\mathbf{R}_n}{d\mathbf{x}_n})^{-1} = \mathbf{S}_n = (\mathbf{C}^{-1} + \mathbf{K}_n^T.\mathbf{E}^{-1}.\mathbf{K}_n)^{-1}$$

$$= \mathbf{C} - \mathbf{C}.\mathbf{K}_n^T.(\mathbf{K}_n.\mathbf{C}.\mathbf{K}_n^T + \mathbf{E})^{-1}.\mathbf{K}_n.\mathbf{C} \tag{8}$$

Iteration proceeds until the increment $(\mathbf{x}_{n+1} - \mathbf{x}_n)$ is acceptably small.

The matrix $\mathbf{S}_n$ is interesting in its own right, as the value at convergence is an estimate of the error covariance of the retrieved profile. Calculation of $\mathbf{S}_n$ for a range of values of $\mathbf{x}_n$ gives an efficient mechanism for exploring the expected error characteristics of the retrievals (without having to perform simulated retrievals for a large number of cases).

The iteration is initialised with a "first guess" profile. This may in principle be arbitrary, but a good first guess will lead to a more rapid convergence. It is therefore convenient to use a forecast profile as both background and first guess. However it is necessary to distinguish clearly between the roles of the background and the first guess. The background profile (and its error covariance) act as constraints on the inversion, and the retrieved profile, which must satisfy (5), will be sensitive to the background information. The first guess profile however is just the starting point for the iteration; it affects the speed of convergence but not (normally) the profile to which the method converges.

An equivalent form for (6), (7) and (8) which is usually more efficient for computation is:

$$\mathbf{x}_{n+1} = \mathbf{x}_n + (\mathbf{x}^b - \mathbf{x}_n) + \mathbf{W}_n.\{\mathbf{y}^m - \mathbf{y}(\mathbf{x}_n) - \mathbf{K}_n.(\mathbf{x}^b - \mathbf{x}_n)\} \tag{9}$$

where

$$\mathbf{W}_n = \mathbf{C}.\mathbf{K}_n^T.(\mathbf{K}_n.\mathbf{C}.\mathbf{K}_n^T + \mathbf{E})^{-1} \tag{10}$$

This is the form suggested by Rodgers (1976) and is probably adequate for problems which are only weakly or moderately non-linear. However, experiments have shown that the inclusion of cloud parameters in $\mathbf{x}$ makes the problem discussed here so non-linear that the iteration will often oscillate away from the required solution unless we "damp" or "over-constrain" some of the parameters (see section 3). This may be done by replacing $\mathbf{C}$ by $\mathbf{C}^r$ in (8), where $C^r_{ij} = C_{ij}$ except for elements representing parameters to be damped for which $C^r_{ij} \ll C_{ij}$. The correct value of $\mathbf{C}$ is preserved in (6) to ensure that $\mathbf{x}$ solves the appropriate equation. With this modification, (9) and (10) become

$$\mathbf{x}_{n+1} = \mathbf{x}_n + \mathbf{I}^r.(\mathbf{x}^b - \mathbf{x}_n) + \mathbf{W}^r_n.\{\mathbf{y}^m - \mathbf{y}(\mathbf{x}_n) - \mathbf{K}_n.\mathbf{I}^r.(\mathbf{x}^b - \mathbf{x}_n)\} \tag{11}$$

and

$$\mathbf{W}^r_n = \mathbf{C}^r.\mathbf{K}_n^T.(\mathbf{K}_n.\mathbf{C}^r.\mathbf{K}_n^T + \mathbf{E})^{-1}, \tag{12}$$

where

$$\mathbf{I}^r = \mathbf{C}^r.\mathbf{C}^{-1} \tag{13}$$

It is important to note that the convergence criterion applied here differs from that used in many iterative retrieval schemes, in which the iteration proceeds until the measured and calculated radiances agree to within some tolerance. In this scheme, convergence is defined by the solution of analysis equation (5). The degree of fit between measured and calculated radiances in all channels at convergence gives an independent check which is found to provide a powerful mechanism for quality control.

3. APPLICATION TO TOVS DATA

In applying this approach to TOVS data, HIRS and MSU radiances are used in "raw" form; they undergo no pre-processing other than the mapping of MSU data to HIRS locations. To date, HIRS channels 1–8 and 10–15 and MSU channels 1–4 have been used. The profile vector includes all the variables which appear in the radiative transfer problem, i.e. the temperature and humidity profiles, surface skin temperature, pressure and microwave emissivity, and cloud-top pressure and effective fractional amount.

To make the scheme practicable, it has been necessary to develop a fast method for calculating $\mathbf{K}(\mathbf{x})$, the derivatives of the forward model. The TOVSRAD model (Eyre, 1984), which itself is an extension of ITPP algorithms, has been adapted to calculate all the elements of $\mathbf{K}(\mathbf{x})$ in parallel with the evaluation of the radiances $\mathbf{y}(\mathbf{x})$. Details are given by Eyre (1987).

The forward model includes the effects of cloud. At each step in the iteration, the current cloud-top pressure and effective fractional cloud amount (along with the current profile) are used to calculate the corresponding radiances in all infra-red channels. A single-layer cloud model is assumed. Also the use of the same effective cloud amount in all channels implies that cloud transmittance is assumed to be spectrally constant. Cases where the real cloud conditions are more complicated than this will occur, but we rely on the quality control procedure discussed in section 2 to identify cases where the assumptions are grossly deficient.

Cloud is assumed to have no effect on MSU radiances. This approximation is not always valid, as cloud liquid water often has a measurable effect on channel 1. However its effect is similar to that of a change in surface emissivity. Since we do not have sufficient microwave channels to separate these two effects, we can interpret the retrieved "surface emissivity" as an effective value which also compensates for cloud effects.

The treatment of measurement error is more rigorous here than in many retrieval schemes. The matrix $\mathbf{E}$ in section 2 represents expected measurement error but should include both radiometric errors (noise) and any uncorrected errors in the forward model. Even when an effective scheme is in operation for correcting biases in the forward model, there will remain uncorrected random errors which should be allowed for. Values for the standard deviation of error in forward model brightness temperatures are assumed (currently 0.2K

in all channels). These are converted to radiance errors at the appropriate measured brightness temperature, and the variance added to the radiometric error covariance in constructing **E**. This gives a different value of **E** for each retrieval. Depending on the channel and the measured brightness temperature, it is possible for either the radiometric component or the forward model component to be dominant.

The matrix **C** represents the expected covariance of background error. It can be estimated from available statistics of difference between forecast profiles and analyses or radiosonde measurements. Elements of the background profile not provided by the forecast model – cloud parameters and microwave surface emissivity – are assigned a very large value of background error and thus are not effectively constrained by the background values. More details of the method for constructing **C** are given by Eyre (1987) and recent developments in this area are discussed by Watts and McNally (1988).

The forecast profile provides both background and first guess for most elements of **x**. For surface emissivity, an average value is assumed. For cloud parameters, average values are used for the background but, in order to speed convergence, first-guess values are derived from measurements in HIRS channels 7 and 8. This method is described further by Eyre (1987). As explained in section 2, it is necessary to damp the adjustment of some parameters during the iteration. It is found to be necessary, in this case, only for the cloud parameters.

4. SUMMARY OF RESULTS

The method has been studied theoretically through calculations of the matrix **S**, and it has been applied to simulated TOVS radiances. These results are reported fully by Eyre (1987), but the main conclusions were as follows.

In cloud-free cases, the theoretical performance of the scheme is similar to that of other schemes, showing an ability to make a modest but significant improvement on a short-range forecast of reasonable accuracy (i.e. one in error by $\sim$ 2K). In fully cloudy conditions, performance degrades at levels well below the cloud-top; as expected, we have essentially an MSU-only retrieval here. However around and just above the cloud-top, a small improvement is seen in retrieval performance compared with the cloud-free case. The effect results from the sharpening of the HIRS weighting functions by the cloud and is illustrated in Fig.1. This demonstrates a theoretical advantage of retrieving cloud parameters simultaneously with other variables.

Cloud parameters are retrieved with reasonable accuracy under most conditions and particularly well for significant amounts of high cloud (i.e. to better than 20 mb in cloud-top pressure and 5% in fractional amount). Low-level cloud is retrieved less accurately but this uncertainty does not degrade the temperature profile retrieval unduly.

The theoretical retrieval performance is found to be particularly sensitive to the strength of the inter-level correlations of forecast error. The interpretation of this finding is as follows: given the breadth of the weighting functions, forecast errors can only be "seen" by TOVS if they are coherent over some depth of the atmosphere; errors with only small vertical scale cannot be observed and corrected by the inversion process. A thorough understanding of forecast error structures is therefore important, if TOVS data are to be used optimally within NWP systems.

The new inversion method has also been tested successfully on real TOVS data for a small number of cases. The scheme was developed at the Co-operative Institute for Meteorological Satellite Studies (CIMSS) at the University of Wisconsin–Madison. It was applied to TOVS data from January 1986 coincident with the Generation of Atlantic Lows Experiment (GALE) over the eastern USA and western Atlantic. Background profiles for the exercise were obtained from CIMSS' regional model. Details of this study are given by Eyre (1988).

5. FUTURE PLANS

It is planned to continue trials of the new scheme in several ways. It will be applied to more data to test its robustness over a wide range of meteorological conditions and to acquire sufficient collocations with radiosonde data to allow its performance to be examined statistically. It will also be applied to more case studies and its ability to capture features of interest at high horizontal resolution will be investigated. Some theoretical improvements to the present scheme will also be studied.

As mentioned in the introduction, the new scheme may be considered as the first (vertical) part of a split analysis scheme, to be followed by a second (horizontal) part which spreads information to NWP model grid points. The second operation should take into account the correlation of errors between background and retrieval (and hence between adjacent retrievals) introduced by the first stage. Lorenc et al. (1986) have suggested a method for doing this. Weights to be applied to each level of each retrieval are calculated on the basis of the ratio of retrieval and background error variances (i.e. the diagonal elements of matrices **S** and **C**). These data are provided by the new scheme, along with the retrieved and background profiles themselves. The use of these weights will be studied in experiments on horizontal analyses made using these retrievals.

Although applied here to TOVS data, the new scheme is quite flexible and should be suitable for application to many types of data. In particular, the extension of the scheme to Advanced TOVS (HIRS + AMSU) data expected from satellites NOAA-K, –L and –M will be explored.

ACKNOWLEDGEMENTS

This work was started while I was a visiting scientist at CIMSS, University of Wisconsin–Madison. I wish to thank Dr. W.L. Smith and his colleagues at CIMSS for their support.

REFERENCES

Eyre J.R. 1984. User guide to TOVSRAD: a program for calculating synthetic HIRS-2 and MSU equivalent black body temperatures. Met.O.19 Branch Memo 75, Meteorological Office, Bracknell.

Eyre J.R. 1987. Inversion of cloudy satellite sounding radiances by non-linear optimal estimation: theory and simulation for TOVS. Submitted to Q.J.R. Meteorol. Soc., Dec 1987.

Eyre J.R. 1988. Inversion of cloudy satellite sounding radiances by non-linear optimal estimation: application to TOVS data. Submitted to Q.J.R. Meteorol. Soc., Jan 1988.

Eyre J.R., Pescod R.W., Watts P.D., Lloyd P.E., Adams W. and Allam R.J. 1986. TOVS retrievals in the U.K.: progress and plans. Tech. Proc. 3rd Int. TOVS Study Conf.; Madison, Wisconsin; 13–19 August 1986; Report of CIMSS, Univ. of Wisconsin-Madison; Ed.: W.P. Menzel; pp. 60–91.

Eyre J.R. and Watts P.D. 1987. A sequential estimation approach to cloud-clearing for satellite temperature sounding. Q.J.R. Meteorol. Soc., **113**, 1349–1376.

Eyre J.R., Watts P.D., Turner J. and Lorenc A.C. 1985. Research and development on TOVS retrievals in the U.K. Tech. Proc. 2nd Int. TOVS Study Conf.; Igls, Austria; 18-22 February 1985; Report of CIMSS, Univ. of Wisconsin-Madison; Ed.: W.P. Menzel; pp. 94–100.

Lorenc A.C., Adams W. and Eyre J.R. 1986. The analysis of high resolution satellite data in the Met. Office. Proc. ECMWF Workshop on "High Resolution Analysis"; Reading, U.K., 24–26 June 1985; ECMWF Report, pp.69-87.

Purser R.J. 1984. A new approach to optimal assimilation of meteorological data by iterative Bayesian analysis. Preprints 10th Conf. on Weather Forecasting and Analysis; Clearwater Beach, Florida; 25–29 June 1984; American Met. Soc., Boston, pp. 102–105.

Rodgers C.D. 1976. Retrieval of atmospheric temperature and composition from remote measurements of thermal radiation. Rev. Geophys. Sp. Phys., **14**, 609–624.

Watts P.D. and McNally A.P. 1988. The sensitivity of a minimum variance retrieval scheme to the values of its principal parameters. To appear in Tech. Proc. 4th Int. TOVS Study Conf.; Igls, Austria; 16-22 March 1988.

Figure 1.

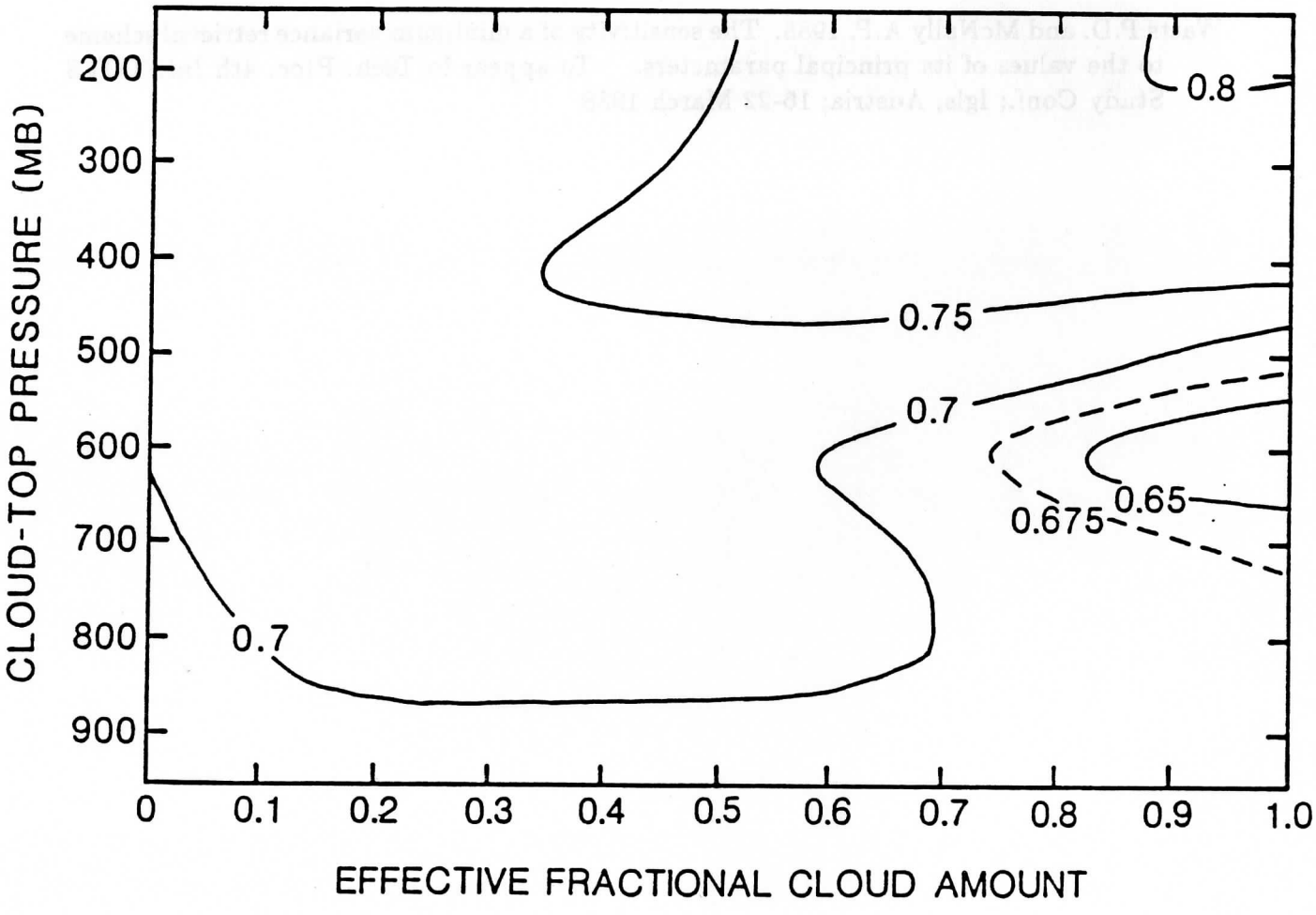

Theoretical errors in retrieved 500 mb temperature expressed as fractional unexplained variance (i.e. retrieval error variance divided by background error variance) as a function of cloud conditions.

GLOBAL USE OF TOVS RETRIEVALS IN NWP AT ECMWF

J. F. Flobert

European Centre for Medium-range Weather Forecasts (ECMWF)

Shinfield Park, Reading, Berkshire RG2 9AX, England

1. INTRODUCTION

NESDIS have provided a dataset of raw radiances (level 1B data; Kidwell, 1986) and retrievals at 80 km resolution, for a period of one month (15 January 1987 - 15 February 1987).

Since December 1986, the 3I code (Chedin et al, 1985; Chedin et al, 1986; Scott et al, 1988), has been implemented, validated and run in global experiments using these data at ECMWF.

After calibration (ITPP3 software, Smith et al, 1983) these data are processed with the 3I code, producing geopotential thicknesses and relative humidities. Cloud top heights, effective cloud amounts and surface temperature are also derived. The complete processing from the level 1B raw counts for two satellites (NOAA-9 and NOAA-10) for a period of six hours requires 23 minutes CPU, using one processor of the Cray XMP48.

2. USE OF 3I PRODUCTS

The data assimilation at ECMWF (Kelly and Pailleux, 1988) is done every 6 hours and uses conventional observations, cloud track winds and satellite determined profiles (Satems). These Satems contain geopotential thicknesses and precipitable water contents at approximately 250 km resolution and are retrieved from the Tiros-N series satellites (NOAA-9 and NOAA-10 during January-February 1987) by NOAA-NESDIS.

The use of 3I in the data assimilation involves the replacement of the present "Satems" with the corresponding 3I products.

The increased horizontal resolution of 3I soundings (100 km) compared to the 250 km resolution of the "Satems" has highlighted the need for a screening, since 30000 3I soundings are produced per analysis cycle (6 hours period). There is currently a practical limit of 20000 soundings in the data assimilation; therefore a strong quality control is presently being investigated.

3. PRESENT RESULTS

3.1 Comparison with collocated radiosondes

The 3I profiles have been collocated with radiosondes, to assess the quality of the retrievals, and a similar comparison has been done for the 80 km "Satems" produced by NESDIS.

The maximum time difference for a comparison is 3 hours, while the maximum distance difference is either 100 km or 150 km. Radiosondes of questionable quality (transmission problems, etc...) have been eliminated for differences greater than 10K. Results are shown for the 1st February 1987 at 12 GMT, for different latitude bands (Figures 1 to 4), retrievals are done with both NOAA9 and NOAA10.

The 3I and NESDIS results appear very similar, if we except the northern latitudes (Fig 4). In particular, the bias pattern is very close, even if 3I results are maybe a little colder. The standard deviations are also very close, if we except the first layer (1000 - 850 mb) for which 3I results are consistently better.

In the northern latitudes, the results appear more different, but the NESDIS results have been screened strongly (the number of collocations is about a third of the one with 3I results, while it is otherwise about three quarters). It apparently does not improve the results, the bias is even worse than in the other cases. However a direct comparison is difficult in this case, the collocation samples being too different.

The same statistics are shown over China (Fig 5). Serious bias problems, mainly in the 30-50 mb layer, appear for both 3I results and NESDIS results: it appears the main reason is the lack of vertical resolution (we can rely only on MSU 4, at these altitudes) more than bias problems resulting from validation of forward models (see Kelly and Flobert, 1988). These problems (as well as high ground retrievals problems) are presently investigated.

3.2 Assimilation of 3I products at ECMWF

A five day assimilation (over the period 30 January - 3 February 1987) of 3I products (approximately 14000 soundings per 6 hour-period: a screening has been applied) has been run recently at ECMWF.

Results will be shown on global maps for the 7th cycle of assimilation (31 January at 12GMT). Three layers are presented: the bottom layer (1000-700 mb) the tropopause layer (300 - 100 mb) and the top layer (30-10 mb). The contours are virtual temperature isolines; the control analysis using NESDIS profiles (SANES), is shown on Figs 6 to 8, the analysis assimilating 3I results (SAIII) is on Figs 9 to 11, the difference maps are on Figs 12 to 14.

At first look, the global maps appear similar, the general shape being the same and the main features well represented in both analyses. However, the difference maps show significant differences, particularly for the bottom layer and the stratosphere, the results in the thick layer around the tropopause (300 - 100 mb) appearing closer to each other.

In the lowest layer, both analyses are almost identical over land (satellite retrievals are not used below 100 mb). Over sea, there are significant differences on all extra-tropical regions. In the tropopause layer, the same comments apply over land, while the differences remain small over sea. In the stratosphere, the main features (low of -70°C over Europe, high of -35°C over Eastern Siberia) are well retrieved, though significant differences appear on both hemispheres.

4. CONCLUSION

The quality of the statistics between retrieved profiles and collocated radiosondes appear very similar, whereas the assimilation of these temperature and water vapor profiles in the analysis leads to significant changes, particularly in the stratosphere and the low troposphere.

The significant changes in the analyses are likely to cause changes in the forecasted fields: nevertheless it is presently too early to foresee if assimilating 3I results leads to an improvement, or a degradation. We need a deeper investigation (comparison of a number of forecasts after several days of assimilation of 3I results, impact of the higher resolution) before drawing any definitive conclusions. This investigation has started, the first conclusions are expected in summer 1988.

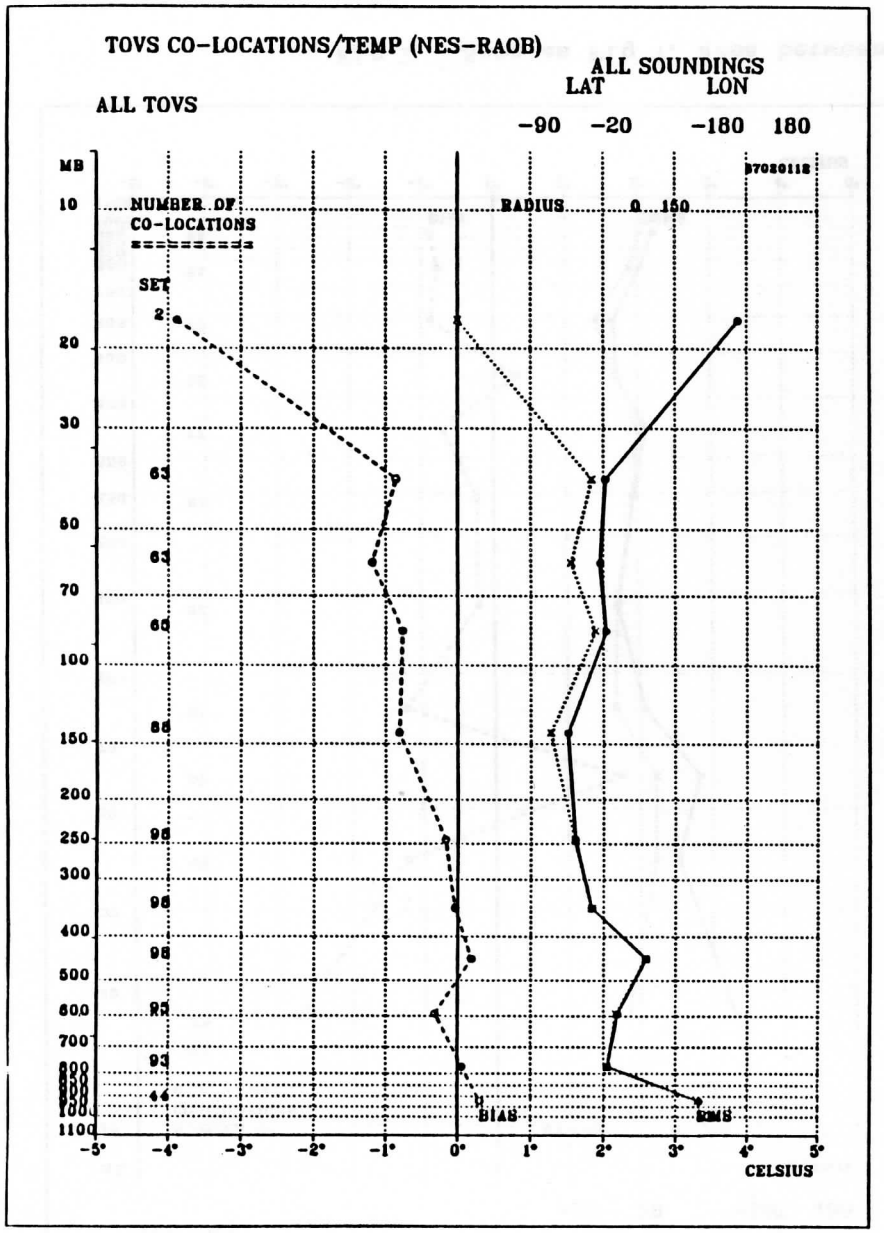

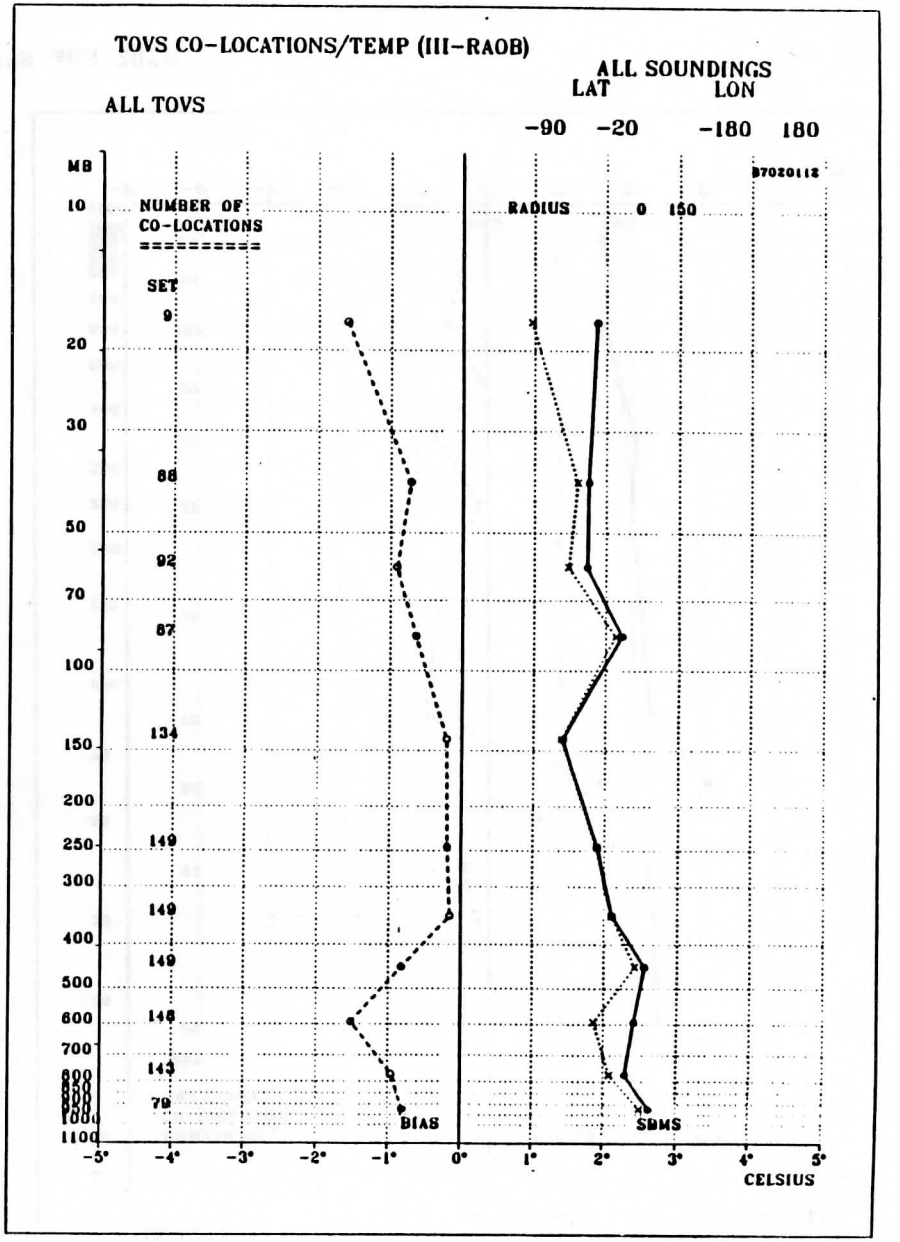

Fig 1 Statistics with collocated radiosondes: area between 90°S and 20°S, the maximum distance difference is 150 km.
Solid line: RMS, dotted line: standard deviation, dashed line: bias

a) 80 km "Satems" produced by the NESDIS

b) "Satems" produced with the 3I method

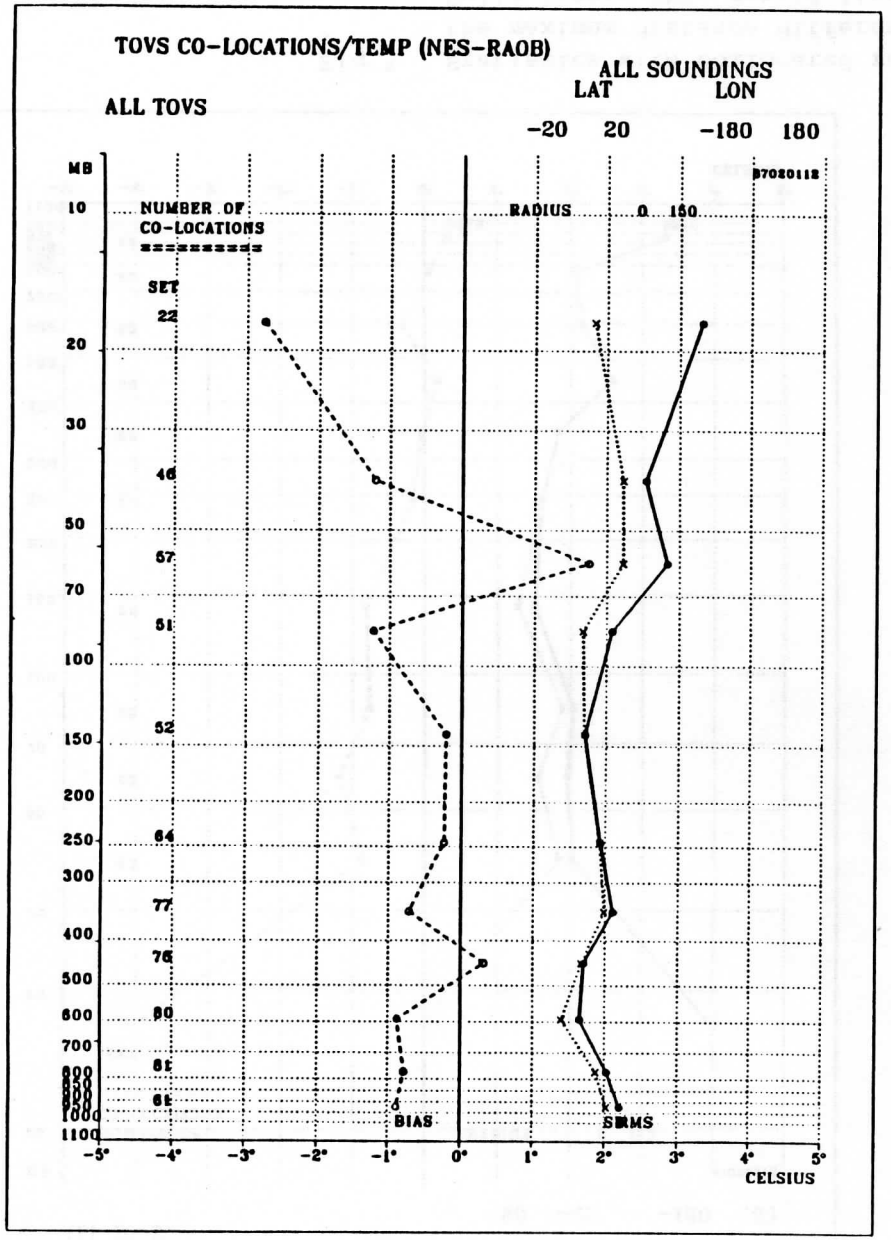

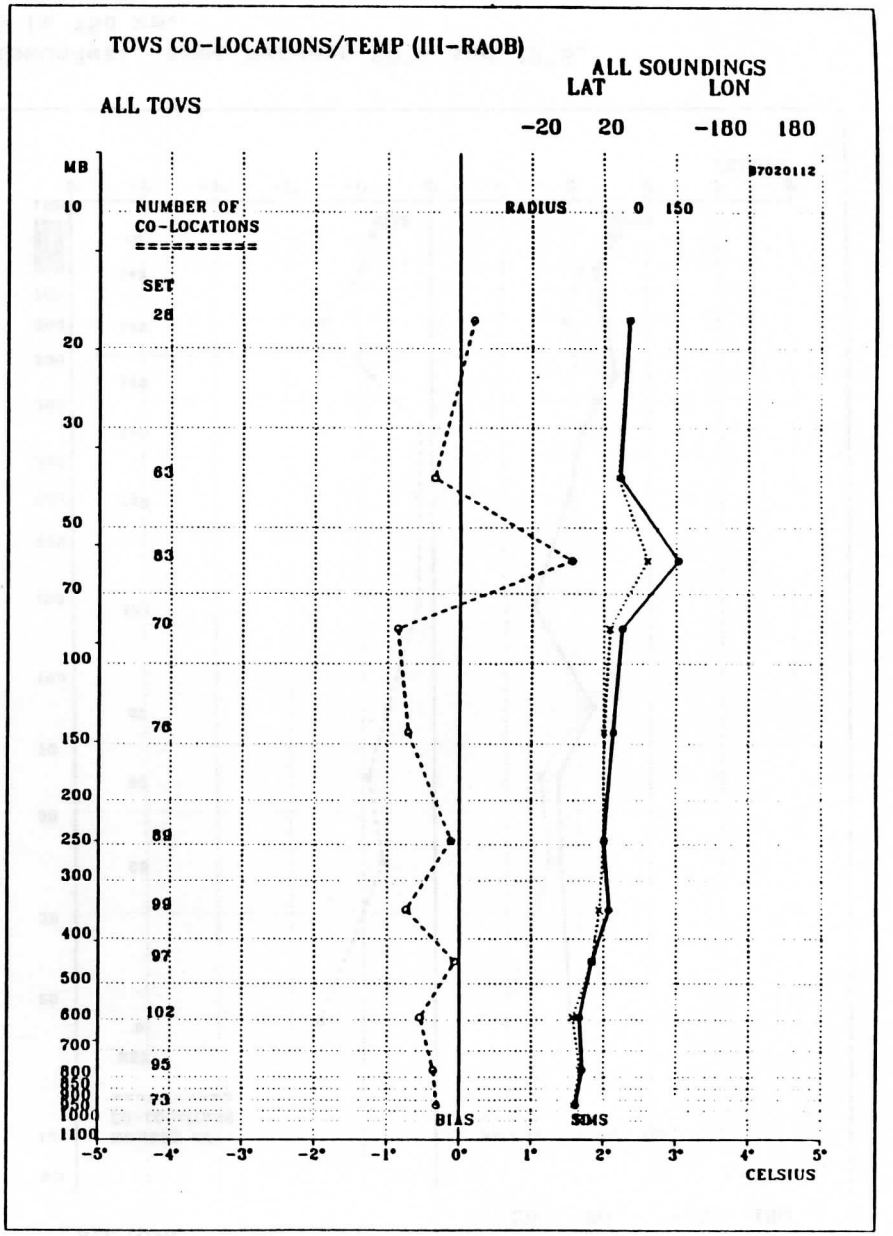

Fig 2 Same as Fig 1, area between 20°S and 20°N

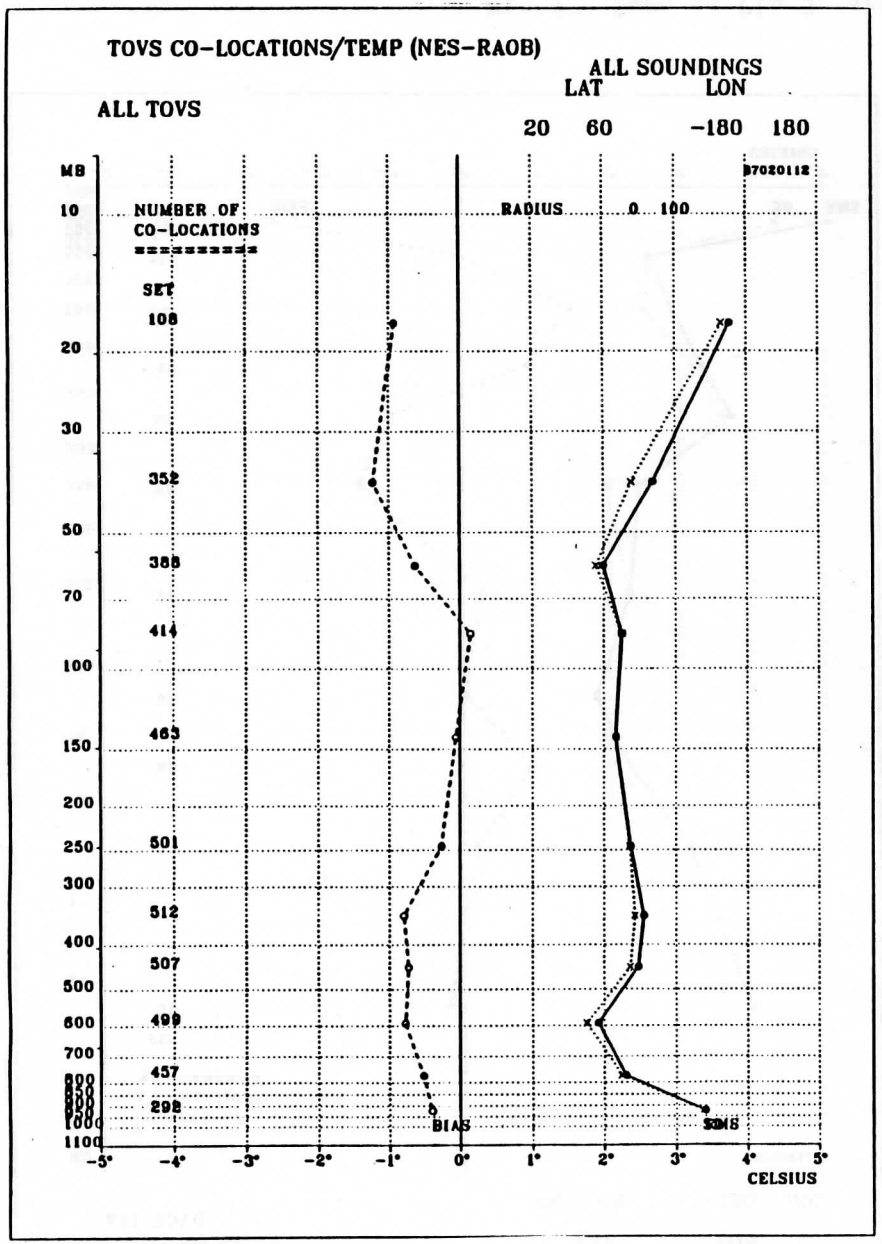

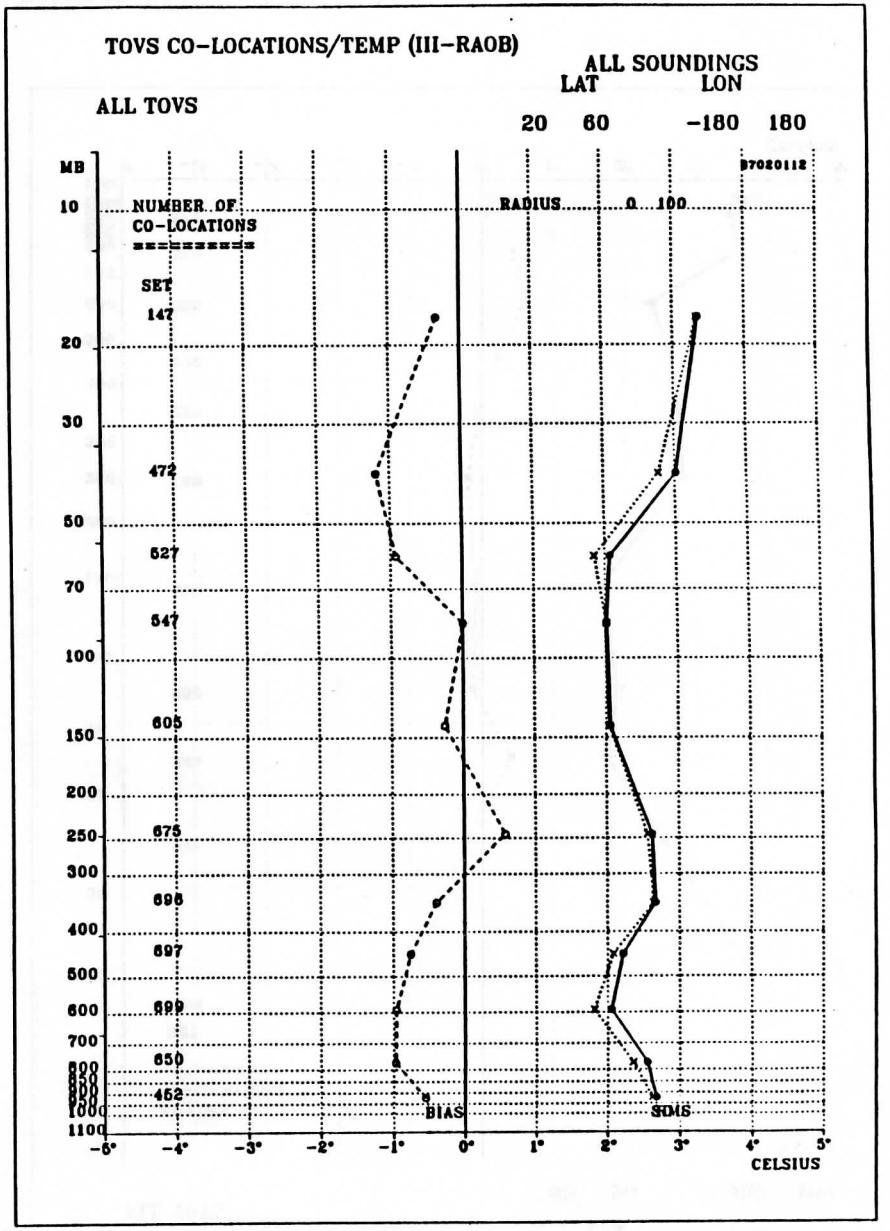

Fig 3 Same as Fig 1, area between 20°N and 60°N, the maximum difference is 100 km.

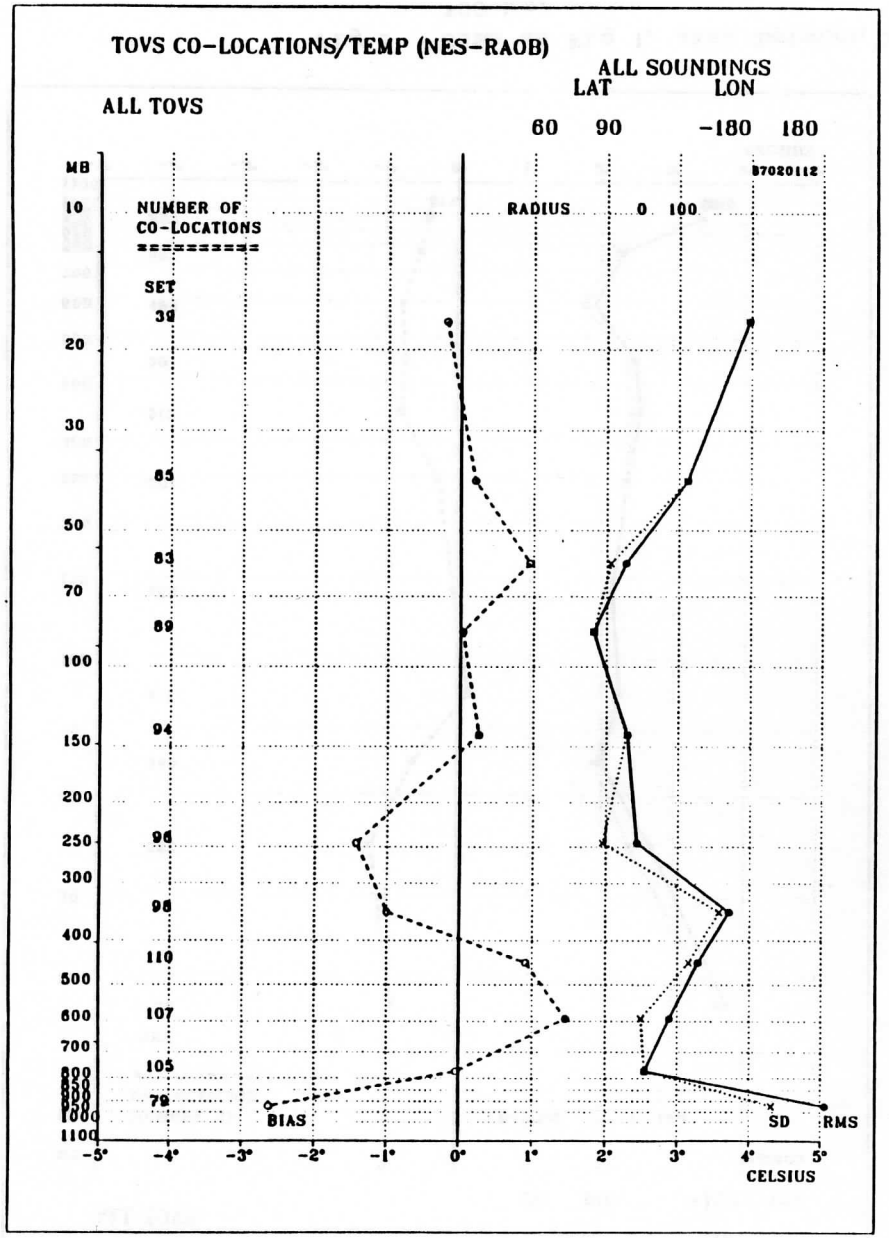

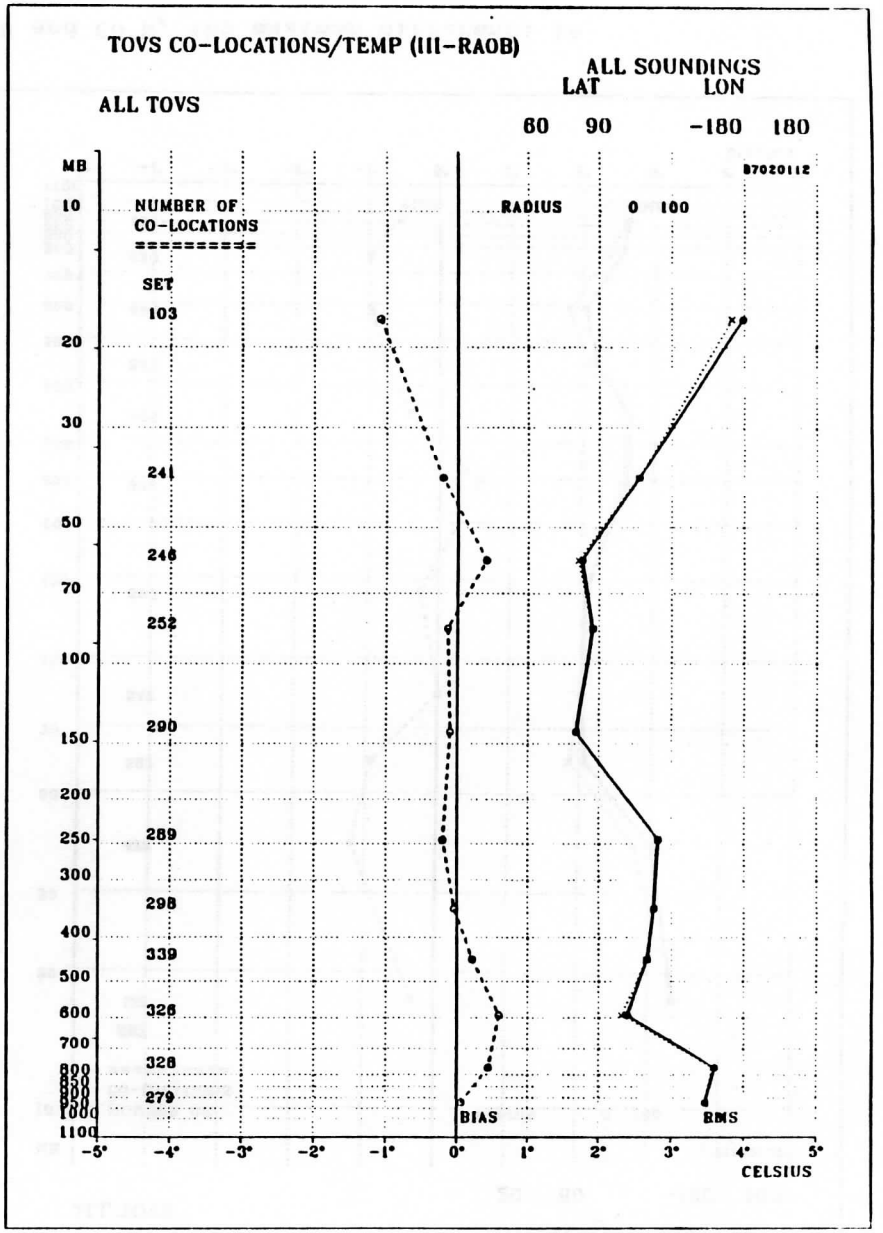

Fig 4 Same as Fig 3, area between 60°N and 90°N

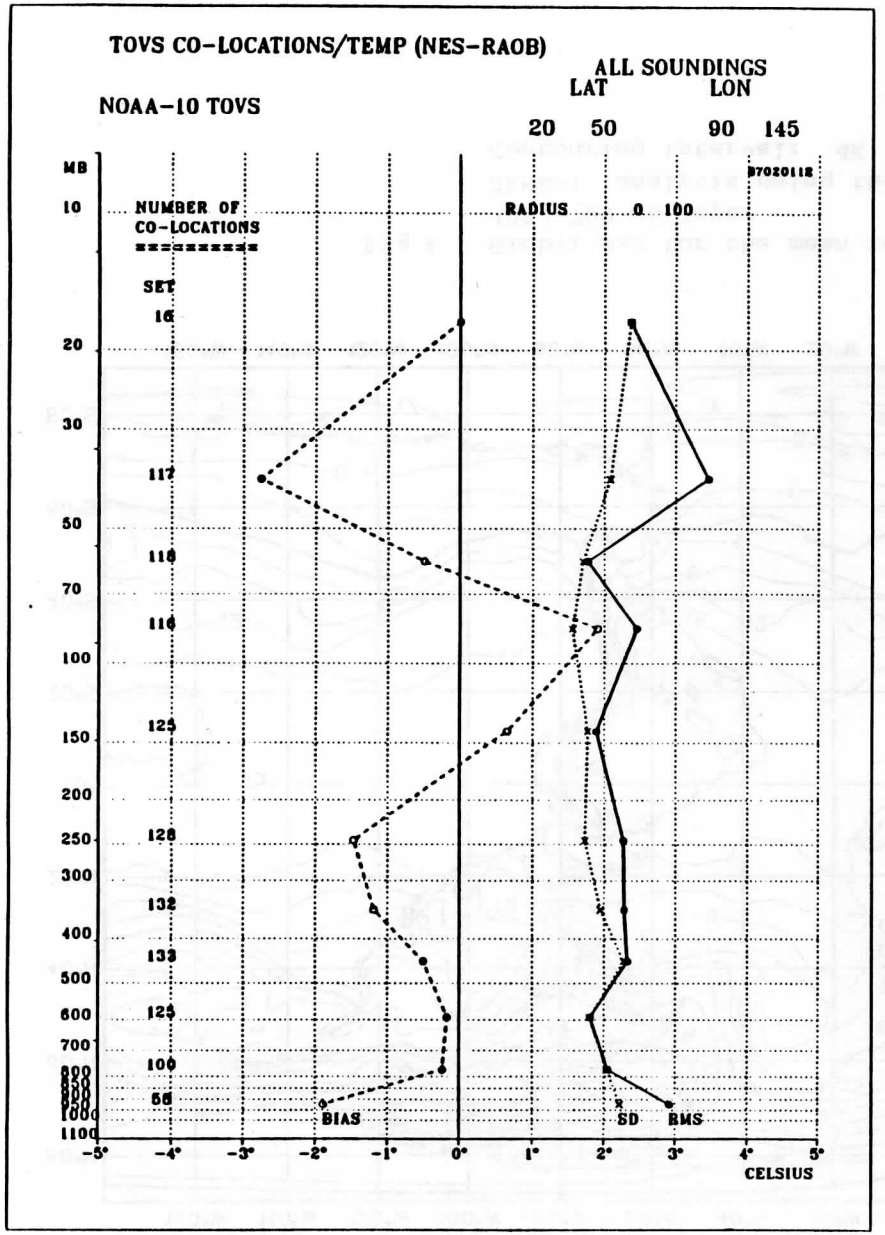

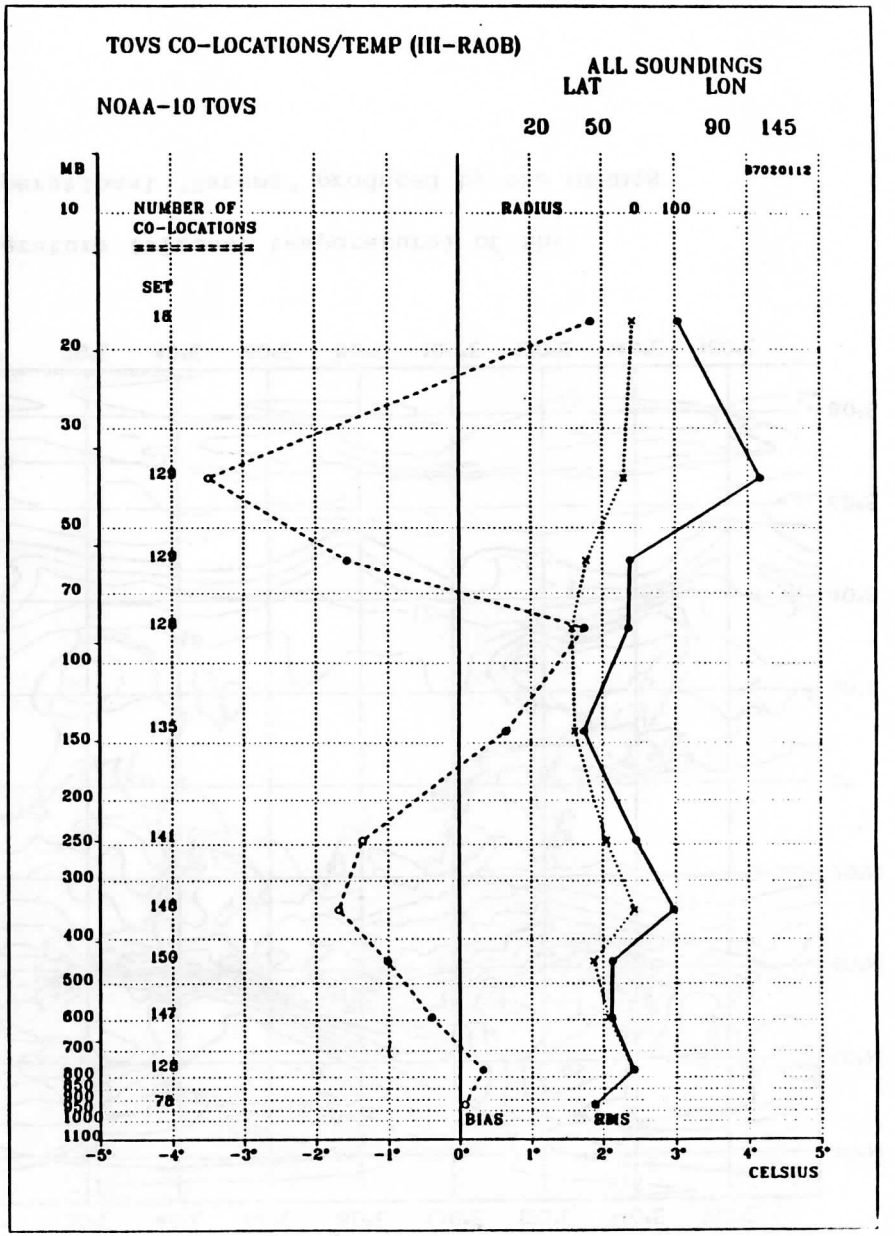

Fig 5 Same as Fig 4, area over China: latitude between 20°N and 50°N, longitude between 90°E and 145°E.

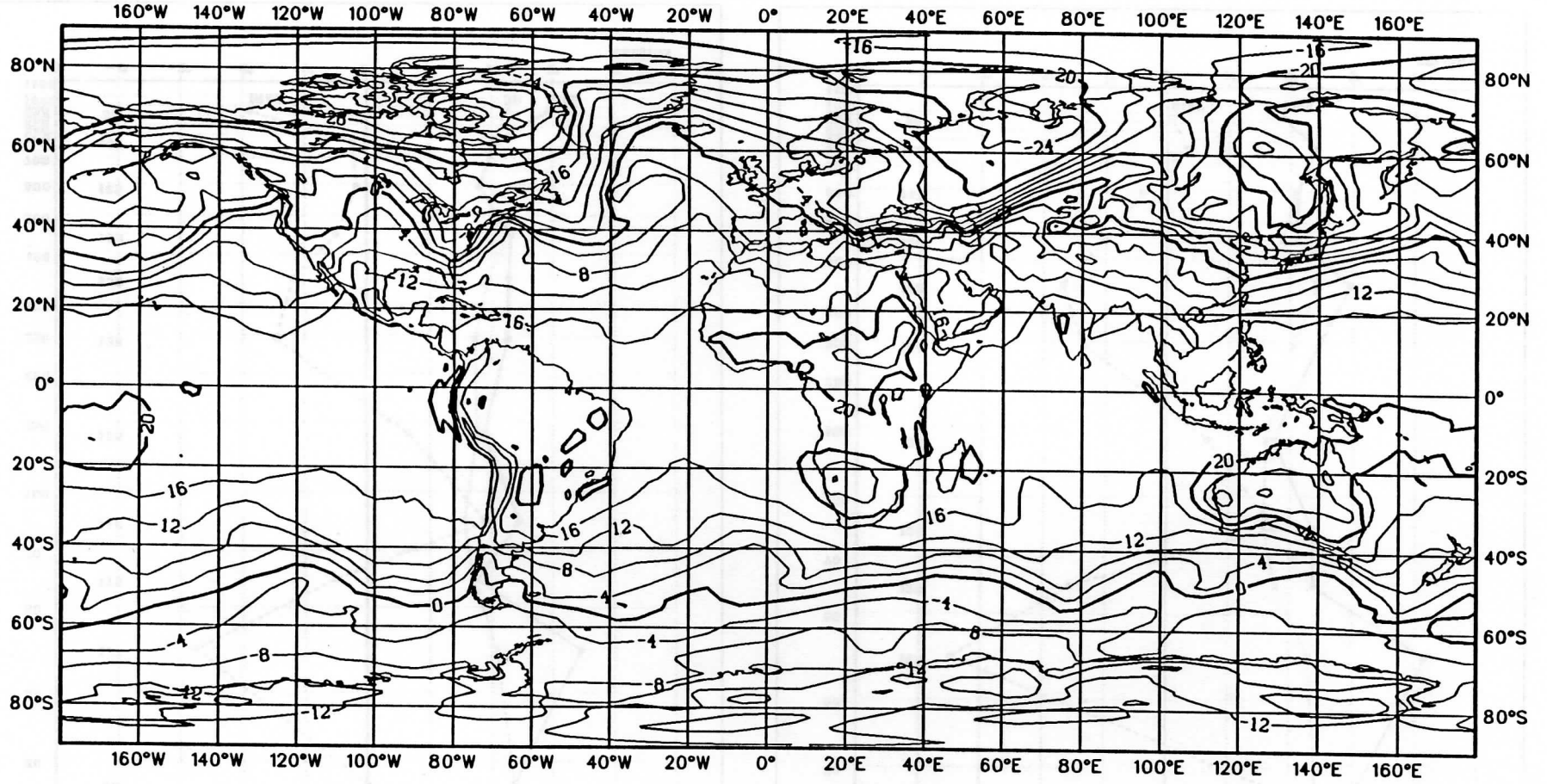

Fig 6 Global map for the mean temperature (virtual temperature) of the 1000-700 mb layer
SANES: analysis using the operational "Satems" produced by the NESDIS
Contouring interval: 4K

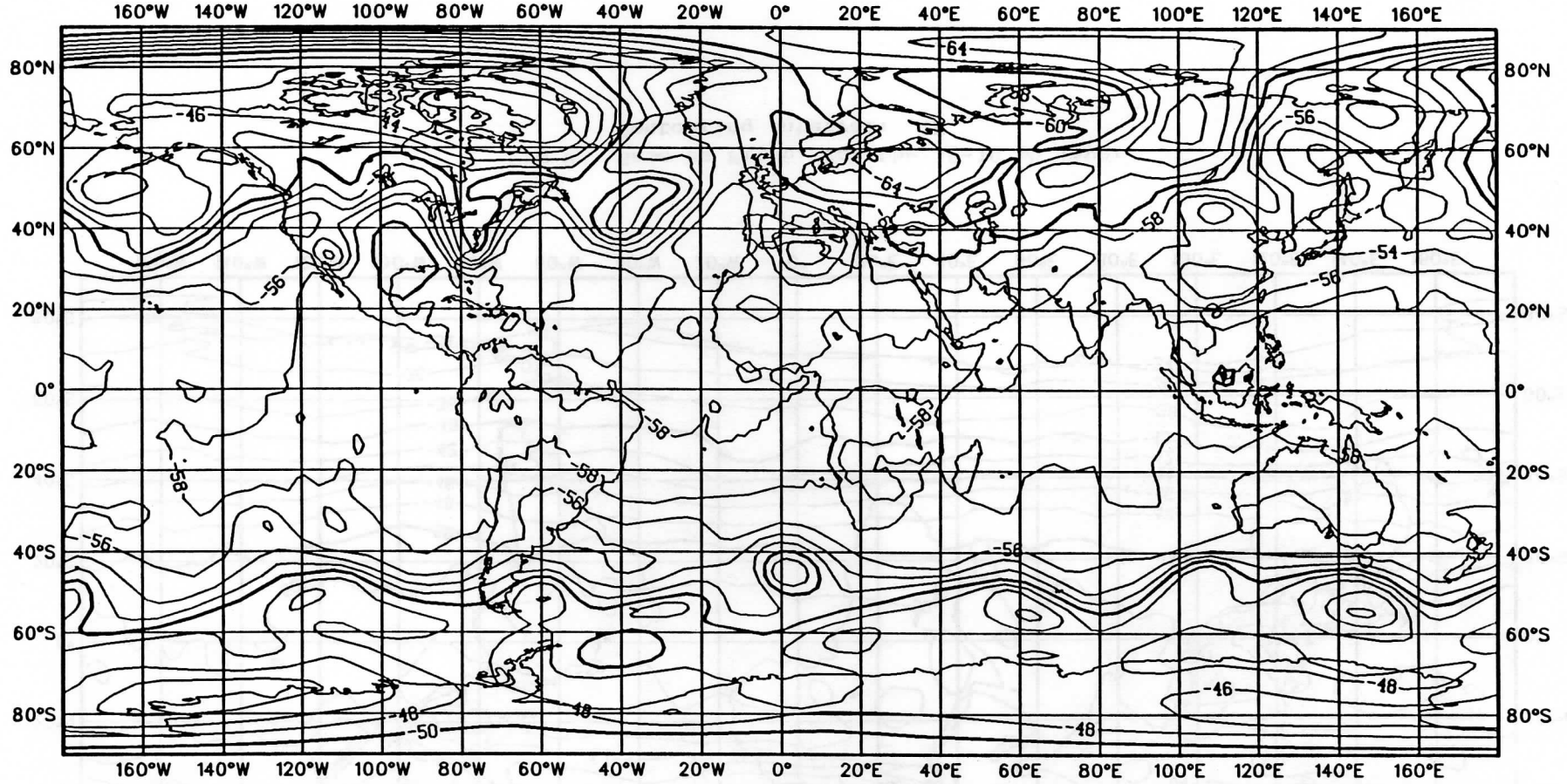

Fig 7 Same as Fig 6, for the 300-100 mb layer
Contouring interval: 2K

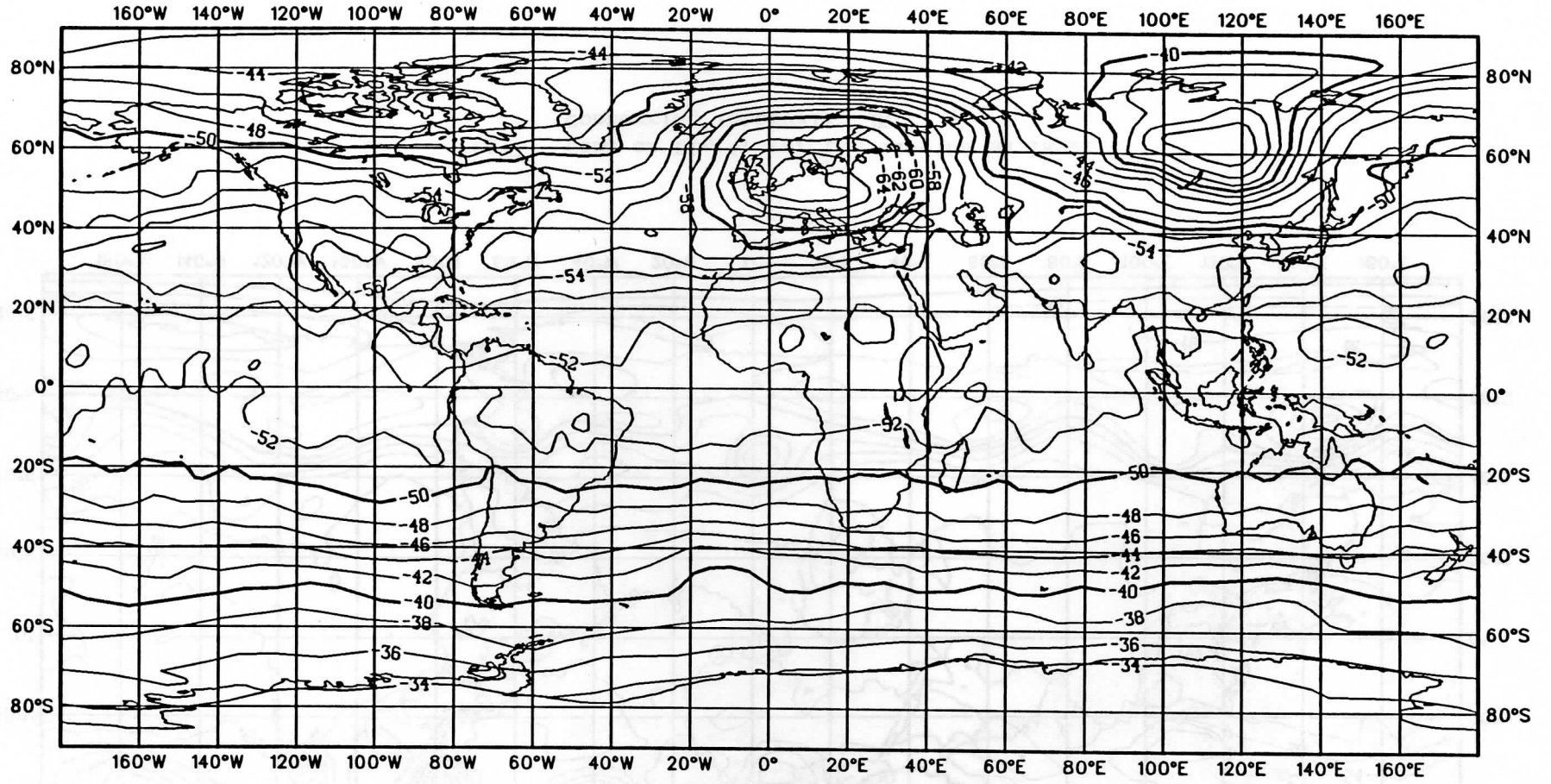

Fig 8 Same as Fig 6, for the 30-10 mb layer
Contouring interval: 2K

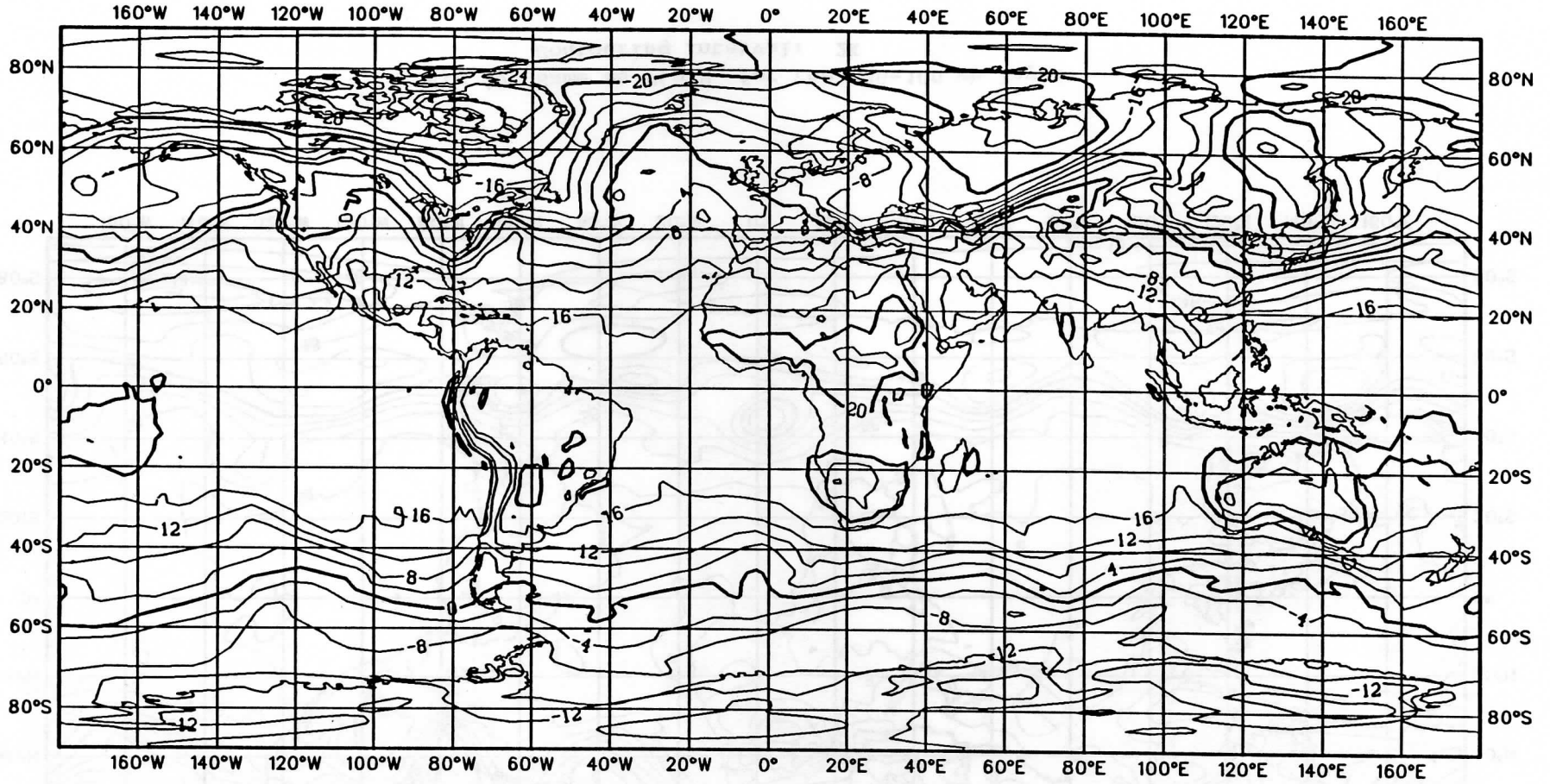

Fig 9 Global map for the mean temperature (virtual temperature) of the 1000-700 mb layer.
SAIII: analysis using the "Satems" produced by the 3I method
Contouring interval: 4K

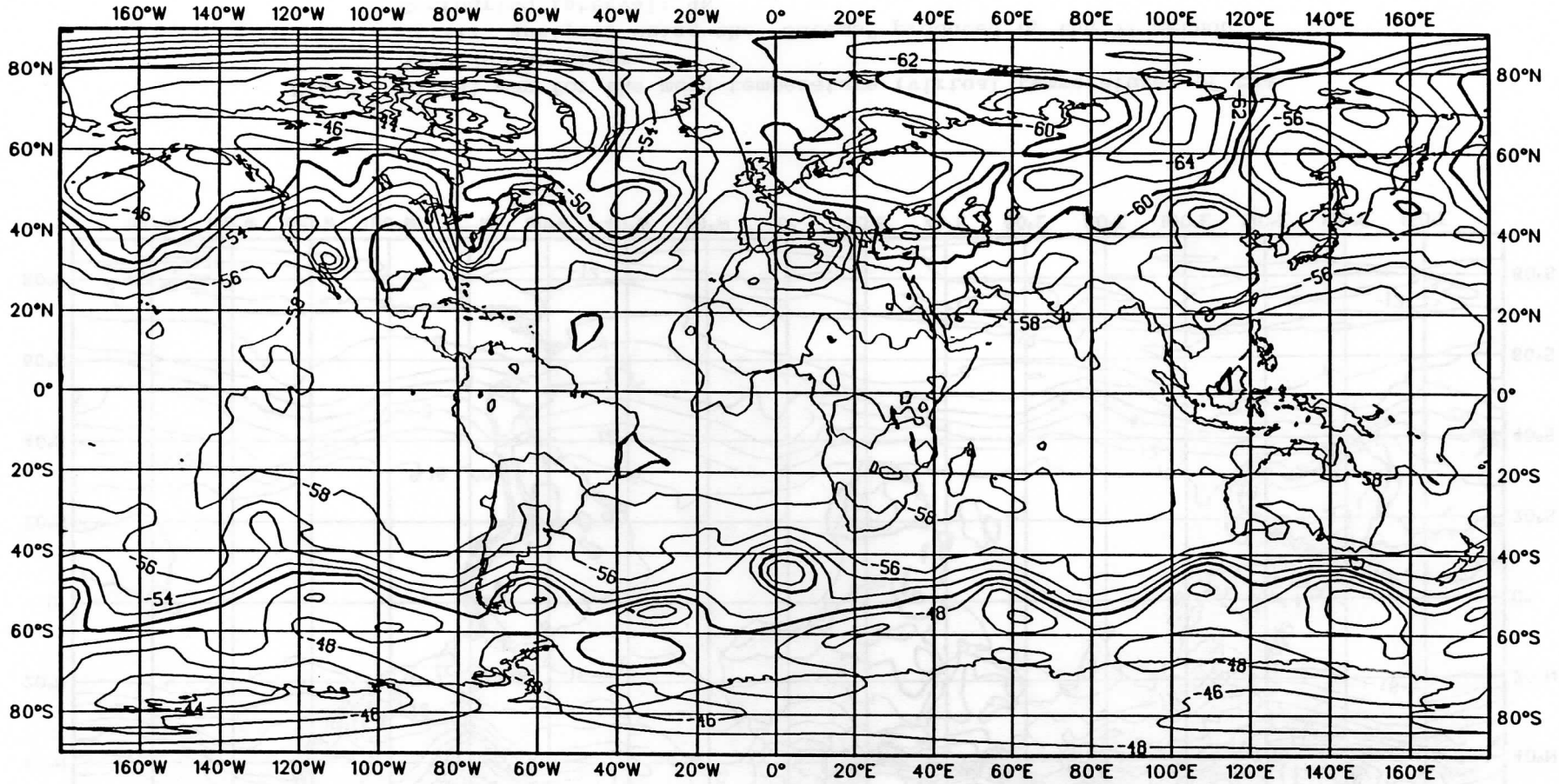

Fig 10 Same as Fig 9, for the 300-100 mb layer
Contouring interval: 2K

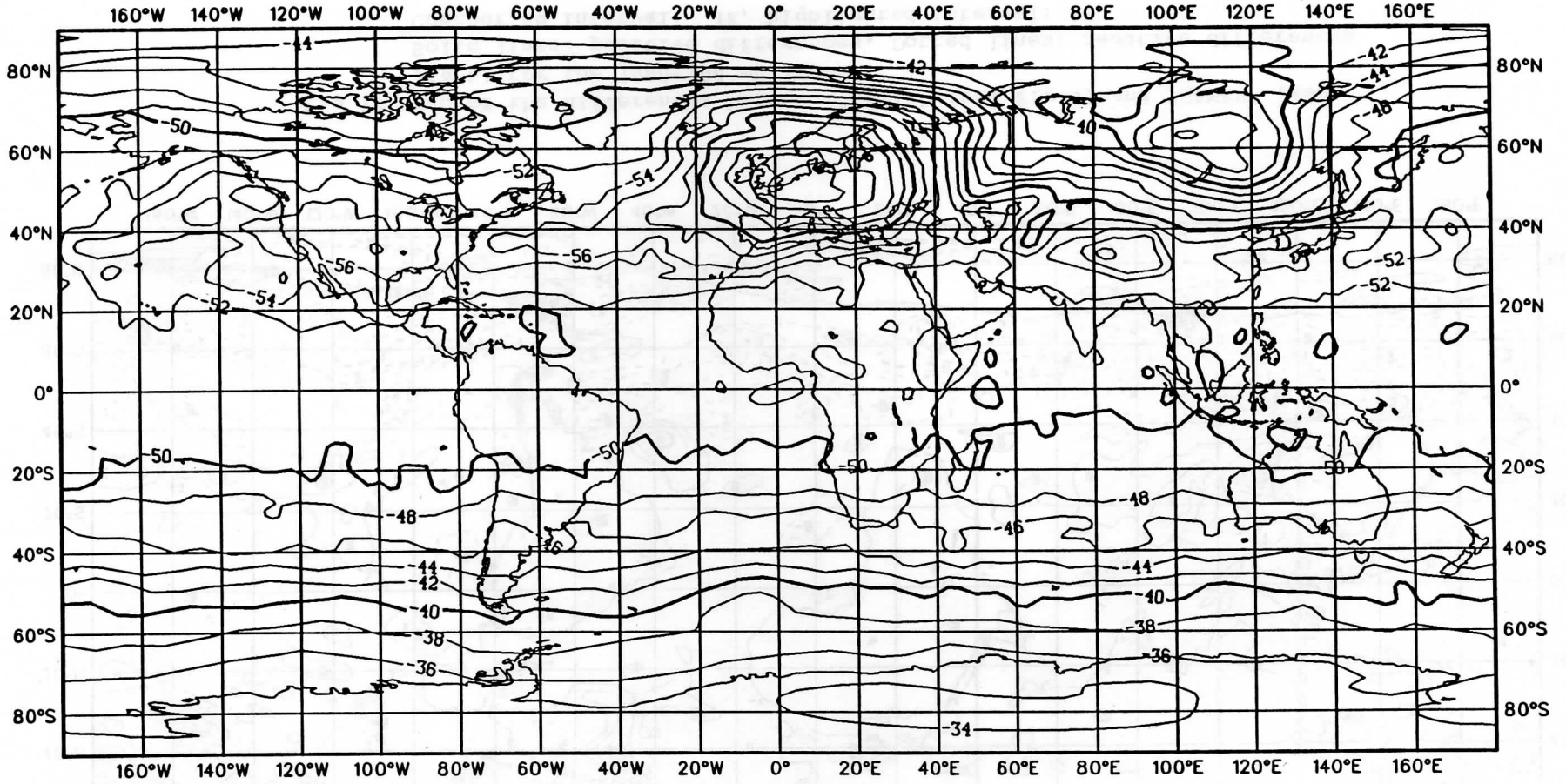

Fig 11 Same as Fig 9, for the 30-10 mb layer
Contouring interval: 2K

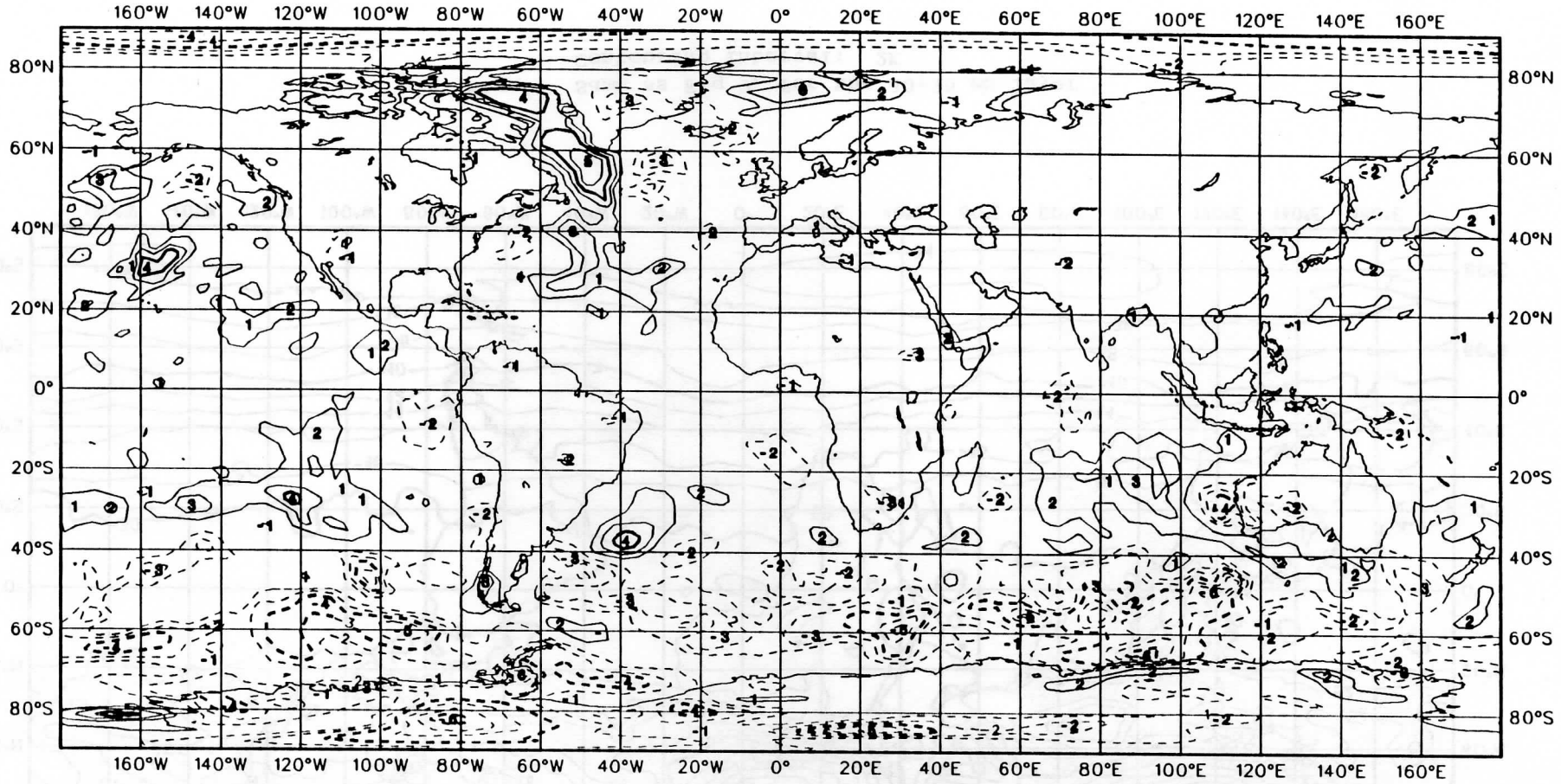

Fig 12 Map of the differences between "SAIII" (see Fig 9) and "SANES" (see Fig 6) for the 1000-700 mb layer
Solid lines: positive differences. Dotted lines: negative differences
Contouring interval: 1K, highlighted interval: 3K.

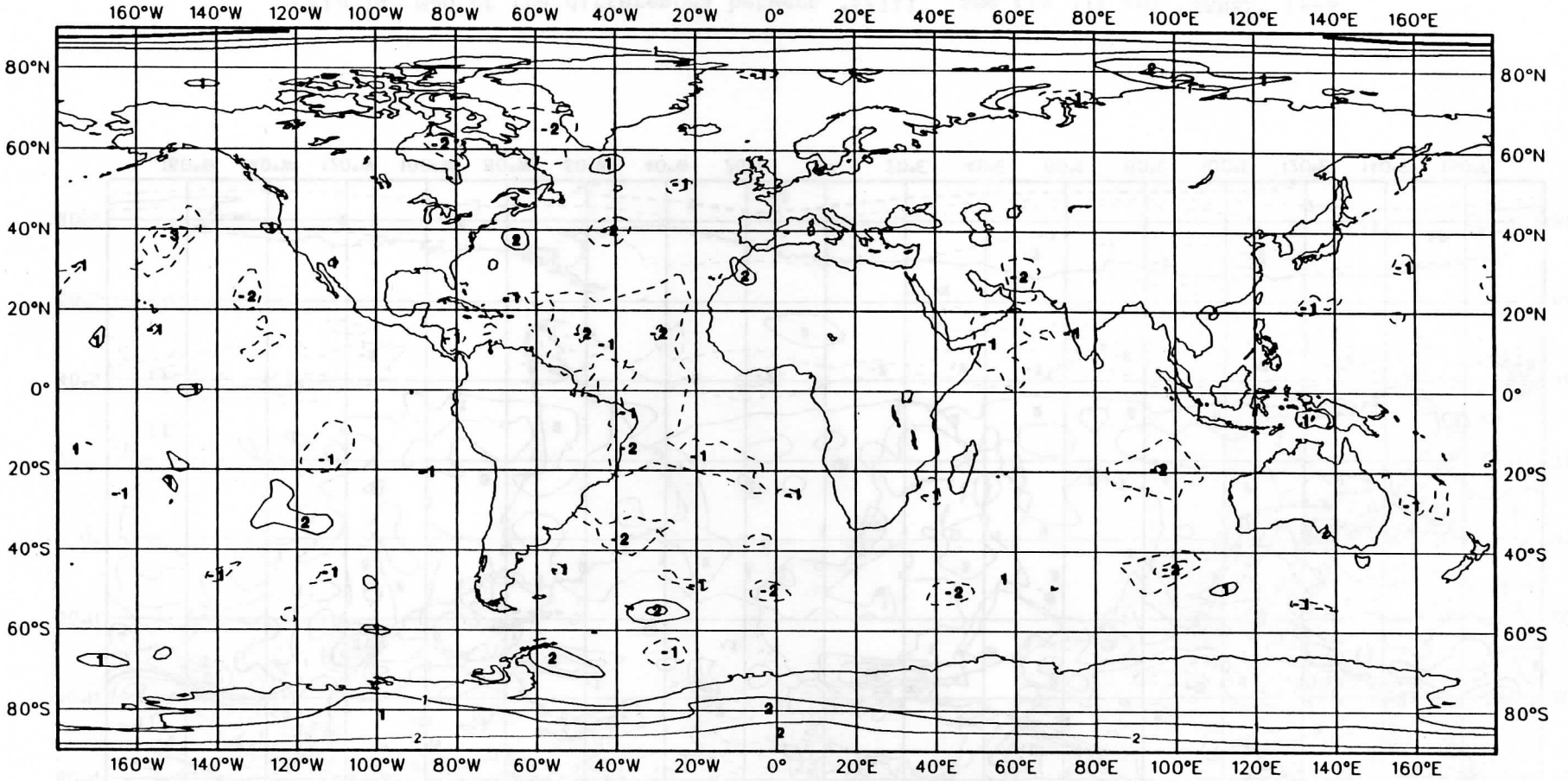

Fig 13 Map of the differences between "SAIII" (see Fig 10) and "SANES" (see Fig 7) for the 300-100 mb layer
Solid lines: positive differences. Doted lines: negative differences
Contouring interval: 1K, highlighted interval: 3K

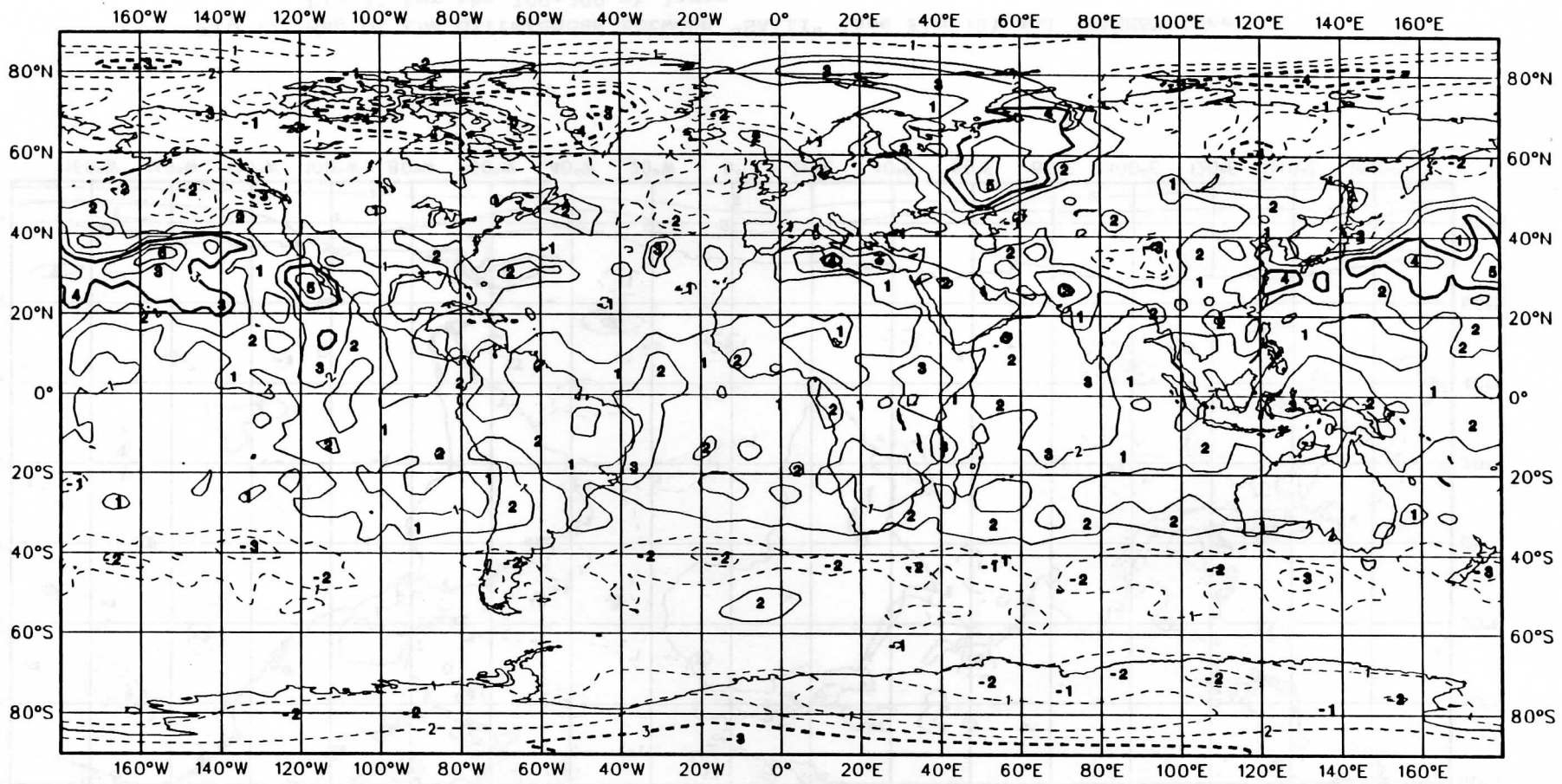

Fig 14 Map of the differences between "SAIII" (see Fig 11) and "SANES" (see Fig 8) for the 30-10 mb layer
Solid lines: positive differences. Dotted lines: negative differences
Contouring interval: 1K, highlighted interval: 3K

5. REFERENCES

Chedin, A, N A Scott, C Wahiche and P Moulinier, 1985: The Improved Initialization Inversion method: a high resolution physical method for temperature retrievals from the Tiros-N series. J Clim Appl Meteor, 24, 124-143.

Chedin, A, N A Scott, C Claud, J F Flobert, N Husson, C Levy, P Moine, G Rochard, J Quere and T Phulpin: Recent Progress in the determination of meteorological parameters from the satellites of the TIROS-N series. Proceedings of the 3rd International TOVS Study Conference. Madison, USA, August 1986, 6-44.

Kelly, G and J Pailleux: Use of satellite vertical sounder data in the ECMWF analysis system. Proceedings of the 4th International TOVS Study Conference. Igls, Austria, March 1988.

Kelly, G and J F Flobert: Radiance tuning. Proceedings of the 4th International TOVS Study Conference. Igls, Austria, March 1988.

Kidwell, K, NOAA Polar Orbiter Data Users Guide. December 1986.

Scott, N A, A Chedin, F M Breon, C Claud, J F Flobert, N Husson, C Levy, Y Tahani, G J Prangsma and G Rochard: Recent advances in the retrieval of meteorological parameters through the "3I" system. Proceedings of the 4th International TOVS Study Conference. Igls, Austria, March 1988.

Smith, W L, H M Woolf, C M Hayden, A J Schreiner: The simultaneous retrieval export package. Proceedings of the 2nd International TOVS Study Conference. Igls, Austria, February 1985, 224-253.

NOAA - 9'S RADIOMETRIC ATLAS OF EUROPE

Dr. J. R. Givri
Direction De La Meteorologie
Centre De Meteorologie Spatiale
BP 147 - 22302 Lannion Cedex - France

ABSTRACT

A TIROS NOAA-9's 1986 orbit set is presented as an annual atlas. Each orbit is considered as cloud-free on the whole Europe, including North Africa and Greenland. The atlas consists of a grid of 1/6 degree of latitude by 1/6 degree of longitude, covering the zone from 75°W to 35°E and from 20°N to 80°N.

Each point of the mesh contains topographic informations and AVHRR calibrated data, averaged inside the HIRS-2 ellipse. The periodicity of the atlas is seasonal.

1. METHODOLOGY

Sixty NOAA-9 clear cloud sceneries have been selected manually, corresponding to five orbits per month, day and nighttime altered and giving 30 daytime orbits and 30 nighttime orbits.

The selection has been made by monthly qualitative analysis in a first time, confirmed by a geographical analysis in order to prevent the data redundancy and to get, if possible, a complementary covering of the whole atlas zone.

Each 1986 clear cloud orbit picture has been cut in squares of four degrees of latitude by four degrees of longitude. The surfaces, obtained by concatenation of squares for three successive months is an admittable optimum. In fact, it seems to be not realistic to get down first because of the seasonal variability of surface parameters on biggest squares, and second, because of the HIRS spot quantity would not be subsequent for processing, if we consider a possible high ellipse rejecting rate in the case of "hard declouding".

For each month and for each orbit selected that month, a "squares-diagram" is dressed. It collects the clear zones, day and nighttime. Then, the five most representative orbits are selected. If it happens more clear daytime orbits than nighttime, the repetition may be: three clear daytime orbits for two clear nighttime orbits. If it happens that month only clear daytime orbits, the five selected orbits are daytime. That technique is a tentative way to take in account the random variable designated as "cloud cover on a given geographical area".

2. OPERATIVE MODE

From that 60 situations set, 60 x 2 CCT magnetic tapes of "CHAMP-4" type and 60 x 2 CCT magnetic tapes of "MASTER-TOVS" type have been made by Center

of Space Meteorology (C.M.S.) -Lannion, France. Excepted headers, each "CHAMP-4" magnetic tape contains:

- TOVS file set (HIRS-2, MSU & SSU) on the whole considered scenery dressed from HRPT Telemeasure.

- File of a maximum of 95 lines of AVHRR data averaged in HIRS ellipses in accordance with the subscenery selected before, HIRS calibration period does not appear in that file. (The first 45 lines are printed on the first magnetic type. The second one contains lacking lines).

Excepted headers, once more, each "MASTER-TOVS" magnetic tape contents is:

- TOV files set (the same as "CHAMP-4's"),

- AVHRR subscenery file with the start and end time of the clear zone scenery selected before.

The atlas grid is a 360 lines of 480 points array where it is necessary to locate the HIRS ellipses accurately. The first question consist in integration of HIRS calibration period inside the AVHRR lines file. FOR each HIRS ellipse, the geometry (inclination, excentricity, diameters) is computed in the atlas reference frame, is center being located before. The atlas points, inside the ellipse, are affected with the radiometric channel value under consideration. The geographical location process accuracy is about 1/12 degree, that is approximately nine kilometers in mid-latitude countries. Taking in account sizes of HIRS ellipse and atlas mesh, respectively, it is not realistic to get a more accurate instrument for determining at the atlas scale following parameters, for cloud-free sceneries:

Channel 1: Daytime surface mapping and albedo
Channel 2: idem
Channel 3: Nighttime surface temperature
Channel 4: Day and nighttime surface temperature
Channel 5: idem

More precisely, channel one monitors energy inside the yellow-green band of visible light. Channel 2 monitors the near infrared portion of the electromagnetic waves spectrum, allowing observation of clouds, lakes, shorelines, snow and ice. Comparison of data from these two channels gives informations about the vegetation index studied with two formulas:

- The Normalized Difference Vegetation Index (NDVI) computed form Channel 1 and 2 albedos, designated A1 and A2, as follows:

$$NDVI = \frac{A2 - A1}{A1 + A2}$$

and Channel 1 and 2 albedos ratio, calculated as follows:

$$RA = A2/A1.$$

Seasonal albedo studies are possible. A1 and A2 are corrected from solar elevation as follows:

$A1 = A1/\cos\theta$; $A2 = A1/\cos\theta$,

where is the zenithal solar angle of the viewed spot (ground, forest, plain). That data is available into each of the HIRS orbit file.

The other three channels operate entirely within the infrared band, depending upon which AVHRR instrument is being used. They detect the heat radiation from , and hence, the temperature of land, water, sea surface of top of clouds.

It has been noted that AAVHRR's channel 3 is noisy when the satellite is aging. It has been observed that channel 3 noise is dependent upon and varies as the "noise conductance" of the thermal equilibrium condition of the radiometer radiant cooler.

Furthermore, even in the case where noise is not discernable, i.e., at beginning of the satellite's life, channel 3 is quite uneasy to process daytime scenarios. 1986 has been a particular year where that effects can be neglected. Channel 3 must be anyway corrected form solar irradiance effects.

3. ATLAS PRESENTATION

After declouding by day/nighttime procedures, the sixty orbits set has been reduced to a 42 orbits set, containing the radiometric days and stored into the atlas file. The atlas content, for winter, spring, summer, autumn and the 1986, are the following averaged values:

- Albedos in channels 1 and 2: A1, A2
- Albedos' ratio: A2/A1
- Normalized Difference Vegetation index: $(A_2 - A_1)/(A_1 + A_2)$
- Far infrared temperature difference: T4 - T5.
  (that last parameter remains uneasy to use).

Future developments will concern the ground temperature and differences between infrared temperatures, day and nighttime, in order to get an emmissivity atlas on the considered geographical zone.

Grid of topography of the European Atlas : color being brighter when altitude is increasing.

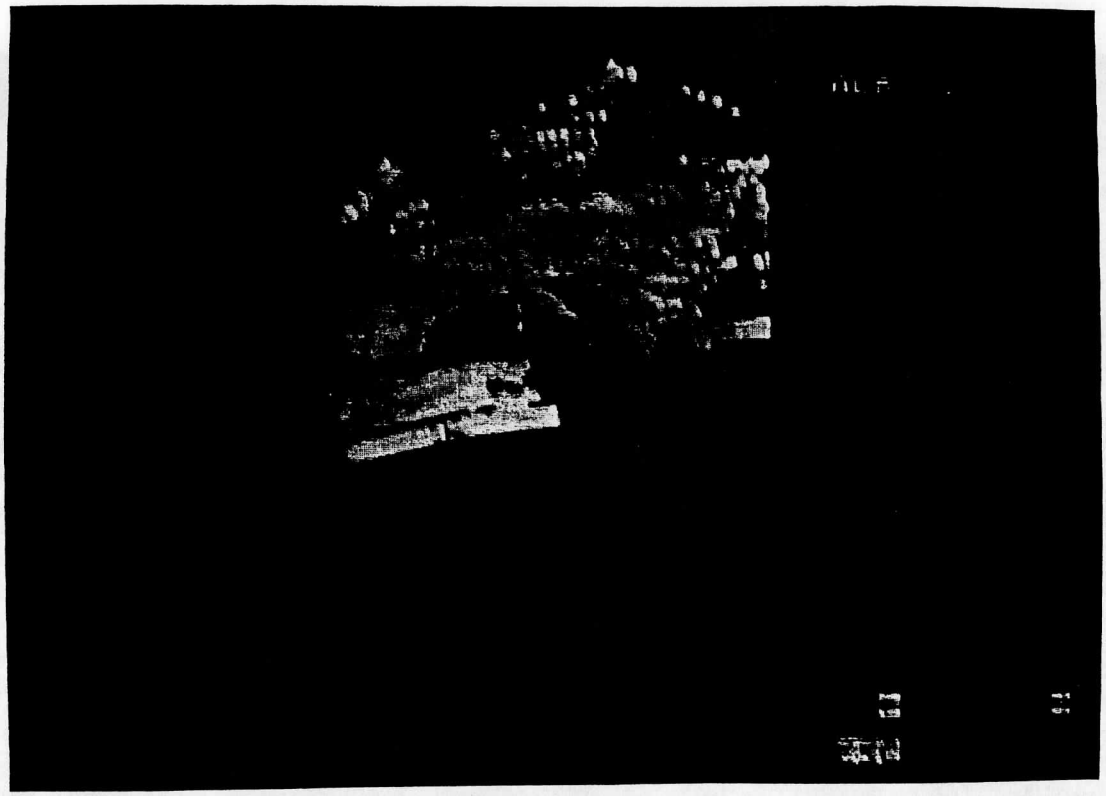

AVHRR Channel 1 albedo annual mean value.

AVHRR Channel 2 albedo annual mean value

AVHRR Channels 2 to 1 albedos ratio mean value, between
(dark) and (bright)

Temp. difference T4 - T5 annual mean value, sensitive to atmospheric absorption.

1986's 1st trimester NDVI mean values.

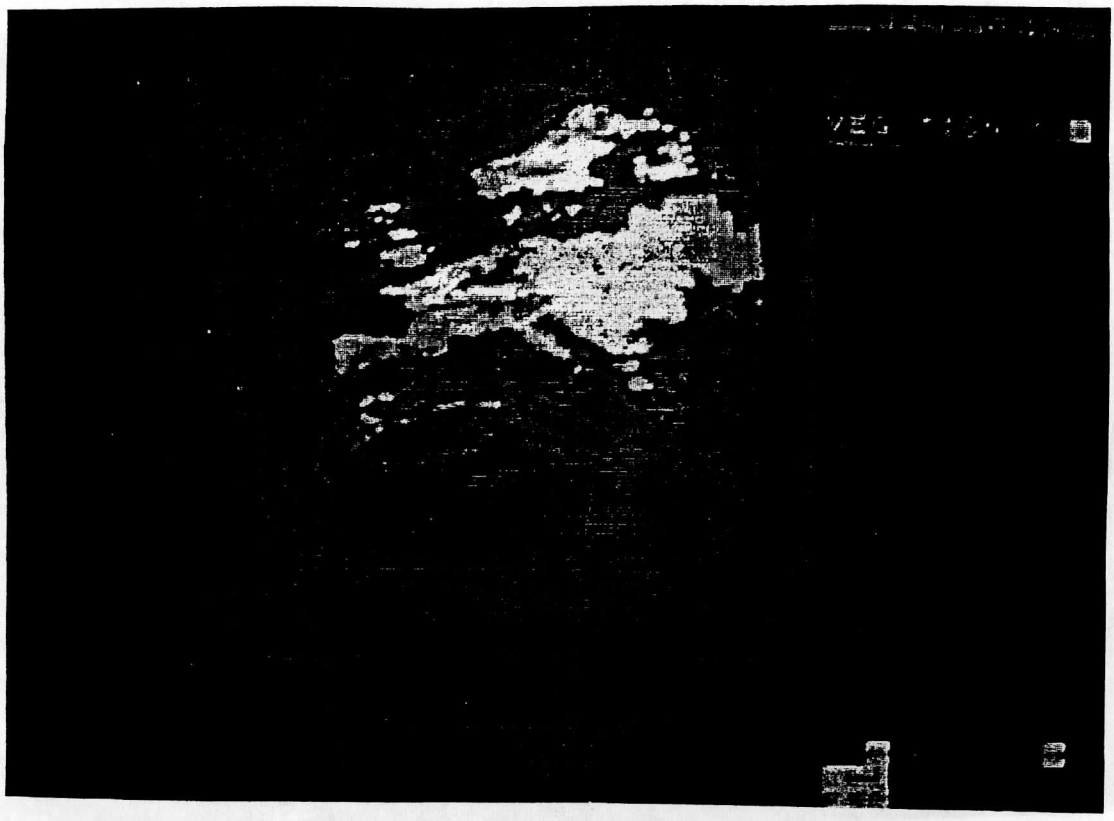

1986's 2nd trimester NDVI mean values

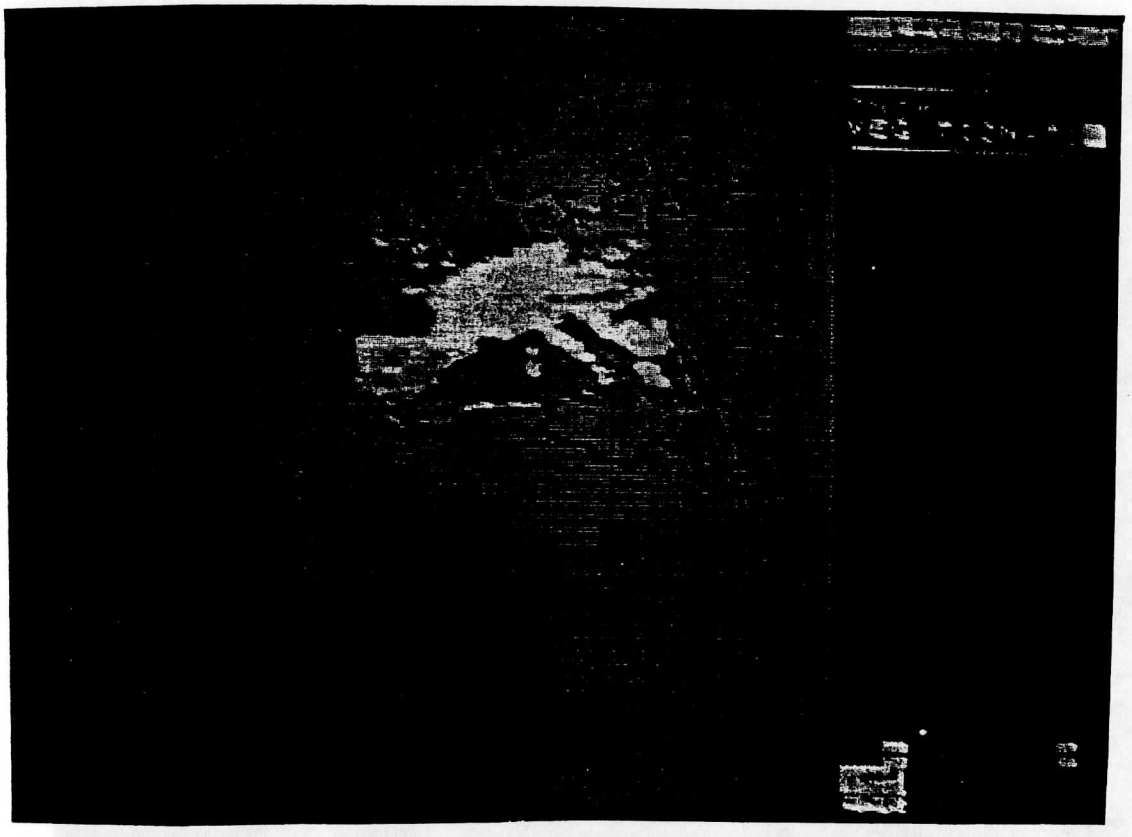

1986's 3rd trimester NDVI mean values

1986's last trimester NDVI mean values.

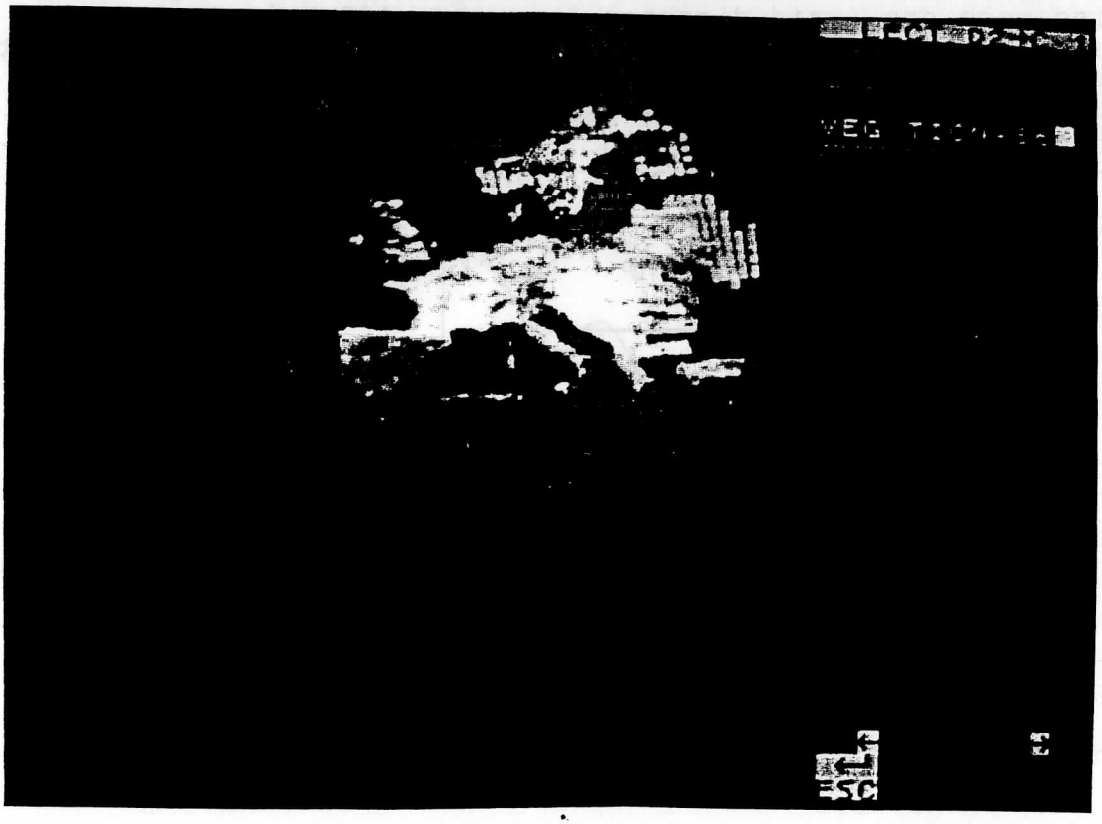

1986's NDVI mean values.

EXPERIENCES WITH TOVS MEASUREMENTS DURING ALPEX-1

Güldner, J. and D. Spänkuch

Meteorological Service of the GDR, Main Meteorological Observatory, Telegrafenberg, Potsdam, GDR-1561

I. INTRODUCTION

It is not a simple task to evaluate the impact of satellite geopotential retrievals on meteorological analyses and forecasts correctly. The impact depends on (i) the capacity of the numerical model used, e.g., how it handles the data assimilation problem, (ii) the geographical region, i.e. whether it is data-rich or data-sparse and whether -for that region- the satellite measurements are made around synoptic standard observation hours or not, (iii) the meteorological situation, and finally (iv) the general organisation within a Meteorological Centre. The findings are, therefore, not unambiguous. The impact is generally considered to be marginal. There are cases with a definitely positive impact, others with a negative and again others with a negligible impact at least.

For a National Meteorological Centre (NMC) of Central Europe embedded in an area of a dense aerological network with distances between radiosonde stations of 100 to 200 km over land and with a coarse-mesh region as A of Fig. 1 and a fine-mesh one (grid distance less than 150 km) similar to region B satellite temperature retrievals are less important than in other geographical areas with data-sparse surrounding. Even with drastic changes of analysis products in the North Atlantic area D of Fig.1 as a result of satellite temperatures no significant and definite changes in the 24 hour geopotential

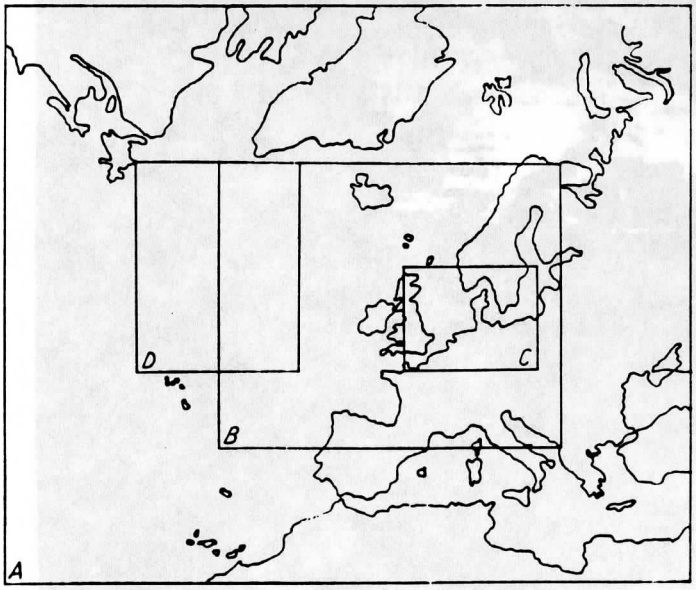

Fig. 1: Areas of the NMC; A-coarse-mesh area, B- fine-mesh area, C- verification area, D- area of drastic changes in analyses due to SIRS data (after Kluge and Petzold 1978)

forecast for Central Europe (area C of Fig. 1) were observed (Kluge and Petzold 1978). Kluge's and Petzold's satellite input temperatures based on SIRS[1)] data with a rather coarse spatial resolution (at the surface about 200 km) caused as a rule only large-scale corrections in the geopotential fields of remote areas. These corrections gradually disappeared in the data-rich areas under the weight of the aerological information with the weather ships OWS R and L having played an essential role. The growing need to forecast subsynoptic scale processes and phenomena has again raised the problem of incorporating in the analysis and forecasting procedures satellite retrievals, and that of high spatial density as, for example, at present offered by the TOVS measurements.
An NMC with its limited resources and possibilities has thoroughly to evaluate expense and benefit of each meteorological observational subsystem used including the corresponding technological aspects. If the present aerological network in Central Europe with a density of about 100 to 200 km distance between the stations is to be maintained in the future, satellite retrievals must add substantial mesoscale information to be considered in the technological run within a Central European NMC. A considerable number of aerological stations has, however, only a reduced sounding programme, i.e. one or two ascents per day. Satellite retrievals are beneficial already if they can satisfactorily trace temporary changes in the geopotential fields. The incorporation at the NMC could be either direct by its own receiving station or via teleconnections from a regional receiving station or indirect by corresponding meteorological products (e.g., analyses, forecasts) obtained at the competent Regional Meteorological Centre (RMC). As long as the question wether or not substantial mesoscale information is contained in TOVS data cannot definitely be answered case studies such as ALPEX are a suitable tool to tackle this problem. We have should, however, to emphasize that this question can adequately be answered only (i) by a comparison with verified mesoscale analysis products or (ii) if simultaneously high-spatial-density TOVS data (spot by spot) and mesoscale features, recognized by means of conventional observations are available, including TOVS data of the current operational systems with some spatial filtering. Generally, none of these conditions are met. Conventional analysis products of RMCs or NMCs do in general not contain meso-α features. Hence, if differences between retrievals and analysis products with gridpoint distances of 150 km or 300 km occur they cannot directly be used as an evidence of mesoscale information in TOVS data unless they are manifested by further meteorological development.
This study is a modest approach at our NMC to become familiarize with the sounding of single-spot TOVS measurements.

[1)] SIRS: Satellite Infrared Spectrometer, flown on Nimbus 3 and 4.

Due to the lack of sufficient mesoscale verification means the evaluation is, however, restricted to the impact of the TOVS subsystems HIRS and MSU at a synoptic-scale analysis by comparing analysis products with the corresponding retrieval results. It is not the purpose of this paper to assess the influence of TOVS data on numerical models and forecasting.

II. RETRIEVALS FROM THE ALPEX DATA AND COMPARISON WITH NUMERICAL ANALYSES PRODUCTS

Let us now discuss the experiences made with TOVS data of the ALPEX period of 4 and 5 March, 1982. The TOVS data were made available on magnetic tape by the Cooperative Institute for Meteorological Satellite Studies (CIMSS) of the Space Science and Engineering Center of the University of Wisconsin Madison and included all HIRS/2- and MSU-measurements of two consecutive orbits on 4 March at about 12^{00} and on 5 March 1982 at about 00^{00} UTC. Additionally, the tape contained fast computer programmes for transmittance calculations with the corresponding coefficients. For further details see Weinreb et al. 1981.

The synoptic situation was characterized by a low-pressure system of 975 hPa, over the northern North Sea and southern Norway (4 March 00^{00} UTC) which weakened to 995 hPa and moved to the Gulf of Finland (5 March 00^{00} UTC). At the same time, a wave disturbance at the frontal system of this depression moving from Central France to the Gulf of Genoa developed into a separate low-pressure system with 1010 hPa making way for a ridge of high pressure over Western and part of Central Europe. Fig. 2, according to the analysis of the European Centre of Medium Weather Forecasting (ECMWF) showing the 500/1000 hPa thickness of 4 March, 12^{00} UTC (full lines) and 5 March, 00^{00} UTC (dashed lines) demonstrates this meteorological development. The tongue of cold air over Britain and Northern France, shifting eastwards, extended up to the Mediterranean.

The following discussion concentrates on the analysis of the boxes D10 and D17 of Fig. 2 where TOVS data of both days were available. The dimension of D10 with 10 scan lines and of D17 with 17 scan lines are 2400 km x 400 km and 2400 km x 700 km. Marked thickness changes from 4 to 5 March are within D17 and lesser ones are within D10. Temperature retrievals were made for each spot with 56 HIRS and 11 MSU spots per scan line using (i) only the HIRS channels 1 to 8 (HIRS), (ii) only the MSU channels 2 to 4, and (iii) both data sets (HIRS + MSU). MSU channel 1 and the HIRS channels within the 4.3 um region were deliberately omitted to avoid the problems connected with the unknown microwave surface emittance of the ground and the scattered light at 4.3 um.

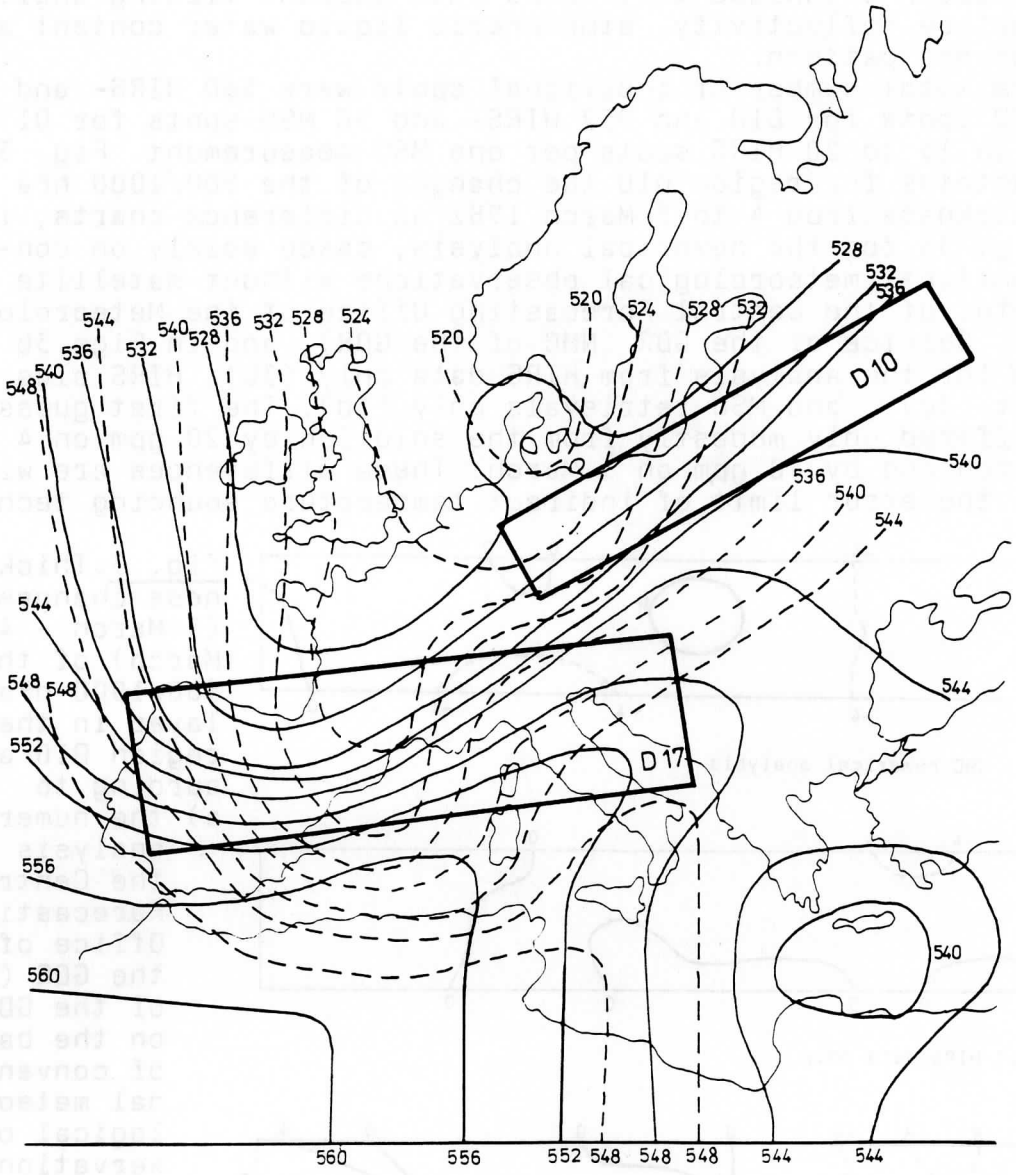

Fig. 2: 500/1000 hPa thickness analysis of the European Centre of Medium Weather Forecasting (ECMWF) of 4 March, 12^{00} UTC (——) and 5 March, 00^{00} UTC (– – –) (from Rizzi 1984). The discussion in the paper is concentrated of the boxes D10 and D17.

The MSU data were already 'limb-corrected' based on a regression technique that takes into account viewing angle, surface reflectivity, atmospheric liquid water content and antenna pattern.
The total number of individual spots were 560 HIRS- and 35 MSU spots for D10 and 952 HIRS- and 50 MSU-spots for D17 with 15 to 20 HIRS spots per one MSU measurement. Fig. 3 contains for region D10 the changes of the 500/1000 hPa thickness from 4 to 5 March 1982 as difference charts, in Fig. 3a for the numerical analysis, based solely on conventional meteorological observations without satellite data, of the Central Forecasting Office of the Meteorological Service of the GDR (NMC of the GDR), and in Figs.3b to 3d for the analysis from HIRS data only (3b), HIRS plus MSU dat (3c) , and MSU retrievals only (3d). The first guess differed only modestly from the solution by 20 gpm on 4 March and by 40 gpm on 5 March. These differences are within the error limit of indirect temperature sounding tech-

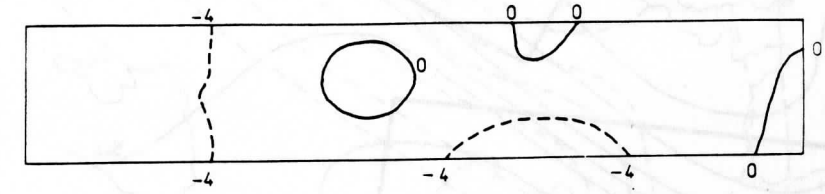

a) NMC numerical analysis

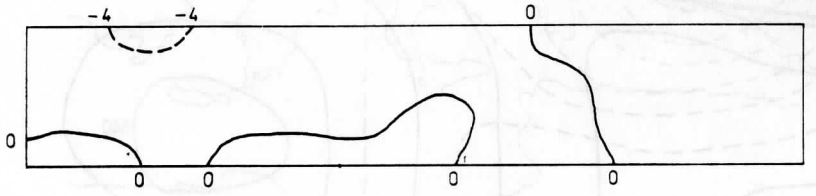

b) HIRS data only

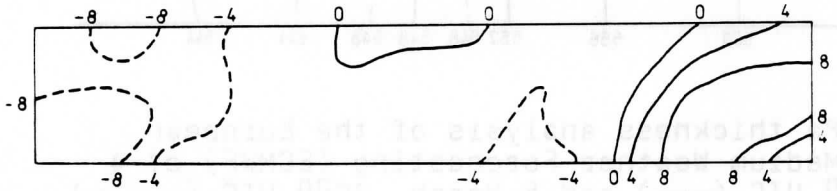

c) HIRS plus MSU data

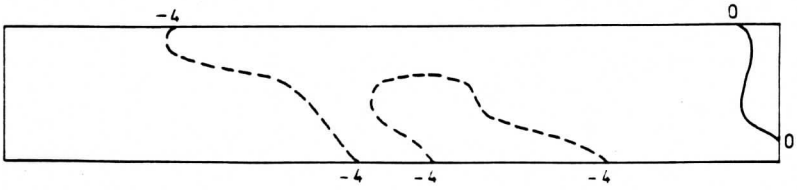

d) MSU data only

Fig. 3: Thickness changes (5 March - 4 March) of the 500/1000 hPa layer in the region D10 according to
a) the numerical analysis of the Central Forecasting Office of the GDR (NMC of the GDR) on the basis of conventional meteorological observations only without any satellite information
b) HIRS data only
c) HIRS plus MSU data
d) MSU data only

niques. A substantial improvement of the first guess can, therefore, not be expected. High-level cloudiness (p_c 500 hPa) was estimated with 68 and 23 per cent on 4 and 5 March, and cloudless conditions with 24 and 43 per cent. The meteorological situation in D10 is characterized by small temporal change and small thickness gradients. There are, according to the numerical analysis, only two regions with thickness changes greater than 4 gpdm. These changes are best reflected by the analysis of the MSU retrievals. For HIRS- plus MSU data the analysis is similar to the numerical analysis for 4 March, but there are larger differences on 5 March resulting in a much more detailed structure in the thickness change map 3c compared with 3a. The meteorological situation of D10 is, however, not appropriate for definite conclusions.

In Figs. 4 to 6 500/1000 hPa thickness analysis products are shown for the region D17, in (a) and (b) of the numerical analysis of the ECMWF and of the NMC of the GDR (b), and based on HIRS data only (c), HIRS plus MSU data (d), and MSU data only (e). Figs. 4 and 5 are for 4 and 5 March, respectively, and Fig. 6 shows the thickness change of 5 March minus 4 March. The first-guess thickness differs from the 'solution' (NMC numerical analysis) with, on the average, 65 gpm and 84 gpm on 4 and 5 March remarkably, high cloudiness was estimated to be 60% on 4 March and 47% on 5 March, and cloudless spots to be 37% for both days.

Note the different numerical analyses of ECMWF and of the NMC in subsynoptic scale (Fig. 7). With regard to the analysis on the basis of the retrievals we would like to point out that the isolines could be drawn only after some spatial filtering. The meteorological situation in D17 is dominated by a trough with southward movement, recognised also in the difference maps (Figs. 6a and b) with negative amounts in the centre and especially in the southern part of D17, and positive amounts in the western part. With regard to 'satellite products' the thickness maps based solely on HIRS data are most difficult to interpret. This is due to the large variability of the retrieval results as temperature sounding with infrared channels only is most complicated in case of high cloudiness. The trough displacement can, however, be identified especially in the difference chart 6c. The combined use of HIRS plus MSU data furnishes extreme deviations from the numerical analysis in the western part of D17 on 4 March with strong thickness gradients. Both data sets are probably not well adapted and a preselection to identify questionable measurements was not made so that in some cases instabilities occurred in the retrieval procedure. Nevertheless, the trough displacement can be recognised in the difference chart 6d. Best agreement with the numerical analysis, i.e. for both days and, therefore, also for the meteorological development is obtained using MSU retrievals only. The agreement is within the limit defined by the ECMWF's and the NMC's numerical analysis (Fig. 7). Both, the southeastward displacement of the trough and the thickness increase to the west are well reflected. We emphasize once again that, strict-

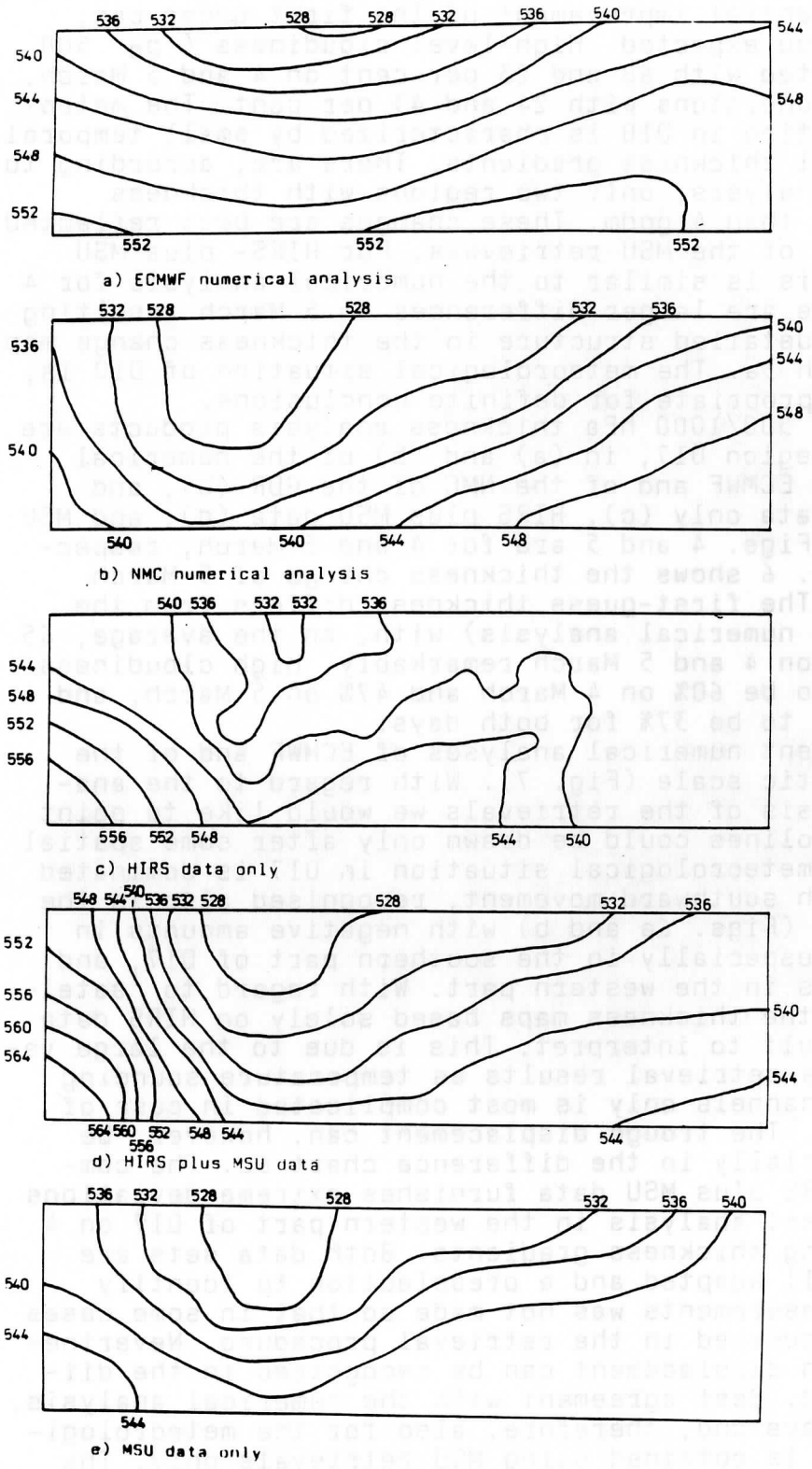

Fig.4:
500/1000 hPa thickness chart of 4 March 1982, 12^{00} UTC for region D17 according to
a) the ECMWF numerical analysis
b) the NMC of the GDR numerical analysis
c) HIRS data only
d) HIRS plus MSU data
e) MSU data only

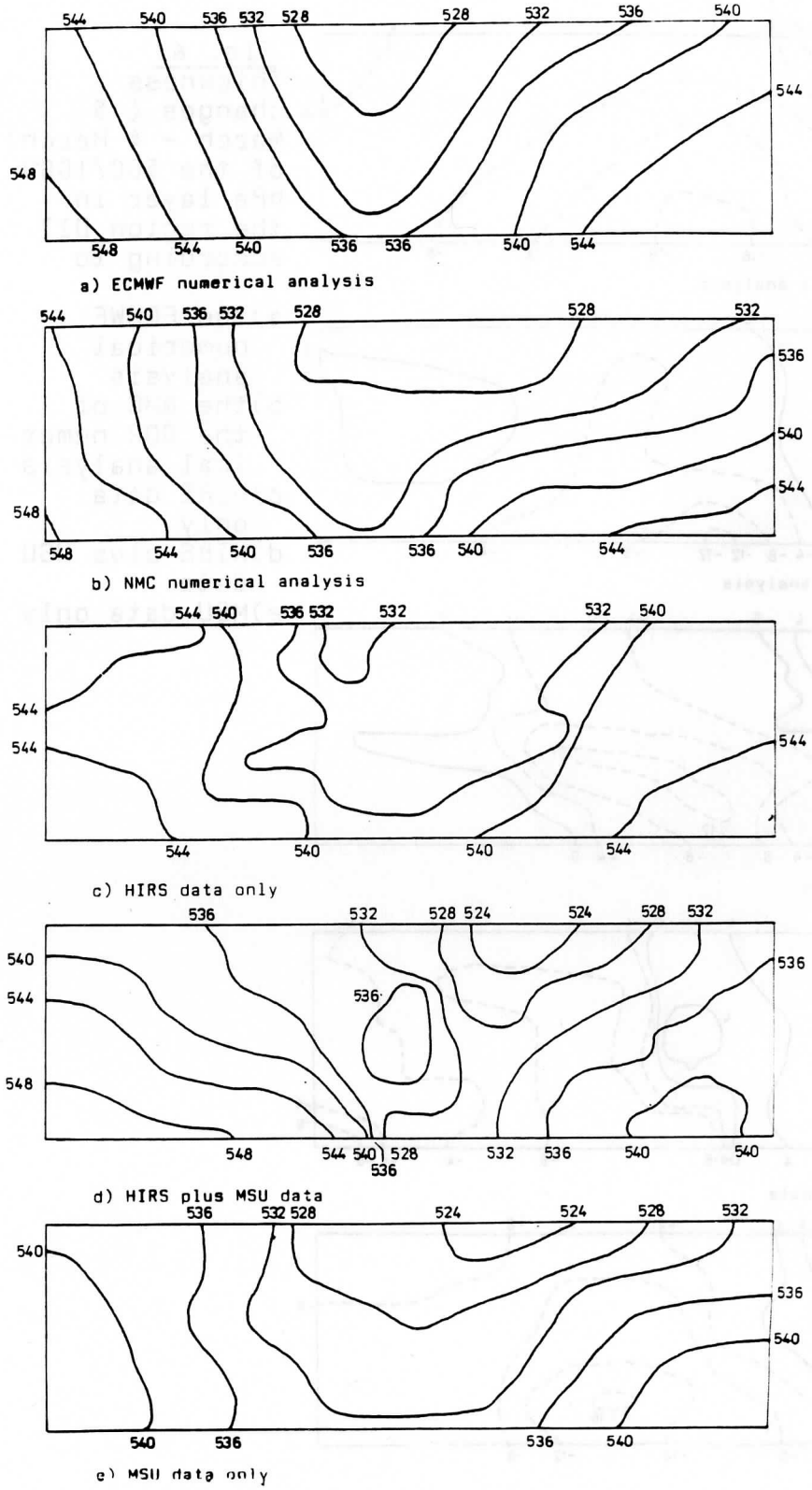

Fig 5: As for Fig. 4, but for 5 March 1982, 0000 UTC

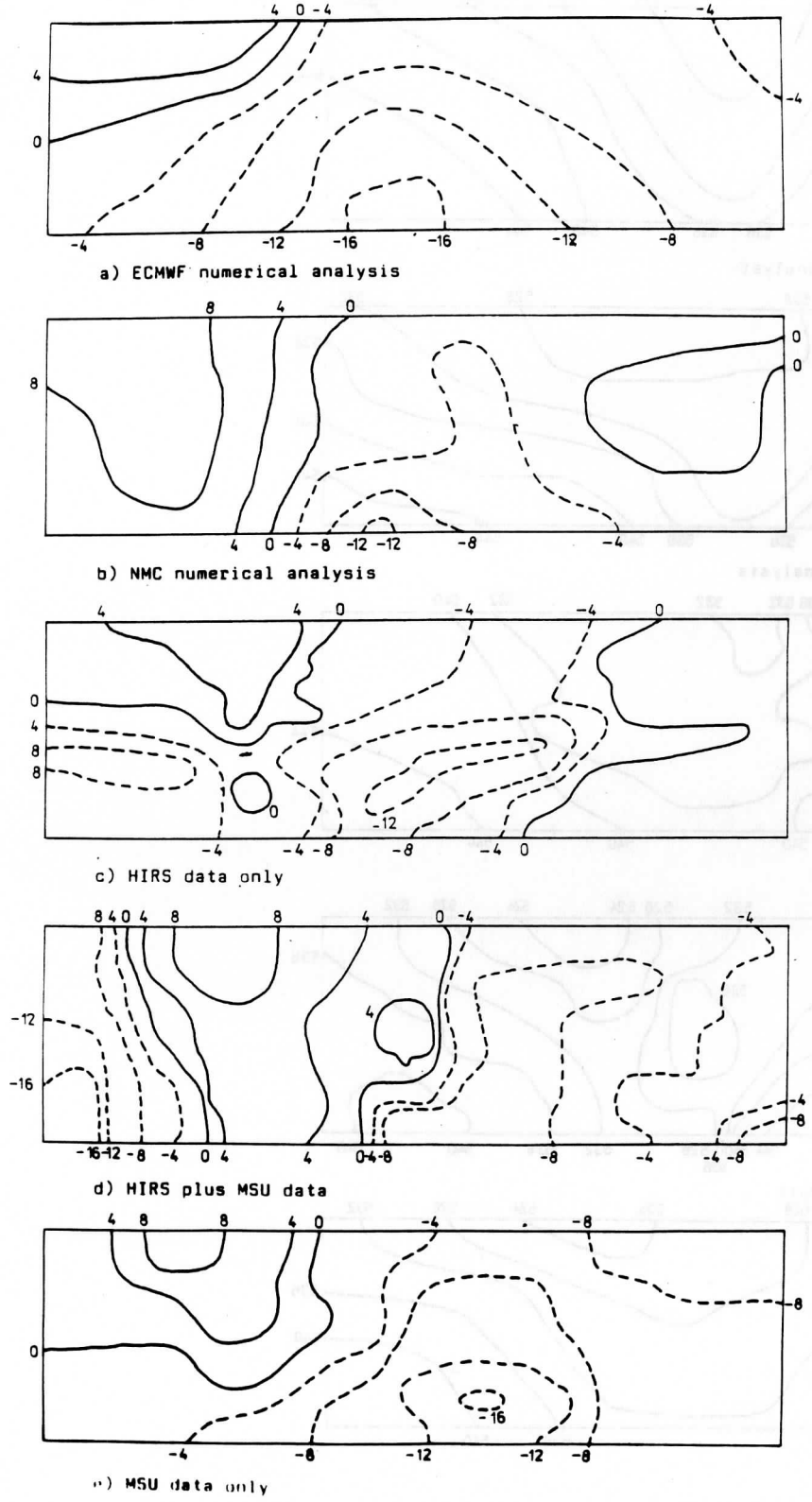

Fig. 6:
Thickness changes (5 March - 4 March) of the 500/1000 hPa layer in the region D17 according to

a) the ECMWF numerical analysis
b) the NMC of the GDR numerical analysis
c) HIRS data only
d) HIRS plus MSU data
e) MSU data only

Fig. 7: Difference charts of 500/1000 hPa thicknesses, NMC minus ECMWF numerical analysis (top), NMC analysis minus analysis from MSU data (bottom)

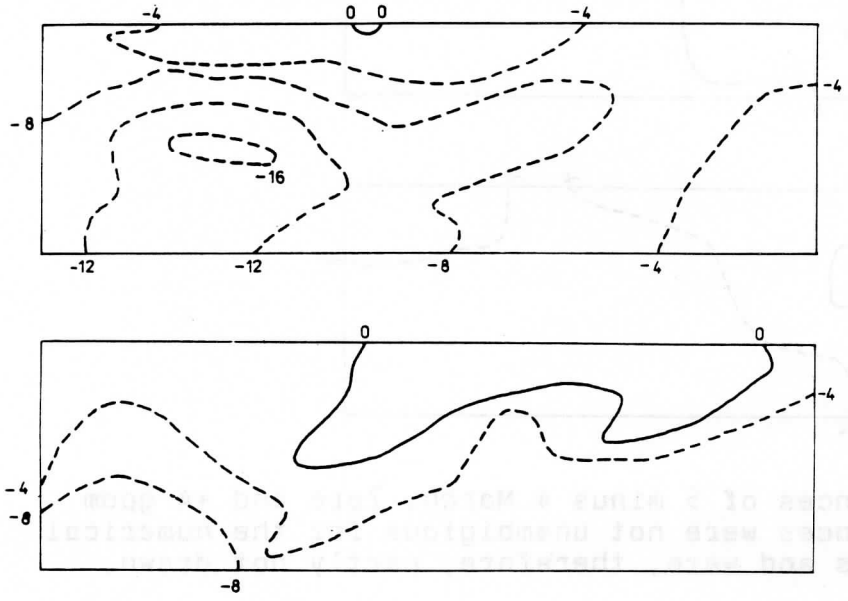

a) 4 March 1982, 00^{00} UTC

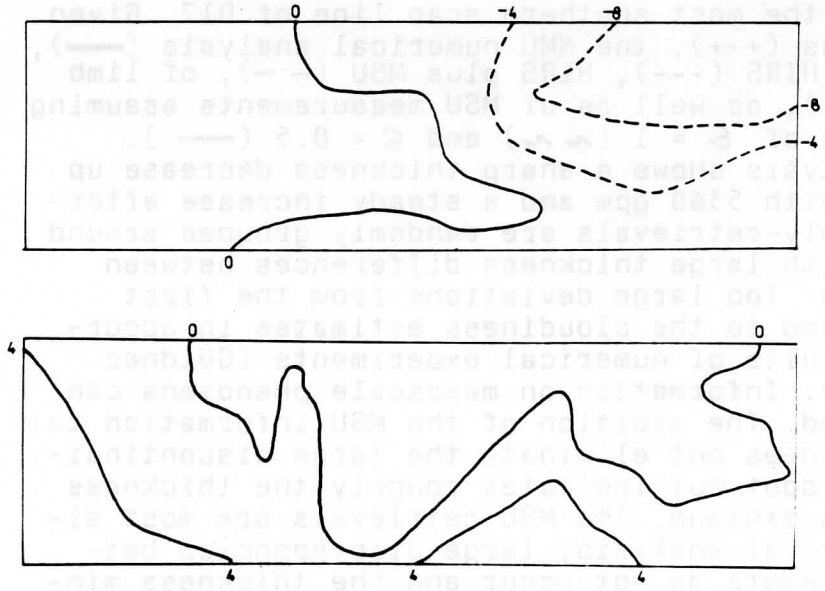

b) 5 March 1982, 12^{00} UTC

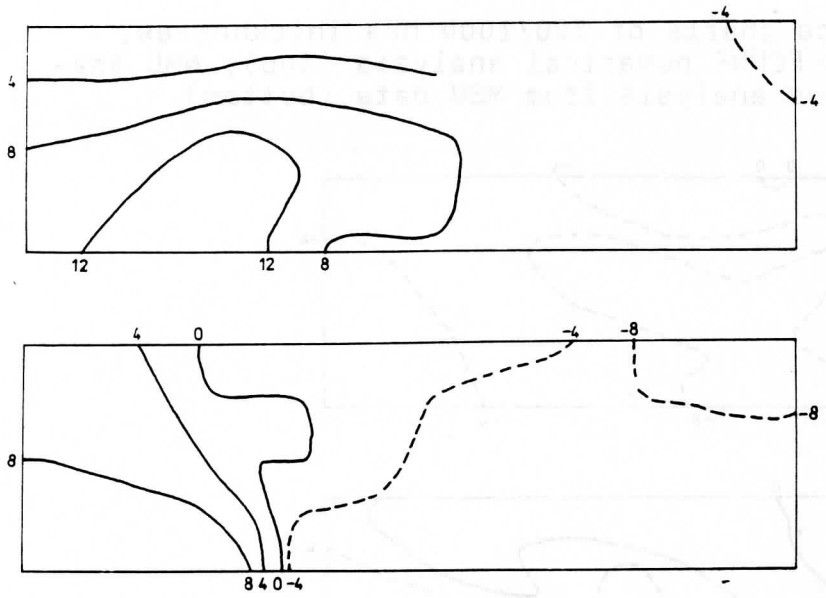

Fig. 7c: Differences of 5 minus 4 March. Zero and +4 gpdm differences were not unambigious for the numerical analyses and were, therefore, partly not drawn.

ly speaking, verification is not possible and that the impact of retrieval on meteorological analysis and forecasting must be evaluated by means of appropriate numerical models.
To shed some more light on the characteristics of TOVS retrievals Fig. 8 presents the 500/1000 hPa thickness of one single scan line, the most southern scan line of D17. Given are the first guess (+++), the NMC numerical analysis (——), and retrievals of HIRS (---), HIRS plus MSU (—·—), of limb corrected MSU (···), as well as of MSU measurements assuming a ground emittance of ε = 1 (∼∼) and ε = 0.5 (——).
The numerical analysis shows a sharp thickness decrease up to spot number 8 with 5360 gpm and a steady increase afterwards. The HIRS-only-retrievals are randomly grouped around the first guess with large thickness differences between neighbouring spots. Too large deviations from the first guess are attributed to the cloudiness estimates in accordance with the results of numerical experiments (Güldner and Spänkuch 1989). Information on mesoscale phenomena can hardly be extracted. The addition of the MSU information to the HIRS channels does not eliminate the large discontinuities from spot to spot but indicates roughly the thickness variation with its minimum. The MSU retrievals are most similar to the numerical analysis, large discrepancies between neighbouring spots do not occur and the thickness minimum is well reflected. The thickness differences between retrievals with ε = 1 and ε = 0.5 are a function of the scan angle and can be as great as 2 gpdm. The thickness retrievals with limb-corrected MSU data are similar but they

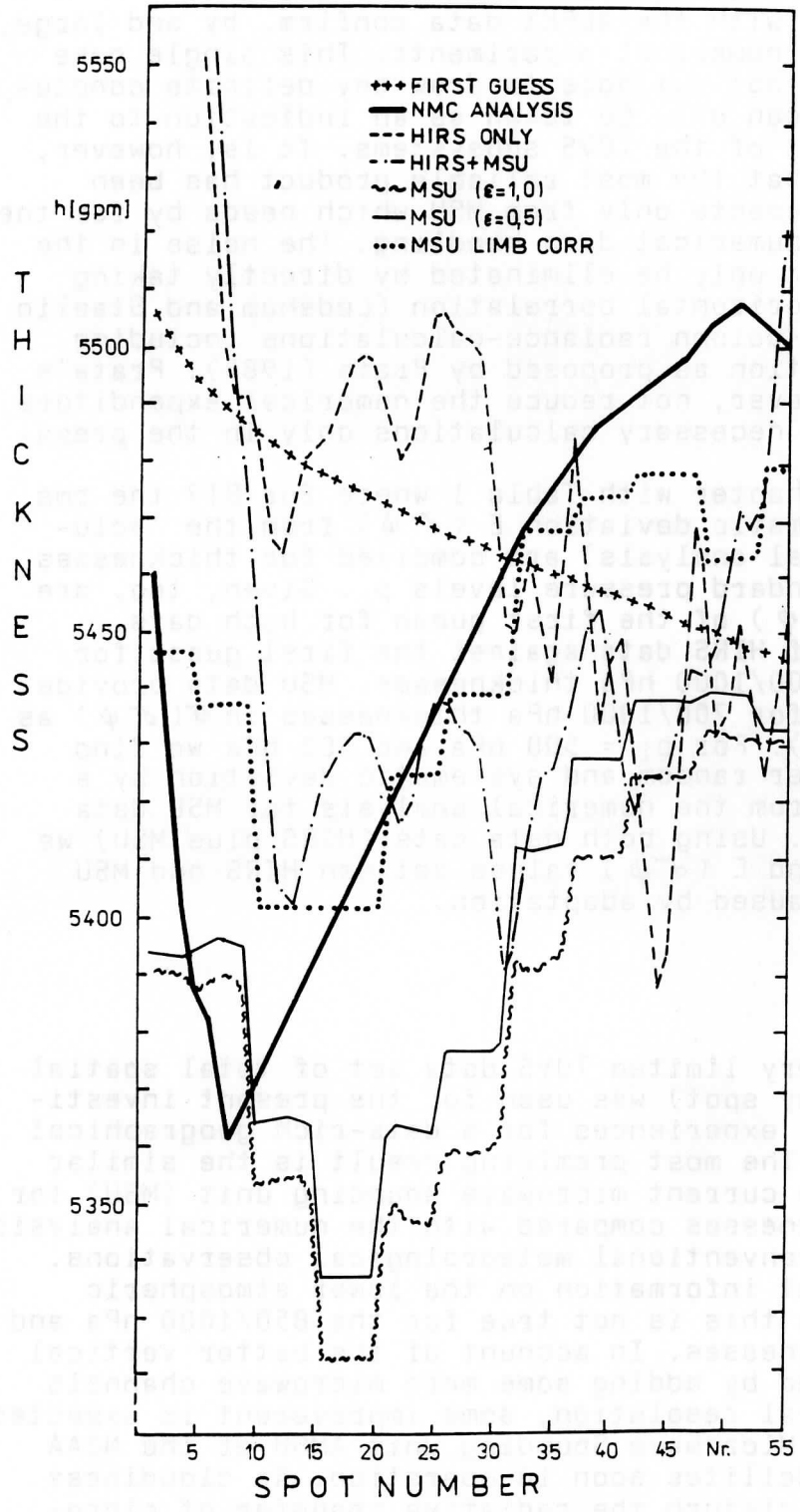

Fig. 8: 500/1000 hPa thickness along a scan line

are higher by about 5 to 7 gpdm due to the additional atmospheric attenuation having been taken into account.

The experiences with the ALPEX data confirm, by and large, the results of the numerical experiments. This single case study is, however, not suitable to draw any definite conclusion. The outcome can only be taken as an indication to the information content of the TOVS subsystems. It is, however, worth mentioning that the most reliable product has been achieved by measurements only from MSU which needs by far the least troublesome numerical data handling. The noise in the HIRS retrievals can only be eliminated by directly taking into account the horizontal correlation (Ledsham and Staelin 1978), or by clear-column radiance-calculations including horizontal correlation as proposed by Prata (1985). Prata's proposal does, however, not reduce the numerical expenditure but transforms the necessary calculations only in the preparatory phase.

We conclude this Chapter with Table 1 where for D17 the rms $\sigma(\sigma\phi)$ and systematic deviation $E(\sigma\phi)$ from the 'solution' (NMC numerical analysis) are compiled for thicknesses $p_i/1000$ hPa at standard pressure levels p_i. Given, too, are $\sigma(\sigma\phi)$ and $E(\sigma\phi)$ of the first guess for both days. There is no gain of HIRS data against the first guess for 850/1000 hPa and 700/1000 hPa thicknesses. MSU data provide already some gain for 700/1000 hPa thicknesses in $\sigma(\sigma\phi)$ as well as in $E(\sigma\phi)$. For p_i = 500 hPa and 300 hPa we find considerably smaller random and systematic deviation by a factor of 2 to 3 from the numerical analysis for MSU data than for HIRS data. Using both data sets (HIRS plus MSU) we obtain $\sigma(\sigma\phi)$ and $E(\sigma\phi)$ values between HIRS and MSU results,probably caused by adaptation.

III. CONCLUSIONS

Although only a very limited TOVS data set of total spatial resolution (spot by spot) was used for the present investigation some useful experiences for a data-rich geographical region were made. The most promising result is the similar information of the current microwave sounding unit (MSU) for 500/1000 hPa thicknesses compared with the numerical analysis that uses solely conventional meteorological observations. Due to insufficient information on the lower atmospheric layers in MSU data this is not true for the 850/1000 hPa and 700/1000 hPa thicknesses. In account of the better vertical resolution obtained by adding some more microwave channels of improved spectral resolution, some improvement is expected from the Advanced Microwave Sounding Unit AMSU of the NOAA polar orbiting satellites soon in operation. As cloudiness does not severely disturb the radiative transfer of microwave radiation, there is no need for cumbersome cloud elimination procedures as in case of temperature sounding with infrared channels. Temperature retrievals of single-spot HIRS measurements are pretty noisy and need, additionally to

Table 1: Mean E ($\sigma\phi$) and rms deviation $\sigma(\sigma\phi)$ in gpm of estimated layer thicknesses from the NMC numerical analysis ϕ_{AN} $\hat{\phi}$ above 1000 hPa for standard pressure levels p_i using different TOVS measurements. Region D17 for 4 and 5 March, 1982. The corresponding deviations of the first guess ϕ_{FG}, are also included.

p_i (hPa)	4 March 1982, 12^{00} UTC $\hat{\phi} - \phi_{AN}$		$\phi_{FG} - \phi_{AN}$		5 March 1982, 00^{00} UTC $\hat{\phi} - \phi_{AN}$		$\phi_{FG} - \phi_{AN}$	
	$\sigma(\sigma\phi)$	E ($\sigma\phi$)	$\sigma(\sigma\phi)$	E ($\sigma\phi$)	$\sigma(\sigma\phi)$	E ($\sigma\phi$)	$\sigma(\sigma\phi)$	E ($\sigma\phi$)
850	19.5	- 2.4	13.3	- 1.5	16.8	- 0.7	14.3	- 8.5
700	44.0	- 13.8	32.2	- 16.4	31.5	- 13.2	30.0	- 2.6
500	100.8	- 49.7	95.4	- 65.4	64.0	- 39.4	95.3	- 84.0
300	176.1	-100.2	186.3	-145.5	120.0	- 83.6	187.6	-169.6
				HIRS				
850	21.8	- 14.0	13.3	- 1.5	17.3	- 8.4	14.3	- 8.5
700	38.3	- 9.5	32.2	- 16.4	29.6	- 5.1	38.1	- 32.1
500	78.7	- 17.9	95.4	- 65.4	53.6	- 13.0	95.3	- 84.0
300	136.2	- 67.6	186.3	-145.5	94.5	- 55.2	187.6	-169.6
				HIRS plus MSU				
850	17.3	- 14.5	13.3	- 1.5	18.9	- 13.8	14.3	- 8.5
700	20.4	- 10.5	32.2	- 16.4	27.5	- 18.1	38.1	- 32.1
500	37.3	- 15.3	95.4	- 65.4	34.0	- 15.0	95.3	- 84.0
300	81.9	- 63.0	186.3	-145.5	50.6	- 11.3	187.6	-169.6
				MSU				

the cloud elimination, spatial filtering. This spatial filtering can mask existing subsynoptic features. The HIRS measurements with their high spatial density do not yield analysis products of reliable mesoscale structure as the horizontal resolution power of sounding systems is intimately related to their vertical resolution power. For passive sounding systems the vertical resolution power is, however, generally limited. Mixing of MSU and HIRS measurements is anticipated to supply best accuracy but further efforts are needed to improve adaptation.

References

Fritz, S., Wark, D.Q., Fleming, H.E., Smith, W.L., 1970: Temperature sounding from satellites. NOAA Technical Report NESS 59, Washington, D.C., 49 p.

Güldner, J., Spänkuch, D., 1989: Evaluation of TOVS measurements made during ALPEX-1. Z. Meteorol. (in press)

Kluge, J., Petzold, M., 1978: Nachträgliche Korrektur numerischer Analysen durch SIRS-Daten und einige Ergebnisse zur Abschätzung von deren Informationswert. Z. Meteorol. 28, 145 - 151

Kondrat'ev, K.Ja., Timofeev, Ju.M., 1978: Meteorologičeskoe zondirovanie atmosfery iz kosmosa, Gidrometeoizdat Leningrad

Ledsham, W.H., Staelin, D.H., 1978: An extended Kalman Bucy filter for atmospheric temperature profile retrieval with passive microwave sounder. J. Appl. Meteor. 17, 1023 - 1033

Prata, A.J., 1985: Clear column radiances by optimal estimation. Technical Proceedings of the Second International TOVS Study Conference, Igls, Febr. 1985, 201 - 207

Rizzi, R., 1984: Satellite sounding over the ALPEX area. Proceedings of the First International TOVS Study Conference, Igls, August, 1983.Ed. P. Menzel, 210 - 218

Weinreb, M.P., Fleming, H.E., McMillin, L.M., Neuendorffer, A.C., 1981: Transmittances for the TIROS Operational Vertical Sounder. NOAA Technical Report NESS 85, Washington, D.C.

TOVS PROCESSING AND EVALUATION AT THE NORWEGIAN METEOROLOGICAL INSTITUTE (DNMI)

Mariken Homleid and Jens Sunde
DNMI, Box 43, Blindern, N-0313 Oslo 3, Norway

1. INTRODUCTION

Since 1978 polar orbiter HRPT data has been read down at the local receiving ground station at DNMI in Oslo. AVHRR pictures are processed operationally. During 1987 ITPP has been implemented. We will here give a short overview of system configuration and numerical forecasting models operated at DNMI. Further we will present some ideas about data evaluation and show some preliminary results, before we end up with our future plans

2. SYSTEM CONFIGURATION AND CURRENT CAPABILITIES

Figure 1 shows the data aquisition area covered by the receiving station at DNMI, Oslo. The HRPT-data are read down to a NORD-100 computer where AVHRR-pictures are processed operationally. TIP-data are transferred to an IBM-4341 where ITPP-3.1 are implemented. Two limited area weather prediction models are running operationally on the IBM-4341, LAM50 and LAM150. The meshwidths are 50 and 150 km respectively. Figure 2 shows the areas covered by the numerical models. The present data assimilation system is based on a three dimensional multivariate successive correction sheme. All conventional observations including radiosonde observations from the area of interrest are collected and stored.

3. DATA EVALUATION

Presently we are able to process TOVS data through ITPP. The calculations seems reasonable for the different parameters. What about the quality ? Which soundings are the good ones ? To answer these questions we are now working on software and methods for data evaluation. As no method fits every purpose, it is important to look at data in different ways.

1) visually comparisons - TOVS / AVHRR
2) graphically - TOVS / numerical models / radiosondings
3) summary statistics - TOVS / numerical models / radiosondings

Figure 3 - 4 shows some preliminary results.

4. FUTURE PLANS FOR TOVS ACTIVITIES

We are continuing the work on evaluation of TOVS data quality, and assimilation experiments. As a small country with few persons working on TOVS data we also think it is important to follow the development in other countries.

Our goal is operationally processing and assimilation of TOVS data. As we are dependent on data from the northern regions, we attend to consentrate on research and development conserning special problems in arctic and subarctic regions.

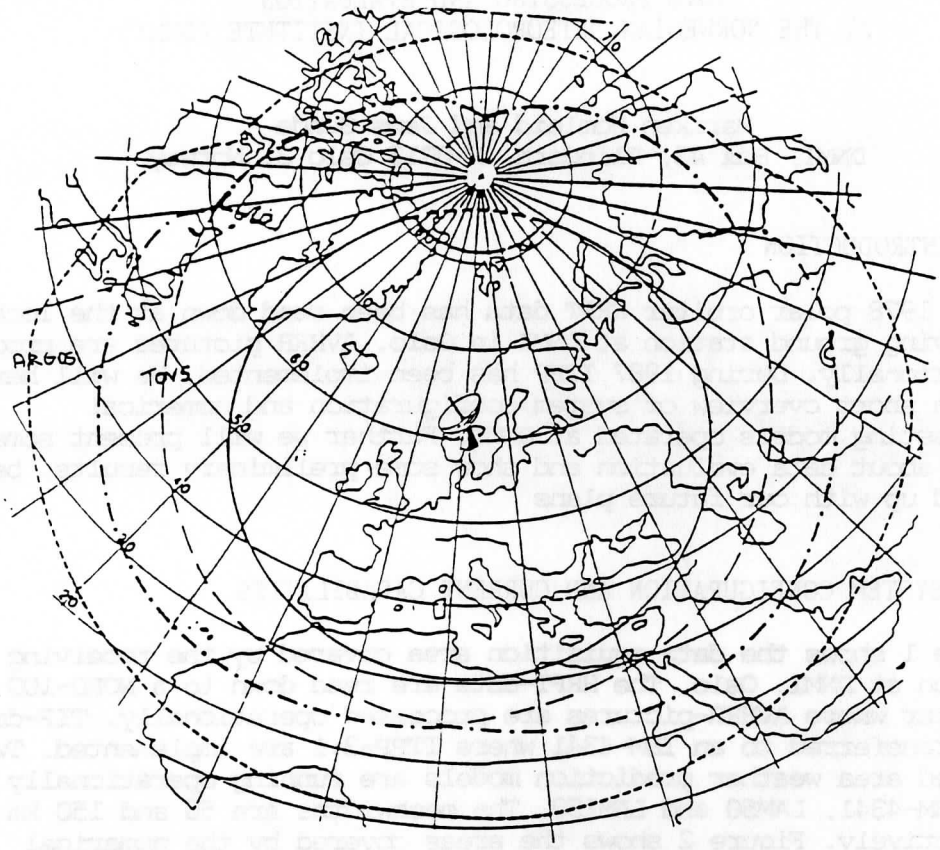

Figure 1.

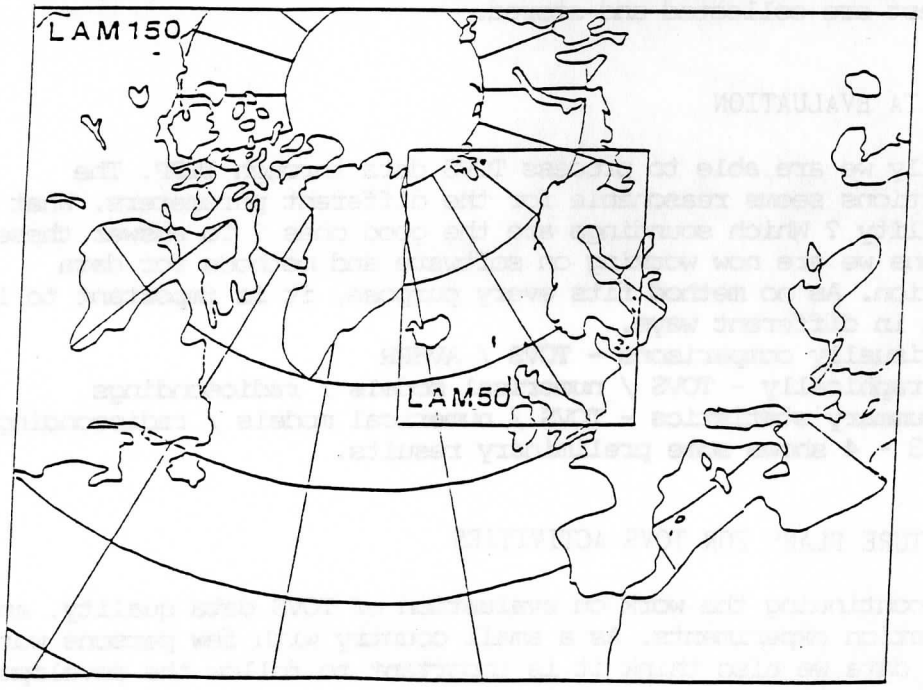

Figure 2.

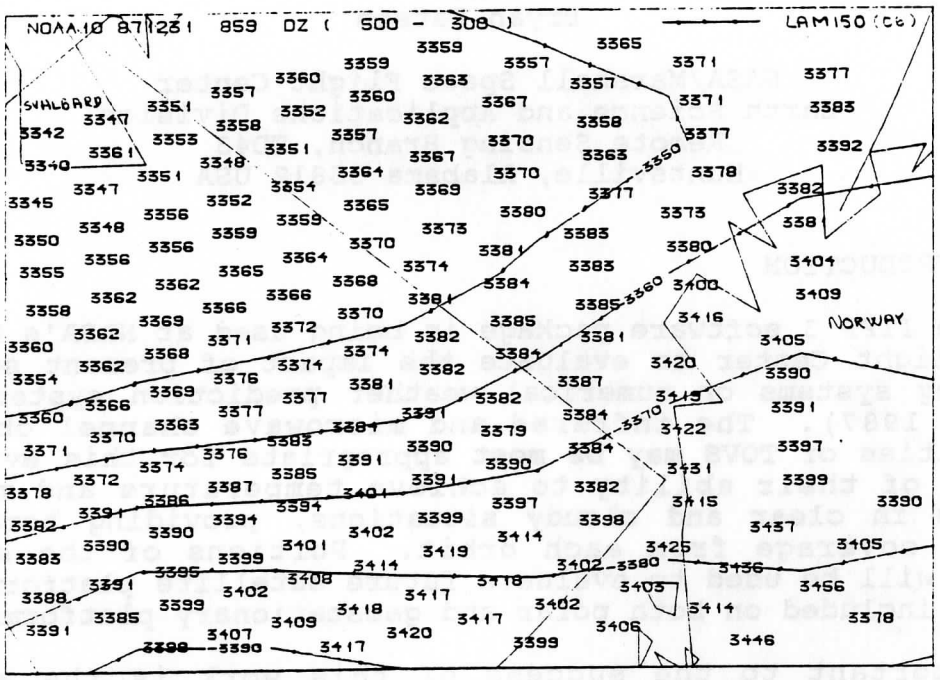

Figure 3.

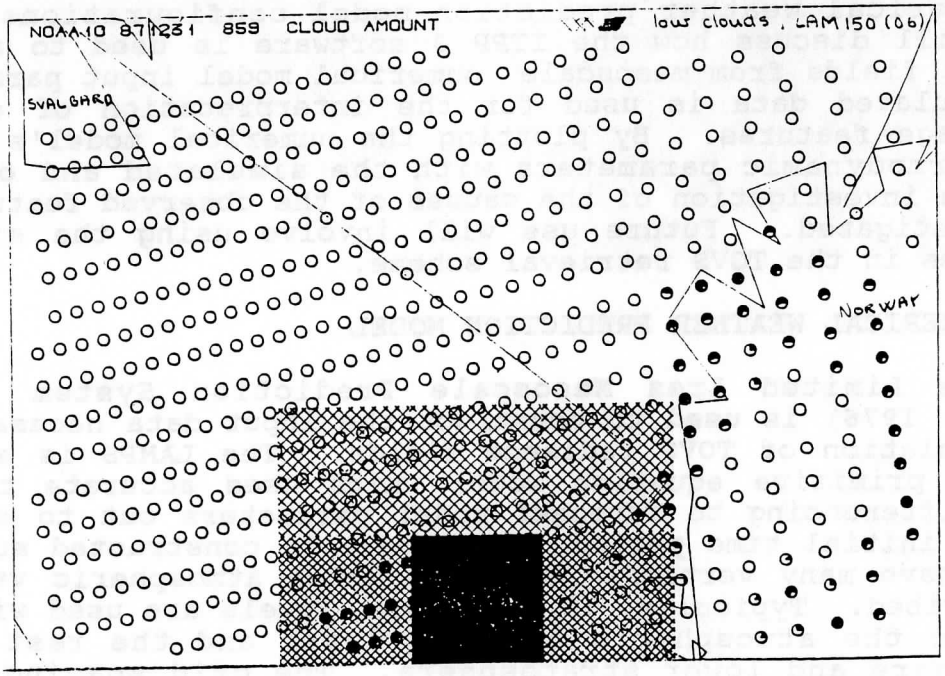

Figure 4.

INTERPRETATION OF OBSERVED TOVS IMAGERY FROM SIMULATED RADIANCE FIELDS

Gary J. Jedlovec
and
Bryan Batson

NASA/Marshall Space Flight Center
Earth Science and Applications Division
Remote Sensing Branch, ED43
Huntsville, Alabama 35812 USA

1. INTRODUCTION

The ITPP 3 software package is being used at NASA's Marshall Space Flight Center to evaluate the impact of present satellite observing systems on numerical weather prediction systems (Kalb et al., 1987). The infrared and microwave channel observing capabilities of TOVS may be most appropriate for this evaluation because of their ability to achieve temperature and mositure profiles in clear and cloudy situations, providing homogeneous spatial coverage from each orbit. Portions of the software package will be used to evaluate future satellite platforms which will be included on both polar and geostationary platforms.

Important to the success of this work is the accurate simulation of radiances and brightness temperatures from prescribed atmospheric parameters for representative case studies and numerical weather prediction model configurations. This paper will discuss how the ITPP 3 software is used to simulate radiance fields from mesoscale numerical model input parameters. The simulated data is used for the interpretation of observed TOVS image features. By plotting the numerical model's dynamic and thermodynamic parameters with the simulated and observed data, an investigation of the causes of the observed features can be investigated. Future use will involve using the simulated radiances in the TOVS retrieval scheme.

2. NUMERICAL WEATHER PREDICTION MODEL

The Limited Area Mesoscale Prediction System (LAMPS) (Perkey, 1976) is used to construct the input data necessary for the simulation of TOVS radiance fields. The LAMPS is a hydrostatic, primitive equation model which uses accurate time and space differencing to forecast model parameters out to 48 hours from an initial time period. The model is constructed such that it can have many vertical levels at which atmospheric variables are ascribed. Typically, 15 - 20 model levels are used with 6 of those in the atmospheric boundary layer and the rest in the troposphere and lower stratosphere. The grid spacing can be varied with application between 25 and 140 kilometers. Typical domain sizes are from 80 - 120 grid points in each horizontal direction.

A number of special model features make its application to TOVS simulations appropriate. First, multilevel optimal interpolation is used to provide a detailed description of atmospheric temperature and moisture structure, particularly in the lower portion of the troposphere. Second, the model carries resolvable (gridscale) cloud and rainwater at all levels throughout the forecast cycle. This allows the effects of clouds to be explicitly included in the radiative transfer calculations. Third, the LAMPS uses a parameterization scheme for sub-grid scale convective cloud water and precipitation. Large amounts of precipitation in liquid and ice phases can affect microwave radiances in the lower frequency MSU channels. Thus the modelled precipitation can be used to represent these effects in the simulated data. It should be noted that clouds and precipitation are parameterized rather than being described by detailed microphysics. Therefore smaller scale clouds and cloud systems (sub-grid scale) may not be adaquately represented in the radiance fields.

3. SIMULATED HIRS AND MSU RADIANCES

A modification of the ITPP 3 software package is used to simulate radiances in the 19 HIRS and 4 MSU channels. The ITPP simulation code (forward radiative transfer calculation) was modified to use the LAMPS gridded fields (initial and/or forecast conditions) instead of a guess or radiosonde profile. The numerical prediction model parameters used in the simulation code are listed in Table 1. The temperature and moisture described by the model was interpolated to the standard TOVS pressure levels (40). Surface information used for the lower boundary is that forecasted by the model itself. Additional model parameters for clouds and precipitation are also used.

Table 1

Numerical prediction model parameters used at every gridpoint in the radiative transfer simulation code

Date, time (of model grid data)
Latitude, longitude, elevation (of each gridpoint)
Surface parameters: P, T, Td, T_{skin}
Land/Ocean flag
Zenith angle (satellite to gridpoint)
Total Ozone
Cloud parameters: level, thickness, water/precipitation content
Temperature, T(p)
Dewpoint, Td(p)
Pressure, P(z)

The radiative transfer simulation code was also modified to incorporate clouds and precipitation into the simulation process. Schematic diagrams showing these processes are presented in Figs.

1 and 2. In the absence of clouds (case 1, Fig. 1), the simulation process remains unchanged from the original ITPP version. Thus the simulated radiances in each channel are expressed as the sum of the surface and atmospheric terms of the radiative transfer equation

$$R_s = R_{s\nu} = \varepsilon_{s\nu}\beta(T_s)\tau_\nu(p_s,0) + \int_{p_s}^{0} \beta\{T(p)\}\frac{\partial\tau_\nu(p)}{\partial p}\,dp \qquad (1)$$

The input LAMPS data serves to define the lower boundary condition, T_s, and the atmospheric temperature and moisture profile. The ITPP radiance simulation code uses empirical relationships between modelled parameters and atmospheric transmittance for fast transmittance determination (Weinreb et al., 1981). For infrared radiances, the emissivity of the surface in each channel, $\varepsilon_{s\nu}$ is approximately equal to unity. In the presence of opaque clouds (case 2, Fig. 1), the infrared radiative transfer equation must incorporate the effect of the cloud top temperature. The appropriate radiative transfer equation can be expressed as

$$R_c = R_{c\nu} = \varepsilon_{c\nu}\beta(T_c)\,\tau_\nu(p_c,0) + \int_{p_c}^{0} \beta\{T(p)\}\frac{\partial\tau_\nu(p)}{\partial p}\,dp \qquad (2)$$

where $\varepsilon_{c\nu}$ is the effective cloud emissivity in channel ν, and T_c is the cloud top temperature. When $\varepsilon_{c\nu} < 1.0$ (case 3, Fig. 2), the simulated radiances are represented by a combination of equations (1) and (2) above, and expressed as

$$R_T = R_c + \{\varepsilon_{s\nu}\beta(T_s)\tau_\nu(p_s,0) + \int_{p_s}^{0} \beta\{T(p)\}\frac{\partial\tau_\nu(p)}{\partial p}\,dp\}(1-\varepsilon_{c\nu}) \qquad (3)$$

It is easily seen that for $\varepsilon_{c\nu} = 1.0$, (3) reduces to (2). In this formulation, the emissivity of model diagnosed cirrus clouds (infinitely thin) is based upon their cloud water content. For multiple layers of clouds, the emissivity of the uppermost cloud layer is estimated and the lower level clouds are not considered in the simulated infrared radiances.

For the microwave region, only precipitation is allowed to effect the simulated radiances. The effect of both scattering and emission from rainwater and ice is empirically included in the transmittance calculations based on the total rainwater content of the cloud and its vertical distribution.

The simulated radiance data from the model input grids can be displayed in several forms using the Marshall Space Flight Center's McIDAS. Typically all simulated channels are displayed in a 24 panel (19 HIRS, 4 MSU, and a cloud/precipitation image)

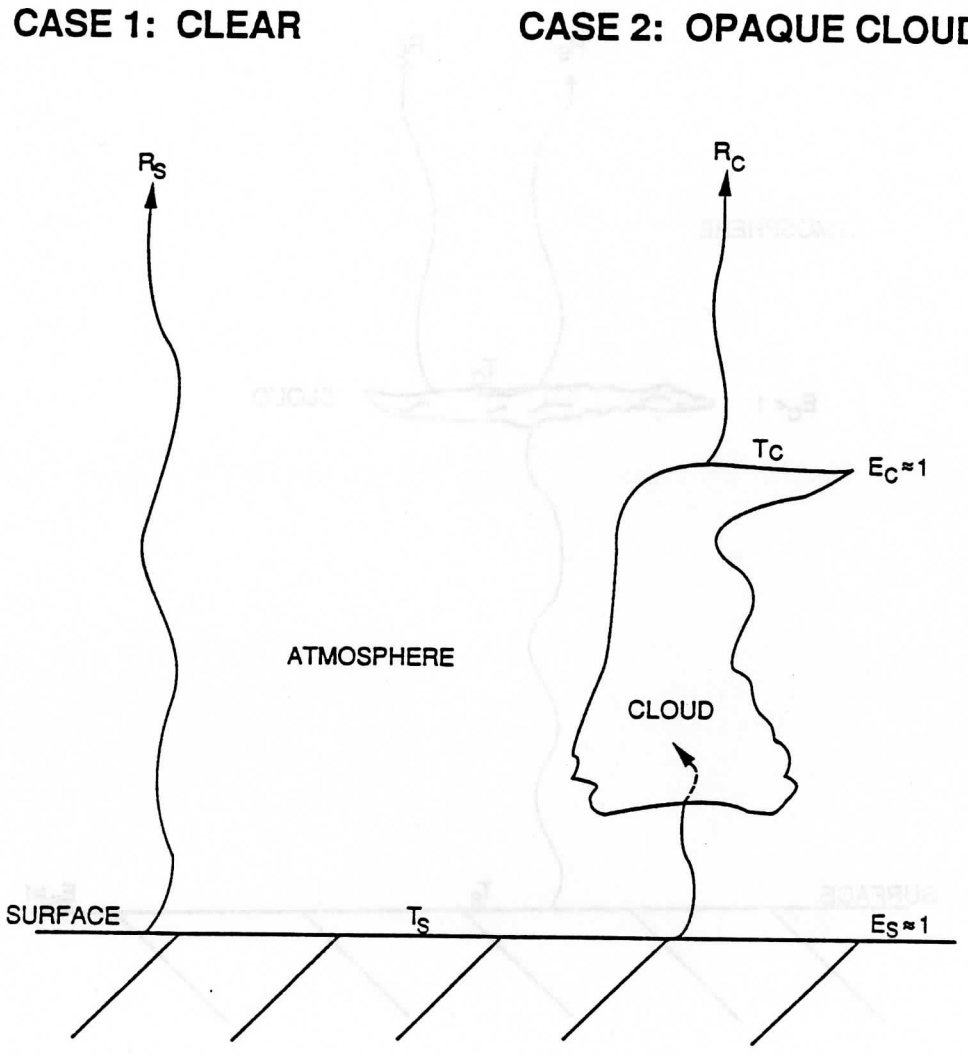

Figure 1. Schematic diagram of radiative transfer processes in the absence of clouds and in "thick" cloud environments.

CASE 3: SEMI-TRANSPARENT CLOUD

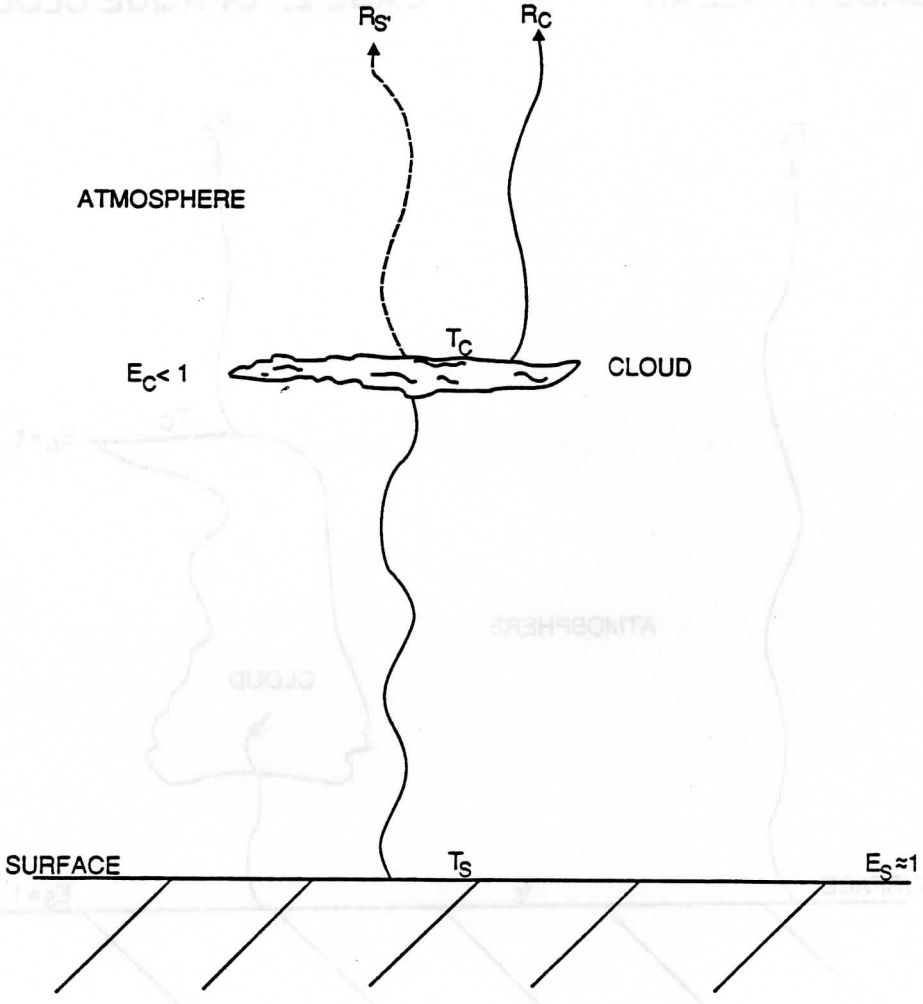

Figure 2. Schematic diagram of radiative transfer processes in the presence of "thin" clouds.

image. With simulated radiances from a number of model forecast periods, features in these radiance fields can be animated to simulate the evolution of storm and image features. Figure 3 presents a display of 3 simulated images and a cloud/precipitation image for 2000 UTC on 23 January 1986. This time period represents an 8 hour forecast with LAMPS from 1200 UTC inital conditions. The model grid spacing is approximately 46 km in each direction and the model domain covers a 4500 by 5300 km region over the eastern half of the United States and adjacent Atlantic Ocean. A map is superimposed on the upper right hand panel for geographic orientation. The upper left-hand image in Fig. 3 presents a map of cloud (grey) and precipitation (white) regions as determined by the LAMPS forecast. The precipitation regions include both gridscale and sub-gridscale precipitation. The clouds and precipitation are assumed to cover the entire grid box (46 x 46 km) and therefore the entire simulated HIRS footprint. In the absence of clouds, water (ocean) is denoted as black and the land is a dark grey shade.

The synoptic regime for the simulated imagery at 2000 UTC on 23 January 1986 is presented in Fig. 4. A cold front stretched from New Foundland southwest through Florida and on into the Gulf of Mexico. A high pressure system was building in from Canada (Fig. 4a), causing mostly northern flow over the eastern United States. Precipitation associated with the cold front was over the Atlantic, although some convective activity remained near Florida (not shown).

Analysis of the LAMPS 8 hour forecast fields (2000 UTC) indicates that the dynamical support associated with the geopotential height trough at 500 mb (4b) had advanced ahead of the cold air in the lower troposphere (4c) providing significant cold air advection over the eastern United States. As indicated in Fig. 4b, the upper level trough was positioned over the Atlantic seaboard at this time. The 850 mb temperature map (Fig. 4c) shows a cold trough aligned southward from the Ohio Valley through Texas. This tendency for cold air to tilt eastward with height is believed to inhibit the early states of storm development. Another significant feature is the upper level low in Canada which is causing considerable cloudiness and precipitation in the northwest portion of the model domain. More details of these features and their evolution are discussed in Mercer and Kreitzberg (1986).

The upper right-hand image of Fig. 3 represents the HIRS 12 (6.7 micrometer) radiance field. This channel senses upwelling energy which is absorbed and re-radiated by atmospheric water vapor in the middle troposphere. Dry (radiometrically warm) regions are denoted as dark features and moist/cloudy (radiometrically cool) regions are denoted with the brighter grey shades. Much horizontal structure is associated with these water vapor variations. These variations are related to thermodynamic and dynamic processes represented in the numerical forecast model. The lower left-hand image represents HIRS 8 (11

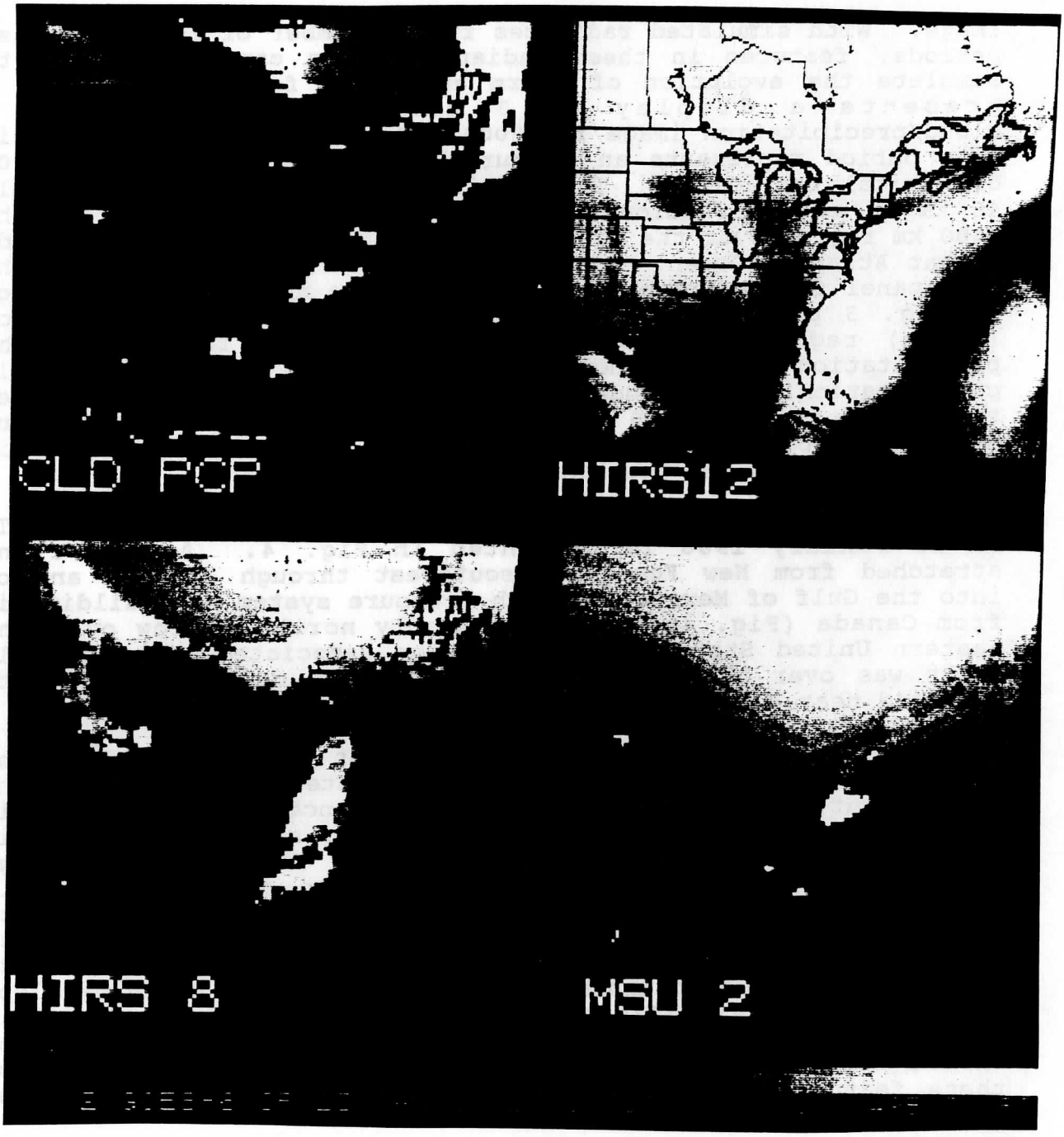

Figure 3. Display of simulated HIRS and MSU channel data for 2000 UTC on 23 January 1986. The four sub-images represent (clockwise from upper left), a) a cloud/ precipitation image, b) the HIRS 12, 6.7 micrometer channel, c) the MSU 2, 53 ghz channel, and d) the HIRS 8, 11 micrometer channel. Simulated channel data does not incorporate any orbital geometry.

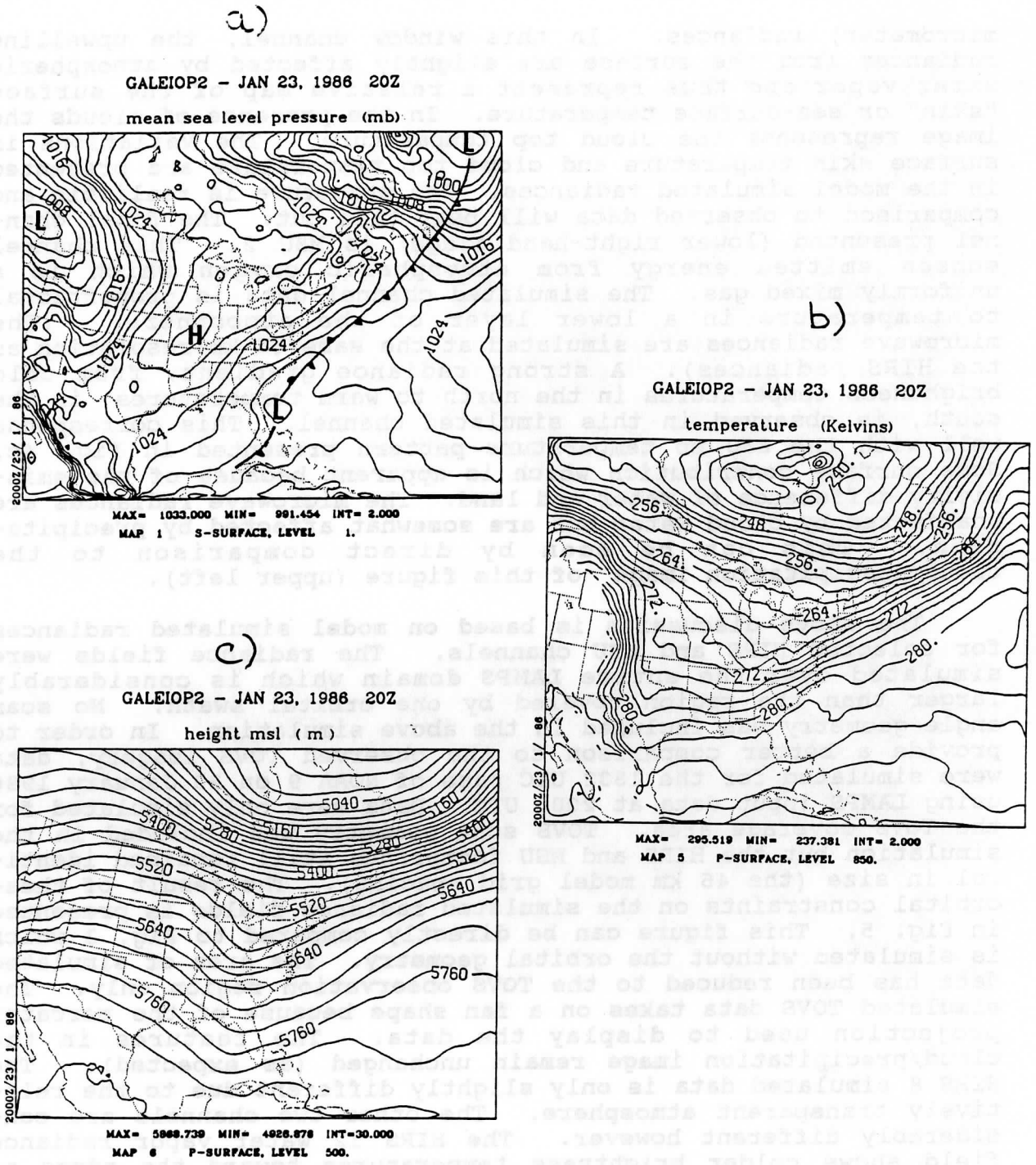

Figure 4. Synoptic situation for 2000 UTC on 23 January 1986 based on an 8 hour forecast from the LAMPS model. The three diagrams present the a) surface pressure analysis, b) the 850 mb temperature pattern, and c) the 850 mb geopotential height field.

micrometer) radiances. In this window channel, the upwelling radiances from the surface are slightly affected by atmospheric water vapor and thus represent a relative map of the surface "skin" or sea-surface temperature. In the presence of clouds the image represents the cloud top temperature. The variations in surface skin temperature and cloud top temperature are presented in the model simulated radiances. The structure is realistic and comparison to observed data will bear this out. The final channel presented (lower right-hand image) is MSU 2. This channel senses emitted energy from atmospheric oxygen which is a uniformly mixed gas. The simulated channel data is proportional to temperature in a lower layer of the atmosphere. (The microwave radiances are simulated at the same 46 km resolution as the HIRS radiances). A strong radiance gradient, from cold brightness temperatures in the north to warm temperatures in the south, is observed in this simulated channel. This corresponds well with the 850 mb temperature pattern presented in Fig. 4c. Some surface contribution which is apparent because of the emissivity difference of water and land. The microwave radiances are unaffected by cloud water but are somewhat affected by precipitation. This can be seen by direct comparison to the cloud/precipitation image of this figure (upper left).

The above discussion is based on model simulated radiances for selected HIRS and MSU channels. The radiance fields were simulated over the entire LAMPS domain which is considerably larger than the region covered by one orbital swath. No scan angle geometry was included in the above simulation. In order to provide a better comparison to the observed TOVS imagery, data were simulated for the 1832 UTC pass of NOAA 9 on 23 January 1986 using LAMPS input data at 2000 UTC. Data were only simulated for the TOVS coverage area. TOVS scan geometry was included in the simulation but the HIRS and MSU footprints still remained identical in size (the 46 km model grid spacing). The result of these orbital constraints on the simulated radiance fields is presented in Fig. 5. This figure can be directly compared to Fig. 3 which is simulated without the orbital geometry. The area of simulated data has been reduced to the TOVS observation region only. The simulated TOVS data takes on a fan shape because of the mercator projection used to display the data. The features in the cloud/precipitation image remain unchanged (as expected). The HIRS 8 simulated data is only slightly different due to the relatively transparent atmosphere. The other two channels are considerably different however. The HIRS 12 water vapor radiance field shows colder brightness temperatures toward the edges of the scan. This is due to the increased path length and water vapor absorption with increased scan angle.

For the microwave channel the scan angle effect is more dramatic. Details of the thermal structure seen in Fig. 3 are masked by this limb brightening effect. Along the nadir track (where the scan angle is zero) the thermal gradient is the same as in the previous image. Out on the edge of the scan, the

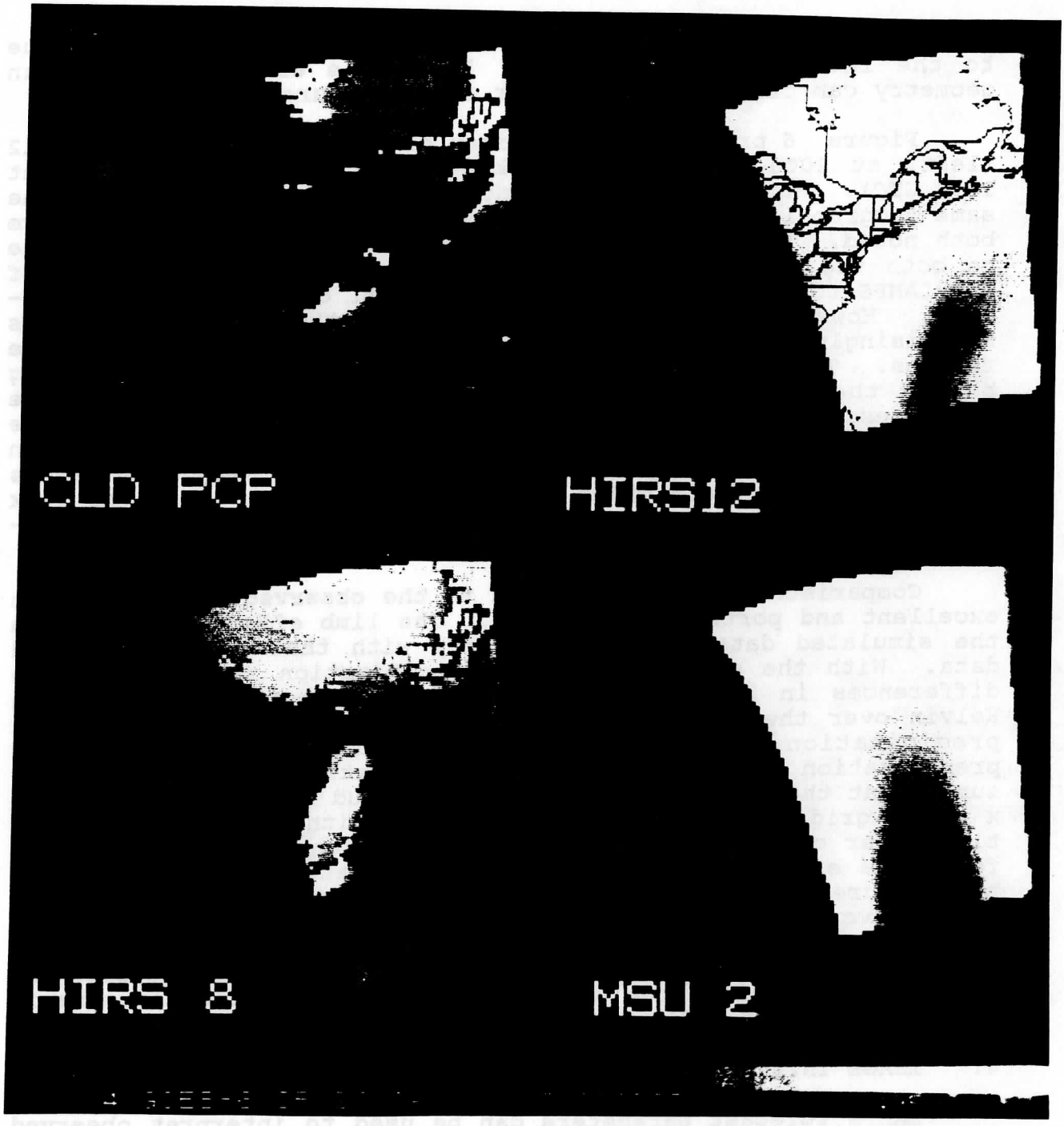

Figure 5. Display of simulated HIRS and MSU channel data for the 1832 UTC TOVS pass on 23 January 1986. The four sub-images represent (clockwise from upper left), a) a cloud/ precipitation image, b) the HIRS 12, 6.7 micrometer channel, c) the MSU 2, 53 ghz channel, and d) the HIRS 8, 11 micrometer channel. The simulated data incorporates the NOAA orbital and TOVS scan geometry with 46 km horizontal resolution. Data is simulated only for the region covered by the TOVS orbit.

brightness temperature gradient looks considerably different due to the increased path length. Thus, the effect of the scan geometry can often hide important image features.

Figure 6 presents a comparison of the the simulated HIRS 12 (left, at 2000 UTC) with the observed HIRS 12 data (right, at 1832 UTC). Both images are in the same projection and cover the same geographical region. Image differences and similarities are both noted. Some differences occur where clouds are present due to both the time difference of the imagery and the inability of the LAMPS to forecast the details of small clouds and cloud systems. However, the general agreement of the cloudy regions is surprisingly good. Better agreement occurs in the cloud free regions. The simulated radiances accurately pinpoint the drying behind the frontal zone off the east coast of the U.S. The brightness temperature differences in non-cloudy regions indicate that the simulated data is several degrees drier (warmer) than the observed. This may be due to the effect of very thin cirrus in the observed field which the model can not resolve, the lack of good initial moisture data above 400 mb, or enhanced subsidence in the model.

Comparisons of the simulated to the observed MSU 2 data are excellent and portrayed in Fig. 7. The limb effect prominent in the simulated data matches precisely with that of the observed data. With the exception of the precipitation region, absolute differences in brightness temperature are less than one degree Kelvin over the entire image. The larger discrepancies in the precipitation regions are due to the size of the simulated precipitation region. Currently the radiative transfer code assumes that the precipitation producing cloud covers the entire 46 x 46 km grid region. In nature, storms with intense precipitation cover only a small fraction of a region this size. Therefore, the simulated effect of the precipitation on the microwave temperatures is exaggerated. Future modifications will take the storm coverage into effect. In general, these comparisons are consistent on two counts; first that the LAMPS is properly forecasting large scale atmospheric features, and second that the radiance simulation code is adaquately representing atmospheric transmittance and radiance in these channels.

4. IMAGE INTERPRETATION

LAMPS forecast parameters can be used to interpret observed and simulated TOVS image features. As an example, Fig. 8 presents an analysis of model derived specific humidity at 500mb for 2000 UTC on 23 January 1986. This time corresponds to the imagery presented in Fig. 6. It is believed that there is a high correlation between this absolute moisture parameter and 6.7 micrometer radiances fields. For the most part, Fig. 8 supports this statement. In observed and simulated data, regions of cold brightness temperatures (bright grey shades) correspond to relatively high values of specific humidity and vice versa. For extremely dry regions ($q < 0.2$ gm/kg), specific humidity values are

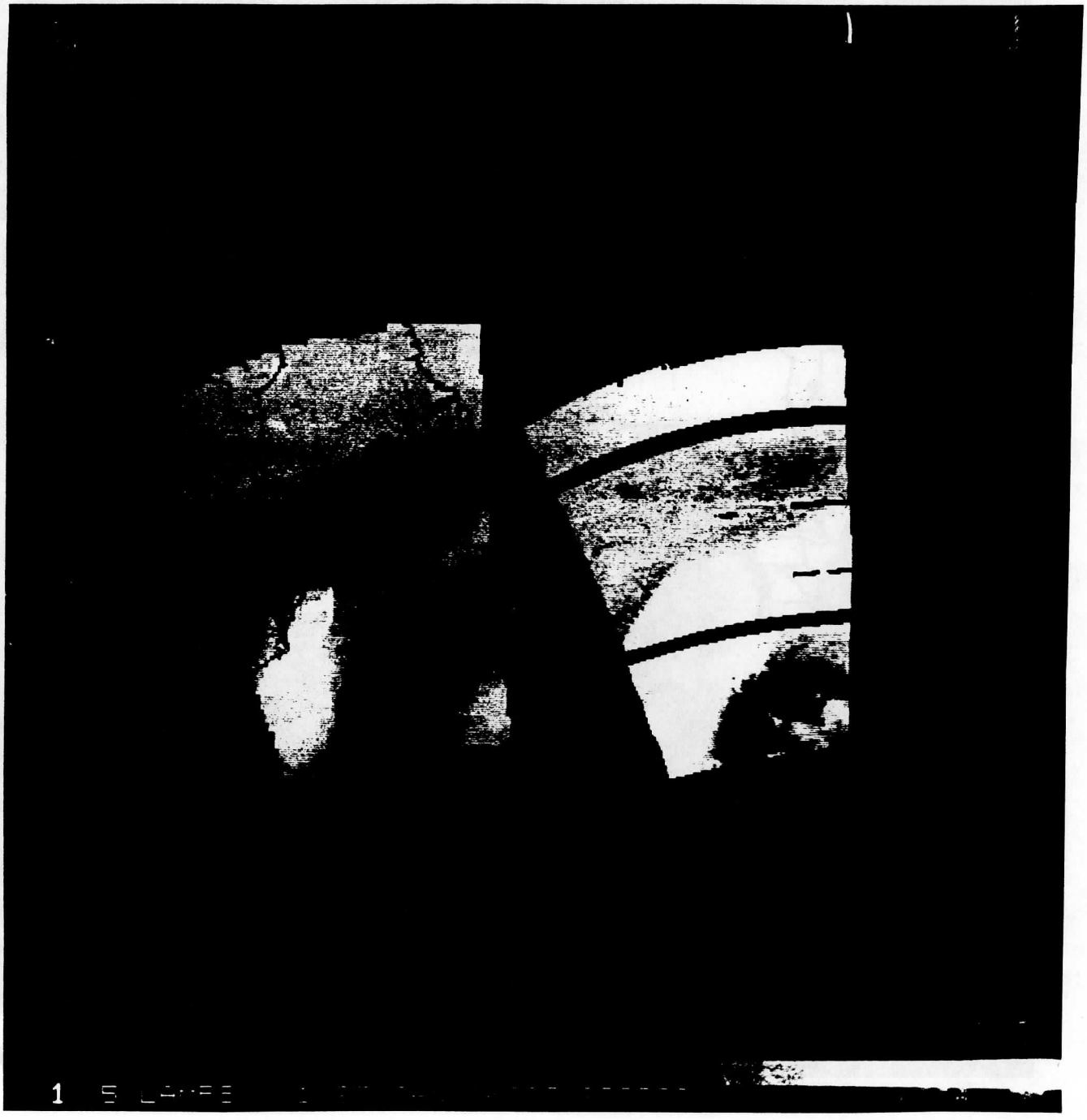

Figure 6. Simulated (left) and observed (right) HIRS 12, 6.7 micrometer data for the afternoon of 23 January 1986. Each image covers the same geographical region. The simulated data incorporates the NOAA orbital and TOVS scan geometry of with 46 km horizontal resolution. Data is simulated only for the region covered by the TOVS orbit.

Figure 7. Simulated (left) and observed (right) MSU 2, 53 ghz data for the afternoon of 23 January 1986. Each image covers the same geographical region. The simulated data incorporates the NOAA orbital and TOVS scan geometry with 46 km horizontal resolution.

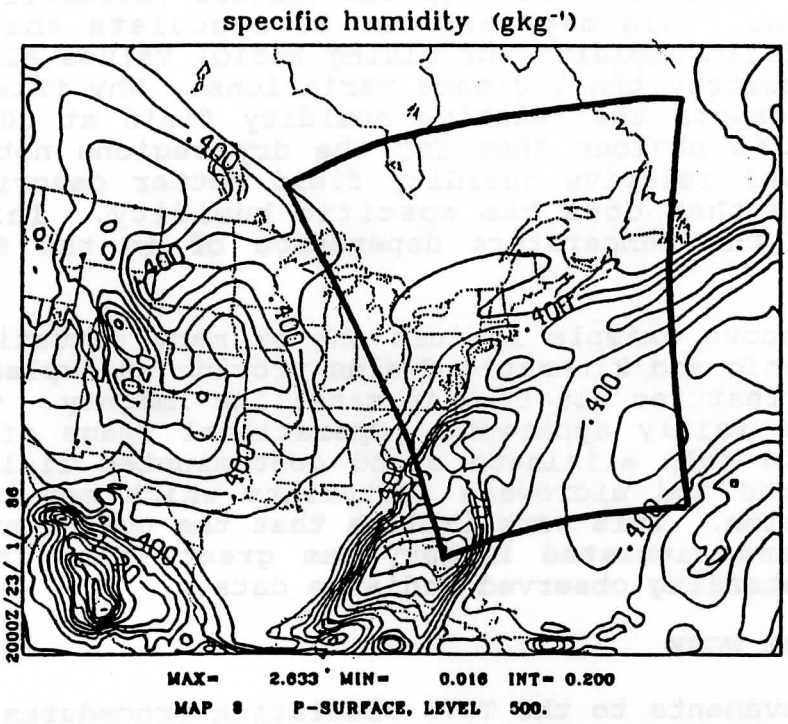

Figure 8. LAMPS forecast field of 500 mb specific humidity at 2000 UTC on 23 January 1986. Units are gm/km times.

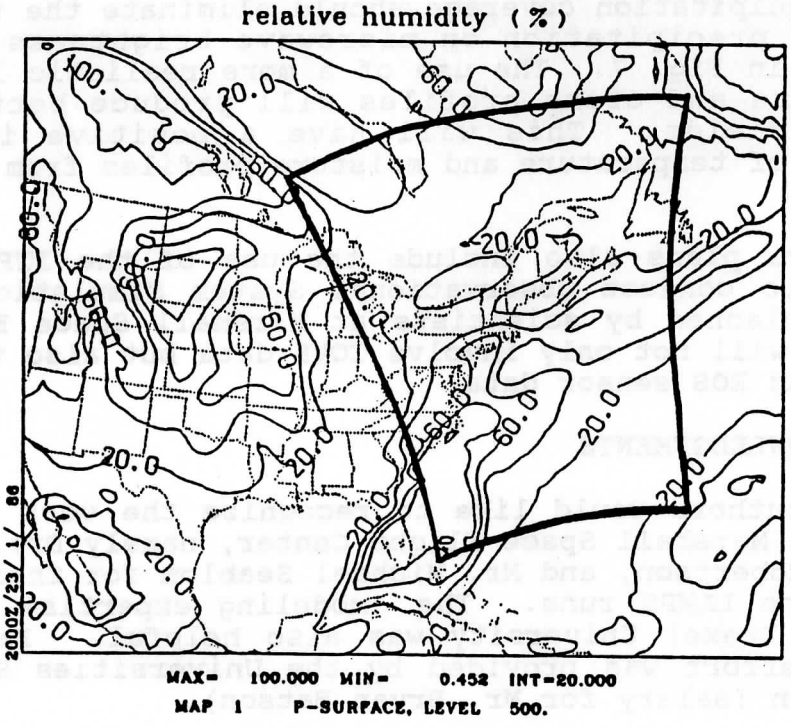

Figure 9. LAMPS forecast field of 500 mb relative humidity at 2000 UTC on 23 January 1986. Units are in percent.

invariant. However, there is substantial variability in the TOVS image data. This may lead one to speculate that that single layer specific humidity (or mixing ratio) values alone do not accurately portray the radiance variations. Why this may be true, Fig. 9 presents the relative humidity field at 500 mb for this time. It is obvious that for the dry regions noted above, the single level relative humidity field better describes the image variations than does the specific humidity. This could be a result of the temperature dependence of in the 6.7 micrometer channel.

The above example is just one of many situations where the LAMPS dynamic and kinematic fields provide an explanation for interesting features observed in satellite imagery. Other areas of impact are fairly apparent. Operational usage of such a technique could help eliminate cloud contaminated fields of view in the infrared and microwave footprints which may be effected by precipitation. This work implies that the use of numerical model products and simulated imagery has great value in interpreting and understanding observed radiance data.

5. FUTURE WORK

Improvements to the TOVS simulation procedures are on going. Several areas of changes include incorporating cloud and precipitation fractional grid coverage, using a physically modelled skin-sea-surface temperature in the calculations, and varying total ozone spatial across the LAMPS domain. The fractional precipitation coverage should eliminate the the exagerated effect of precipitation on microwave brightness temperatures presented in Fig. 7. The use of a more realistic lower boundary temperature and ozone profiles will produce better simulated radiance fields. This will have a positive impact on the retrieval of temperature and moisture profiles from the simulated data.

Future plans also include the use of the ITPP 3 retrieval software to conduct Observational System Simulation Experiments (OSSE's) planned by scientists at Marshall Space Flight Center. This work will not only involve TOVS data but also the simulation of AMSU and EOS sensor data.

6. ACKNOWLEDGEMENTS

The authors would like to recognize the work of their colleagues at Marshall Space Flight Center, namely Drs. Michael Kalb and Pete Robertson, and Mr. Michael Seablom for their fine execution of the LAMPS runs. The modeling expertise of Dr. Donald Perkey at Drexel University was also helpful. Partial support for this effort was provided by the Universities Space Research Association (salary for Mr. Bryan Batson).

7. REFERENCES

Kalb, M., F. Robertson, G. Jedlovec, and D. Perkey, 1987: Use of simulated satellite radiance data from a mesoscale numerical model to understand kinematic and dynamical processes. Preprints Conference on Mesoscale Analysis and Forecasting, AMS, Boston, .

Perkey, D. J., 1976: Prediction of convective activity using a system of parastic-nested numerical models. NASA CR-2761, 160pgs.

Weinreb, M. P., H. E. Fleming, L. M. McMillin, and A. C. Neuendorfer, 1981: Transmittances for the TIROS Operational Vertical Sounder. NOAA Technical Report NESS 85, 60 pgs.

Mercer, T. J., and C. W. Kreitzberg, 1986: Genesis of Atlantic Lows Experiment (GALE): Field Program Summary. Department of Physics and Atmospheric Science, Drexel University, Philadelphia, 443 pgs.

TOVS DATA IMPACT STUDIES OF THE PERIDOT NWP SYSTEM ON THE 7 JUNE 1987 CASE

R. Juvanon du Vachat*, M. Imbard*, Y. Durand**

*EERM/CRMD
**SCEM/PREVI-NUM

Météorologie Nationale
2 avenue Rapp 75007 Paris

1. INTRODUCTION

On the Seventh June 1987 in the afternoon, a very active squall line crossed over Southwestern France, causing the death of several people and a great amount of material damage. This violent squall line developed ahead of a front parallel to the french "Landes" coast (oriented North-South), which was the consequence of a secondary development along a primary front oriented SouthWest/NorthEast. The sudden development of such a severe weather event was such that it has been impossible to forecast some hours before.

The development of such a squall line is probably out of scope of the Péridot (35 Km grid mesh) model prediction (cf. Figure 1) but we could expect it to give an indication of the secondary development and of a strong frontal structure.

Thus we've done some impact studies with the Péridot NWP system in order to understand :

a) what is crucial for conditioning the development of such a squall line with the Péridot model ?

b) what is the optimal configuration of the Péridot NWP system which could have been used for operational warning ?

We've to mention that the operational Péridot system (Imbard et al. 1987 ; Geleyn et Jarraud, 1988) makes prediction only with 0 Z data including a few TOVS data, those which are observed before 3 Z and with a 12 hours assimilation cycle. There is only an analysis with 12 Z data, including the TOVS data which are observed before 14.30 Z but not prediction due to limited computer resources.

As in the case of the operational forecasting (which was run on the smaller domain 51x51 on 7 June 1987) trials with 0 Z data (but with the actual 95x95 domain (cf. Figure 1)) were not successfull in building any indication even of a slight secondary development or frontal structure. On the contrary, starting with 12 Z data gave far better results, thus giving an answer on the question a) (Imbard et al., 1988). But since such a forecast would have arrived too late to be useful for operational warning we've also considered the Péridot simulations starting with 6Z data in order to answer on the question b). In the following we report the results of the simulations starting with 12 Z data, or with 6 Z data with special emphasis on the use or not of TOVS data in the starting analysis. We refer the papers in the previous International TOVS Conferences for the technique of "direct assimilation of radiances" in the Péridot fine-mesh analysis (Durand et Juvanon du Vachat, 1983, 1985, 1986 ; see also Durand, 1985 and Durand et Bougeault, 1987). We only mention that TOVS data mean HIRS-2 + MSU + AVHRR information for NOAA 10, and the same data without MSU for NOAA 9.

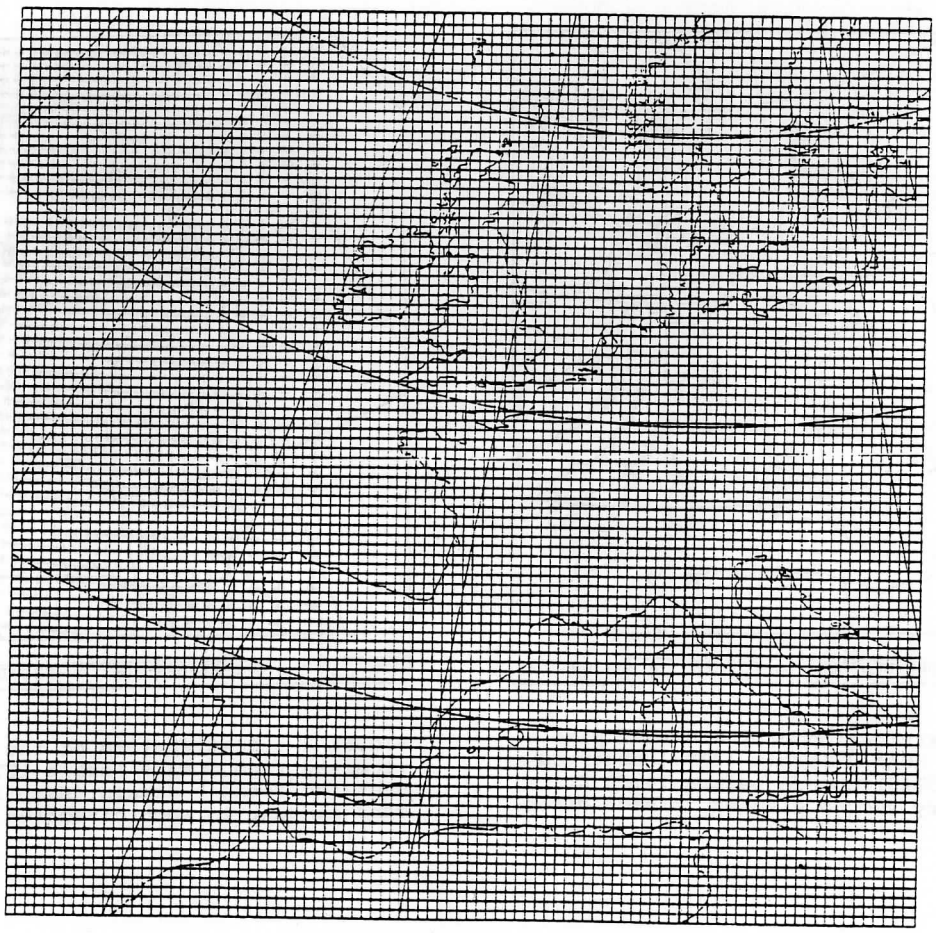

FIGURE 1 : The Péridot domain with the grid-point distribution (Δx = 35 Km, 95x95 grid-points).

2. SIMULATIONS STARTING WITH 12 Z DATA

We've run different Péridot simulations with using the following initial states at 12 Z :

a) Péridot analysis with 12 hours large-scale forecast as guess field.
b) Péridot analysis with 12 hours Péridot forecast as guess field.
c) Same as b) but with including only the TOVS data received from NOAA 9 (orbit 12796) and observed over the old 51x51 domain before 14.30 Z (as in operational mode).
d) Same as b) but with including the TOVS data received from NOAA 9 (orbit 12797) observed over the Péridot domain.

The Figures 2 and 3 show the location of the HIRS-2 pixels used in the cases c) and d). They include respectively 77 and 1062 radiances (sampling : every second element in each direction). These data have been observed between 12.56 Z and 13 Z in the case c) and between 14.35 Z and 14.44 Z in the case d).

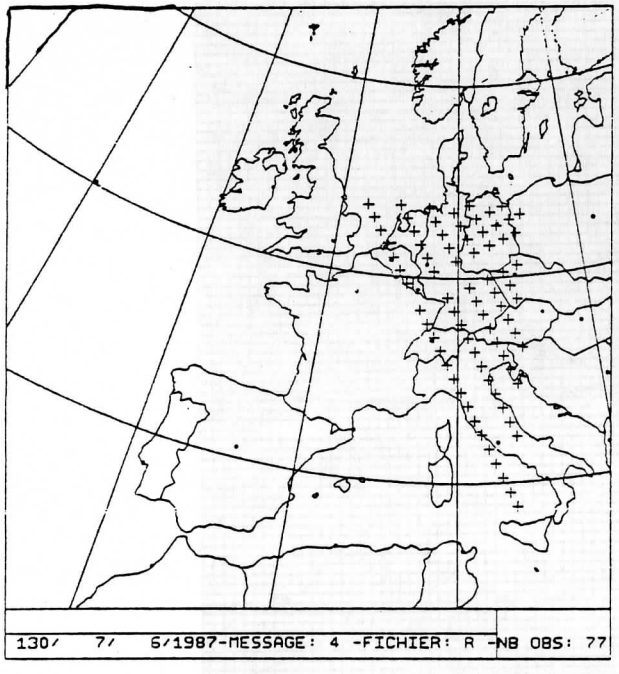

FIGURE 2 : Distribution of the HIRS-2 pixels received from NOAA 9 (orbit 12796) observed over the old 51x51 domain before 14.30 Z (sampling every second element in each direction).

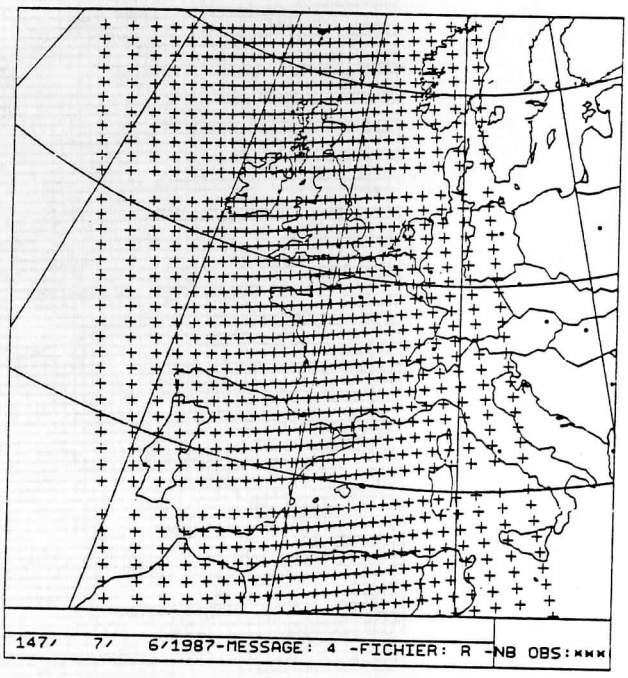

FIGURE 3 : Distribution of the HIRS-2 pixels received from NOAA 9 (orbit 12797) observed over the Péridot domain (sampling every second element in each direction).

Due to spin-up problems, the model evolution is lagging behind the real one. Thus we compare the forecasted fields from these a, b, c and d, simulations at 6 hours range, at the time 18 Z of the day. We've chosen the following surface fields : planetary boundary layer (PBL) moist equivalent potential temperature θ'w (Figure 4), wind at 10 m (Figure 5), 3 hours rain amount (Figure 6). From these Figures the following conclusions can be drawn :

+ The strongest gradient of θ'w (1°C/15 Km across the front) is observed in the Southwestern France in the case d), with all ingredients of a fine-mesh analysis ... including TOVS data observed approximately at the time of the phenomenon. For this parameter the impact of using TOVS data (d) against b)) is smaller than the impact of change in the guess field (b) against a)) but can be clearly seen. The fact of using those TOVS data which are observed before 14.30 Z (c)) has a very small impact on this parameter (because of the very small number of radiances).

+ Concerning the wind at 10 m the change in the guess field (b) against a)) change the wind in Brittany but in Southwestern France there is no obvious impact when using TOVS data.

+ Concerning the precipitation it is clear that the four Figures a), b), c) and d) show a different configuration of the two frontal systems : in Northern France and Belgium the system oriented SouthWest/NorthEast and the system oriented South/North in the Southwest France. In the cases b), c) and d) the two systems are well separated on the contrary of a).

  Obviously there is no important difference between b) and c) (same reason as before). At last the simulation d) describes well the two frontal systems. Why such differences between b) and d) ? We've to mention that together with TOVS data, AVHRR information (channel 4) is used too along a process defined in (Derrien, Phulpin, 1987). This last information gives indication of clouds in each HIRS-2 pixel and in some cases a "bogus" of 100 % relative humidity is imposed, which stimulates irreversible processes in the model evolution. That is also the reason why including TOVS data can give an impact on "physical fields" rather than on "dynamical fields", like 10 m wind field. A conclusion that has been drawn in previous tests (Durand et Juvanon du Vachat, 1985).

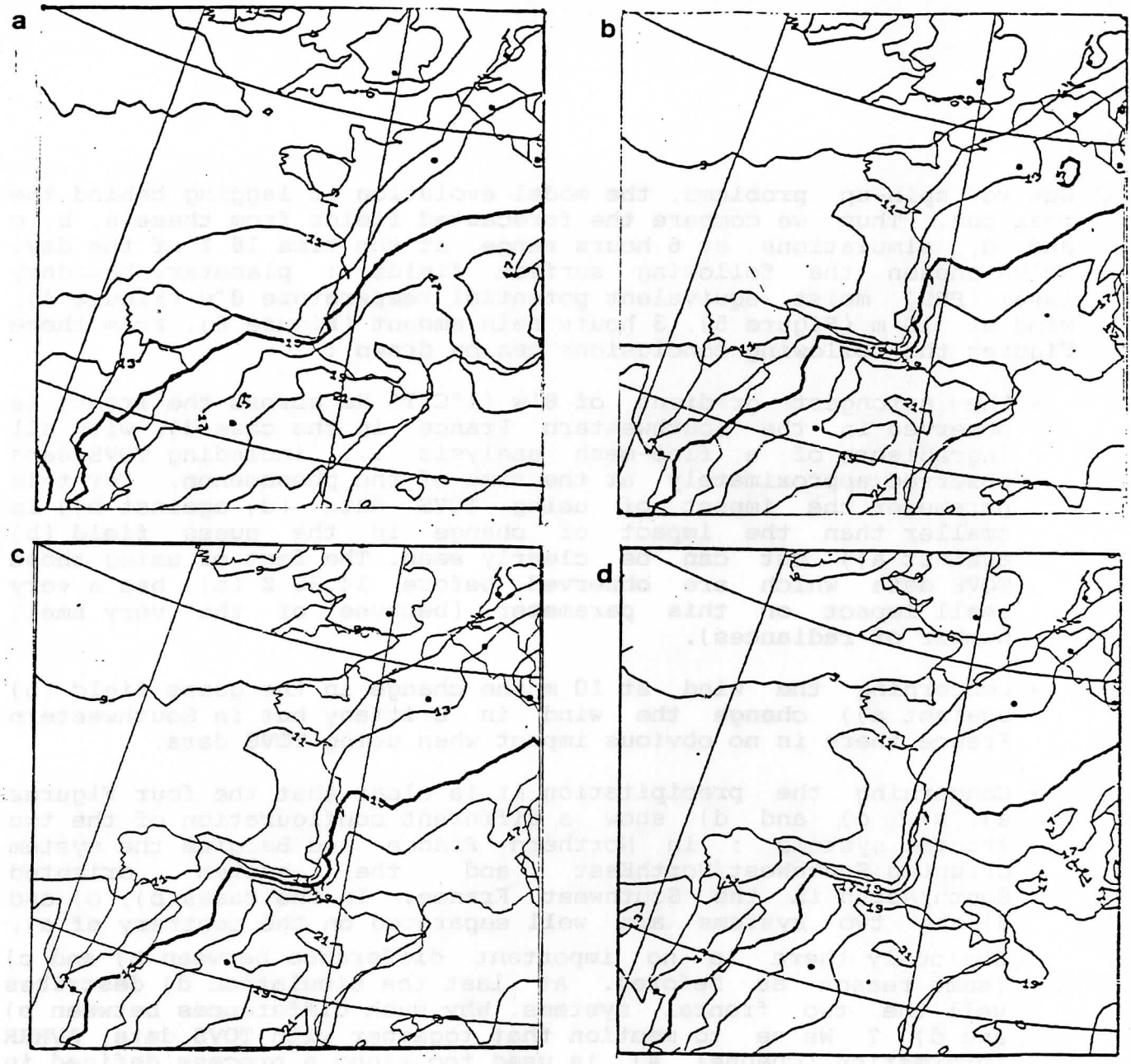

FIGURE 4 : Maps of 6 hours forecasts of PBL moist equivalent potential temperature verifying 7/6/1987 18 Z. The forecasts differ only by their initial states at 12 Z :

a) Péridot analysis with 12 hours large-scale forecast as guess field.b) Péridot analysis with 12 hours Péridot forecast as guess field.

c) Same as b) but with including only the TOVS data received from NOAA 9 (orbit 12796) and observed over the old 51x51 domain before 14.30 Z (as in operational mode).

d) Same as b) but with including the TOVS data received from NOAA 9 (orbit 12797) observed over the Péridot domain.

Contouring interval 2°C. Only part of the Péridot domain is shown here.

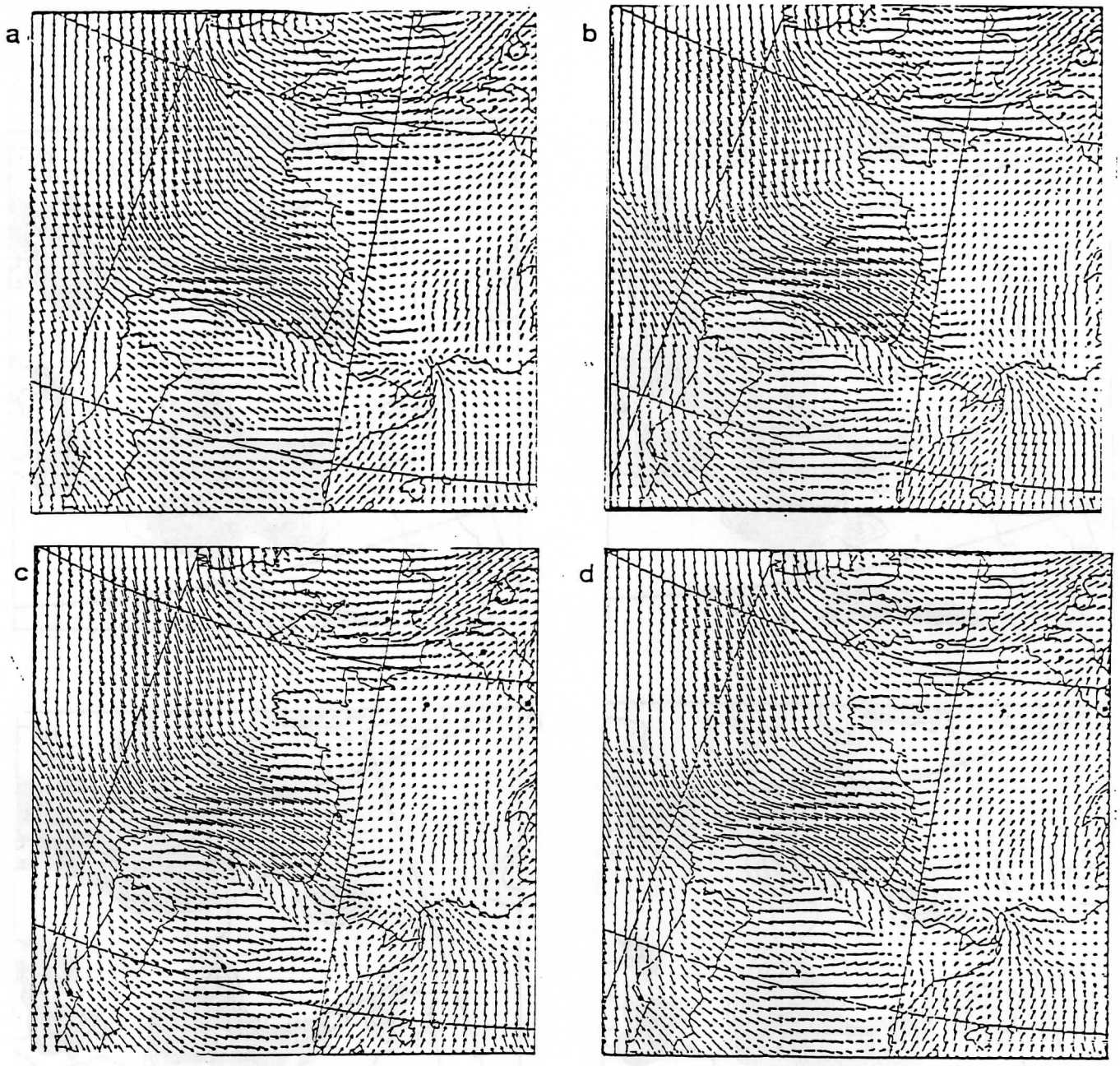

FIGURE 5 : As Figure 4 but for the 10 m wind field.

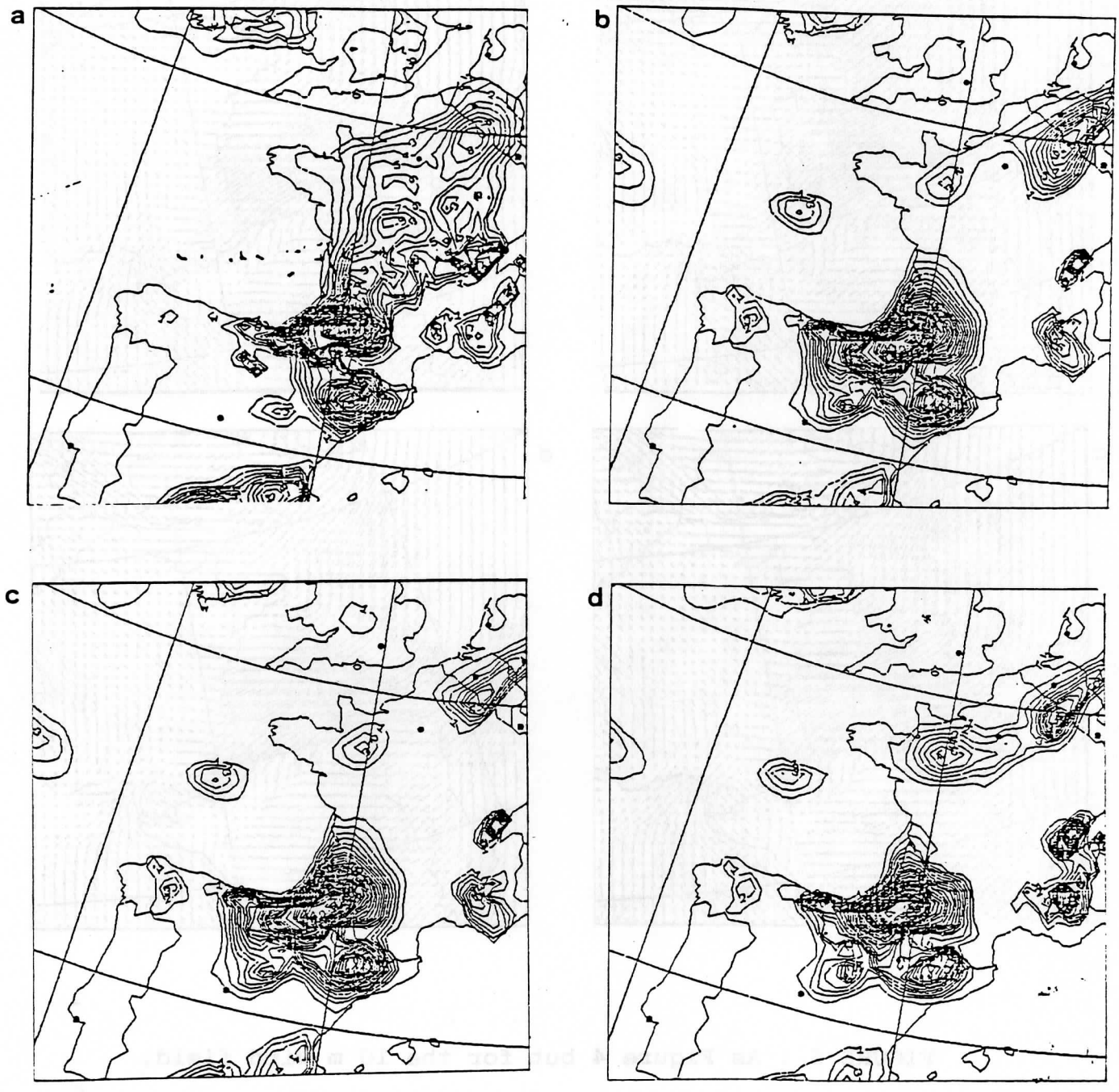

FIGURE 6 : As Figure 4 but for the 3 hours rain amount.

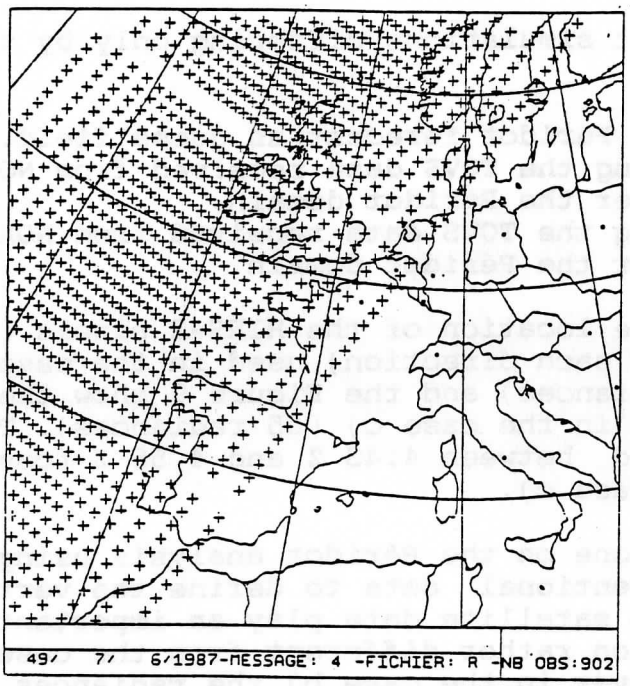

FIGURE 7 : Distribution of the HIRS-2 pixels received from NOAA 9 (orbit 12791), observed over the Péridot domain (sampling : every second element in each direction).

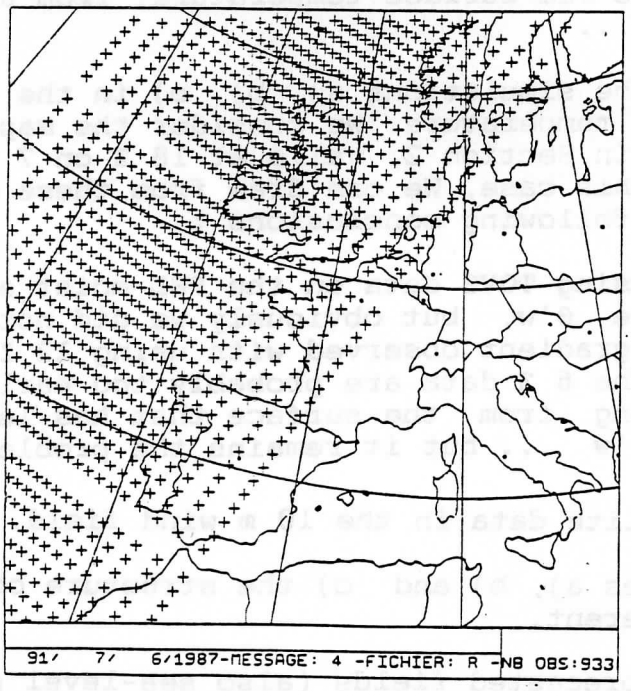

FIGURE 8 : Same as Figure 7 but for NOAA 10 (orbit 3735).

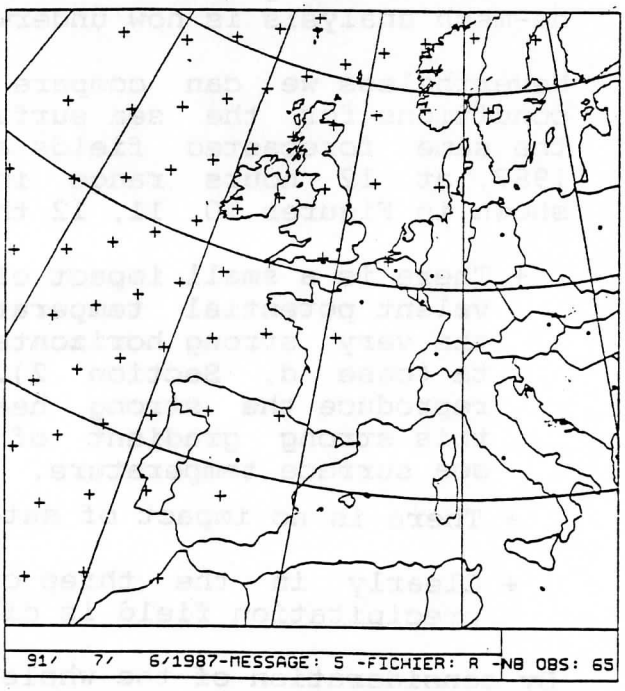

FIGURE 9 : Distribution of the MSU pixels received from NOAA 10 (orbit 3735) observed over the Péridot domain.

3. SIMULATIONS STARTING WITH 6 Z DATA

We've run the following Péridot simulations differing only by their initial states at 6 Z :

a) Péridot analysis with 6 hours Péridot forecast as guess field.
b) Same as a) but with including the TOVS data received from NOAA 9 (orbit 12791) and observed over the Péridot domain.
c) Same as a) but with including the TOVS data received from NOAA 10 (orbit 3735) and observed over the Péridot domain.

The Figures 7 and 8 show the location of the HIRS-2 pixels (sampling : every second element in each direction) used in the cases b) (922 radiances) and c) (933 radiances) and the Figure 9 show the location of the MSU pixels used in the case c) (65 radiances). These HIRS-2 data have been observed between 4.43 Z and 4.56 Z (case b) and between 8.58 Z and 9.11 Z (case c).

At first some remarks must be done on the Péridot analysis using 6 Z data. Since there is no conventional data to define the vertical structure of the atmosphere, the satellite data play an important role in this analysis, a situation rather different from the cases of using 0 Z or 12 Z data. Moreover in the case b) the radiances have been considered as on nighttime, but in the case c) they have been considered as on day-time, like in the cases c) and d) in Section 2.

By considering the process of selecting the data in the analysis we notice that there is a lot of rejection of the following HIRS-2 channels 6, 7, 11 (low-level) and 8, 10, 18 (window). After inspection, it appears that may be due to the misuse of sea surface temperature, which was chosen from a climatological data bank. A more complete test with using a more realistic sea surface temperature, from a fine-mesh analysis is now underway...

Nevertheless we can compare the simulations a), b), c) in the same conditions for the sea surface temperature. We consider the maps of the same forecasted fields as in Section 2, valid at 18 Z on 7 June 1987, at 12 hours range in this case. We can draw from these maps shown in Figures 10, 11, 12 the following conclusions :

+ There is a small impact of using TOVS data on the PBL moist equivalent potential temperature $\theta'w$, but obviously we did not get the very strong horizontal gradient observed with using 12 Z data (case d, Section 2). The 6 Z data are probably too early to reproduce the strong heating from the surface that has led to this strong gradient of $\theta'w$ ... but it remains the problem of sea surface temperature.

+ There is no impact of satellite data in the 10 m wind field.

+ Clearly in the three cases a), b) and c) the structure of the precipitation field is different.

By consideration of the whole forecasted fields (also sea-level pressure, temperature at 2 m...) the case b) when using NOAA 9 satellite data, observed before 6 Z and considered as on nighttime appear as the best, but far from the results obtained with 12 Z data (case d, Section 2).

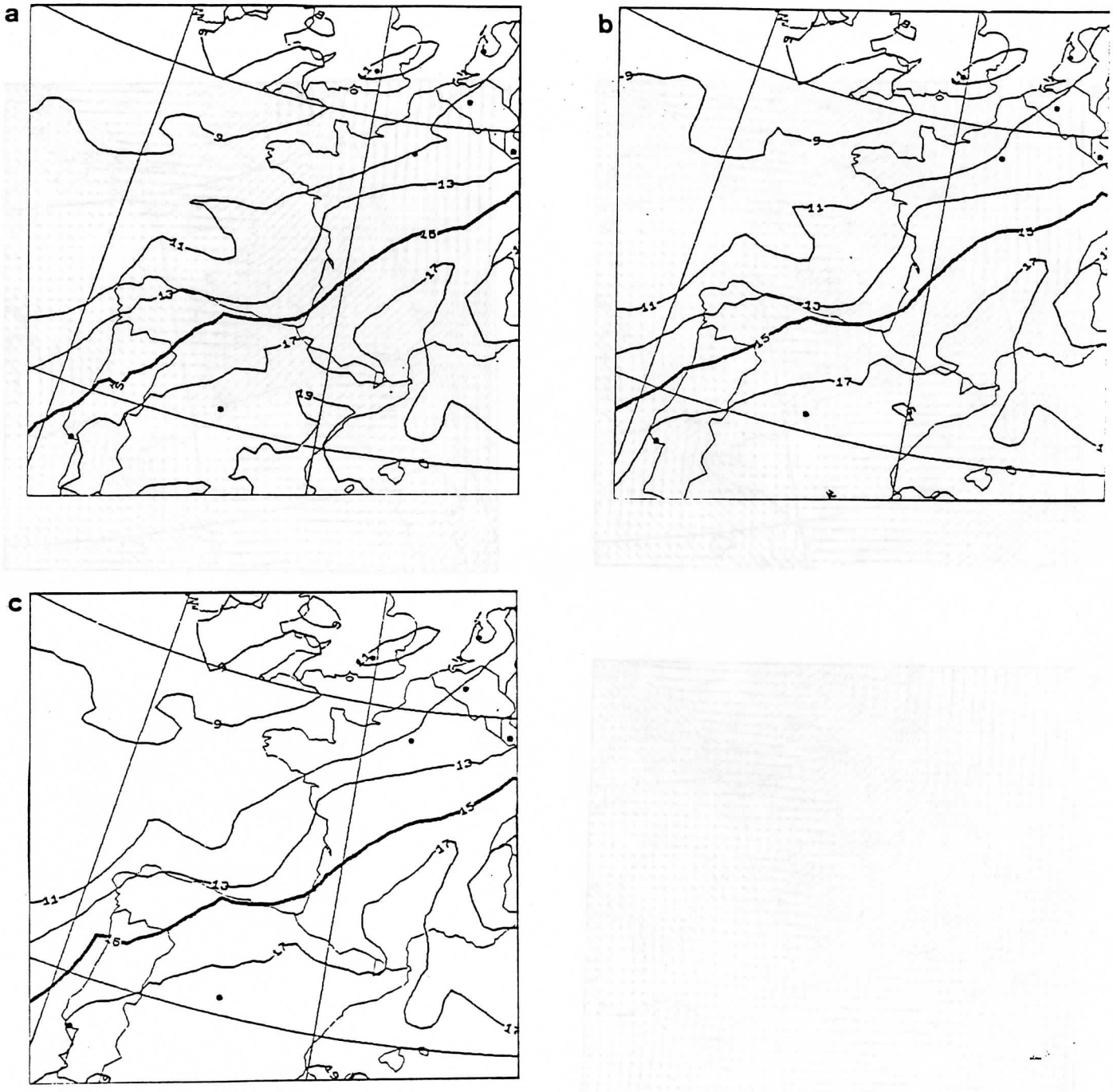

FIGURE 10 : Maps of 12 hours forecasts of PBL moist equivalent potential temperature verifying 7/6/1987 18 Z. The forecasts differ only by their initial states at 6 Z :

a) Péridot analysis with 6 hours Péridot forecast as guess field.
b) Same as a) but with including the TOVS data received from NOAA 9 (orbit 12791) and observed over the Péridot domain.
c) Same as a) but with including the TOVS data received from NOAA 10 (orbit 3735) and observed over the Péridot domain.

Contouring interval 2°C. Only part of the Péridot domain is shown here.

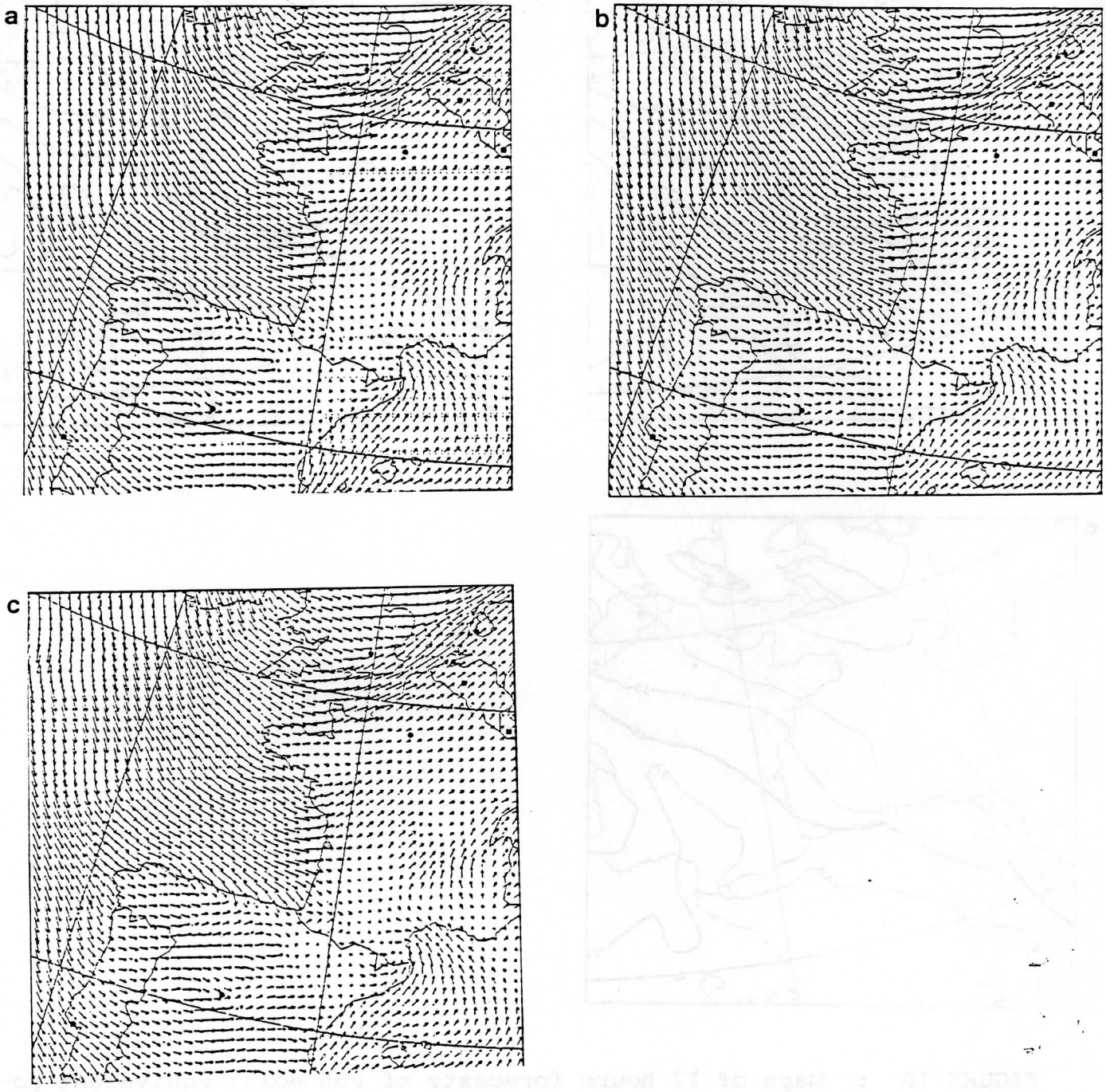

FIGURE 11 : As Figure 10 but for the 10 m wind field.

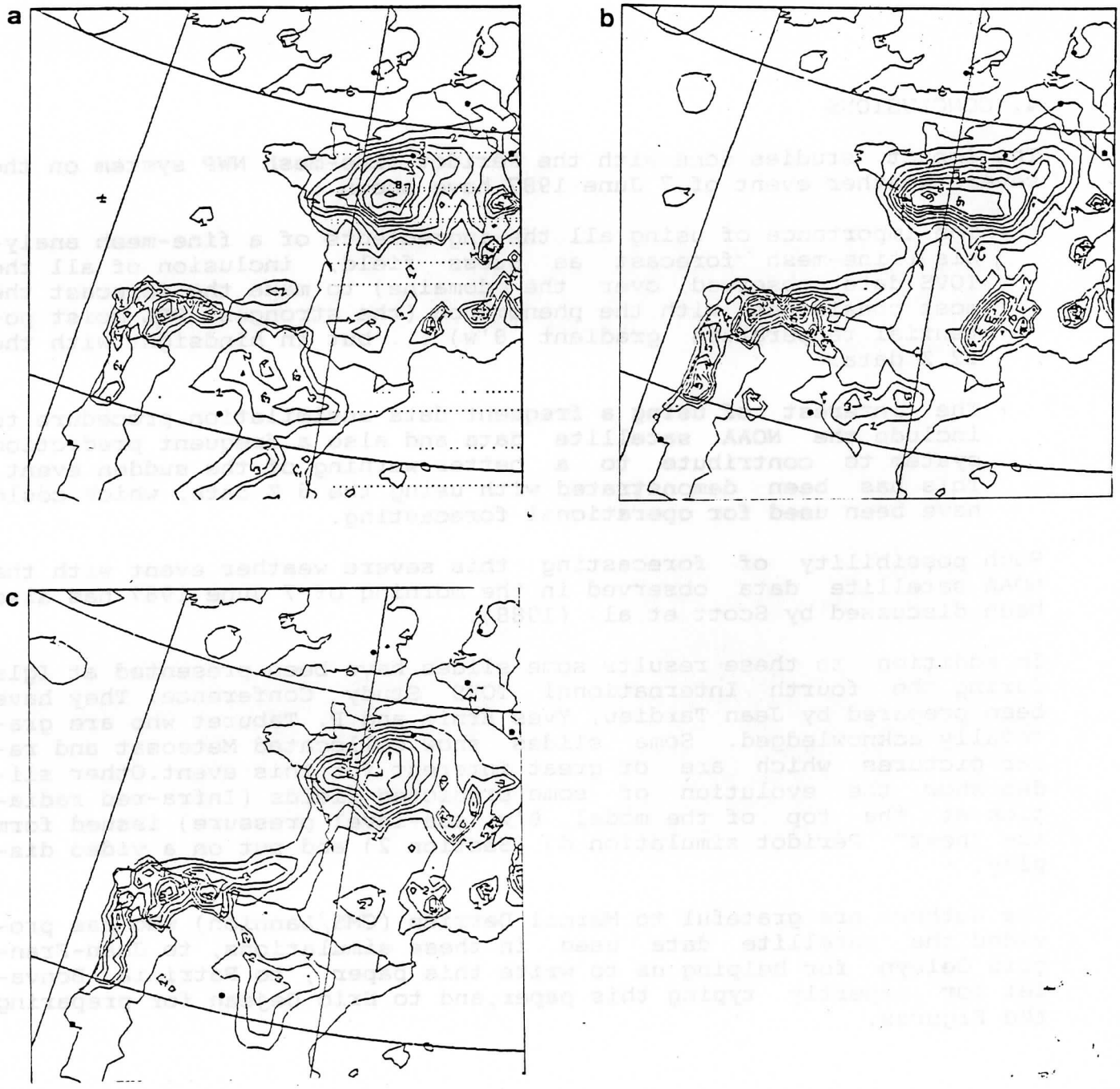

FIGURE 12 : As Figure 10 but for the 3 hours rain amount.

4. CONCLUSIONS

The impact studies done with the Péridot fine-mesh NWP system on the severe weather event of 7 June 1987 have shown :

+ The importance of using all the ingredients of a fine-mesh analysis (fine-mesh forecast as guess field, inclusion of all the TOVS data observed over the domaine) to make the forecast the most consistent with the phenomenon (the strongest PBL moist potential temperature gradient $\theta'w$) ... but in hindsight with the 12 Z data.

+ The interest of using a frequent data assimilation procedure to include the NOAA satellite data and also a frequent prediction system to contribute to a better warning of the sudden event. This has been demonstrated with using the 6 Z data, which could have been used for operational forecasting.

Such possibility of forecasting this severe weather event with the NOAA satellite data observed in the morning of 7 June 1987 has also been discussed by Scott et al. (1988).

In addition to these results some slides have been presented at Igls during the fourth International TOVS Study Conference. They have been prepared by Jean Tardieu, Yves Ernie and P. Taburet who are gratefully acknowledged. Some slides show collocated Meteosat and radar pictures which are of great interest for this event.Other slides show the evolution of some predicted fields (Infra-red radiation at the top of the model, $\theta'w$, sea-level pressure) issued form the "best" Péridot simulation d) (Section 2) and put on a video display.

The authors are grateful to Marcel Derrien (CMS/Lannion) who has provided the satellite data used in these simulations, to Jean-François Geleyn for helping us to write this paper , to Patricia Bonvalet for expertly typing this paper,and to Eric Dejean for preparing the Figures.

5. REFERENCES

Derrien M., T. Phulpin, 1987 : Fourniture de données satellitaires TOVS/AVHRR (canal 4) à l'analyse Péridot. Note de travail EERM N° 189.

Durand, Y., Juvanon du Vachat, R., 1983 : Mesoscale analysis using satellite information. Proc. of the First Int. TOVS Study Conf., Igls, September 1983, 80-93.

Durand, Y., Juvanon du Vachat, R., 1985 : Developments of a mesoscale analysis using raw satellite data. Proc. of the Second Int. TOVS Study Conf., Igls, February 1985, 39-57.

Durand, Y., 1985 : The use of satellite data in the French high resolution analysis. Proc. of ECMWF Workshop on High Resolution Analysis, 89-128.

Durand, Y., Juvanon du Vachat, R., 1986 : New developments in the French mesoscale analysis in the use of raw satellite data. Proc. of the Third Int. TOVS Study Conf., Wisconsin, August 13-19, 1986, 45-59.

Durand Y., Bougeault Ph., 1987 : L'analyse objective Péridot. Note de travail EERM N° 193.

Geleyn, JF., and Jarraud, M., 1988 : Recent changes in the French NWP operational systems Emeraude and Peridot. Proc. of the Eighth AMS Conf. on Numerical Weather Prediction, Baltimore, Maryland, 22-26 February 1988, 314-317.

Imbard, M., Juvanon du Vachat, R., Joly, A., Durand Y., Craplet A., Geleyn, JF., Audoin, JM., Marie N., Pairin, JM., 1987 : The Peridot fine-mesh numerical weather prediction system. Description, evaluation and experiments. Journal of the Meteorological Society of Japan. Special Issue. 1987. 455-465.

Imbard M., A. Craplet, Ph. Degardin, Y. Durand, A. Joly, N. Marie and JF. Geleyn, 1988 : Fine-mesh limited area forecasting with the French operational "Péridot" system. Proc. of ECMWF Workshop on the nature and prediction of extratropical weather systems, 7-11 Sept. 1987.

Scott, N.A., A. Chedin, F.M. Bréon, C. Claud, JF. Flobert, N. Husson, C. Levy, Y. Tahani, G.J. Prangsma, G. Rochard, 1988 : Recent advances in the retrieval of Meteorological parameters through the "3I" System. This volume.

RADIANCE TUNING

G.A. Kelly and J-F. Flobert
ECMWF, Shinfield Park, Reading

At ECMWF various satellite retrieval methods are being tested in order to determine their impact on global ten day forecasts. It is important that care is taken to reduce any biases in the temperature retrievals with respect to the local radiosonde data otherwise the analysis will be degraded. Radiance tuning has been discussed by other workers (Susskind et al. (1983, 1986)) (Steenbergen et al. (1986)), (Chedin et al. (1986)), (Uddstron, (1986) and (Eyre et al. (1986)). It appears that the radiance biases are air mass dependent and the purpose of this study is to show the geographical extent of these variations. A daily global time series of the observed minus calculated radiances showed little variation during a period of one month. It is now generally considered (McMillin (1988)) that much of the problems are due to radiosonde radiation effects but there are other sources of error.

1. INTRODUCTION

Almost all temperature and humidity physical retrieval methods require a priori knowledge of the atmospheric transmittance. The exceptions are direct regression techniques, however, these methods cannot take advantage of use of the physical processes associated with radiative transfer. Errors arise in several areas in physical temperature retrievals. The first is with atmospheric transmittance which only known to about five to ten percent (Flemming et al. (1986). In order to correct these errors the usual practice is to collect radiosonde data within a small distance in both space and time from the satellite measurement and from a match set. Unfortunately, radiosondes are another source of error particularly at high levels. These errors are discussed by (McMillin (1988)) and are large in the stratosphere and a function of air mass, day-night and cloud cover. A third error source is due to the match space/time separation. In general these errors are not systematic and can be reduced with large statistical samples.

2. DATA

In order to study the problem two match data sets were obtained from NESDIS for NOAA9 and NOAA10 for JAN/FEB 87.

The radiosondes were pre-processed by NMC Washington and a day-night corrections applied. The clear radiances were obtained from the TOVS operational processing (McMillin et al. (1982)) and the collocations are restricted to time differences of six hours or less and space difference that is less than a maximum value which varies with location according to the density of radiosondes and is less than 300 km. Figs. 1(a) and (b) show the global distribution of the radiosonde/radiance pairs for both NOAA9 and NOAA10. In general there is good coverage with the exception of the Antarctic continent and the tropics.

3. TRANSMITTANCE MODELS

At ECMWF two fast transmittance models are used in satellite inversion methods. The first is the model (ITPP) contained in the ITPP package (Smith et al. (1985)) and based on work of (Weinneb et al. (1981)). The other is the 3R model and described in papers by (Flobert et al. (1986)) and (Chedin et al. (1986)). Both models are approximations to more accurate line by line calculations and require empirical adjustments for particular satellite instruments. Initially the two models were tuned on different match data sets. In all the following calculations all free model parameters (gammas and deltas) were kept fixed and the aim of the study is to adjust these free parameters for both models.

All radiosonde data are required to be extrapolated to 0.1 mb and to reduce the effect of this extrapolation only sondes reaching 20 mb and above were used. Another test was made on the lowest reported level of the sonde, it was required to be within 5°C of the HIRS channel 8 after a water vapour correction was applied. If this was not done the noise increased in many of the channels with weighting functions in the lower troposphere.

4. RESULTS

Figs. 2(a), (b) and (c) show scatter plots of the brightness temperature differences, as a function of latitude for the ITPP model. In order to compare the spatial variation a least square cubic spline was fitted. This curve shows a marked variation with latitude with a decrease in the noise at the equator and a larger noise value in the northern hemisphere. The channels HIRS 3, 15 and MSU 4 show the largest noise level, in particular, in

the northern latitudes whereas the lower tropospheric channels HIRS have generally less scatter. The water channel HIRS 12 shows larger errors with a strong latitude dependence.

Similar plots Fig. 3(a), (b) are shown for 3R calculations and same spatial variations are observed. There are some bias differences between ITPP and 3I model, however, the general pattern is similar.

In order to study the effect of longitude on transmittance calculations the data was grouped in the latitude band 50°N to 90°N and scattered as a function of longitude. At these longitudes there was a large air mass variation, particularly in the stratosphere during this period. A large cold stratospheric vortex was centred over Europe and a warm vortex located above Siberia. (Flobert (1988)). Fig. 4(a) and (b) show marked longitude variations and changes in the pattern between channels, HIRS 4 and MSU 3. The variation in MSU 3 is almost linear with longitude whereas MSU 2 and 4 show a sine pattern. Similar results were found using 3R model (Figs. 5a, b).

Finally, in an attempt to reduce the noise in the calculations an area was chosen over North America. Figs. 6(a) and (b) show a much reduced scatter of the forward calculations. In this region there is only one radiosonde type, however, there is still a marked variation from pole to equator in all channels.

5. DISCRIMINATE ANALYSIS OF BIAS

The concept of air mass classification is a practical way of reducing the bias of the forward radiance calculation. Three stratospheric channels, HIRS 3 and MSU 3 and 4, were chosen to produce an air mass classification using an iterative discriminate analysis (Kelly et al. (1976)). The classification has been applied to an ECMWF analysis of 12Z 1/2/87, Fig. 7. The overall effect is the reduced bias and standard error of the radiance calculations in most channels. Work is still proceeding in this area.

6. CONCLUSION

This study is only the start at ECMWF in a program to monitor the bias in forward radiance calculations. It is still unclear the nature of the errors, radiosondes, transmittance models or satellite instruments, however, a corrective procedure is important for physical retrieval methods.

It is strongly recommended that all groups involved in the operational use of TOVS data set up their own radiance tuning procedures, otherwise the packages like ITPP or 3I will not produce reliable retrievals.

This was clear there is good general agreement between the ITPP and 3R forward models.

7. REFERENCES

Chedin, A. and N.A. Scott, 1983: Improved initialization inversion procedure ("3I"). In Technical proceedings of the first international TOVS Study Conference. 14-79, 29 August-2 September, Igls, Austria, Pub. CIMSS, University of Wisconsin.

Chedin, A., N.A. Scott, C. Claud, J-F. Flobert, N. Hussen, C. Long, P. Moine, G. Rochard, J. Quere and T. Phulpin, 1986: Present progress in the determination of meteorological parameters from the satellites of the TIROS-N Series. Technical proceedings third international TOVS Study Conference 13-19 August 1986; Madison, Wisconsin.

Eyre, J.R., R.W. Pescod, P.D. Watts, P.E. Lloyd, W. Adams, and R.J. Allan, 1986: TOVS retrievals in the UK: Progress and plans technical proceedings third international TOVS Study Conference. 1 13-19 August 1986; Madison, Wisconsin.

Fleming, H.E., D.S. Crosby and A.C. Neuendorffer, 1986: Correction of satellite temperature retrieval errors due to errors in atmospheric transmittances. J. Climate Appl. Meteor. 25, 869-882.

Flobert, J-F., N.A. Scott and A. Chedin, 1986: A fast model for TOVS radiances computation. Proceedings of the 6th Conference on Atmospheric Radiation. Williamsburg, USA, p. 186-189.

Flobert, J-F., 1988: Global use of TOVS retrievals in NWP at ECMWF. Technical proceedings 4th international TOVS Study Conference. March 1988; Igls, Austria.

Kelly, G.A., P.E. Powers, and F.J. Gauntlett, 1976: Temperature and water vapour retrievals from the NOAA-4 satellite in the southern hemisphere. Proceedings of the symposium on meteorological observations from space: Their contribution to the first GARP Global Experiment, June 8-10, 1976, Philadelphia, Penna., USA, COSPAR, 77-84.

McMillin, L.M. and C. Dean, 1982: Evaluation of a new operational technique for producing clear radiances. J.Appl.Meteor., 21, 1005-1014.

McMillin, L.M., 1988: A method of use satellite retrievals as a transfer standard to determine systematic radiosonde errors. Mon.Wea.Rev., 116, 1091-1102.

Smith, W.L., H.M. Woolf, C.M. Hayden and A.J. Schreiner, 1985: The simultaneous retrieval export package. In technical proceedings of the second international TOVS Study Conference. 224-253, February 18-22, Igls, Austria, Pub CIMSS, University of Wisconsin.

Steenbergen, J.D., B.T. Greaves and Yip Tsoi-Ching, 1986: Simultaneous retrieval of temperature and relative humidity using empirical orthogonal functions. Technical proceedings third international TOVS Study Conference, 13-19 August, 1986; Madison, Wisconsin.

Susskind, J., J. Rosenfeld, D. Reuter, and M.T. Chahine, 1984: Remote sensing of weather and climate parameters from HIRS/MSU on TIROS-N. J.Geophys.Res., 89, 4677-4697.

Susskind, J., J. Rosenfield and D. Reuter, 1983: An accurate radiative transfer model for use in the direct physical inversion of HIRS-2 and MSU temperature sounding data. J. of Geophys. Res., Vol. 88, 8550-8568.

Uddstrom, M.J., 1986: Synthetic and real data applications of the typical shape function simultaneous physical retrieval algorithm, 1986: Technical proceedings third international TOVS Study Conference, 13-19 August 1986; Madison, Wisconsin.

Weinreb, M.P., H.E. Fleming, L.M. McMillin and A.C. Neuendorffer, 1981: Transmittances for the TIROS operational vertical sounder. NOAA Tech. Rep. NESS 85, 60 pp.

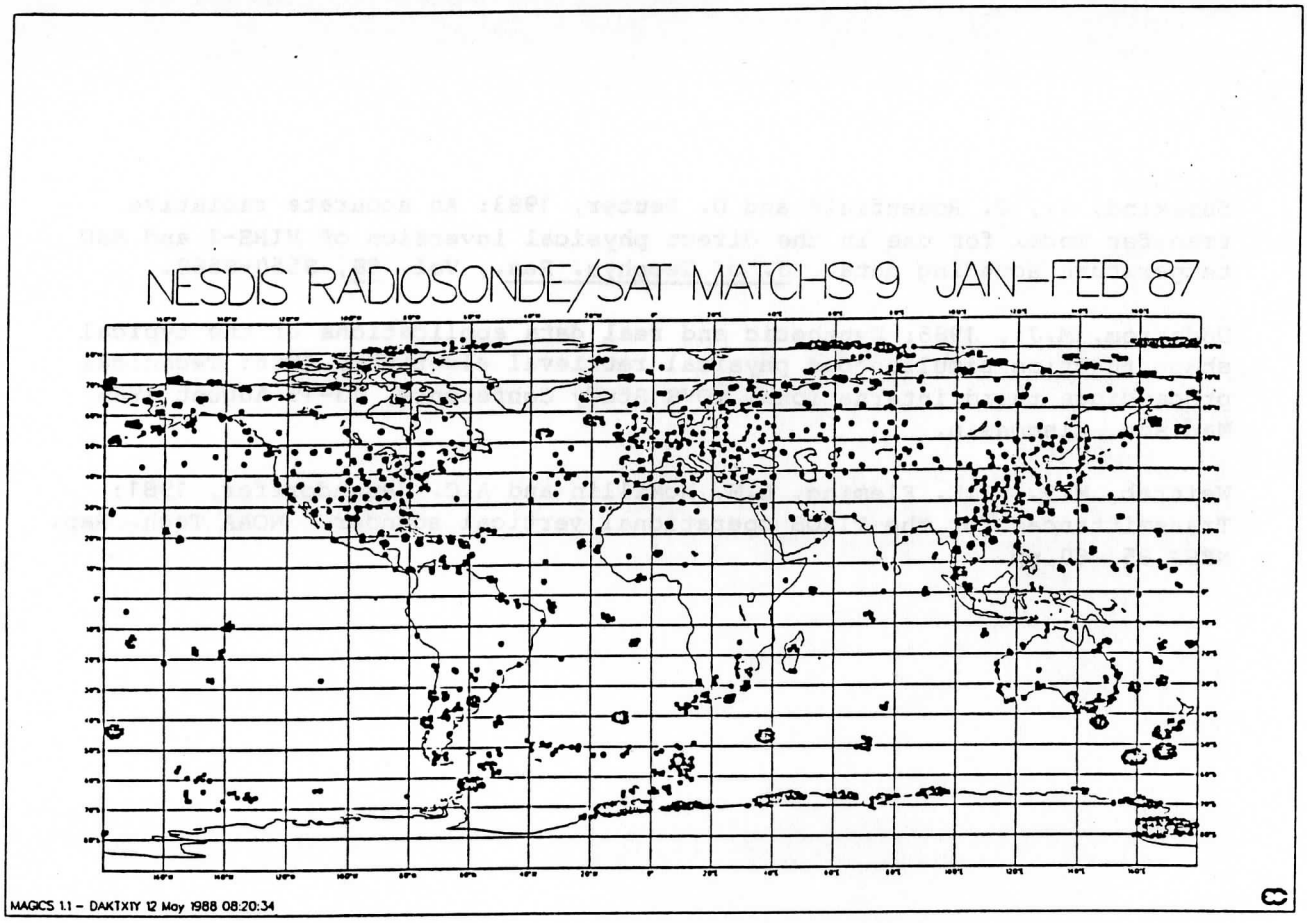

Fig. 1(a) Plot of NOAA-9 matched radiosonde/clear radiances for the January Febraury period.

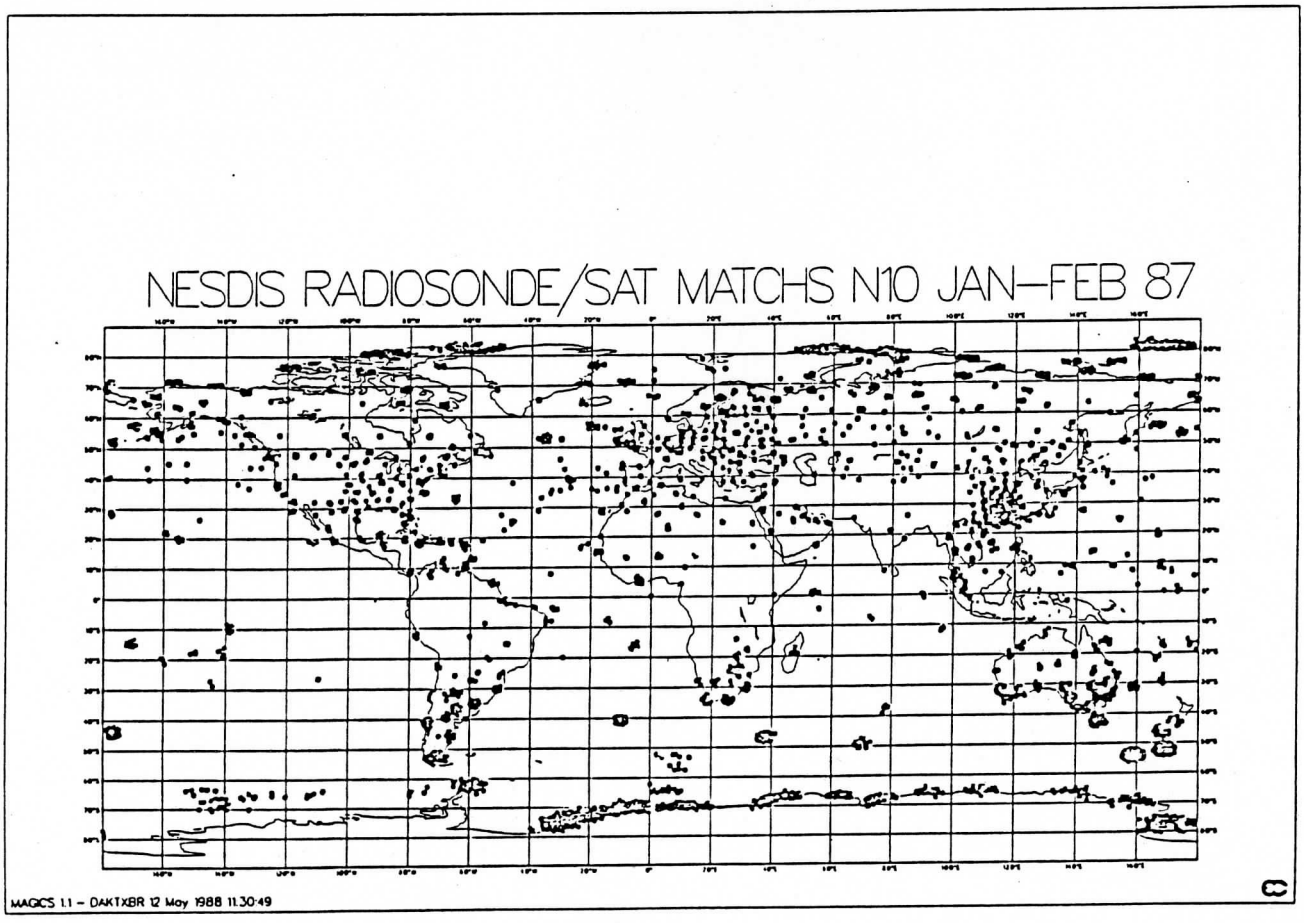

Fig. 1(b) Same as Fig. 1(a) for NOAA-10.

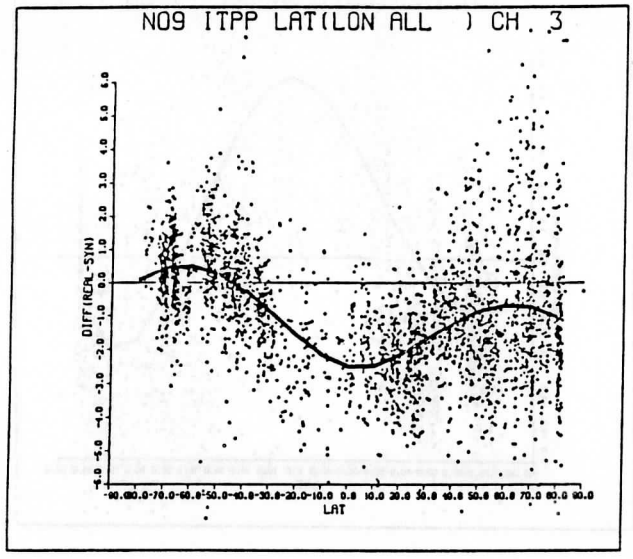

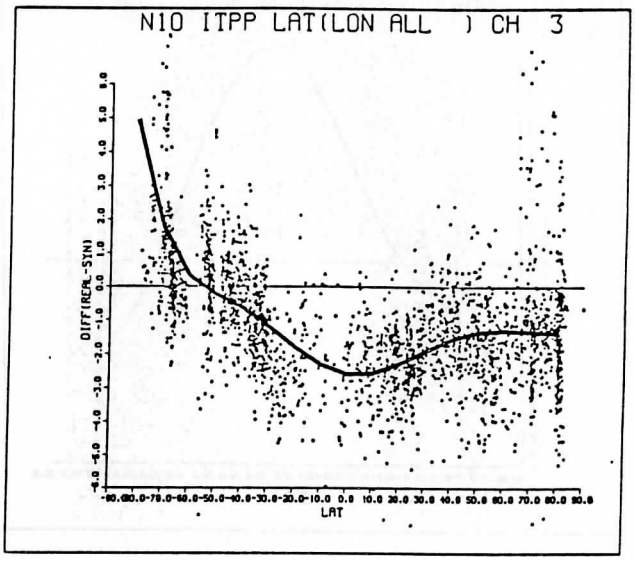

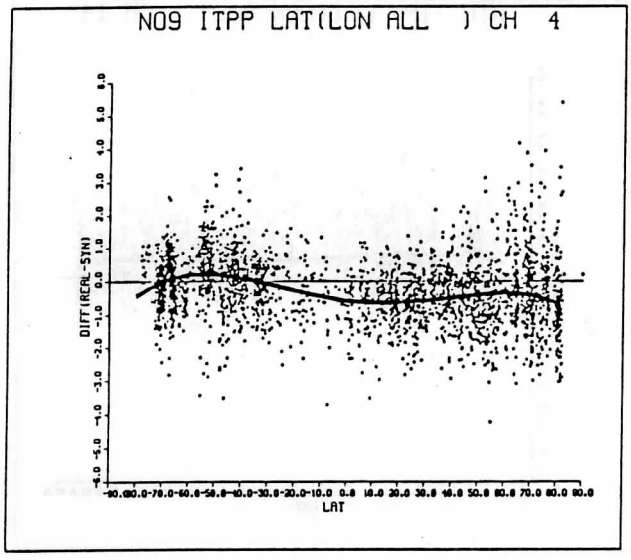

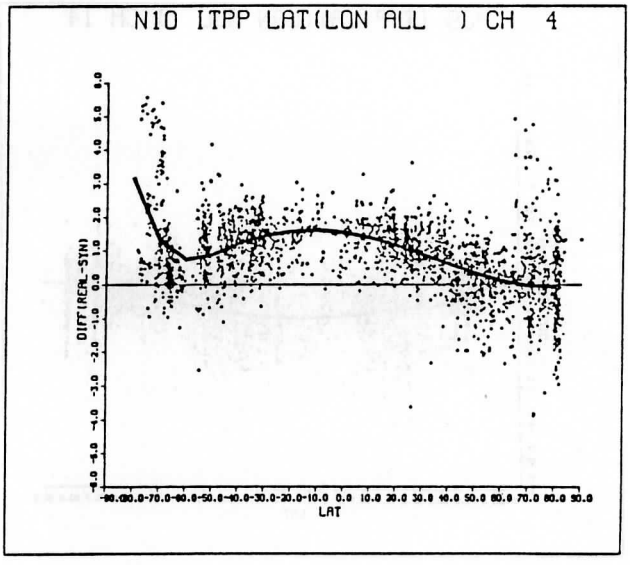

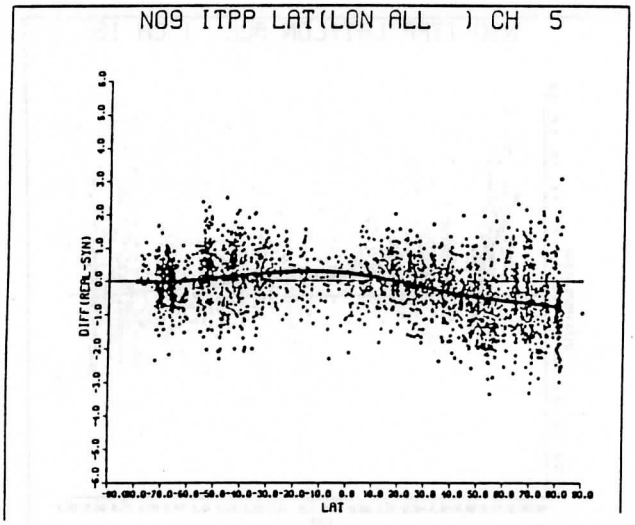

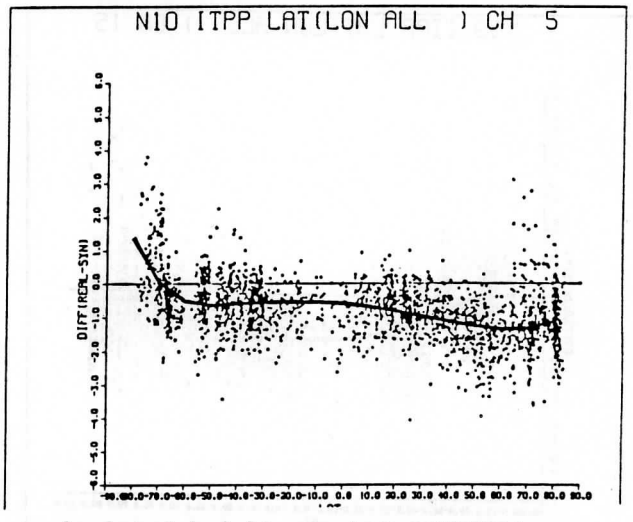

Fig. 2(a) Scatter plots of observed minus calculated brightness temperatures (ITPP model) as a function of latitude. The solid curve is a least square piecewise cubic spline to the data points. Results shown for HIRS channels 3, 4 and 5 for NOAA-9 and NOAA-10.

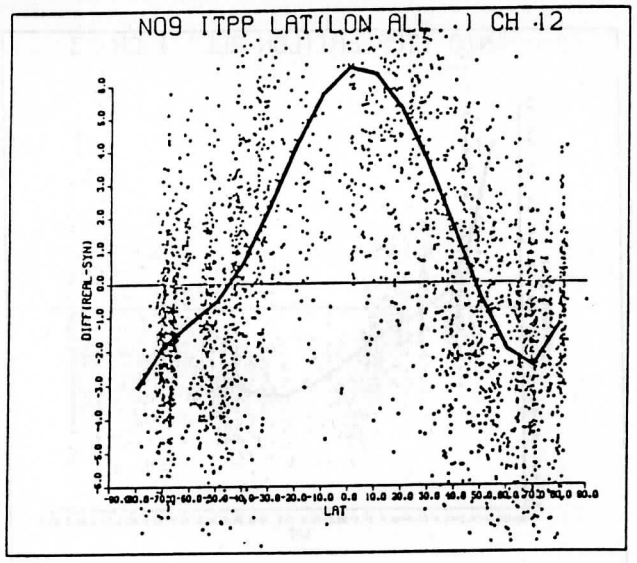

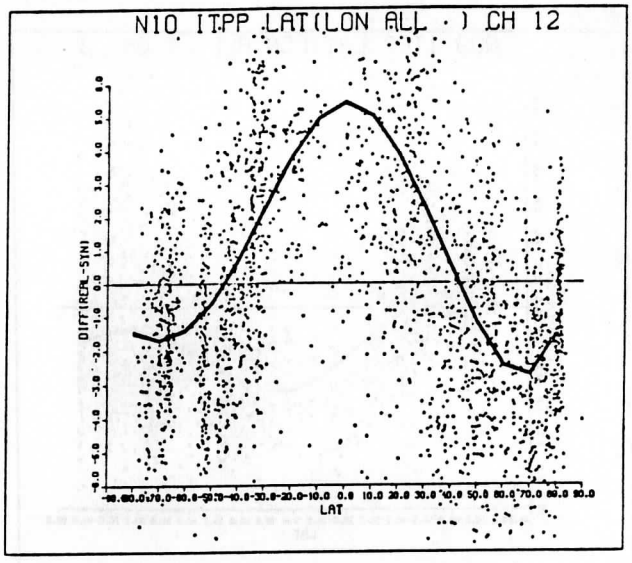

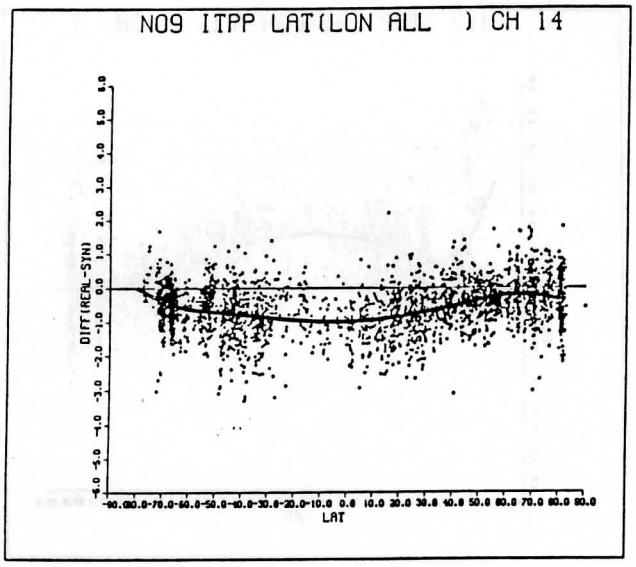

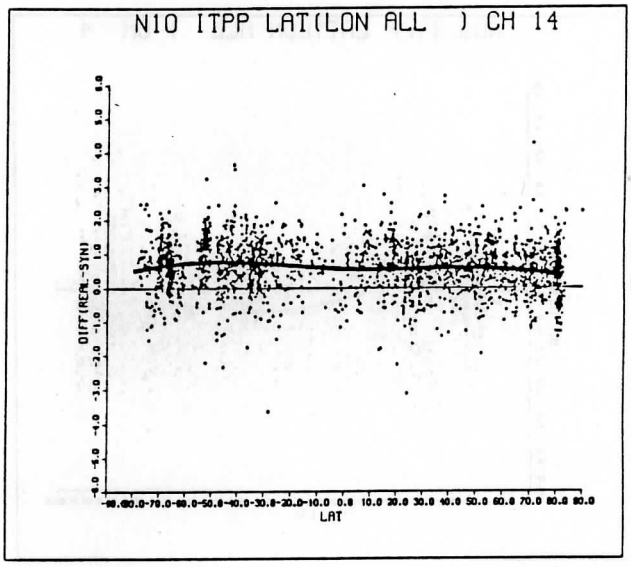

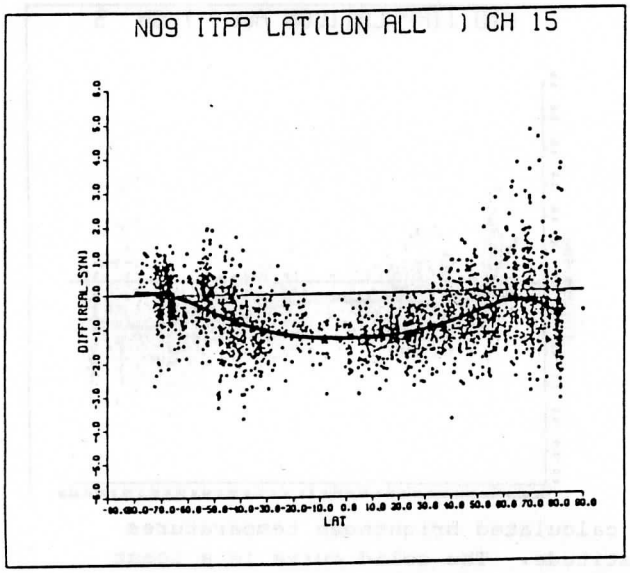

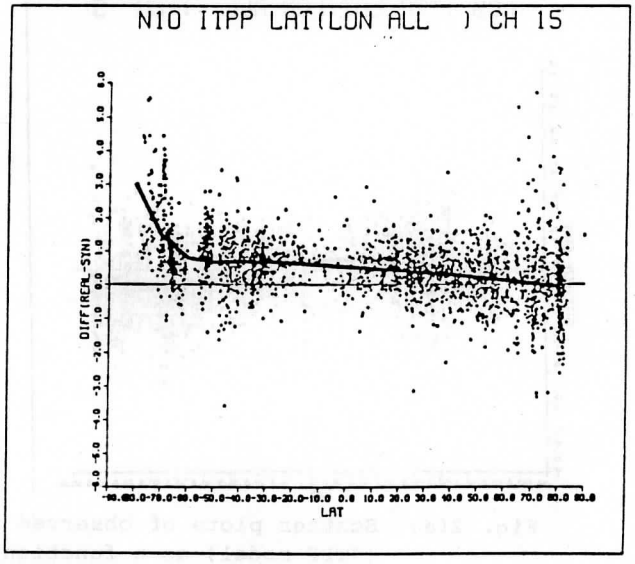

Fig. 2(b) Same as Fig. 2(a) for HIRS channels 12, 14 and 15.

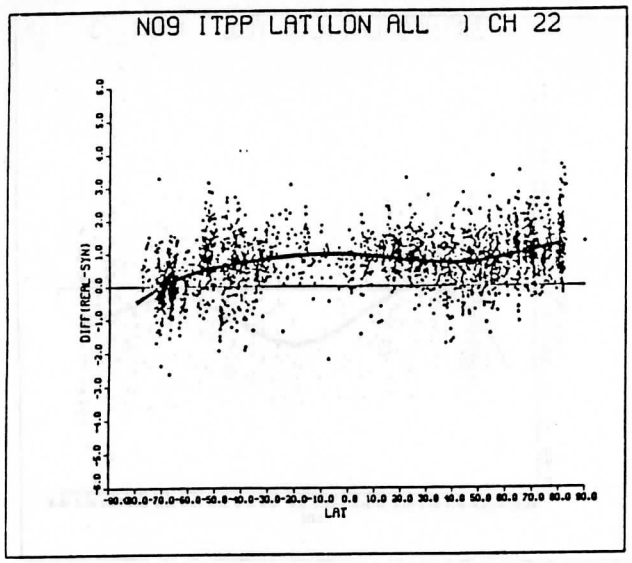

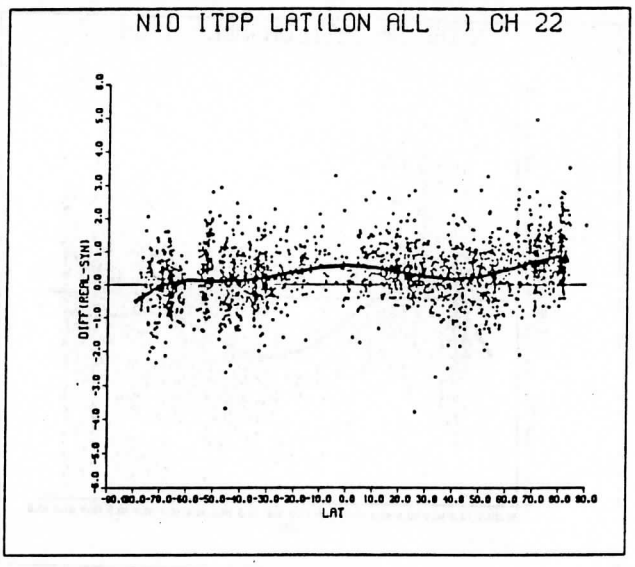

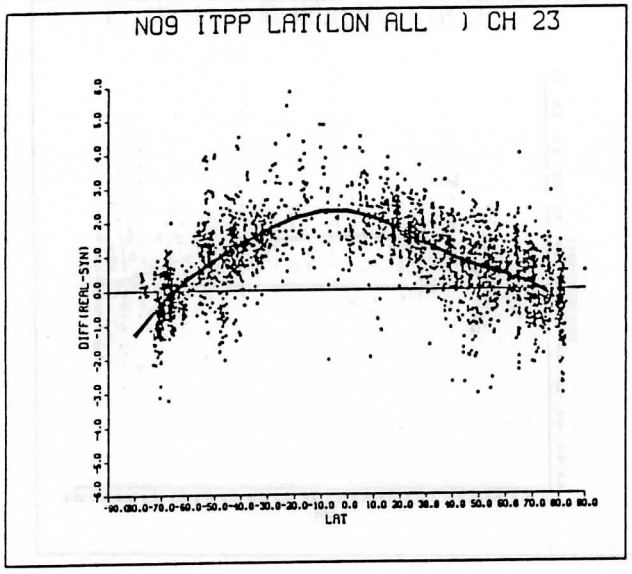

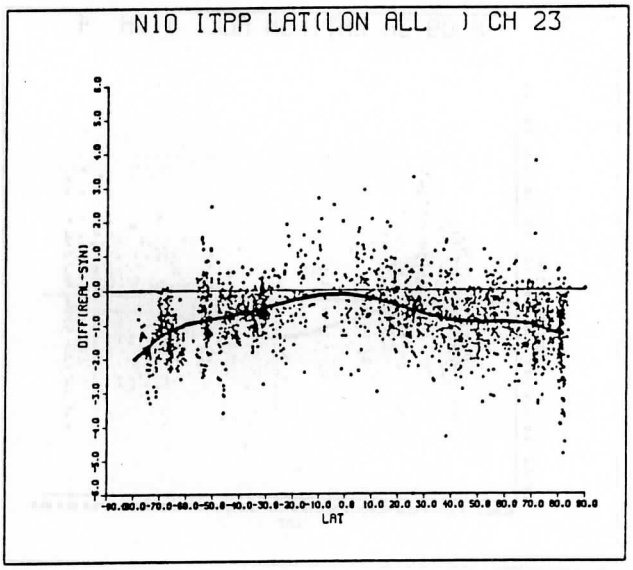

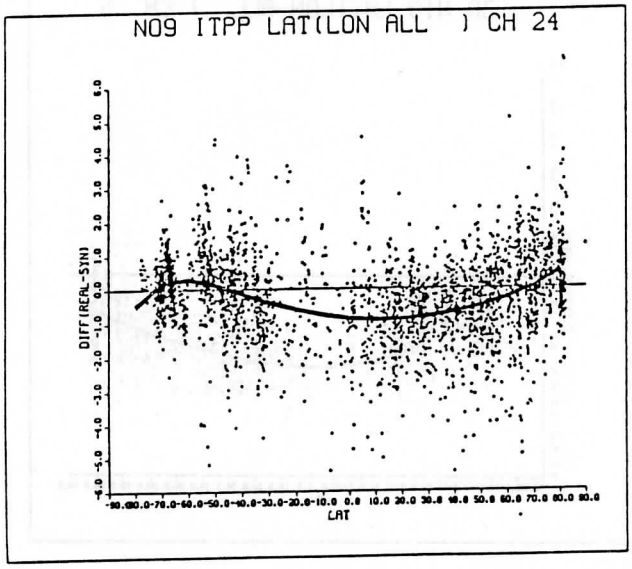

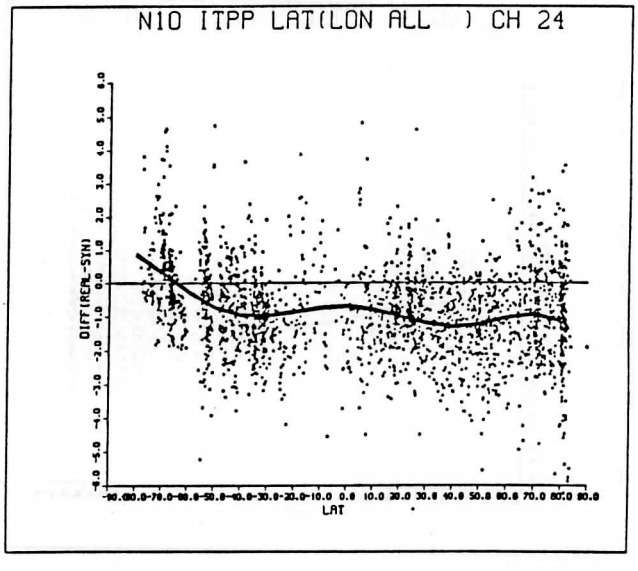

Fig. 2(c) Same as Fig. 2(a) for MSU channels 2, 3 and 4 (labelled 22, 23 and 24).

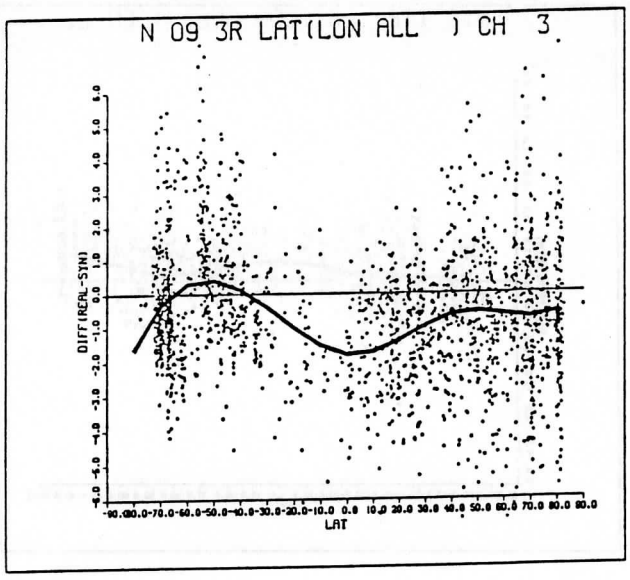

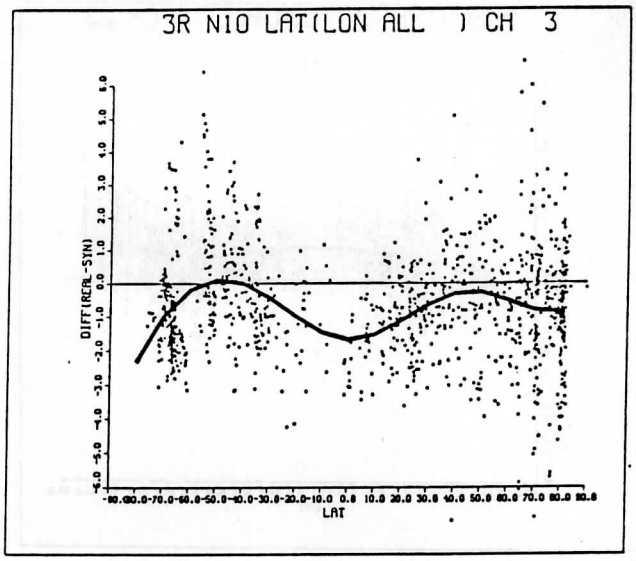

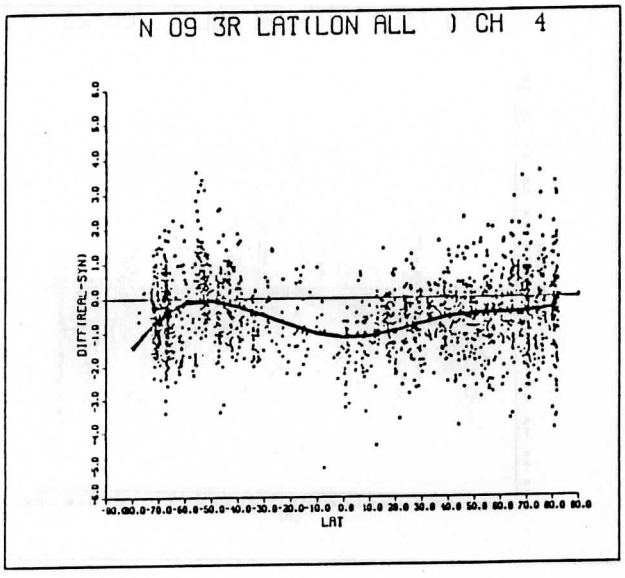

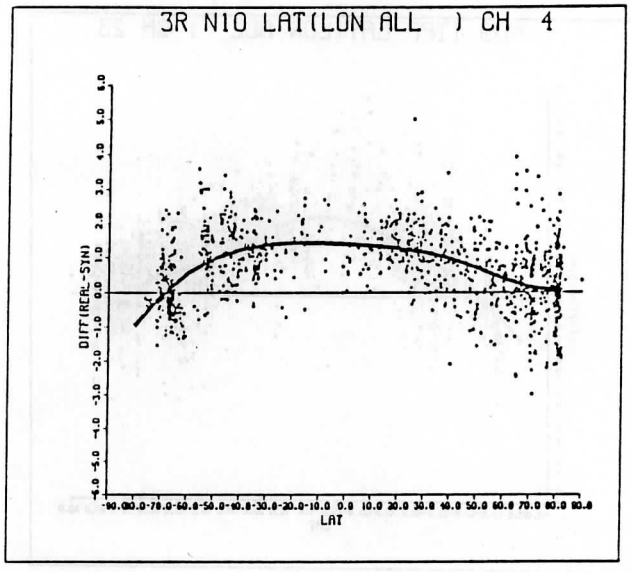

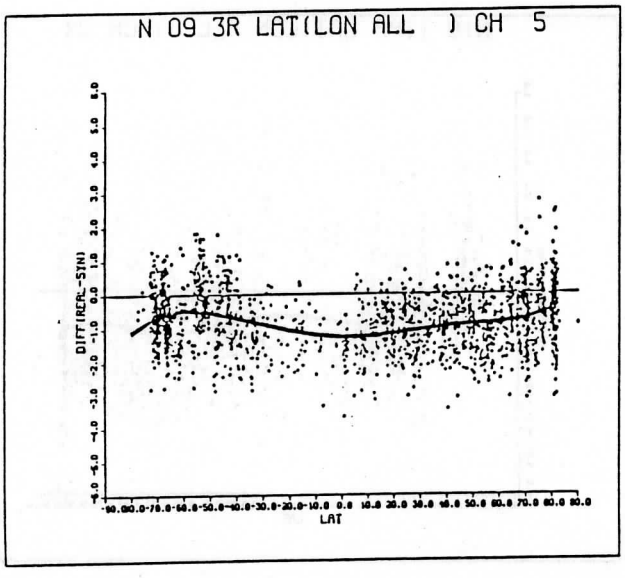

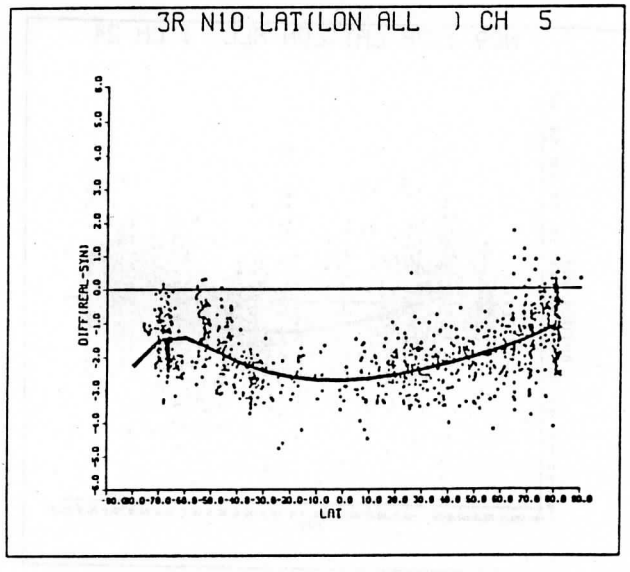

Fig. 3(a) Same as Fig. 2(a) using 3I model.

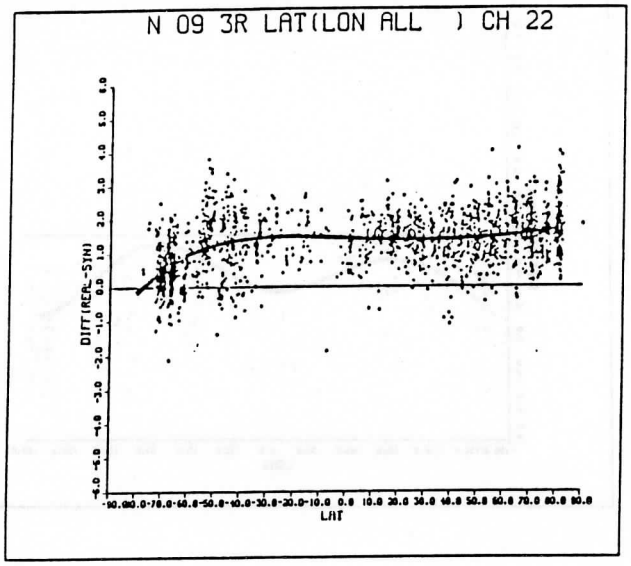

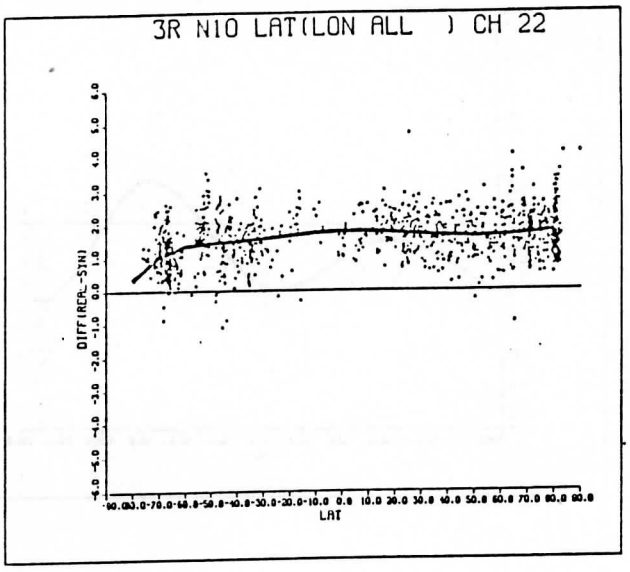

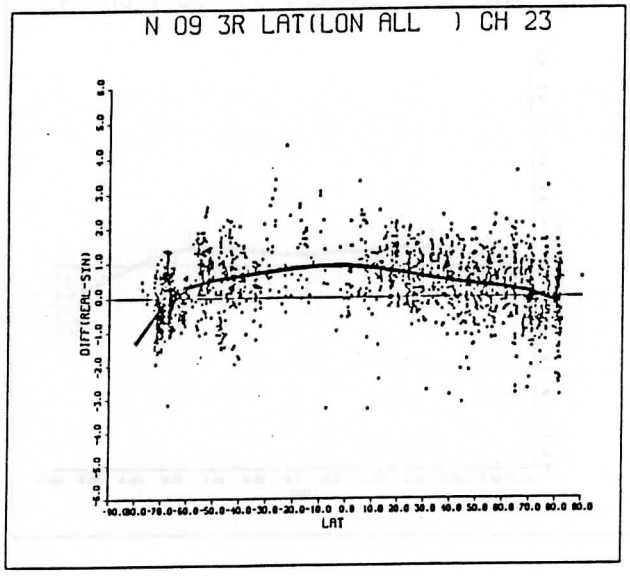

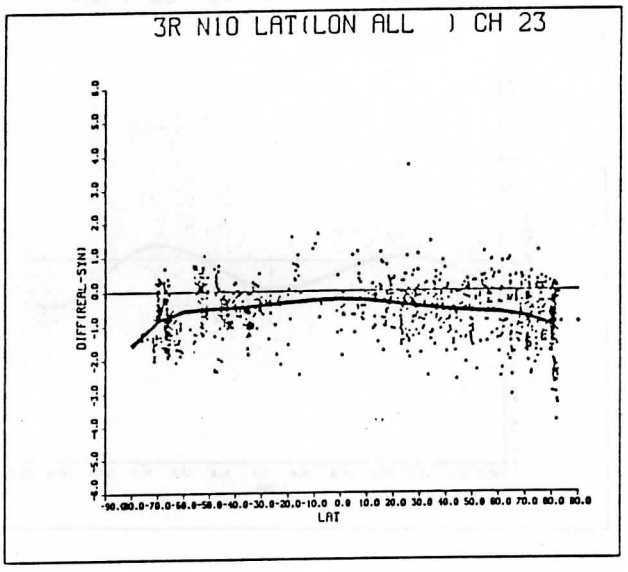

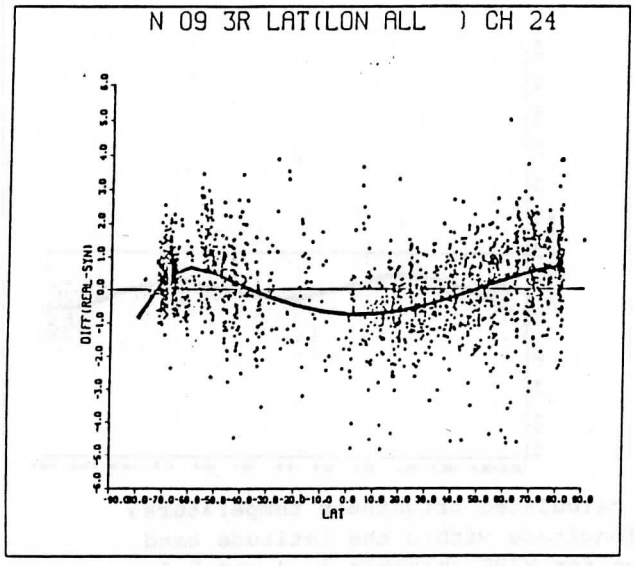

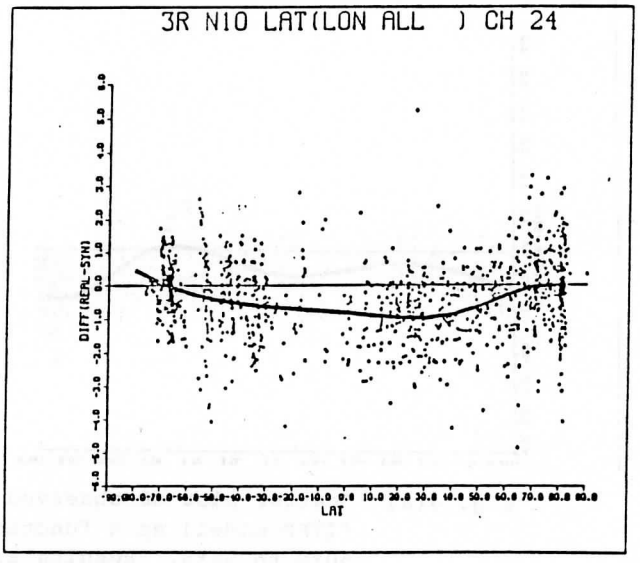

Fig. 3(b) Same as Fig. 3(a) for MSU channels 2, 3 and 4.

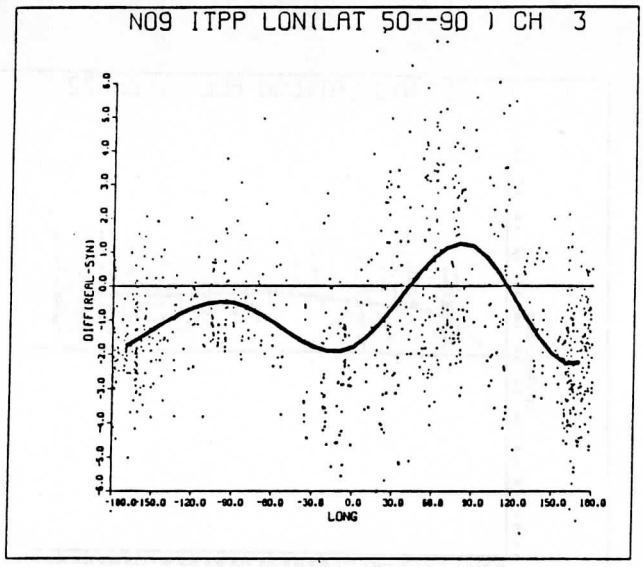

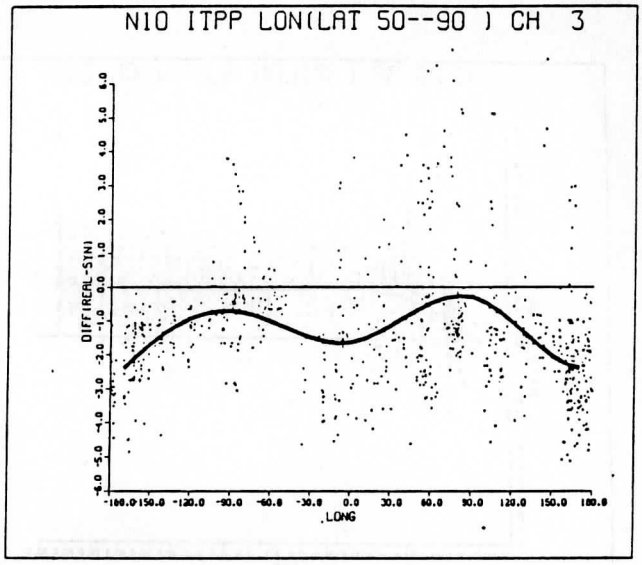

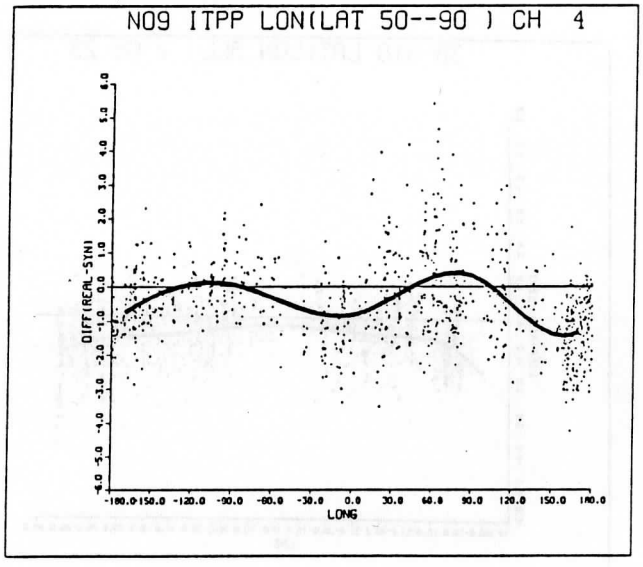

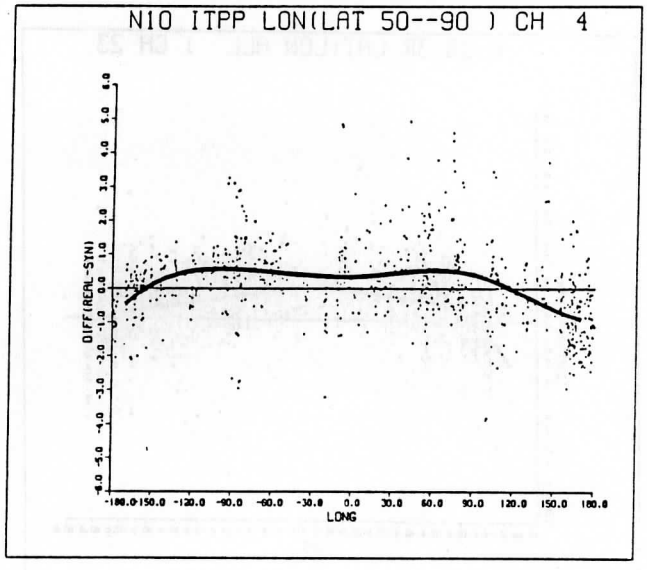

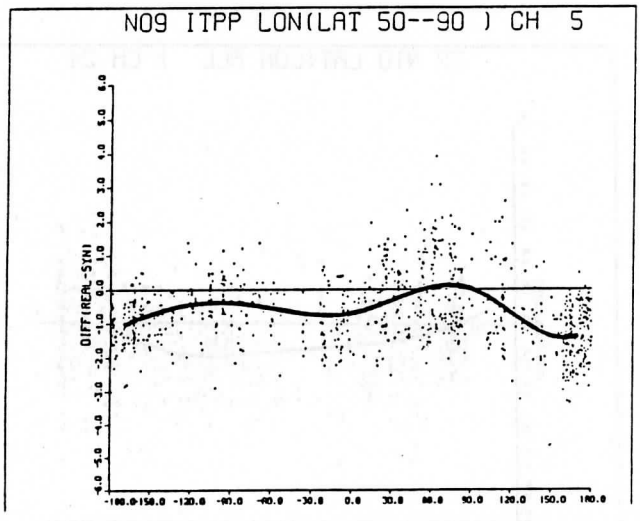

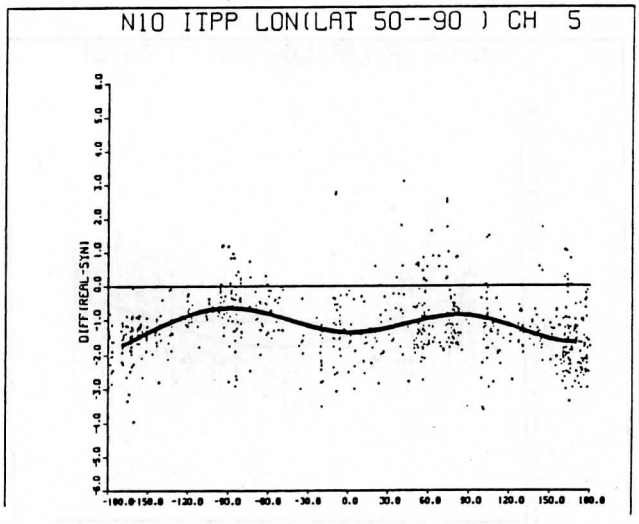

Fig. 4(a) Scatter plot of observed minus calculated brightness temperatures (ITPP model) as a function of longitude within the latitude band 50°N to 90°N. Results are shown for HIRS channels 3, 4 and 5 for NOAA-9 and NOAA-10.

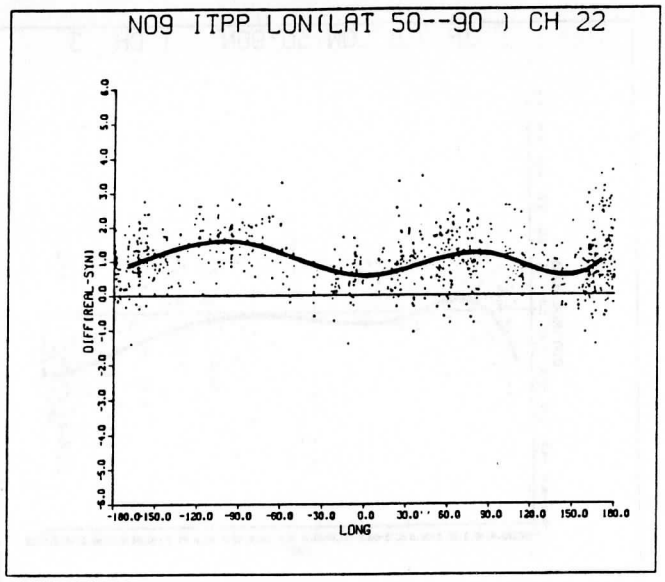

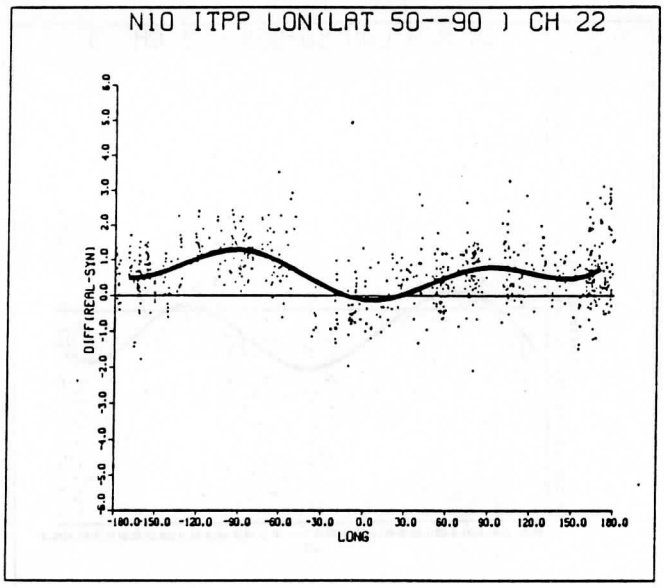

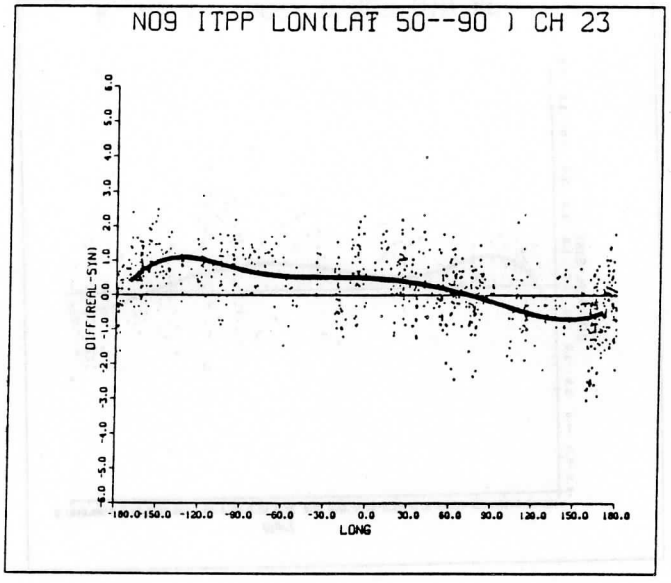

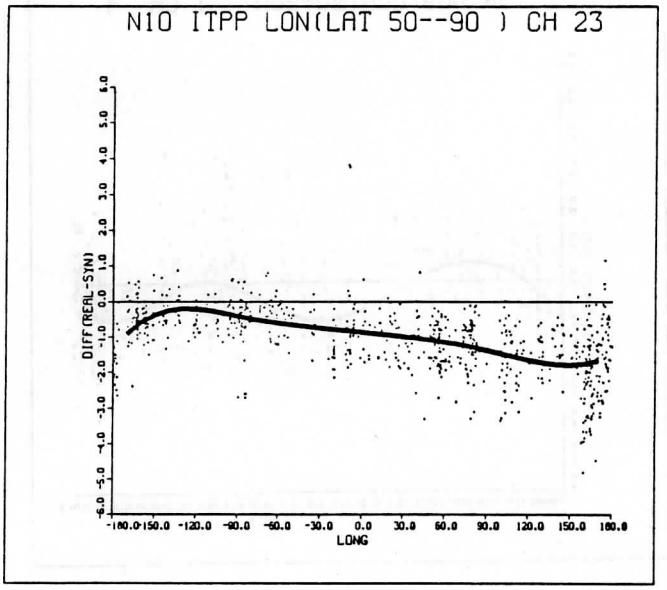

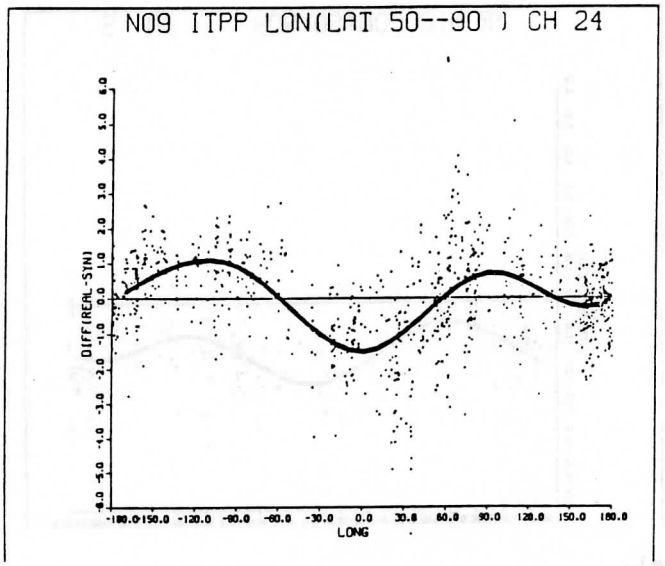

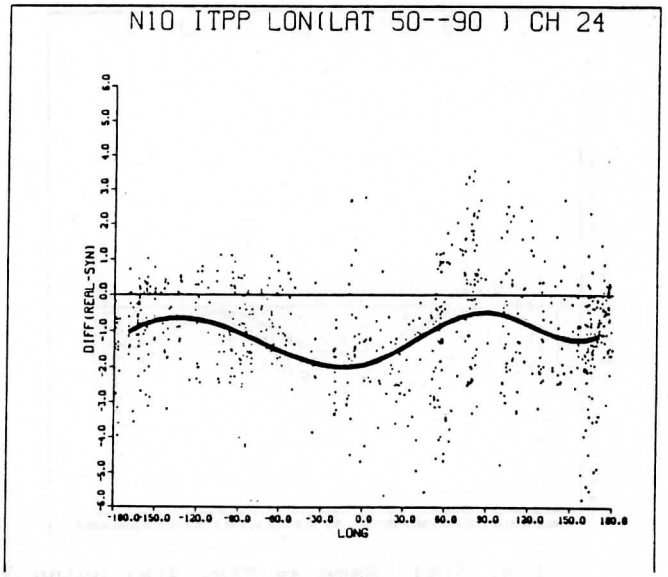

Fig. 4(b) Same as Fig. 4(a) for MSU channels 2, 3 and 4 (labelled 22, 23 and 24).

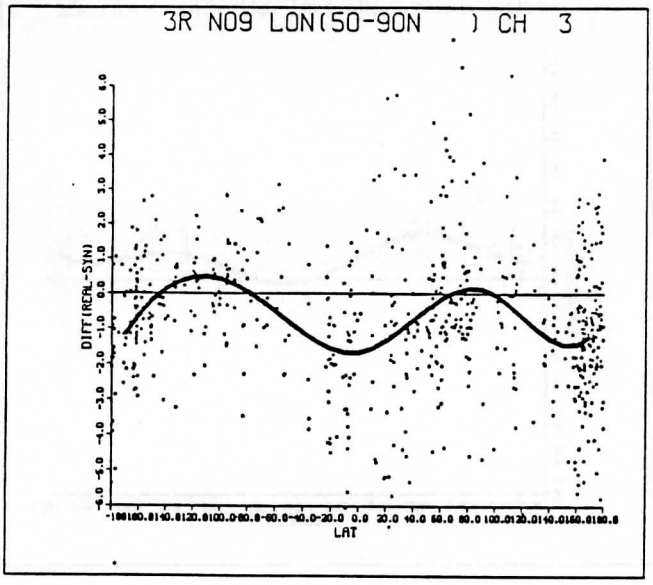

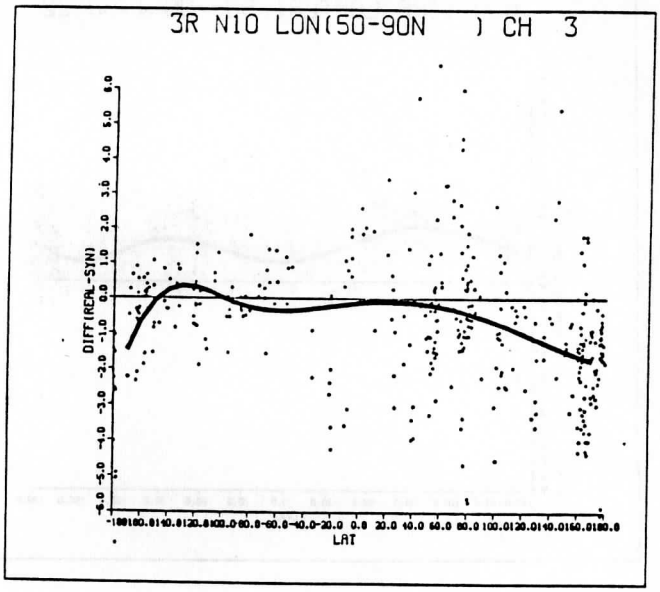

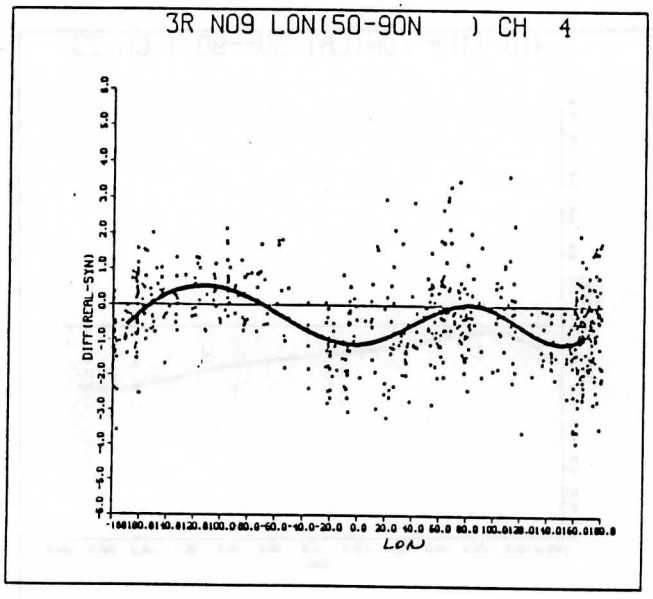

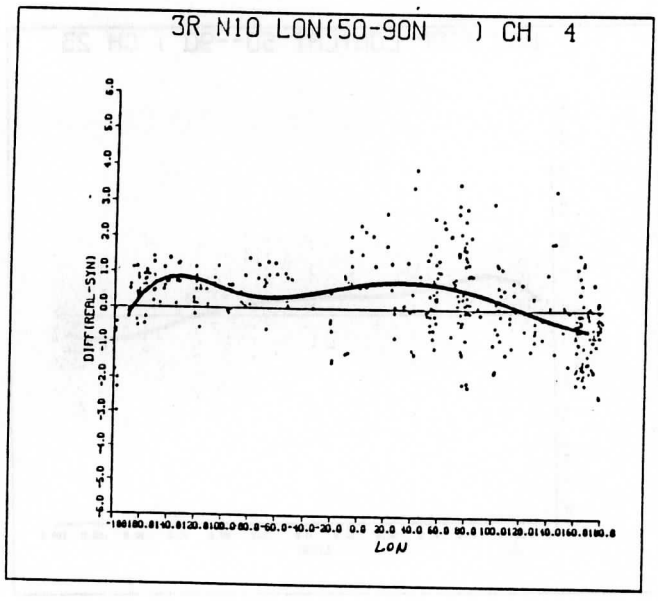

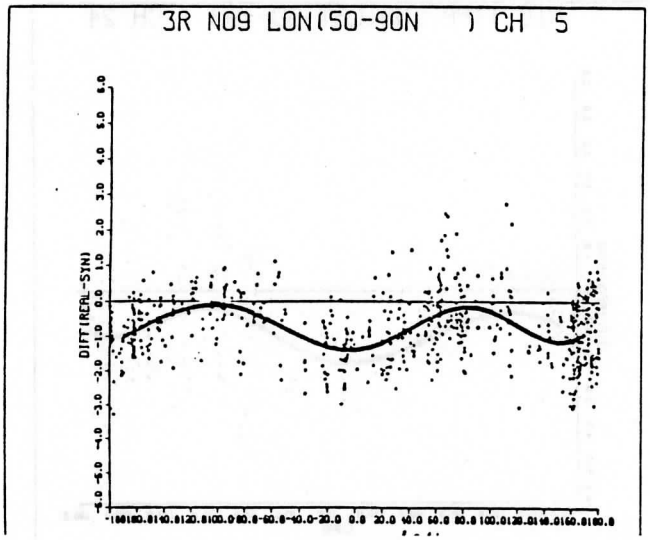

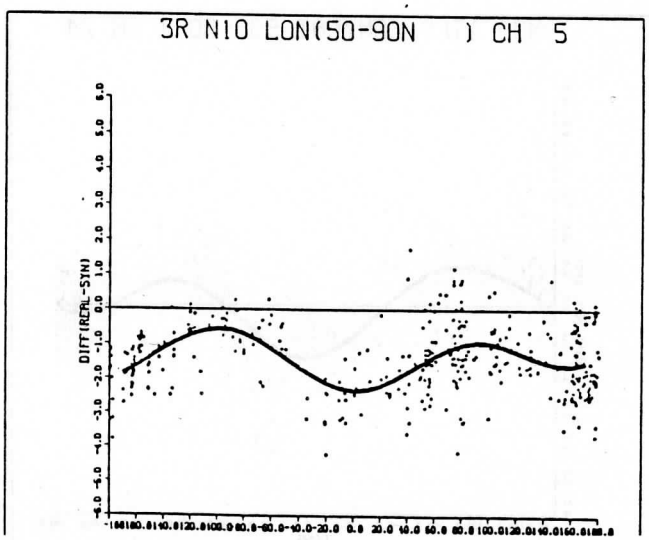

Fig. 5(a) Same as Fig. 4(a) using 3I model.

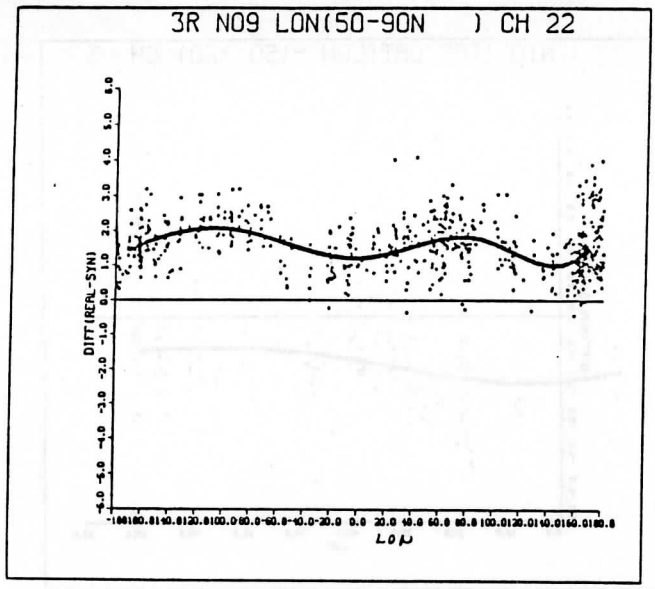

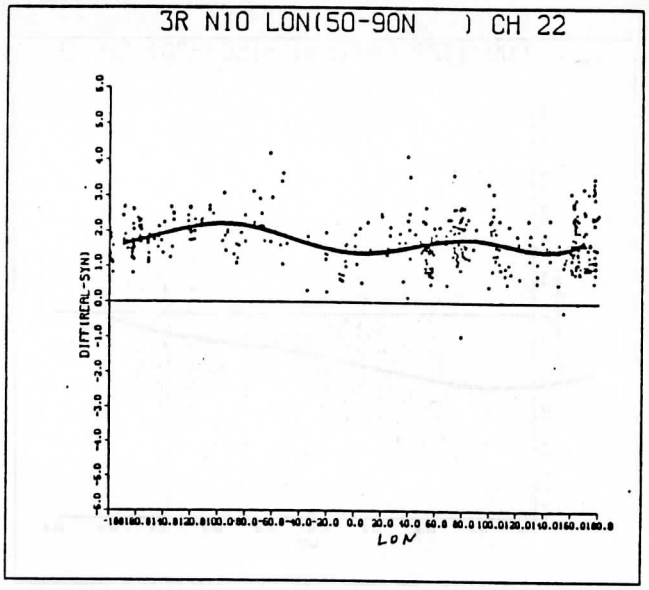

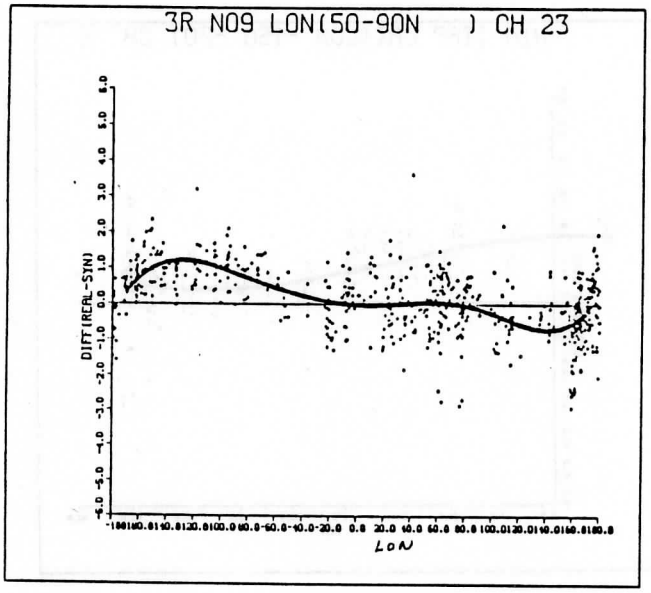

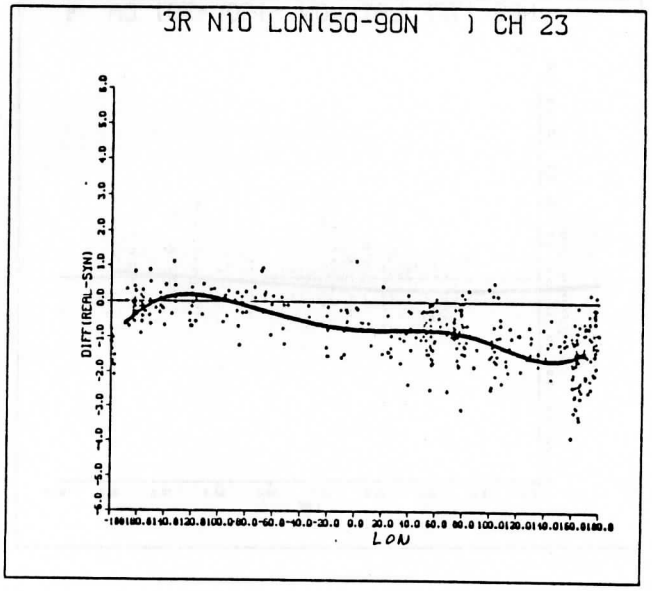

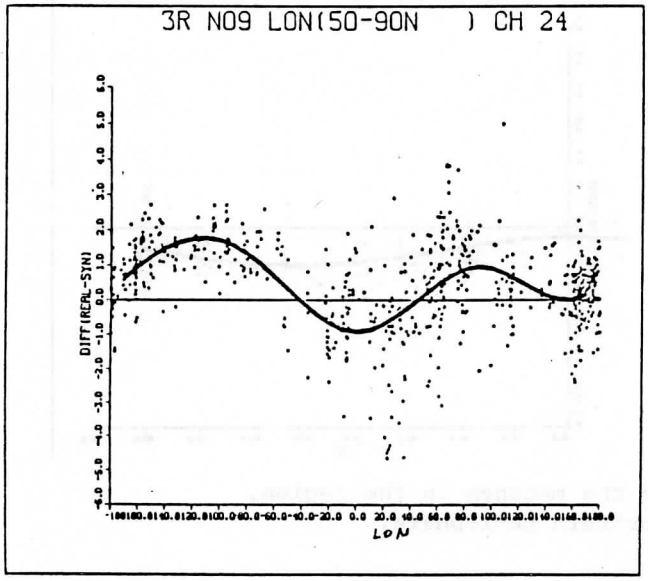

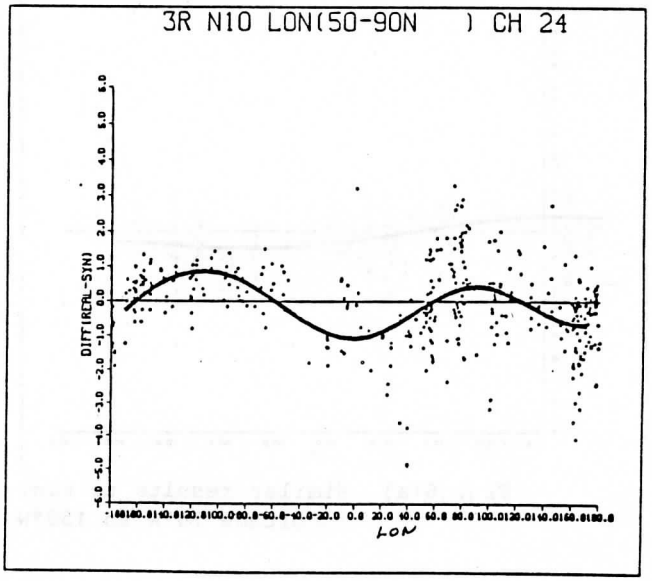

Fig. 5(b) Same as Fig. 4(b) using 3I model.

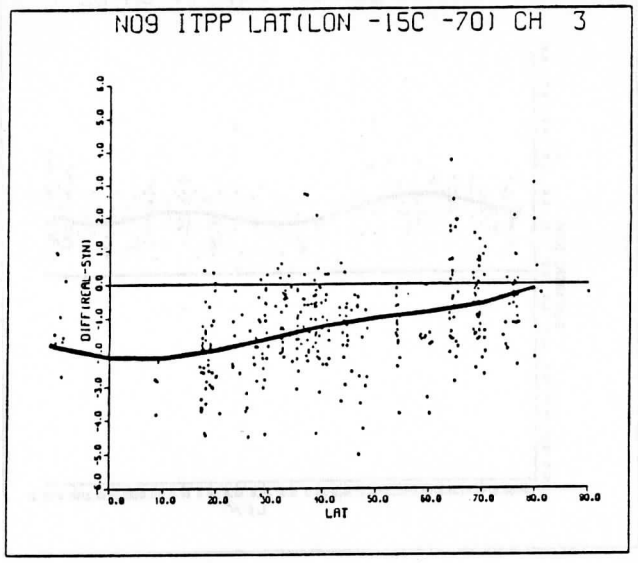

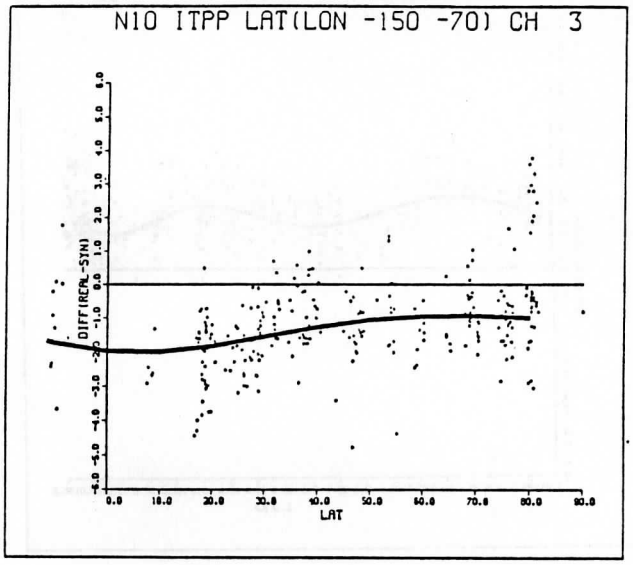

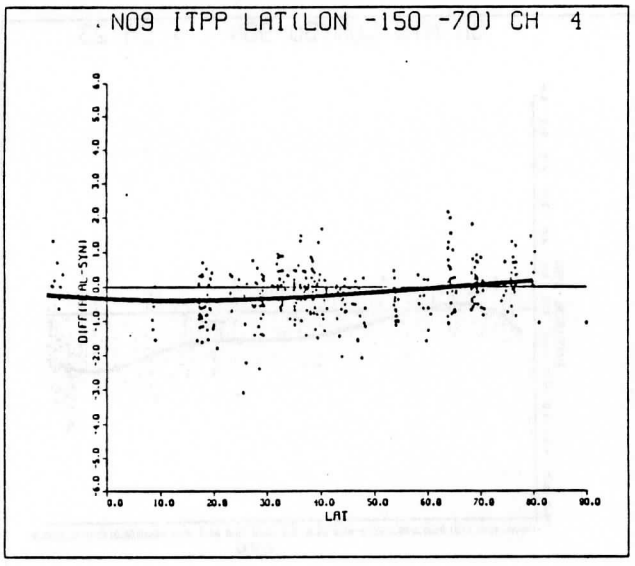

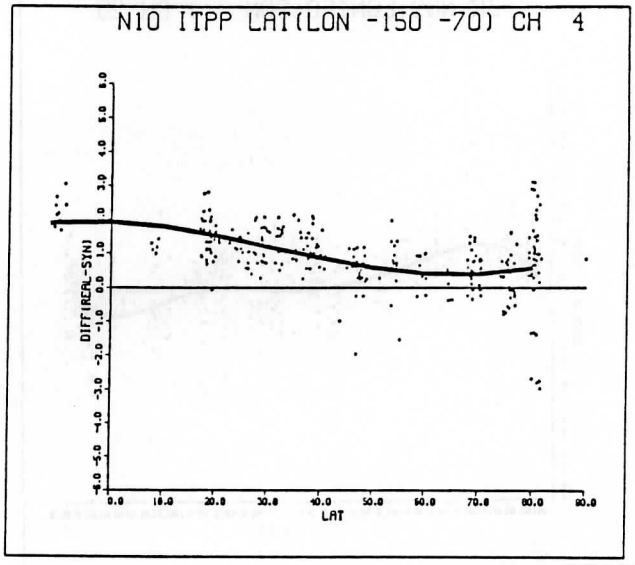

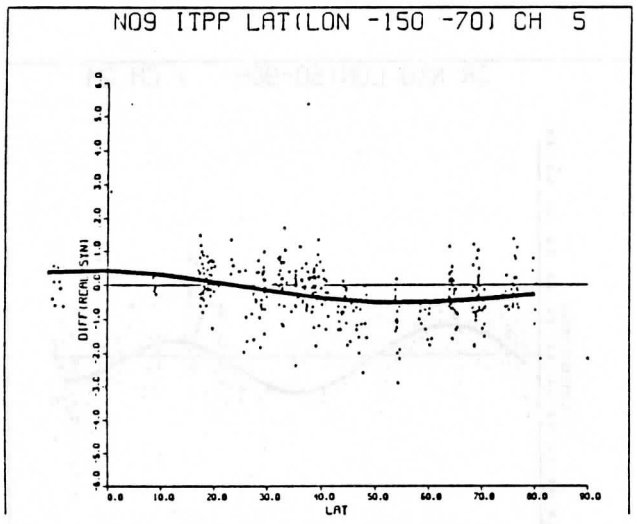

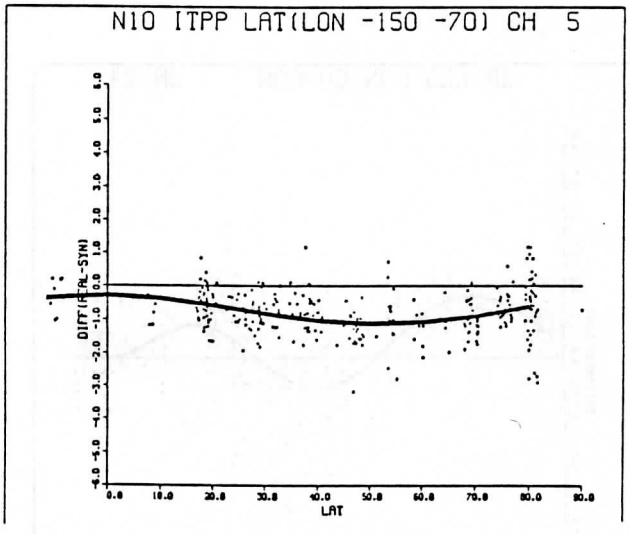

Fig. 6(a) Similar results to Fig. 2(a) with the matches in the region, longitude 70°W to 150°W and in northern hemisphere.

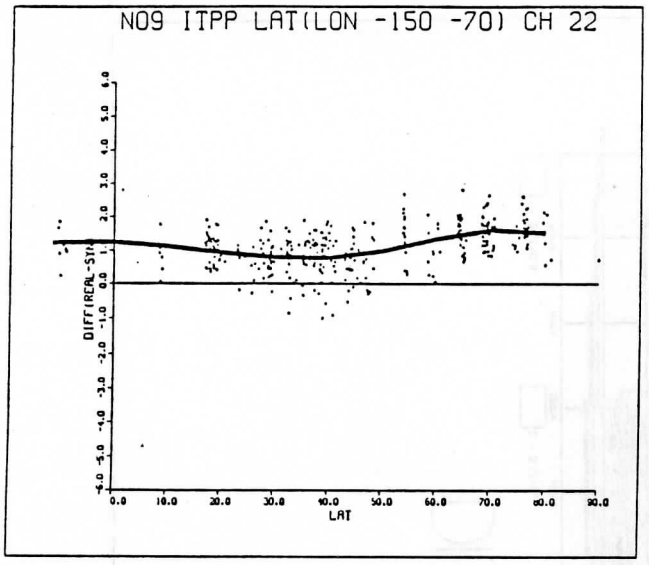

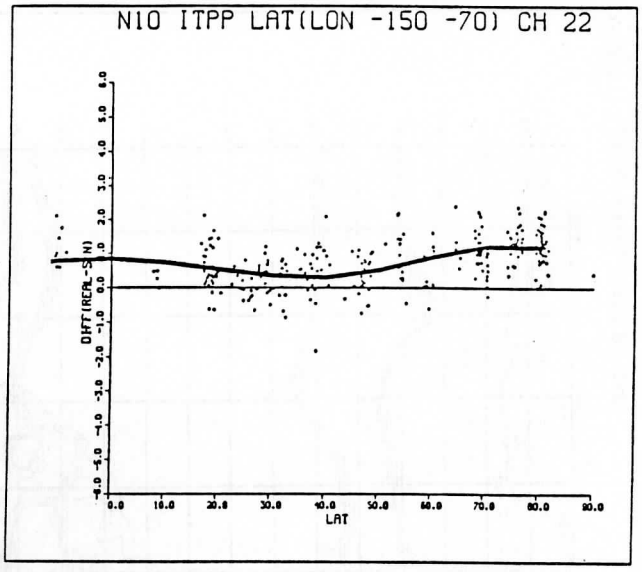

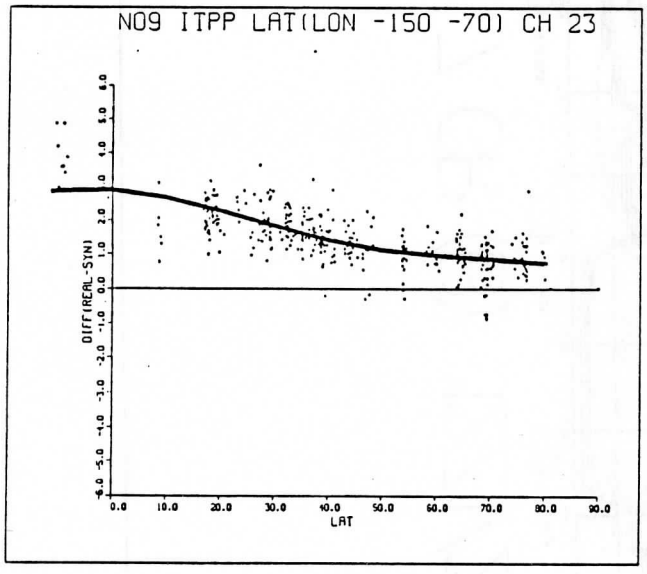

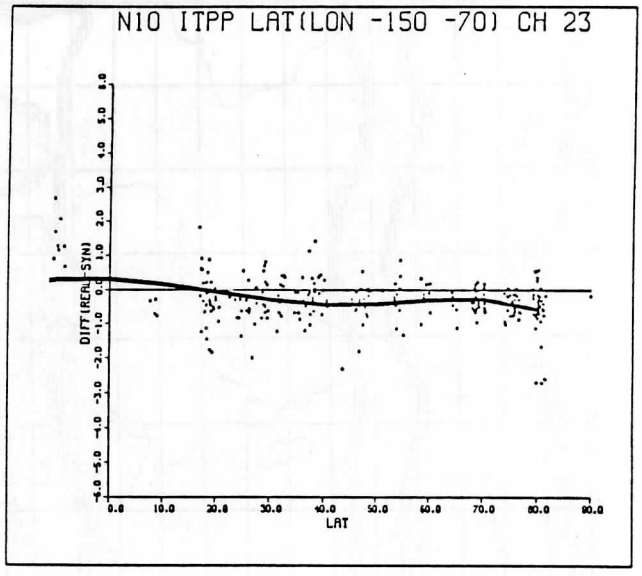

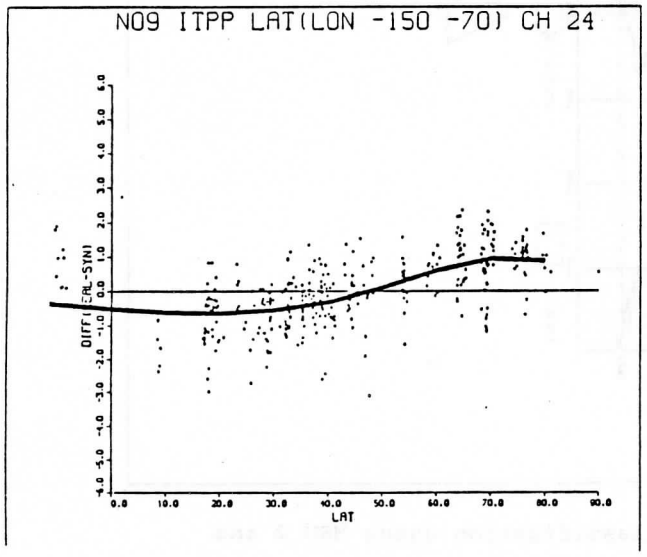

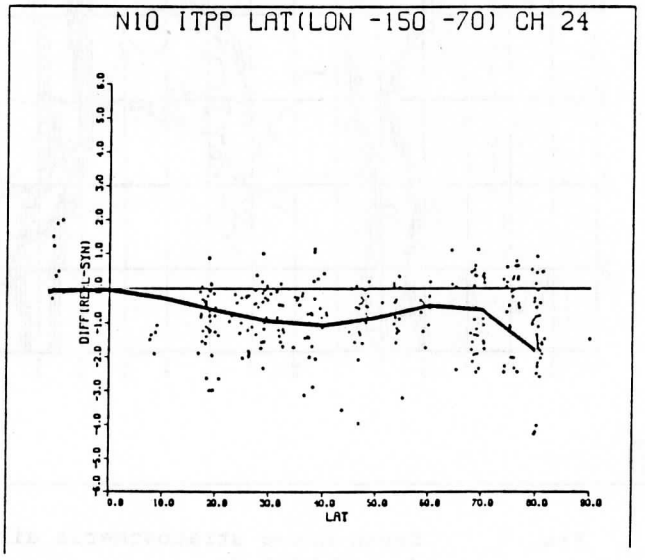

Fig. 6(b) Same as Fig. 6(a) for MSU channels 2, 3 and 4.

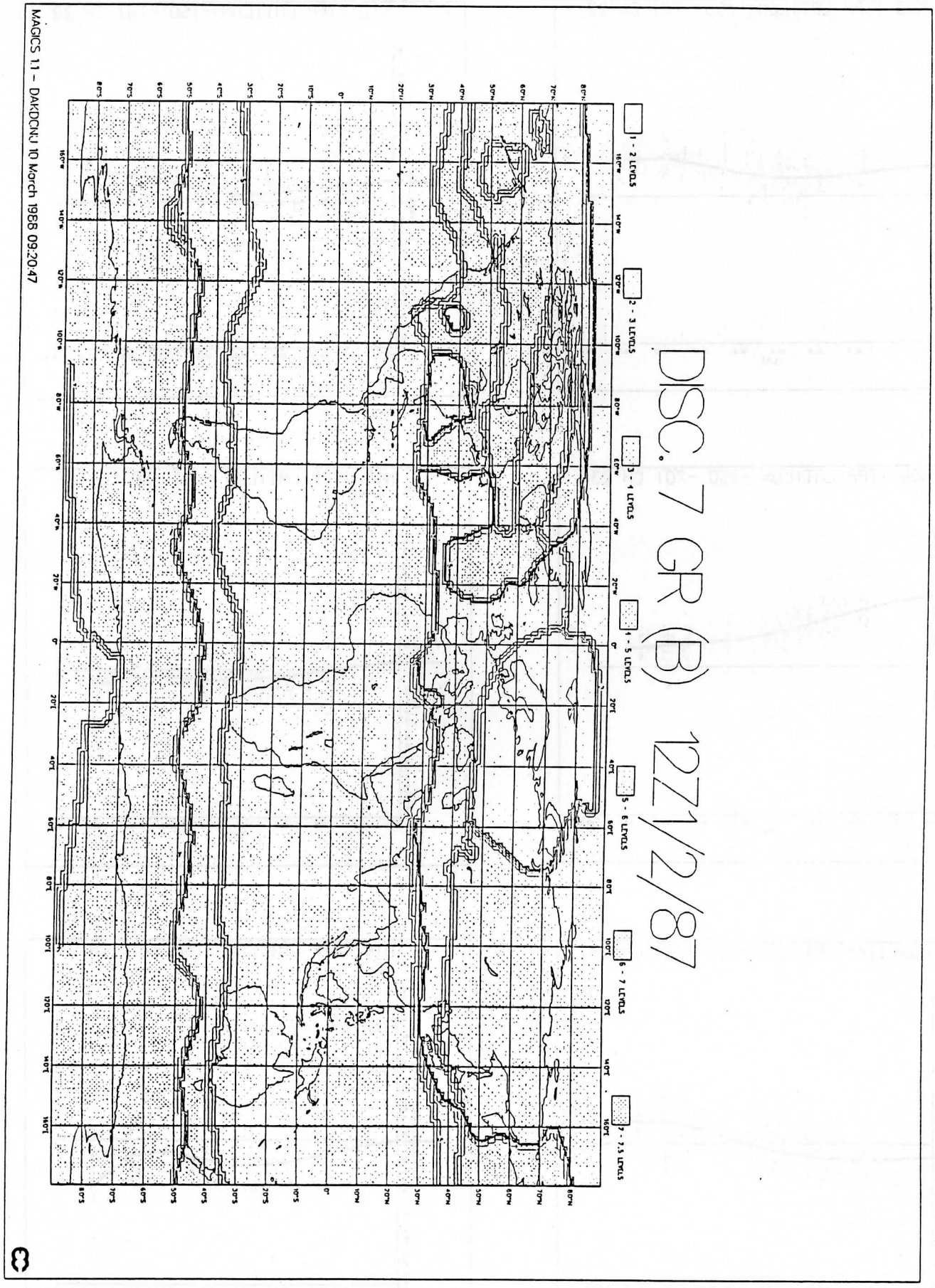

Fig. 7 Seven group stratospheric air mass classification using MSU 2 and 4, and HIRS 3.

Determination of Precipitable Water with the AVHRR

Thomas J. Kleespies
Air Force Geophysics Laboratory/LYS
Hanscom AFB, Bedford MA 01731

Larry M. McMillin
National Oceanic and Atmospheric Administration
National Environmental Satellite, Data, and Information Service
Washington D.C. 20233

1. INTRODUCTION

The "split window" technique was originally derived for the determination of surface skin temperature, specifically sea surface temperature (Anding and Kauth, 1969). The technique makes use of two differentially absorbing channels in the 11- to 12- μm region to remove the contaminating effect of water vapor and thus arrives at an improved estimate of the skin temperature. See McMillin and Crosby (1984) for a detailed discussion of the split window technique and an extensive review of the literature.

More recently the channels used for the split window have been applied to the retrieval of precipitable water (Chesters, et al, 1983, Chesters et al, 1987). Whereas these methods seemed to produce internally consistent fields of "low level water vapor", they required *a priori* knowledge of the mean air temperature and empirical adjustment of the absorption coefficients in order to bring the results in agreement with in situ observations.

In this paper we present the results of an extension to the split window technique such that precipitable water can be retrieved with a minimum of *a priori* information.

2. THEORETICAL DISCUSSION

Kleespies and McMillin (1984,1986) have presented a theoretical discussion of this extension to the split window technique. Summarized briefly, the upwelling longwave infrared radiance emitted from a plane parallel, non scattering atmosphere in local thermodynamic equilibrium and a surface with unit emissivity can be expressed as

$$I = B_s\tau_s + \int_{\tau_s}^{1} B \, d\tau \qquad (1)$$

where I is the radiance measured by the satellite, B is the Planck radiance, τ is the transmittance from a given level to the top of the atmosphere, the subscript s refers to the surface of the earth, and the integral is the radiance originating from the atmosphere alone. Equation (1) may also be written as

$$I = B_s\tau_s + \bar{B}_a(1-\tau_s) \qquad (2)$$

where $\bar{B}$ is a weighted average given by

$$\bar{B}_a = \frac{\int_{\tau_s}^{1} B \, d\tau}{\int_{\tau_s}^{1} d\tau} \qquad (3)$$

Consider observations of the earth under conditions where the surface contribution to the outgoing infrared radiance varies markedly, but where the atmospheric contribution changes very little. We can now write a set of four equations, one for each of the two channels, and one for each of the different surface observing conditions:

$$I_{11}^{1} = B_{s_{11}}^{1}\tau_{s_{11}} + \bar{B}_{a_{11}}(1-\tau_{s_{11}}) \qquad (4a)$$

$$I_{12}^{1} = B_{s_{12}}^{1}\tau_{s_{12}} + \bar{B}_{a_{12}}(1-\tau_{s_{12}}) \qquad (4b)$$

$$I_{11}^2 = B_{s_{11}}^2 \tau_{s_{11}} + \bar{B}_{a_{11}}(1-\tau_{s_{11}}) \quad (4c)$$

$$I_{12}^2 = B_{s_{12}}^2 \tau_{s_{12}} + \bar{B}_{a_{12}}(1-\tau_{s_{12}}) \quad (4d)$$

where the superscripts 1 and 2 refer to the viewing conditions and the subscripts 11 and 12 refer to the nominal 11 and 12 micrometer channels in the split window. We can eliminate the atmospheric term $\bar{B}_a$ by differencing to yield two equations

$$\Delta I_{11} = \Delta B_{s_{11}} \tau_{11} \quad (5a)$$

$$\Delta I_{12} = \Delta B_{s_{12}} \tau_{12} \quad (5b)$$

where for compactness we have written the delta quantities as

$$\Delta I_{11} = I_{11}^1 - I_{11}^2 \quad (6a)$$

$$\Delta B_{11} = B_{11}^1 - B_{11}^2 \quad (6b)$$

The ratio of transmittances in the two channels may be formed by dividing Eqs. (5) to yield

$$\frac{\tau_{11}}{\tau_{12}} = \frac{\Delta I_{11}\, \Delta B_{s_{12}}}{\Delta I_{12}\, \Delta B_{s_{11}}} \quad (7)$$

Following the approach of McMillin (1971), Eq. (7) can be linearized by converting from radiances to temperatures, the ΔB_s become ΔT_s and cancel, and after expanding the delta quantities we are left with

$$\frac{\tau_{11}}{\tau_{12}} = \frac{T_{11}^1 - T_{11}^2}{T_{12}^1 - T_{12}^2} \quad . \quad (8)$$

It has been shown that this ratio can be related to "low level water vapor" i.e., precipitable water (Chesters, et al, 1983).

The observing conditions under which the surface contribution to the upwelling radiances can change markedly but the atmospheric contribution can change very little fall into two general categories; that of variation in time, and that of variation in space. Consecutive observations of a land surface from a geosynchronous satellite during the heating cycle of the day would be one example. Another would be observations from either a geosynchronous or polar orbiting satellite of immediately adjacent land and water surfaces with contrasting skin temperatures.

Kleespies and McMillin (1984) discuss the theoretical application of this extension to the Visible Infrared Spin Scan Radiometer (VISSR) Atmospheric Sounder (VAS), and in their 1986 paper describe, again in theoretical terms, its application to Advanced Very High Resolution Radiometer (AVHRR) split window data. In ensuing sections, application of this technique to the AVHRR instruments is demonstrated with real data.

3. APPLICATION TO SATELLITE RADIOMETER DATA

The test of a retrieval algorithm is to apply it to real data and to somehow verify it with ground truth. However this is fraught with difficulties, including cloud contamination, aerosol problems, collocation inaccuracies, and errors in the satellite instrument and the in situ measurements. In the following sections we apply this technique to measurements made with the AVHRR. In all cases where atmospheric transmittance was computed or radiative transfer was performed, the wide-band radiative transfer model described by Weinreb and Hill (1980) was used.

Global Area Coverage (GAC) data from the AVHRR were collected from NOAA-7 for 11 June 1982. GAC data has a nominal resolution of 4 km and is distinguished from the nominal AVHRR sensor 1 km resolution by the fact that four pixels are averaged along scan and four scans are skipped to make a GAC scan line. Bands 4 and 5 have the nominal wavelength of 10.7- and 11.8- μm respectively. Nighttime data over North America was used in order to be as close as possible to radiosonde launch time and in order to avoid convective cloudiness. The orbits were from four hours to one hour prior to synoptic time. Cloud free areas were selected at the AFGL Interactive Meteorological System (AIMS) (Gustafson et al, 1987) workstation by examining 24-bit multispectral imagery created from AVHRR bands 3, 4 and 5 (d'Entremont and Thomason, 1987). In this imagery opaque clouds appear white, low clouds and fog appear bright red against a brown background, and thin cirrus appears cyan, yielding a fairly unambiguous rendition

of clear/cloudy regions. Contrasting surface temperatures were determined by selecting a body of water (lake, river, coastline) which at nighttime in the late spring was relatively warm compared to the surrounding countryside. A 3×3 array of GAC spots were selected for both the warm water surface and the cooler countryside surrounding it. Since many of these water surfaces did not fill the 3×3 array of GAC pixels, a method was developed to determine the "best" combination of warm and cold brightness temperatures. A comparison of two ensembles of 3×3 arrays yields 81 possible combinations. The brightness temperature differences between these 81 combinations were sorted in descending order for each of the two channels. The sum of the rank order of the pixel pairs between the two scenes and the two channels was used as a "quality measure", the idea being to maximize the brightness temperature difference between the warm and the cold scenes for both channels. A truncated normal type of filter was applied to the pixel pairs with the top ten "quality measures". The mean and standard deviation of the transmittance ratio as determined by Eq. 8 was computed. Any transmission ratio outside of one standard deviation was discarded and the mean recomputed from the remaining ratios. The effect of this procedure was to objectively eliminate outliers. The next step is to computes precipitable water from the transmission ratio. This was done by synthetic regression. Two hundred and ninety six North American radiosondes were collected from three consecutive synoptic times beginning at 12Z 8 June 1982. Transmittances were computed for these radiosondes and regressed against the radiosonde precipitable water. The line of best fit and error statistics are given in Figure 1.

Next the precipitable water determined with the AVHRR was compared with the 12Z radiosondes. Collocation distance was 300km and collocation time depended upon the orbit, and varied from one to four hours. This comparison is given in Figure 2. Given the large collocation window these results are quite good, with a correlation of .7077, mean difference of 0.11 cm and standard difference of 0.552 cm. However the large collocation window can certainly be improved upon. For example, one of these "collocations" was between an AVHRR observation near Pittsburgh, PA and a radiosonde near Washington DC, which was on the other side of the Appalachian mountains and on the opposite side of a cold front.

As an attempt to bring some of the gradient information from the radiosondes into the comparison, the radiosonde precipitable water observations were analysed to a 2x2 degree grid using a Cressman analysis. The analysed precipitable water was bilinearily

interpolated to the AVHRR location. The comparison between the AVHRR observations and the analysed radiosonde precipitable water is given in Figure 3. There are more comparisons in Figure 3 than in Figure 2 because Figure 2 had a maximum separation of 300 km. The comparison here is quite good, yielding a correlation of .8253, effectively no bias and a standard difference of 0.397 cm. The comparison appears even better when the analysis error is examined in Figure 4. Here it is seen that the radiosondes compared with their own analysis have a mean difference of -0.02 cm, a standard difference of 0.463 cm, and a correlation of .8906. These statistics are similar to those given in Figure 3.

4. DISCUSSION

The comparison between precipitable water deduced from the AVHRR and analysed radiosondes is quite good, especially considering the fact that there is a difference in observing time of up to four hours, and that the analysis error is only slightly less than the difference between the AVHRR and the analysed radiosonde. It is clear that this technique has potential for determining precipitable water from radiometric observations using *a priori* information only in setting up synthetic regression. However, this particular method of obtaining the contrasting skin temperatures is unwieldy and requires considerable manual effort. While this method may be useful for limited area work of case studies, it's usefulness for large scale applications will probably be limited.

Recently, Jedlovec (1987) has proposed an extension to this technique, where he determines the transmission ratio to be the ratio of the spatial variance of the channel brightness temperatures, and demonstrated it's usefulness with the Multispectral Atmospheric Mapping Sensor (MAMS), an airborne instrument with a resolution of 100m. The Jedlovec technique may be useful in large scale applications, but it remains to be demonstrated if it will work with an instrument such as the AVHRR.

Potentially the most useful platform for this technique is the geosynchronous satellite. Kleespies and McMillin (1988) presented preliminary results from the VISSR Atmospheric Sounder (VAS) on the GOES satellites which indicate that it may be possible to deduce precipitable water in clear air by observing the earth's surface heat up and cool down during the diurnal heating cycle. The geometric considerations of geosynchronous orbit are very amenable to automated techniques. If the difficulties in using the more noisy VAS instrument can be resolved, then truly useful precipitable water measurements can be made from split window observations.

ACKNOWLEDGEMENTS

The authors wish to thank Mssrs. Mike Weinreb and Mike Hill of NOAA/NESDIS for providing the radiative transfer code used in this study. The authors also express their appreciation to Mr. Robert d'Entremont of AFGL Satellite Meteorology Branch for his assistance with the AVHRR GAC data.

REFERENCES

Anding, D., and R. Kauff, Atmospheric Modeling in the Infrared Spectral Region: Atmospheric Effects on Multispectral Sensing of Sea Surface Temperature from Space, *Rep 2676-1-P, Willow Run Lab., Inst. Sci. Technol.,* Univ. Mich. Ann Arbor, Mich., 1969.

Chesters, Dennis, Louis W. Uccellini and Wayne D. Robinson, 1983: Low Level Water Vapor Fields from the VISSR Atmospheric Sounder (VAS) "Split window" Channels. *J. Clim. Appl. Met.,* Vol 22, No. 5. pp 725-743.

Chesters, Dennis, Wayne D. Robinson and Louis W. Uccellini, 1987: A Note on Optimized Retrievals of Precipitable Water from the VAS "Split Window", *J. Clim. Appl. Met.,* Vol 26, No. 8. pp 1059-1066.

d'Entremont, Robert P. and Larry W. Thomason, 1987: Interpreting Meteorological Satellite Images Using a Color-Composite Technique, *Bull. Am. Met Soc.,* Vol 68, No.7, pp762-768.

Gustafson, G., D. Roberts, C. Ivaldi, R. Schechter, T. Kleespies, K. Hardy, R. d'Entremont, G. Felde and R. Lynch, 1987, The AFGL Interactive Meteorological System, *Preprints, Third International Conference of Interactive Information and Processing Systems for Meteorology, Oceanography, and Hydrology,* 12-16 January 1987, New Orleans, LA.

Jedlovec, G., 1988: Determination of Low-Level Precipitable Water Variability from Split Window Channel Radiance Data, *Preprints, Third Conference on Satellite Meteorology and Oceanography.* Anaheim,CA., Am. Met. So

Kleespies, Thomas J. and Larry M. McMillin, 1984: Physical Retrieval of Precipitable Water Using the Split Window Technique, *Preprints, Conference on Satellite Meteorology/ Remote Sensing and Applications,* Clearwater Beach FL, Am. Met. Soc.

Kleespies, Thomas J. and Larry M. McMillin, 1986: An Extension of the Split Window Technique for the Retrieval of Precipitable Water. *Preprints, Second Conference on Satellite Meteorology/ Remote Sensing and Applications,* Williamsburg VA., Am. Met. Soc.

Kleespies, Thomas J. and Larry M. McMillin, 1988: An Extension of the Split Window Technique for the Retrieval of Precipitable Water: Experimental Verification. *Preprints, Third Conference on Satellite Meteorology and Oceanography.* Anaheim,CA., Am. Met. So

McMillin, L. M. and D.S. Crosby, 1984: Theory and Validation of the Multiple Window Sea Surface Temperature Technique, *J. Geoph. Rsch.* Vol 89, No. C3, pp 3655-3661.

Weinreb, Michael P. and Michael L. Hill, 1980: Calculation of Atmospheric Radiance and Brightness Temperatures in Infrared Window Channels of Satellite Radiometers, *NOAA Technical Report NESS 80,* 40 pp.

Figure 1.

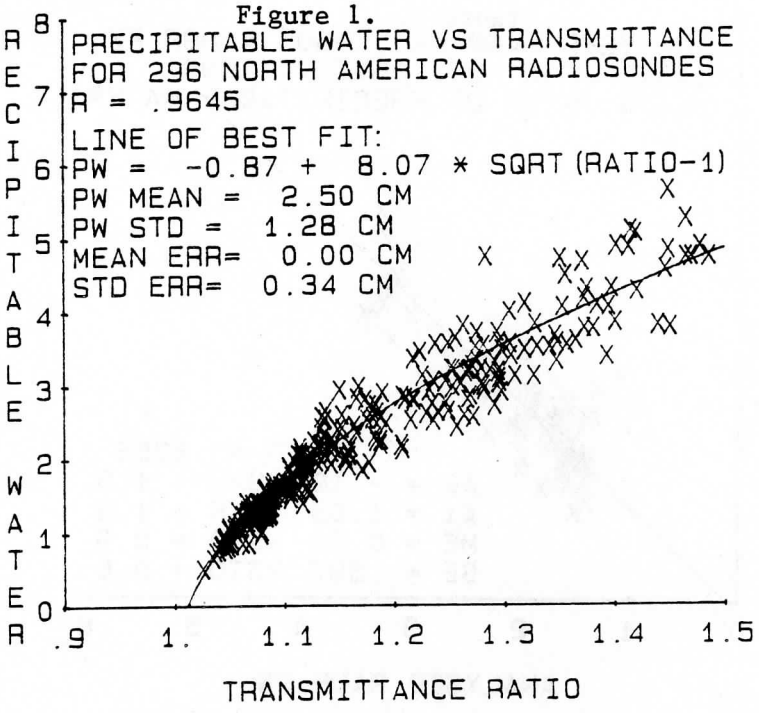

Figure 2.

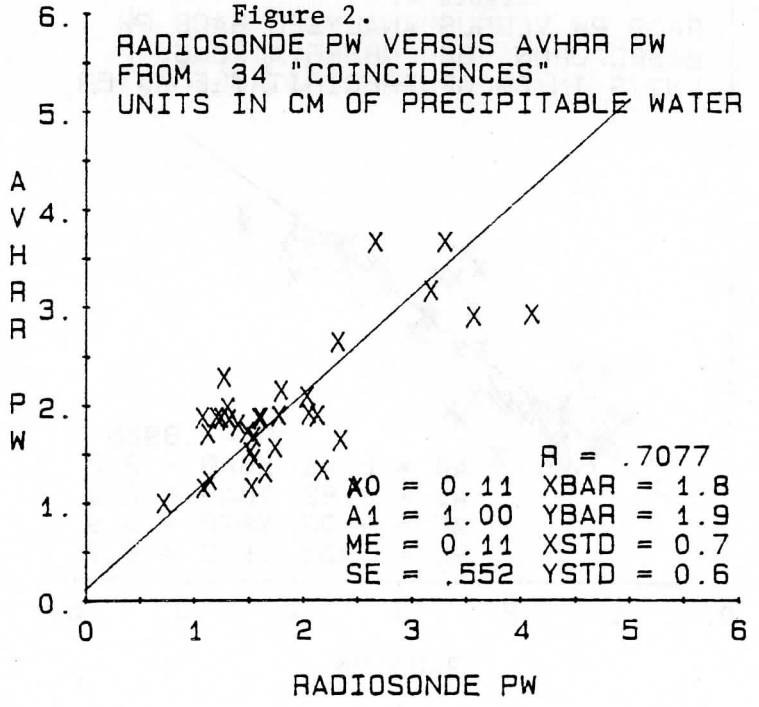

Figure 3.

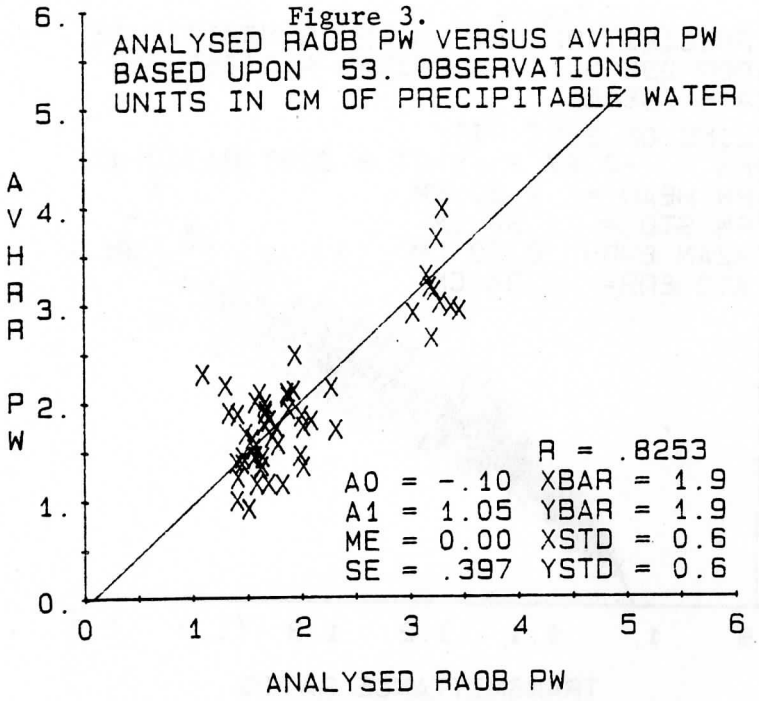

Figure 4.

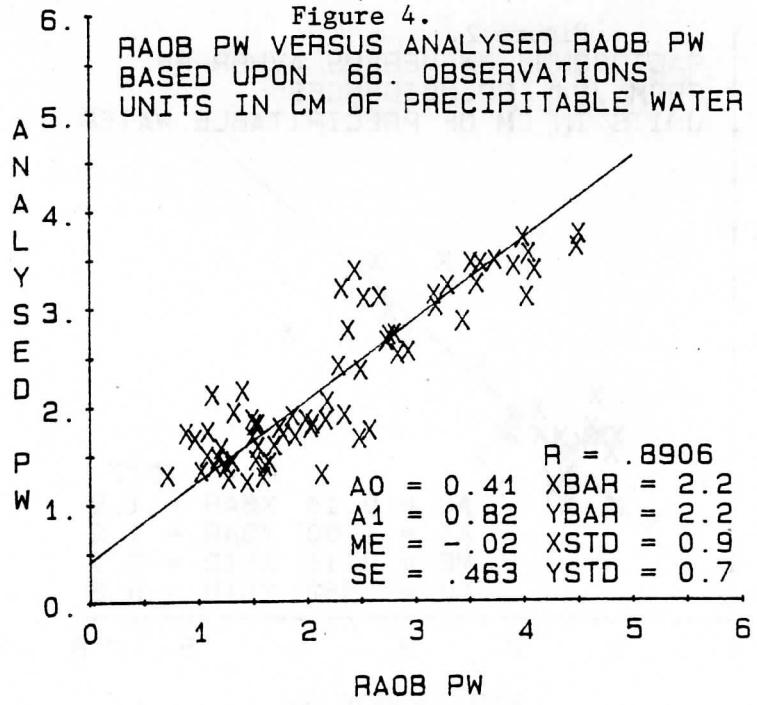

CATHIA: A DATA SET FOR CLOUD CLASSIFICATION AND HIRS CLOUD CLEARING

L.Lavanant,P.Brunel,M.Derrien,J.Quéré,H.Le Gléau,G.Rochard

Météorologie Nationale
Centre de Météorologie spatiale
22302 Lannion.France

1. INTRODUCTION

A HIRS2 cloud clearing scheme,using AVHRR data,is undergoing to be implemented at C.M.S Lannion.The first step is to use AVHRR brightness temperatures to estimate the cloud cover type,the cloud top temperature,its emissivity at AVHRR wavelengths ,the fractional cloud cover in the HIRS2 field of view (F.O.V).The second step is to get these cloud parameters for each HIRS2 channel and specially to compute the cloud emissivities for each HIRS2 wavelength regions.This should be possible by using the results of a statistical study on the CATHIA data set which is a compilation of collocated data (radiosonde profiles and TOVS/AVHRR measurements).A summary of the approach used in the C.M.S cloud clearing scheme is described here.Some parts are already implemented,like the CATHIA data set or parts of the first step.Some others have to be more carefully consirered, like a third step (not described here) for synthetic cloud free radiances estimation with HIRS2 cloud parameters.

2. AVHRR CLOUD PARAMETERS

The analysis of the cloud cover with the AVHRR data is done in boxes of 34*39 pixels around the centers of the HIRS2 F.O.V.

A discrimination between the ground,the sea and the clouds is done with a threshold technique applied every AVHRR pixel,like the one described by SAUNDERS (ref 1).For an operational use of the scheme,the threshold values are now updated to take into account seasonal and zonal effects.The results of this step are,for a partially cloud covered HIRS F.O.V,the surface brightness temperature Ts and the channel(4)-channel(5) brightness temperature difference DTS,in clear-sky conditions,which is a function of the atmospheric absorption.

For a black-body cloud layer,the cloud top temperature is directly estimated from the coldest brightness temperature in the ellipse.For a semi-transparent cloud layer,the bidimentional histogram (channel(4) against channel(4)-channel(5)) is processed to obtain the cloud top brightness temperature.For that,we assume that the emissivity E of the clouds may be expressed as an exponential function of cloud thickness:

$$E = 1 - \exp(-\beta z) \qquad (1)$$

where β is the extinction coefficient and z the cloud thickness.

The cloudy equation for channel i (i=4 or 5) is:

$$I = (1-N*Ei)*Isi+N*Ei*Ici \quad (2)$$

where I is the measured radiance,Is the clear-sky radiance,Ic the upwelling blackbody radiance and N the cloud amount in the pixel.

From these equations and assuming N=1 for a semi-transparent cloud layer,the brightness temperature difference T4-T5 is related to the surface brightness temperature channel(4) Ts and the cloud top brightness temperature Tc by the equation:

$$T4-T5 = (1- A -(1 -A))*(Ts-Tc) + DTS *(1 -A) \quad (3)$$

with A =(T4-Ts)/(Tc-Ts) and b = β_5/β_4 ratio of extinction coefficients for channels 5 and 4.

The values of the two unknown parameters,Tc and b,are determined by a least-square fit of the curve on the bidimentional histogram (T4/(T4-T5)).

With the averaged AVHRR measured radiance in the HIRS2 F.O.V,the blackbody cloud and surface radiances,it is quite easy to compute the effective emissivity N*E of the cloud by using equation (2).

With two cloud layers,we directly determine the top brightness temperature of the lower cloud when this one is thick enough and we get the temperature of the highest cloud by fitting the curve (3) on the modified bidimentional histogram (the pixels corresponding to the low cloud having been suppressed).

3 HIRS2 CLOUD PARAMETERS

In a HIRS2 cloud clearing scheme,it is necessary to obtain the cloud parameters for all HIRS2 channels;ie,the same parameters than those determined in HIRS2 F.O.V from AVHRR pixel processing except that the cloud emissivity,function of the vawenumber,have to be computed now for all HIRS2 channels.

We assume that a simple relation,probably function of the cloud type,may exist between emissivities for different wavelenght regions and that it can be got one time for all with a statistical methcd..If it is true,it will then be possible,in an operational scheme to use this relation,to compute HIRS2 cloud emissivities from AVHRR emissivities determined in the previous step.

The CATHIA (*) data set is a compilation of collocated data (radiosonde profiles,TOVS/AVHRR measurements) and will be used to get the relation between the emissivities.

By applying the AVHRR processing,previously described ,to each satellite situation,the cloud type,the surface temperature Ts,the cloud top temperature Tc and the effective emissivities N*E(AVHRR) are determined.

To each radiosonde profile and incidence angle corresponding to collocated TOVS measurements,the 4A radiative transfer model (ref 2) have been applied.It gives,for all HIRS2,MSU and AVHRR channels,the atmospheric transmittances from the satellite to

---

(*) CATHIA :Calcul Automatique des Températures et Humidités Incluant le AVHRR

each of the 40 pressure levels of the model.

For each HIRS2 channel,the clear-sky radiance Is is computed by using the surface temperature Ts and the whole atmospheric transmittance from the satellite to the surface.The upwelling blackbody radiance Ic is obtained from the cloud top temperature Tc and the atmospheric transmittance from the satellite to the pressure corresponding to Tc (given by the radiosonde profile).So,with the measured upwelling radiance I,the effective emissivity N*E(HIRS2) is calculated from equation (2).That will give the relation emissivities for different wavelength regions.

4. THE CATHIA DATA SET

A data set of 1333 situations has been created containing:
.satellite AVHRR/TOVS data (1333 ellipses) from 143 orbits.
.151 collocated radiosonde profiles and their respective AVHRR/TOVS synthetic cloud-free radiant energies.

The data for each profile consist of pressure,air temperature and dew-point temperature.They have been selected from different campaigns,some of them specifically made for the CATHIA data set which means:a perfect temporal collocation of the satellite-radiosonde measurements and the largest cloud type diversity as possible.For marine radiosonde observations,a sea surface temperature,measured at the station or in the vicinity,has been assigned to the profile.Concerning the situations over land,the concidered surface temperature is that of the lowest-level pressure measurement.

The satellite data for each situation consist of TOVS measurements ,HIRS2,MSU (corrected by ITPP) and SSU interpolated in the ellipse, and AVHRR measurements collocated in the ellipse (33*38 box centered on the ellipse with the data around set to 0).For a given radiosonde observation,the nearest NOAA orbit,in space and time,is considered.Several HIRS2 ellipses have been selected around the radiosonde station (often in a square 3*3 around the station) in order to have the largest diversity in cloud types,cloud amount and number of cloud layers.For that,we assume that the atmospheric profile was the same over a few tenths of kilometers around the station.

Tables 1 and 2 give some statistics,respectively over the radiosonde profiles and the selected cloud types.More details,and specially a photograph compilation for all the situations,can be found in the CATHIA data set report (ref 3).

The 4A radiative transfer model is applied to synthetic computations of atmospheric transmittance over 40 pressure levels (from 0.05 mb to 1013 mb) and radiant energies.In most of the cases,the balloon-borne instruments transmitted data up to pressures of about 100-50 mb.Therefore,the profiles have been extended to a 0.05 mb pressure by using the TIGR data set (ref 4) with a nearest neighbouring technic.Surface emissivities used in 4A computation method and details in the processing are given in the CATHIA data set report (ref 3).

5. SUMMARY

The CATHIA data set of coincident satellite data-radiosonde profile has been created in order to get the relation between cloud emissivities in different wavelength regions.This relation is probably dependant of the type of cloud layer but we expect that it will be stable for each cloud type in order to use it in an operational scheme.

A lot of work has to be done in the future.The AVHRR processing scheme which has only been tested,at the present time,during night and over sea,have given a good improvement of the cloud top temperature achievement,specially for high level layers.The processing of the CATHIA data set is only at its beginnig but the first results seem to be encouraging.

REFERENCES:

1.R.W.SAUNDERS,K.T.KRIEBEL:'An improved method for detecting clear sky and cloudy radiances from AVHRR data.'Int.J.of Remote Sensing vol 9 n°1,123-150 (1988)

2.N.A.SCOTT,A.CHEDIN:'A fast line-by-line method for atmospheric absorption computations:The automatized atmospheric absorption atlas'.J. Appl. Meteor. 20,802-812 (1981)

3.C.M.S. lannion:'The CATHIA data set' Vol 1 and 2.Internal Technical Report. (1988)

4.A.CHEDIN,N.A.SCOTT:'Improved initialization inversion procedure (3I).First International TOVS Study Conference. (1983)

SEA	77
LAND	36
COAST	38
DAY	87
NIGHT	64
WINTER	8
SPRING	73
SUMMER	33
FALL	37
TROPICAL	1
MID-LATIT.	142
POLAR	8

TABLE 1:statistics on radiosonde profiles (in number of profiles)

CLEAR	20%
SINGLE LAYER	60%
TWO LAYERS	15%
MORE	5%
Sc	25%
Cu	25%
St	8%
Ci	23%
Cn	8%
Ac	8%
fog	17 ellipses

TABLE 2:statistics on cloud types

AN INTERCOMPARISON OF TEMPERATURES AND MOISTURE FIELDS DERIVED FROM TIROS OPERATIONAL VERTICAL SOUNDER DATA BY DIFFERENT RETRIEVAL TECHNIQUES-CLEAR RADIANCE CASE

J. F. Le Marshall and M. Y. Chee

Satellite Section, Bureau of Meteorology, Melbourne, Australia

ABSTRACT

Fields of temperature, thickness and precipitable water derived from common sets of TIROS Operational Vertical Sounder (TOVS) radiance data using different retrieval techniques have been previously intercompared for the Second International TOVS Study Conference (ITSC-II). This document describes the verification statistics for that study associated with temperature and moisture fields derived from cloud free or clear fields of view. It also provides a comparison of the statistics for these clear soundings with those associated with the clear and cloudy soundings of the previous study. In this study, the results in general point to a small increase in the accuracy of the temperature and moisture sounding data for the cloud free case.

1. INTRODUCTION

Several participants at the three International TOVS Study Conferences to date, provided temperature and moisture profiles retrieved by different techniques, for an intercomparison study. These temperature and moisture profiles were for three test areas, namely the Alpine Experiment (ALPEX) region, the Tasman Sea and the United States (US). Basic verification statistics were derived and reported by Le Marshall (1985). The general conclusions were that, notwithstanding the recognized advantages of a physical retrieval scheme, the general accuracy and consistency of the retrieved soundings at the scale examined were to a significant degree independent of the retrieval scheme used. This was, however, no indication that the advantages of physical schemes, compared to some commonly used statistical ones, are insignificant in areas such as limb correction (Le Marshall and Schreiner, 1985) and for example in the explicit accounting for elevation and skin temperature in the profile solution. Overall it was found that both operational and research processing of TOVS radiance data indicated that the instrument is capable of providing temperature soundings with an rms difference near 2K compared to ECMWF analysis and RAOB data, from 850 hPa to the tropopause region. There was an increase in the magnitude of the difference near the tropopause and surface. This was contributed to by the inherent smoothing of the TOVS profile in these regions of sharp vertical temperature gradient. These differences were changed considerably by ancillary data (e.g. surface data) or constraints. In fact, the surface differences appeared to be more a function of ancillary data or constraints rather than the retrieval scheme. It is important to note that these statistics

included differences due to radiosonde error, colocation differences, analysis errors and other factors.

The basic statistics associated with the retrieval of moisture were also calculated by Le Marshall (1985). In general, differences between radiosonde and ECMWF precipitable water estimates and TOVS estimates were thirty to forty percent of the total precipitable water. Again these differences include those which arose from the comparison of fields with high spatial and temporal variability and also from errors in the measurement of moisture by radiosonde.

It was recommended at ITSC-III (Menzel and Lynch, 1986) that the quantitative intercomparison for the ALPEX case study should be repeated for clear only radiances. As a result this paper extends the statistics in Le Marshall (1985) by providing statistics for those soundings which were derived using only cloud free fields of view.

2. THE CONTRIBUTORS TO THE INTERCOMPARISON :

A complete list of contributors is found in Table 1. In the comparison between clear and total ensemble (clear and cloudy) statistics, only those contributors who provided a fully described ensemble of clear, cloudy and microwave soundings were used. In the ALPEX case, these were from NASA/GLAS, United States (ALNA), Laboratoire de Meteorologie Dynamique, France (ALFR), the British Meteorological Office (ALUK), CIMSS, University of Wisconsin (ALWI2) and WAIT, Western Australia (ALWA). In the Tasman Sea case, contributions were from the Australian Bureau of Meteorology (TAAU) and the New Zealand Meteorological Service (TANZ), while for the US case the contributors came from the Atmospheric Environment Service, Canada (USCA), the British Meteorological Office (USUK) and CIMSS, Wisconsin (USWI).

3. THE INTERCOMPARISON :

Fields nominated for intercomparison at the First International TOVS Study Conference were temperature at fifteen standard levels, geopotential thickness and precipitable water in the layers 1000 to 400 hPa, 850 to 400 hPa, 700 to 400, and 500 to 400 hPa. For cloud free cases, these fields have been compared to their respective ECMWF fields interpolated to the sounding position in time and space. They have also been compared to colocated (within 150 km) radiosondes (RAOBs). Bias, standard difference, rms difference, standard deviation and correlation coefficient have been computed.

The basic statistics are summarised in this paper with the results for the ALPEX study being shown in Figures 1 through 10. This case is regarded as more representative of a clear versus cloudy comparison because of the larger number of retrievals involved, compared to the US case for instance and because of the larger number of retrievals and amount of verification data available compared to the Tasman Sea case (see Le Marshall, 1985). The US cases, however, are illustrated in Figures 11 through 16. Due to the availability of data sets from only two institutions and very sparse RAOB data in the Australian/New

Zealand region, results for the Tasman Sea study are not presented here.

4. THE BASIC STATISTICS

(a) ALPEX case

Figures 1 and 2 show the basic statistics for temperature for both the previously reported mixed (clear and cloudy) cases and the clear cases, compared to ECMWF data. Some differences can be discerned. To examine these further, the data sets consisting of clear, cloudy and microwave-only data, were used to produce mean values for clear and mixed ensembles (Fig. 3). A small improvement in agreement with the ECMWF analyses for the clear case can be seen for the rms difference and standard difference at most levels. The mean standard deviation is higher for the clear case (compared to the mixed ensemble) below the tropopause and the opposite above. This is true for the associated ECMWF data as well. The correlation coefficient for the clear case shows a clear improvement at and below 250 hPa with little difference above 150 hPa. The differences between the mean clear and mixed statistics are plotted in Fig. 4.

The corresponding basic statistics and related differences from a comparison with RAOB data, for mixed and clear soundings, are seen in Figures 5 through 8. A small improvement compared to RAOB data is seen for bias for the troposphere, while standard difference is improved near the surface but not so for the remainder of the troposphere. Rms differences for the clear and mixed cases fluctuate in relative accuracy from level to level. However, the correlation coefficient for the clear case in general shows improvement through most of the atmosphere. Again the mean standard deviation for the clear soundings is greater than the mixed soundings for most of the troposphere with a tendency to reverse near and above the tropopause. This is also true for the associated radiosonde data.

In the case of precipitable water (Figs. 9 and 10), the rms statistics for the lowest layer (1000/400hPa) indicate the clear soundings to be in better agreement with radiosondes, while a small improvement for the mixed case is seen for the less water burdened layers examined below 400hPa. It should be noted that the moisture statistics from the three data sets examined are drawn from fields that vary rapidly in time and space. This, combined with the errors associated with the measurement of moisture by radiosonde (Nash et al, 1985), the colocation criteria employed and the influence of the cloud field or radiosonde data may result in the basic statistics not fully reflecting the comparative skill of the clear and cloudy data. It should also be noted that the statistics for these cases are also a function of the way clouds are handled in the retrieval scheme. For example, while in some statistical schemes, (eg. ITPP1) the N* technique (Smith and Woolf, 1986) is used to provide clear radiances for use in moisture retrievals. Some physical schemes (those based on ITPP3) use cloud height and cloud amount information to influence the moisture retrievals (saturating cloud top in the first guess) and subsequently solve the retrieval problem by using transmittances consistent with the

presence of cloud.

(b) United States case.

Data sets were examined for the United States region and some of the basic statistics for the clear and mixed cases are shown in Figs. 11 to 16. For the standard level temperatures, comparison of clear and mixed rms differences indicate, apart from the two lowest levels, that the clear data were in closer agreement with the ECMWF analysis fields through most of the troposphere. The mean standard deviations below the tropopause generally appear larger for the clear case.

In comparison with RAOB data, better agreement in terms of rms difference was found for the clear data. Also, in this case the standard deviation of the temperatures is smaller through much of the troposphere.

With regard to precipitable water (Figs. 15 and 16), rms differences in comparison to ECMWF fields generally indicate better agreement for the clear case, despite a larger bias, particularly in the lower layers. Comparisons with RAOB data show an improvement in agreement in the lowest two tropospheric layers examined.

SUMMARY AND CONCLUSIONS :

Several sets of sounding data generated using different retrieval techniques have been intercompared to gauge the comparative accuracies of soundings from clear and mixed fields of view. As in Le Marshall (1985), no attempt has been made, nor is there any intention to rank the retrieval schemes relative to one another. As noted earlier, the statistics presented are not simply a function of basic retrieval method but are related in a complex way to the number of retrievals (and, eg. editing), the characteristics of the first guess field, the use of ancillary data (eg. surface data or AVHRR data), the resolution of the retrieval scheme and a variety of other factors.

It should again be noted that the character of the clear and cloudy soundings may be different for different retrieval schemes. For example, some retrieval schemes use the N* technique (Smith and Woolf, 1976) to give estimates of clear radiances in cloudy fields of view and soundings are based on these radiances, while some physical schemes use calculated cloud height and amount to influence the moisture retrievals and to determine the temperature at cloud top levels.

With these considerations in mind, however, some general comments about basic statistics for clear and mixed groups of soundings in this study, can be made.

For this study, in the case of level temperatures, a small improvement in the agreement between the sounding data and ECMWF analyses was seen for clear data in the troposphere for both the ALPEX and US cases. This improvement was between 0.1K and 0.2K in an rms sense. In comparison to RAOB data, a similar result was found for the US case but no clear result was evident in the

ALPEX case. However, in the latter case an improvement in the correlation coefficient at almost all levels for the clear case was seen.

The basic statistics associated with the retrieval of precipitable water show an improvement generally in the rms differences compared to ECMWF and RAOB data for the 1000/400 hPa layer. For this layer, the reduction in rms difference ranged between 2 and 20 (cm x 100) of precipitable water. This represents between 5 and 20 percent of the precipitable water in the layer 1000/400 hPa.

Examination and significance testing of the population means and variance for the different levels studied however, indicated that further sampling is warranted to establish the extent of the difference between the clear and mixed sounding populations examined confidently.

In summary, for this study a small overall improvement in retrieval accuracy has resulted from the determination of temperature profiles from cloud free fields of view. It was also found that the precipitable water content of the lower atmosphere (1000/400 hPa) was also better determined in the cloud free case. An evaluation of the differences, between the clear and mixed populations, however, indicates that further study is required to establish their magnitude with confidence. It is hoped that these differences will be refined and related a little more directly to particular retrieval techniques by further intercomparisons, in particular the two recommended for study by ITSC-IV.

A separate document with complete statistics for each set of cases has also been prepared, but for reasons of brevity this information was not included in this document.

ACKNOWLEDGEMENTS
Many thanks are due to Julia Gorman, who helped in the preparation of this manuscript.

REFERENCES

LE MARSHALL, J. F., An Intercomparison of Temperature and Moisture Fields Retrieved for TIROS Operational Vertical Sounder Data. Technical Proceedings of the Second International TOVS Study Conference, Igls, Austria, 1985. Report from CIMSS, SSEC, University of Wisconsin, Madison, Wisconsin, 53706.

LE MARSHALL, J. F., and SCHREINER, A.J., 1985. Limb effects in satellite temperature sounding. J. Clim. and Appl. Meteor., 24, 287-290.

MENZEL, W. P., and M. J. LYNCH, 1986: A Report on the Third International TOVS Study Conference, Madison, Wisconsin. A report from the Cooperative Institute for Meteorological Satellite Studies, Space Science and Engineering Center, University of Wisconsin, Madison, Wisconsin, 82pp.

NASH, J., KITCHEN, M., and PONTING, J. F., Comparison of relative humidity measurements from Phase 2 of the WMO International

Radiosonde Comparison. WMO/TD-50 Third WMO Technical Conferences on Instruments and Methods of Observation (TECIMO III), Ottawa, Canada, 8-12 July, 1985, 25-32.

SMITH, W. L., WOOLF, H. M. 1976, The use of eigenvectors of statistical covariance matrices for interpreting satellite sounding radiometer observations, J. Atmos. Sci. 33., 1127-1140.

TABLE 1

Summary of contributions to the intercomparison study. (Note T represents temperature data, Z represents thickness data and P represents precipitable data, ITPP1, ITPP2, and ITPP3 represents International TOVS Processing Package 1, 2 and 3 respectively, RFG represents regression first guess, CFG represents climatology first guess, MFG represents first guess fields derived from a forecast model, SD indicates the use of surface data in the retrieval scheme, AVHRR represents the use of locally generated regression coefficients and NRC indicates the use of NESDIS regression coefficients.)

DATA ORIGIN	ALPEX	CONTENT	DATA	TOT. NOBS	NOBS (CLEAR)	RET. SCHEME
British Met. Office	ALUK	T, Z, P	clear, cloudy, and microwave	~695	~420	Statistical (Modified ITPP1, NRC)
CIMSS/NOAA-NESDIS Wisconsin	ALWI1	T, Z, P	clear only	~1719	~1719	Physical (Iterative, ITPP2, RFG, SD)
	ALWI2	T, Z, P	clear, cloudy, and microwave	~1819	~1333	Physical (One step, ITPP3, CFG, SD)
	ALWI3	T, Z, P	clear only	~1828	~1828	Physical (One step, ITPP3, RFG, SD)
DFVLR West Germany	ALDF	T, Z, P	clear only	~1389	~1389	Physical (Iterative, modified ITPP2, RFG, SD)
Laboratoire de Meteorologie Dynamique France	ALFR	T, Z	clear, cloudy, and microwave	~4180	~1879	Physical/ Statistical
NASA/GLAS United States	ALNA	T, Z, P	clear, cloudy, and microwave	~903	~614	Physical (Relaxation, MFG)
NOAA/NESDIS Washington	ALNE	T, Z	clear only	~223	~223	Statistical (Operational Algorithm)
University of Bologna Italy	ALIT1	T, Z, P	cloudy only	~1517	-	Physical (Iterative, modified ITPP2)
	ALIT2	T, Z, P	clear only	~1757	~1757	Physical (Iterative, modified ITPP2, SD)
Western Australian Institute of Tech.	ALWA	T, Z, P	clear, cloudy, and microwave	~2808	~1757	Statistical (Modified ITPP1, NRC)

DATA ORIGIN	TASMAN	CONTENT	DATA	TOT. NOBS	NOBS (CLEAR)	RET. SCHEME
Bureau of Meteorology Australia	TAAU	T, Z, P	clear, cloudy, and microwave	~2037	~859	Physical (Modified ITPP3, RFG)
CIMSS/NOAA-NESDIS	TAWI	T, Z, P	clear only	~1626	~1626	Statistical (ITPP2, RFG, SD)
NOAA-NESDIS	TANE	T, Z	clear only	~229	~229	Statistical (Modified ITPP1, NRC)
New Zealand Meteorological Service	TANZ	T, Z, P	clear, cloudy, and microwave	~2049	~1329	Statistical (Operational Algorithm)

DATA ORIGIN	US	CONTENT	DATA	TOT. NOBS	NOBS (CLEAR)	RET. SCHEME
Atmospheric Environment Services (AES) Canada	USCA	T, P	clear, cloudy, and microwave	~192	~95	Statistical (Modified ITPP1, NRC)
British Met. Office	USUK	T, Z, P	clear, cloudy, and microwave	~163	~83	Statistical (Modified ITPP1, NRC)
CIMSS/NOAA-NESDIS	USWI	T, Z, P	clear, cloudy, and microwave	~134	~42	Physical (Iterative, AVHRR)

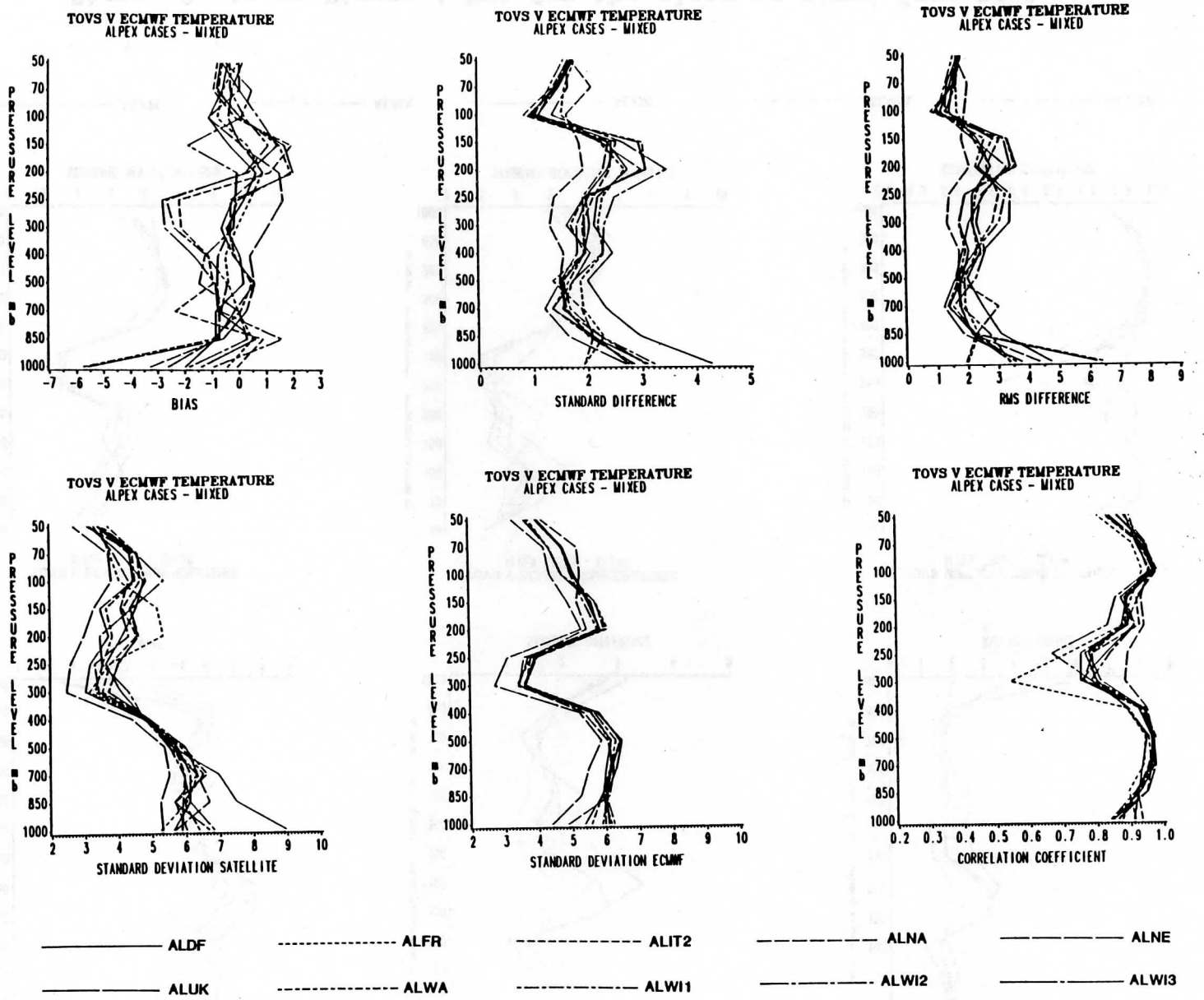

Figure 1. Basic Statistics for TOVS retrievals compared to ECMWF data for the ALPEX case. Temperatures in degrees K and the legend used Table 1 acronyms.

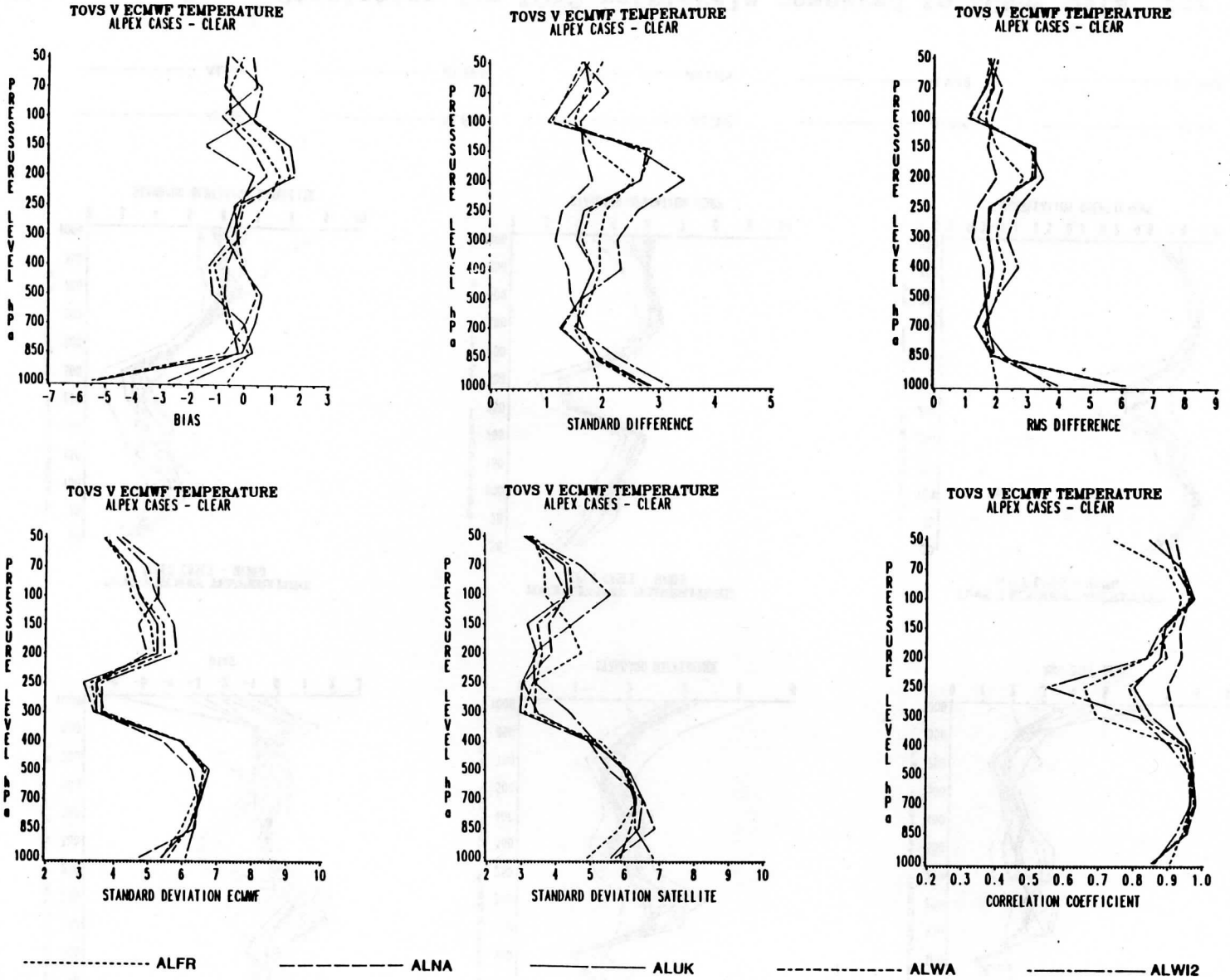

Figure 2. As in Figure 1 but for the clear or cloud free case.

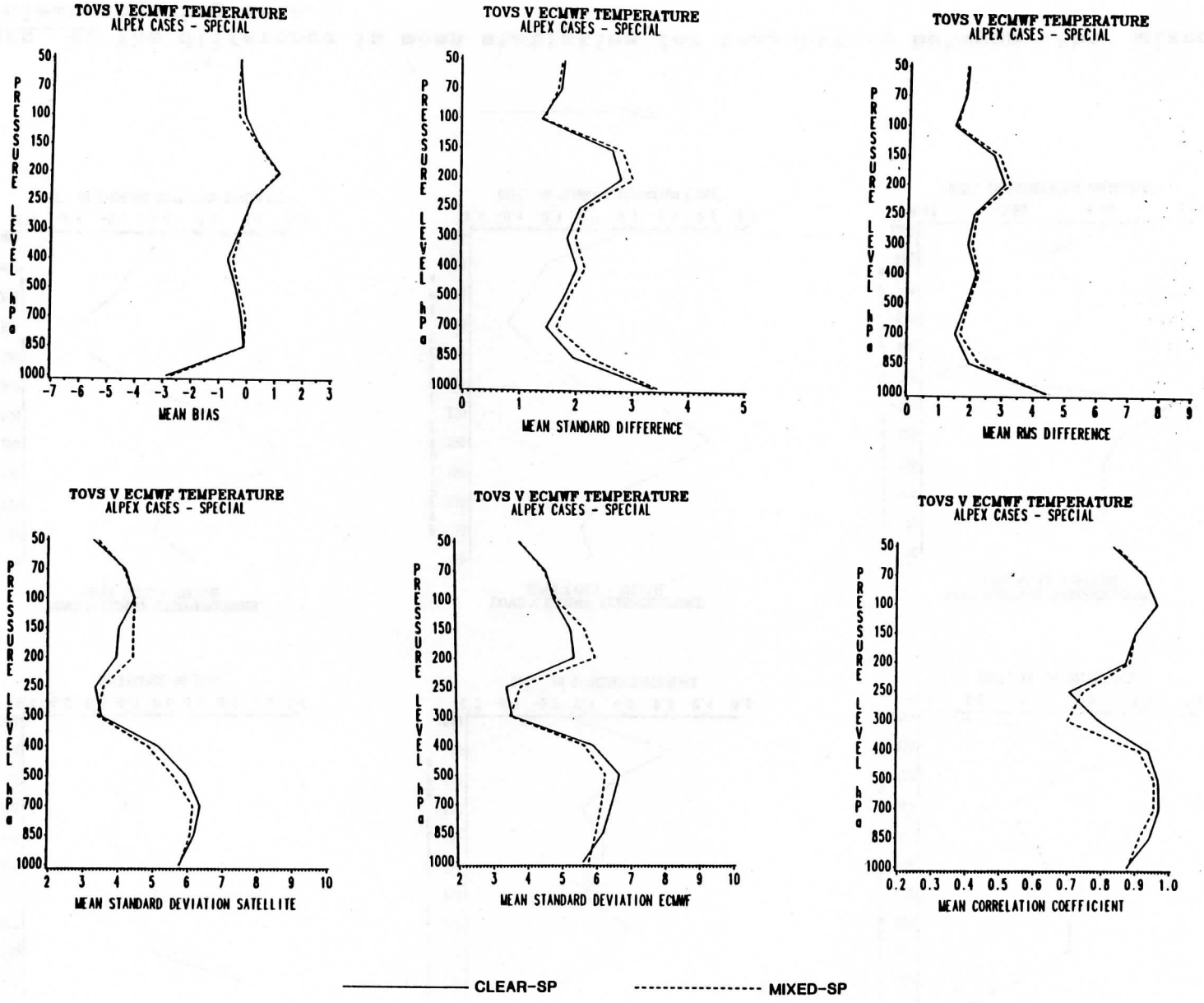

Figure 3. Mean statistics for temperature for clear and mixed (clear plus cloudy) sounding sets from the contributors to Figure 2.

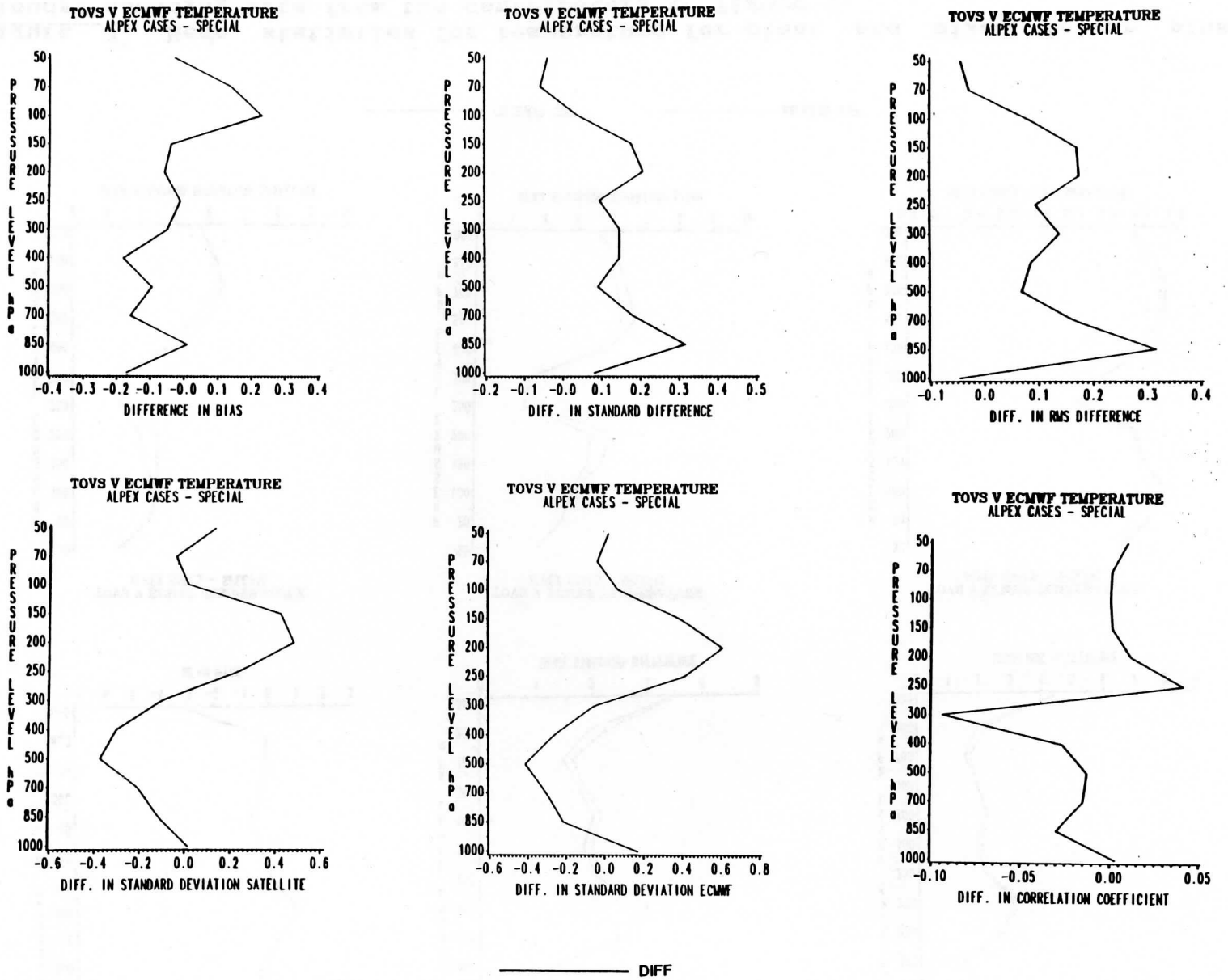

Figure 4. The difference in mean statistics for temperature between the mixed and clear sounding sets.

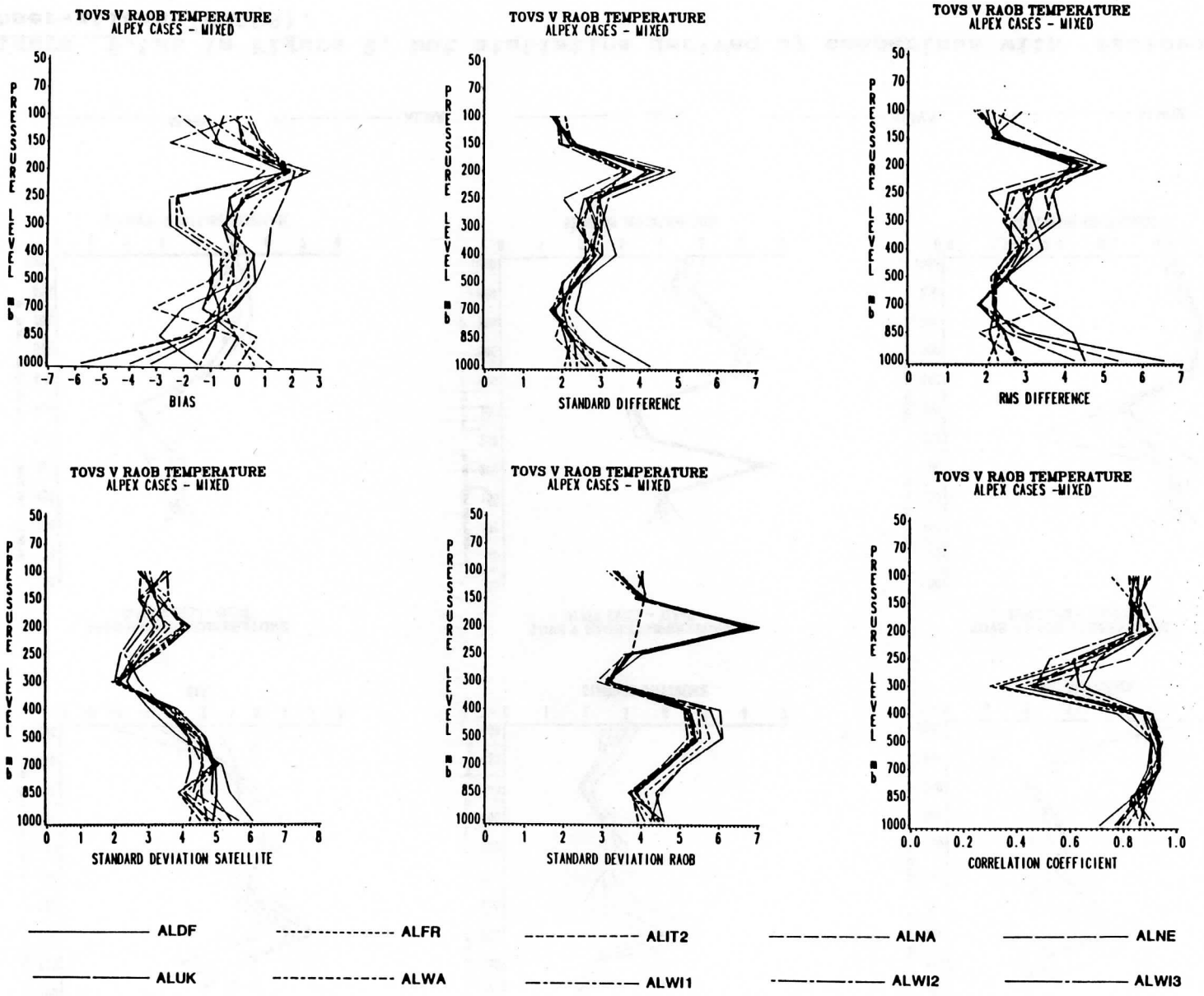

Figure 5. As in Figure 1, but statistics derived by comparison with radiosonde observation (RAOBS).

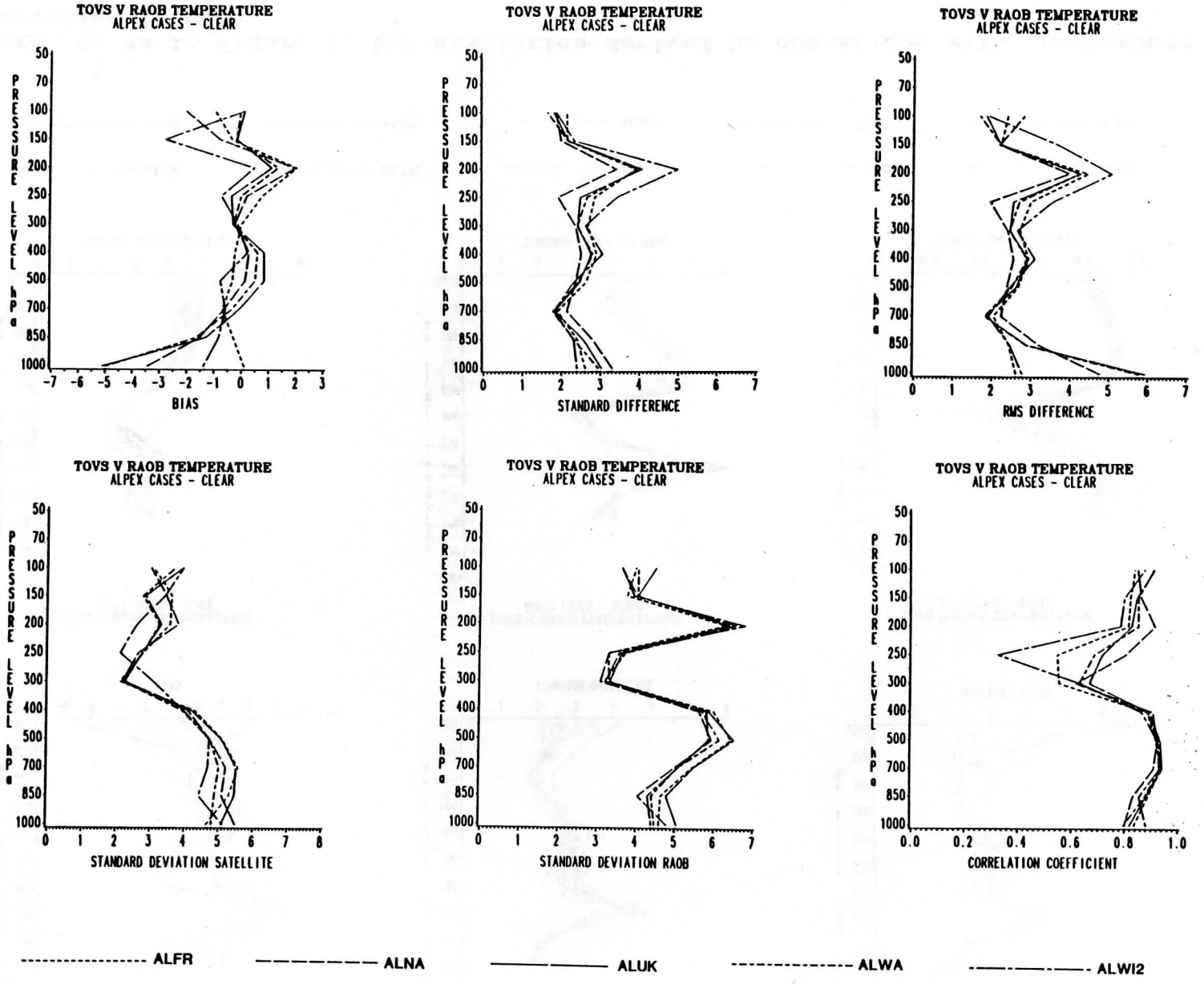

Figure 6. As in Figure 2, but statistics derived by comparison with radiosonde observations (RAOBS).

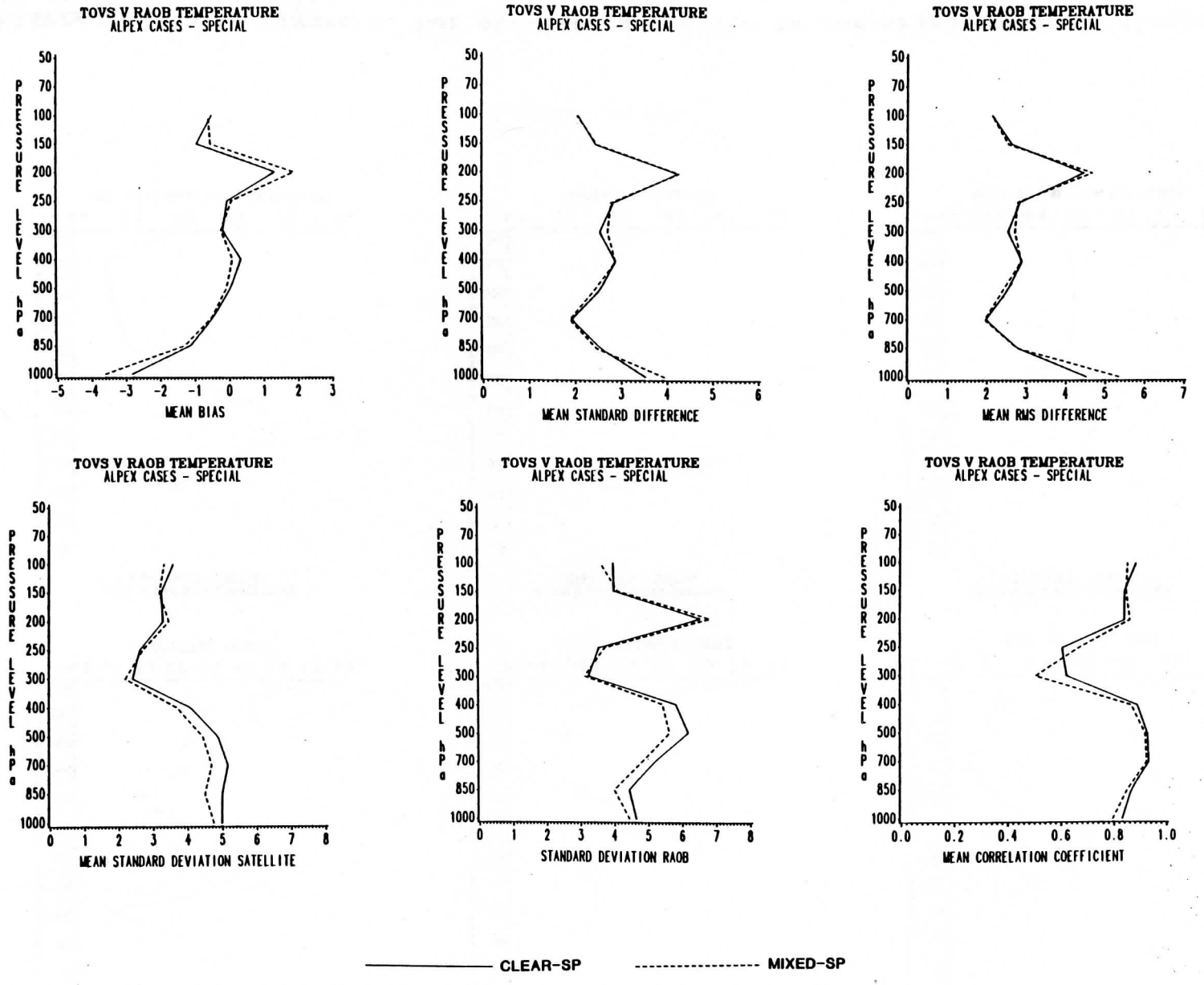

Figure 7. As in Figure 3, but statistics derived by comparison with radiosonde observations (RAOBS).

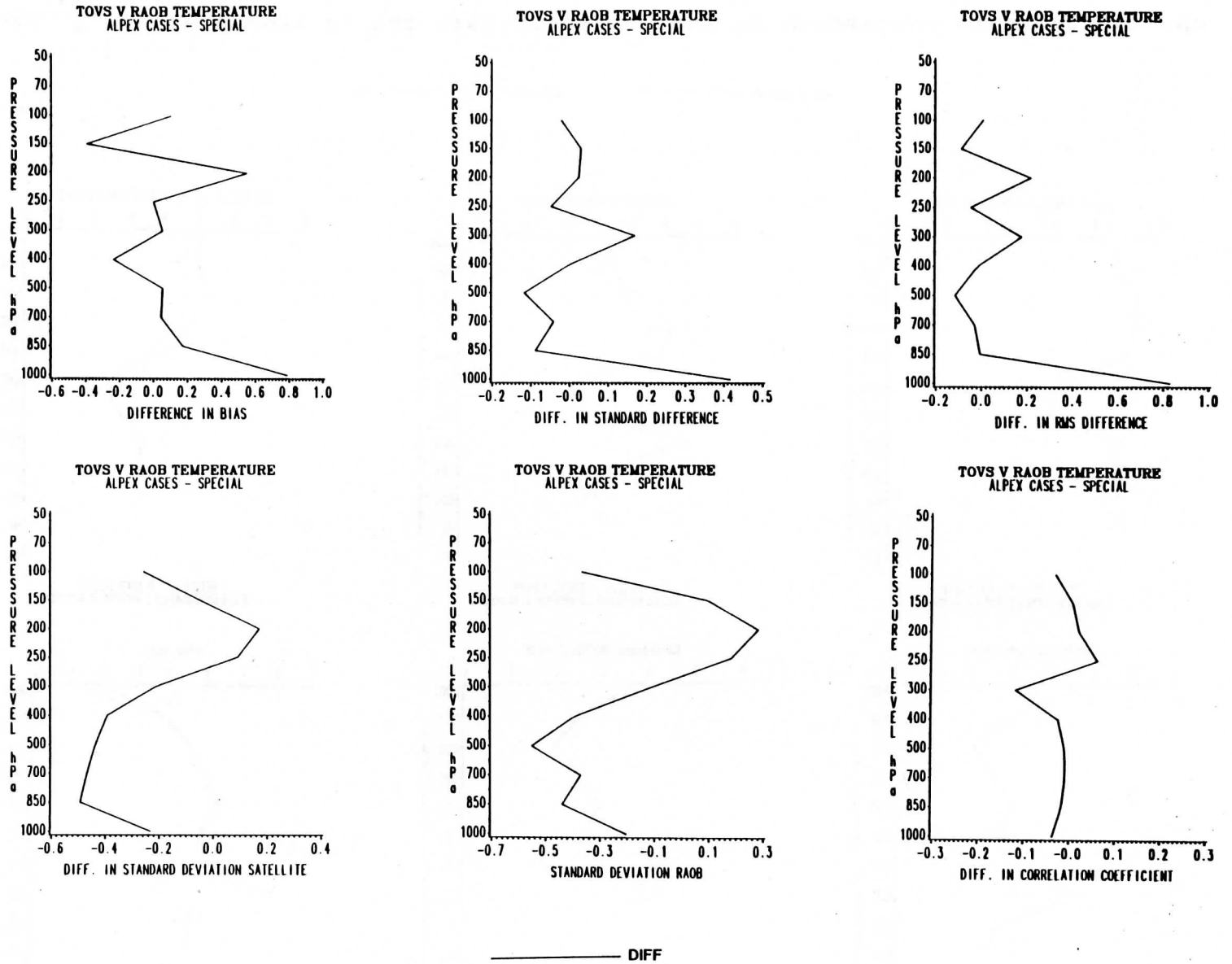

Figure 8. As in Figure 4, but statistics derived by comparison with radiosonde observations (RAOBS).

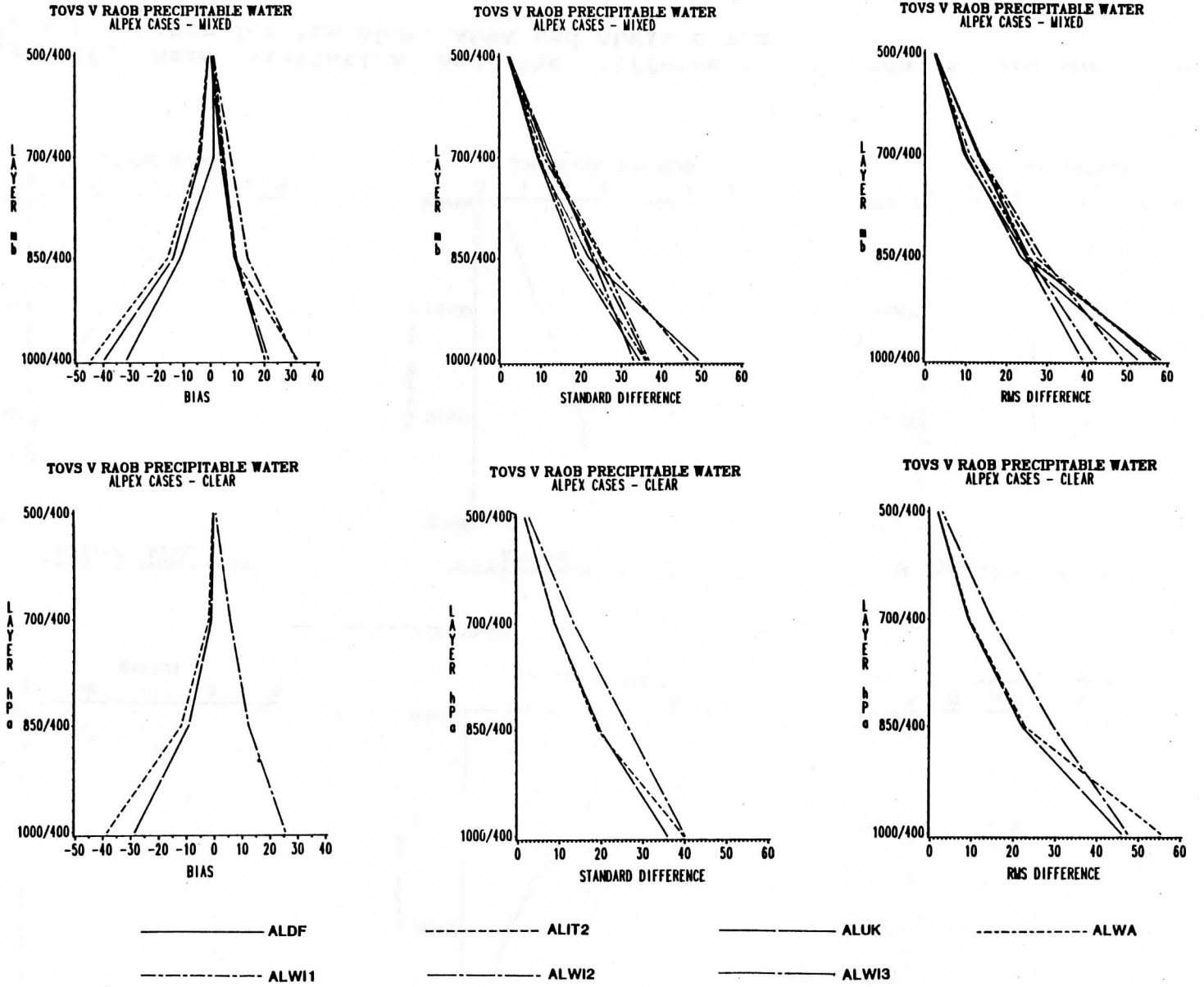

Figure 9. Basic statistics for TOVS retrievals compared with radiosondes for precipitable water observations for both the mixed and clear case. Precipitable water units (cm x 100)

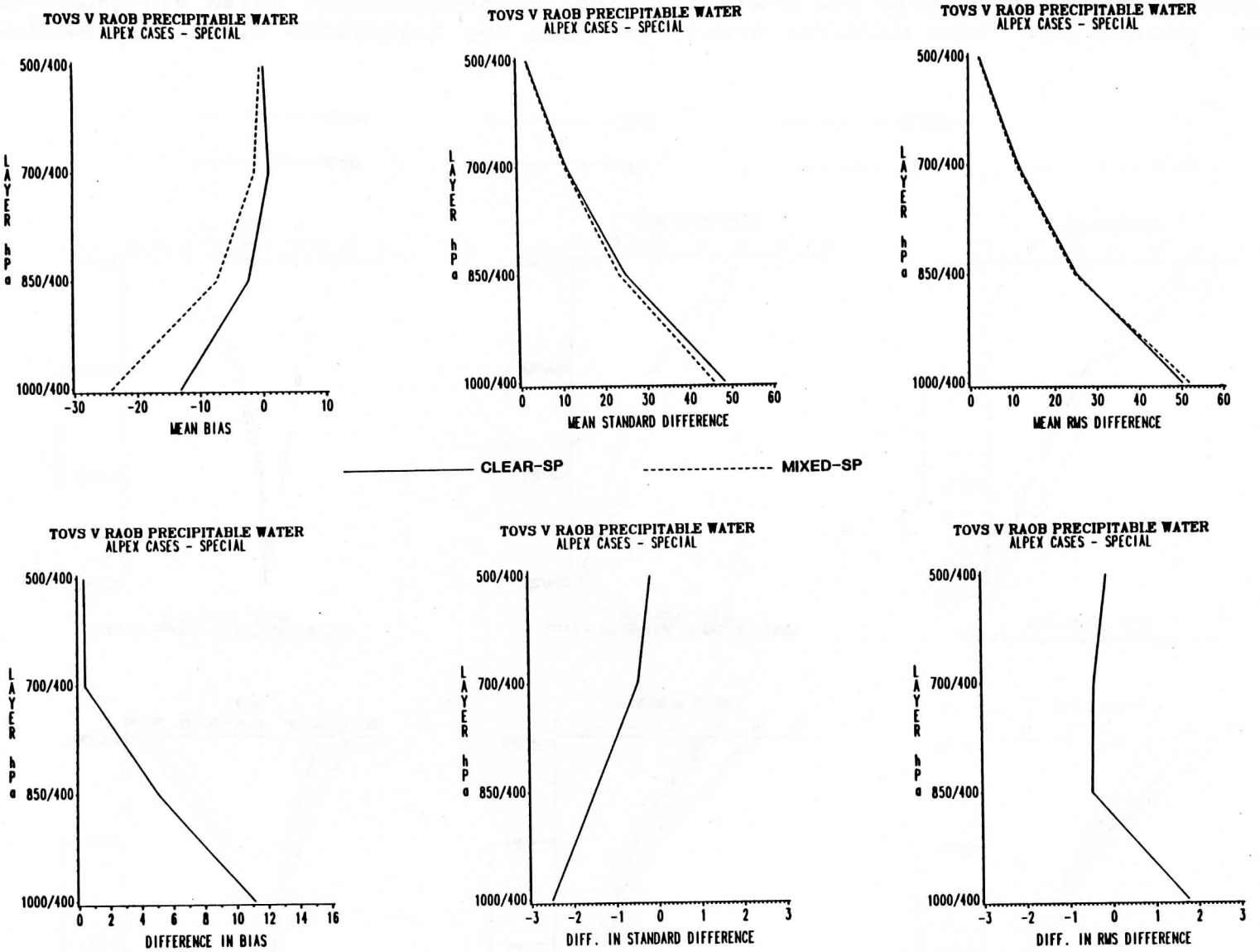

Figure 10. Mean statistics and the difference in mean statistics for precipitable water for the ALUK, ALWA and ALWI2 cases.

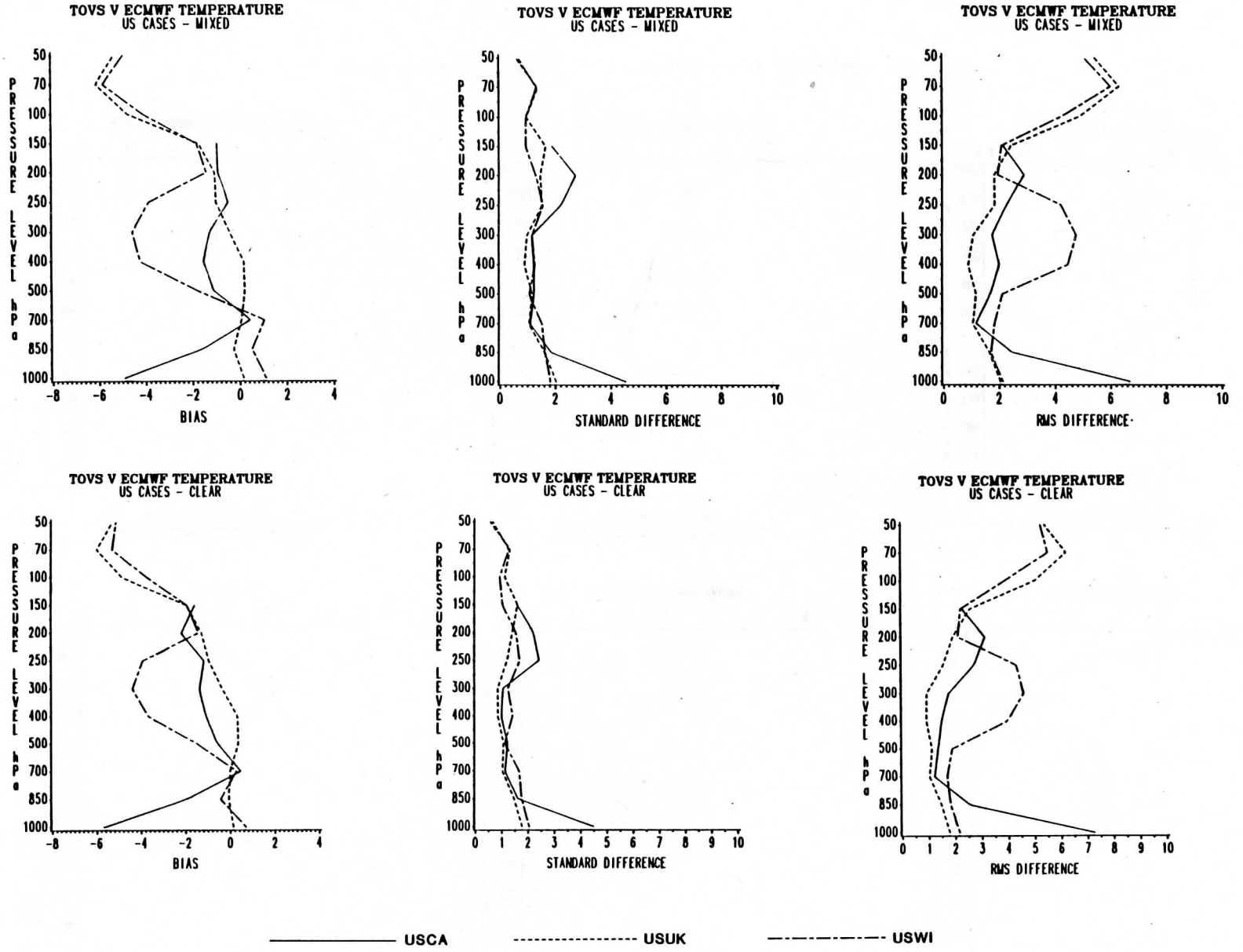

Figure 11. Basic statistics for temperature compared to ECMWF data, for mixed and clear TOVS retrievals for the US case.

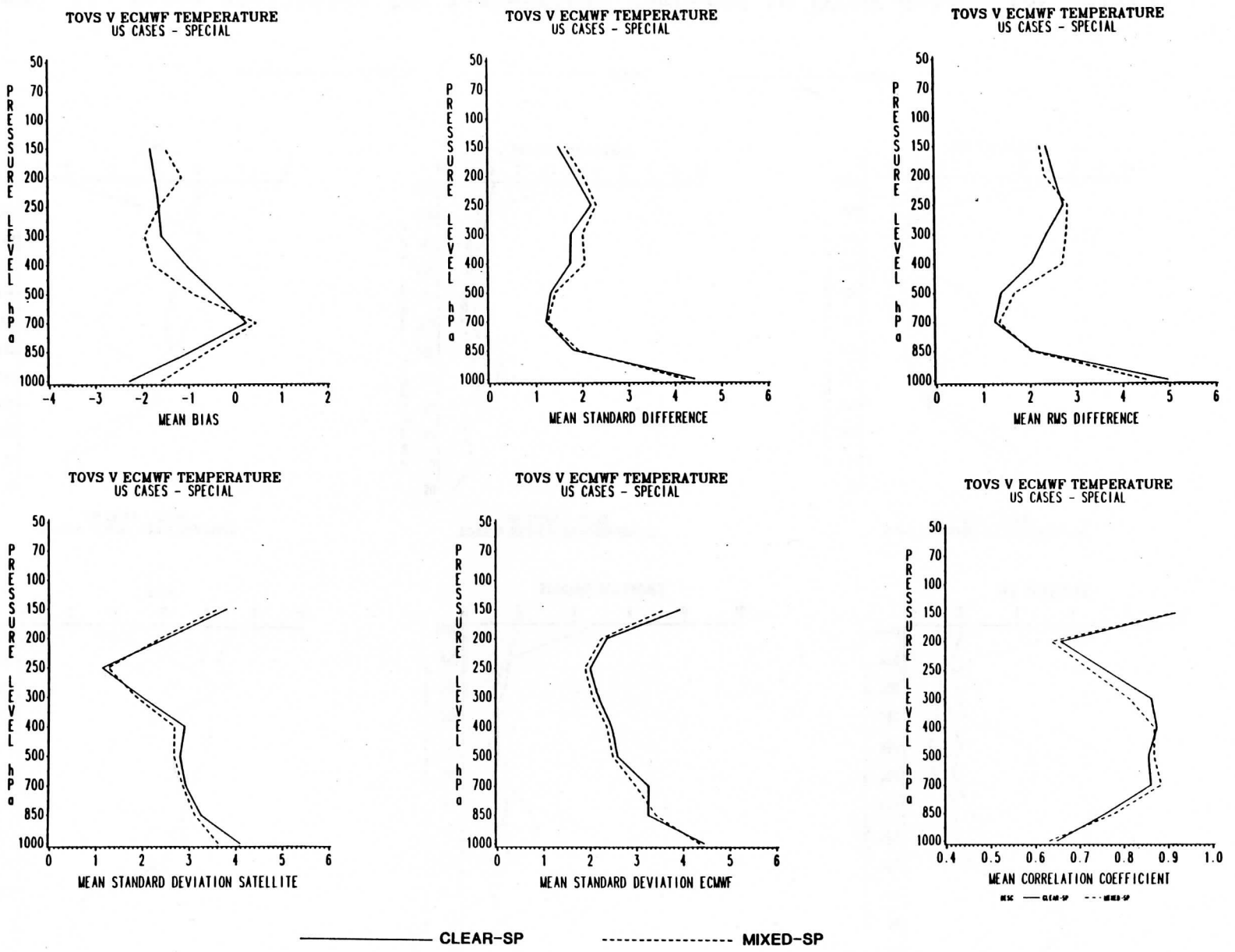

Figure 12: Mean basic statistics for temperature, compared to ECMWF data, for mixed and clear TOVS retrievals for the US case.

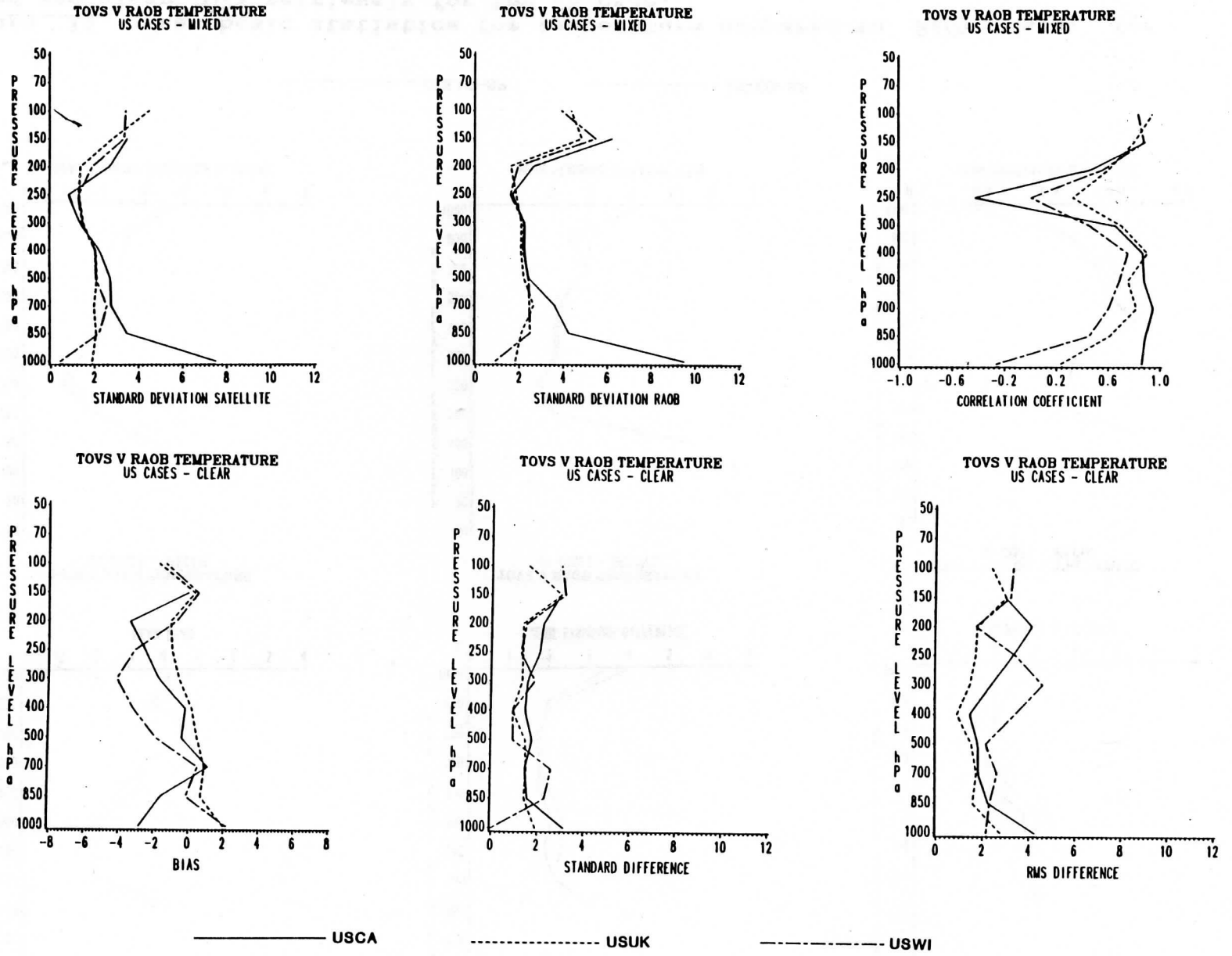

Figure 13. Basic statistics for temperature compared to RAOB data, for mixed and clear TOVS retrievals for the US case.

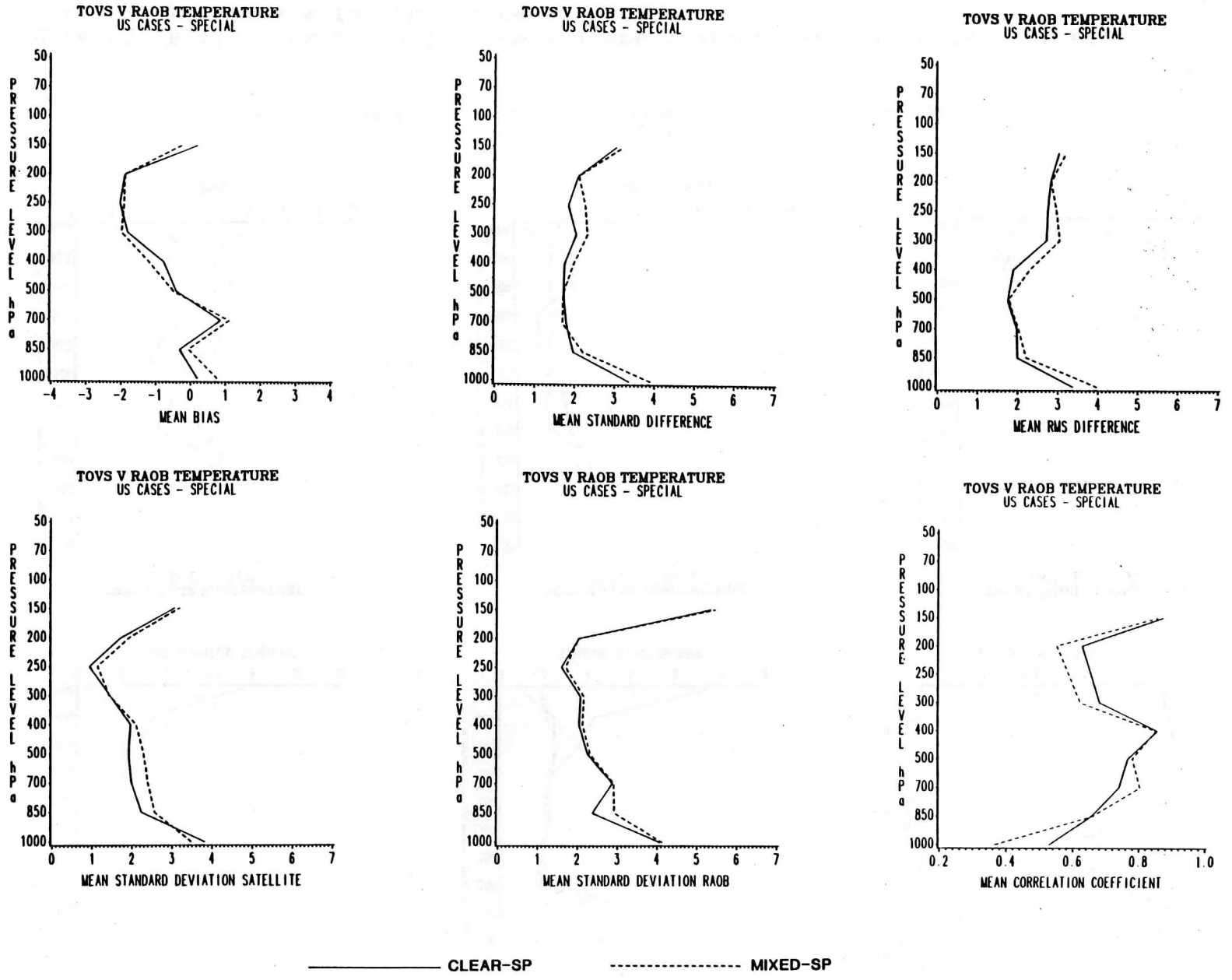

Figure 14. Mean basic statistics for temperature compared to RAOB data, for mixed and clear TOVS retrievals for the US case.

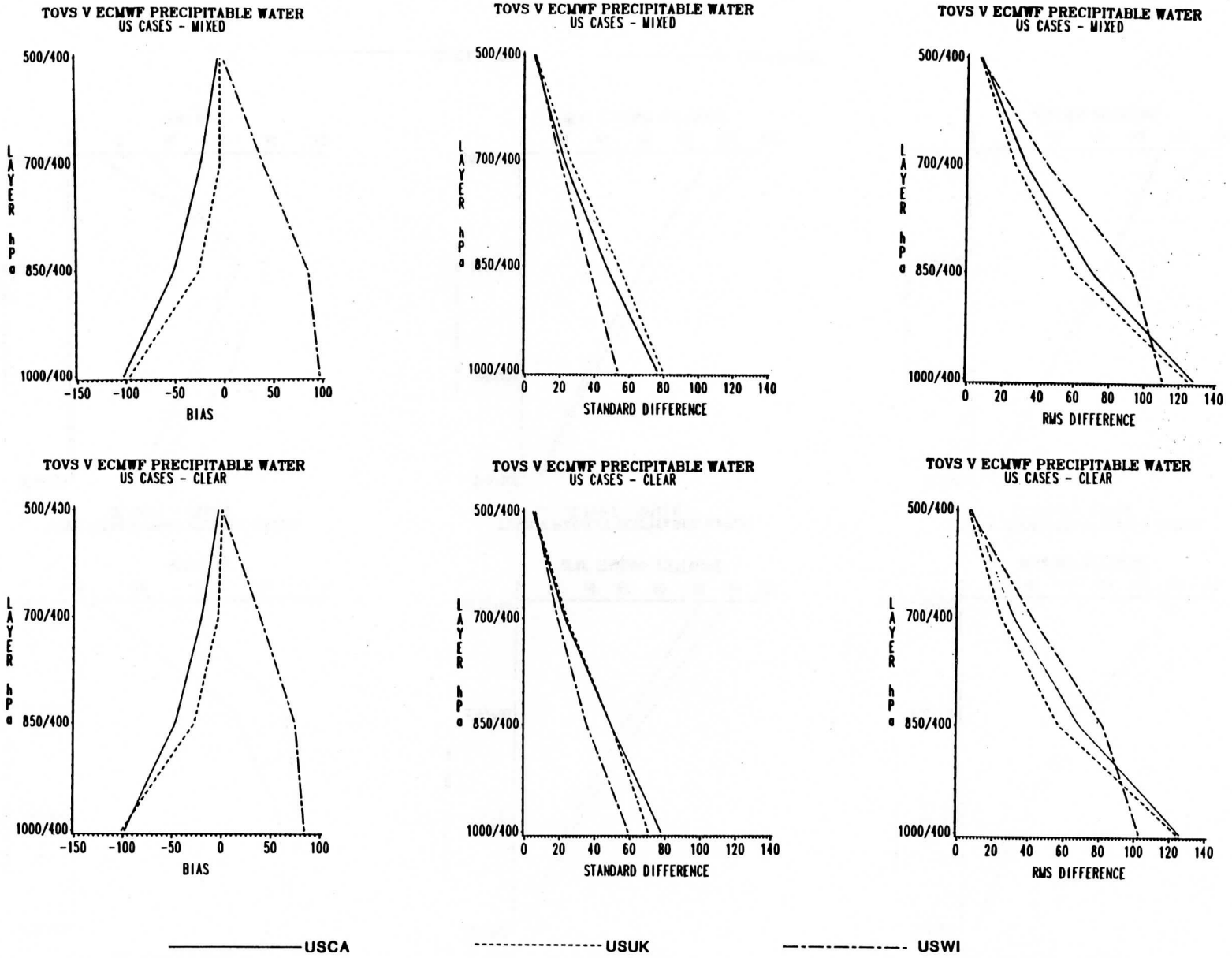

Figure 15. Basic statistics for precipitable water compared to ECMWF data, for mixed and clear TOVS retrievals for the US case.

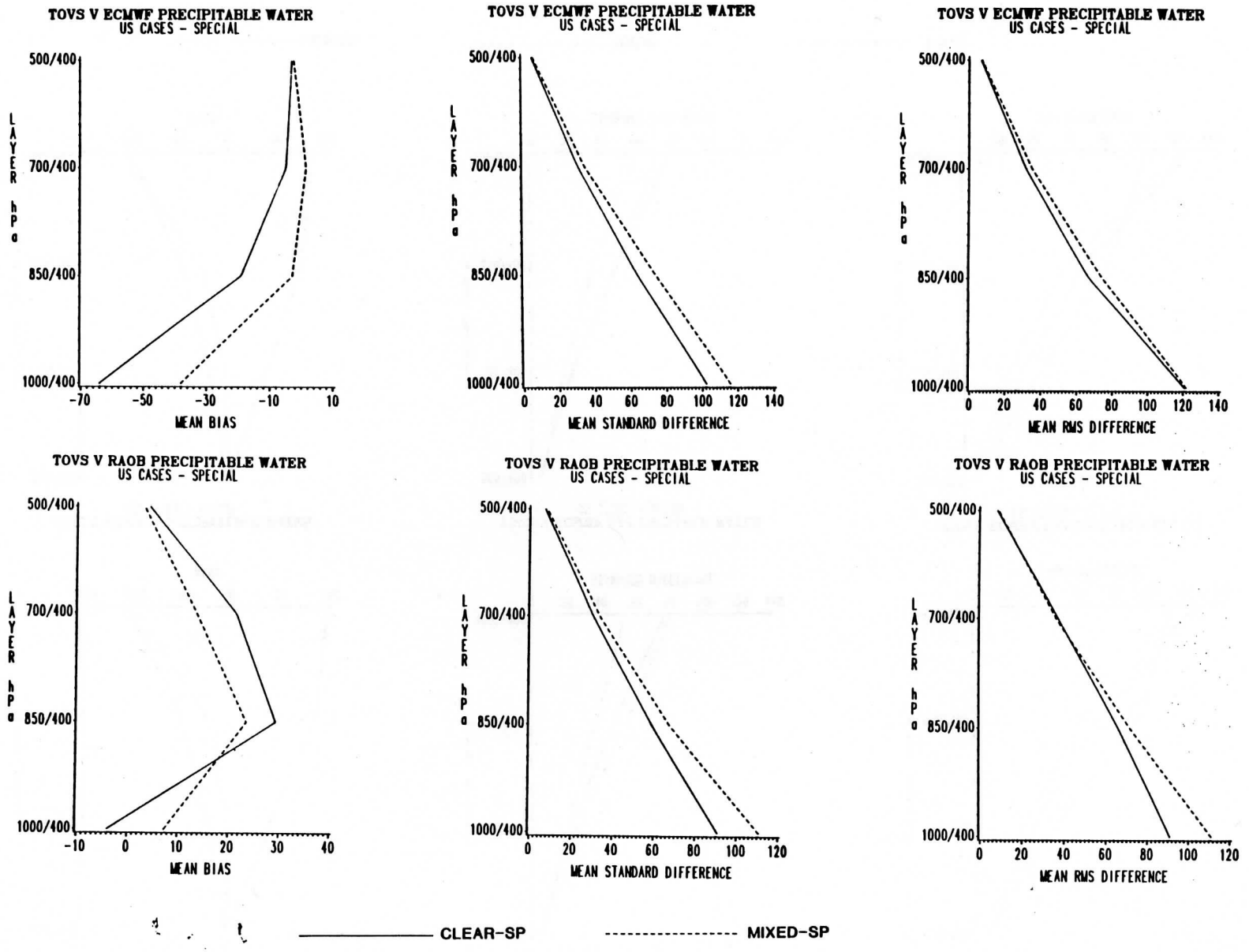

Figure 16. Mean basic statistics compared to ECMWF and RAOB data, for mixed and clear TOVS retrievals for the US case.

A PHYSICALLY BASED OPERATIONAL ATMOSPHERIC SOUNDING SYSTEM FOR THE AUSTRALIAN REGION.

J.F. Le Marshall, R. F. Davidson, M. C. Willmott, P. E. Powers

Bureau of Meteorology
Melbourne, Australia

ABSTRACT

The Australian Bureau of Meteorology has recently implemented a physically based real time TOVS processing system. This provides atmospheric temperature and moisture soundings, surface, ozone and cloud information for the Australian Region. The scheme uses either a statistically based, or an operational numerical weather prediction (NWP) model derived, first guess for temperature and moisture fields. Numerically forecast first guess surface temperature and surface moisture fields are also used. Numerical analysis and prognosis fields are used to control the quality of the processing of radiance data onto meteorological parameters. Instrument bias and transmittance corrections are determined locally. This system has now been running in real time from late 1987 and provides real time data to the ARM system which is used by the National Meteorological Centre and research workers.

1. INTRODUCTION

Since Christmas Day, 1963, when the Australian Bureau of Meteorology (BoM) first received satellite imagery, analysis and forecasting in the Australian region have depended heavily on satellite data. These data have been used continuously by forecasters for operational purposes and also used within the National Meteorological Centre (NMC). From the early 'seventies, use of the data at NMC was via subjective cloud picture interpretation (Guymer, 1978), providing quantitative estimates of MSLP and 1000 - 500 hPa thickness for the operational numerical analysis and prognosis system. In the mid 'seventies, after the utility of satellite vertical temperature profiles was established, clear column radiance data from the VTPR instrument, carried on the NOAA polar orbiting satellites, was processed in NMC and used in the operational hemispheric analysis.

The benefit of profiles from the second generation of sounders on the TIROS-N series of satellites is long established (Kelly et al., 1978 and Bourke et al., 1982) and these data have assumed an ever increasing role in the numerical analysis and prognosis system of the BoM. This role has been enhanced since May, 1980 by the ability to receive and process these data locally in real time (Le Marshall et al., 1985). Initially, the retrieval system involved a statistical procedure closely coupled to the operational analysis and prognosis scheme. The regression

coefficients were determined principally by the latitude of the soundings being produced. This system was later replaced by one which used the microwave radiances and discriminant analysis to select regression coefficients, thereby selecting by synoptic type rather than latitude bands.

In late 1985, partly as a result of a long standing collaborative research program with the University of Wisconsin, the BoM implemented the Australian Region McIDAS (ARM) (Le Marshall et al., 1987). This system was established in such a way that it provided real time access to a very extensive historical and real time data base (the NMC data base). The system also provided an extensive number of application programs to enable use to be made of the data base for operational and research purposes. It was within this environment that this physically based operational atmospheric sounding system for the Australian Region was introduced. The retrievals in this system were made by using a simultaneous solution of the radiative transfer equation similar to that described by Smith et al., 1985, with locally calculated instrument bias and transmittance corrections.

This paper notes the advantages of a physical retrieval scheme compared to a statistical one and the particular advantages of a scheme which provides simultaneous retrieval of temperature and moisture profiles and skin temperature. It describes the retrieval methodology and the salient features of the new real time system. It also provides some verification data and illustrates some of the products produced on the system.

2. THE RETRIEVAL METHODOLOGY

To date, local processing of TOVS data has been done using a statistical retrieval scheme which has used information from the operational analysis / prognosis system to enhance and "quality control" the retrieval process (Le Marshall et al., 1985). The inherent advantages of a physically based retrieval scheme are, however, well known (see for example Smith et al., 1983). These advantages include explicit treatment of surface parameters such as skin temperature, emissivity and elevation, the estimation of cloud height and amount in the processing scheme and the proper treatment of non-nadir radiances to avoid the problems inherent in statistical limb correction (Le Marshall and Schreiner, 1985). With these considerations in mind and noting the results from previous intercomparison studies (Le Marshall, 1985), it was decided to implement a physically based operational retrieval scheme. Being aware of the chance of positive error feedback in some physical solutions which solve for temperature and moisture profile sequentially, and noting the advantages of solving simultaneously for skin temperature and atmospheric temperature and moisture (Smith et al., 1984) a system based on a perturbation solution of the radiative transfer equation similar to that of (Smith et al., 1985) was chosen. Using these methods, the difference between the observed and estimated brightness

ϵ represents cloud emissivity. The effective cloud amount is then given by

$$n\epsilon_i = I_i - I_i^{cl} / \int_{Ps}^{Pc} \tau_i(p) \frac{\partial B}{\partial p} \, dp$$

Several alternative formulations using additional cloud channels are under consideration while the use of AVHRR in the cloud algorithm will be evaluated as soon as real time AVHRR becomes operationally available.

Ozone

Total ozone amount is being calculated in real time using a system similar to that described by Ma et al., 1984. An effort is being made to improve this technique in the Australian Region, by using Dobson spectrophotometer data from Melbourne, Hobart, Brisbane, Perth and Macquarie Island, to provide estimates of total ozone and Umkehr profiles. Ozone sonde flights from Melbourne are also being used.

3. THE OPERATIONAL TOVS DATA UTILIZATION SYSTEM

3.1 Reception and Processing Hardware

TOVS data in Manipulated Information Rate Processor (MIRP) form are acquired directly in digital HRPT format in Melbourne and Perth. These MIRP data contain information from the TOVS package as well as ARGOS, Solar Environment (SEM) and other environmental packages. A schematic diagram showing the groundstations in Melbourne and Perth, their connections to the Fujitsu M180 mainframe in Melbourne and other hardware components in the data utilization system is presented in Figure 1. The data are processed by an automatically scheduled job within the ARM system and the products are put into a cyclic data set for access by NMC and other users within 20 minutes of satellite overpass.

3.2 The Operational Processing System

An overview of the present TOVS processing scheme is given in Figure 2. An ensemble of eleven programs is necessary to fully process the data, using over twenty reference data files to filter and adjust the raw input data into three main production files. The ensemble can be split into three main sections: preprocessing, sounding radiance preparation, and retrieval. The preprocessing is done by the first four programs whose activities are listed in Figure 2. DCP data, which includes buoys, fixed platforms and Antarctic Stations is also processed by this system.

temperature recorded by each channel of the satellite instrument is given by

$$\delta T^* = \delta Ts \frac{\frac{\partial B}{\partial Ts}}{\frac{\partial B}{\partial T^*}} \tau_s - \int_{Ps}^{o} \delta\mu \left[\frac{\partial T}{\partial p} \frac{\partial \tau}{\partial \mu} \frac{\left(\frac{\partial B}{\partial T}\right)}{\left(\frac{\partial B}{\partial T^*}\right)} \right] dp + \int_{ps}^{o} \delta T \left[\left(\frac{\partial \tau}{\partial p} - \frac{\partial \tau}{\partial T}\right) \frac{\frac{\partial B}{\partial (T)}}{\frac{(\partial B)}{\partial T^*}} \right] dp$$

where T, U and B represent temperature, precipitable water and the Planck function respectively.

In addition, τ represents transmittance while the subscript s refers to the surface and T* denotes brightness temperature.

This equation is solved for δu, δT and δTs from the radiance observations, after expressing the perturbation profiles in terms of arbitrary pressure functions, which in this case are the weighting function for HIRS Channels 7, 11 and 12 for the water vapour basis functions and HIRS Channels 1, 3, 7 and MSU Channels 2, 3 and 4 for the temperature profile basis functions.

First Guess

In the operational scheme, the first guess is provided by the operational regional forecast model or regression, using the previous statistical technique which incorporates discriminant analysis. The important first guess surface temperature and moisture fields are derived from the regional optimum interpolation scheme of Keenan et al., 1986. This system uses a modeled diurnal cycle to provide a first guess for surface fields in consecutive three hour analyses.

Transmittances

The basic transmittance functions used by the system are similar to those of Smith et al., 1985. However, a local correction technique is in use. After breaking the radiances into discriminant groups using a method similar to that of Le Marshall et al., 1985, estimates of instrumental bias, a correction to atmospheric transmittance and noise are calculated from the regional satellite and radiosonde match data.

Cloud

In the operational scheme partly cloudy radiances are used to determine the cloud pressure (Pc) which minimizes the expression

$$(I_i - I_i^{cl})\epsilon j \int_{Ps}^{Pc} \tau j(p) \frac{\partial B j}{\partial p} dp - (I_j - I_j^{cl})\epsilon_i \int_{Ps}^{Pc} \tau_i(p) \frac{\partial B_i}{\partial p} dp$$

(after Smith and Platt, 1977), where i and j are typically HIRS Channels 5 and 7. I represents a clear column radiance and

Sounding radiance preparation is achieved by the fifth program. The sixth program is the simultaneous retrieval algorithm described in the previous section which produces skin temperature, atmospheric temperature and moisture profiles, cloud height and amount and total ozone estimates. These are automatically edited using operational analysis and prognosis data. Most of the remaining programs edit and filter the data and also generate wind and geopotential height fields.

The final program provides a TOVS archive procedure and initiates the recording of satellite and sonde match data. These can be used to generate regression coefficients and correction data for the transmittance functions.

4. RESULTS

The new retrieval scheme has been running in real time since late 1987. An example of bias, standard difference and RMS difference plots compared to independent NMC analyses, interpolated to the satellite time, are seen in Figure 3. The retrievals for a recent 500 hPa temperature field and the related independent operational NMC analysis are seen in Figure 4, along with a scatter diagram showing the relationship between the two fields. In general the scheme has performed with few problems during its initial period. It was found necessary, however, during the implementation of the scheme, to locally calculate instrument bias and transmittance corrections to reduce bias and RMS differences. This scheme shows some differences compared to the previous operational scheme, particularly in the moisture and stability fields. A report showing quantative differences between the two schemes will be completed later this year.

Use of the data in NWP has to date consisted of a number of mid-latitude and tropical case studies, using the new regional data assimilation scheme (RASP), (Seaman and Mills, 1988). However, it is anticipated that this assimilation scheme will be operationally implemented in September and will subsequently use data from this new physical retrieval scheme.

Some early indication of the impact of these data on operational analyses may be gained by examination of Figures 5 and 6. Here assimilation analyses generated using the new RASP scheme are presented. Figures 5 (a) and (b) show frontal cross sections for both the NMC operational analysis and an assimilation analysis with the new TOVS data, while 6 (a) and (b) show the 1,000 - 500 hPa thicknesses for the same cases. In both cases the representation is closer to that expected for a summertime cold front when high resolution TOVS data is used.

Verification of cloud data will be assisted by a lidar based observation program planned for July, 1988 while verification of ozone data is well underway. Running values of total ozone for Melbourne from both TOVS and a Dobson spectrophotometer may be seen in Figure 7.

5. CONCLUSION

A physically based atmospheric sounding system designed for operational use has been running in real time since late 1987. Results to date indicate the scheme is robust, free from gross errors and able to produce sounding data of good quality. It has been found necessary to include in the scheme corrections for instrumental bias and atmospheric transmittance. The application of the data to NWP has been examined in a number of case studies and is about to be tested in an operational environment in the BoM's new regional NWP system. Data from the system has also proved useful for several other applications including estimating total ozone and, for instance, for calculating temperature anomalies associated with tropical cyclones (Le Marshall et al., 1988).

6. REFERENCES

BOURKE, W.P., PURI, K. and R. SEAMAN, 1982: Numerical Weather Prediction Studies from the FGGE Southern Hemisphere Data Base. Mon. Wea. Rev. 110, 1787-1800.

GUYMER, L.B., 1978: Operational Application of Satellite Imagery to Synoptic Analysis in the Southern Hemisphere. Technical Report 29, Bureau of Meteorology, Australia.

KEENAN, D.W., DAVIDSON, N.E. and KELLY, G.A., 1986: Screen Level Analyses of Temperature and Dewpoint in the Australian Region. Aust. Meteor. Mag. V34(4).

KELLY, G.A., MILLS, G.A., and SMITH, W.L. 1978: Impact of Nimbus-6 Temperature Soundings on Australian Region Forecasts. Bull. Amer. Meteor. Soc. 59, 393-405.

LE MARSHALL, J.F., 1985: An Intercomparison of Temperature and Moisture Fields retrieved from TIROS Operational Vertical Sounder Data. Technical Proceedings of the Second International TOVS Study Conference, Igls, Australia, 1985. Report from CIMSS, SSEC, University of Wisconsin, Madison, Wisconsin, 53706.

LE MARSHALL, J.F., KELLY, G.A., POWERS, P.E. and DAVIDSON, R.F., 1985: The Operational and Research Processing of TOVS data in the Australian Bureau of Meteorology. The Technical Proceedings of the Third International TOVS Study Conference,Madison, Wisconsin, U.S.A. A Report from the CIMSS, SSEC, University of Wisconsin, Madison, Wisconsin 53706, 224-273.

LE MARSHALL, J.F. and SCHREINER, A.J., 1985: Limb Effects in Satellite Temperature Sounding. J. Clim. and Appl. Meteor., 24, 287-290.

LE MARSHALL, J.F., STIRLING, L.J., DAVIDSON, R.F. and HASSETT, M.J., 1987: The Australian Region McIDAS. Aust. Met. Mag. 35, 55-64.

LE MARSHALL, J.F, KHAW, A., MILLS, G and DAVIDSON, R., 1988: An analysis of the environment about a tropical cyclone using temperature, moisture and wind data sensed by satellite. Proceedings of the Australian Physics of Remote Sensing Conference, Canberra, Feb., 1988

MA, X., SMITH, W.L., WOOLF, H.M., 1983: Total Ozone from the NOAA Satellites - A Physical Model for Obtaining Observations with High Spatial Resolution. JCAM,4

SEAMAN, R.S. and MILLS, G.A., 1988: An Operational Limited Area Data Assimilation System. In preparation.

SMITH, W.L., WOOLF, H.M., HAYDEN, C.M. and SCHREINER, A.J., 1985: The Simultaneous Retrieval Export Package. Technical Proceedings of the Second International TOVS Study Conference, Igls, Austria, 1985, Report from CIMSS, SSEC, University of Wisconsin, Madison, Wisconsin 53706.

SMITH, W.L., and WOOLF, H.M., 1984: Improved Vertical Soundings from an Amalgamation of Polar and Geostationary Radiance Observations. Preprints Volume: Conference on Satellite Meteorology/Remote Sensing and Applications, 25-29, June, 1984, Clearwater Beach, Florida. Published by the American Meteorological Society, Boston, Massachusetts.

SMITH, W.L., WOOLF, H.M., HAYDEN, C.M., SCHREINER, A.J. and LE MARSHALL, J.F., 1983: The Physical Retrieval TOVS Export Package. Tech. Proc. First International TOVS Study Conference, Igls, Austria. A Report from the Cooperative Institute for Meteorological Satellite Studies, Space Science and Engineering Centre, University of Wisconsin-Madison, 352 pp. 227-278.

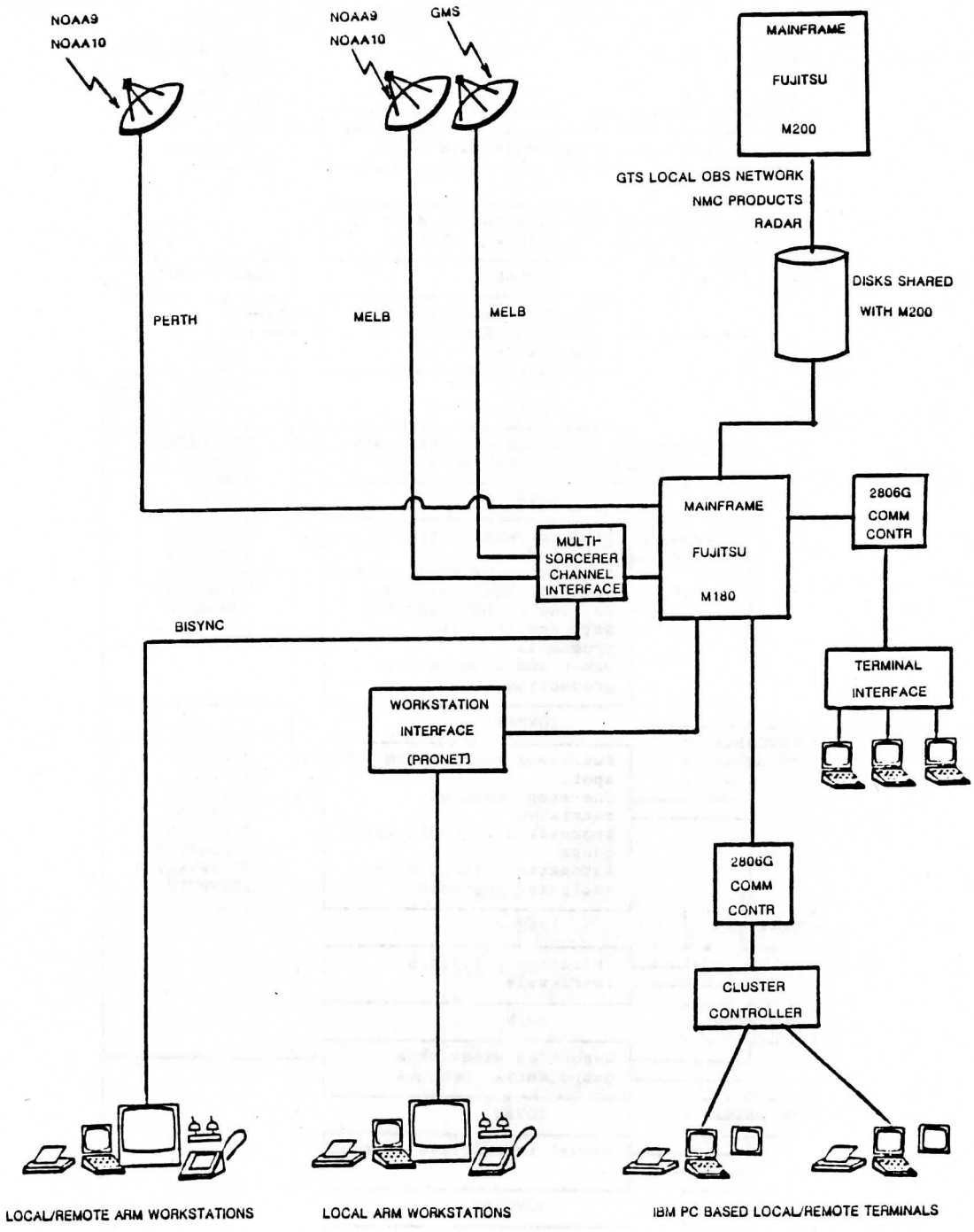

Figure 1

TOVS data utilisation/ARM system diagram.

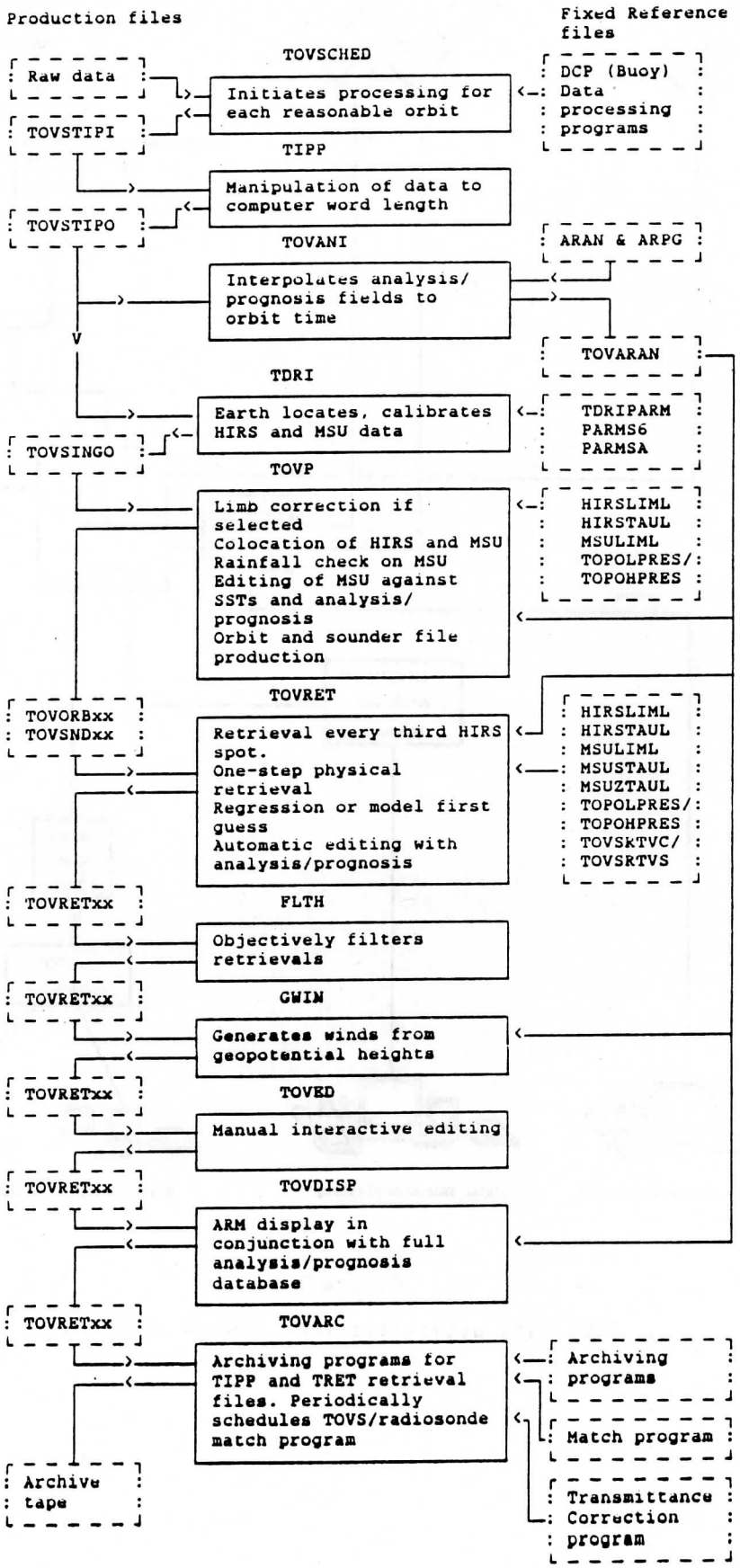

Figure 2

The present TOVS processing scheme.

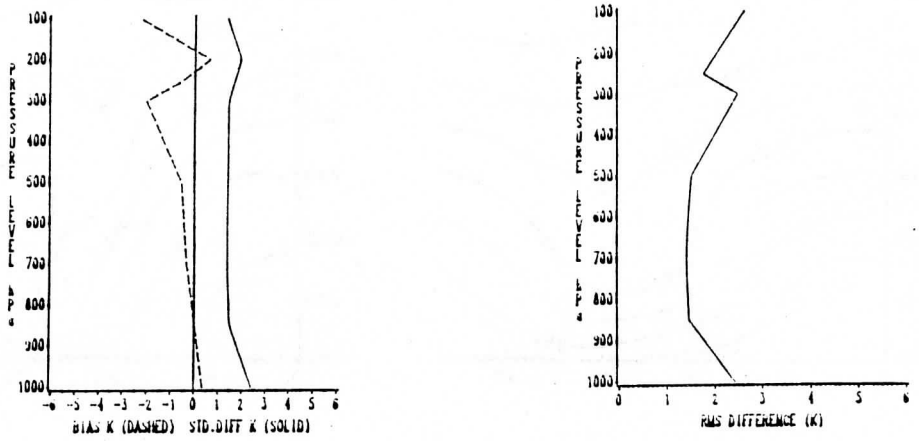

(a) (b)

Figure 3

Bias and standard differences (a) and RMS differences (b) comparing NMC temperature analyses to NOAA 10 for 1-3-88.

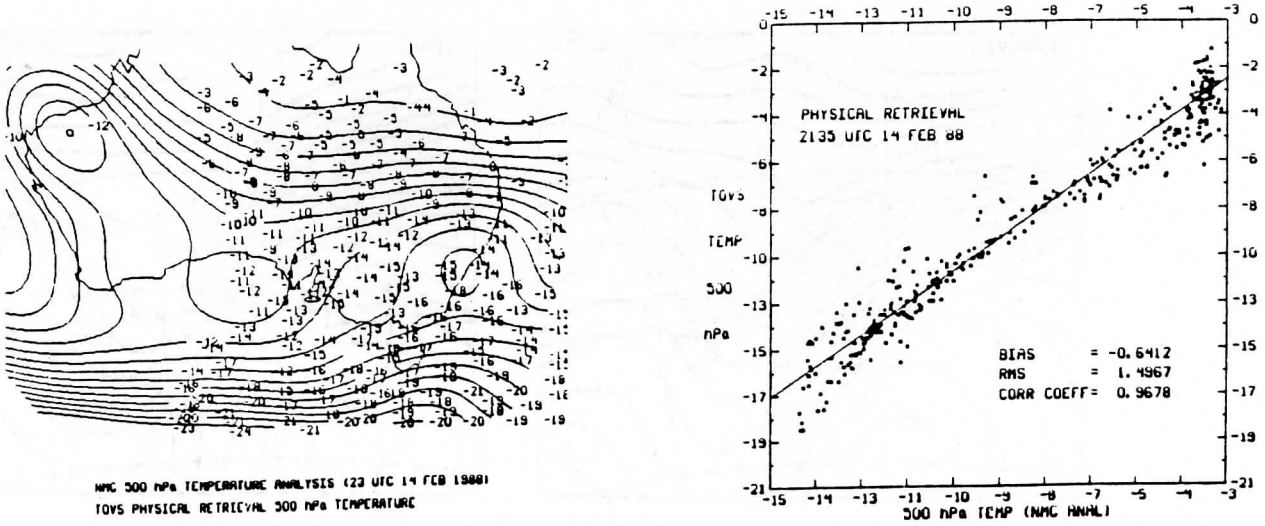

(a) (b)

Figure 4

500hPa TOVS temperature analysis with the related NMC analysis (a) and corresponding scatter diagram and statistics (b).

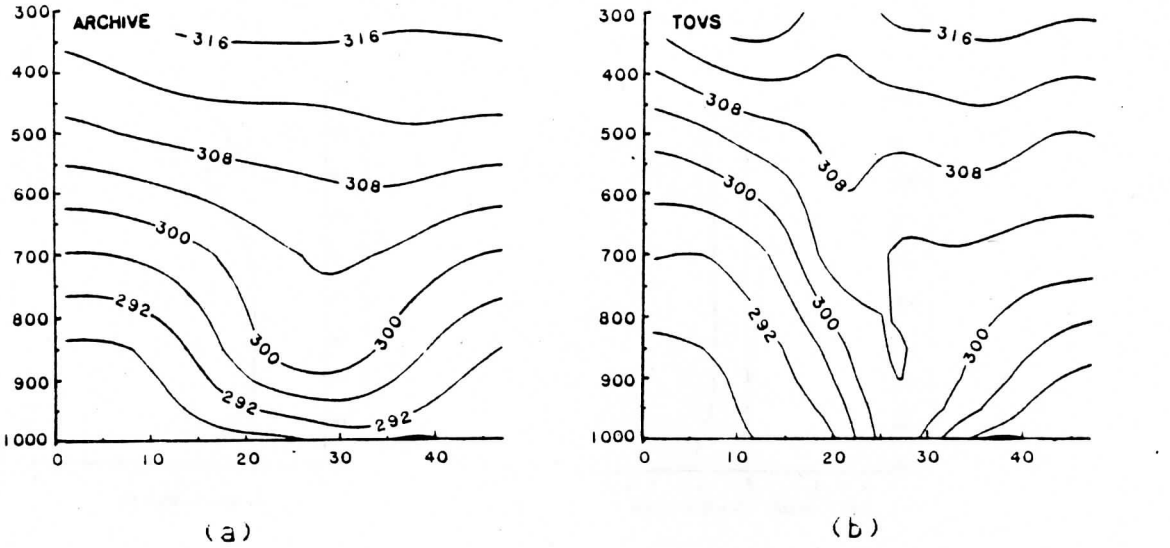

Figure 5

Frontal cross section from the NMC archive (a) and the corresponding assimilation analysis with high resolution TOVS data (b), for 12UTC on 22nd November 1981.

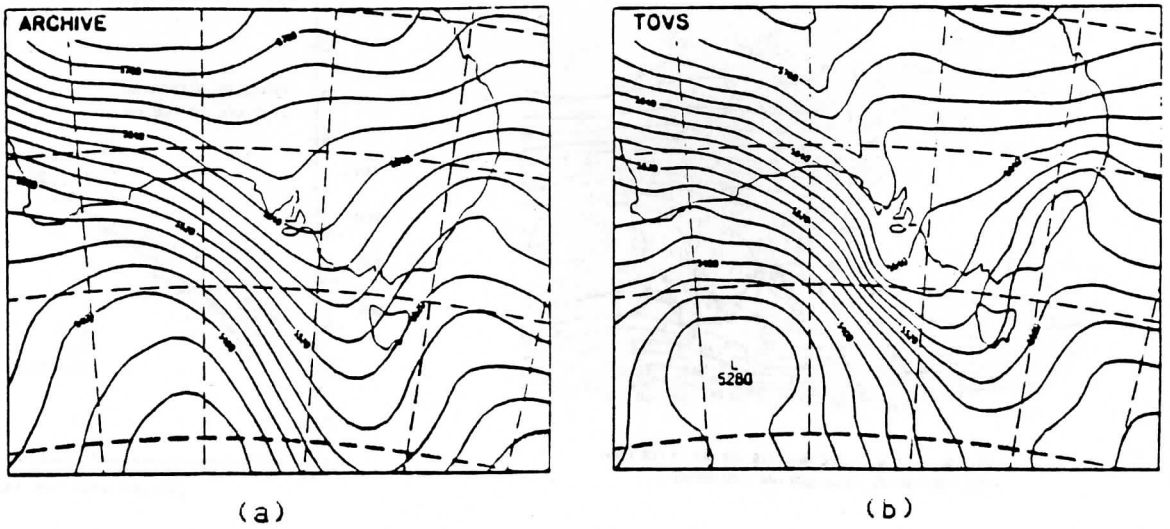

Figure 6

1000-500hPa analyses for the cases noted in figure 5.

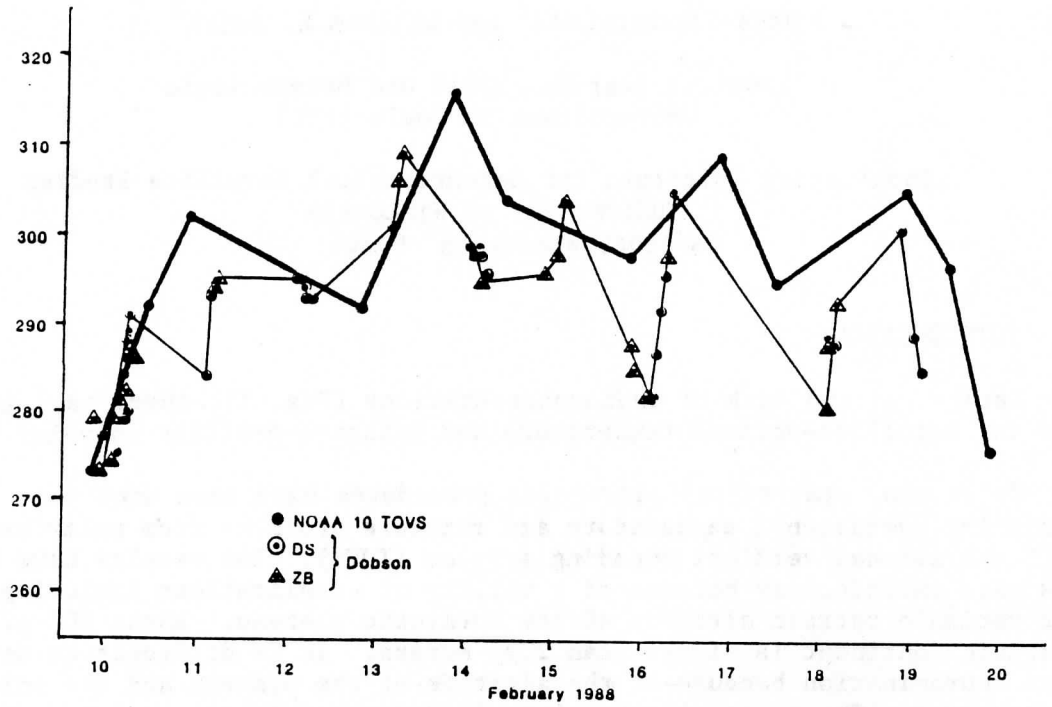

Figure 7

Total Ozone data for Dobson spectrophotometer and NOAA 10 data at Melbourne for the period 10th to 20th February 1988

TOVS OVER POLAR REGIONS

Hans-Joachim Lutz[1] and William L. Smith[2]

[1]Institut fuer Geophysik und Meteorologie
Universitaet zu Koeln (FRG)

[2]Cooperative Institute for Meteorological Satellite Studies
University of Wisconsin
Madison, Wisconsin 63706 USA

1. INTRODUCTION

Because of the lack of radiosonde-stations (Fig. 1), there is a great need for satellite-derived temperature and moisture profiles in polar regions.

Up to now, statistical regression procedures have been used for retrieving operational temperature and moisture profiles from polar orbiting TIROS operational vertical sounding systems (TOVS). The results have been less than satisfactory because of a variety of complications including the high variable terrain altitude of the Antarctic plateau. About 80% of the Antarctic continent is higher than 2000 meters. It is difficult to detect cloud contamination because of the altitude of the plateau and the cold temperatures. There are also problems in detecting temperature inversions, which are often found in polar regions.

In this paper, improvements are made in using the simultaneous TOVS retrieval algorithm (Huang and Smith, 1986) in polar regions. Results from the modified procedure are compared with radiosonde profiles for several orbits over southern polar regions (December 1 and 21, 1987; February 4, 1988), and for one orbit over northern polar regions (February 4, 1987). The retrieved temperature profiles show a good agreement with radiosonde profiles, especially in the troposphere.

2. CLIMATE OF THE ANTARCTIC CONTINENT

The Antarctic continent is a cold desert. For example, the plateau station VOSTOK has an annual mean temperature of -60°C with a precipitation of 30mm per year. The coastal area is much warmer (-10°C to -20°C) and has also more precipitation.

Some other features of the Antarctic climate are the coreless winter and pointed summer. Coreless winter means that the temperature is nearly constant during the winter from the end of March to the end of September, especially on the plateau. Very often, katabatic winds transport cold air down to the coast. In the winter, the temperature profiles show strong inversions. At the end of winter, the continent is surrounded by an ice-area of about 18.8 million square kilometers. The short summer reaches its highest temperature in the beginning of January. On the plateau, the summer starts in mid-December and ends in mid-January. After reaching the peak, the temperature drops until the winter starts again at the end of March (Fig. 2). In summer, small inversions are found on the plateau. The sea-ice surrounds only parts of the continent, especially on the Weddell Sea. The surface air pressure

shows a circumpolar pattern. A trough surrounds the continent between 60°S and 73°S. Over the plateau, a stationary high pressure area is found. The climate of the Antarctica is described in more detail by Schwerdtfeger (1984).

The features of the polar climate provides an indication of what to expect from satellite measurements. In particular, the high terrain of the plateau and the temperature inversions cause problems. Because of the dry atmosphere over polar regions, it is expected that channel 8 (11.1 micron, atmospheric window) and channel 10 (8.3 micron, water vapor of the lower troposphere) will show approximately the same brightness temperature.

3. CALIBRATION AND DATA VALIDATION

At the beginning, an attempt was made to validate the ITPP-3 in polar regions. The package was used without any changes, except for the acknowledgment of high altitude terrain. A radiosonde profile from this area was used as a first guess. The retrieved temperature profile was compared with the original radiosonde. The results can be seen in Figs. 3 and 4.

Afterwards several radiosonde profiles from polar stations were used to calculate brightness temperatures using the radiative transfer equation. These calculated brightness temperatures were compared with measured brightness temperatures to test the calibration algorithm and validation of the transmission functions. As shown in Table 1, there are significant differences in several channels. For the window channels 18 and 19 (4.0 and 3.7 micron) reflected sunlight causes these large differences. Because of the high altitude of the Antarctic plateau (at cloud level 1) and the ice and snow coverage, the 4.5 micron channels 13 to 17 are also contaminated with reflected sunlight. This causes an inconsistency of the 4.5 micron channels compared with the 15 micron channels. Therefore, the 4.5 micron channels are inappropriate for retrieving temperature profiles in polar regions during daylight.

For channels 1 and 2 (15 micron, upper atmosphere), it is difficult to compare measured and calculated brightness temperatures. Very often, the radiosondes reach only the 20 hPa level. Therefore, it is necessary to use temperature values from a polar standard atmosphere to interpolate the missing levels. Nevertheless, it seems that a gamma adjustment of the transmission function (Tau=Tau**Gamma) is useful because the measured brightness temperatures are always higher than the calculated values. This means that the peaks of the weighting function in channels 1 and 2 are at a higher (warmer) level.

Comparisons between retrieved profiles and radiosonde profiles show that a change of the transmittances using a gamma adjustment is required for channels 6 and 7 (15 micron, lower troposphere).

Another large discrepancy is observed between channel 10 (8.3 micron, water vapor in the lower troposphere) and channel 8 (11.1 micron, atmospheric window). Because of the dry atmosphere in polar regions, it is expected that channel 10 will have nearly the same temperature as channel 8. But as soon as the surface temperatures are below 250 Kelvin, the brightness temperature of channel 10 is higher than in channel 8. This fault is caused by using the space view in the calibration procedure. The TOVS calibration procedure shows

that, by using space view and warm blackbody temperatures, the calculated cold blackbody temperatures for all channels are too warm compared with the actual blackbody temperature. For channel 10, this temperature is much too warm (Table 2). After changing the calibration procedure (i.e., using the cold and warm blackbodies), the brightness temperature in channel 10 is not only consistent with the brightness temperature in channel 8, but also the comparison with the calculated brightness temperature from the radiosonde profiles shows an agreement within 1 Kelvin (Table 3).

4. RETRIEVAL RESULTS

The results from the modified procedure are compared with radiosonde profiles for several orbits of NOAA-10. Three orbits over the southern polar regions (December 1 and 21, 1987; and February 4, 1988), and one orbit over the northern polar regions (February 4, 1988) are chosen. The time of the satellite overpass is near the launch time of radiosondes (00z and 12z).

After the improvements described above were made, a radiosonde profile again was used as a first guess. As it is shown in Figs. 5 and 6, the retrieved profile and the radiosonde profile are in agreement as should be expected. Only the moisture profile shows some significant differences.

With a regression first guess, the errors in the retrieved profile are much larger (Fig. 7). Using a special climatology profile in southern polar regions (south of 60°S) as a first guess, the results become more acceptable (Fig. 8). This is also shown for coastal stations (Figs. 9 and 10). Only in the high atmosphere are larger differences between retrieved profiles and radiosondes found.

For retrieving temperature and moisture profiles over all chosen orbits, the climatology profiles were used as a first guess. In northern polar regions, good agreement between retrieved profiles and radiosondes is also found (Figs. 11 and 12).

After retrieving temperature and moisture profiles, the 500 hPa and 200 hPa heights were calculated. The radiosonde stations were located in the orbit (Fig. 13) and the retrieved and measured heights were compared. As can be seen, there are still problems with the navigation near the pole. Figures 14 and 15 show the results for 500 hPa and 200 hPa, respectively. The heights calculated from satellite measurements are within 100 meters of the radiosonde measurement.

5. SUMMARY

The physical simultaneous retrieval approach has been modified to operate in polar regions. Because of discrepancies in observed radiances arising from the space view, the calibration procedure was altered to use only cold and warm blackbody views. The calculated transmittances have been tuned using gamma adjustments. Because of the reflected sunlight problem, channels 13 to 17 (4.5 micron) and channels 18 and 19 (4.0 and 3.7 micron) are not used in the retrieval algorithm. A special climatological profile is used as a first guess in southern polar regions (south of 60°S).

The results from the modified procedure are compared with radiosonde profiles for several orbits over southern polar regions (December 1 and 21, 1987; February 4, 1988) and one orbit over northern polar regions (February 4, 1988). The retrieved temperature profiles are within 2 Kelvin of the radiosonde measurements over most of the troposphere and they are less accurate in the higher atmosphere.

6. REFERENCES

Schwerdtfeger, W., 1984: Weather and climate of the Antarctic. Devel. Atmos. Sci., 15, Elsevier.

Smith, W. L., H. M. Woolf, C. M. Hayden, A. J. Schreiner, J. M. LeMarshall, 1983: The physical retrieval TOVS export package. Tech. Proc. of the First International TOVS Study Conf., W. P. Menzel (ed.), 227-278.

Smith, W. L., H. M. Woolf, C. M. Hayden, A. J. Schreiner, 1985: The simultaneous retrieval export package. Tech. Proc. of the Second International TOVS Study Conf., W. P. Menzel (ed.), 224-253.

Smith, W. L., H.-L. A. Huang, 1986: An extension of the simultaneous TOVS retrieval algorithm - the inclusion of cloud parameters. Tech. Proc. of the Third International TOVS Study Conf., W. P. Menzel, (ed.), 118-130.

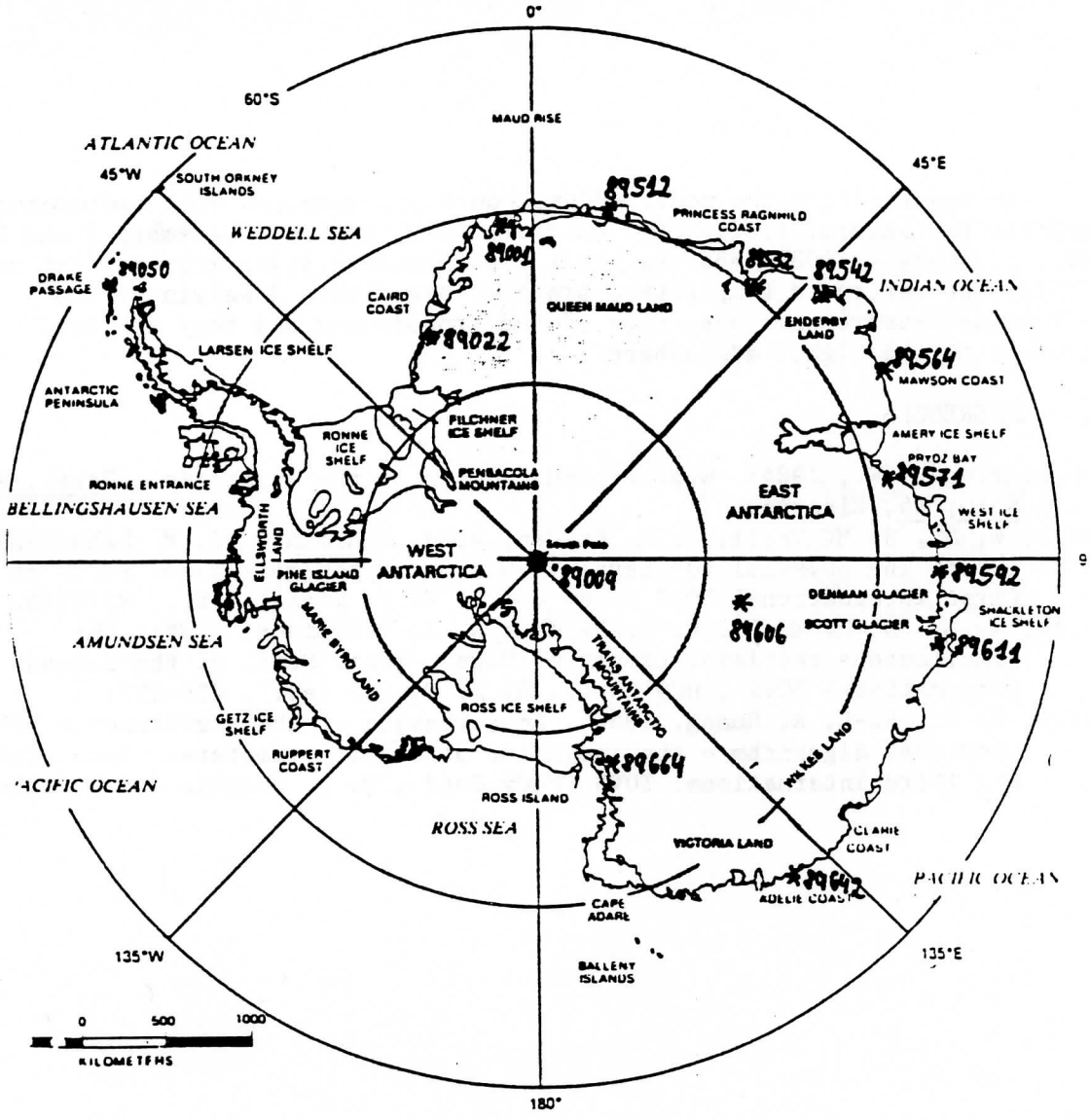

Fig. 1. The antarctic continent with the location of the radiosonde stations.

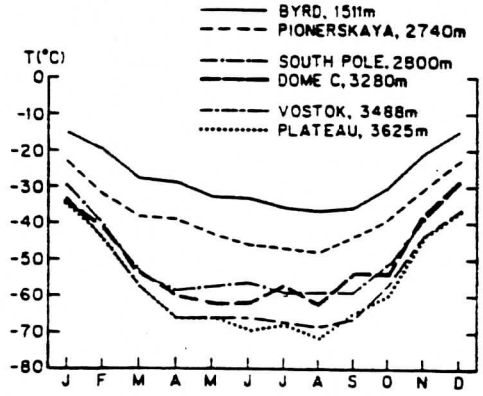

Fig. 2. Annual course of surface temperature at several antarctic stations.

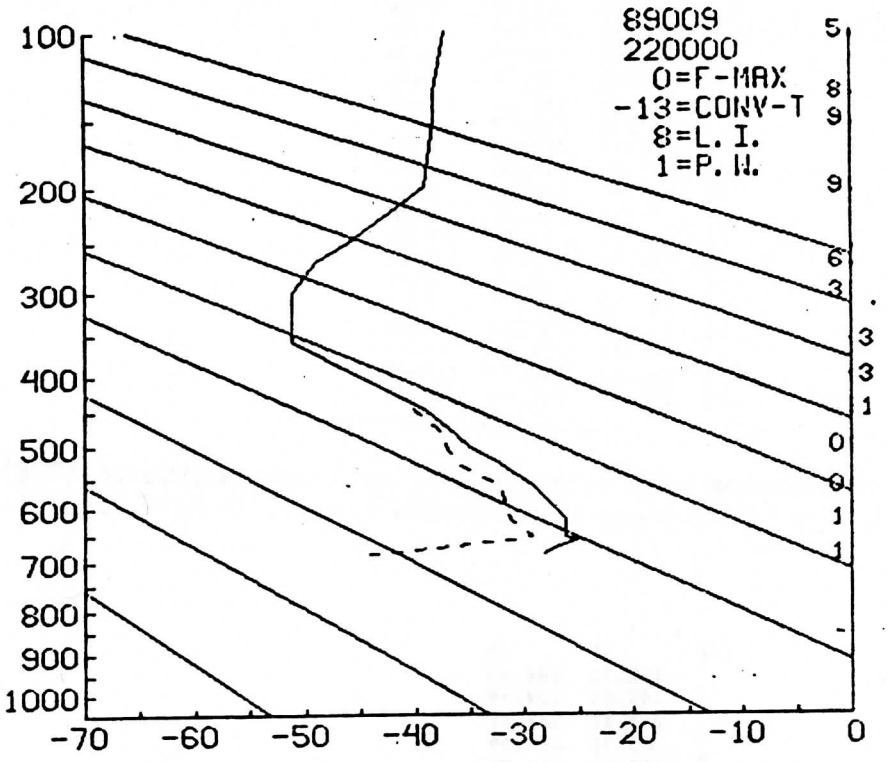

Fig. 3. Radiosonde profile from December 22, 1987 (time: 00z). Station: 89009 (Southpole).

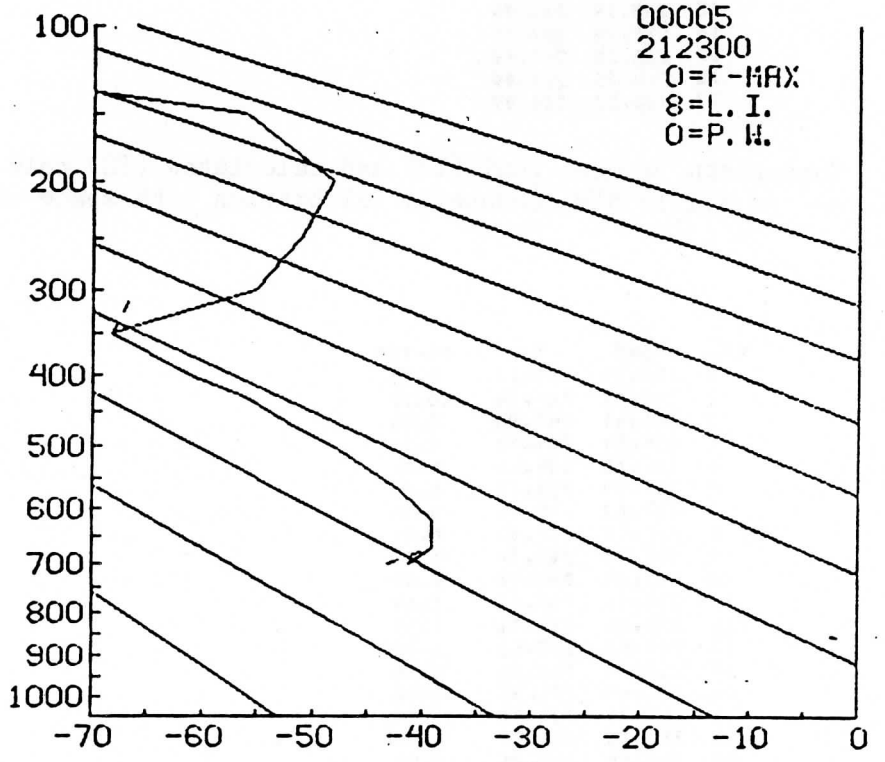

Fig. 4. Retrieved profile, orbit from December 21, 1987 (time: 23z). First guess: RAOB profile.

CH.	TSAT	TBB	TN-TBB
1	257.61	248.77	8.84
2	245.17	242.73	2.44
3	242.07	240.99	1.08
4	236.74	236.00	0.74
5	237.53	236.77	0.76
6	237.32	237.12	0.20
7	239.31	239.72	-0.41
8	242.04	242.03	0.01
9	243.94	242.04	1.90
10	243.69	241.19	2.50
11	238.38	238.14	0.24
12	231.60	232.73	-1.13
13	241.08	238.03	3.05
14	236.59	235.78	0.81
15	237.72	235.55	2.17
16	243.34	237.82	5.52
17	261.12	254.35	6.77
18	260.83	241.42	19.41
19	274.81	241.86	32.95

Table 1. Comparison between measured (TSAT) and calculated (TBB) (from radiosonde data) brightness temperatures for all 19 HIRS channels.

CH	TG	TM
1	265.15	264.99
2	265.05	264.99
3	265.16	264.99
4	265.21	264.99
5	265.24	264.99
6	265.27	264.99
7	265.28	264.99
8	265.28	264.99
9	265.39	264.99
10	265.94	264.99
11	265.19	264.99
12	265.14	264.99
13	265.27	264.99
14	265.22	264.99
15	265.19	264.99
16	265.24	264.99
17	265.25	264.99
18	265.26	264.99
19	265.30	264.99

Table 2. Comparison between real (TM) and calculated (TG) cold blackbody temperatures for all 19 HIRS channels; calibration with space view and warm blackbody.

CH.	TSAT	TBB	TN-TBB
1	256.96	253.17	3.78
2	244.82	244.94	-0.12
3	241.61	240.98	0.63
4	235.99	235.97	0.02
5	236.75	236.64	0.11
6	236.59	236.59	0.00
7	238.62	238.96	-0.34
8	241.34	241.33	0.01
9	242.91	241.34	1.57
10	241.24	240.55	0.69
11	237.81	236.32	1.49
12	231.10	229.71	1.39
13	239.97	237.63	2.34
14	235.24	235.54	-0.30
15	236.40	235.49	0.90
16	242.36	237.82	4.54
17	260.75	254.35	6.41
18	260.49	240.76	19.73
19	274.71	241.18	33.53

Table 3. Comparison between measured (TSAT) and calculated (TBB) (from radiosonde data) brightness temperatures for all 19 HIRS channels after the improvements were made.

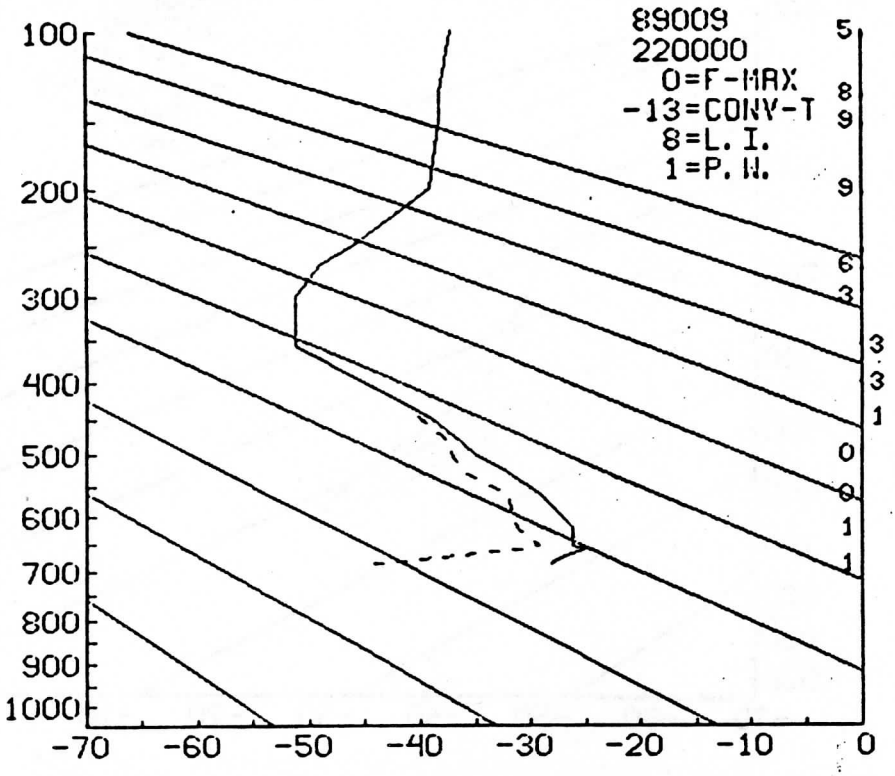

Fig. 5. Radiosonde profile from December 22, 1987 (time: 00z). Station: 89009 (Southpole).

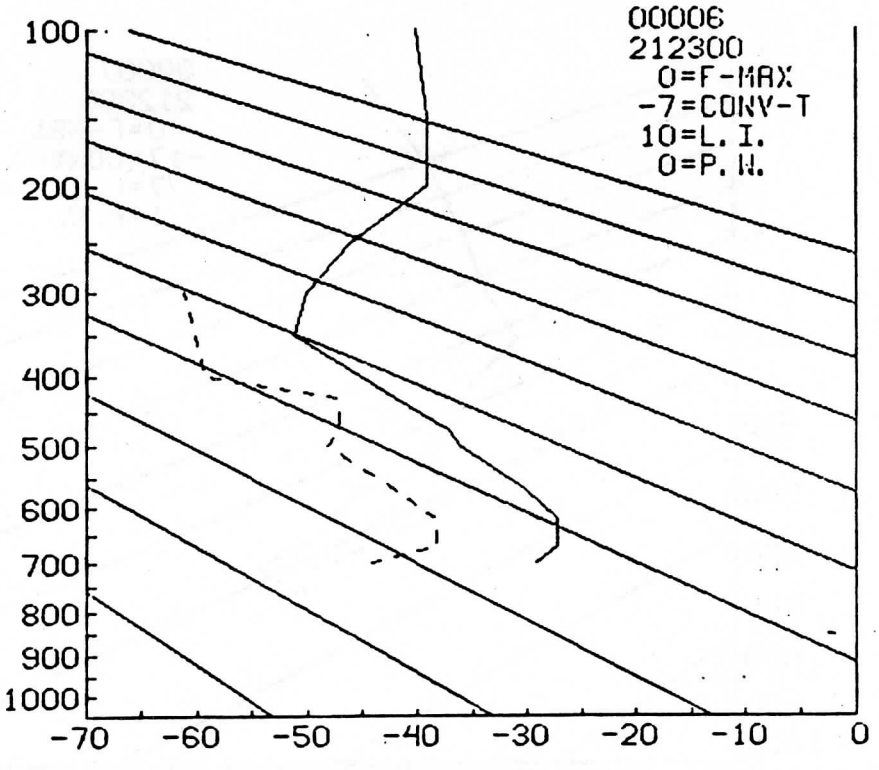

Fig. 6. Retrieved profile after changes were made. Orbit from December 22, 1987 (time: 23z). First guess: RAOB profile.

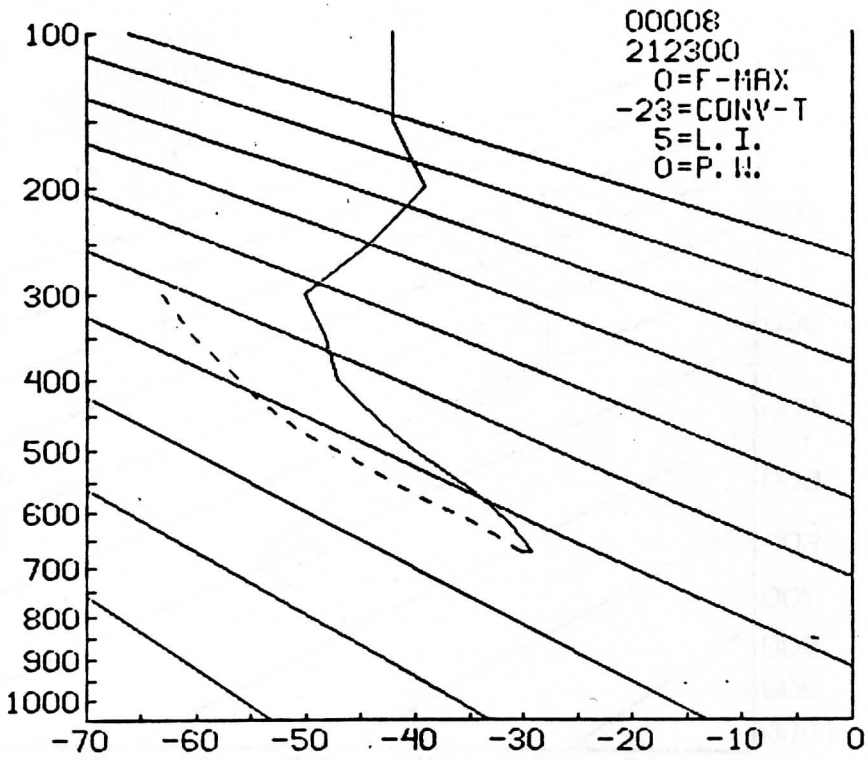

Fig. 7. Retrieved profile like in Fig. 6, but with a regression first guess.

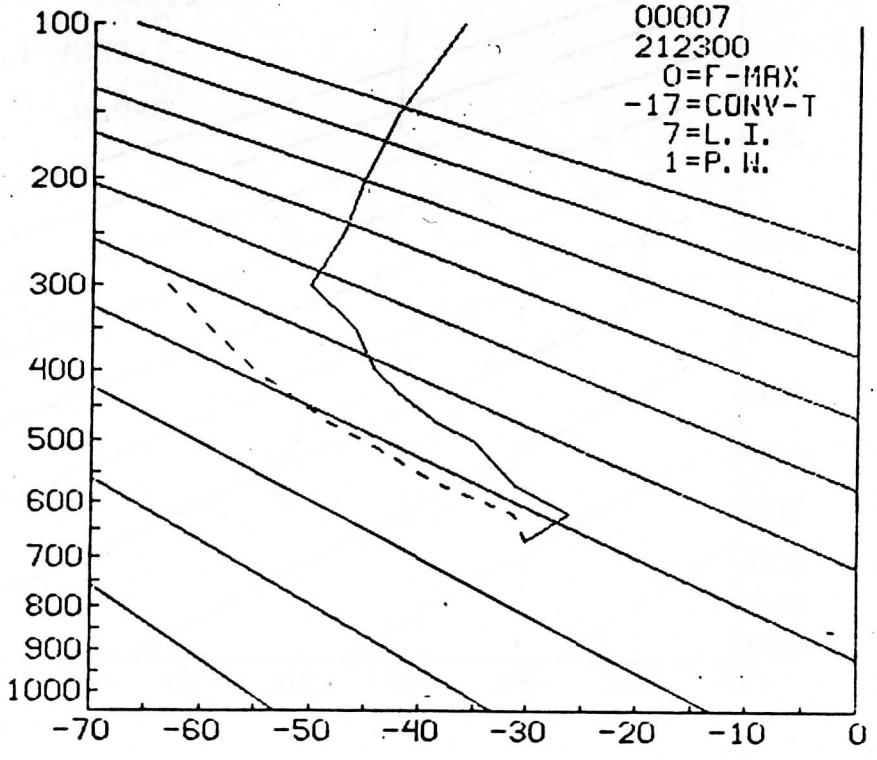

Fig. 8. Retrieved profile like in Fig. 6, but with a climatological profile as a first guess.

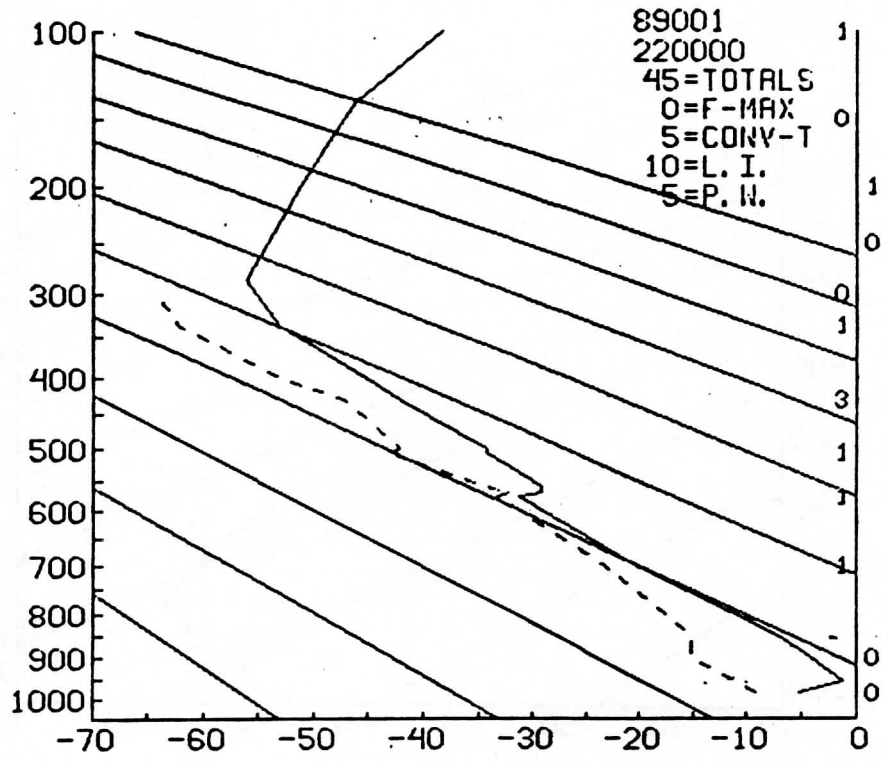

Fig. 9. Radiosonde profile from December 22, 1987 (time: 00z). Station: 89001 (SANAE).

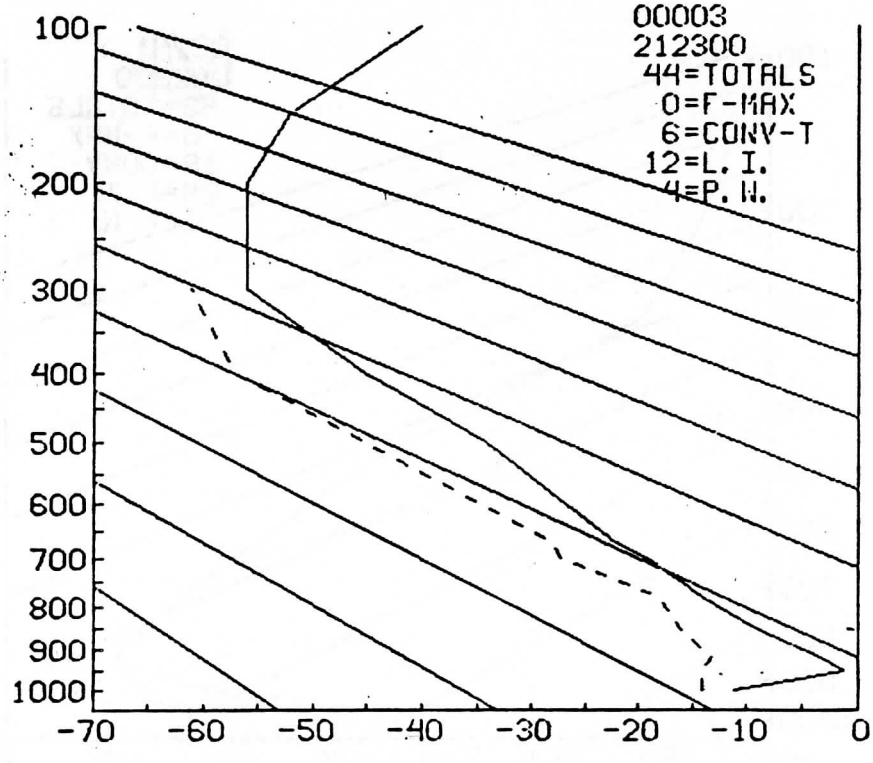

Fig. 10. Retreived profile, orbit from December 22, 1987 (time: 23z). First guess: climatological profile.

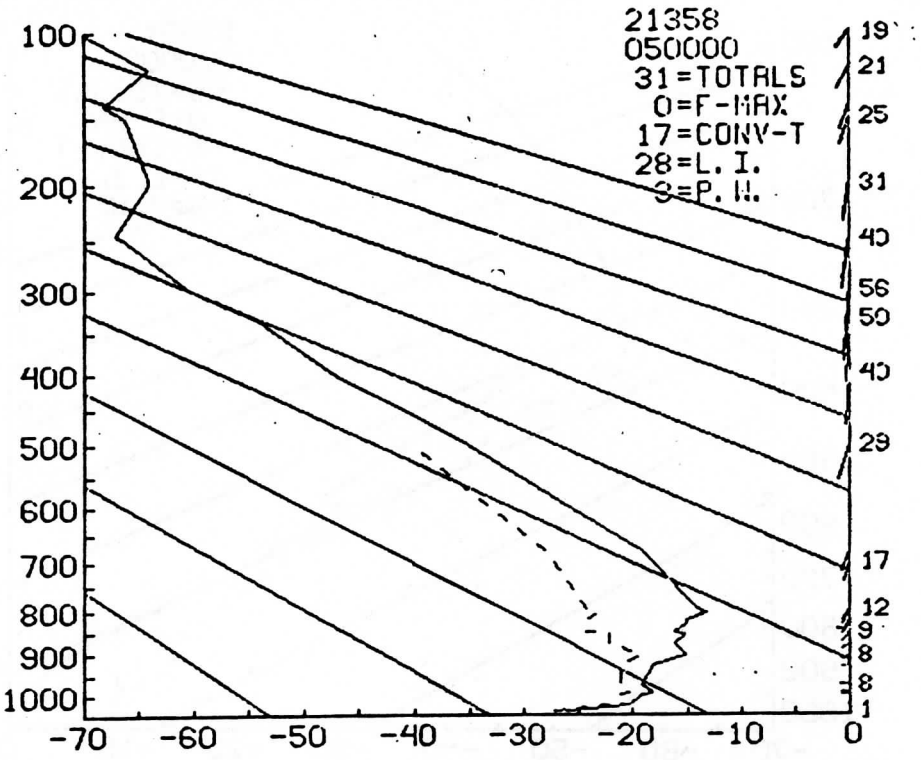

Fig. 11. Radiosonde profile from February 5, 1988 (time: 00z). Station: 21358 (northern Siberia).

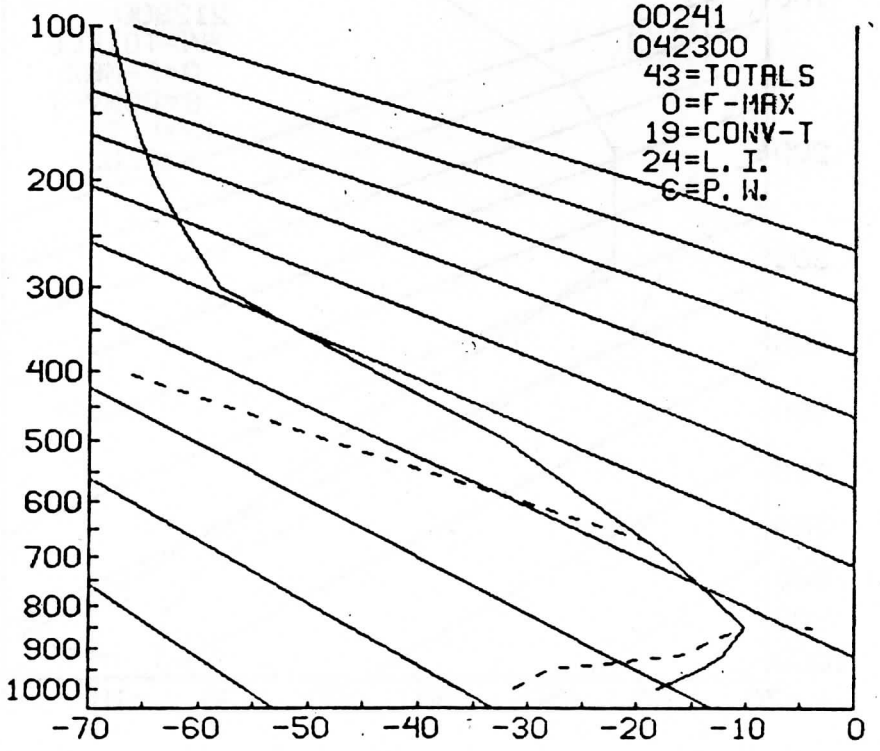

Fig. 12. Retrieved profile, orbit from February 4, 1988 (time: 23z). First guess: climatological profile.

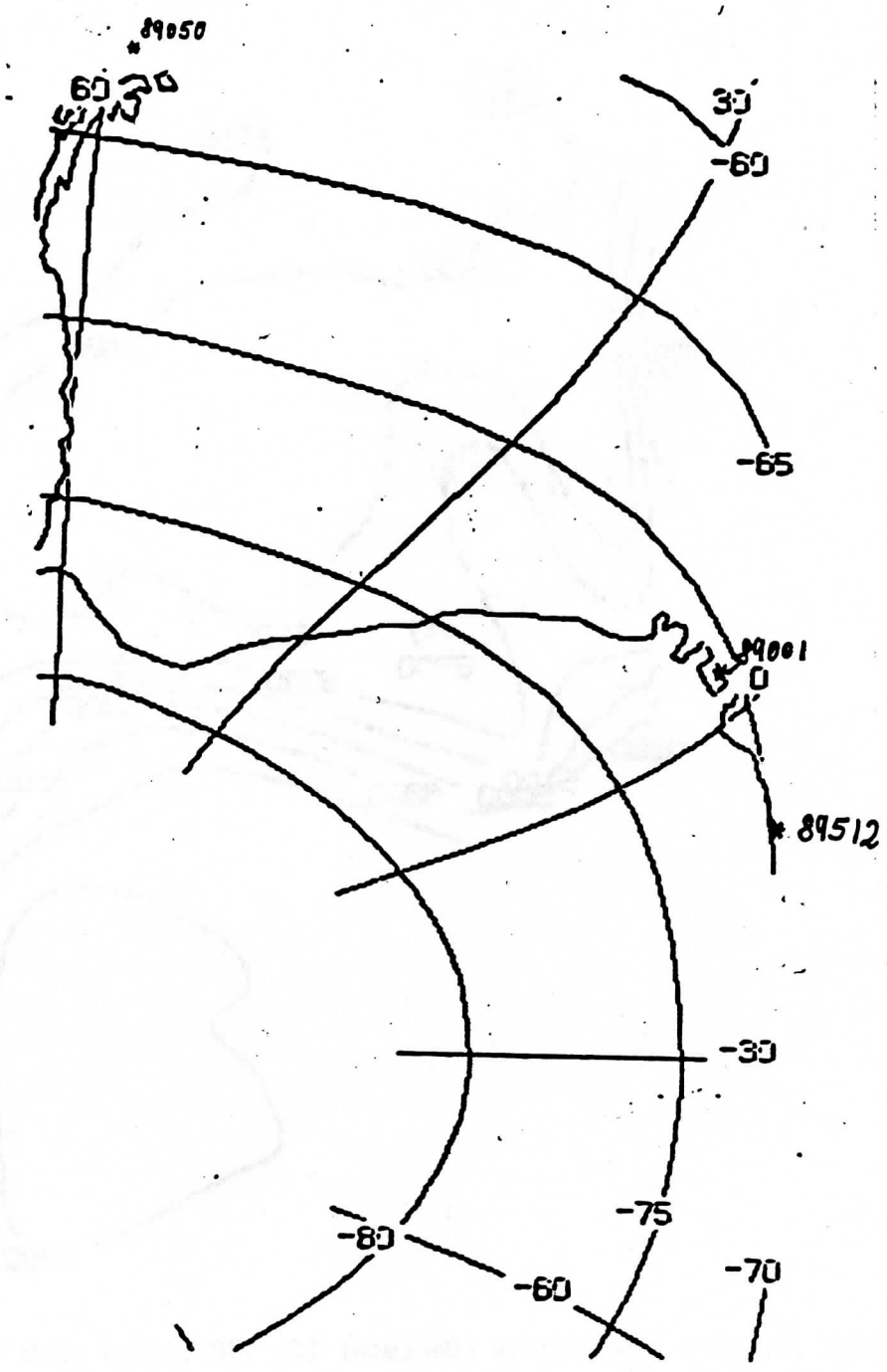

Fig. 13. Location of the orbit from December 21, 1987 (time: 23z) over the Antarctic region and the location of Station 89001 SANAE, Station 89050 Bellinghausen, Station 89512 Novolazar.

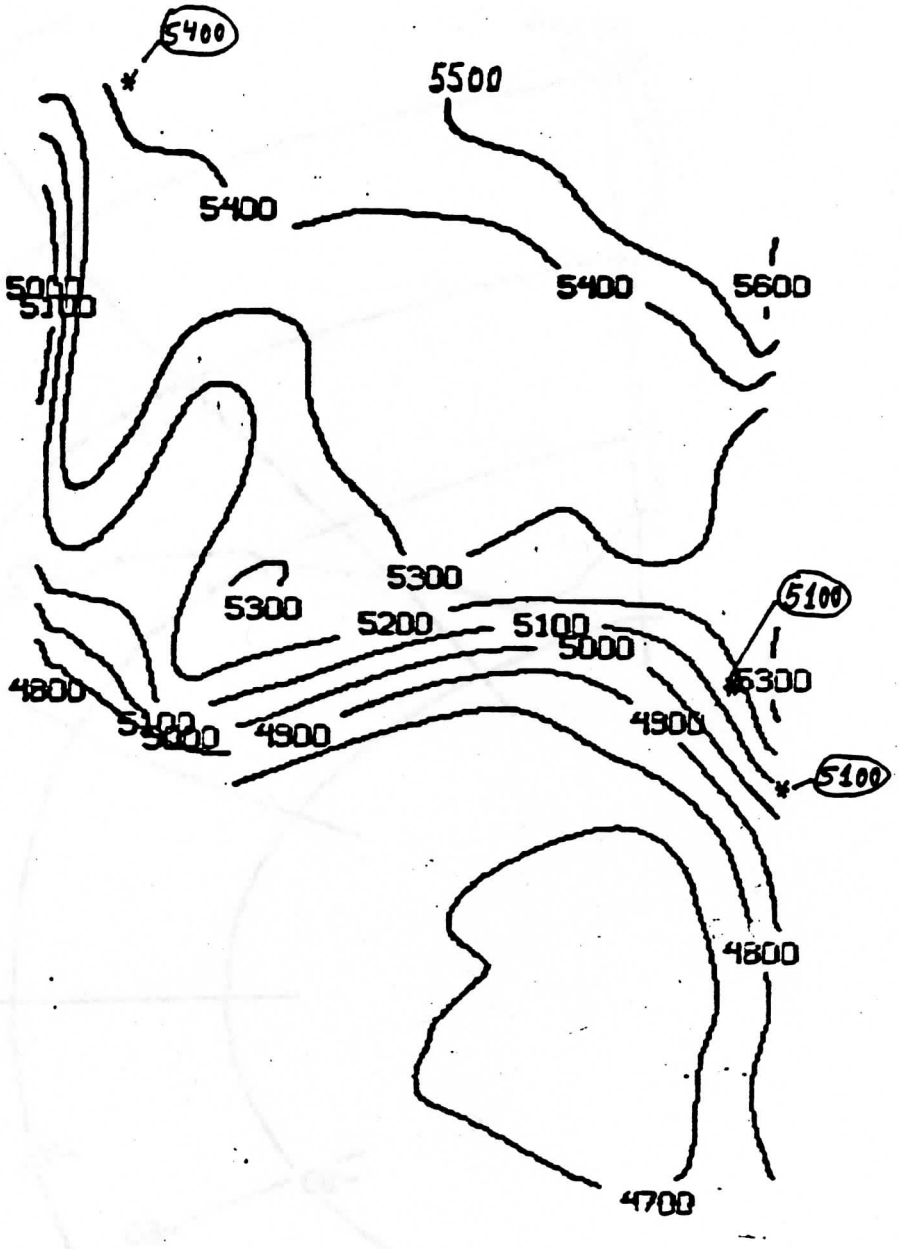

Fig. 14. 500 hPa heights (December 22, 1987, 23z) with the location and results of the three radiosonde stations (encircled) in that area.

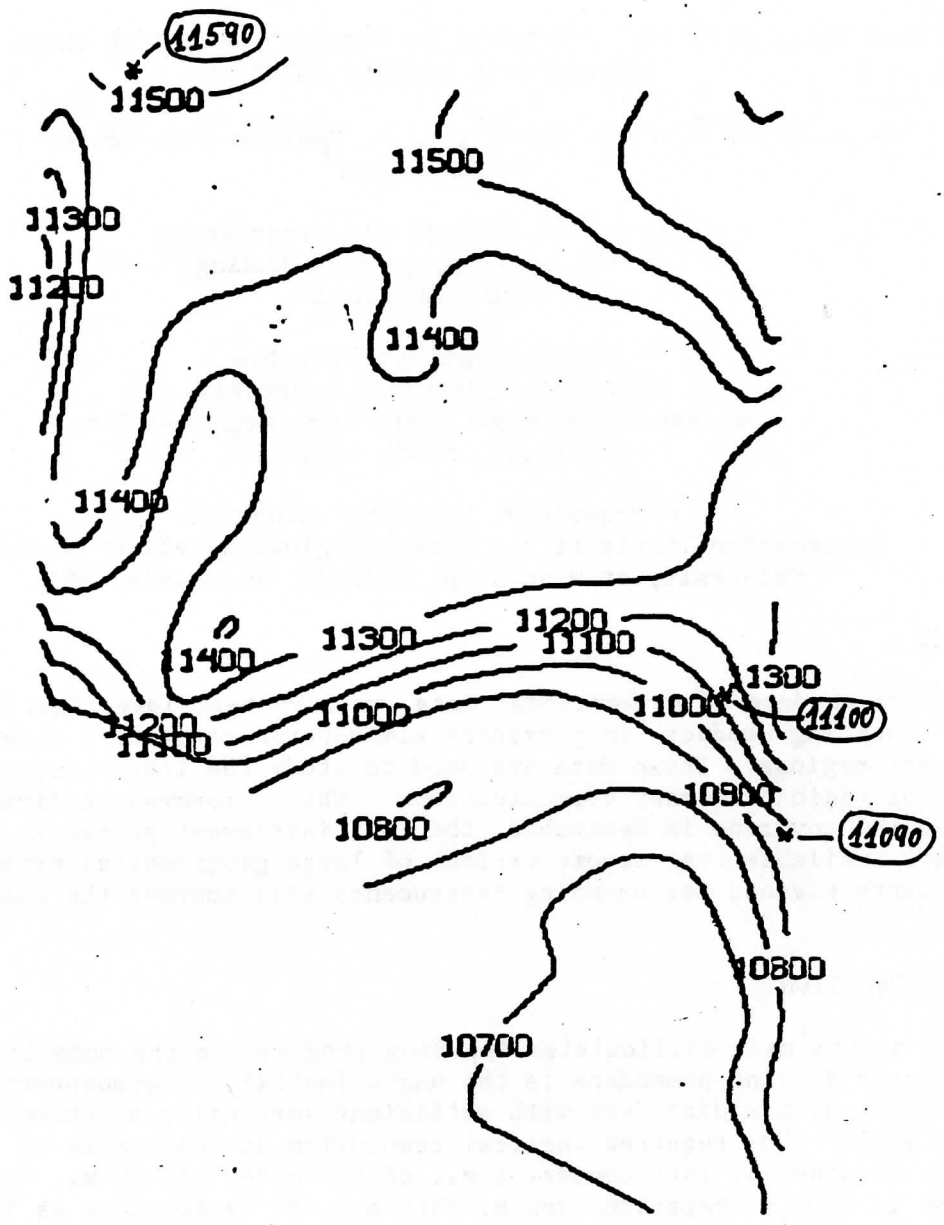

Fig. 15. 200 hPa heights (December 21, 1987, 23z) with the location and results of the three radiosonde stations (encircled) in that area.

USE OF NOAA POLAR ORBITING SATELLITES TO PROVIDE REFRACTIVE INDEX PROFILES FOR TROPOSPHERIC DUCTING MODELLING

M. J. Lynch[+x], P. W. Baker[*], J. D. Penrose[+], L. Gumley[+], and P. Mountford[+]

[+]School of Physics and Geosciences
Curtin University of Technology
Perth, Australia

*Communications Division
Electronics Research Laboratory
Defense Science and Technology Organisation
Salisburg, South Australia

[x]Presently, Visiting Scientist
Cooperative Institute for Meteorological Satellite Studies
University of Wisconsin, Madison, Wisconsin, USA

ABSTRACT

In the absence of conventional data, we have been investigating the use of TOVS sounding products in providing atmospheric refractive index profiles over ocean regions. These data are used to study the likely occurrence of the ducting of radio frequency communications. While improved vertical resolution and temporal coverage is desirable, the TOVS instrument presently provides the only data available over remote regions of large geographical extent. Future developments planned for sounding instruments will improve the quality of data.

1. INTRODUCTION

One of the main difficulties impeding progress in the modelling of tropospheric ducting phenomena is the unavailability of atmospheric temperature and humidity data with sufficient vertical resolution over large spatial areas. The required vertical resolution is comparable to that normally obtained by radiosondes, i.e., of the order of 100 m. However, in the case of some propagation events, this may not be adequate as it has been shown theoretically that for very intense microwave ducting events to occur sharp refractive gradients over heights of the order of metres are required. In meteorological parameters, this translates into sharp lapses in water vapour (humidity) content and/or temperature inversions. However, the refractive index is more sensitive to water vapour decrements than temperature increments. Radiosonde data have been shown to be useful for modelling purposes (but usually only providing enough data for one-dimensional modelling). For satellite sounding, a vertical resolution requirement equivalent to that of the radiosonde is the desired goal.

One important potential benefit from satellite remote sensing of refractive index is the delineation of horizontal gradients or slopes in the duct boundaries. It has been suspected from the propagation measurements across the Great Australian Bight that horizontal gradients are a necessary ingredient to maximize transfer of energy between the elevated duct and the ground terminals.

2. TWO CASE STUDIES

Curtin University supplied temperature and dewpoint profiles for 18 NOAA-9 orbits over the Great australian Bight (Figure 1) for the period January to March 1986. These profiles were produced using the VAX/VMS version of the International TOVS Processing Package (ITPP Version 3) distributed by CIMSS, University of Wisconsin. The simultaneous physical retrieval scheme using regression first guess was utilised. Near the surface profile values were calculated at pressure levels of 1000, 960, 920 and 850 mbars in an attempt to extract the maximum resolution possible from the retrievals. The data were then interpolated by ERL across an experimental VHF/UHF transmission path between Albany (WA) and Salisburg (SA), (a distance of 1800 km). Two particular orbits showing significant structure in the derived refractive profiles are discussed further below.

Attached are profiles derived from two NOAA-9 orbits, numbers 5456 and 5752. These show regularly spaced profiles along a path between Albany and Adelaide across the Great Australian Bight (obtained by gridding the data supplied by Curtin). The full-scale range of each curve is between the tick marks above the horizontal axis (maximum) and the adjacent tick mark below the axis (minimum). The refractivity shown in the middle curve is given by

$$N = (77.6\ P/T + 3.73 \times 10^5\ e/T - 1) \times 10^6$$

where N is the refractivity in N units, P is the pressure (millibars), T the temperature (K) and e is the partial pressure of water vapour (millibars). The lower curve is the modified or "flat earth" refractive index given by

$$M = N + h/R \times 10^6$$

where h is the height and R is the radius of the earth.

Height intervals where dM/dh is negative indicate the presence of radio ducting and the horizontal extent of these gradients is a major interest in this study. Orbit No. 5456 (Figure 2) shows the presence of gradients approaching, and even exceeding, negative values right across the bight which suggests the presence of a radio duct. However, there were no amateur radio operator reports of propagation. Of course, it is quite possible that a propagation opening was missed by operators. The other interesting case occurred on 21/1/867 (orbit no. 5752). The satellite profiles (Figure 3) suggest a duct with sloping walls at both terminals. Such a structure has been postulated to be the likely candidate to support propagation across the Bight. Amateur radio reports confirmed strong propagation on this day, hence this initial result is encouraging.

3. FUTURE WORK

The retrieved profiles were processed without the inclusion of surface data. There was not one ship surface observation in the region on the 18 days investigated. The data will be reprocessed using sea surface temperatures from climatology. Sensitivity to the humidity guess will be examined.

A useful set of 20 ship sondes coincident with satellite overpasses are presently under analysis. The sondes were released during scientific cruises on HMAS Cook and HMAS Franklin off the Western Australian coast (Figure 1). While the sondes will provide only point verification of the satellite retrievals, they will be a useful guide to the confidence which should be attached to the boundary layer refractive index profiles for the larger region.

4. FUTURE PROSPECTS

The limitations of satellite sounders in this work have been mentioned above. In data sparse ocean regions, however, they remain the only source of information on refractive index behaviour.

Without doubt, the higher spectral resolution sounder (e.g., AIRS - Atmospheric Infra-red Sounder) proposed for the Earth Observing System offers the prospect of a substantial improvement in the vertical resolution of atmospheric soundings. It will be possible with these new generation instruments to obtain improved structural information on the marine boundary layer adequate for identifying mesoscale situations in which ducting is favoured. The temporal coverage of a given region provided by polar orbiters will continue to be a severe limitation to studying the development of gradients in the boundary layer. Geostationary sounders of high vertical resolution, when available over the Australian region, will address this concern.

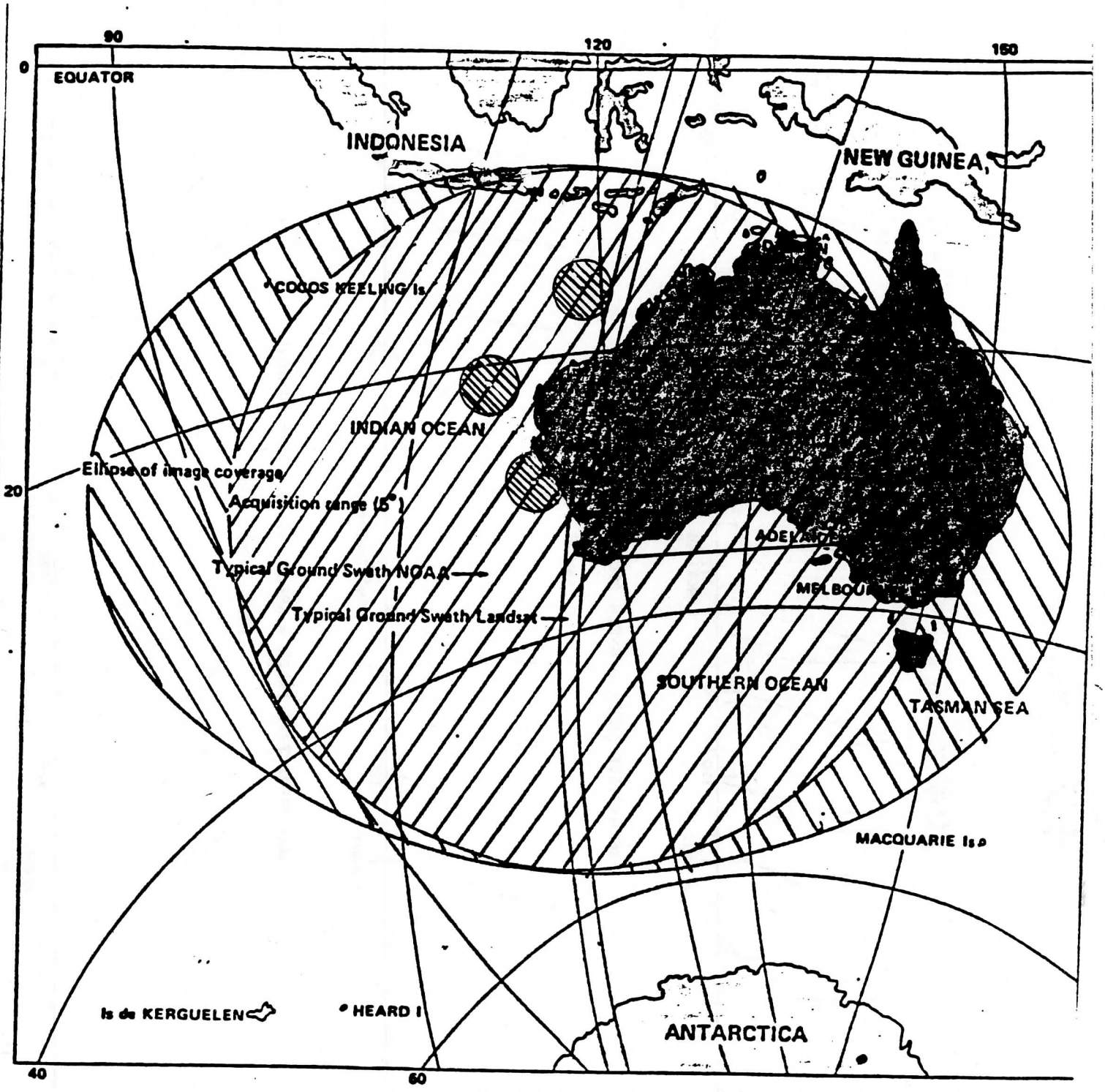

FIGURE 1:AREAS OF IN-SITU, SATELLITE AND RADIOSONDE DATA COLLECTION [ ].

ORBIT NO. = 5456
DATE :- 03-01-86
GMT TIME : 632 TO 640

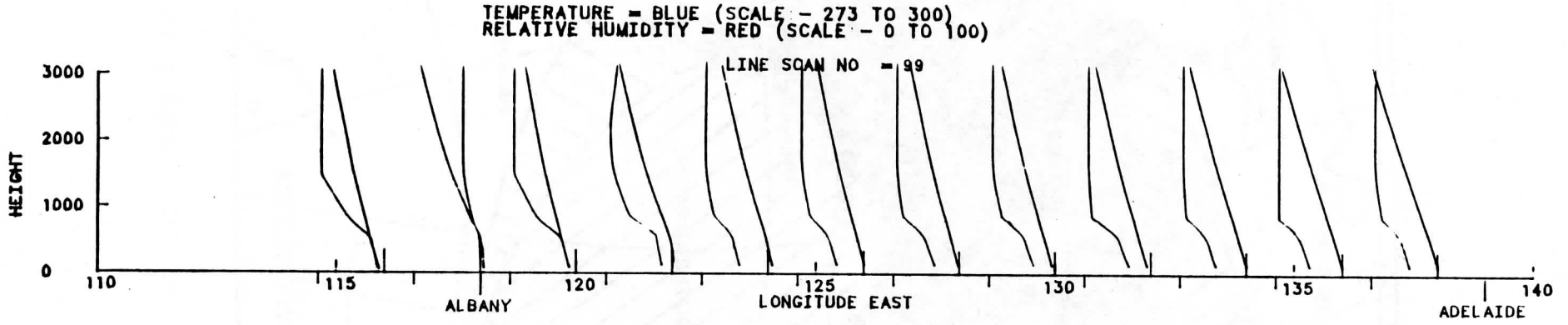

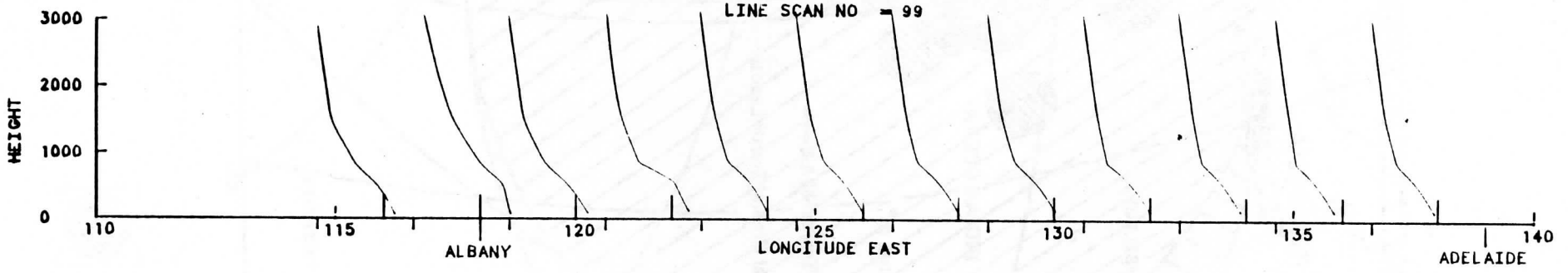

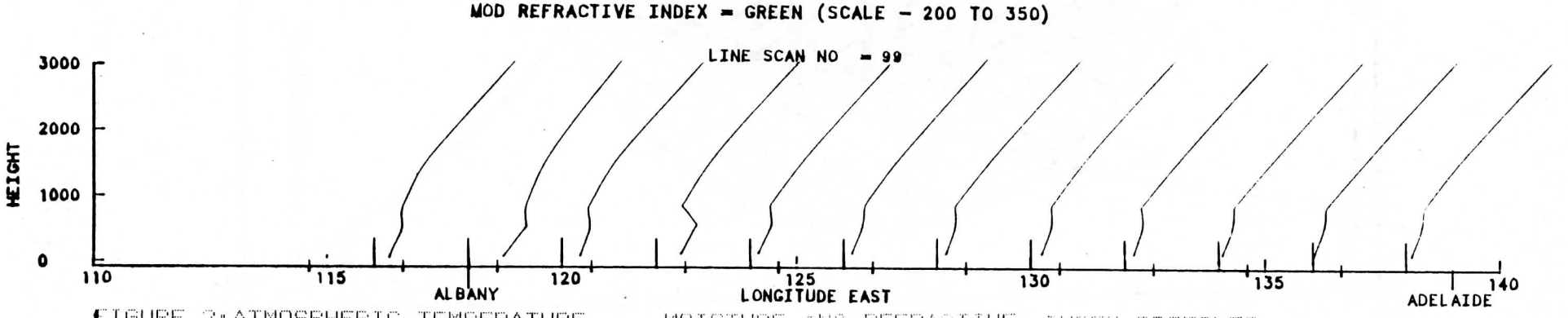

FIGURE 2:ATMOSPHERIC TEMPERATURE , MOISTURE AND REFRACTIVE INDEX PROFILES.

ORBIT NO = 5752
DATE = 24-01-86
GMT TIME 609 TO 617

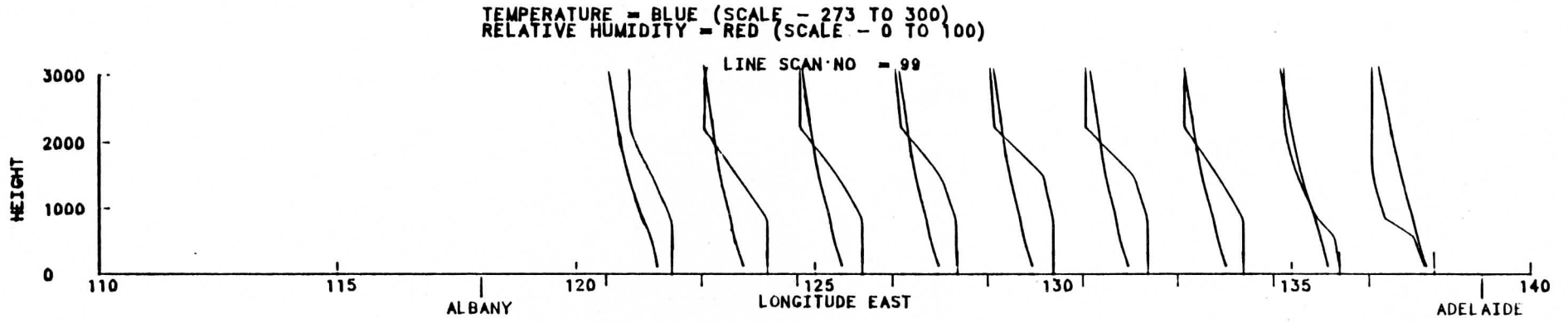

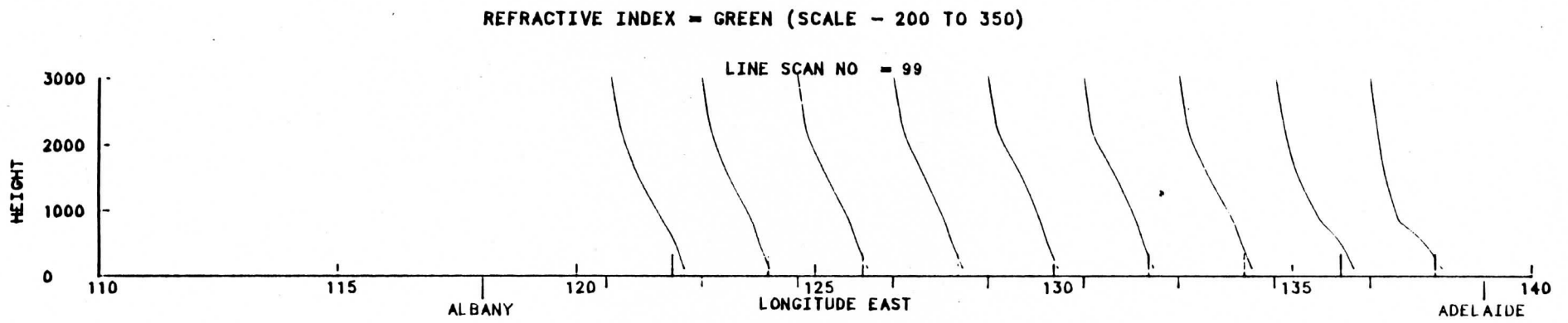

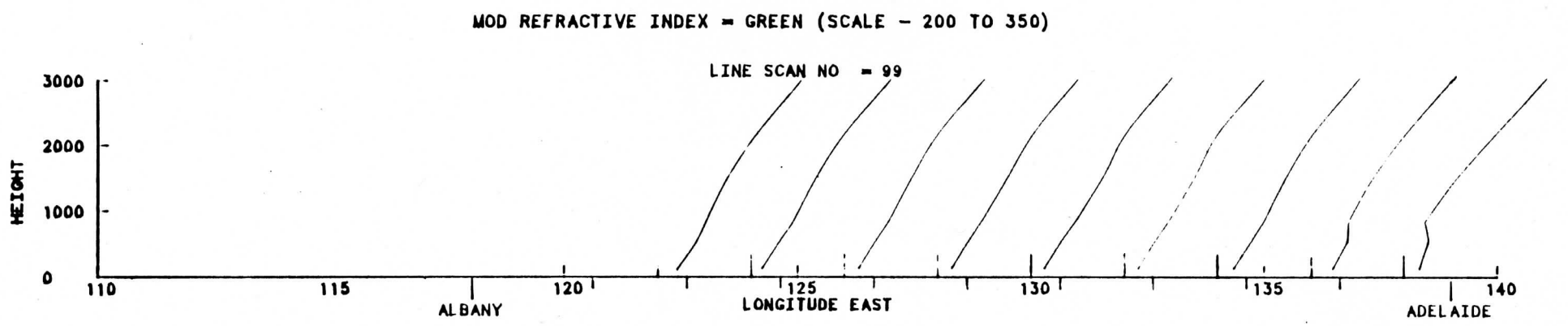

FIGURE 3: ATMOSPHERIC TEMPERATURE, MOISTURE AND REFRACTIVE INDEX PROFILES.

AN ATMOSPHRIC CORRECTION METHOD FOR AVHRR INFRARED DATA USING HIRS/2 DATA

Y. Minowa, W. D. Sun, and M. Takagi

Institute of Industrial Science, University of Tokyo

Institute of Industrial Science, University of Tokyo
7-22-1, Roppongi, Minato-ku, Tokyo 106, Japan

ABSTRACT

The atmospheric effect of remotely sensed data must be compensated for sea surface temperature(SST) obsevation. The observed data of HIRS/2 sensor on board NOAA satellites contain vertical information and are observed at the same time of AVHRR data. To correct SST's, this vertical observations of the atmosphere are useful. In this paper, a correction method using HIRS/2 data to correct the atmospheric effect in AVHRR data is proposed. This method is applied to the NOAA-10 imagery, using seven HIRS/2 channels and one AVHRR infrared channel. And these SST's are compared with the in-situ SST's in weather report by the Meteorological Agency of Japan. In the results of this atmospheric correction, error average is –0.283°C, standard deviation is 0.449°C, and correlation is 0.997.

1. INTRODUCTION

The distribution of the sea surface temperature(SST) observed by the infrared sensors of the satellite is contaminated by the atmosphere. In general, remotely observed SST's are about 2~6°C cooler than in-situ ones. The causes are mainly emission, absorption and scattering by the atmosphere. To determine the SST's on better accuracy, it is necessary to compensate the atmospheric effect. Many kinds of method have been proposed so far to compensate the effect.(Ref.3–7,12,14,15) The major method is multichannel correction method which is the most widely accepted atmospheric correction method. It requires two infrared channels at least.(Ref.5) The NOAA satellite has two(3.7μm and 11μm) or three(3.7μm,11μm and 12μm) infrared channels in AVHRR. Using these channels, it can correct the SST's on good accuracy (biases 0.3°C and rms deviations 0.5°C).(Ref.12) Two other infrared sensors(HIRS/2 and SSU) are on board NOAA satellites , and HIRS/2 is used with the AVHRR sensor for the multichannel SST procedure,(Ref.13,14) and the method using HIRS/2 data to estimate the water vapor effect with AVHRR infrared data is better than using only AVHRR infrared data.(Ref.13) In these multichannel correction method, the atmospheric effects are corrected by a linear equation which is derived from the relationship between remotely sensed and in-situ SST's. This regression analysis method is a very simple and fast in correcting. But there are some difficult problems to get the relationship between in-situ and remotely sensed SST's, because ships and buoys measure pin-point temperature, and satellite sensors observe average surface temperature in large area. And this method needs many in-situ SST's (collecting these data isn't easy.) to update the regression equation.

Other methods to correct the SST's are climatological correction or model correction methods, in which the statistical constructions of the atmosphere are approximately expressed by some models, and the atmospheric effects are reduced by the radiative transfer equation in this model.(Ref.3,8) As no in-situ SST's are needed for this method(of course,they are needed to verify the accuracy and effectivity.), the measurement errors of the in-situ SST's don't influence the accuracy of correction. And it is sufficient for the statistical analysis of SST distribution in a special time and a special place, the local vertical construction of the atmosphere. In this time must be known simultaneously.

On the NOAA satellites, the AVHRR sensor is used for observing the earth surface, and the HIRS/2 sensor is used for sounding the atmospheric vertical construction in the same time. So the atmospheric effects in the AVHRR data can be compensated by using vertical information in HIRS/2 data.

In this paper, a new atmospheric correction method for AVHRR infrared data by using of HIRS/2 data is proposed. This method is applied to NOAA-10 image of northwest Pacific Ocean for 9 May 1987, and the results of those experiments show that the atmospheric effects included in AVHRR data can be removed.

2. ATMOSPHERIC CORRECTION METHOD

In a cloud free nonscattering atmosphere, the remotely sensed brightness temperatures are affected by the radiation and absorption of the atmosphere. Under local thermodynamic equilibrium, the radiative transfer equation for the upwelling total radiance of the atmosphere observes at the top of atmosphere can be written as

$$\int_0^{p_s} \delta I_\nu \tau_\nu(\theta,p)dp=-\int_0^{p_s} B_\nu(T)sec\theta\tau_\nu(0,p)^{sec\theta-1}W_\nu(p)dp \tag{1}$$

where K_ν is the atmospheric absorption per unit pressure at frequency ν , $\rho(p)$ is the absorber's density at the pressure p, $B_\nu(T)$ is the Planck function at frequency ν for emitted radiance of blackbody at temperature T , $\tau_\nu(\theta,p)$ is the atmospheric transmittance from pressure p to the top of the atmosphere at frequency ν and zenith angle θ, subscript S means the value at the earth surface, and $W_\nu(p)$ is the weighting function which can be written as

$$W_\nu(p)=\frac{d\tau_\nu(0,p)}{dp} \tag{2}$$

The remotely sensed radiance R_ν at the top of the atmosphere is the sum of the radiance from the earth surface and the radiance of the atmosphere. So it can be written as

$$R_\nu=\varepsilon_\nu B_\nu(T_s)\tau_\nu(0,p_s)^{sec\theta}-\int_0^{p_s} B_\nu(T)sec\theta\tau_\nu(0,p)^{sec\theta-1}W_\nu(p)dp \tag{3}$$

where ε_ν is the emittance of the earth surface at frequency ν. The property of ε_ν changes greatly in the different spectrum regions. In microwave region, it strongly depends on the surface conditions. In infrared region, it can be regarded as a constant, and the value is about 0.95 in the 11μm window region, and 0.98 in the 3.7μm window region on the sea surface.

In this method, the atmosphere is simplified by assuming that the optical properties of the atmosphere vary only in the vertical direction, that is, the distribution of atmospheric constituents in the horizontal direction is assumed to be homogeneous. Such kind of atmosphere is known as a plane-parallel atmosphere. On this assumption, eq.(3) can be rewritten as

$$R_\nu=\varepsilon_\nu B_\nu(T_s)\tau_\nu(0,p_s)^{sec\theta}-\sum_{i=1}^{n} B_\nu(T_i)sec\theta\tau_\nu(0,p)^{sec\theta-1}W_\nu(p)\Big|_{p=p_i}\Delta p_i \tag{4}$$

where n is the total layers of the atmosphere, p_i and T_i are the pressure and the

temperature of the i-th layer respectively. And then, $W'_\nu(p_i)$, and $\tau_\nu(0,p)$ can be determined by the atmosphere model.

To calculate the temperature of the earth surface and vertical temperature distribution, Planck function $B_\nu(T)$ can be expanded at certain reference temperature T_0 and reference frequency ν_r And substituting this function with eq.(4) is written as

$$R_\nu=\varepsilon_\nu\left\{B_\nu(T_0)+\frac{\partial B_\nu(T)}{\partial B_{\nu_r}(T)}\Big|_{T=T_0}(B_{\nu_r}(T_s)-B_{\nu_r}(T_0))\right\}\tau_\nu(0,p_s)^{sec\theta}$$

$$-\sum_{i=1}^{n}\left\{B_\nu(T_0)+\frac{\partial B_\nu(T)}{\partial B_{\nu_r}(T)}\Big|_{T=T_0}(B_{\nu_r}(T_i)-B_{\nu_r}(T_0))\right\}sec\theta\tau_\nu(0,p)^{sec\theta-1}W'_\nu(p)\Big|_{p=p_i}\Delta p_i \tag{5}$$

where

$$W'_\nu(p)=\frac{\partial\tau_\nu(0,p)}{\partial p} \tag{6}$$

is an approximated weighting function. finally, defining that

$$\begin{cases} A_\nu^0=\varepsilon_\nu\dfrac{\partial B_\nu(T)}{\partial B_{\nu_r}(T)}\Big|_{T=T_0}\tau_\nu(0,p_s)^{sec\theta}, \\ A_\nu^i=\dfrac{\partial B_\nu(T)}{\partial B_{\nu_r}(T)}\Big|_{T=T_0}sec\theta\tau_\nu(0,p)^{sec\theta-1}\dfrac{\partial\tau_\nu(0,p_i)}{\partial p}\Big|_{p=p_i}\Delta p_i \quad (i=1,2,\ldots,n), \\ B_\nu=R_\nu-\varepsilon_\nu(B_\nu(T_0)-\dfrac{B_\nu(T)}{\partial B_{\nu_r}(T)}\Big|_{T=T_0}B_{\nu_r}(T_0))\tau_\nu(0,p_s)^{sec\theta} \\ \quad +\sum_{i=1}^{n}(B_\nu(T_0)-\dfrac{B_\nu(T)}{\partial B_{\nu_r}(T)}\Big|_{T=T_0}B_{\nu_r}(T_0))sec\theta\tau_\nu(0,p_i)^{sec\theta-1}W'_\nu(p)\Big|_{p=p_i}\Delta p_i, \\ X_i=B_{\nu_r}(T_i) \quad (i=0,1,\ldots,n). \end{cases} \tag{7}$$

And making those substitutions into eq. (5) yield

$$B_\nu=\sum_{i=0}^{n}A_\nu^iX_i \tag{8}$$

Solving this simultaneous equations, $B\nu_r(T_i)$ can be decided, so the temperature of each layer T_i is known by the solution of the inverse-Planck function.

3. CHANNEL COMBINATION BETWEEN AVHRR SENSOR AND HIRS/2 SENSOR FOR THE ATMOSPHERIC CORRECTION

In this paper, the observation data of HIRS/2 sensor are used to calculate the atmospheric absorption and radiation for the atmospheric correction of AVHRR infrared data. The HIRS/2 sensor has 19 channels in infrared region. To use above correction method, it is necessary to consider the accuracy of the approximation of eq.(5) and the balance of the atmospheric layers disposition. The possible channel combination between AVHRR channels and HIRS/2 channels for the atmospheric correction can be decided as table 1. To use AVHRR ch-3, we have to compensate the effect of the scattering and sun glint on the sea surface, so it can not be used easily in daytime. As the AVHRR/1, which is onboard the even number NOAA satellites, does not have ch-5. This channel can only be used on the odd number satellites.

To use the HIRS/2 ch-10 ~ ch-12, these are very important channels because the main absorber is water vapor, which is an important factor of the absorption of AVHRR infrared

channels. And the weighting functions shift by the difference of the vertical water vapor distribution. So it is necessary to estimate the shift and adjust these weighting functions. The profile of weighting functions are shown in Figure 1.

Table 1. Channel Combination of AVHRR and HIRS/2

AVHRR sensor	HIRS/2 sensor
CH 4	CH 1 ~ CH 7
CH 5	CH 1 ~ CH 7
CH 3	CH 13 ~ CH 17
CH 3	CH 10 ~ CH 17

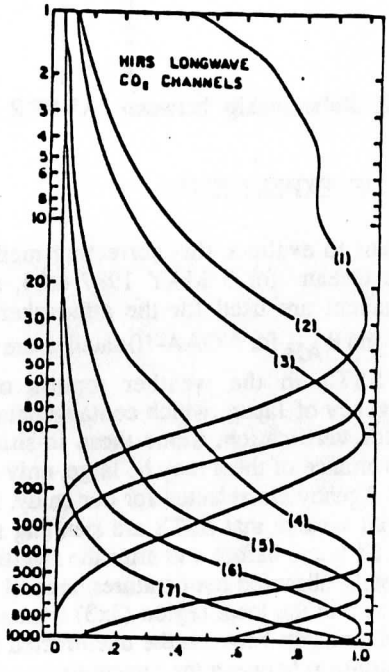

Figure 1. The Weighting Functions (Normalized) (Ref.2)

4. THE RELATIONSHIP BETWEEN AVHRR SENSOR COORDINATE SYSTEM AND TOVS SENSOR COORDINATE SYSTEM

To use HIRS/2 data related with AVHRR data, it is necessary to decide the pixel to pixel correspondence. Figure 2 shows the relationship of between AVHRR sensor coordinate system and HIRS/2 sensor coordinate system. This coordinate relationship can be expressed with parameters θ_{AH},θ_A,ΔI,ΔJ. But θ_A is very small, so it can be omitted from consideration. So the relationship can be expressed as

$$\begin{cases} X_H = 28.5 \dfrac{X_A - 1024.5 - \Delta J}{\cos(\theta_{AH})\,\Delta X}, \\ Y_H = \dfrac{Y_A - \Delta I + (X_A - 1024.5 - \Delta J)\tan(\theta_{AH})}{\Delta Y} \end{cases} \tag{9}$$

where (X_A, Y_A) and (X_H, Y_H) are pixel number and line number on each sensor image. ΔX and ΔY are the resolution ratio between the two sensors.

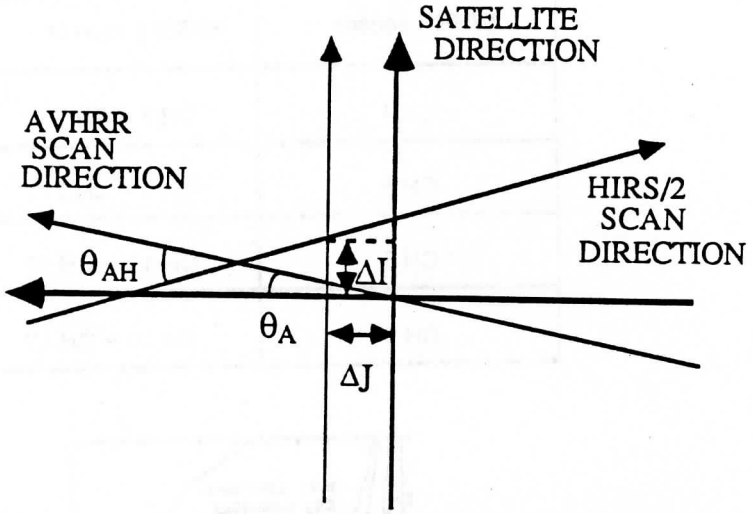

Figure 2. Relationship between AVHRR Sensor and HIRS/2 Sensor

5. RESULT OF EXPERIMENTS

The experiment to evaluate this correcting method, the NOAA-10 satellite image of northwest Pacific Ocean for 9 MAY 1987 6:44, and HIRS/2 ch-1,2,...,7 channels and AVHRR ch-4 channel are used for the atmospheric correction. The sensor coordinate parameters ΔI, ΔJ and θ_{AH} for NOAA-10 satellite are used as –0.5, 2.5 and 0.00 respectively.

The in-situ SST's in the weather reports of northwest Pacific Ocean by the Meteorological Agency of Japan, which contains data observed by many kinds of ships and buoys, are used for verification. Since these in-situ SST's spread very widely, and it is expected that the variance of them may be large, only the in-situ SST's observed by the ships of Meteorological Agency are selected for our study. In general, the SST's do not change so quickly, and we can assume that SST's are standing still in two days. Thus the in-situ data observed between 24 hours before and after the satellite observation. For selecting the cloud free area, the remotely observed temperatures, around which the difference of maximum and minimum temperature in the local region (3x3) is smaller than 2.0°C, are compared with the in-situ data. the relationship between the uncorrected remotely sensed SST's and this in-situ ones, and the relationship between the atmospheric corrected remotely sensed SST's and the in-situ ones are shown in Fig.3a, Fig.3b, Fig.4a and Fig.4b respectively. The statistical parameters are shown in Table 2 and Table 3.

Table 2. Relation between the Uncorrected Remotely Observed Temperature and Sea-Truth

	MIN. ERROR	MAX. ERROR	AVG. ERROR	STD. DISTRIBUTION	CORRELATION
ALL POINTS	-9.841	-0.117	-4.031	1.764	0.944
SELECT POINTS	-5.477	-0.362	-3.498	1.303	0.987

(MAY 9 1987, 6:44, UNCORRECTED)

Table 3. Relation between the Corrected Remotely Observed Temperature and Sea-Truth

	MIN. ERROR	MAX. ERROR	AVG. ERROR	STD. DISTRIBUTION	CORRELATION
ALL POINTS	-2.585	3.835	-0.026	1.279	0.972
SELECT POINTS	-1.272	0.432	-0.283	0.449	0.997

(MAY 9 1987, 6:44, CORRECTED)

6. CONCLUSION

In this paper, an atmospheric correction method for AVHRR infrared data using HIRS/2 data has been proposed and the result of some experiments have been shown. It has been shown from our experiments that the average error is -0.026°C, standard deviation is 1.279°C and correlation is 0.972 for all points, and average error is –0.283°C, standard deviation is 0.449°C, correlation is 0.997 for selected points.

In this paper, the in-situ SST's are the bulk temperatures,but satellite sensor only observes the skin surface. It is necessary to estimate the relationship between bulk and skin surface temperature as discussed in some papers, and in usual, skin surface temperatures are 0.1 ~ 0.5 °C cooler than bulk temperatures.(Ref.16,17) And the standard distribution depends on the selection method of cloud free area. For research of the distribution of SST's and monitoring the ocean current, it is necessary to keep the average error less than 0.5°C, So this result satisfies it and can be used for many kinds of research work.

The main remaining problems are the cloud correction method, skin and bulk SST estimation, and the usage consideration of the water vapor channels for the atmospheric correction.

REFERENCES

1. L. Lauritson, et al 1979, Data Extraction and Calibration of TIROS-N/NOAA Radiometers, *NOAA Technical memorandum NESS 107.*
2. A. werbowetzki 1981, Atmospheric Sounding Users Guide *NOAA Technical Report NESS 83.*
3. A. Deepak 1980, *Remote Sensing of Atmospheres and Oceans*, Academic Press.
4. S. M. Singh 1982, Sea Surface Temperature from Infrared Measurements, *Remote Sensing Applications in Marine Science and Technology*, D. Reidel Publishing Company, pp.213-262.
5. C. Prabhakara, et al 1974, Estimation of Sea Surface Temperature from Remote Sensing in the 11- to 13-μm Window Region, *Journal of Geophysical research*, Vol.79, No.33, pp.5039-5044.
6. G. Dalu 1985, Emittance Effect on the Remotely Sensed Sea Surface Temperature, *INT. J. Remote Sensing*, Vol.6, No.5, pp.733-740.
7. N.Castagne, et al 1986, Operational Measurement of Sea Surface Temperature at CMS Lannion from NOAA-7 AVHRR data, *INT. J. Remote Sensing*, Vol.8, No.7, pp.953-984.
8. F.X.Kneizys, et al 1983, Atmospheric Transmittance/Radiance Computer code LOWTRAN6, *AFGL-TR-83-0187 Air Force Geophysics Laboratory.*
9. T.Aoki et al 1983, Summary of TOVS Data Processing System, *Meteorological Satellite Center Technical Note (special issue)*, March.
10. J. Susskind 1984, Vertical Temperature Sounding of the Atmosphere, *Satellite Sensing of a Cloudy Atmosphere*, Tayler & Francis Ltd., pp.167-202.
11. T.Aoki 1986, Procedure and Results of AVHRR-HIRS Picture Matching, *Proc. of the 1st Australian AVHRR Conference*, pp.280-285.

12. McClain, et al 1985, Comparative Performance of AVHRR-Based Multichannel Sea Surface Temperatures, *Journal of Geophysical Research*, Vol.90,No.C6, pp.11587-11601.
13. P.Schluessel et al 1987, Comparison of Satellite-Derived Sea Surface Temperatures With in Situ Skin Measurements, *Journal of Geophysical Research*, Vol.92, No.C3, pp.2859-2874.
14. T.Aoki, et al 1982, Remote Measurement of the Sea Surface Temperature by Multichannel Observation from Orbital Satellite, *Journal of the Meteorological Society of Japan*, Vol.60, No.6, pp.1238-1248.
15. T.Takashima, et al 1981, Estimation of Sea Surface Temperature from Remote Sensing in the 3.7μm Window Region, *Journal of Meteorological Society of Japan*, Vol.59, No.6, pp.876-891.
16. Y.Takayama, et al 1982, Measurements of the Water Surface Temperature at the 11μm Window region, *Papers in Meteorology and Geophysics*, Vol.33, No.2 pp.79-83.
17. I.S.Robinson, et al 1984, The Sea Surface Thermal Boundary Layer and its Relevance to the Measurement of Sea Surface Temperature by Airborne and Spaceborne Radiometers, *Int. J. Remote Sensing*, Vol.5, No.1, pp.19-45.
18. G.Rochard, Status Report on Calibration Problems, *The Technical Proceedings of The Third International TOVS Study Conference*,pp.235-242.

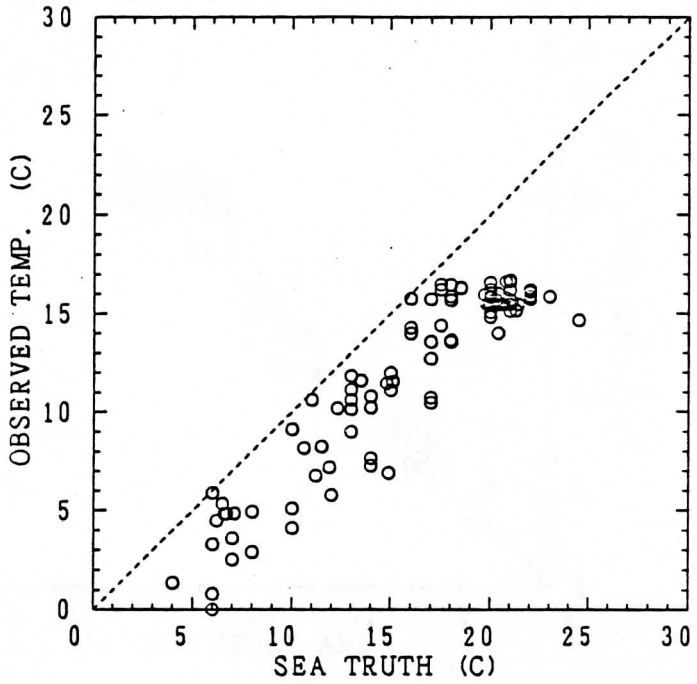

Figure 3a. Relation between the Uncorrected Remotely Observed Temperature and Sea-Truth(All Points)

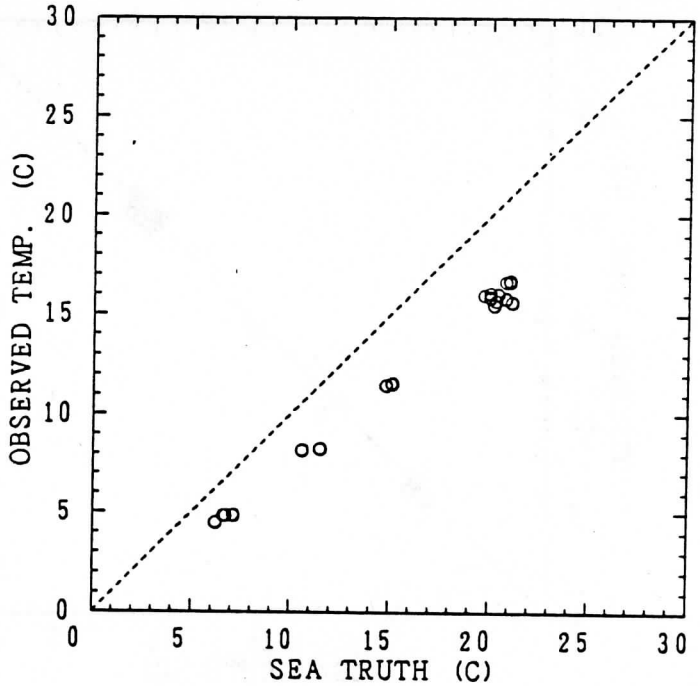

Figure 3b. Relation between the Uncorrected Remotely Observed Temperature and Sea-Truth(Selected Points)

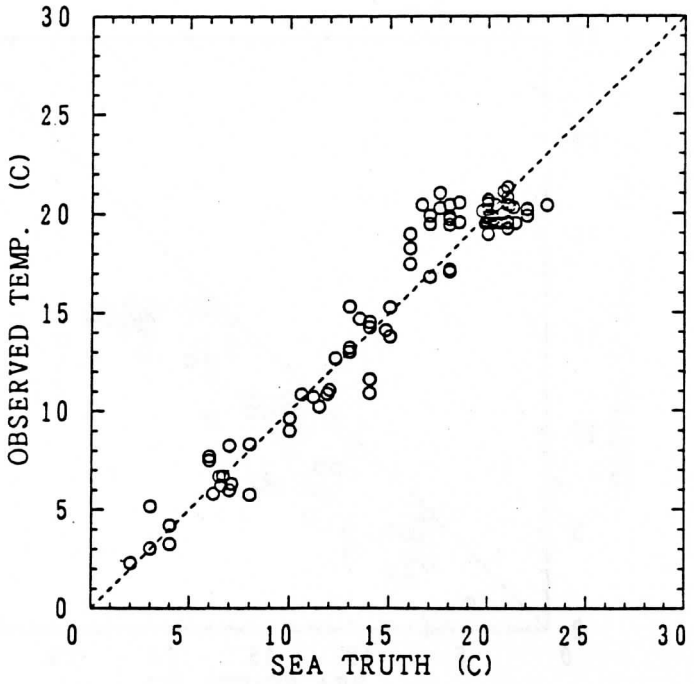

Figure 4a. Relation between the Corrected Remotely Observed Temperature and Sea-Truth (All Point)

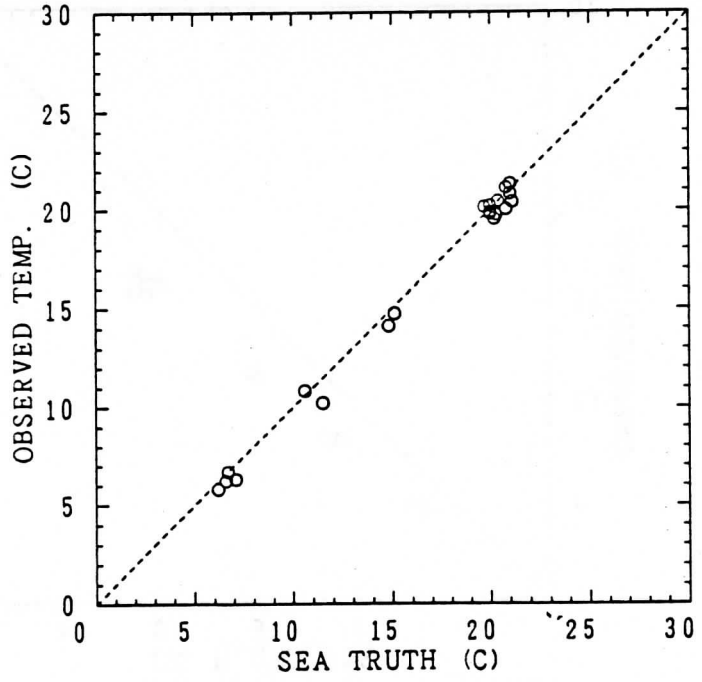

Figure 4b. Relation between the Corrected Remotely Observed Temperature and Sea-Truth(Selected Points)

SATELLITE NAVIGATION AND DE-NAVIGATION

F. W. Nagle
NOAA/NESDIS Systems Design and Applications Branch
1225 West Dayton Street
Madison, Wisconsin 53706 USA

ABSTRACT

The term NAVIGATION has several connotations, but among satellite meteorologists it refers to the process whereby one applies a set of known orbital parameters, along with the scanning characteristics of an on-board instrument, to compute the position of a satellite in space at some future instant, and also the point(s) on the ground which the satellite will view at that moment.

One may ask if this process can be inverted. Thus, if we are given a set of points on the Earth's surface viewed by the satellite in the recent past, sometimes called the "footprint", is it then possible to drive the navigation algorithm backward in order to recover the orbital characteristics? And if it is possible, why would anyone wish to derive the orbital characteristics from a set of Earth locations? This inverse process will be termed 'de-navigation' in this paper, and it is our purpose to discuss its feasibility and usefulness.

1. TEMPORAL AND SPATIAL COORDINATES

1.1 Time Units

To forestall confusion involving certain terms, we shall review the temporal and spatial units used below. The term Julian Day Number is a measure of time, and it denotes the numbers of days and fraction thereof which have elapsed since 12 o'clock Universal Time on 1 January 4713 BC. The reader may wonder at this seemingly strange date as the origin of the Julian Day chronology. It is not our purpose here to explain this origin, and the reader is referred to Durant (3) for a full explanation of this choice, as well as the reason for the name 'Julian', which has nothing to do with the Julian calendar or with Julius Caesar. The term Julian Day Number is unfortunately confused with a similar term, Julian Date, which is used both in civilian and military computer systems to mean simply the two-digit year indicator, followed by a three-digit sequential day of the year, e.g. 85365 to mean 31 December 1985. One must keep in mind that a day within the Julian Day Number (JDN) chronology begins at noon, not midnight, the reason being that historically European astronomers preferred that all observations made in the course of a single night be ascribed to the same Julian Day number, which of course would not be so had the date changed at Greenwich midnight rather than noon. The JDN which began at 12 UT on 3 August 1987 was 2447011, from which the reader may deduce the JDN for

any other calendar date.

On a computer system such as an IBM 4381, a double-precision quantity has a resolution comparable to about 17 decimal digits, so that by storing time expressed in JDN within double precision words, one can achieve a resolution in time of the order of a billionth of a day, easily adequate for most satellite navigation.

One can readily see the advantages of reducing measurements of time to a single scalar value, allowing us to dispense with months which may have 31, 30, 28 or sometimes 29 days, with leap years and common years, the distinction between the Julian and Gregorian calendars, etc.

1.2 Spatial Coordinates

The point in the sky which the sun occupies at the instant when it crosses the Equator from south to north about 22 March is called the Vernal Equinox, or sometimes the First Point of Aries, an old astrological name. Using the center of the Earth as the origin, the Vernal Equinox to define the x-axis, the North Pole to define the z-axis, and a point on the Equator 90 degrees east of the Vernal Equinox as the y-axis, one can construct a dextral (right-hand) orthonormal coordinate system which we call the celestial coordinate system. Since the Vernal Equinox is almost a fixed point in the sky, much like a seemingly-fixed star, the celestial coordinate system appears to rotate westward with respect to the Earth at the rate of 360 degrees per sidereal day, and in fact it is by the motion of the Vernal Equinox that a sidereal day is defined (1).

The terrestrial coordinate system is analogous to the celestial system, having the same origin and the same z-axis, but with an x-axis fixed to the Earth and directed toward the longitude of Greenwich in the plane of the Equator, and with a y-axis oriented 90 degrees east of Greenwich. Clearly the terrestrial and celestial systems rotate with respect to one another, and a transformation of a position vector in one system to the other at any time T is effected by a matrix equation of the form:

$$V_1 = \begin{vmatrix} \cos(a) & -\sin(a) & 0 \\ \sin(A) & \cos(A) & 0 \\ 0 & 0 & 1 \end{vmatrix} V_2 \qquad (1)$$

where A, the instantaneous longitude of the Vernal Equinox, is given by

$$A = -215.465 - 360.9856473(T - 2442348) \qquad (2)$$

The angle A is expressed in degrees, and T in Julian Day Number. The matrix is orthogonal, i.e. its inverse is also its transpose, so that the direction of the transformation depends merely on the sign of the

angle A. The constant 360.9856473 is the westward rate of movement of the vernal equinox in degrees per mean solar day.

The more common terrestrial coordinates of latitude and longitude are polar variations of the Cartesian terrestrial system, and are readily deducible from the latter by simple trigonometric relationships. The distinction must be kept in mind between geodetic and geocentric latitudes, as described elsewhere (1).

2. DE-NAVIGATION

The path of an orbiting satellite such as the NOAA or DMSP series when expressed in celestial coordinates is very nearly a great circle, at least over a short period of time. The orbit of a sun-synchronous satellite, if it is to remain sun-synchronous, must precess 360 degrees per year in order that an ascending pass always present the same relationship to the sun. This amounts to just less than one degree per day, or about a fourteenth of a degree per orbit. Hence, over any significant fraction of an orbit, the path of the satellite is very close to a true great circle, and if it is necessary to consider the precession of the orbit, the needed adjustment is not difficult.

Let us assume that we are given a set of sub-satellite points on the Earth's surface, presumably expressed in terms of latitude and longitude, together with the times associated with those points, and constituting at least one complete orbit including two Equator crossings, not necessarily consecutive. If the latitudes are geodetic, these must be converted to geocentric, but otherwise the given coordinates are easily converted to terrestrial Cartesian coordinates by straightforward trigonometry. Each of the three-dimensional Cartesian vectors thus obtained is in turn easily changed to celestial coordinates by using (1). Alternatively, the terrestrial longitude of the Vernal Equinox is known as a function of time, and is given by (2) above, so that we could first have converted terrestrial longitude to celestial longitude, and thence to celestial Cartesian coordinates.

From Kepler's third law we know that the semi-major axis of an orbit is proportional to the two-thirds power of the period, where the constant of proportionality estimated by the author from orbital data stored on the NAS 9000 computer at NMC is 330.9982746. The semi-major axis is expressed in kilometers, and the period in minutes. The period itself is found by interpolating a set of known sub-satellite positions to the times of two or more Equator crossings. We now have an accurate estimate of semi-major axis, although as we shall see presently, we shall not use it except perhaps as a reasonableness test of the period. Next, we can compute the cross product of any two non-collinear satellite position vectors which by its orientation in celestial space gives us the orientation of the orbit. This vector cross product, normalized to a length of one, is called hereafter the Vector Orbital Plane (VOP). It is of course perferable if the two non-collinear satellite positions are nearly normal to each other to maximize the accuracy of their cross product. The angle between VOP and its own

projection in the plane of the Equator, added to 90 degrees, is the inclination of the orbit. The angle between the same projection and the celestial x-axis, added to 90 degrees, is the right ascension of the ascending node, that is, the angle measured eastward along the Equator from the Vernal Equinox to the point of northward Equator crossing of the satellite.

Of the six classical orbital elements (semi-major axis, eccentricity, orbital inclination, right ascension of the ascending node, argument of perigee, and mean anomaly) we have now determined three. The remaining three in principle could be found, though in practice it is difficult or impossible to do so with much accuracy. Kepler's second law stating that the areal velocity of a satellite is constant can be written as

$$C = r^2 \dot{\theta}$$

and since $\dot{\theta}$ can be estimated from the successive positions of the satellite along the ground, the radius vectors from the center of the Earth to the satellite can be obtained. To these known radii, an ellipse could be fitted by some least-squares means. The point in the orbit with the shortest radius is the perigee, and that with the longest, presumably diametrically opposite to perigee, is the apogee. The sum of these two radii is the major axis. The center of the ellipse evenly divides the major axis, and the distance between the center of the ellipse and the center of the Earth (which is a focus of the ellipse) can be used to determine the eccentricity. If the epoch is taken to be the moment when the satellite is at perigee, then the mean anomaly can be set to zero, and in principle we now know the six classical elements, at least for the case of a pure two-body Keplerian orbit.

In practice, the foregoing procedure is of little value because the known Earth locations are rarely precise enough to allow the needed calculations to be accomplished without introducing large errors in the radius vectors. The eccentricity of a NOAA or DMSP satellite is roughly .0015, and the reader by using this value in the equation of an ellipse may satisfy himself that the difference between the semi-major and semi-minor axes is a mere 8 meters, whereas the mean diameter of the orbit is in the neighborhood of 14000 kilometers. Another technique was therefore preferred.

As noted, knowledge of the vector orbital plane (VOP) at a given time provides us with the orbital inclination and right ascension of ascending node. Since the rate of change of the right ascension is roughly known, or better, can be accurately inferred by noting the change in VOP over a period of several days, and since the inclination is almost invariant, we can find the orientation of the orbit at any time in the near future, i.e. for a span of several weeks ahead.

Let us next make the inaccurate assumption that the satellite moves about the Earth with a period found by observing successive

Equator crossings, with a constant angular velocity in a purely circular path, and with an epoch chosen as the moment of one of the northward Equator crossings, i.e. ascending node. The Earth locations resulting from this assumption will contain serious errors, say, of the order of of 50 kilometers. However, the errors are easily decomposed into harmonic components as a function of nodal anomaly, by which we mean the angle in the orbital plane between ascending node and instantaneous satellite position. We show a typical decomposition for the case of the DMSP-7 satellite on 4 August 1987:

Along-track errors:

0	.83	.00	.83	.00
1	1.36	7.41	7.54	79.59
2	.02	3.32	3.32	44.81
3	-.07	-.05	.08	-49.08
4	-.02	.84	.84	22.88
5	.07	.03	.07	5.09
6	-.08	-.42	.43	-16.78
7	-.02	-.08	.08	-14.75
8	.03	.91	.91	11.01
9	.07	.03	.08	2.71

Cross-track errors:

0	.59	.00	.59	.00
1	2.07	-.94	2.27	-24.44
2	.57	.16	.59	7.86
3	-.05	2.85	2.85	30.35
4	-.18	.01	.18	44.52
5	-.09	-1.94	1.94	-18.50
6	.09	.00	.09	.15
7	-.01	1.22	1.22	12.90
8	-.01	-.08	.08	-11.98
9	.01	-.79	.79	-9.89

showing ten harmonics, the zeroth through the ninth, for both along-track and cross-track errors. The fourth column of values given above for along-track amplitudes is of greatest interest. As seen, there is a constant term correction of .83 kilometers, a first harmonic component of 7.54 km, and a second harmonic of 3.32 km. Thereafter the higher harmonics are all very small, suggesting that the assumption of a purely circular motion, corrected by removing the zeroth through the second harmonics of the error, results in errors which are generally of the order of a kilometer. In fact, in this case, the remaining error, compared against the given Earth locations, had an RMS value of only 1.59 kilometers, a discrepancy which is marginally acceptable for a high-resolution Earth-viewing instrument such as AVHRR, and easily acceptable for a sounding instrument such as HIRS, MSU, or SSTI aboard the NOAA or DMSP spacecraft.

The foregoing table shows that cross-track errors tend to be much

smaller than the along-track errors, though again they could be easily removed by a harmonic correction. Column 5 shows the phase angles of the along-track and cross-tracks errors.

This case displaying the harmonic error components for the DMSP-7 satellite is of interest, for it represents a practical and necessary instance of de-navigation. The author has experienced great difficulty in obtaining the classical orbital parameters from the Air Force, not because the latter is unwilling to release them as a matter of policy, but simply because their distribution is not the routine responsibility of any individual, and as a result they are usually obtainable only by special request and for a limited time only. On the other hand, the Earth-located micro-wave retrievals from the DMSP-7 can be accessed on a daily basis from the NAS 9000 system at Suitland, Md, through the McIdas system at the University of Wisconsin. Although these data are intended for meteorological use, not for navigational purposes, it has become both feasible and necessary to de-navigate the Earth locations in order to compute future positions of satellite for planning purposes. An immediate disadvantage of the foregoing technique, however, is that it affords no information of satellite altitude.

On the other hand, there is another reason for de-navigating Earth locations even for satellites like those of the NOAA series for which the orbital elements are widely published and distributed. One of the most frequently used orbital prediction models is the Brouwer-Lyddane model (2,4), which is a lengthy and involved program, and which may be unavailable at many computer sites. It is relatively slow in execution owing to its complexity, and is itself not free of error. Its size and complexity are even more disadvantageous on a small computer, such as a personal computer (PC) or lap-top model, than on a larger system such as the NAS-9000 or IBM 4381.

By de-navigating the Earth locations, we have obtained period, vector orbital plane, and the zeroth through the second error components, so that we can then apply a very simple and fast algorithm, as described below, to compute future (and past) satellite positions with an accuracy competitive with that of a classical prediction model, and with easy adaptability to a small computer system. Moreover, if our original Earth location data are accompanied with information about satellite altitude, then that too can be harmonically resolved so that we now obtain predictions of height as well as of sub-satellite locations. The computer language in which the simple model was written on the SSEC McIDAS computer, Madison, is High Level Fortran (HLF), which incorporates vectors and matrices as variable types, thus allowing the code to be written concisely in 3-dimensional vector notation (5).

Let us review and quantify the foregoing. Firstly, we are given a set of Earth-locations representing the sub-satellite points for a polar-orbiting satellite, encompassing at least two Equator crossings in the same direction, so that we can estimate the nodal period of the satellite. Normally, none of the sub-satellite points will fall exactly on the Equator, so it may be necessary to do a bit of careful

interpolation to find the precise moments of Equator crossing.

Let us introduce the following notation, where the superior arrow will be used to express a vector quantity. We use the unit vectors $\vec{I}$, $\vec{J}$, and $\vec{K}$ to denote a right-hand orthonormal basis in the celestial system, where $\vec{I}$ lies in the equatorial plane pointing from the center of the Earth toward the Vernal Equinox, $\vec{J}$ toward a point 90 degrees eastward of the Vernal Equinox, and $\vec{K}$ toward the North Pole. Let $\vec{N}$ denote the unit vector pointing toward the satellite's ascending node, and $\vec{E}$ a unit vector in the equatorial plane pointed 90 degrees east of the ascending node $\vec{N}$. Clearly, the angle between $\vec{I}$ and $\vec{N}$ is the right ascension. $\vec{P}$ denotes the unit vector orbital plane, and can be computed as the normalized cross product of any two non-collinear satellite positions. Let $\vec{P}'$ be the projection of $\vec{P}$ onto the equatorial plane, and let $\vec{M}$ be a unit vector in the orbital plane pointing toward the northernmost position of the satellite. We denote the epoch T_o as the time of first equator crossing, and by A the angular rate of change of the right ascension in degrees per day. Finally, let U be a unitizing operator which normalizes any vector by dividing it by its own components of an arbitrary vector. Then at the initial time T

$$\vec{P} = U(\vec{S}_1 \times \vec{S}_2)$$

where S_1 and S_2 are two non-collinear satellite position vectors, perferably chosen so that they are approximately orthogonal, or separated by about 25 minutes in time. Moreover,

$$\vec{P}' = P(I)\vec{I} + P(J)\vec{J} + 0\vec{K}$$

$$\vec{N} = U(\vec{P}' \times \vec{P})$$

$$\vec{E} = \vec{K} \times \vec{N}$$

$$\vec{M} = \vec{P} \times \vec{N}$$

At some later (or earlier) time T, the following relationships obtain:

$$\vec{N}(T) = \text{cosine}(At)\,\vec{N} + \text{sine}(At)\,\vec{E}$$

$$\vec{P}'(T) = \vec{N}(T) \times \vec{K}\ \text{mag}(P')$$

$$\vec{P}(T) = P'(I)\,\vec{I} + P'(J)\,\vec{J} + P(K)\,\vec{K}$$

$$\vec{M}(T) = \vec{P}(T) \times \vec{N}(T)$$

where $t = (T - T_o)$, and the mag( ) operator denotes the magnitude (length) of a vector. The three vectors $\vec{N}(T)$, $\vec{M}(T)$, and $\vec{P}(T)$ constitude an orthonormal basis, with two of them ($\vec{N}(T)$ and $\vec{M}(T)$) lying in the orbital plane. If W is the nodal period of the satellite, inferrable from the times of successive equator crossings,

an approximate position of the satellite can be estimated at time T as

$$\vec{S}(T) = \text{cosine}(360\ t/W)\ \vec{N}(T) + \text{sine}(360\ t/W)\ \vec{M}(T)$$

The discrepancy between this crudely-estimated position, and the known Earth location can be obtained, i.e.

$$\vec{X}(T) = \vec{S}(T) - \vec{S}$$

Let us use the lower case letters $\vec{i}$, $\vec{j}$, and $\vec{k}$ to denote an orthonormal coordinate system attached to the moving satellite, where $\vec{k}$ is a unit vector pointing downward toward the center of the Earth, i points in the direction of motion of the satellite, and j points to the right of the motion. We have:

$$\vec{k}(T) = -U(\vec{S}(T))$$

$$\vec{i}(T) = \vec{k}(T) \times \vec{P}(T)$$

$$\vec{j}(T) = \vec{k}(T) \times \vec{i}(T)$$

Then the discrepancy vector can be resolved into vertical, along-track, and cross-track components by:

$$x(T) = \vec{X}(T) * \vec{i}(T)$$

$$y(T) = \vec{X}(T) * \vec{j}(T)$$

$$z(T) = \vec{X}(T) * \vec{k}(T)$$

where * is the dot product operator. These three error components can be resolved by a Fourier analysis as a function of the nodal anomaly (360 t/T), and the resulting coefficients then used to correct the approximate position S(T) with a more precise one:

$$\vec{S}(T) = \vec{S}(T) + \vec{i}\ (c0 + c1\ \text{cosine}(A-e_1) + c2\ \text{cosine}((2(A-e_2)) \qquad (3)$$

The values c0, c1, and c2 are cosine coefficients obtained from the Fourier analysis, and e_1 and e_2 are corresponding phase angles. We have now corrected the satellite position vector S(T) for the along-track error associated with the first approximation. Similar corrections may be applied to remove cross-track and vertical errors as well, though these are usually far smaller than the along-track error. In fact, for the NOAA-10 satellite on 10 September, the Fourier error components were:

harmonic	x	phase	y	phase	z	phase
0	5.33	180.00	0.02	0.00	4.30	0.00
1	14.65	107.04	0.74	61.88	8.24	16.50
2	0.72	-46.29	0.01	39.36	1.47	-0.21
3	0.04	-9.75	0.02	40.44	0.01	29.90
4	0.03	13.94	0.01	37.48	0.01	24.16
5	0.01	29.63	0.01	-21.90	0.01	-25.34
6	0.02	-26.19	0.01	-5.25	0.01	-7.44
7	0.02	-8.70	0.01	4.12	0.01	2.75
8	0.02	-6.02	0.01	-12.45	0.01	-7.60
9	0.02	3.61	0.00	19.44	0.01	11.21

showing that the amplitude of the along-track error was 14.65 kilometers, whereas the cross-track amplitude was .74 km. The maximum vertical amplitude, if we care to remove it, is 8.24 km. The biases and RMS errors of the satellite positions, predicted five days into the future, i.e. for 15 Sepetmebr 1987, expressed in kilometers, were:

x,y,z	BIAS:	4.09	0.02	-0.04
	RMS:	5.55	0.56	2.06

where a positive x-bias means that the satellite position predicted by equation (3) was ahead (further along the orbit) than the true position. This result compares favorably with the position predicted by the Brouwer-Lyddane model, which had 10.38 km as the along-track RMS error, versus 5.55 km for the simple model.

3. SUMMARY

De-navigation of Earth-located satellite data affords not only a means to obtain orbital characteristics which may otherwise be difficult to obtain, but also allows the use of a much simplified navigation algorithm, suitable for small computers, faster than the classical Keplerian-Newtonian models, and competitive with the latter in accuracy.

REFERENCES

1. Bowditch, N., 1977, 'American Practical Navigator', Pub. No. 9, Vol I, Defense Mapping Agency Hydrographic Center, p. 371

2. Brouwer, D., November 1959, 'Astronomical Journal', Vol 64, No. 1274, p.378

3. Durant, W., 1935, 'The Story of Civilization', Simon and Schuster, New York

4. Lyddane, R.H., October 1963, 'Astronomical Journal', Vol 68, p. 555

5. Nagle, F., 1987, 'High-Level Fortran', unpublished document available on request, Madison.

PLANS FOR TOVS PROCESSING AND DISTRIBUTION AT THE ITALIAN METEOROLOGICAL SERVICE

P. Pagano - Italian Meteorological Service, Rome - Italy

Abstract

A HRPT receiving station has been operational at the Italian Meteorological Service since January 1988. The plans for the use of the station include the implementation of ITPP software for TOVS processing on a dedicated VAX system.

Raw and/or processed TOVS data will be available to users in real time through a connection with the facilities of Rome RTH, while historical data will be part of the Earthnet archive.

The possibility of disseminating TOVS data by means of the MDD mission is also suggested.

1. INTRODUCTION

A HRPT station has been implemented at the Italian Meteorological Service in 1987 and it is operational since January 1988. The station, whose block diagram is shown in fig. 1, is based on a steering 3.5 m antenna, with the receiving chain backed by a PDP 11/44. Full automatic program tracking allows to track every useful pass up to seven days, limited only by the degradation of precision in the TBUS-derived orbit propagation for tracking.

2. PLANS FOR AVHRR AND TOVS PROCESSING

Since the setting up of the station, AVHRR images are being extracted and used for supporting in qualitative way meteorological operations. The plans for the use of the station in near future are based, as a first priority, on the quantitative use of AVHRR data, by means of a numerical treatment of imagery data for multispectral analysis and identification of particular features. A specific program foresees the tailoring of high resolution sub-sectors for areas of specific interest and some pseudo-images, obtained as a result of a numerical treatment, to be formatted in a WEFAX format and disseminated via landlines to local meteorological offices.

As a second priority TOVS data elaboration is considered, by means of the International TOVS Processing Package (ITPP), acquired from the University of Wisconsin, Madison, USA.

The first step for TOVS processing will be based on the production of maps of thicknesses and hence of actual profiles, to be used, in a qualitative way, by the operational forecasters to support nowcasting activity.

Eventually, the use of TOVS profiles as an input for the fine-mesh limited area model, under development at the Italian Meteorological Service, would be considered.

So far ITPP, IBM version, has been acquired, and its implementation on the system already started. However the final operational version for TOVS processing is planned to run on a dedicated VAX system; therefore the present activity should be rather considered as an exercise, to experience how the package works and what major problems for its implementation have to be faced.

The implementation on the VAX system will start as soon as the new ITPP, VAX version, will be made available to users.

3. AVAILABILITY OF TOVS DATA

a. Archive data

Since January 1988, the Rome HRPT station is part of the Earthnet network for TIROS data archive. This archive, managed by ESA/ESRIN, Earthnet Programme Office, located in Frascati, Italy, is based on a network of three receiving stations, the other two being Maspalomas ans Tromsoe.

The coverage of NOAA receiving station network is shown in fig. 2.

Therefore TOVS data, extracted from HRPT data stream, are made available to users through the distribution channels of ESRIN, which is taking over the responsibility of the data service.

The Earthnet archive is still in an experimental phase and, for the time being, the Rome station is supplying it with one pass/day (afternoon pass), but the amount of data is planned to increase up to 4-6 pass/day as soon as it will become operational, at the end of 1988.

b. real time data

The real-time availability of TOVS data from Rome station is based on the concept of data circulation at the Italian Meteorological Service, which is shown in fig. 3, as it will be at the end of 1988.

According to this concept, TOVS data received from the HRPT station, will be extracted from the data stream and transferred from the receiving station onto the system (a micro-VAX 3500), on which the processing will take place.

Processed data, as well as raw data (depending on users' requests), will therefore be sent to the Rome RTH (based on cluster of two VAX 8250 computer). Hence the data will be transferred to the data bank, in the IBM environment, for temporary storage (tipically 1 day), and eventually to the IBM Series 1 computers.

Remote users, other than those connected locally to the central facility (IBM 3090 and/or 4381), will be allowed to get TOVS data either through a scheduled transmission programme, or (the qualified users) via a direct request to the data bank, using a dedicated or switched line in a DECNET, X-25 or IBM 3270 environment.

4. DATA DISSEMINATION VIA MDD

With the launch of METEOSAT MOP-1, scheduled for the end of 1988, the MDD (Meteorological Data Distribution) mission will be set up.

The concept of the MDD mission is to complement the GTS, mainly in those countries lacking ordinary telecommunication links, such as Africa.

It is based on two uplink stations, one to be located in Rome at the Italian Meteorological Service, the other at the British Met. Office in Bracknell, U.K. The two stations will uplink onto the Meteosat alphanumeric as well as facsimile charts on two channels, 2400 BPS. In the nominal case the Rome station will transmit alphanumeric data, while the Bracknell station will handle facsimile charts; at any rate each station is intended to be used as a back-up of the other. The data will be relayed by Meteosat to any user, in the Meteosat field of view, operating a SDUS-type station properly equipped.

Being the MDD mission operational, it would be worth considering the opportunity of including in the dissemination schedule also TOVS processed data, possibly not only the Italian ones, in order to provide users with a wide coverage of high resolution soundings in near real time for nowcasting purposes.

Of course the scheme for this operation needs to be supervised by EUMETSAT and possibly coordinated with WMO, to define standardized procedures and formats for TOVS processing and assure the proper quality level of end product.

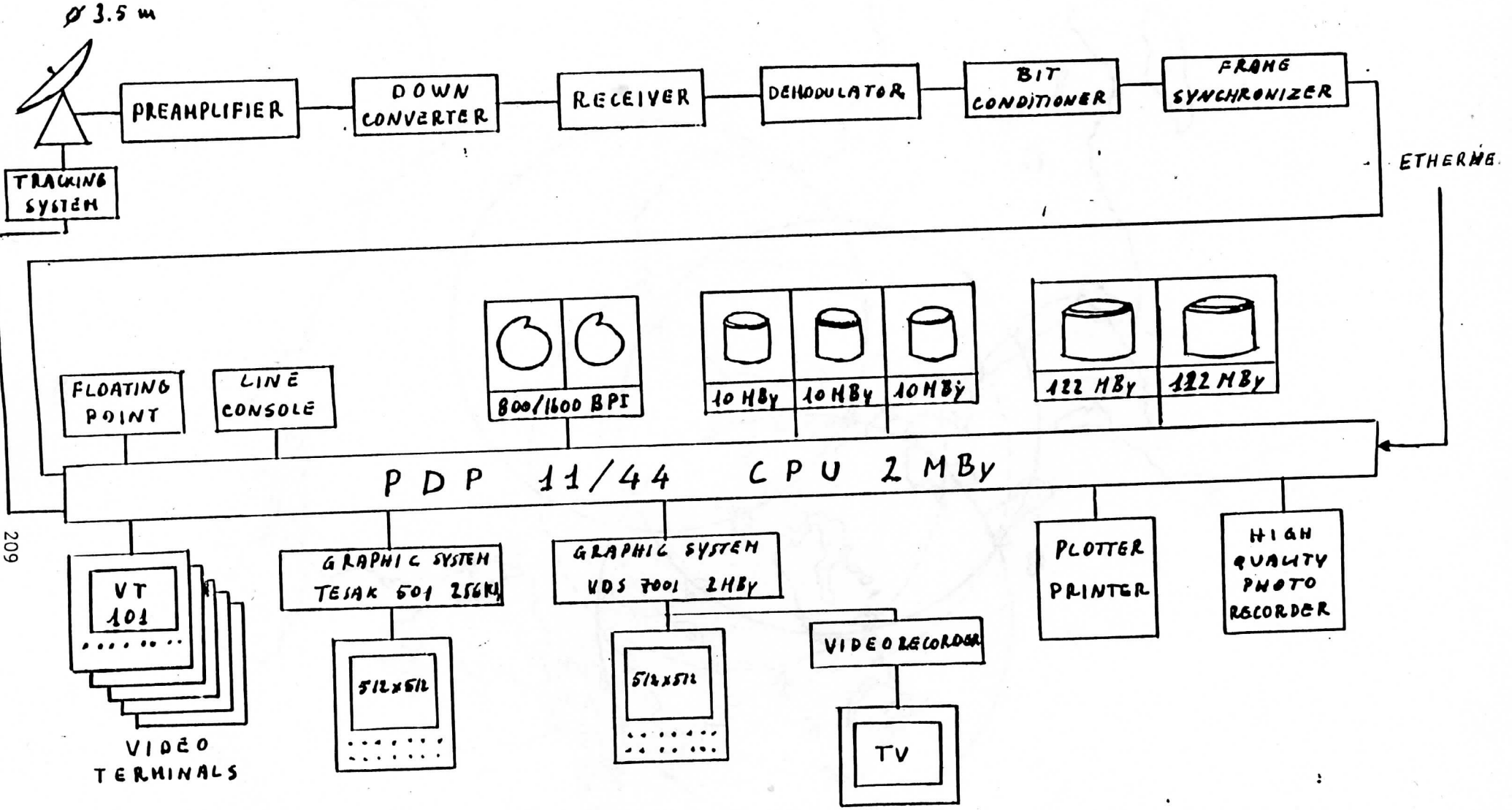

Fig. 1 - HRPT receiving station

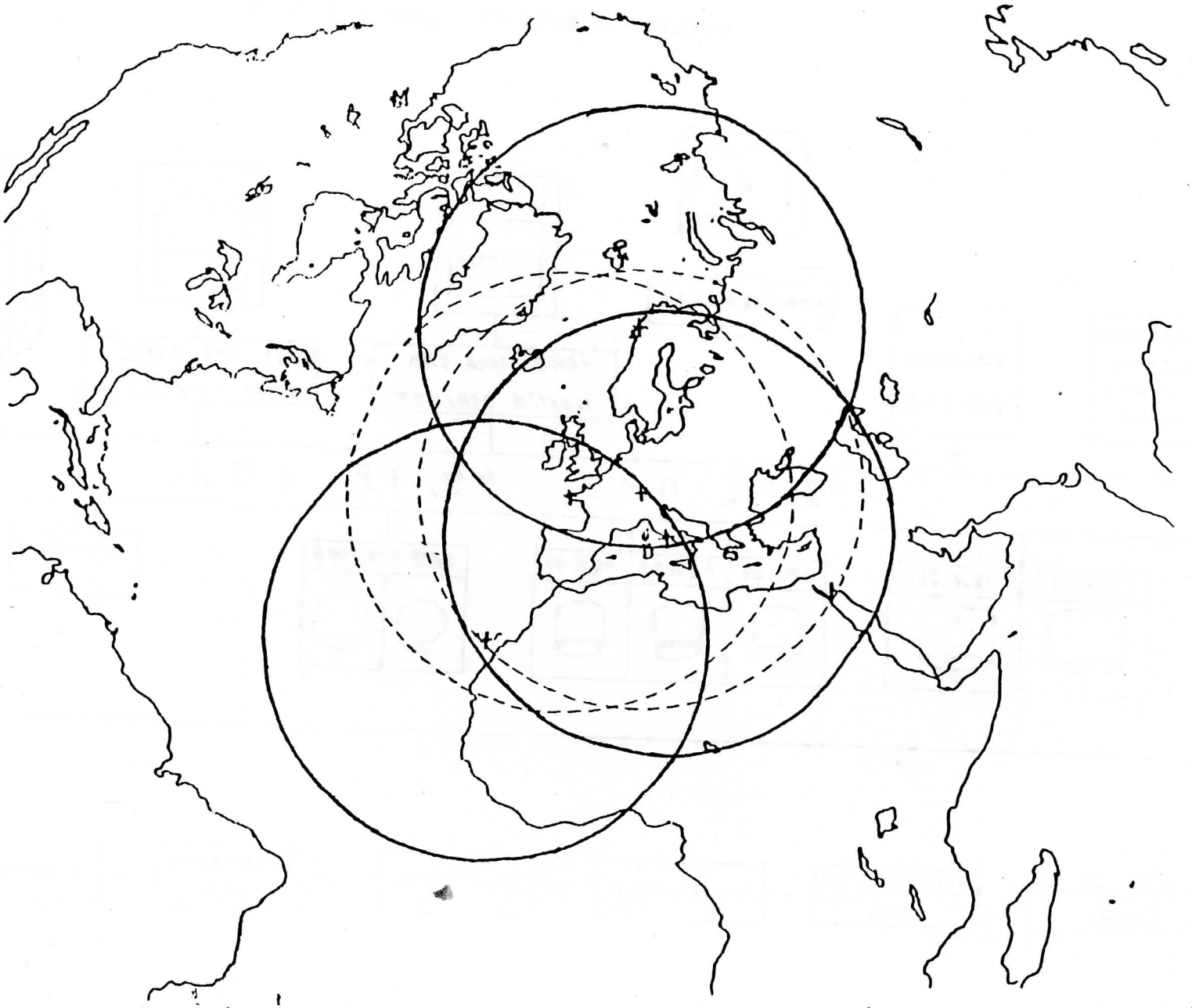

FIG. 2 - ——— Coverage of NOAA receiving stations network (Roma, Maspalomas, Tromsoe)

- - - - Coverage of possible other stations (Lannion, Oberpfaffenhofen)

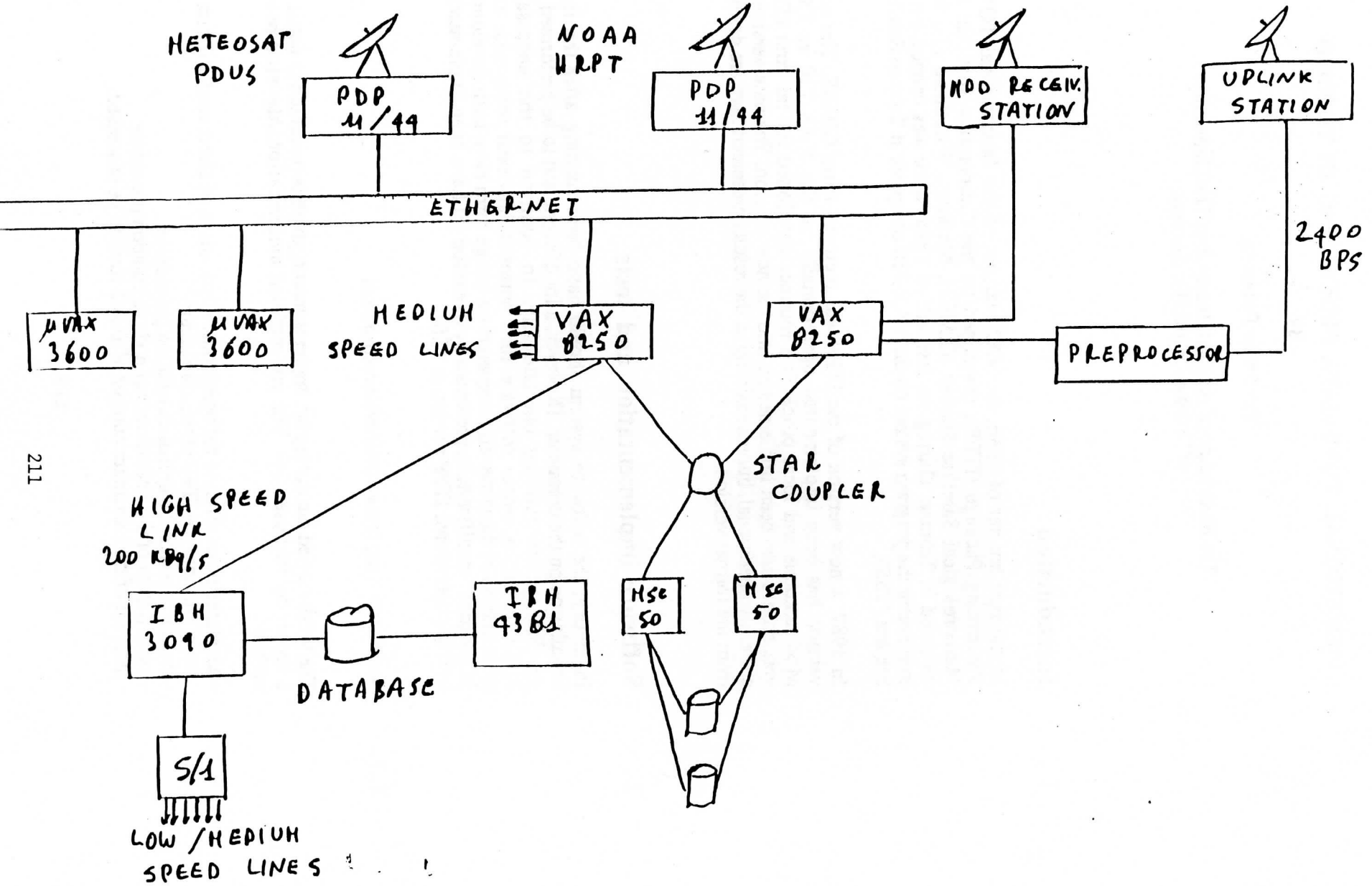

Fig. 3 - Data circulation scheme at the Italian Meteorological Service (end 1988)

OPERATIONAL TOVS DATA PROCESSING IN TROMSØ

By

Jan-Petter Pedersen,

The Foundation of Applied Research at The University
of Tromsø (FORUT), Norway.

1. Introduction

In the first quarter of 1986, the VAX version of the International TOVS Processing Package (ITPP), developed by the Cooperative Institute for Meteorological Satellite Studies (CIMSS), Madison, Wisconsin [3], was received in Tromsø. During the last half of 1986, work was carried out to implement the program system on the VAX-730 computer at Tromsø Satellite Station (TSS).

In 1987, a new version of the ITPP was recieved from CIMSS. The new version has been implemented operationally on the VAX-730 at TSS. Modifications and local processing routines developed for the first ITPP version has also been implemented into the new version. The new version is currently operational, but the majority of the results presented here are derived from the former version.

2. Software implementation and tests

In theory, the software system should have been running after the first installation on the computer. However, a lot of work had to be performed to get the system running operationally. In addition to the necessary implementation work, software for optional full/local retrievals, and presentation of the retrieved parameters on image form have been developed. In addition, modifications presented by Svensson [5] have been implemented into the operational ITPP version at TSS.

2.1. Software implementation/development

The work carried out during the implementation phase is presented in detail in a report by Pedersen [4]. The pre-retrieval modifications/developments include :

- development of routines for operational applications of direct read-out data from TSS into the ITPP processing chain
- modifications of the orbital calculation procedures
- modification of the satellite orbital node calculation procedure
- increase of the maximum number of TOVS lines to be processed.

Retrieval procedure modifications include :

- increase of the maximum number of sounding spots to be processed
- correction of system bug for handling data from latitudes exceeding the satellite tangential latitude (π - inclination)
- development of routines for subsequent local retrieval surrounding specified geographical locations

Post-retrieval development includes a routine for presentation of retrieval parameters on image form including relevant annotation, grid and landcontours.

2.2. System performance tests

After the modifications and new developments had been implemented, real NOAA/TOVS data read out at TSS, were applied for testing the performance of the ITPP when dealing with data from the Arctic. All four first guess options have been applied in the presented work. The resulting satellite retrievals have been compared with radiosondes data from some of the Norwegian meteorological stations in the Arctic region [4].

Figure 2.1 shows the locations of the meteorological stations for which the data comparisons have been made. Using the developed local processing option, the satellite sounding spot closest to the geographical position of the actual station is determined from the preprocessed data.

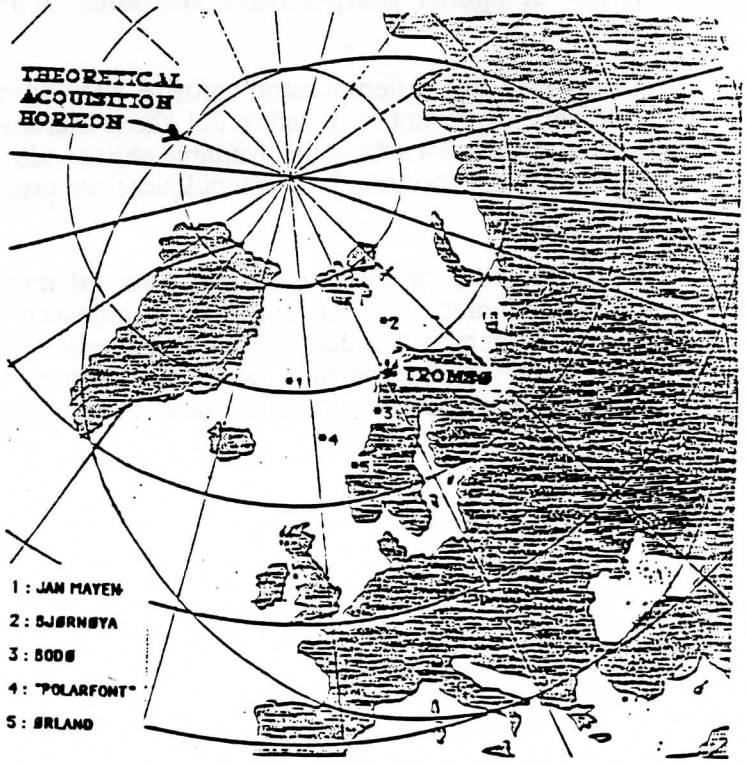

Figure 2.1 : Location of meteorological stations in the Arctic applied for data comparisons. Also presented in the figure is the theoretical 0 deg. elevation acquisition horizon for Tromsø Satellite Station (TSS).

The data comparison results are presented as RMS differences for the four modes at the available pressure levels. RMS curves have been derived for the temperature and the dewpoint temperature profiles. Notice, however, that the statistical material used for generation of the RMS curves is limited to maximum 12 comparable radiosonde versus satellite profiles for each first guess mode. Figure 2.2 and 2.3 present the derived RMS temperature and dewpoint temperature profiles.

2.2.1. RMS temperature profile statistics discussion

The conclusion that can be made from the presented RMS temperature statistics is that although the average absolute RMS differences presented in figure 2.2 are somewhat increased compared to results presented by others [2, 6], three of the different processing modes seem to give reasonable results for operational temperature profiling by applying the available processing system.

Although the non-surface data climatology mode is the one giving the best RMS coincidence with the radiosonde in the uppermost layers, and in the mid-atmosphere, the RMS values observed towards 1000 mb are too coarse for operational applications.

From the four different modes, the two regression modes seem to give the overall best results. Compared to the surface data climatology mode, the overall performance is approximately constant 0.5 deg. Kelvin better for the two regression modes for all levels except 1000 mb.

2.2.2. RMS dewpoint temperature statistics discussion

Compared to the temperature profile RMS statistics, the dewpoint RMS differences presented in figure 2.3 show increased both relative as well as absolute deviations from the available radiosonde profiles. From the presented data it is observed that best coincidences are present at 300 mb, and towards 1000 mb.

From the four processing modes, none of them can be identified as the uniquely better one. The important conclusion that can be made from the presented data is that due to the overall poor coincidences between satellite and radiosonde dewpoint data, the present ITPP system has limited operational aspects regarding dewpoint profiling in our Arctic regions.

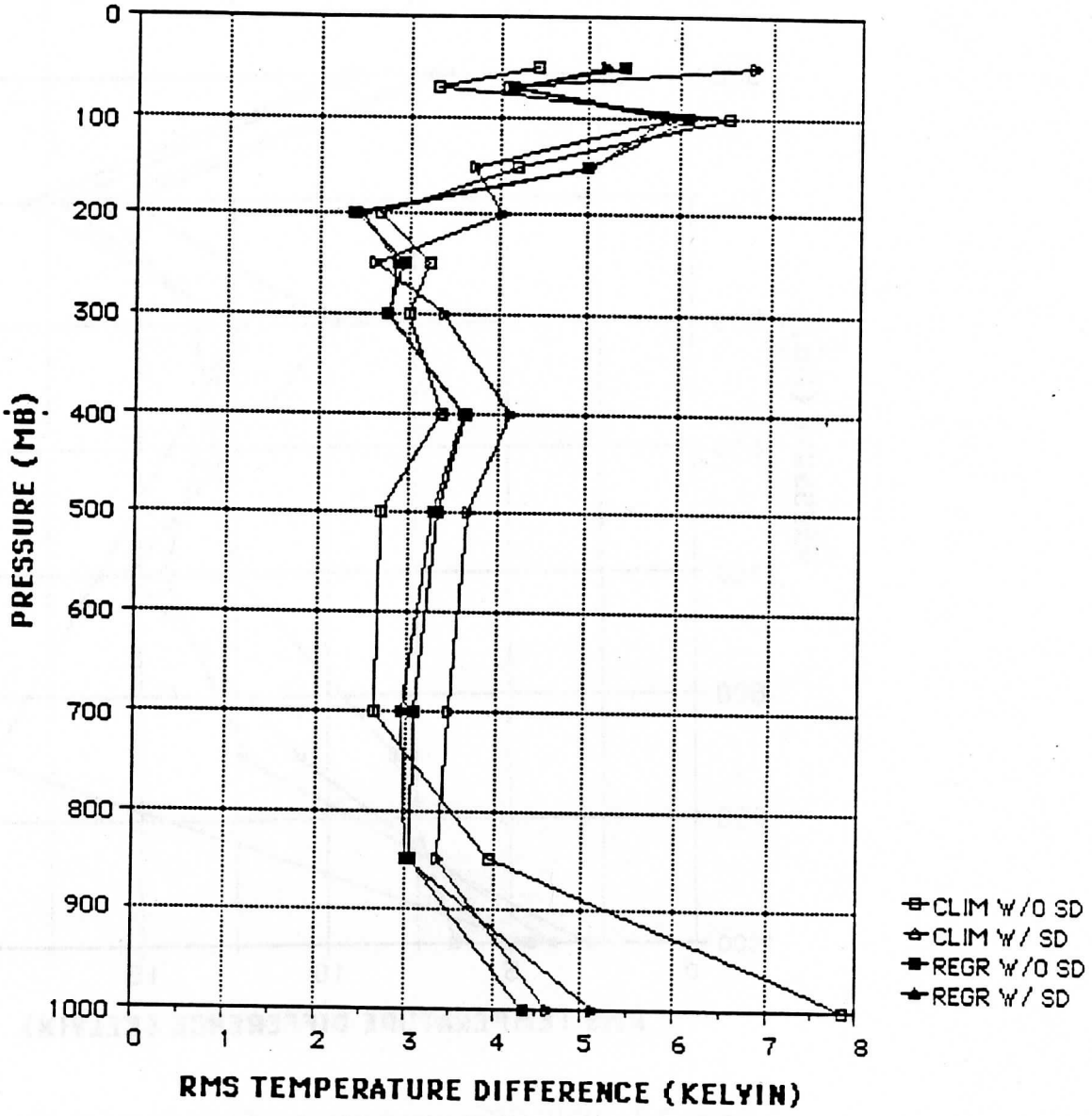

Figure 2.2: RMS differences between radiosonde and satellite retrieval mode temperature profiles.
CLIM W/O SD: Non-surface data climatology, N=12 soundings
CLIM W/ SD: Surface data climatology, N=8 soundings
REGR W/O SD: Non-surface data regression, N=8 soundings
REGR W/ SD: Surface data regression, N=8 soundings.

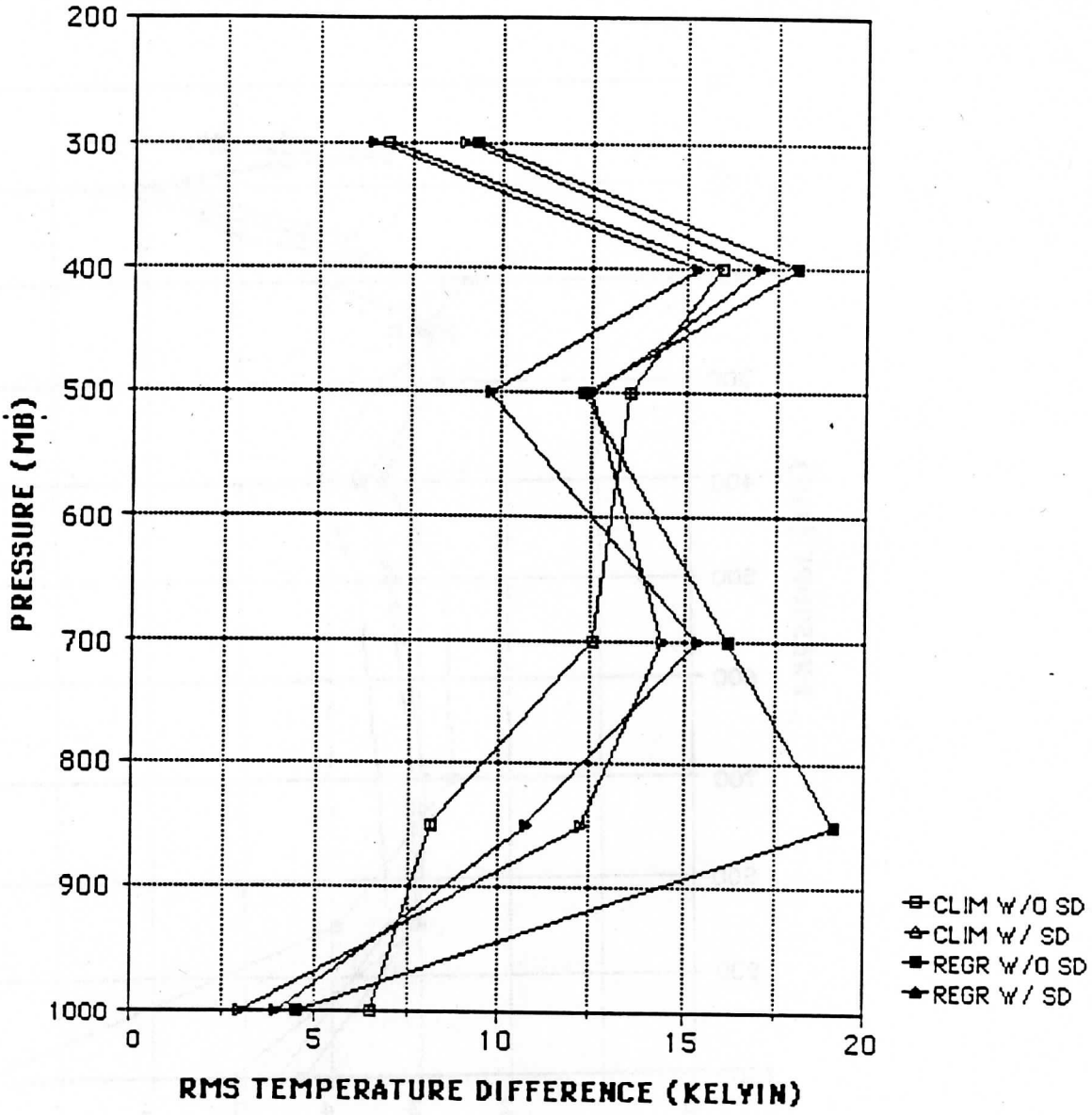

Figure 2.3 : RMS differences between radiosonde and satellite retrieval mode dewpoint temperature profiles.
CLIM W/O SD: Non-surface data climatology, N=12 soundings
CLIM W/ SD: Surface data climatology, N=8* soundings
REGR W/O SD: Non-surface data regression, N=8* soundings
REGR W/ SD: Surface data regression, N=8* soundings.

3. Operational applications of NOAA/TOVS data.

3.1. Studies of the atmospheric Ozone content in Arctic regions.

Since January 1987 the total atmospheric Ozone content has been studied at certain locations in the Arctic from NOAA/TOVS data read out at TSS. Using

the local processing option, TOVS data from Longeyarbyen (Spitzbergen), Tromsø, Oslo (Norway) and Sodankyla (Finland) have been processed daily. This project is performed in personal cooperation with S. Larsen at the Physical Institute at the University of Oslo (UiO). All ground measurements have been provided by Larsen [1], while all satellite measurements have been provided from Tromsø.

From January until March 1987 NOAA-9/TOVS data read out at TSS was applied. After the serious NOAA-9 MSU calibration trouble occured in March 1987, the ozone content study project temporarily ended. In late autumn 1988 the project was restarted again, using the TOVS system onboard NOAA-10.

The satellite derived Ozone contents have been compared to corresponding ground measurements. The ground measurement is always performed at 1200 GMT, while the satellite masurement time can differ from day to day. Therefore, the variable measurement time difference has to be kept in mind when comparing the data.

The results from the data comparisons are presented in figures 2.4 - 2.6. In figure 2.4 the results from the comparisons of ground measured and NOAA-9/TOVS measured Ozone contents for Oslo for the period January 1987 until March 1987 are presented. The data comparison for this period shows that on average the satellite underestimates the Ozone content by 12-13 % [1].

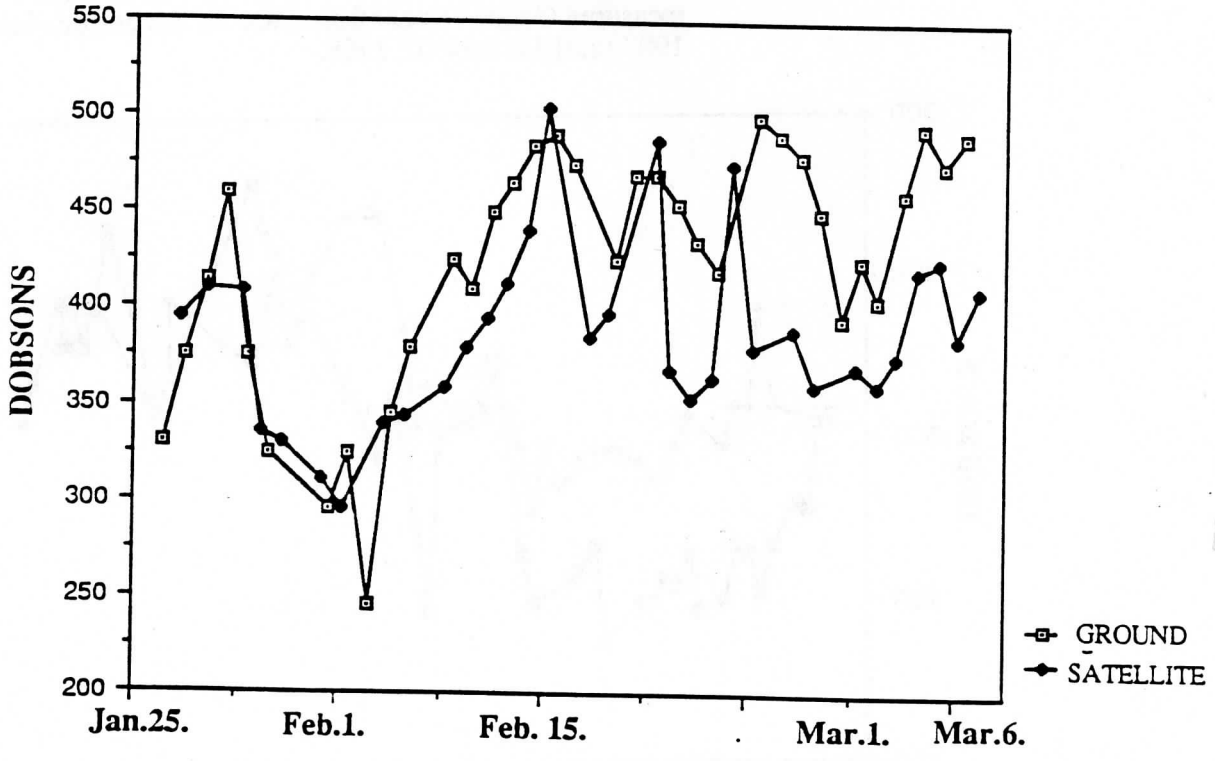

Figure 2.4 : Comparison of ground measured and NOAA-9/TOVS measured ozone content from Oslo for the period January 25. until March 6. 1987.

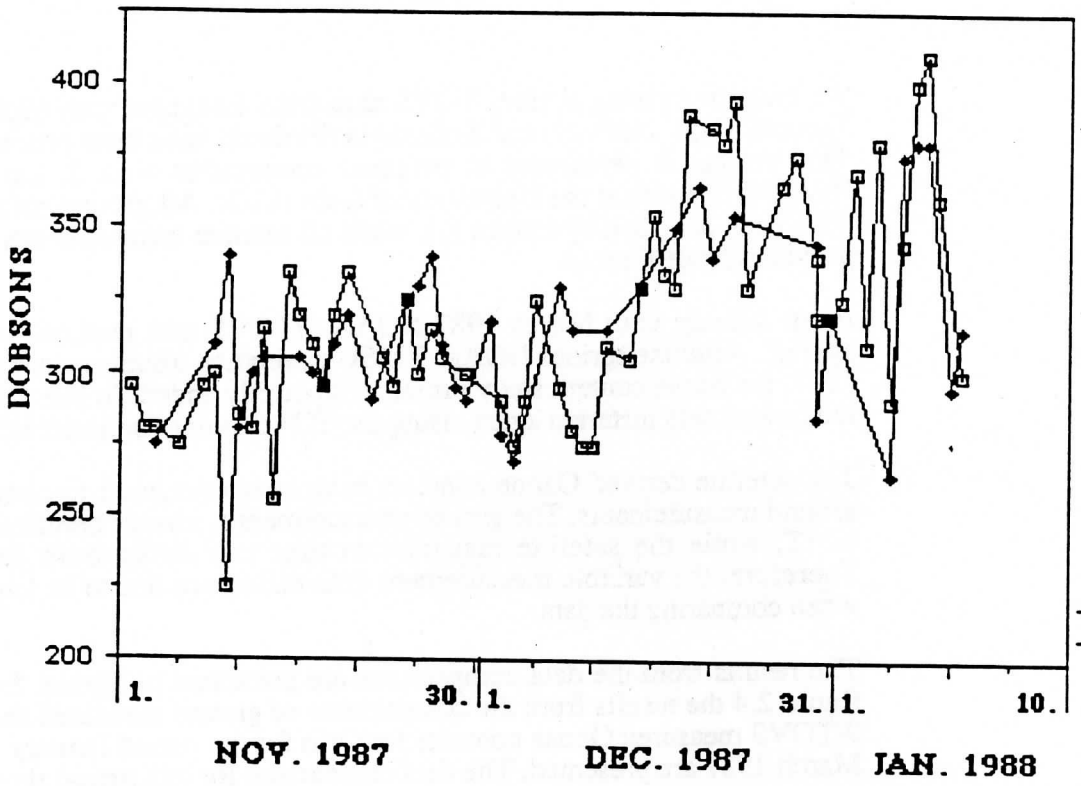

Figure 2.5 : Comparison of ground measured and NOAA-10/TOVS measured Ozone content from Oslo for the period November 1. 1987 until January 10. 1988.

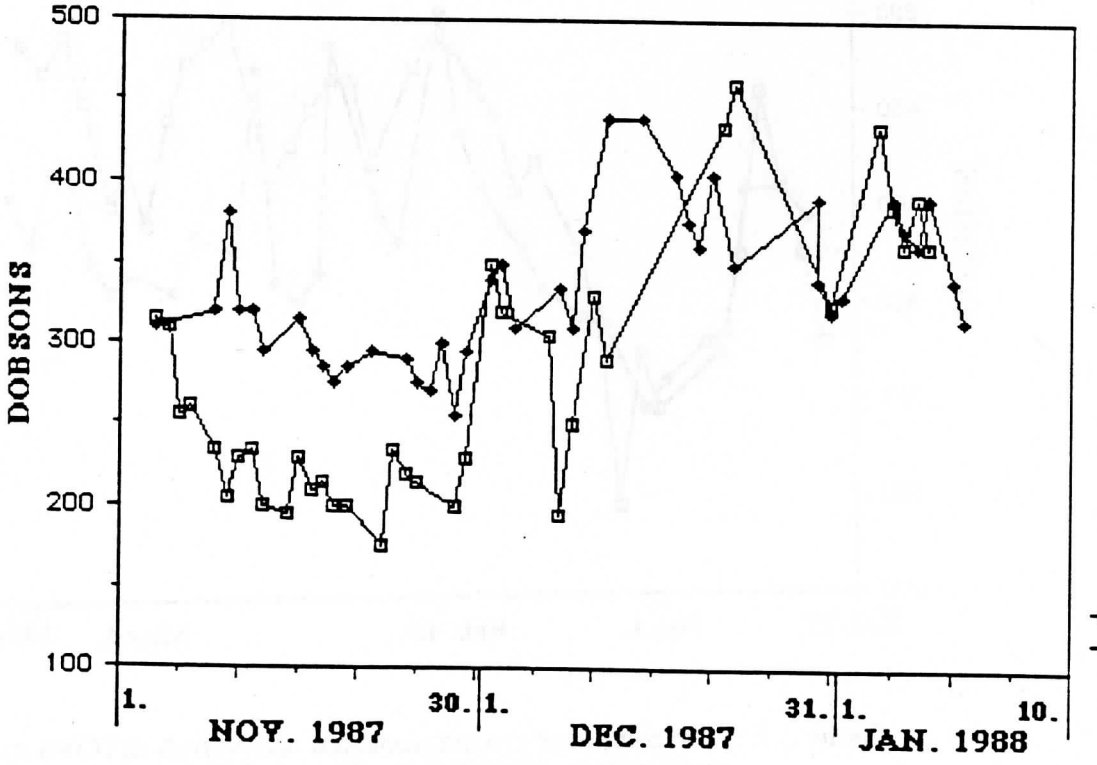

Figure 2.6 : Comparison of ground measured and NOAA-10/TOVS measured Ozone content from Tromsø for the period November 1. 1987 until January 10. 1988.

From the data presented in figures 2.5 and 2.6, the RMS deviations between ground and satellite measurements have been derived for respectively Tromsø and Oslo. The results are presented in table 2.1.

Location	RMS deviation (Dobsons)	Number of comparisons
Tromsø	16	26
Oslo	5	33

Table 2.1 : RMS deviation between ground measured and NOAA-10 measured Ozone contents for Tromsø and Oslo for the period November 1. 1987 until January 10. 1988.

Comparing the RMS deviations for Oslo and Tromsø shows that the observed deviation for Tromsø is increased by a factor > 3 compared to that for Oslo, from 5 Dobson units until 16 Dobson units. The observed difference may be explained from ground measurement uncertainties since the sun is below the horizon in the actual period in Tromsø. The RMS result observed for Oslo shows coincidence within 5 Dobson units between ground and satellite measurements.

In addition to the Ozone studies for the certain locations, developed routines [4] have been applied for studies of the spatial Ozone distribution. Figure 2.7 shows the Ozone content in Northern Europe derived from NOAA-9/TOVS data on February 23. 1987. The white areas represent the lowest contents, while the darkest areas represent the highest.

Visible from the figure is low Ozone content in the Northernmost areas, and also a number of local, small areas of minimum Ozone contents. South of Scandinavia is observed an extended minimum content area. Comparing the derived Ozone contents with corresponding visible data shows that some of the areas of minimum Ozone content coincide with cloud covered areas. Therefore, from this data set it looks like some of the observed features can be explained from the present cloud cover.

Another interesting feature observed from figure 2.7 is that the low content area in the Northernmost region coincides with the TOVS scan lines. Studying a sequence of images (not presented here) shows that minimum Ozone contents are systematically detected at the beginning of the satellite passes before the first sensor calibration cycle. The image presented in figure 2.7 is generated from a descending satellite pass. In order to document the observation, data from an ascending pass are presented in figure 2.8. In this figure the low Ozone content area is at the bottom of the image. An explanation of this observation is that for all data preceeding the first calibration cycle, mis-calibration of the HIRS channels applied for the Ozone retrieval give resulting minimum contents.

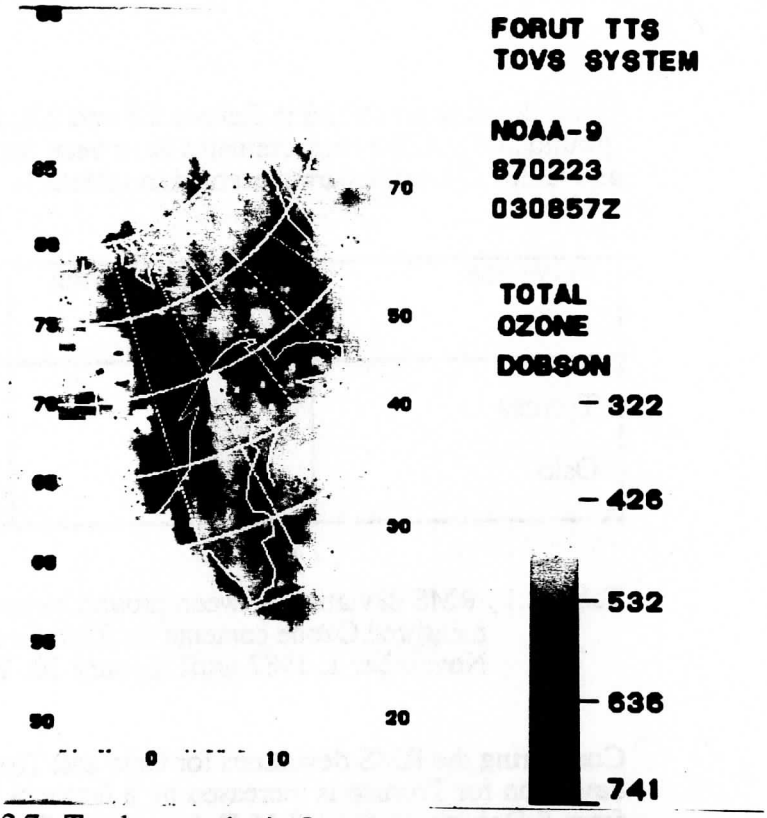

Figure 2.7 : Total atmospheric Ozone content in Northern Europe on February 23. 1987. Data from NOAA-9 read out at TSS. Notice the minimum content area at the top.

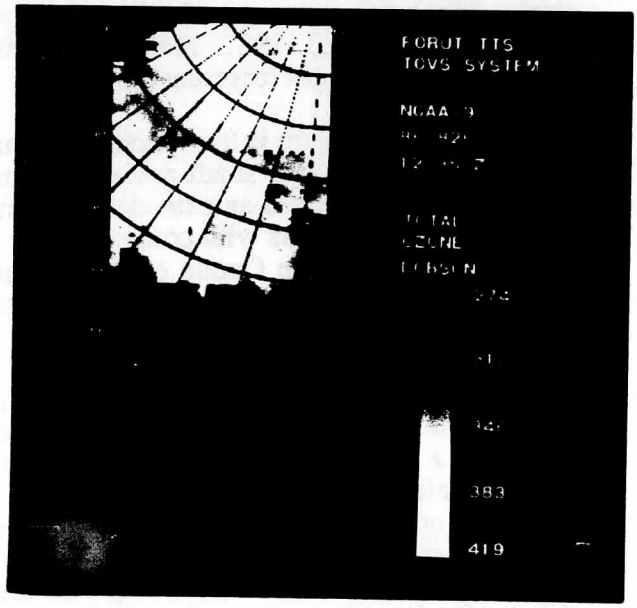

Figure 2.8 : Total atmospheric Ozone content in Northern Europe on August 26. 1986. Data from NOAA-9 read out at TSS. Notice the minimum content area at the bottom.

3.2. TOVS based atmospheric corrections of AVHRR surface temperatures.

The absolute surface temperatures are obtained from inversion of the equation of radiative transfer [4] :

$$R(\lambda, p, \mu, \phi) = \tau(\lambda, p_s, \mu, \phi)\, \varepsilon(\lambda, \mu, \phi)\, B(\lambda, T(p_s)) + \int_{\tau(\lambda, ps, \mu, \phi)}^{1} B(\lambda, T(p))\ \delta\tau(\lambda, p, \mu, \phi) \qquad (1)$$

The equation of radiative transfer is implemented operationally in a NOAA data processing software system at TSS. From knowledge about the atmospheric composition, its influence on the detected satellite signal represented by the atmospheric transmittance $\tau(\lambda, p_s, \mu, \phi)$ and the second term in equation (1) may be computed and corrected for. For the operational implementation of equation (1), the surface is assumed to be a perfect black-body, i.e. $\varepsilon(\lambda, \mu, \phi) = 1.0$.

For demonstration of the effects from atmospheric corrections of sea-surface temperature derivation from thermal infrared satellite observations, non-atmospheric and atmospheric corrected tables for conversion of AVHRR digital counts into temperatures have been generated. Also given is a comparison of conversion tables based respectively on radiosonde and TOVS profiles as input to the atmospheric correction procedure.

Data from the island Jan Mayen was applied for the actual study. NOAA satellite data read out at TSS and radiosonde data from the meteorological station on the island was available. The satellite data was acquired on August 26. 1986 at 1350 GMT, while the radiosonde was launched from the island at 1200 GMT.

Using the operational TOVS data processing system, the atmospheric profiles were derived from the NOAA-9 data. Figure 2.9 presents the satellite derived and the corresponding radiosonde temperature and dewpoint temperature profiles in a (standard) sonde diagram.

From the different profiles presented in figure 2.9, the total atmospheric transmittances have been calculated for wavelengths corresponding to the NOAA/AVHRR thermal infrared channel 4. Figure 2.10 presents the total transmittance versus wavelength for the two source profiles.

Using the radiosonde and the TOVS temperature and humidity profiles also the integrated atmospheric path radiance represented by the second term in equation (1) can be calculated. Knowing all parameters in equation (1), a table for conversion of AVHRR digital counts into atmospheric corrected absolute sea-surface temperatures have been generated. The conversion table is presented on figural form in figure 2.11. For comparison is also a conversion curve for non-atmospheric corrected surface temperatures presented in the figure.

Studying the curves in figure 2.11 shows that the radiosonde and the TOVS input profiles give coinciding conversion tables. This is also expected, due to the small differences in the calculated atmospheric transmittance values presented in figure 2.10. The most interesting observation made from figure 2.11 is the difference between the non-atmospheric and the atmospheric corrected conversion tables.

Observe that the atmospheric correction shows the most significant influence for the highest temperatures. This observation is expected, and can be explained mainly from that the relative contribution from the atmospheric path radiance term increases with increasing temperature.

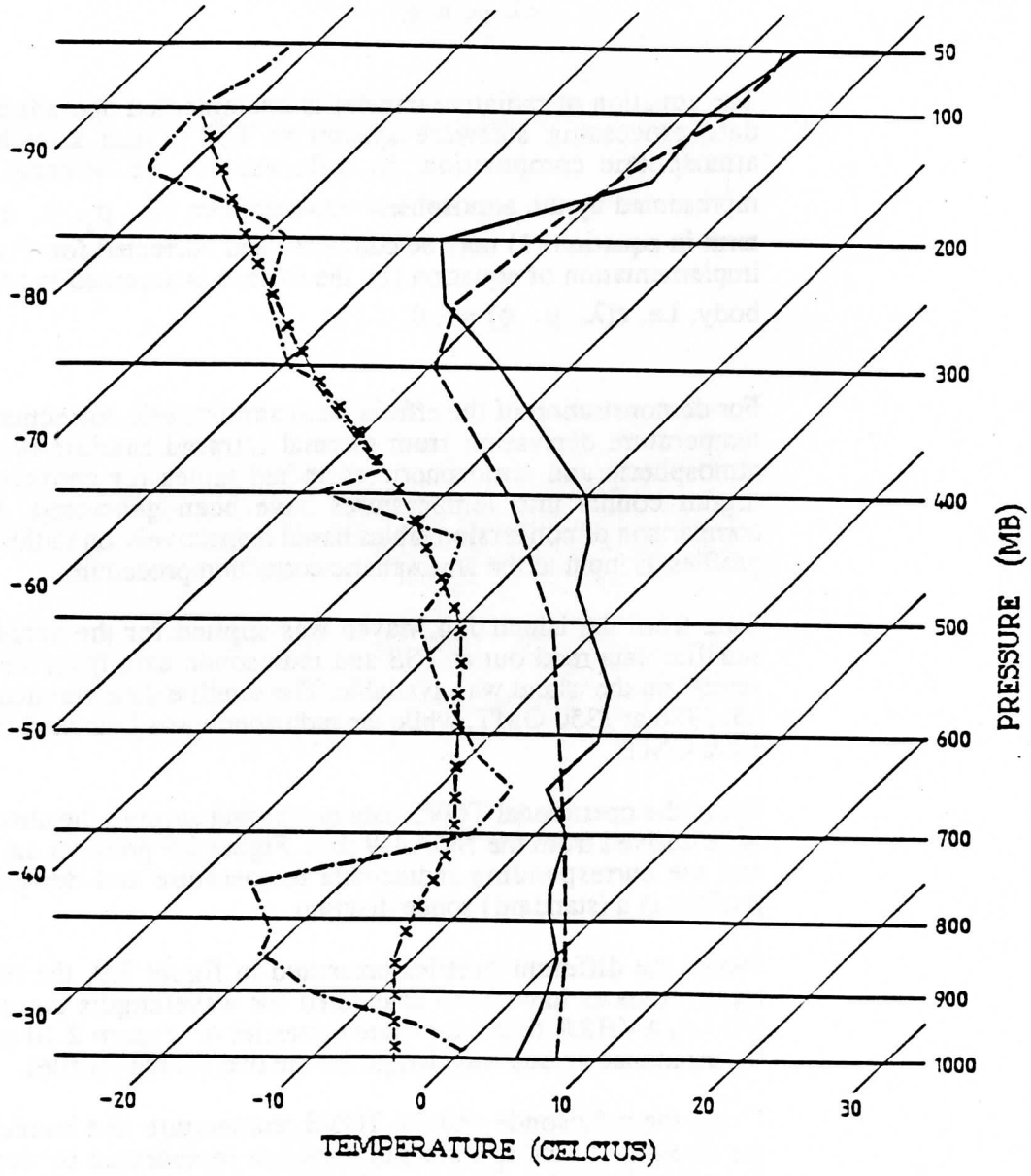

Figure 2.9 : Satellite and radiosonde temperature profiles acquired on August 26. 1986.

——— radiosonde temperature profile
-·-·- radiosonde dewpoint temperature profile
- - - - satellite temperature profile
-x-x- satellite dewpoint temperature profile

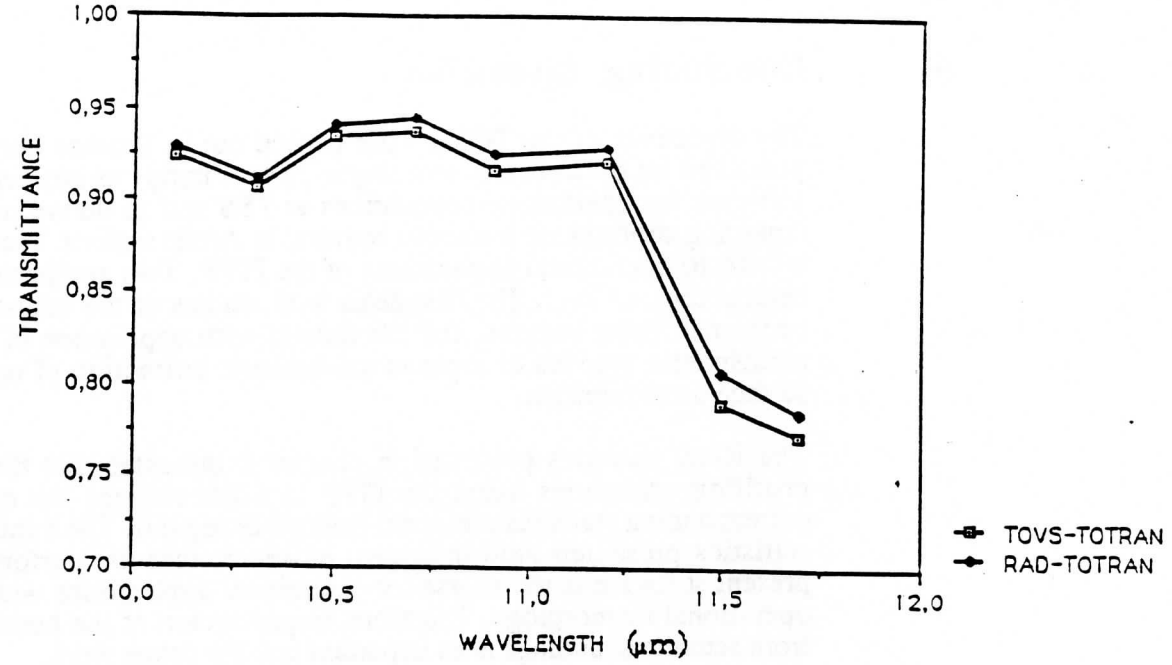

Figure 2.10 : Total transmittance versus wavelength for radiosonde (RAD-TOTRAN) and satellite (TOVS-TOTRAN) atmospheric profiles.

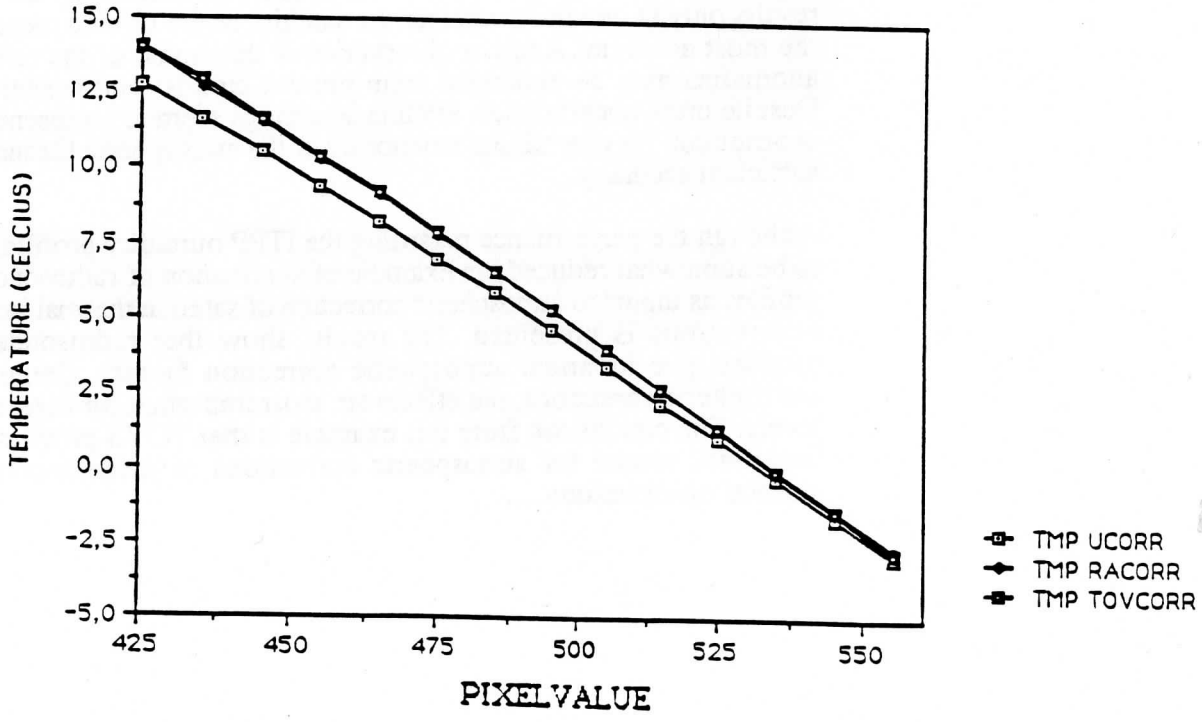

Figure 2.11 : Relationship between AVHRR digital pixelvalue and surface temperature in deg. Celcius, for:
a : No atmospheric corrections (TMP UCORR)
b : Radiosonde atmospheric corrections (TMP RACORR)
c : TOVS based atmospheric corrections (TMP TOVCORR).

4. Concluding discussion

The objectives of the TOVS work carried out in Tromsø during the recent years can be divided into two major parts. Firstly, to implement the ITPP software for operational applications at TSS and to derive initial statistics regarding atmospheric parameter retrieval in Arctic regions. The second part is related to operational applications of the ITPP. Two application areas have been presented here. The first deals with studies of the atmospheric Ozone content in Polar regions, and the second with application of TOVS based atmospheric profiles as input to atmospheric correction of optical satellite surface measurements.

The RMS statistics presented in chapter 2 indicates that the temperature profiling accuracies using the ITPP in Polar regions are comparable to corresponding statistics presented from other regions. The humidity profiling statistics presented here indicates, however, that the performance of the present software is too coarse for operational applications within fields like operational meteorology. Therefore, improvement of the humidity profiling from satellite soundings is an important task for future work.

The results presented from the Ozone content studies show that satellite observations coincide within 5-16 Dobson units with ground measurements. The presented results indicate that the coincidence changes with the seasons, depending upon the sun elevation. It is difficult based only on the presented results only to conclude whether the satellite or the ground measurements are the most accurate. Another observation is that some of the retrieved Ozone anomalies may be explained from present clouds (and sensor calibration). Despite these uncertainties, satellite soundings seem to represent an important contribution for operational monitoring of the atmospheric Ozone content with sufficient accuracy.

Although the performance regarding the ITPP humidity profiling is observed to be somewhat reduced, an example of application of radiosonde and TOVS profiles as inputs to atmospheric correction of satellite thermal infrared surface observations is presented. The results show that radiosonde and TOVS profiles give identical atmospheric correction factors. Compared to non-atmospheric corections, the effects are most important for higher temperature levels. The conclusion from this example is that TOVS profiles represent an important source for atmospheric corrections of simultaneously acquired surface observations.....

5. References

1. Larsen, S. : Physical Institute, Univ. of Oslo, Personal communication, 1987.

2. LeMarshall,J.F. : "An Intercomparison of Temperature and Moisture Fields Retrieved from TIROS Operational Vertical Sounder Data", Paper presented at ITOVS-2, Igls, Austria, February 1985, CIMSS.

3. Nelson, J.P. : "Documentation of the TOVS Bangladesh data processing software", CIMSS Report, February 1985.

4. Pedersen, J.P. : "Atmospheric parameter retrieval from satellites - Theory, implementation and application of a NOAA/TOVS data processing system -", FORUT Report IT5003/26-87.

5. Svensson, J. : SMHI, Norrkøping, Sweden, Personal communication, 1986.

6. Svensson, J. et al. : "Towards an Operational TOVS Processing Package", SMHI, FoU-Notiser, No. 50, February 1987.

MESO-SCALE ANALYSIS AND THE USE OF TOVS
A CASE STUDY USING 3I RESULTS

by G.J. Prangsma
KNMI, De Bilt, Netherlands

ABSTRACT

TOVS derived upper-air information for use in weather forecasting is generally fed into a numerical atmosphere model. This is commonly considered to be the most profitable, if not the best way to apply TOVS data.

An entirely different approach, based on theoretical work of Sutcliffe (1947), is presented here. In this method meteorological developments are linked to properties of the thickness field of a standard atmospheric layer. It can be applied both in manual, synoptic forecast techniques and in numerical models.

For this method to be used, TOVS retrievals should be as evenly spaced as possible. This requires a retrieval method that is insensitive to the presence of clouds. Two case studies are presented, in which the results of the 3I-inversion method are used to illustrate the application of Sutcliffe's theory.

1. INTRODUCTION

During a visit at the Atmospheric Radiation Analysis (ARA) group of the Laboratoire de Météorologie Dynamique (LMD) in Palaiseau (France), the present author analyzed TOVS data, taken by the NOAA-9 polar orbiting satellite, using the 3I (Improved Initialization Inversion) system (*cf.* Chedin *et al.*, 1985). The reception station of the French National Meteorological service at Lannion made available TOVS data for 2 consecutive afternoon passes three times a week during a 6 week period. Moreover, the central forecasting office in Paris asked for the analysis of some situations of interest from the operational point of view. In total, data for 55 satellite passes have been analyzed.

Following a brief outline of the relation between satellite retrievals and the work of Sutcliffe (section 2), in section 3 results for two cases are presented. These results are discussed in section 4, along with some concluding remarks.

2. SATELLITE SOUNDINGS AND DEVELOPMENT OF ATMOSPHERIC SYSTEMS

Weather forecasting throughout its existence has been and will continue to be based on observations of the thermodynamical state of the atmosphere. These observations encompass a wide variety of variables, such as temperature, humidity, wind, pressure, etc.

Until the introduction of satellite sensors, these observations - by the nature of the sensors and technology used - are local, point measurements, both in time and space. Only recently (see *e.g.* Isaacs *et al.*, 1986) it has been fully appreciated that remotely sensed data (and especially satellite-borne radiation measurements) have an essentially different character: basically they are mean values over some volume, the size of which is determined by the instrumental details.

For satellite sounder retrievals this implies that the derived results are area-mean thicknesses of atmospheric layers, *e.g.* 1000-500 hPa. Some sub-division of these layers can be shown to be relevant, but satellite retrievals must be expected to show considerably less detailed structure in the vertical than obtainable with modern radiosonde systems.

On the other hand, satellite soundings provide us with a wealth of detail in horizontally coherent structures (see *e.g.* Chedin *et al.*, 1987, Prangsma *et al.*, 1987, Claud *et al.*, 1988), which gives hitherto unknown opportunities in meso-scale meteorology.

As a first step, a self-consistent presentation of the satellite-derived thickness can make use of the theory developed by Sutcliffe (1947), describing surface cyclogenisis (or cyclo-lysis) in terms of the so-called thermal vorticity of the 1000-500 hPa layer.

If V and V_o are the winds at 500 and 1000 hPa, V' is the thermal wind for the 1000-500 hPa layer, f the Coriolis parameter, Φ' the vorticity of V' (*i.e.*, the thermal vorticity), and Φ_o the vorticity of the 1000 hPa wind, Sutcliffe derived the following relation between the divergences at 500 and 1000 hPa (*i.e.*, the cyclo-genesis/cyclo-lysis) and the vorticities:

$$f \left(\mathrm{div}_p\, V - \mathrm{div}_p\, V_o \right) = - V' \frac{\delta}{\delta s} \left(f + \Phi' + 2\, \Phi_o \right) \qquad (1)$$

where the derivative $\delta/\delta s$ is taken along the thermal wind (V') direction.

If we note that, generally, the divergence of the 500 hPa winds virtually vanishes, eq. (1) gives the surface cyclogenesis ($\mathrm{div}_p\, V_o$) in terms of the advection of planetary, thermal and surface vorticity. In some simplified short-range forecast models this is an essential ingredient to take developments into account (L. Heijboer, private communication; see also Heijboer *et al.*, 1987).

Since TOVS retrievals yield thickness fields, the Sutcliffe-type analysis seems fit to provide the framework for presenting satellite soundings, both for numerical atmosphere models and for combination with standard operational synoptic methods. The first results of this technique (*cf.* Prangsma *et al.*, 1987) were so promising that the same method has been applied to some of the cases selected by the French National Meteorological service.

3. ANALYSIS OF THREE ORBITS OF NOAA-9 ON 7 AND 8 DECEMBER 1986

3.1 Development of a small, violent depression on 7-8 December 1986 (NOAA-9 orbits 10224 and 10237).

In the cold front of a large depression near Iceland, a frontal wave is observed being formed off the Bay of Biscay: the frontal wave has not been distinguished in the standard 0.00 GMT surface analysis (fig. 1a) nor in the upper-air analysis (fig. 1b) of the same time, yet the 12.00 GMT analyses (fig. 2) of the same day (7 December 1986) clearly mark the development being in progress.

The satellite image (NOAA-9, orbit 10224 around 05.00 GMT, fig. 3) is typical for frontal wave activity near 20W. Atypical in this image is a cloud structure from roughly 46N, 30W extending westward to about 47N, 35W.

The thickness distribution retrieved with the 3I-method from the TOVS radiances indicate the presence of a complex structure to the north of this cloud band with considerably more detail than is revealed by the standard thickness analysis (figs. 1b and 2b, dotted lines)

The vertical structure of this feature can be assessed by considering thinner layers. One then clearly finds the feature to exist above 850 hPa (figs. 4b-c), being most pronounced between 700 and 500 hPa. In the 500-300 hPa thickness map (fig. 4d), an isolated cold cell around 53N, 32W hints at some of this structure extending into the upper troposphere, with its vertical axis slightly tilted.

Analyses of the next day (8 December 1986, 0.00 GMT, figs. 5a-b) and the satellite image received around 03.30 GMT (NOAA-9, orbit 10237, fig. 6), show that the frontal wave has developed into a small, but violent depression with force 10 winds being reported on its western flank.

The TOVS derived thickness maps for this orbit (figs. 7a-b) show that much of the detailed structure has been dissipated, with hardly any vertical differentiation being left.

Now the question must be adressed whether the available data, and more

specifically the TOVS products, can explain at least in a qualitative way, the rapid developments observed.

To this end, the thermal vorticity field for the 1000-500 hPa layer has been computed as a basic ingredient in the Sutcliffe-type approach. The result (fig. 8a) reveals the existence of sharp gradients between positive (cyclonic) and negative (anticyclonic) vorticity structures in the area just north of the the cloud feature at 05.30 GMT on December, 7. These thermal vorticity gradients along with the thermal winds for the same layer (fig. 8b) could induce the rapid development of a surface depression at the entrance of the Channel, according to eq. (1).

3.2 A double cloud band structure south of Iceland on December, 8, 1986.

On December, 8, 1986 around 15.00 GMT the NOAA-9 satellite in orbit 10244 revealed an uncommon double cloud band structure over the North Atlantic ocean south of Iceland (fig. 9).

The standard surface and upper-air analyses (figs. 10a-b) of 12.00 GMT on that day, indicate the presence of a frontal zone in this area, but give little explanation for a double band of clouds of the type observed. The French National Meteorological service therefore asked to investigate, whether such a structure is detectable in the TOVS analyses.

Since the swath of the TOVS instruments is narrower than the AVHRR swath width, we expect to find the signature of the structure considered at or near the edge of the available data. Due to a numerical limitation currently existing in the contouring software, we therefore have to rely on the thermal wind plots as produced by the 3I-system.

Careful inspection of these plots shows (figs. 11a-b) that indeed a double structure is present in the 700-500 hPa (fig. 11a) and 500-300 hPa (fig. 11b) layers, whereas in the lower layers in the area of concern only a single, wider cold tongue is found. This result shows the ability of the method to resolve structure of limited vertical extent.

In order to assess the potential dynamical implications of such double structures, we computed the thermal vorticity for the layers cited above, as well as for the standard 1000-500 hPa layer. The results are shown in figs. 12a-c. Apart from boundary effects induced by the numerics of the contouring package, some sharp vorticity gradients are clearly delineated, indicative of potential surface cyclogenesis.

4. DISCUSSION

Sutcliffe's theoretical approach has been applied to coherently present the results of TOVS retrievals. Since this theory is primarily based on gradients in the thermal vorticity field (eq. 1), the representation of these gradients is essential. This requires a reasonably homogeneous spatial distribution of the available observational data. In other words, the TOVS retrieval scheme must provide evenly distributed results under all meteorological conditions.

From the results presented in section 3, we conclude that the 3I-system is fully capable to fulfill this distribution requirement: no discontinuities are found between clear and cloudy areas.

The Channel depression development (section 3.1) in particular, shows the potential of the method to provide early warning for sudden and/or violent developments. This application requires the timely availability of the results (*cf.* figs. 8a and 12a) to the operational forecaster. Current experimental results indicate that the 3I-system can generate these products within at most one hour after observation time.

Two cautionary notes are in place here. Firstly, TOVS derived upper-air information is not fully exploited in such a "manual" approach; the assimilation into a numerical atmosphere model is essential to provide a complete forecast, which - among other things - confirms (or cancels) the early warning.

Secondly, the presented results look rather promising. Nevertheless, more rigorous and systematic investigations are needed to establish to what extent "false alarms" are introduced. *I.e.*, research is needed to show that the early warnings provided by the Sutcliffe-type presentation are generally followed by the severe weather conditions implied by the warning.

The case studies (section 3) show the potential of the 3I-method to delineate detailed atmospheric structures with horizontal scales unobtainable with classical observation techniques. We therefore conclude that the field of TOVS retrieval has matured to a state, where dense and robust data sets are becoming available for use in meso-scale meteorology, both in a research and in an operational mode, and also in manual/synoptic techniques as well as numerical models.

REFERENCES

Sutcliffe, R.G., 1947.
A contribution to the problem of development.
Quart. J. Roy. meteor. Soc. London, 73, 370-383.

Isaacs, R.G., R.N. Hoffman and L.D. Kaplan, 1986.
Satellite remote sensing of meteorological parameters for global numerical weather prediction.
Rev. Geophys., 24, 701-743.

Chedin, A., N.A. Scott, C. Wahiche and P. Moulinier, 1985.
The Improved Initialization Inversion method: a high resolution physical method for temperature retrievals from satellites of the TIROS-N series.
J. Climate and Appl. Meteor., 24, 128-143.

Chedin, A., N.A. Scott, J. Flobert, N.Husson, C. Levy, G. Rochard, J. Quere, B. Bellec and J. Simeon, 1987.
Analysis of thickness fields retrieved from NOAA-7 observations through the "3I" inversion method. Interest for weather forecasting.
Proc. Symp. Mesoscale Analysis and Forecasting, (Vancouver, Canada, 17-19 August 1987), ESA SP-282, 97-101.

Prangsma, G.J., A. Chedin, N. Husson, N.A. Scott, J. Quere and G. Rochard, 1987.
Observation of the development of mesoscale systems by operational meteorological satellites.
Proc. Symp. Mesoscale Analysis and Forecasting, (Vancouver, Canada, 17-19 August 1987), ESA SP-282, 117-122.

Claud, C., A. Chedin, N.A. Scott, J.C. Gascard and G.J. Prangsma, 1988.
Retrieval of mesoscale meteorological parameters from NOAA-9 over Greenland and Barents Seas for three consecutive days of June 1986.
Preprint-volume AMS Conf. on Arctic Oceanography and Meteorology, (Madison, USA, 29-31 March 1988).

Heijboer, L.C., H. Timmerman and A. van der Hoek, 1987.
An hourly analysis, updating and short-range forecasting system.
Proc. Symp. Mesoscale Analysis and Forecasting, (Vancouver, Canada, 17-19 August 1987), ESA SP-282, 297-301.

Fig. 1 Synoptic analysis for December 7, 1986 at 0.00 GMT.
a. Surface
b. 500 hPa heights (full lines), 500 hPa winds and 1000-500 hPa thickness (dashed lines).

Fig. 2 As fig. 1, but for December, 7, 1986 at 12.00 GMT.

Fig. 3 NOAA-9 Infrared (channel 4) image for orbit 10224, December, 7, 1986, 05.30 GMT.

Fig. 4 Thickness fields in dam, derived from TOVS data using the "3I" inversion method for NOAA-9 orbit 10224, December, 7, 1986 at 05.30 GMT.
a. 1000-500 hPa b. 850-700 hPa c. 700-500 hPa d. 500-300 hPa

Fig. 5 As fig. 1, but for December, 8, 1986 at 0.00 GMT.

Fig. 6 As fig. 3, but for orbit 10237, December, 8, 1986 at 03.38 GMT.

Fig. 7 As fig. 4, but for orbit 10237.
a. 1000-500 hPa b. 500-300 hPa

Fig. 8 a. Vorticity (in 10^{-4} sec^{-1}) of the thermal wind field for the 1000-500 hPa layer for NOAA-9 orbit 10224 (December, 7, 1986, 05.30 GMT).
b. Thermal winds obtained for the same layer.
(Numbers give thickness in dam above 500 dam)

Fig. 9 As fig. 3, but for orbit 10244, December, 8, 1986, 15.10 GMT.

Fig. 10 As fig. 1, but for December, 8, 1986 at 12.00 GMT.

Fig. 11 Thermal wind fields for NOAA-9 orbit 10244, December, 8, 1986 at 15.10 GMT.
a. 700-500 hPa (Numbers give thickness in dam above 200 dam)
b. 500-300 hPa (Numbers give thickness in dam above 300 dam)

Fig. 12 Vorticity (in 10^{-4} sec^{-1}) of the thermal wind for NOAA-9 orbit 10244, December, 8, 1986 at 15.10 GMT.
a. 700-500 hPa (Numbers give thickness in dam above 200 dam)
b. 500-300 hPa (Numbers give thickness in dam above 300 dam)
c. 1000-500 hPa (Numbers give thickness in dam above 500 dam)

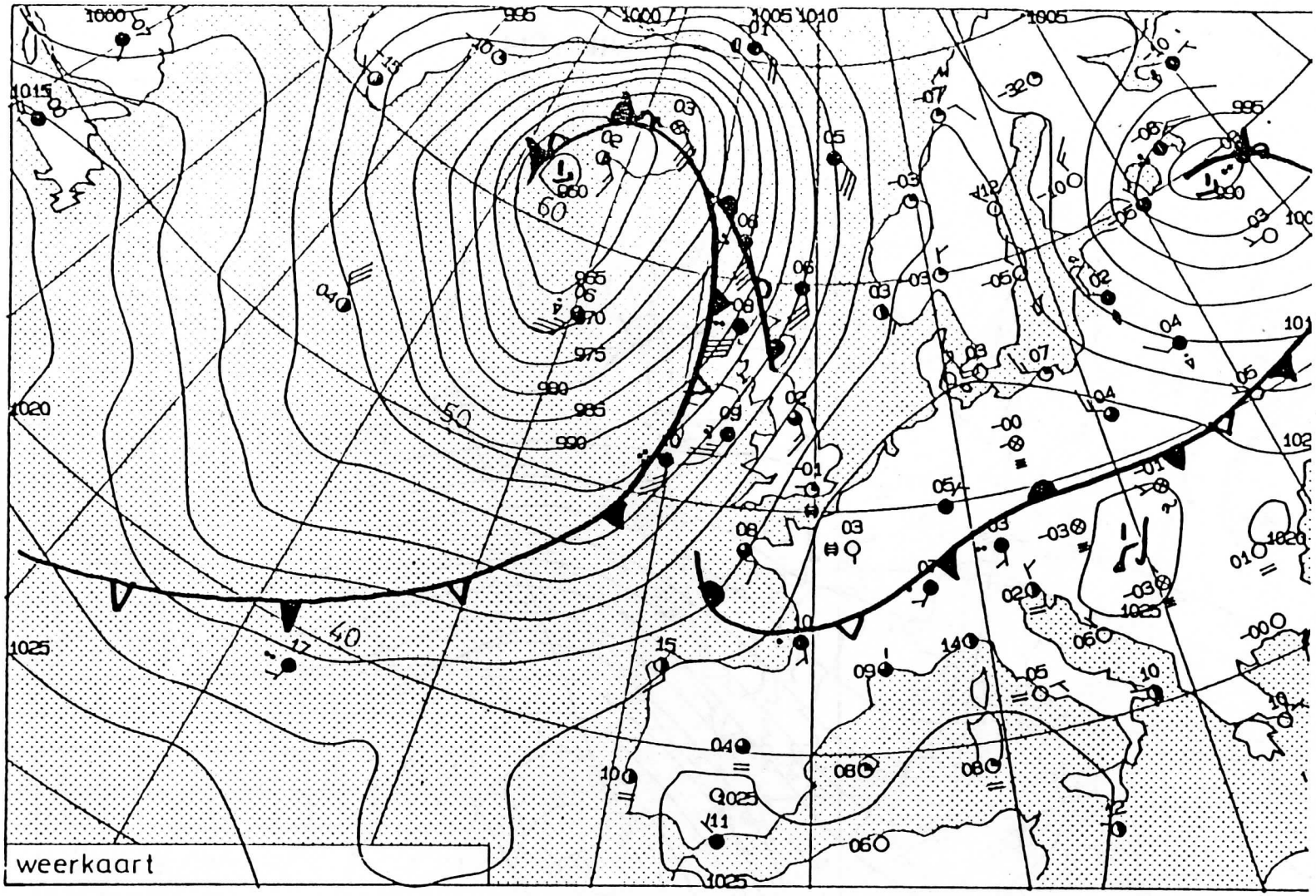

Fig 1a

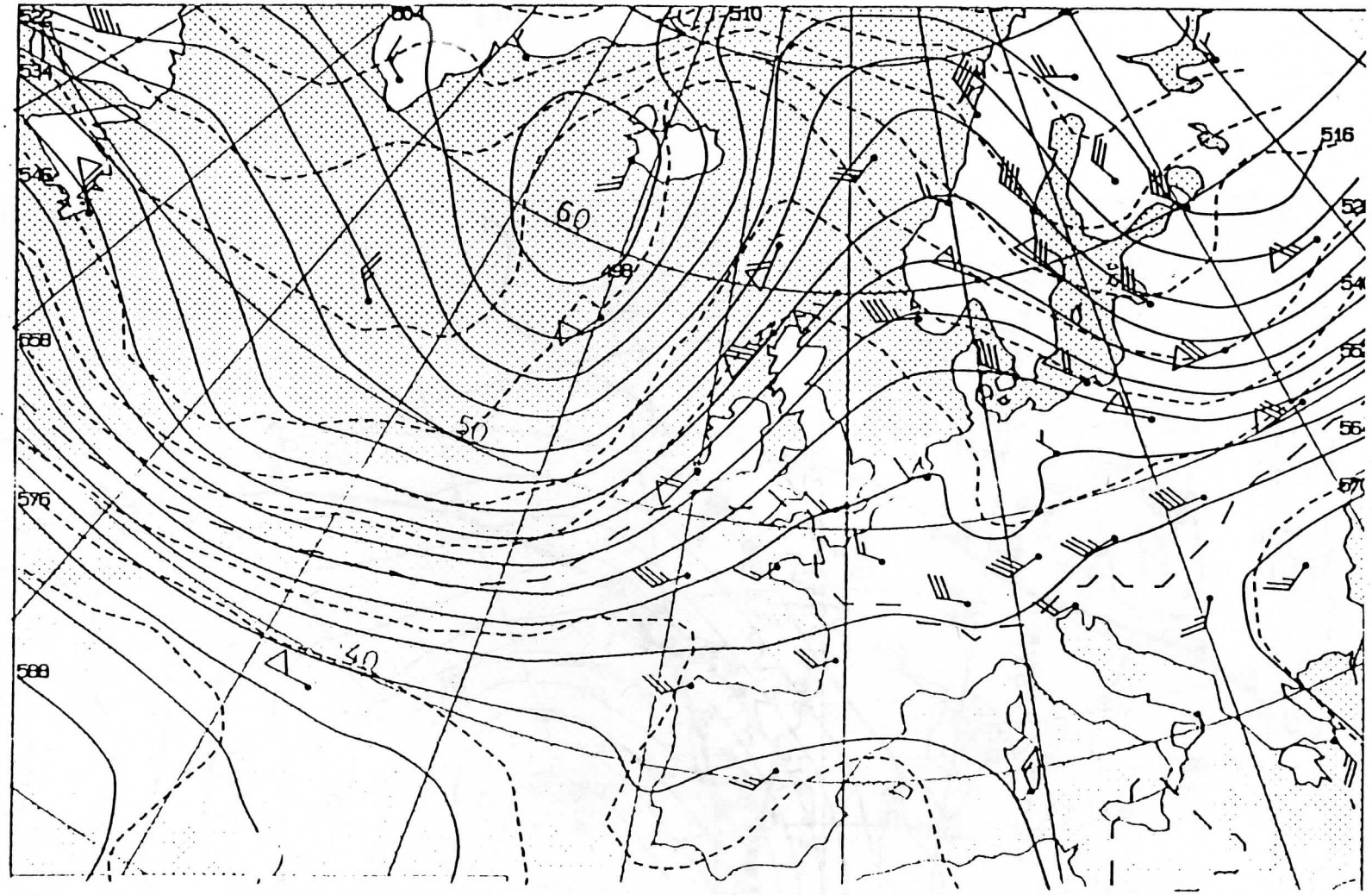

Fig 1b

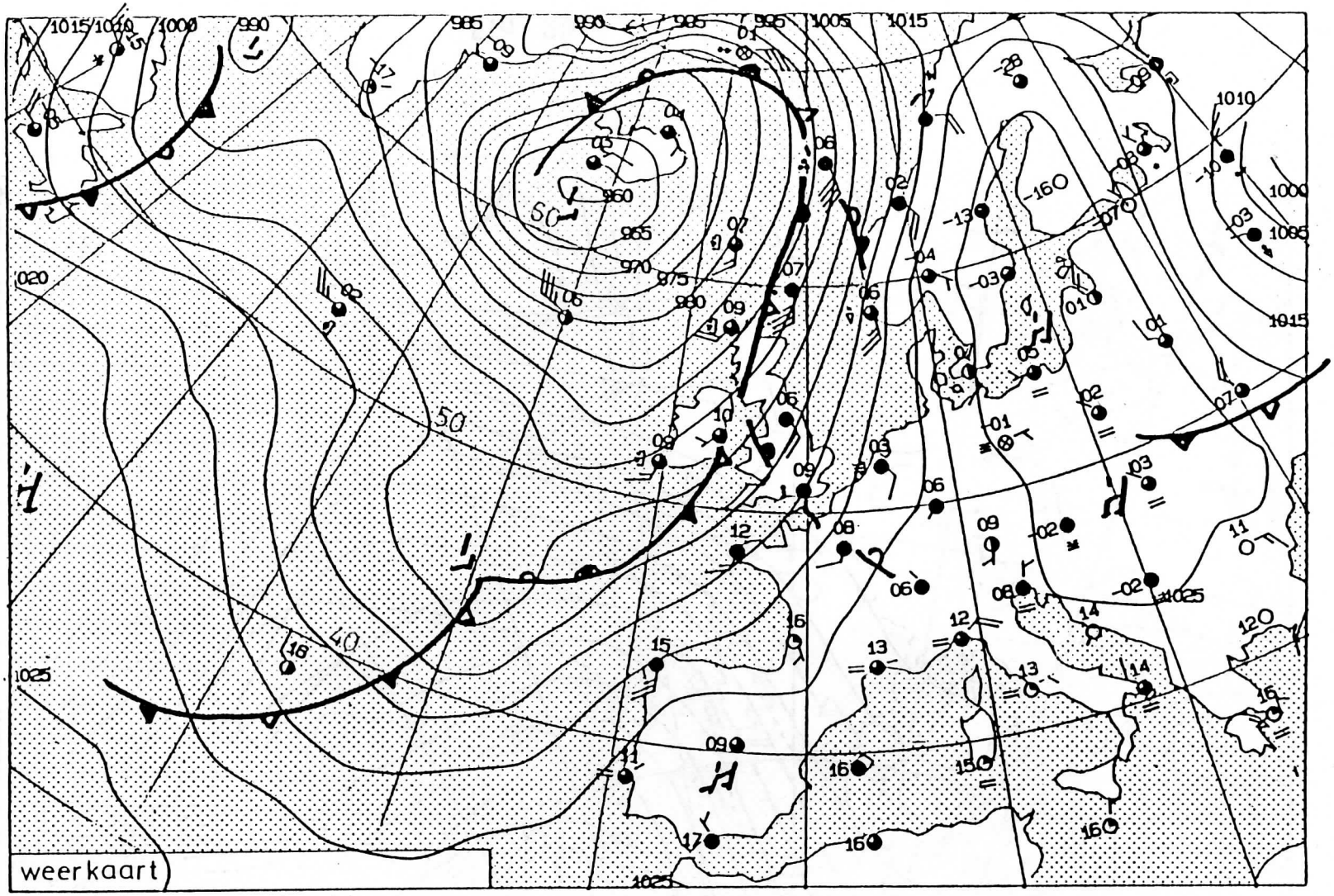

Fig 2a

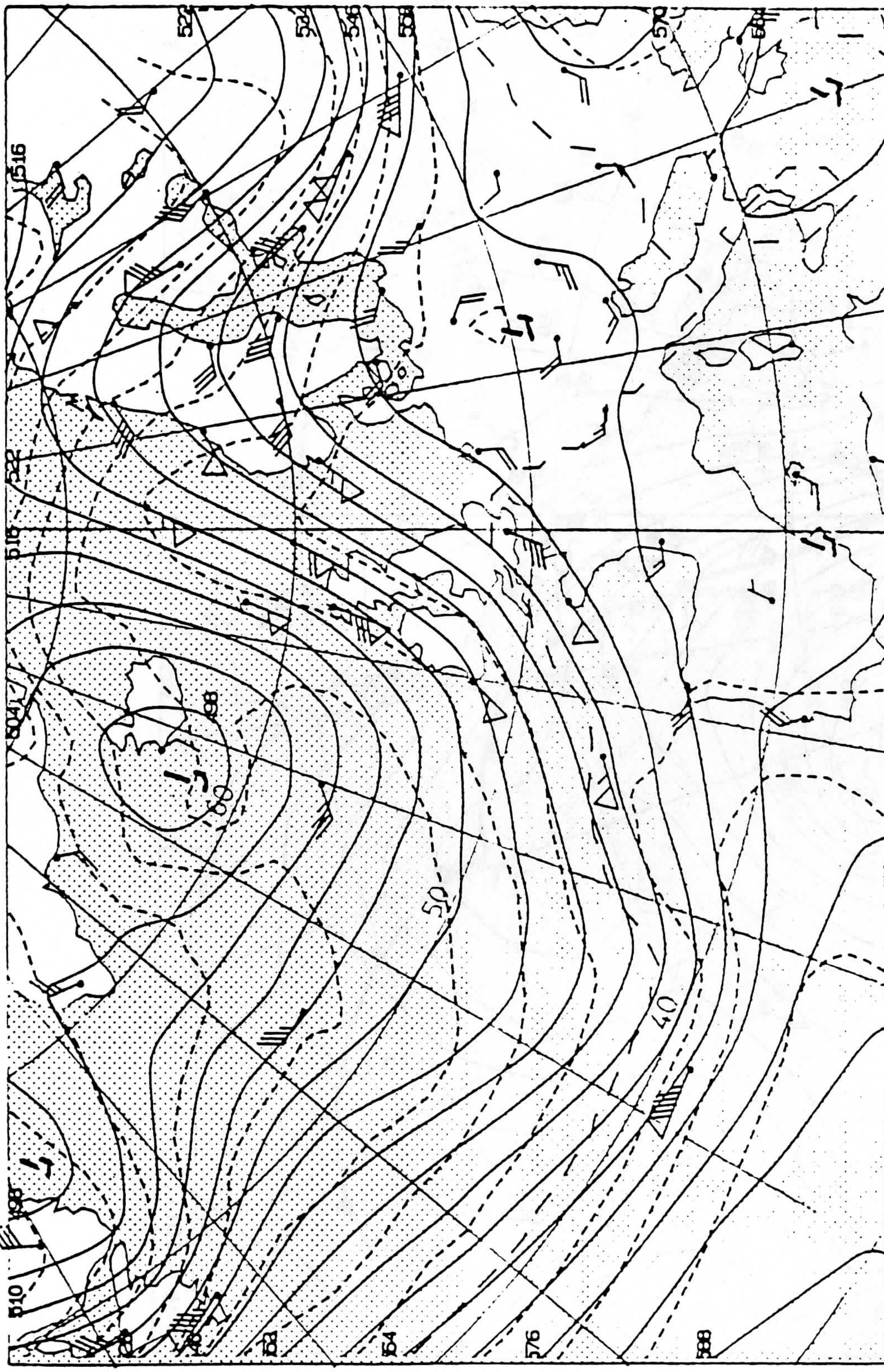

Fig 2b

Fig 3

NOAA- 9 224 1:1 XXXX RT R2-S11-1554 LPMX1 G=10 861207 5:28:40
79.48N 21.48O IR4 ENH: 2 DT= 0
40.64N 32.58W ST: 0
+30 +20 +10 00 -10 -20 -30 -40 -50

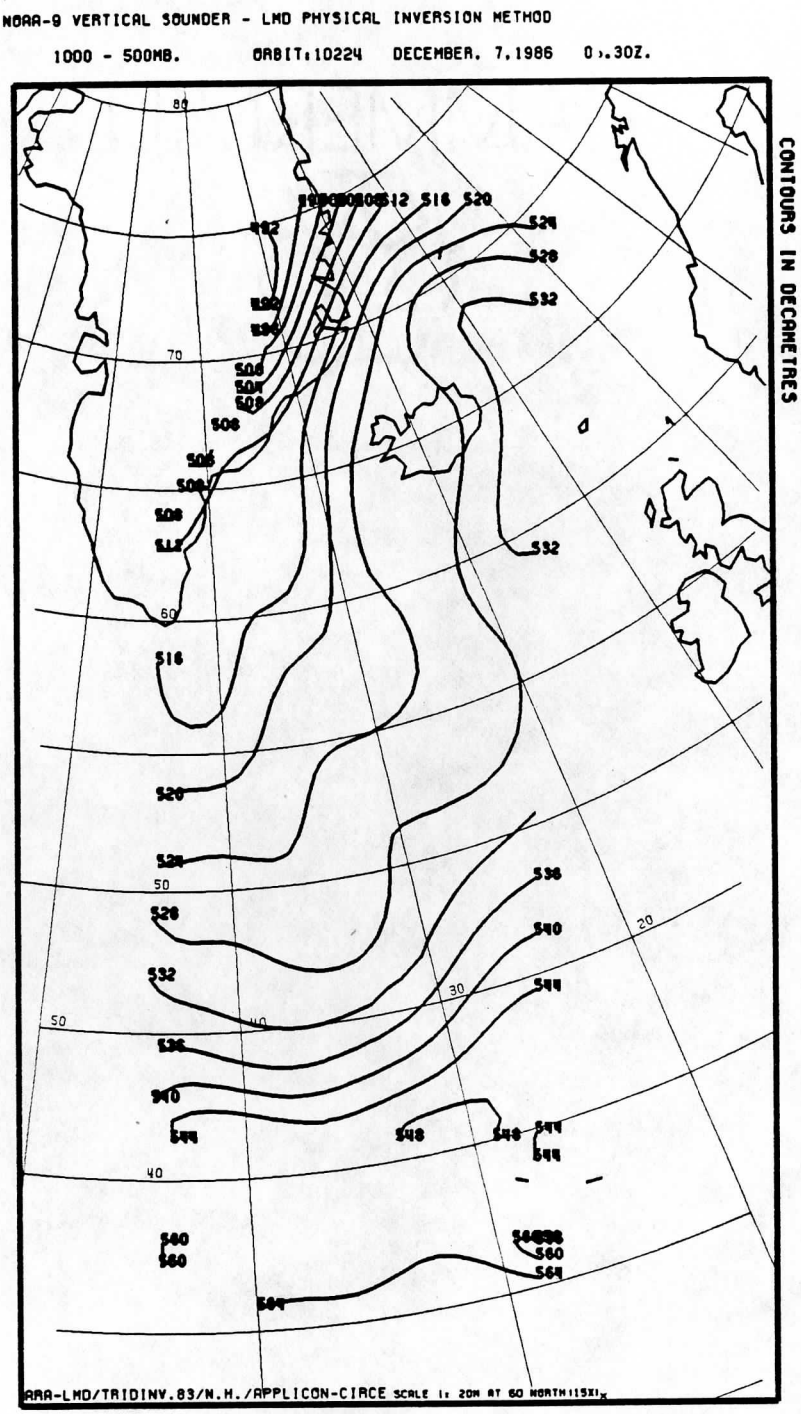
NOAA-9 VERTICAL SOUNDER - LMD PHYSICAL INVERSION METHOD
1000 - 500MB.
ORBIT:10224
DECEMBER. 7,1986
0 >.30Z.
CONTOURS IN DECAMETRES
516
520
524
528
532
536
540
544
548
560
564
80
70
60
50
40
30
20
NOAA-LMD/TRIDINV.83/N.H./APPLICON-CIRCE SCALE 1: 20M AT 60 NORTH

Fig 4a

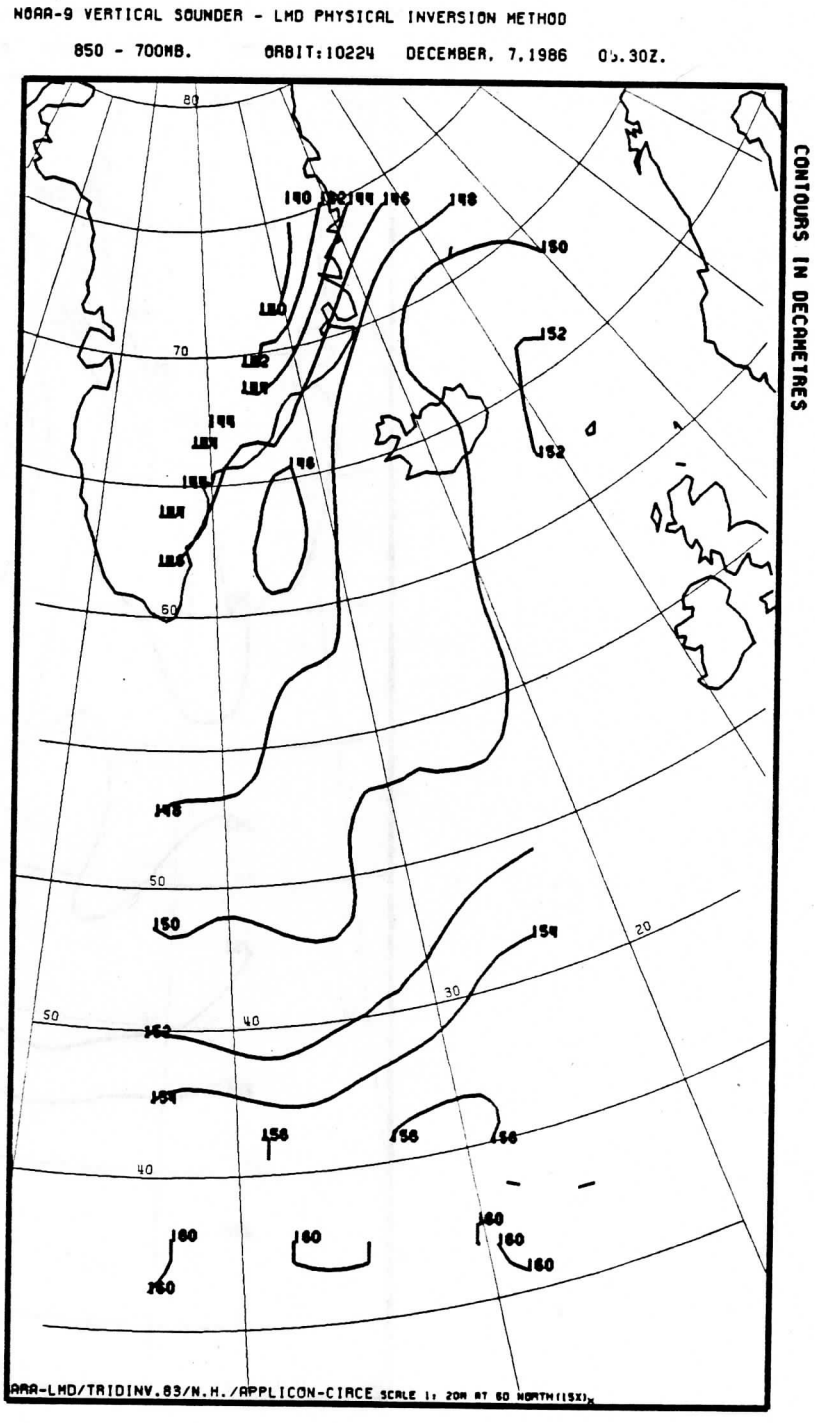
NOAA-9 VERTICAL SOUNDER - LMD PHYSICAL INVERSION METHOD
850 - 700MB. ORBIT:10224 DECEMBER, 7,1986 05.30Z.
CONTOURS IN DECAMETRES
80
70
60
50
40
20
30
140
142
144
146
148
150
152
154
156
158
160
NOAA-LMD/TRIDINV.83/N.H./APPLICON-CIRCE SCALE 1: 20M AT 60 NORTH(1SX)

Fig 4b

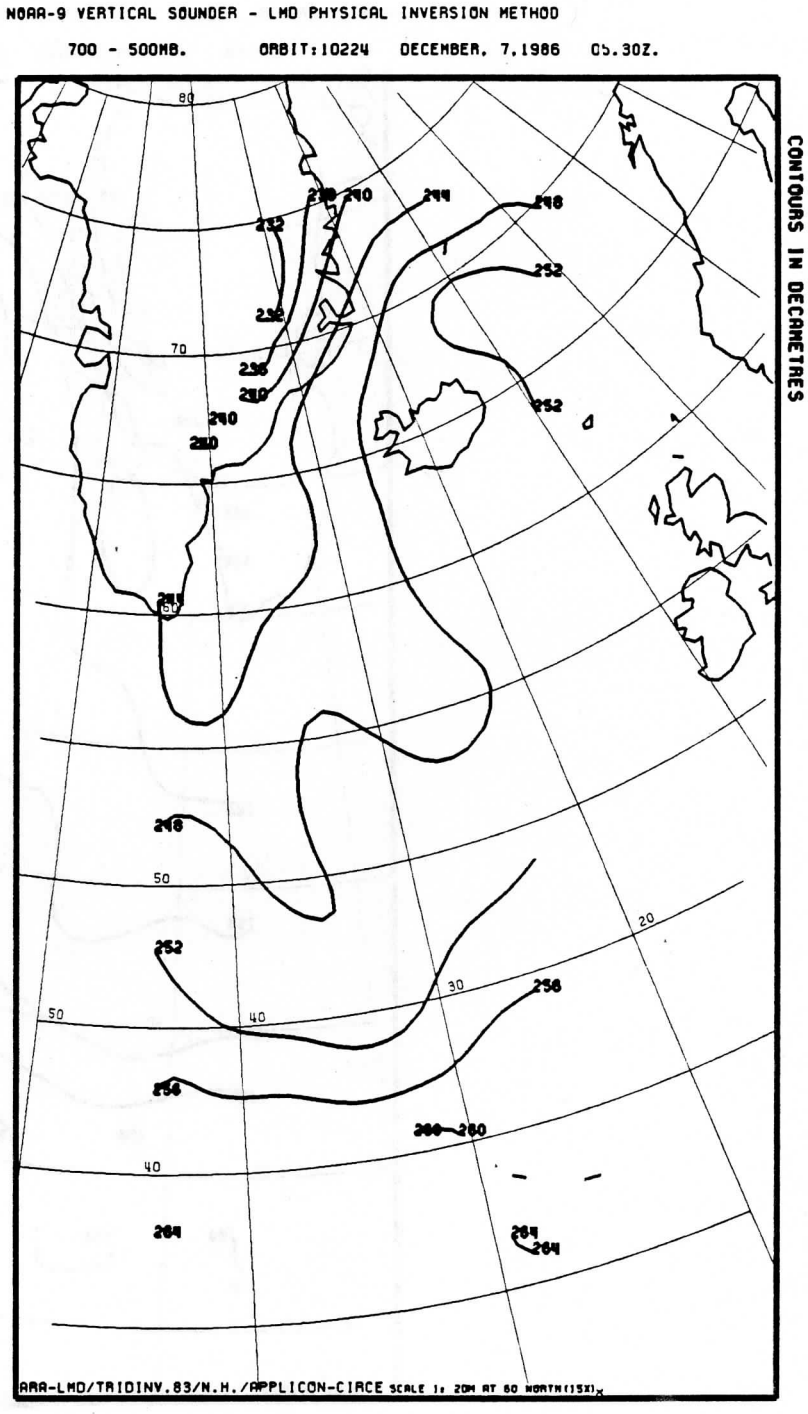
NOAA-9 VERTICAL SOUNDER - LMD PHYSICAL INVERSION METHOD
700 - 500MB. ORBIT:10224 DECEMBER, 7,1986 05.30Z.
CONTOURS IN DECAMETRES
80
70
60
50
40
30
20
50
40
232
236
240
244
248
252
256
260
264
AAA-LMD/TRIDINV.83/N.H./APPLICON-CIRCE SCALE 1: 20M AT 60 WORTH(15X)

Fig 4c

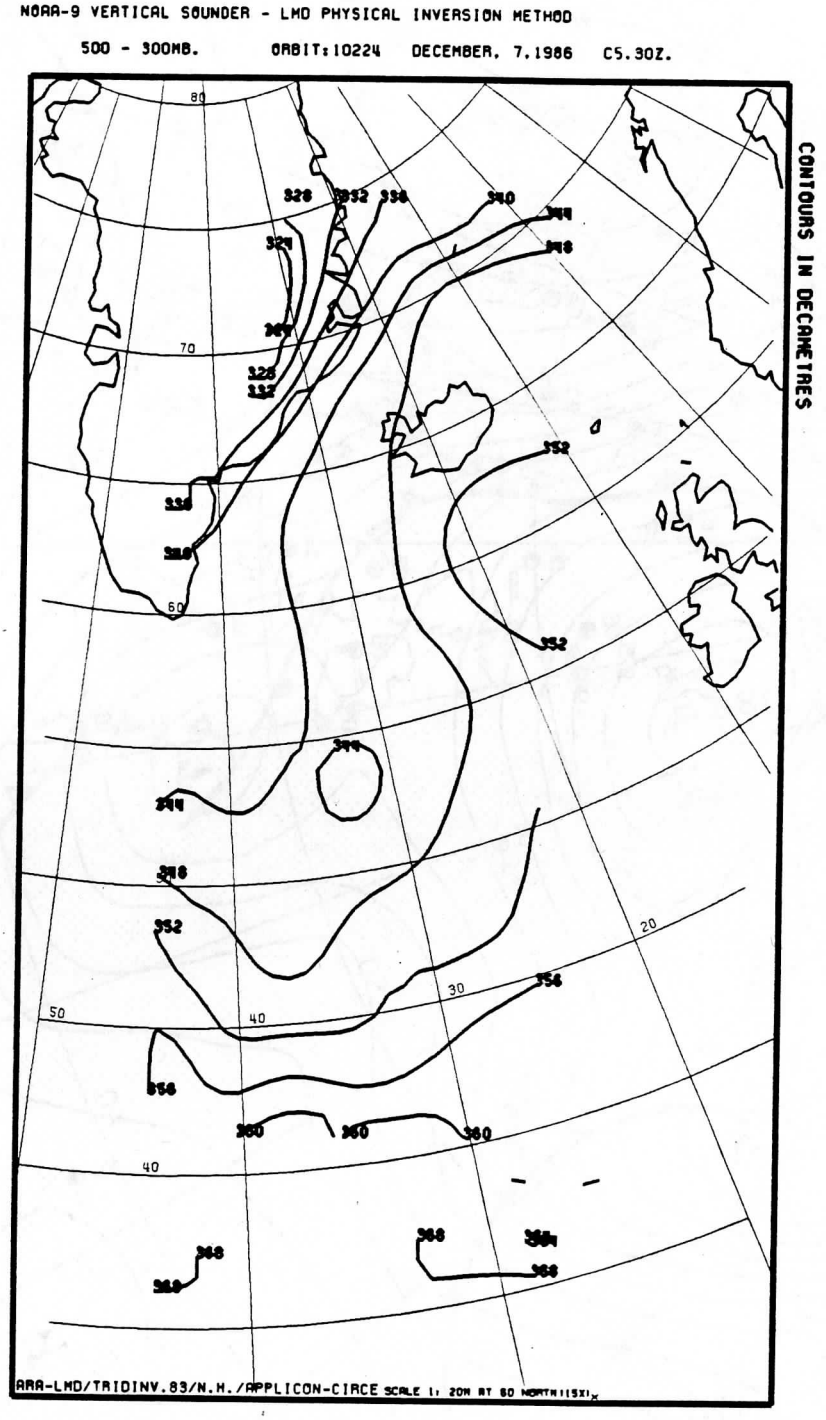
NOAA-9 VERTICAL SOUNDER - LMD PHYSICAL INVERSION METHOD
500 - 300MB. ORBIT:10224 DECEMBER, 7.1986 05.30Z.
CONTOURS IN DECAMETRES
80
70
60
50
40
30
20
40
AAA-LMD/TRIDINV.83/N.H./APPLICON-CIRCE SCALE 1: 20M AT 60 NORTH(1SX)

Fig 4d

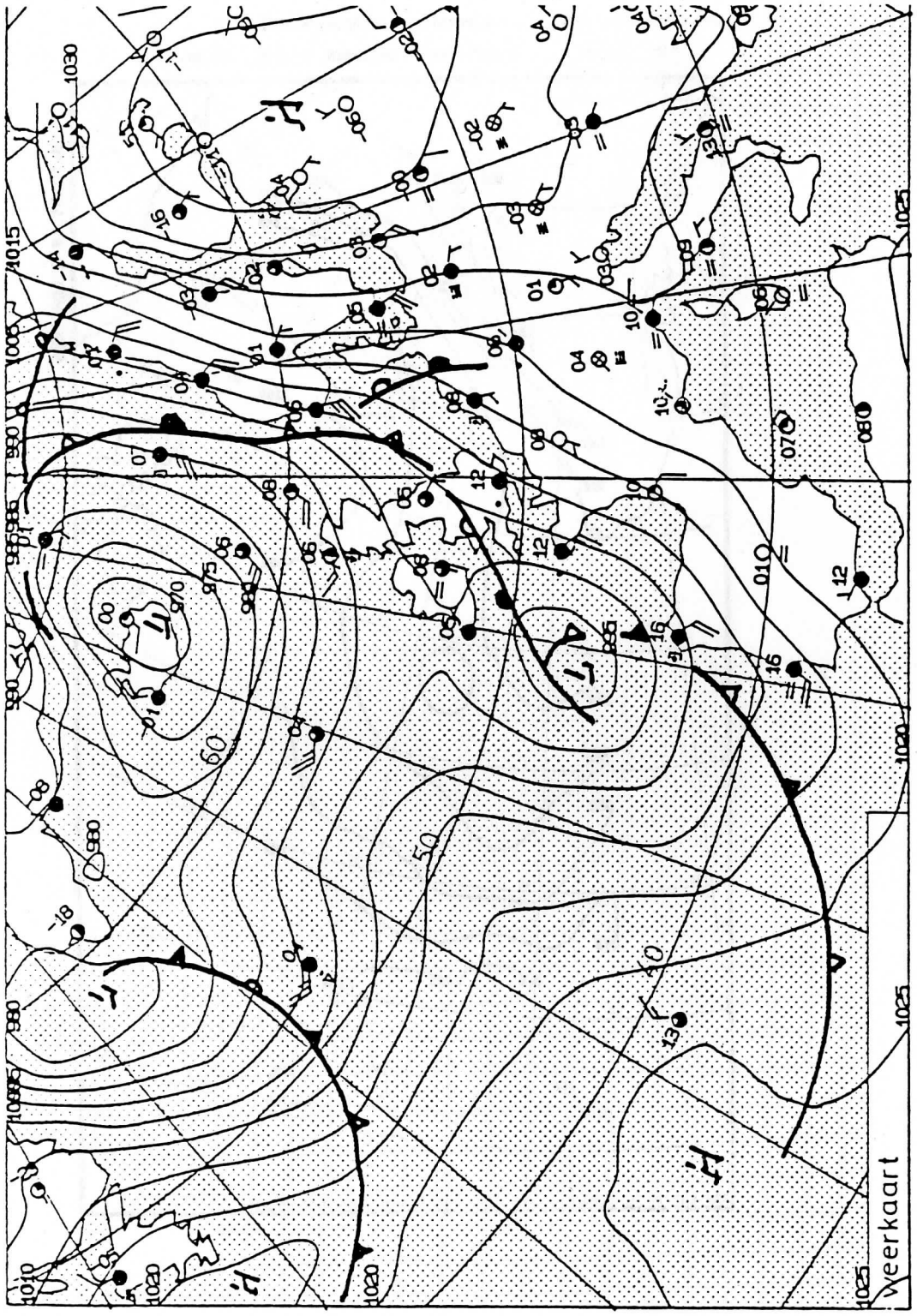

Fig 5a

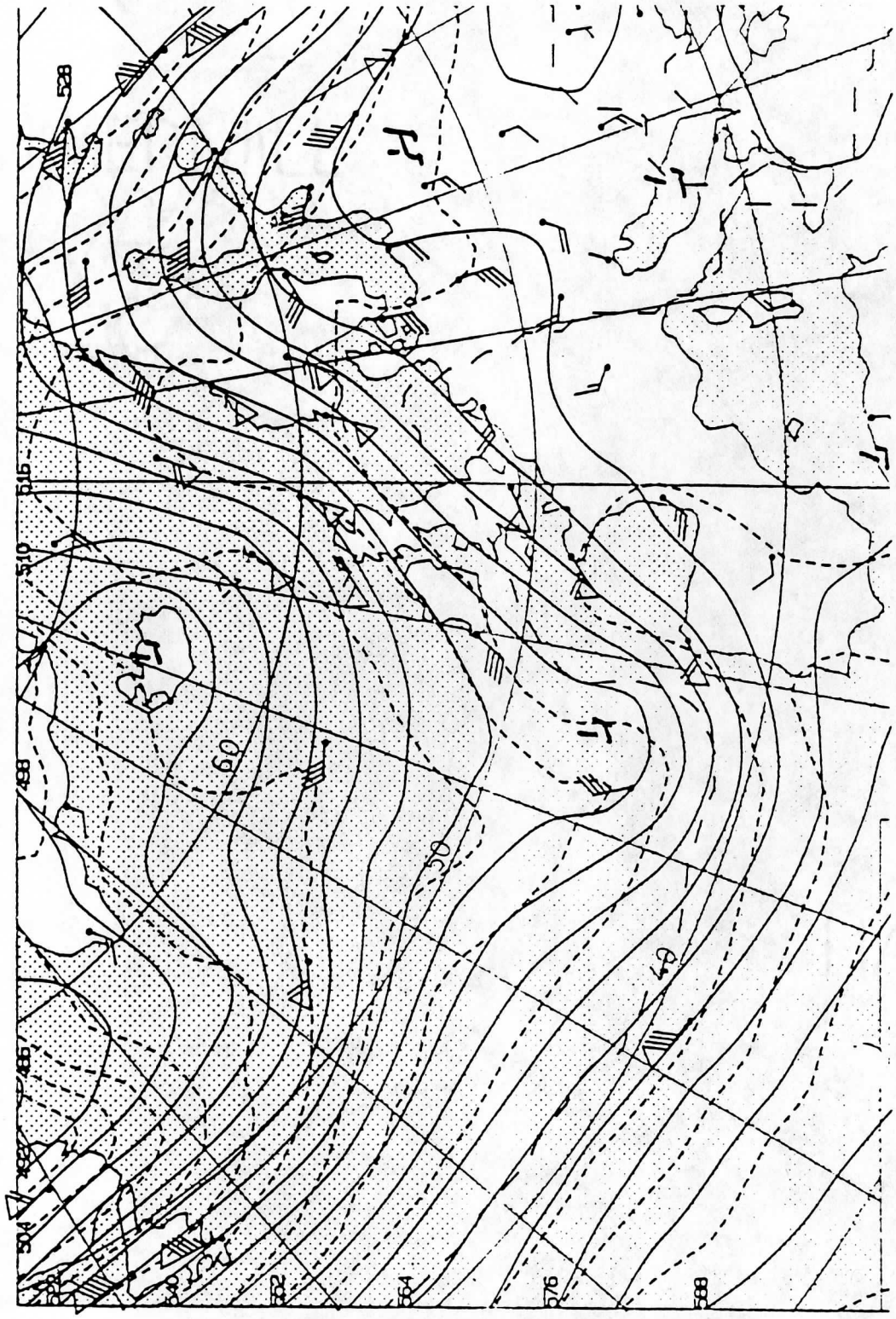

Fig 5b


NOAA- 9 237 1:1 XXXX RT R1-S 1- 777 LPMX1 G=10 861208 3:36:37
77.52N 36.59O IR4 ENH: 2
26.11N 8.73W
DT= 1
ST: 0
+30 +20 +10 00 -10 -20 -30 -40 -50

Fig 6

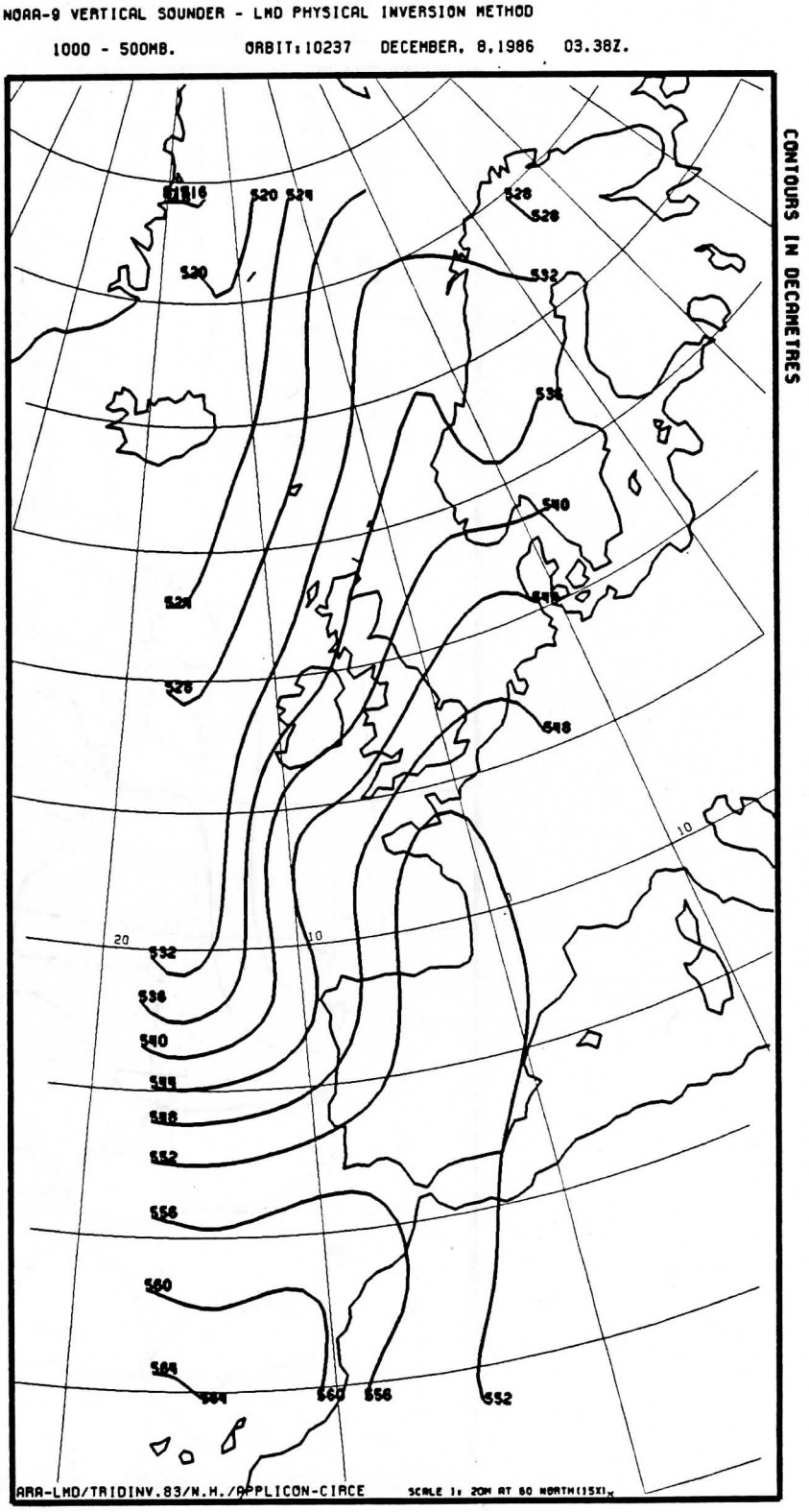
NOAA-9 VERTICAL SOUNDER - LMD PHYSICAL INVERSION METHOD
1000 - 500MB. ORBIT:10237 DECEMBER, 8,1986 03.38Z.
CONTOURS IN DECAMETRES
516
520
524
528
532
536
540
544
548
552
556
560
564
ARA-LMD/TRIDINV.83/N.H./APPLICON-CIRCE
SCALE 1: 20M AT 60 NORTH(15X)

Fig 7a

NOAA-9 VERTICAL SOUNDER - LMD PHYSICAL INVERSION METHOD

500 - 300MB. ORBIT:10237 DECEMBER, 8,1986 03.38Z.

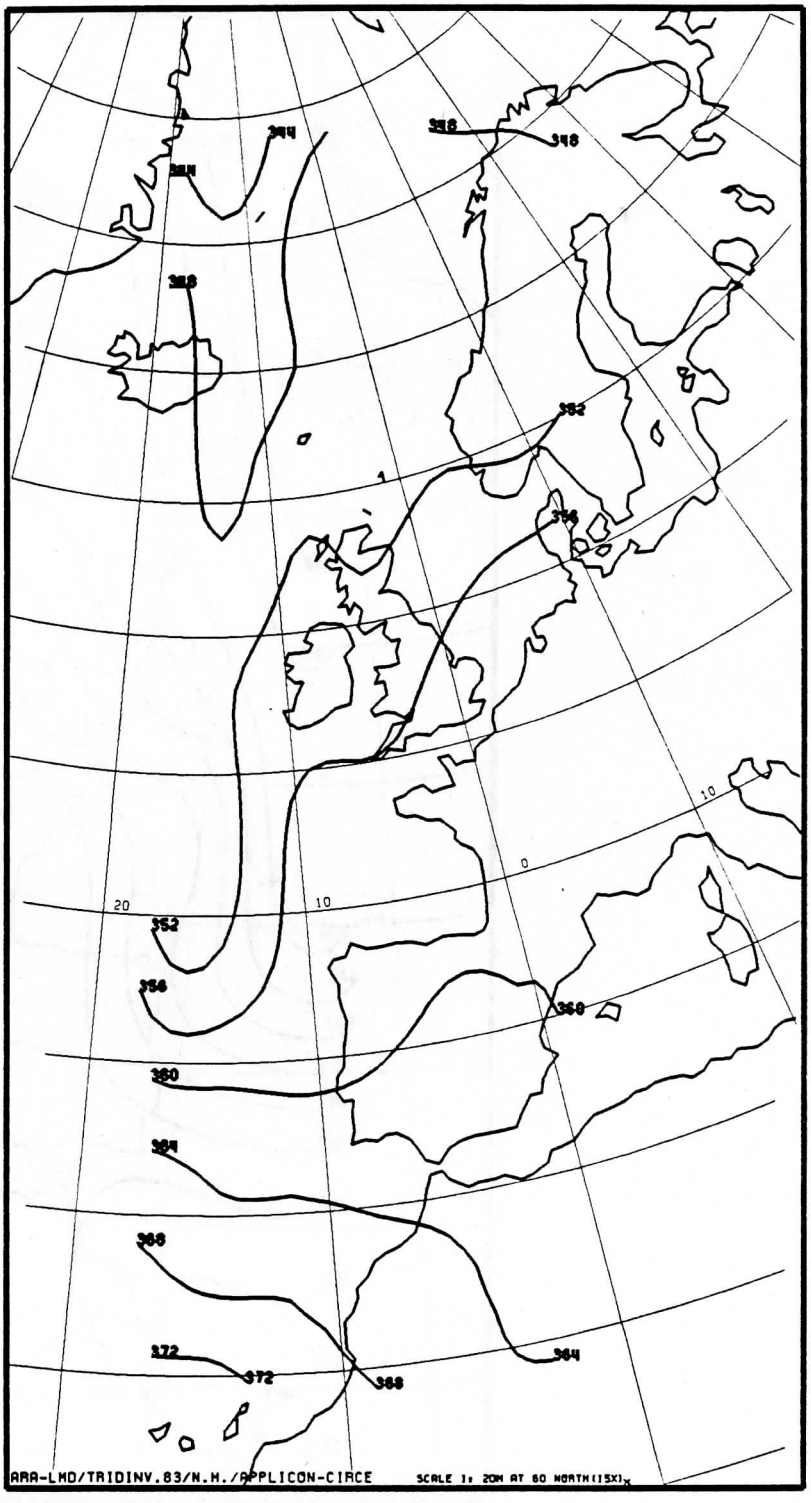

Fig 7b

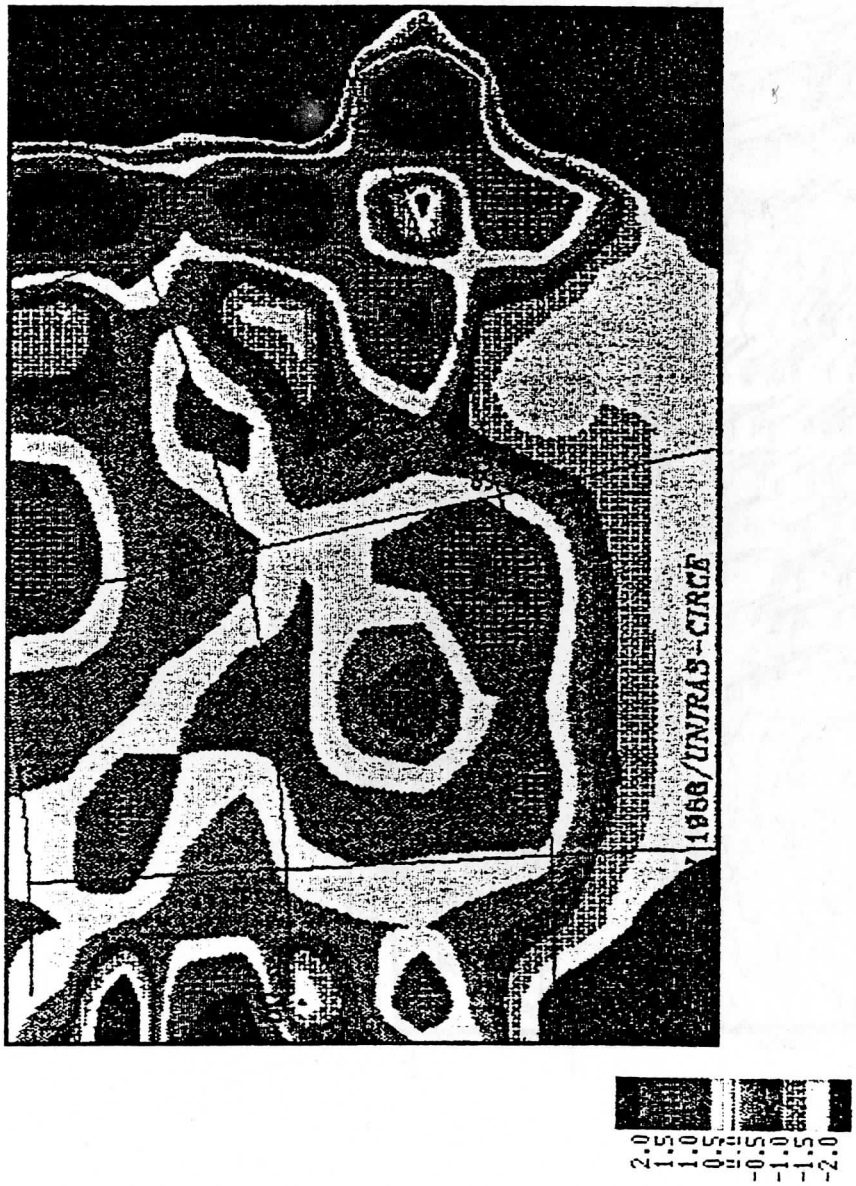

Fig 8a

NOAA-7 VERTICAL SOUNDER - LMD PHYSICAL INVERSION METHOD - CATHIA

1000 - 500MB THICK.(DAM) AND THERMAL WINDS(M/S). ORBIT:10224 DECEMBER, 7,19

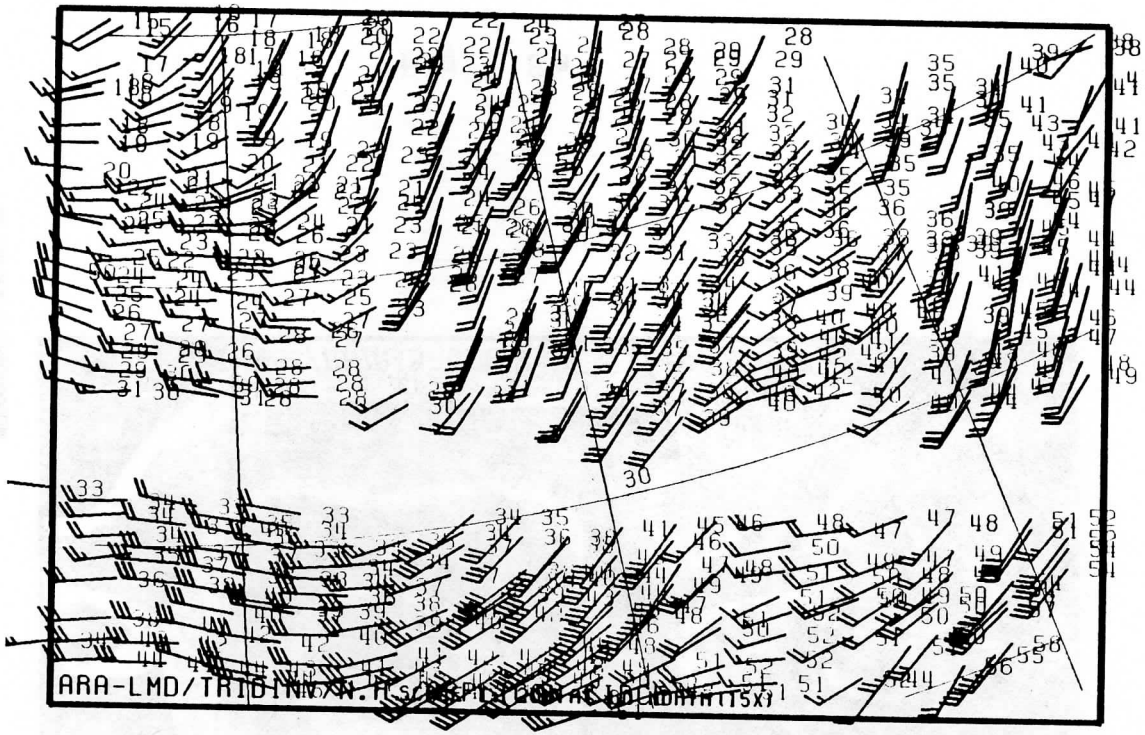

Fig 8b


NOAA- 9 244 1:1 XXXX RT R1-S 3- 777 LPM*1 G=10 861208 15:11:14
72.21N 35.91W IR4 ENH: 2
28.49N 7.94W
BT=-13
ST: 0
+30 +20 +10 00 -10 -20 -30 -40 -50

Fig 9

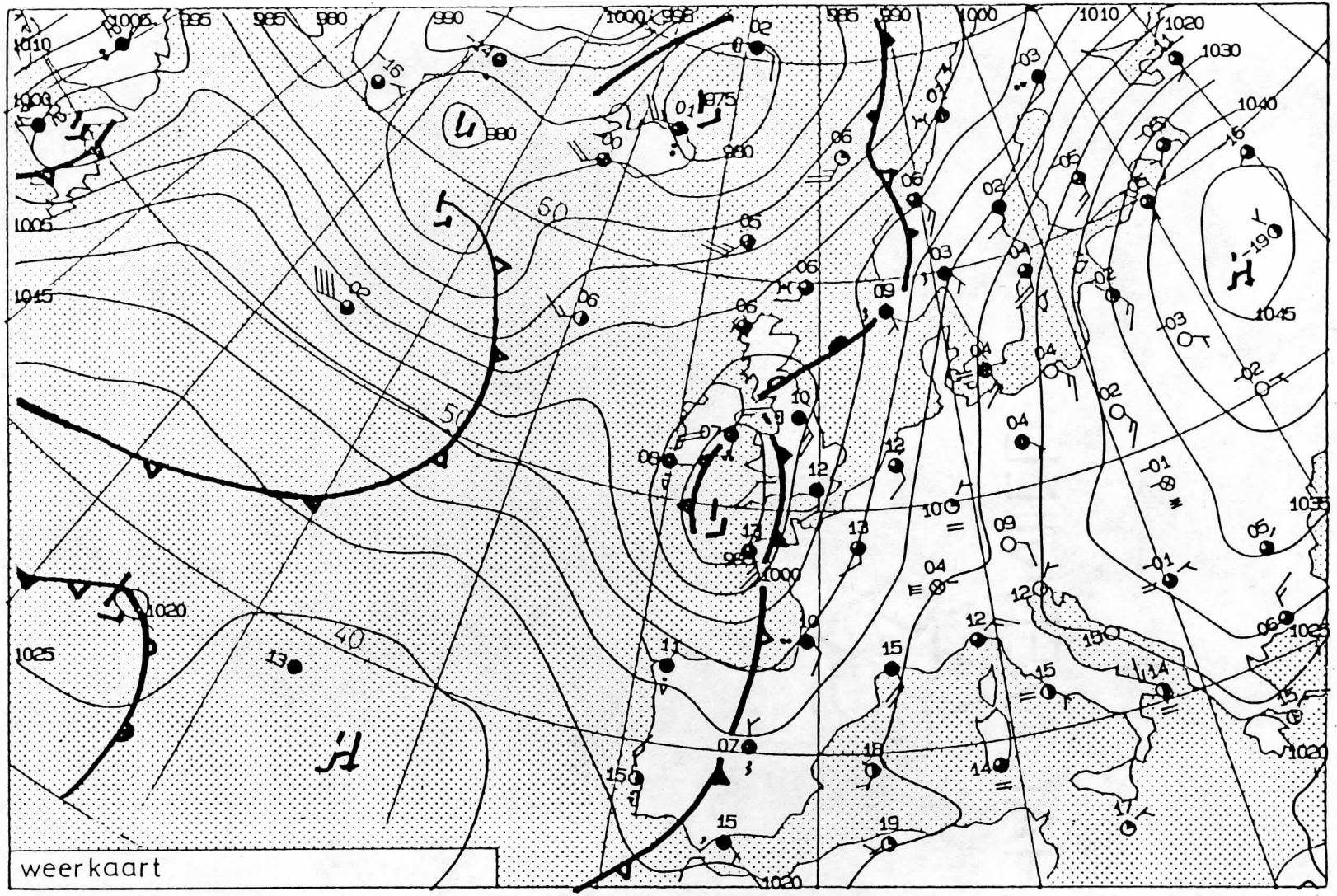

Fig 10a

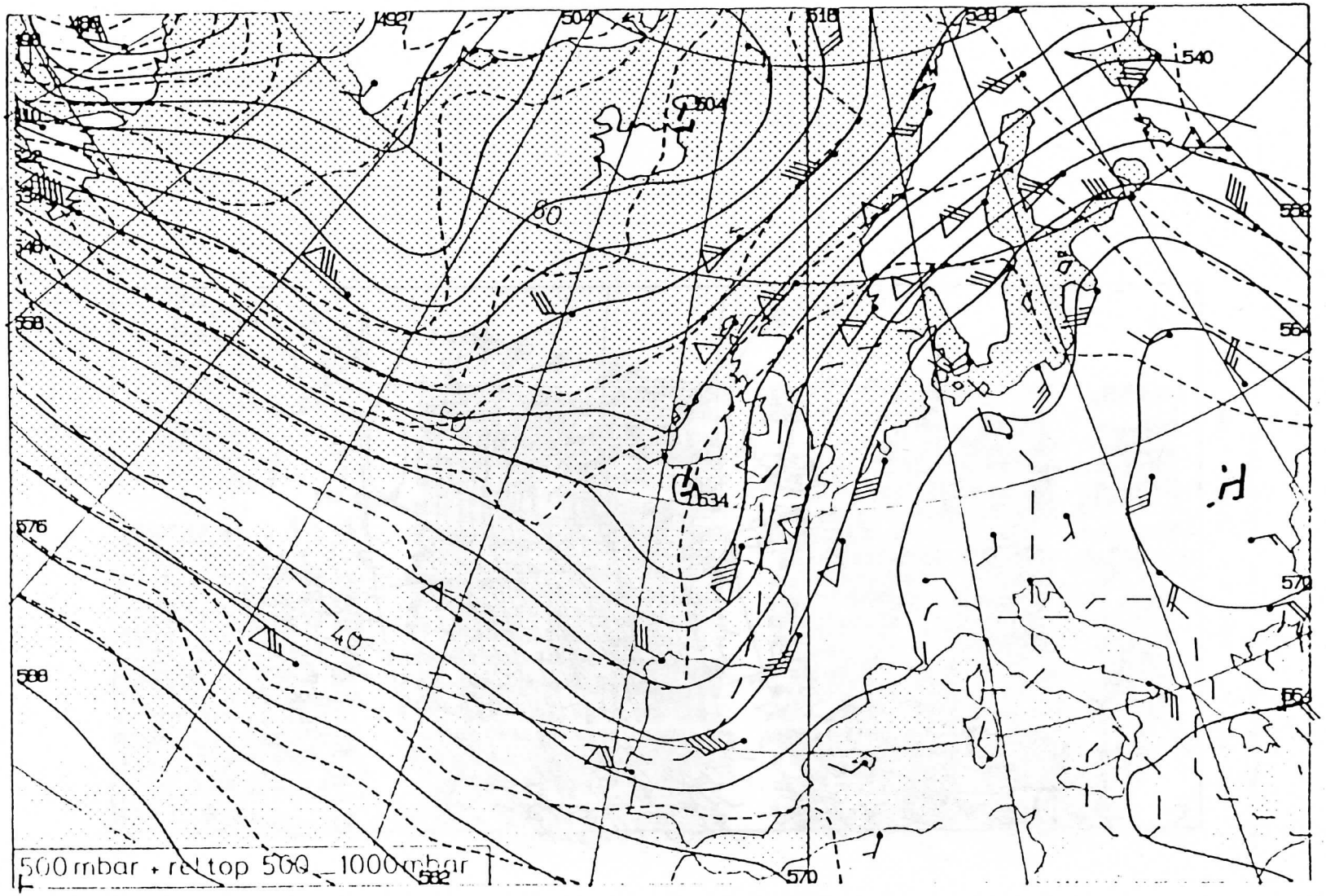
492
504
516
528
540
504
552
564
576
588
582
570
534
H
80
60
40
500 mbar + rel top 500 - 1000 mbar

Fig 10b

NOAA-9 VERTICAL SOUNDER - LMD PHYSICAL INVERSION METHOD

700 - 500 HB. ORBIT: 10244 DECEMBER, 8, 1986 15.10Z.

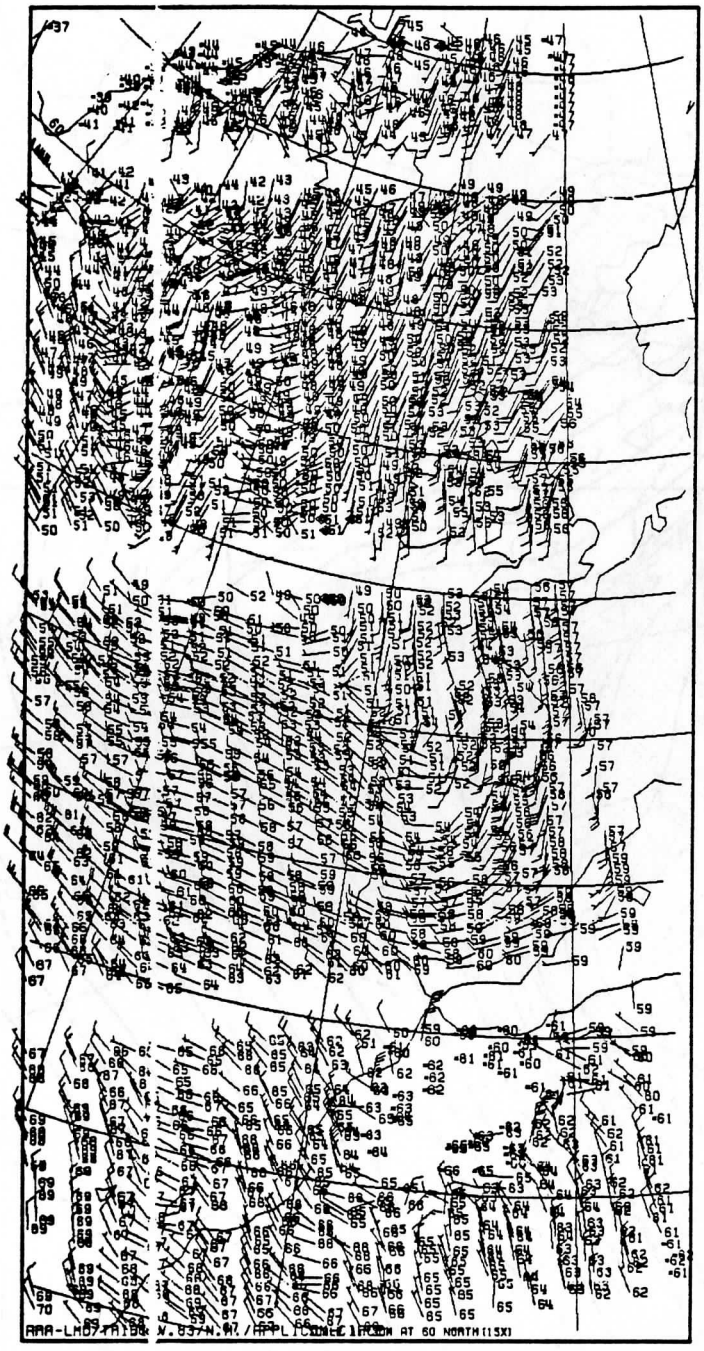

Fig 11a

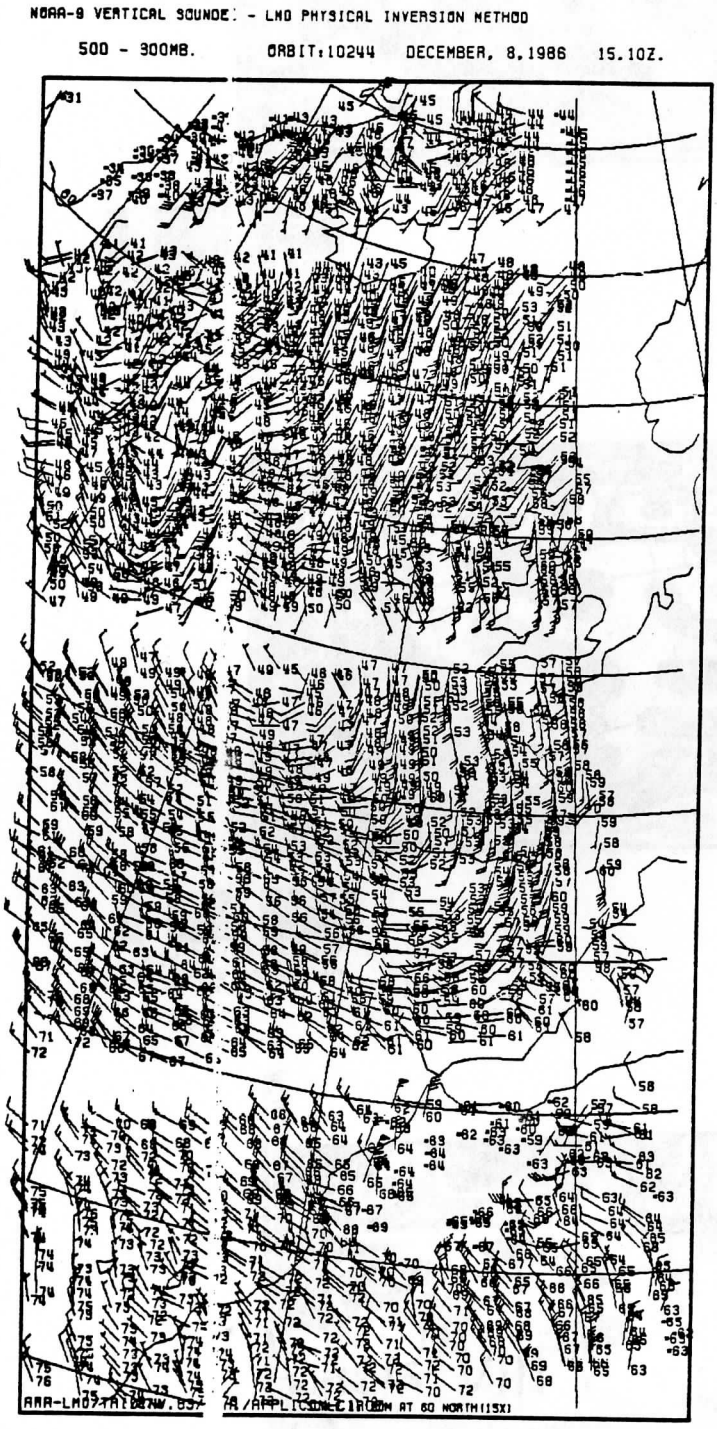
NOAA-9 VERTICAL SOUNDE - LMD PHYSICAL INVERSION METHOD
500 - 300MB. ORBIT:10244 DECEMBER, 8,1986 15.10Z.

Fig 11b

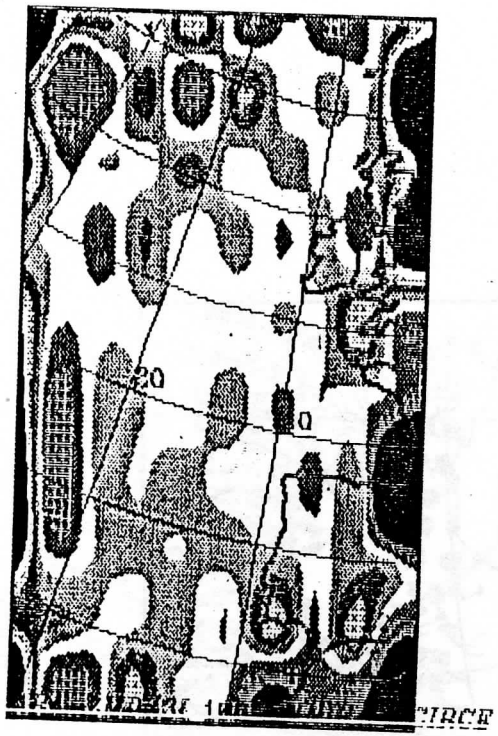

Fig 12a

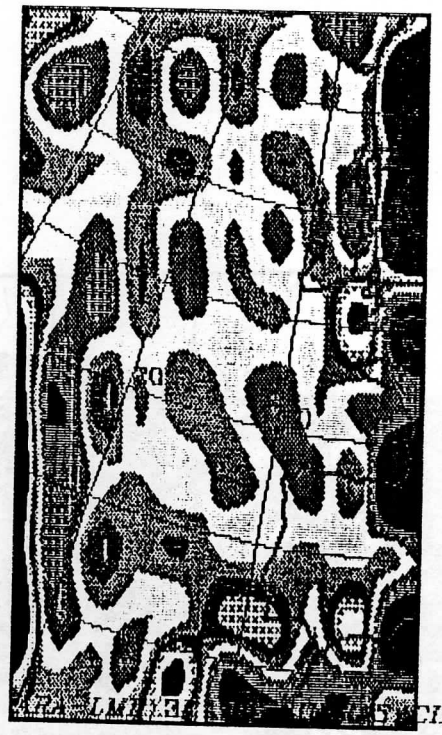

Fig 12b

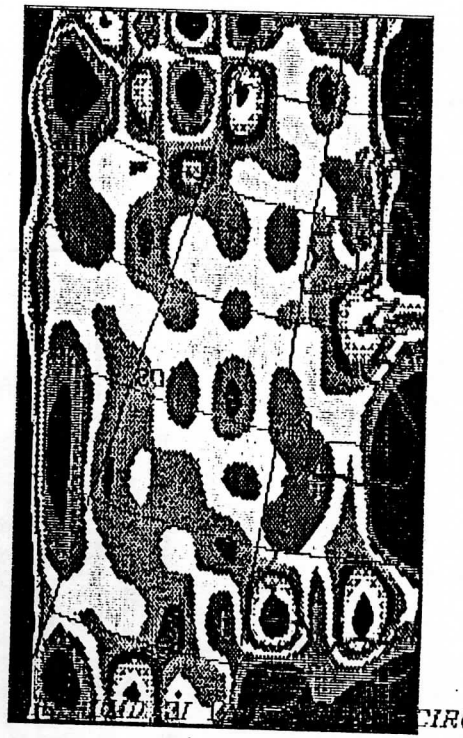

Fig 12c

TOWARDS OPERATIONAL USE OF TOVS IN THE NETHERLANDS

by G.J. Prangsma
KNMI, De Bilt, Netherlands

ABSTRACT

An overview is presented of the preparatory work at KNMI as part of the introduction of TOVS data in the so-called "Automatic Production Line" (APL) for the operational weather service. The arguments for the selection of an inversion method for the radiance data as received from the NOAA-TIROS series of polar orbiting satellites are discussed.

The development of the APL is briefly outlined, emphasizing the role of TOVS data in the basic system.

1. INTRODUCTION

Background

After the installation of a HRPT[1] receiving station at the Dutch Meteorological service (KNMI[2]) in 1981, a lot of experience has been gained in the manual interpretation of cloud imagery, originating from the AVHRR[3] instrument. Gradually the need for a more quantitative use of these data resulted in a development project aiming at the implementation of a package for the numerical treatment of imagery data. Along with the basic analysis system, a variety of useful products has been developed (see *e.g.* Prangsma and Roozekrans, 1988).

As a second phase, in early 1986 a project has been defined aiming at the implementation of the quantitative use of TOVS[4] data in operational and research work. The need arose to choose an adequate TOVS inversion algorithm, suited for both operational and research needs, with the possibility for linkage with the already existing AVHRR package and experience.

Selection of a TOVS inversion algorithm

For the selection of an inversion algorithm of the radiances as coming from the TOVS instruments, several obvious candidates were available:

- the International TOVS Processing Package (ITPP), developed by the group at the University of Wisconsin
- the operational method of NOAA/NESDIS[5]
- the 3I (Improved Inversion Initialization) system, developed by the ARA[6] group at LMD[7], Palaiseau.

As outlined above, the criteria in this selection exercise stemmed from operational as well as research needs. These needs can be rephrased in the following requirements:

---

[1] HRPT High Resolution Picture Transmission
[2] KNMI Koninklijk Nederlands Meteorologisch Instituut
[3] AVHRR Advanced Very High Resolution Radiometer
[4] TOVS TIROS Operational Vertical Sounder
TIROS Thermal InfraRed Operational Satellite
[5] NOAA National Oceanographic and Atmospheric Administration
NESDIS National Environmental Satellite, Data, and Information Service
[6] ARA Analyse de Rayonnement Atmosphérique / Atmospheric Radiation Analysis
[7] LMD Laboratoire de Météorologie Dynamique

the method must
- have a clearly understandable physical and mathematical basis
- must be independant of an operational forecast model and/or operational/climatological data base
- be flexible and easily adaptable.

An extra, but not necessarily decisive, consideration is the possibility to establish a cooperation with the group, where the method has been developed, within reach even with limited travelling budgets.

Why choose the 3I method?

As an outcome of this selection study, which used available literature and reports only, the 3I-method has been chosen as -probably- the most viable way to go with the limited staff resources available at KNMI.
This choice is mainly based on the first two criteria presented above:

- sound physical and mathematical basis

and -esteemed of prime importance-:

- independancy of operational or climatological data bases.

This choice being made, contacts have been established with the ARA/LMD group in order to check their willingness to provide us with a copy of their 3I-package and to provide any additional guidance, should the need arise. In this context arrangements have been made under which the present author spent a couple of months in late 1986 and early 1987 at the LMD, during which period he worked on a number of aspects concerning the transportability and the operational use of the 3I system.
During the period from mid-October until mid-December 1986, the satellite reception station of the French meteorological service at Lannion made available TOVS data for two successive satellite passes on Monday, Wednesday and Friday.
Moreover, on a number of occasions the central forecasting service in Paris asked for treatment of special orbits, based on observation of unexpected or remarkable weather developments. In this way, a total of 55 orbits within the range of the Lannion reception station have been routinely treated with the 3I-system. Results for two such situations have been published elsewhere (see Prangsma *et al.*, 1987); two more are presented at this conference.

2. STATUS OF PRESENT WORK AND PLANS FOR FUTURE EXPANSIONS AT KNMI

The Automatic Production Line at KNMI

In the discussion at KNMI on how to use modern technology in the operational weather service, the daily work of the forecaster can been basically split into two parts:
- the interpretation of the output of one or more numerical models
- the manipulation of "classical" meteorological data, such as SYNOPS, charts, satellite imagery, etc.

The first of these tasks can be defined as being the final step in an "Automatic Porduction Line" (APL), whereas the second task in the same spirit can be called an "Interactive Production Line" (IPL).
The natural border-line between these two ways of producing weather forecasts, is the period for which the forecast is produced:
- 0-6 hours ahead is best done in an interactive way
- 6-12 hours ahead can be covered manually as well as by numerical models: simple advection of existing weather systems.

- 12 hours and further ahead requires the inclusion of dynamical processes in the atmosphere and is best cov red by numerical means, that is: a model of sufficient areal extent such as to cover the developments bound to affect the area of interest within the forecast period.

Therefore the period of local forecasting for the next 24 to 36 hours is nowadays generally based on some sort of limited area model, the physical content of which is by and large determined by the output requirements of the meteorological service using the model.

The role of a Limited Area Model in the APL

The main data and information carrier in the automatic production process will naturally be a fine-mesh, limited area model (LAM) of sufficient physical sophistication so as to be able to produce adequate numerical forecasts for 24 to 30 hours ahead as input to other models like storm surge and wave models for areas of local/national interest, PBL* models for air pollution warnings, to name just a few.

At KNMI this central role is played by an in-house adaptation of the ECMWF* LAM, in the near future to be replaced by the model resulting from the international HIRLAM[10] project. From the operational requirements for the Dutch circumstances, a three-hourly update of the forecast cycle is deemed necessary and is therefore a design goal. In order to be able to feed the model at such short intervals with enough information on especially the upper-air situation, satellite data are a vital ingredient.

The place and role of satellite data in APL and IPL

Having said this, it is most important to note that timeliness of the satellite data and regular spatial distribution under all atmospheric conditions are key factors, both for the model runs and for the warning function in the interactive production line.

This illustrates another factor in favour of the 3I inversion method: the results are found to be robust and reliable (see Prangsma *et al.*, 1987), especially in cloudy areas where the weather developments have to be watched as carefully as is possible. In other words: a regular coverage with TOVS derived upper-air data in cloudy, and potential development areas is essential.

Experience has shown, that the NESDIS operational products become scarce and less reliable in areas with heavy clouds (G. Kelly, private communication). Also the ITPP, due to its declouding algorithm (the so-called N-star method), is less performing in this respect, whereas the 3I-system gives evenly distributed results, even under heavy cloudy conditions (see Prangsma *et al.*, 1987).

Status of the KNMI implementation

At the time of writing, the installation of a computer system, linked with the HRPT receiving station, has been finalized, while the software is being adapted to the format of the raw data received by the system in real-time. Both the AVHRR and TOVS data will be treated to give a number of products to be used in the operational weather service as well as in the support of other government branches, KNMI being responsible for the reception and dissemination of operational satellite data within the Dutch national services.

The system is planned to be ready for routine use by the end of 1988 and will be used for further development work and research in the field of satellite meteorology in the coming years.

---

* PBL Planetary Boundary Layer
* ECMWF European Centre for Medium-range Weather Forecasts
[10] HIRLAM HIgh Resolution Limited Area Model

REFERENCES

Prangsma, G.J., and J.N. Roozekrans, 1988.
Using NOAA-AVHRR imagery in assessing water quality parameters.
Int. J. of Remote-Sensing, in press.

Prangsma, G.J., A. Chedin, N. Husson, N.A. Scott, J. Quere and G. Rochard, 1987.
Observation of the development of mesoscale systems by operational meteorological satellites.
Proc. Symp. Mesoscale Analysis and Forecasting, (Vancouver, Canada, 17-19 August 1987), ESA SP-282, pp. 117-122.

FUTURE INSTRUMENTS: NOAA-KLM UPDATE

Anthony L. Reale and H. D. Drahos
NOAA/NESDIS
Washington, DC 29233 USA

The current status of NOAA-K,L,M is summarized in the following tables and figures. NOAA-K,L,M represents a significant upgrade of the current TOVS system (both with regard to instrument and science algorithms). The NESDIS philosophy is to prevent "system shock" by gradually introducing the new software system and science algorithms via System-90 and ultimately the entire upgraded package via System-92. The former represents science and system changes implemented on the TOVS instrument, the latter represents the complete upgrade implemented for AMSU/HIRS-3/AVHRR instrument configuration. AMSU represents a major change since it consists of two units, AMSU-A containing 15 microwave temperature channels at approximately 45 km resolution at nadir and AMSU-B containing five microwave water vapor channels at approximately 15 km resolution at nadir.

Milestones for NOAA-K,L,M are presented in figues 1 and 2. System-90 has slipped to the fourth quarter of 1991 and System-92 to at least the second quarter of 1993. Figure 3 intercompares the data frames of System-90 and System 92. Figure 4 shows a simplified schematic diagram of the flow of satellite data currently planned for NOAA-K,L,M. The return of data to the Data Processing Services System (DPSS) for centralized distribution to all users is significant. Figure 5 shows the current sounding products from the TOVS and the planned addition to those products for System-90 and System-92. The 50,000 soundings per satellite per day available from the high density TOVS system (approximately 10,000 sounding per satellite per day for the low density product) expands to around 250,000 sounding per day per satellite for NOAA-K,L,M in System-92. Figure 6 describes the main features of the science upgrades planned for System-90 and System-92 and their current status. It is important to realize that such lists are subject to change and at best represent a preliminary review of what can be expected.

Overall, a significant effort is presently underway to prepare for NOAA-K,L,M. It is hoped that many of the items can be tested with the current TOVS system prior to System-90. A document "Overview and Capabilities of the NOAA-K,L,M Sounding Products Generation System (Preliminary Design)" prepared by S. M. Systems and Research Corporation (K. Cox, May 1987) is available from NESDIS upon request.

Current Launch Schedule		Software Schedule
NOAA-H (PM)	July 1988	
NOAA-D (AM)	June 1989	
NOAA-I (PM)	October 1990	System-90 - 4th quarter 1991
NOAA-J (AM)	January 1992	System-92 - 2nd quarter 1993
NOAA-K (PM)	June 1993	
NOAA-L (AM)	August 1994	
NOAA-M (PM)	December 1995	

Figure 1: Milestones for NOAA-K,L,M.

Figure 2. Transition from TOVS to System '92

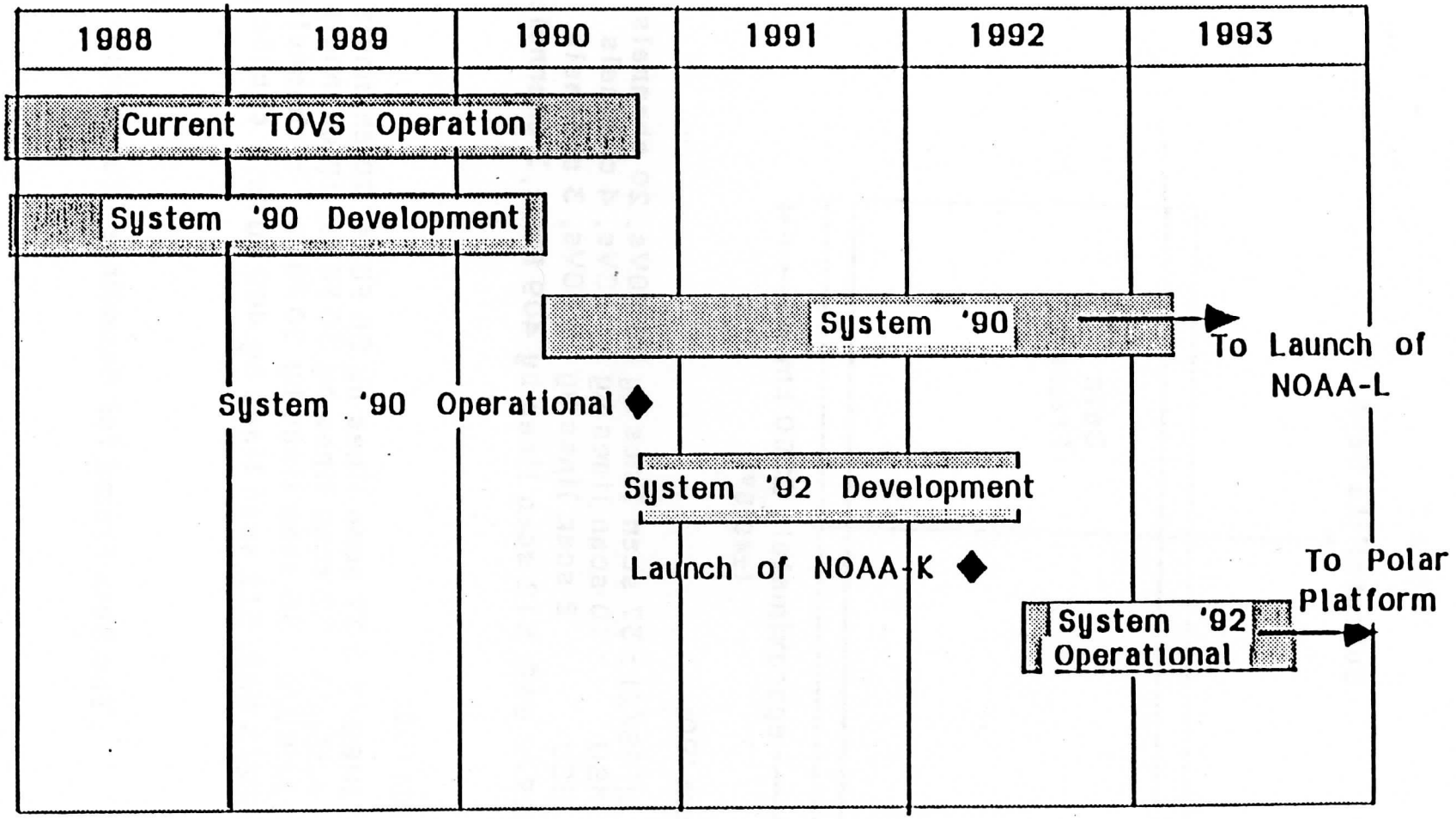

Milestones for the Development of Systems '90 & '92.

Figure 3

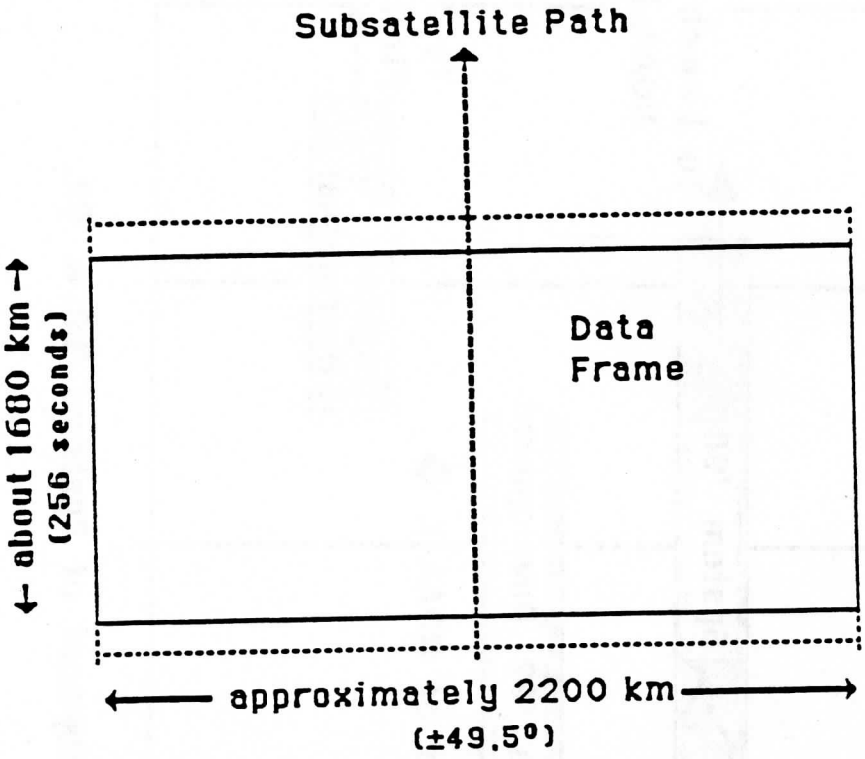

System '90:

HIRS/2I : 37 scan lines by 56 FOVs, 20 channels
MSU : 10 scan lines by 11 FOVs, 4 channels
SSU : 8 scan lines by 8 FOVs, 3 channels
AVHRR/2 GAC: 512 scan lines by 409 FOVs, 3 channels

System '92:

HIRS/3 : 37 scan lines by 56 FOVs, 20 channels
AMSU/A : 32 scan lines by 30 FOVs, 15 channels
AMSU/B : 96 scan lines by 90 FOVs, 5 channels
AVHRR/3 GAC: 512 scan lines by 409 FOVs, 3 channels

The Data Frame for Soundings Processing

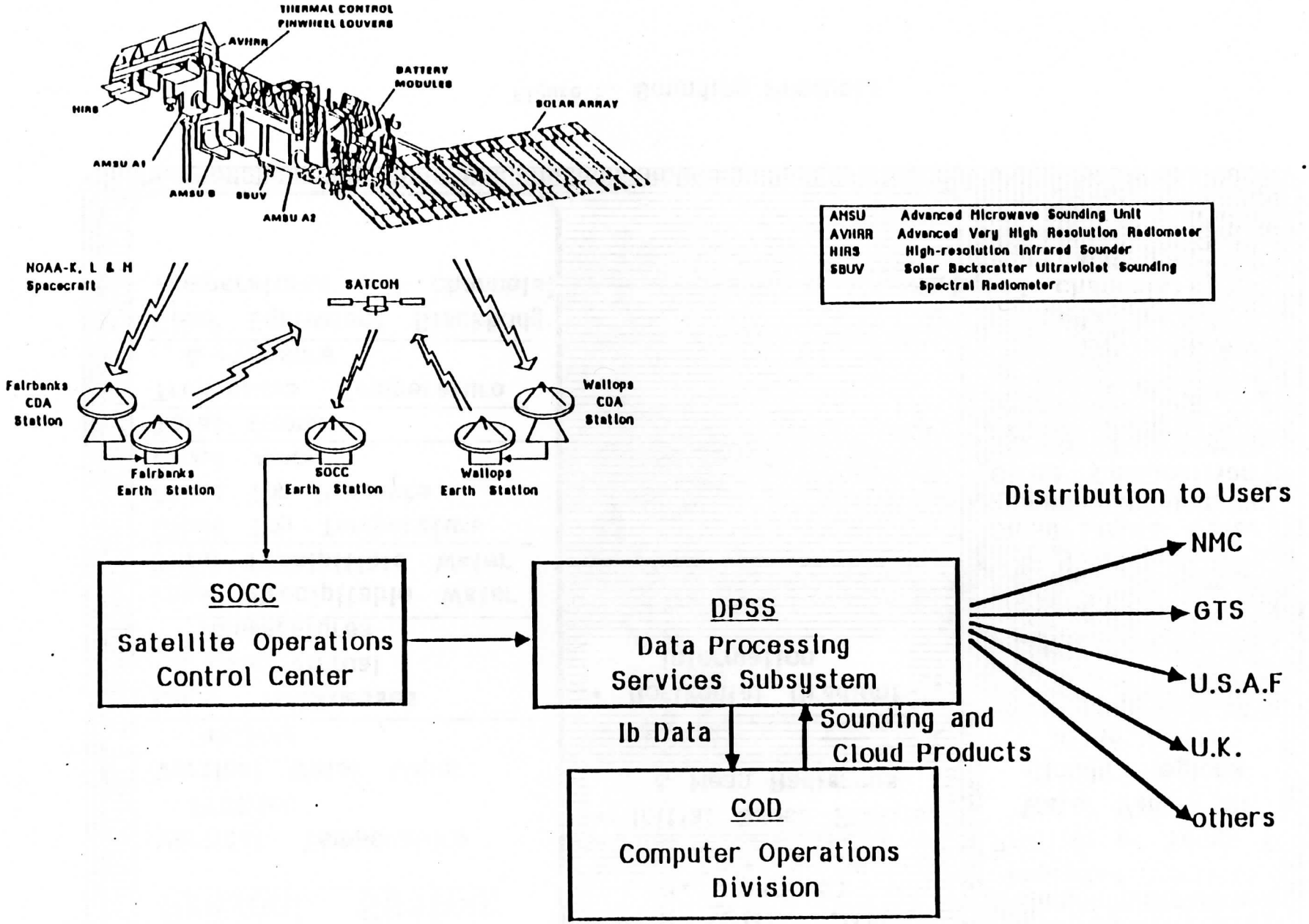

Figure 4. Simplified Schematic of the Flow of the Satellite Data

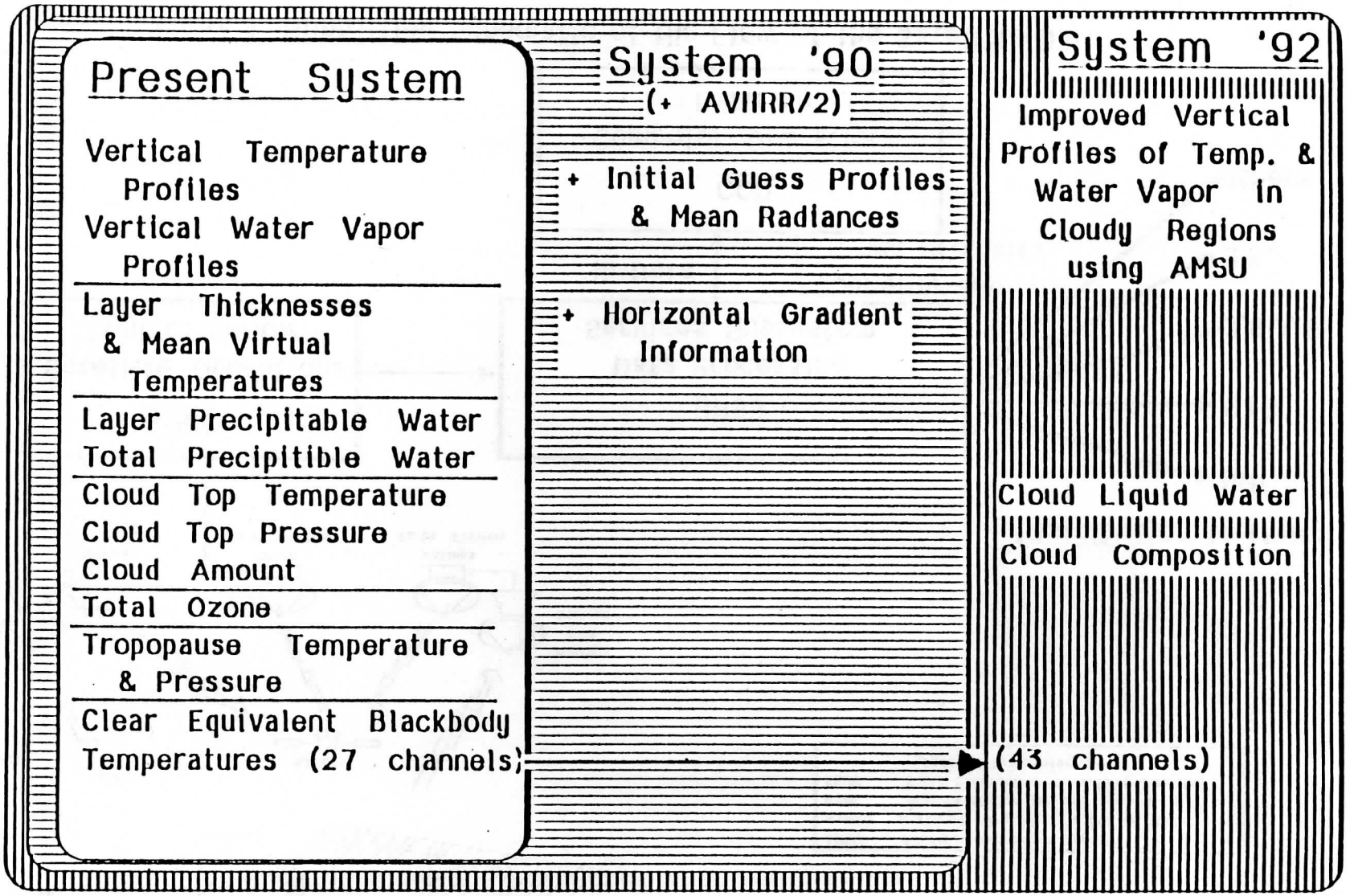

Figure 5. Sounding Products

Figure 6

March 1988 E/RA23:HFD

NOAA-K,L,M SCIENCE CHANGES

New Science	Sys'90	Sys'92
Retrieval Grid	N	Y
Med. Rain Fltr(update/?)	Y	Y
Air Mass		Y
Phys. Retrieval		
HIRS & MSU	Y	N
AMSU & HIRS	N	Y
Limb Correction		
Global	Y	Y
Local	Y	Y
Surface Correction		
Elevation Correction	Y	Y
Emissivity Correction	N	Y
Parameter Mapping		
Optimal Interpolation	Y	Y
Retrievals above clouds		
precip. & ground	Y	Y
Horizontal Gradient		
Information	Y	Y
Cloud Clearing (AVHRR)	Y	Y
Third N* (AVHRR)	Y	Y
Cloud Tests (AMSU)	N	Y
Cldy Water Vap. Ret.	N	Y
Radiosonde from Archive	Y	Y
3-D Checks	Y	Y
Skill Score vs.		
6 hrly Forecast	Y	Y
Calib. Procedure (HIRS)	Y	Y
Earth Location Verify		
Time/Position Comp	Y	Y
Microwave Ck Sys '90	Y	Y
Water Vapor Antenuation	Y	Y
Surface Field Upgrade	Y	Y

BASELINE UPPER AIR NETWORK (BUAN): STATUS OF IMPLEMENTATION

Anthony L. Reale
NOAA/NESDIS
Washington, DC 20233 USA

1. INTRODUCTION

BUAN is an international program to augment operational satellite sounding systems with upper air radiosonde data coincident with the satellite overpass. In March 1987, the final version of the BUAN feasibility test plan (F. Zbar, WMO) was distributed. This document is an assimilation of NMC, NESDIS and WMO inputs.

About 100 candidate stations (83 land raobs, 11 ships (ASAP) and stationary vessels (DSV), and about six rocketsondes) were identified. NESDIS was designated as being responsible for transmitting overpass information, real time processing, and evaluation of BUAN-based sounding products. The WMO responsibility was to coordinate the BUAN launch schedules with the BUAN candidate stations. NMC was given the responsibility to supplement the NESDIS evaluation with collocation studies and perhaps a numerical weather prediction forecast impact study.

2. NESDIS PROCESSING AND ARCHIVING

The BUAN feasibility test began on January 15, 1988. At this time, the Sounding Implementation Branch (SIB) of NESDIS had separate software in place to process sounding products using only the identified BUAN stations for tuning. Tuning includes (1) the weekly update of the small sample mean temperature, moisture and radiance profiles per physical retrieval bin (i.e., the 27 geographical categories used in the NESDIS physical retrieval sounding system), (2) selection of the covariance matrix per bin, (3) computation of the weighting function per bin based on the bin mean temperature and, finally, (4) the daily update of the first guess adjustment procedure (FGAP) raob and sounding match-up file used to compute the first guess. The control system for evaluation of the BUAN soundings was selected to be the NESDIS physical retrieval sounding system.

Software was written to access the BUAN raob reports from the NMC 0Z, 6Z, 12Z and 18Z raob files. Additional software was completed to identify participating BUAN stations (i.e., those launching within 30, 60, and 90 minutes of the scheduled launch), to check the quality of these reports (i.e., completeness, altitude, etc.), and to report on match-ups made.

Software was developed to perform special evaluation of the BUAN based test system versus the control system. This entails special three-way match evaluations in which (1) BUAN raobs are compared to Test and Control system retrievals, (2) conventional raobs are compared to Test and Control system retrievals within one hour and 100 km, and also (3) within three hours and 300 km. Routine evaluation of the products from the Test and Control are also planned using the NESDIS "OLE" off-line interactive graphics display capability.

Finally, a significant effort is also directed toward archiving the BUAN match-ups and the Test and Control products. Since the control system is not operational, it also must be archived. Routine archiving (i.e., daily) incorporates:

(1) BUAN raobs (within +1 hour of scheduled launch)
(2) all test system sounding products (level temperature, moisture, clear column brightness temperature, and first guess) matched to BUAN raobs
(3) 1B level raw satellite radiances corresponding to the sounding products matched to BUAN raobs (after may 1 only)
(4) 1T level raw satellite radiances (corresponding to sounding products matched to BUAN raobs
(5) all BUAN souunding products (identical to layer data distributed by NESDIS to users)
(6) matched raobs and sounding products, 1T raw radiances and all sounding products from the Control system

The archiving task was not identified in the original BUAN feasibility plan and was added later. The requirement for 1B level data archiving was a particularly late requirement, consequently these data will not be available for match-ups before May 1. All other data has been archived since January 15, except the orbital processing products which are not available until late in February. The final archive format is being defined and will be made available at a later date.

3. PRELIMINARY RESULTS

Preliminary results on BUAN reporting, match-up sampling, and orbital product evaluation data are available for the BUAN test. These results cover the period of January 15 through February 29, 1987. The BUAN test is scheduled to run through July 15, 1988. Table 1 shows the radiosondes per TOVS geographic bin for which BUAN match-ups were made and utilized for tuning. Table 2 shows the ample sizes of match-ups collected per TOVS graphic bin. Tables 1 and 2 also reflect the BUAN radiosonde sampling which exists on the 28-day rotating match-up file which is updated each day. This is important for interpreting the performance of the system. Intercomparison of Tables 1 and 2 also point out the problem of duplicate match-ups, that is, match-ups for which a given raob is repeated. This is apparent in bin 8 for which two raob stations were responsible for over 90 match-ups over the 45 day period.

Preliminary match-up collocation statistics are not shown in this report, but they have been generated and indicate no large differences between the Test and Control sounding products. Interactive graphics displays using "OLE" also show reasonable compatibility for several global regions, even those for which the BUAN match-up samples were quite small or zero. More study is needed.

A preliminary report on BUAN will be written and distributed in May. A final report including recommendations for follow-on activities will be available in August. Please communicate with SIB if you wish to receive these reports and/or wish to participate in the writing of these reports.

4. CONCLUSIONS

Conclusions based on preliminary evaluation are:

(1) of approximately 100 candidate BUAN stations (including ships and rockets), about 30 stations are actively participating;
(2) including BUAN stations for which routine synoptic launches fall within one hour of satellite overpass, approximately 60 stations are being matched with soundings to tune the test system;
(3) marginal BUAN participation is occurring for global representation;
(4) there is overall compatibility on a global scale between the Test and Control system sounding (using the NESDIS physical retrieval algorithm);
(5) special archiving of all BUAN radiosonde and satellite sounding match-ups and Test system sounding products is underway.

Table 1

BUAN Raobs Used for Tuning Between 15 Jan and 5 Apr 1988

Bin-Radiosonde Station Identification No.

1 - C7M, 21432, 20046(R)
2 - 70308, 71913, C7L, C7C, ZCSK, VPHA
3 - 71600, ZCSK, FNDR, FNOU, FNPH
4 - 72203, FNOU, 91285, 91245, 47936, 76644, FNPH, 60020, 78861(R), 74794(R)
5 - 61902, 91610, 63985, 78954, 91217, 48698, 91765, 98327
6 - 61901, 91938, 91765
7 -
8 - 93944, 87860
9 - 89050, 89611, 89571

10 - 02963, 71913, 24959, 71957, 71924, 20046(R)
11 - 34560, 71913, 70308, 72747, 10868, 02963, 71600, ZCSK
12 - 72208, 72261, 58457, 72346, 54511, 72402(R)
13 - 72203, 98327, 72261, 58457, 78861(R), 74794(R)
14 - 82193, 48698, 48455, 91610, 78954, 63985, 98327, 80413
15 - 87155, 94326, 94203, 61901
16 - 87860, 94610, 94672
17 - 87860, 61998
18 - 89050, 89611, 89571

19 - 71925, 02963, 71924, 71957, 21432, 24959, 20046(R)
20 - 72747, 70308, 10868, 71913, 28698, 02963, 07145, 71600, VPHA
21 - 72208, 58457, 54511, 72340, 71600, 08001, 72402(R)
22 - 72203, 98327, 76644, 91285, 91245, 72261, 47936, 58457
23 - 48455, 98327, 91765
24 -
25 - 94672
26 -
27 - 89050, 89611, 89571

Table 2

Sample Sizes Per Physical Retrieval Geographic Bin for Two Time Periods (SP1, SP2)

BIN	SP1	SP2	BIN	SP1	SP2	BIN	SP1	SP2
1	30	12	10	8	31	19	167	90
2	50	27	11	43	46	20	135	60
3	10	12	12	62	38	21	97	46
4	38	37	13	37	36	22	86	43
5	31	27	14	41	39	23	53	10
6	2	3	15	34	20	24	0	0
7	4	0	16	18	19	25	35	12
8	53	38	17	27	16	26	0	0
9	12	10	18	54	32	27	12	34

Sampling Periods:
SP1 - 1/15-2/8
SP2 - 2/8-2/29

Bin Definition:
1 - 90N-60N; sea
2-8 - 60-45N, 60-45S; sea
9 - 60-90S; sea
10-18 - same latitudes as above; land, day
19-27 - same latitudes as above; land, night

PLANS FOR TOVS PROCESSING IN THE SPANISH SIVIM SYSTEM

Ricardo Riosalido, José Miguel F. Serdán

Instituto Nacional de Meteorología

Madrid, Spain

ABSTRACT

The Spanish National Institute of Meteorology is developing an Integrated Weather Surveillance System (SIVIM) based on the joint exploitation of satellite, radar and other conventional data sources. One of the most important part of the project is a Satellite Data Reception and Processing System (SAIDAS) for Meteosat, Goes-E and Tiros satellites. The processing and data management is based on the well-known McIDAS system which provides a powerful tool for integrating all types of meteorological data.

During this year, a TOVS processing system will be implemented as part of the project. Taking into account the ability of the McIDAS system to access a wide variety of data sets (NWP products, observations, imagery, etc.) and its interactive capabilities, it becomes the ideal framework for TOVS processing, allowing to perform TOVS retrievals in an interactive way.

These retrievals will provide data for our Limited Area Model in areas with sparse or no data coverage (Atlantic Ocean, Mediterranean Sea, etc.), but also these products will be available for operational weather forecasting in the Regional Forecast Centers through remote McIDAS work-stations. This will allow the forecasters to display, and combine with other data sets, temperature and humidity profiles from TOVS, thickness charts and other derived products (stability indexes, total precipitable water, etc.) to be used as a diagnosis tool, specially in those mentioned data sparse regions.

1. THE SIVIM SYSTEM

SIVIM stands for Integrated Weather Surveillance System; this project was launched a few years ago in order to set up a modern short and very short weather forecasting system; it is being actively developed now; its main components -see also fig. 1- are:

- SAIDAS which is specifically the satellite information processor; furthermore -as we will see in detail- its capabilities on all kind of data adquisition and analisis make it become in some manner the heart of the system.

- SIPREN is the numerical modelling processor; a 48 h. -at 6 h. intervals- high resolution limited area forecast mode is running presently twice a day on a Fujitsu M-382 host computer; there are links to ECMWF -whose global model provides boundary conditions- and other forecast centers; SAIDAS will provide TOVS retrievals.

- SINAT is the telecommunications system; it is based on a Cyber 120/70 with manages up to eight GTS links, a star-like national network with 130 low speed asyncronous lines, links with other european aeronautical networks, and also dial-up capabilities. Via a dedicated link to the Fujitsu it provides conventional data to SAIDAS and SIPREN and from the last gets forecast grids for dissemination.

- SIRAM will be radar integrating processor; based on a VAS 785, from the weather radar network -13 regional radars- it will get a subset of data, and satellite images from SAIDAS, obtaining composite and global products.

- Other subcomponents like lightning detector and automatic station networks will also be included in SIVIM.

2. THE SAIDAS SUBSYSTEM

Is charged on the reception and processing of satellite products; it also supports the large updated data base for the whole system. Its scheme is shown in fig. 2.

The main hardware components are:

- Ingestors for all kind of meteorological data in real time.
- Storing, processing and displaying devices.

The software is an adaptation of the McIDAS system, developed by SSEC an Wisconsin University; it works on the Fujitsu M-382 host computer, and its wide interactive capabilities -handling and combining images, graphics, all kind of data- can be fully exploited by the means of a local-and-remote terminals network, each having a refresh memory and several input-output devices.

The three-satellite ingestion chains for GOES-E, METEOSAT and TIROS high resolution transmissions are quite similar with antenna, down coverter, receptor, bit and frame synchronisers, channel connecting and disk-storage. GOES-E images are already normally received; METEOSAT -first- and TIROS ingestors are now being implemented. Raw METEOSAT data will also be accepted through a 11 m. antenna, and processed, so lowering access time to information; direct TIROS tracking control from SAIDAS will also be posible.

Other ingestors get convencional GTS data from SINAT, analisis-and-forecast grids from SIPREN, and composite images from radars and other sources when available.

3. TOVS PROCESSING

Taking into account the ability of the system to access all type of meteorological data and its interactive capabilities, it becomes an ideal framework for TOVS processing. The software will be implemented during this year and it will be essentially the ITPP software modified in order to be able to use all the capabilities already mentioned of the system, in particular allowing to perform interactively some steps of the retrieval process, mainly in those concerning quality control: cloud clearing, attenuation by precipitation, generation of first-guess, use of ancillary data, etc., where positive impact in the final product quality could be expected.

4. OPERATIONAL USE OF TOVS PRODUCTS

The use of the TOVS products is of particular importance in a country like Spain that is surrounded by extensive areas with no data or poor data coverage (Atlantic Ocean, Mediterranean Sea ...). Meteorological systems like cut-off-lows in the East Atlantic moving toward the Mediterranean sea, the interaction between these systems and subtropical circulations, and the developing of mesoscale convective systems in the Mediterranean area, can produce very heavy rains and flash-floods; and constitute an important forecast problem, mainly because they take place in areas with not enough data coverage to resolve or detect small scale features relevant to these phenomena, and, but in connection with the first reason, because these systems are in general not well conducted by the operational numerical models.

The use of TOVS retrieval can help us in these problems in two ways, first by the asimilation of this data in the limited area model and second, and this is one of the most interesting characteristic of the system, by the direct use of TOVS retrievals and products by the forecaster. In the National Forecast Center, and in the differents Regional Forecast Centers, the forecasters will have access to these products, as soon as generated, through local and remote workstations.

This capability will allow the forecaster to display temperature and humidity profiles, thickness charts or to compute or derive interactively parameters of fields such us stability indices, thermal vorticity, total precipitable water etc., and combine these products with other data sets (imagery or data) in near real time, giving to the forecaster a complementary diagnosis tool. So, apart from the expected improvement in the results of our Limited Area Model, we hope that the direct use of TOVS products by the forecasters can help us, at least, to perform a better diagnosis with positive impact in the short and very-short range forecast.

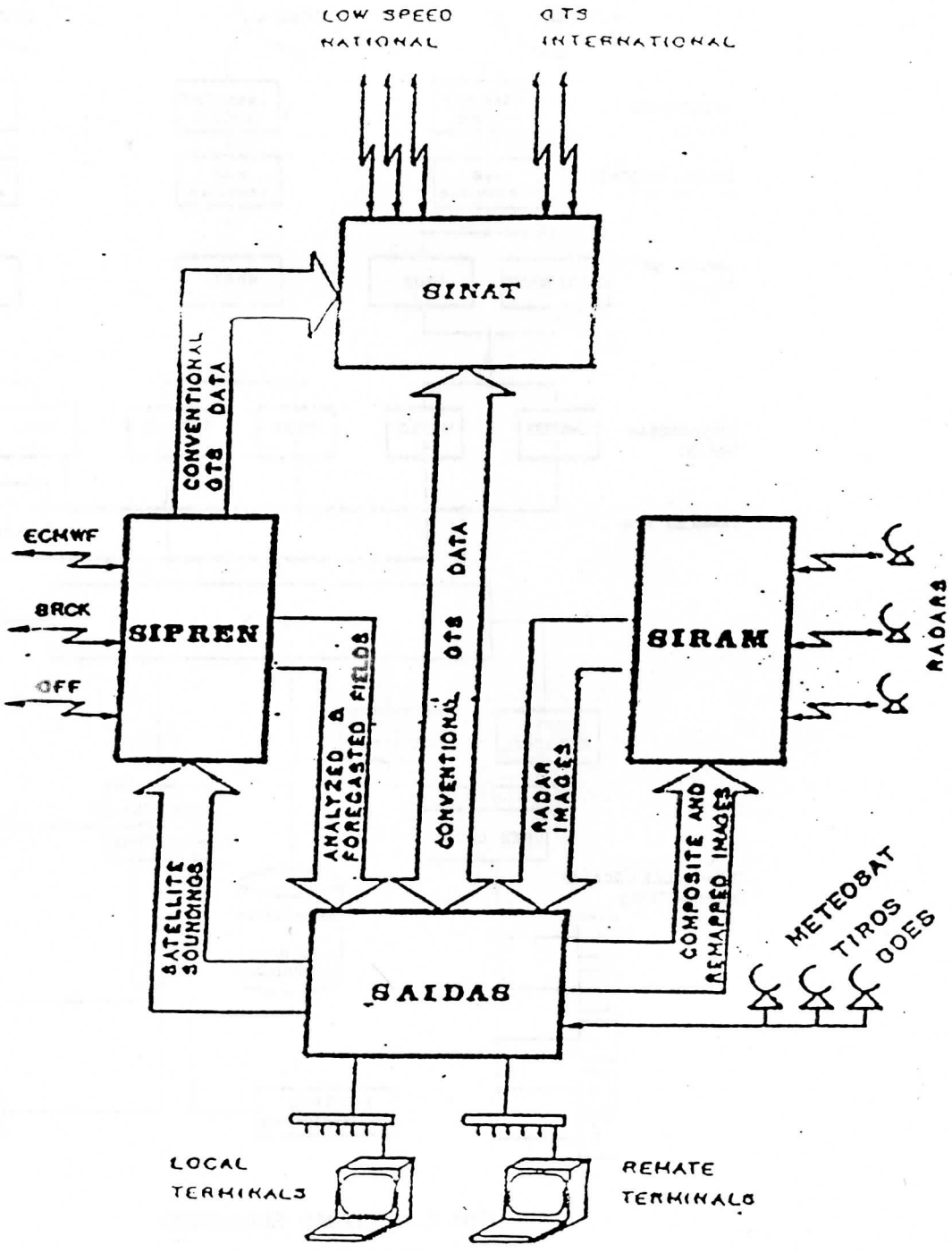

FIG 1.- SIVIM SYSTEM

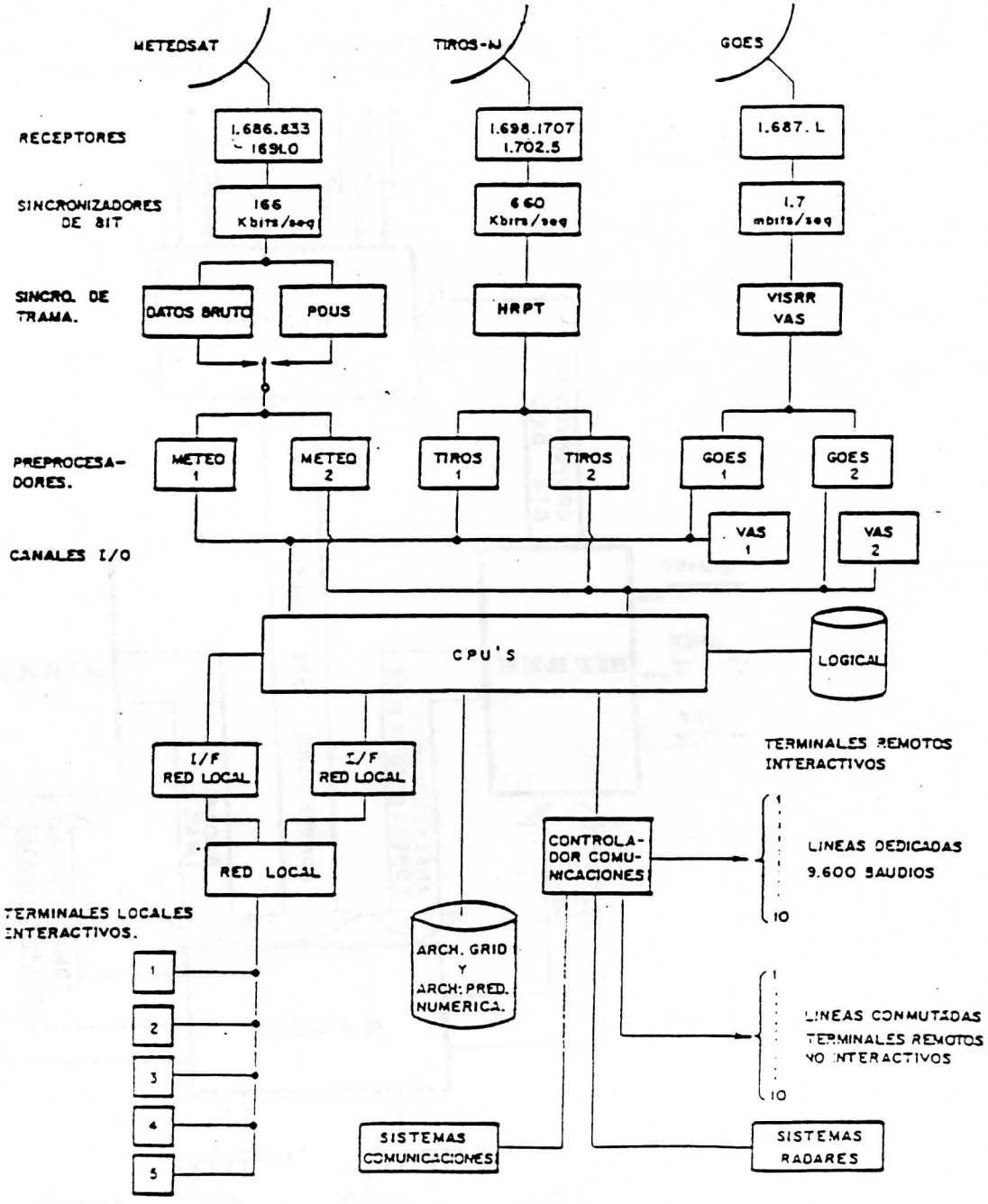

FIG 2.- SAIDAS SUBSYSTEM

OBJECTIVE ANALYSIS OF TEMPERATURE FIELDS OBTAINED FROM CONVENTIONAL AND SATELLITE DATA

Rolando Rizzi and Ennio Tosi
Dipartimento di Fisica
Via Irnerio 46, 40126 Bologna

December 18, 1987

An high resolution objective analysis has been applied to conventional and satellite retrieved temperature profiles to investigate differences among the two sets of data. The case study selected represents the first stages of a rapid cyclone development in the lee of the Alps. It is found, both in statistical and qualitative terms, that satellite data are in good agreement with conventional ones and that a detailed description of the temperature field at surface is of primary importance for an accurate retrieval of satellite soundings, particularly for use in mesoscale meteororology. The time lag between the two different data sets is found to explain a consistent portion of the discrepancies and therefore a full quadridimensional assimilation scheme appears to be essential to pursue the investigation.

The analysis scheme used in this paper (ANBO from now on) was originally devised for the conventional data of the ALPEX dataset (Buzzi et. al. 1985, and Trevisan et. al 1985). It is characterized by a high horizontal resolution (about 50 km), virtual potential temperature θ as vertical coordinate, and an extensive use of surface data to describe the intersection of the θ surfaces with the ground, in particular with the orography. Due to these characteristics, this analysis has been chosen for comparing conventional and satellite upper air data. In particular the performance of satellite data was compared with ALPEX data and the influence of the surface data on the retrival scheme was tested.

The time chosen for the intercomparison is 12 GMT of March 4th 1982. This time is part of an Intensive Observing Period, during which conventional observations were intensified, and two NOAA-7 passes are available at about the same time of upper air conventional observations.

The software used to process the satellite data shown in the present article is a version of what is now called the International TOVS Processing Package and detailed descriptions can be found in Smith et al., 1985. Some changes were made regarding the treatment of conventional surface data inside the inversion algorithm and on the type of bias corrections applied to calculated radiances to reach a satisfying agreement with the measured ones. More details can be found in Rizzi and Tosi, 1988.

1. QUALITATIVE INTERCOMPARISON

The results presented in the following were obtained applying ANBO to the different types of upper air data, conventional and satellite. The analysis at the ground were performed using only conventional type data (SYNOP and SHIP).

Fig. 1a and 1b present pressure at the surface $\theta = 302K$, which is in the zone of the upper level front.

The analysis with satellite data is warmer in the area of the trough and colder in the area of the ridge. These features are visible also in the cross sections (fig. 2) along line A–B drawn in fig. 1a.

The difference between the two kinds of data is very clear (for easier readout the surfaces $\theta = 290K$ and $\theta = 302K$ are dotted). Satellite data are smoother and are not able to resolve the fine vertical structures associated with fronts. The differences in the position of the maxima of thermal gradients, indicated in the description of fig. 1, can be explained in terms of the different steepness of the θ surfaces in the frontal zones. From the θ surfaces it is possible to interpolate on more commonly used pressure surfaces. A visual inspection of geopotential heights at 500 hPa (fig. 3) does not show major differences.

Temperature fields at the same levels (not presented here) show more clearly a pronounced warm ridge in the western part in the satellite analysis extending north to Ireland and Cornwall. The explanation for this discrepancy is complicated by the fact that on one side about 60 satellite soundings coherently bring up

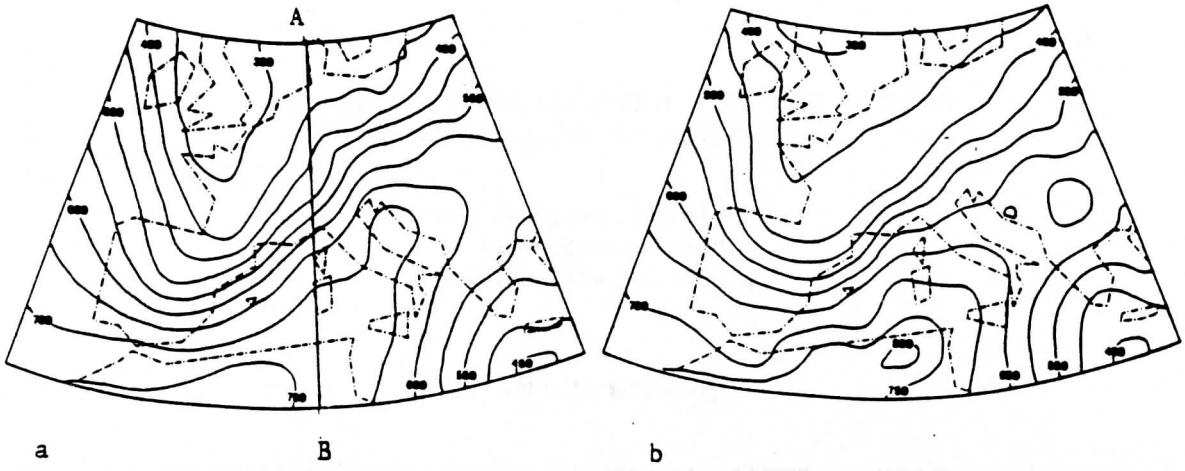

Fig. 1 Analyzed pressure over the 302 K isentropic surface (a. from conventional and b. from satellite data)

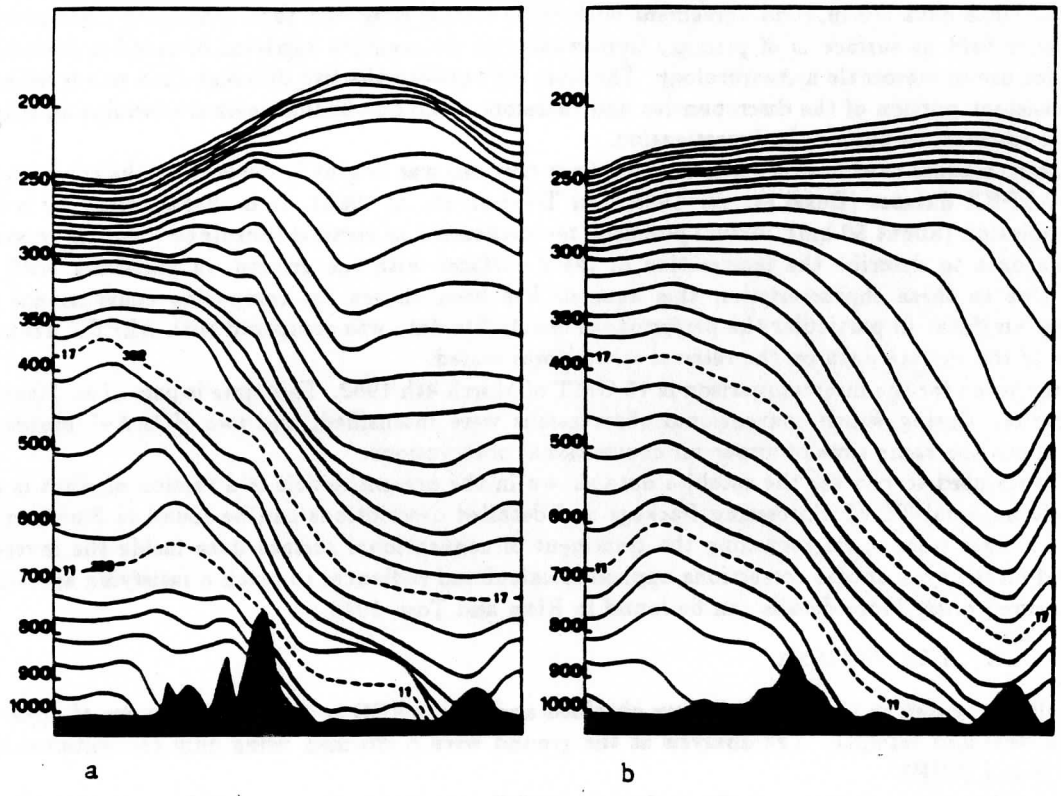

Fig. 2 Vertical cross sections along line A–B (shown in fig.1a) (a. from conventional and b. from satellite data)

the feature, while on the other conventional data are missing over the Atlantic Ocean but over the British Isles several radiosonde profiles are available.

A tentative conclusion may be 1. that the conventional analysis does not conveniently describe the ridge over the oceanic areas and 2. that part of the discrepancy must also be attributed to the difference in time between the conventional and the satellite data (the central and western part of ALPEX area is observed during the second orbit). It must also be reminded that both analyses are forced to the ECMWF operational one for a length of 2 gridpoints from the boundaries. Twelve hour tendency from 12 GMT of March 4 to 00 GMT of March 5 computed after RAOB ascents over Ireland and mid and southern Great Britain show that strongest warm advection is occurring over south–eastern Ireland and over Cornwall, precisely where the discrepancy is largest and cannot be simply explained by the lack of conventional data.

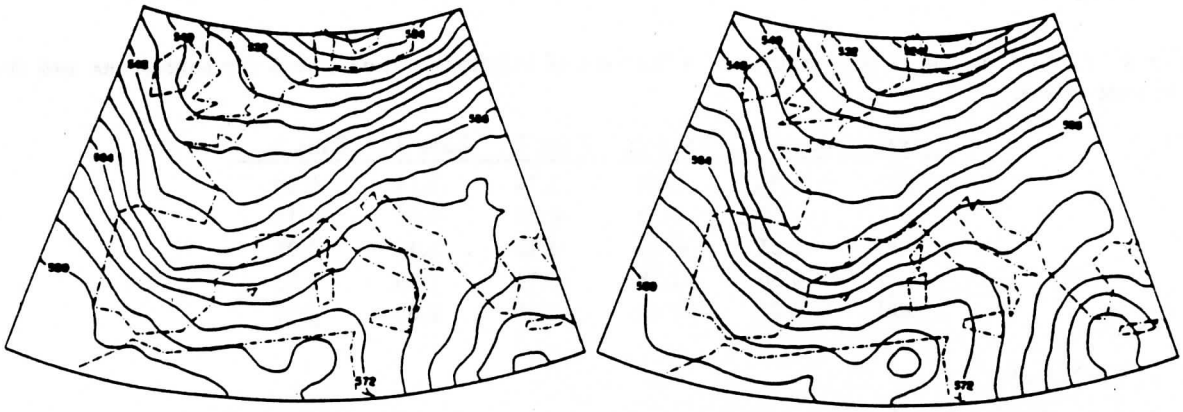

a b

Fig. 8 Geopotential heights in dam interpolated on the 500 hPa pressure surface (a. from conventional and b. from satellite data)

2. STATISTICAL DESCRIPTION

Bias and rms deviations among ANBO analysis of conventional (ACO) and satellite (ASA) temperatures are shown in table 1. Also differences with the ECMWF analysys (ECM) interpolated on ANBO grid, are shown.

Table 1. Bias and rms deviations among ECMWF analysis (ECM) and analysed fields of conventional data (ACO) and satellite soundings (ASA).

level	ACO–ASA		ACO–ECM	
	bias	rms	bias	rms
900	-0.84	1.43	—	—
850	-0.55	1.35	1.05	1.56
500	0.51	1.61	0.40	0.84
500	-0.21	1.85	0.08	0.79
300	1.65	2.52	0.22	0.96

The 1000 hPa surface is mostly under the ground where no information about the temperature is available, and then it is missins in ANBO results. The 900 hPa surface is not standard and is missing in ECMWF analysis. Biases are small at all levels below 300 hPa. In particular biases at low levels are much smaller that the one obtained comparing satellite data to ECMWF operational analysis. The same holds true for the rms differences indicating that the description of the ECMWF analysys is inadequate for the purpose of adding information on layers close to the ground inside a TOVS processing model. Not much needs to be said about results on the 300 hPa surface, since it is fairly well known that present satellite data are not capable to describe any sharp change in stratification, and this is particularly true near the tropopause level.

In table 2 temperature biases are reported for five contigous areas from west to east covering the whole latitude range of ANBO The general trend observed at and above 850 hPa is a change from positive to negative bias, whose magnitude is about $1.5K$.

The effect of the time lag on bias depends on the atmospheric dinamics at the boundaries, in this case a high pressure ridge was entering the area. In the case presented the effect was noticeable in descriptive as well as statistical terms. What seems to be relevant is not the absolute value of the bias (either of temperature or of geopotential) but the relative variation of the bias computed in areas covered by different orbits.

A discussion of the features observed in the geopotential fields would be very similar to what has already been said about the temperature.

Table 2. ACO-ASA bias of temperature as a function of longitude. Zone 1 to 5 are contiguous and span from west to east

level	Zone 1	Zone 2	Zone 3	Zone 4	Zone 5
900	-1.54	-0.63	-0.74	-1.14	-0.34
850	-1.60	-0.35	-0.28	-0.81	0.11
500	-1.05	0.49	0.85	1.41	0.98
500	-0.86	-1.78	-0.34	1.09	0.73
300	1.21	0.59	2.01	2.86	2.05

3. CONCLUSIONS

It is possible to derive some conclusions from the material presented above. First of all a detailed description of the surface temperature fields is of primary importance for an accurate retrieval of satellite soundings, particularly for use in mesoscale meteororology. Without information of the same horizontal scale of the satellite, the conflicts that arise between measured and computed radiances at the ground propagate upward and affect soundings up to 500 hPa. Both in statistical and qualitative terms satellite data are in good agreement with conventional ones.

Root mean square differences among satellite and conventional high resolution analysis are smaller than between satellite and ECMWF 1982 operational analysis which lacks small scale features. The substantial difference between satellite and conventional data is clearly shown by the cross sections. It must be said that the choice of θ as vertical coordinate was made to have the maximum evidentiation of frontal zones, in which are concentrated the highest vertical gradients, and so a comparison with analysis using different vertical coordinates could give more favourable results, at least from the field of view of satellite supporters. The two kinds of data seem mergeable, and a use of satellite to fill spatial gaps of conventional data, particularly large when dealing with mesoscale phenomena, seems possible. In this case the time lag between the two different data sets has very important effects which would otherwise be interpreted either as an addition of information over ocean areas or errors in derived temperature profiles from satellite data in regions where the RAOB network is denser.

REFERENCES

- Buzzi A. and S. Tibaldi, "Cyclogenesys in the lee of the Alps: a case study," Quart. J. Roy. Meteor. Soc. 104, 271–287 (1978).
- Buzzi A., A. Trevisan and E. Tosi,"Isentropic analysis of a case of lee cyclogenesys," Beitr. Phys. Atmosph. 58, 273–284 (1985).
- Rizzi R., "High–Resolution Satellite Soundings over the Alpex Area. The 4–5 March Case Study," Il Nuovo Cimento 7C, 3, 317–337 (1984).
- Rizzi R. and E. Tosi, "Comparison of Temperature Fields obtained from Conventional and Satellite Data using an High Resolution Objective Analysis," submitted to J.C.A.M. (1988)
- Smith W. L. , H. M. Woolf, C. M. Hayden, A. J. Schreiner and J. M. LeMarshall, "The Physical Retrieval TOVS Export Package," Technical Proceedings of the First International TOVS Study Conference, Igls (1985).
- Trevisan A., A. Buzzi, E .Tosi ans S. Rambaldi,"A fine–mesh objective analysis scheme in isentropic coordinates," Nuovo Cimento 8C, 805–821 (1985).

AN UPDATE ABOUT CALIBRATION, NAVIGATION AND FORMATS

Guy Rochard

Centre de Meteorologie Spatiale
BP 147
22302 Lannion Cedex, France

1. INTRODUCTION

This paper is a follow on to the "Status Report on Calibration Problems" (Rochard, Technical Proceedings of ITSC-III, pages 235 to 242) Corrections or comments about the following information are welcomed by the author.

NOAA/NESDIS will publish a revised NESDIS Technical Memeorandum (NTM) 107 and all appendixes B in the summer 1988. (First for NOAA-9, NOAA-10 and NOAA-H).

In addition, a summary of new information will be put on the Electronic Bulletin Board by September 1988. A copy will be also available on request at CMS/Lannion in September 1988.

2. CONCERNING AVHRR

a. In the revised NTM 107, an improvement to the calibration of the AVHRR visible and nearer infrared channels is proposed. Until now, the albedo (expressed as a percentage of that for a perfectly reflecting Lambertian surface) is given by the linear formula:

A = GX + I, where X is the numerical count, G is the gain , and I is the intercept. These values are given in appendix B of NTM 107. In future, the calibration will be written:

$$R = \frac{A}{100} \cdot \frac{F}{\pi W}$$

R is the radiance (W/m^2.sr.micron), F is the solar irradiance weighted by the spectral response of the channel, and W is the equivalent width of the channel. The revised NTM 107 will contain this data.

b. The revised NTM 107 indicates that "the user is cautioned that there is strong evidence that the values of G for the NOAA-7 and the NOAA-9 AVHRR had decreased after two years in orbit by 10 to 20% of their measured pre-launch values for different satellite-channel combinations. Channel degradation in this range has been calculated by Frouin and Gauthier (1987). Aircraft-based observations by Smith et al. (1987) yielded very similar results. Several users of the data have reported evidence consistent with significant reductions in G. There is scant evidence presently available on the dependence of G on time-in-orbit. The evidence suggests that the degradation in G for the NOAA-7 and NOAA-9 AVHRRs is in the 0 to 15% range after one year in orbit and that G tends to stabilize after two years in orbit. Aircraft-based observations of the in-orbit value of G for the NOAA-10 AVHRR in late December 1987 are now (March 1988) being analyzed."

Peter Abel, Land Sciences Branch, Satellite Research Laboratory, NOAA/NESDIS, World Weather Building, Washington is looking into this problem.

c. Concerning channel 3, some work has been done to suppress a part of the noise (using Fast Fourier Transform for example). There is a need for operational software that would be easy to exchange; information exchange could occur in the Electronic Bulletin Board.

d. Concerning the NOAA-9 Nonlinearity Correction Channels 4 and 5, the artifice of using a "corrected" non-zero radiance of space was eliminated. The corrections were calculated for three temperatures of the internal blackbody, 10, 15, and 20°C. To determine the appropriate correction, the user must interpolate in the following tables on the actual blackbody temperature in orbit.

Table 1. NOAA-9 AVHRR Ch. 4 Nonlinearity Correction

Target Temperatures (Deg. K)	Correction at Blackbody Temp. (Deg. C) 10	15	20
320	+2.3	+2.3	+2.3
315	+1.8	+1.9	+1.8
310		+1.4	+1.3
305	+1.3	+1.0	+0.9
295	+0.7	+0.4	+0.2
285	0.0		-0.5
275	-0.5	-0.7	-0.9
265	-0.8	-1.1	-1.2
255	-1.0	-1.3	-1.6
245	-1.1	-1.3	-1.7
235	-1.2	-1.4	
225	-1.3	-1.3	-1.5
215	-1.2	-1.5	-1.4
205	-1.6	-1.5	-0.7

Table 2. NOAA-9 AVHRR Ch. 5 Nonlinearity Correction

Target Temperatures (Deg. K)	Correction at Blackbody Temp. (Deg. C) 10	15	20
320	+0.8	+1.0	+1.2
315	+0.6	+0.9	+0.9
310		+0.7	+0.7
305	+1.1(?)	+0.4	+0.5
295	+0.4	+0.2	+0.1
285	0.0		-0.2
275	-0.3	-0.3	-0.5
265	-0.5	-0.6	-0.7
255	-0.7	-0.8	-1.0
245	-0.8	-0.8	-1.2
235	-1.1	-1.2	
225	-1.2	-1.0	-1.1
215	-1.2	-1.4	-1.4
205	-1.7	-1.6	-1.1

(This constitutes the answer to question 4.a, page 236, in the Status Report on Calibration Problems, Technical Proceedings of ITSC-III).

3. CONCERNING HIRS

a. The HIRS Filters for NOAA-9 and NOAA-10 are now available on 5 1/4 floppy disks. The records are card images.

For NOAA H, the HIRS has been improved (HIRS 2I) and two channels have changed: a new channel 10 has a central wavelength at 797 cm^{-1} and new channel 17 at 2420 cm^{-1}. The floppy disk is also available. The data are available from Michael Chalfant (NOAA/NESDIS) or CMS/Lannion. The plotting of the filter is also available on request.

b. For the HIRS Channel 20 calibration, the revised NTM 107 will give the coefficients for converting the albedo A obtained from gain and intercept into radiance R, using the relation

$$R = \frac{A}{100} \cdot \frac{F}{\pi W} .$$

F is the solar spectral irradiance weighted by the spectral response function and W is the equivalent width of the channel. The gains and intercepts for Channel 20 on the past satellites are listed in Table 3.

Table 3. HIRS 2 Channel 20 All Satellites

	Gain	Intercept
Tiros N	+0.02174	79.80
N6	+0.02972	108.02
N7	+0.018098	65.61
N8	+0.02096	72.17
N9	+0.017622	63.39
N10	+0.02148*	77.11*

*Please note that the values given in Appendix B/N10 February 12, 1986 are wrong (they were N9 values).

c. On NOAA-9, the HIRS 2 radiances of channel 16 are nearly the same as those of channel 14 (0.5°K). Nobody knows exactly why. It is suggested that users avoid channel 16.

d. On the NOAA-9, the HIRS 2 channel 7 central wavelength has been confirmed to be 749.48.

e. On NOAA7, HIRS2, the central wavelengths and band correction coefficients given in Appendix B October 19, 1981 are correct. Filters for channel 6, 9, 10 and 13 also are correct in this Appendix. But the other filters are incorrect. They are filters of model 2 carried by NOAA B (which failed). Michael Chalfant is preparing the corrected filters for users.

An example is shown in Figure 1. The errors (incorrect-correct), using the wrong filters, can be as large as +1° for channel 16, -0.5° for channel 19, +0.3° for channel 12.

4. MATCHING AVHRR AND HIRS 2

a. With the same conventions as listed in the Technical Proceedings of ITSC-III on page 238, the misalignment between AVHRR and HIRS 2 for NOAA 10 is approximately:

$\Delta I \simeq +0.5 \qquad \Delta J \simeq +2.5 \qquad \theta_{AH} \simeq 0$

Note also that there are about 1828 AVHRR pixels between the centers of HIRS 2 spot 1 and spot 56.

b. When using one AVHRR pixel for multispectral analysis, one should take care of the fact that the different channels don't "see" exactly the same area. Figure 2 illustrates this point.

5. CONCERNING MSU ANTENNA PATTERNS

For several years, questions have remained concerning:

(1) how to separate MSU antenna pattern corrections from limb corrections, liquid water content corrections and surface emissivity corrections, and

(2) how to get (if possible) MSU information at the resolution of the HIRS 2 field of view.

An illustration is given in Fig. 3. John Eyre (U.K.) has detailed the questions and both Paul Swanson (JPL) and Norman Grody (NOAA) have contributed to the answers.

The response of Grody follows:

In most applications one only needs to define the antenna pattern in the vicinity of the main lobe. This is the region with 2.5 beamwidths from the center of the beam and represents about 96 percent of the total energy received by the antenna. The 96 percent value is obtained by integrating the antenna gain pattern, $G(\theta,\phi)$, over a spherical volume, $\sin\theta \, d\theta d\phi$, encompassing 2.5 beamwidths, viz.,

$$n = \int \int G(\theta',\phi') \sin\theta' \, d\theta' d\phi' \qquad (1)$$

where n is called the beam efficiency.

An useful expression for the antenna pattern is given by the equation

$$G(\theta) = Co * Exp[-\ln(2)(\sin\theta/\sin\theta o)^2] \qquad (2)$$

θ = angle from beam center
θo = 1/2 beam width

Note that the antenna gain is reduced by 50 percent at the half beam width. This model assumes a symmetrical antenna pattern and neglects sidelobes. Using this model the beam efficiency can be calculated as a function of angle using the relationship

$$n(\theta) = \frac{\int_{\phi}^{\theta} G(\theta') \, \mathrm{Sin}\theta' \, d\theta'}{\int_{\phi}^{w/2} G(\theta') \, \mathrm{Sin}\theta' \, d\theta'} \qquad (3)$$

For most applications, it is necessary to reference the antenna pattern on the earth's surface. This transformation is obtained using the equations $\mathrm{Sin}\theta = r/H$ and $\mathrm{Sin}\,\theta o = L/H$. The parameters r, L and H denote the distance on earth relative to the beam center, half of the field of view, and the satellite altitude, respectively. Substituting these equations into (2) we obtain the final result,

$$G(r) = Go*\mathrm{Exp}[-\ln(2)(r/L)^2] \qquad (4)$$

where $r^2 = x^2 + y^2$. For the MSU instrument L = (110/2) km at nadir.

6. CONCERNING SSU

a. In the Technical Proceedings of ITSC-III, page 240, the correct values of a_0, a_1 and a_2 are given through NOAA-9. Here are the coefficients for the remaining satellites.

NOAA-H (model 8)	a_o=283.901	a_1=5.044x10^{-3}	a_2=1.18x10^{-11}
NOAA-I (model 7)	a_o=284.125	a_1=4.819x10^{-3}	a_2=8.75x10^{-9}
NOAA-J (model D3)	a_o=278.150	a_1=4.989x10^{-3}	a_2-0.003x10^{-9}

b. From Steve Stringer, U.K. Meteorlogical office, the following information has been received.

It has been noticed in the past that a difference in space view counts can be obtained depending on whether the view is part of the normal calibration cycle, i.e., four samples over 16 seconds immediately after a CSP, or subsequent sample taken while the mirror is inhibited in the space view. The effect varies for different channels and models and the reason why it occurs is not understood. However, this can have an effect on calibration and accuracy of retrieved temperatures. Our investigations suggest the correct value for a space view should be obtained from the subsequent samples following the first four samples after a CSP. This is unfortunate since in normal Cal. Auto. mode only the four samples after a CSP are possible. This means that to obtain the correct value an offset has to be applied to the samples normally received. The value of offset is calculated before launch and updated twice a year in orbit (usually May and November) when the SSU mirror is inhibited in space view for five orbits. In the past, the effect has been small, but it seems that as instruments age the effect increases. For F8, to be launched on NOAA-H, the offset if relatively large and will have to be applied give the required temperature accuracy. The offsets for F8 are:

Ch 25	Ch 26	Ch 27
+21.0	+12.0	+18.9

i.e., these offsets are to be added to the space view 8-1 samples (sample 8 minus sample 1) obtained during normal calibration cycles. The effect is to change the calibration slope and offset and hence the retrieved radiances from each earth view, affecting radiances more the lower they are. Figure 4 shows this.

The latest figures available for F5 on NOAA-9 are:

Ch 25	Ch 26	Ch 27
-13.9	-21.8	-7.1

7. NAVIGATION OF THE SATELLITE AND OF THE IMAGES

a. An experiment was conducted in July 1987 to predict the NOAA-9 and 10 positions and to control the real positions. The real positions, using internal ephemerids have been determined both by Jim Ellickson (NOAA/NESDIS) and CLS/ARGOS (Toulouse/France). The results are quite coherent and the difference between the two methods is less that 500 meters for the satellite position. The predicted positions have been computed by Fred Nagle (CIMSS/Madison) using TBUS IV and Brolyd Software, and Pierre-Yves Le Traon (CLS/ARGOS), Anne Marsouin and Pascal Brunel (CMS/Lannion) using ARGOS parameters (from CLS/ARGOS) and MOSAIK software (from CLS/ARGOS). The results (all below) show that with the ARGOS system there are 1 to 2 km errors for one, two, or three days of prediction. In the same time, using TBUS 4 and Brolyd, there are 2 to 3 km errors for one day, 4 to 5 km for two days, and 7km for three days. HRPT stations need only to predict for 24 hours, so both ARGOS and TBUS 4 give near the same results even if ARGOS is a little bit better. An action is being decided by NOAA to propose a Brolyd package for users. News about that will be put in the Electronic Bulletin Board next September.

Those results (for July 87) use the internal CLS/ARGOS ephemerids (which can have 500 meters of difference with NOAA internal high precision ephermerids) as the real position.

Questions about CLS/ARGOS, should be sent directly to:

CLS/ARGOS, CNES, 18 Avenue E. Belin
31055-Toulouse Cedex, France

To date, no detailed information about the satellite attitude precision is available. If anybody has some results, please let us know.

b. Several software packages exist that perform the navigation of the pictures. One of them will be published in the revised NTM 107. Another one is available on request (for AVHRR pixel navigation) from Pascal Brunel, CMS/Lannion, BP 147, 22302 France. The documentation is available in SATMOS Note No. 2 and the software is on floppy disk or on CCT.

Table 4

			ARGOS	TBUS 4
After 24 hours:	mean value of error	N9	1 km	2 km
		N10	0.4 km	.6 km
	RMS	N9	0.6 km	1.2 km
		N10	0.2 km	1.1 km
After 48 hours:	mean value of error	N9	1.1 km	3.9 km
		N10	0.5 km	5.1 km
	RMS	N9	0.7 km	1.8 km
		N10	0.2 km	2 km
After 72 hours:	mean value of error	N9	1.1 km	4.8 km
		N10	0.5 km	7.8 km
	RMS	N9	0.7 km	2.6 km
		N10	0.2 km	3.2 km

It should be noted that a correction has been introduced in the original software of CMS/Lannion (published in Satmos Note No. 2, February 86). Formerly, the local nadir of the satellite was in the orbit plane and perpendicular to the velocity vector. Now, according according to a recommendation of Dr. A Schwalb (NESDIS), the local nadir is obtained using the projection from the satellite on the earth ellipsoid, which is not exactly perpendicular to the satellite velocity.

A new Satmos Note No. 2 and the new software are available on request.

8. ARCHIVE FORMATS IN HRPT DIRECT READOUT STATIONS

Following the first International AVHRR Conference in Melbourne, Fall 86, a questionnaire was sent to HRPT stations and about 20 of them have answered. Most of them archive HRPT raw data directly. However, some of them use level 1-B format as described in NOAA Polar Orbiter Data Users Guide (December 1986). Katherine B. Kidwell, NOAA/NESDIS, Room 100, World Weather Building , Washington.

Two other formats are also used; they are the MASTER format in CMS/Lannion (available on request), and the SHARP format in Earthnet (contact Luigi Fusco, Via Galileo Galilei, 00044 Frascati, Italy).

There may be other formats used, but we are unaware of them. May of the HRPT stations haven't answered the questionnaire yet.

The final report on archive format should be available for International AVHRR conference no. 2.

9. SUMMARY OF INSTRUMENTS

Table 5 summarizes the instruments on past, present, and future NOAA polar orbiters.

Table 5. Summary of Instruments

Satellite	AVHRR Model	HIRS2 Model	MSU Model	SSU Model
TIROS-N	Protoflight 4 channels	Protoflight	2	Protoflight
NOAA-6(A)	103 4 channels	1	Protoflight	2
NOAA-B (failed)	104 4 channels	2	1	4
NOAA-7(C)	201 5 channels	4	3	3
NOAA-8(E)	102 4 channels	3	7	6
NOAA-9(F)	202 5 channels	6	6	5
NOAA-10(G)	101 4 channels	5	5	nothing
NOAA-H	203* 5 channels	HIRS2I 1I	9	8
NOAA-D	204 4 channels	7	4	nothing
NOAA-I	205 5 channels	HIRS2I	10	7
NOAA-J	206 5 channels	HIRS2I 3I	11	D3**
NOAA K,L,M	AVHRR3 (6 channels)	HIRS3	AMSU A AND B	

10. BIBLIOGRAPHY

Collocation of AVHRR/HIRS/MSU fields of view, Technical Memorandum 86/1, CSIRO, Wembley WA 6014 by Fred Prata, Bureau of Meteorology, Melbourne, Australia.

Procedure and results of AVHRR-HIRS picture matching, Tadao Aoki, Meteorological Research Institute, Nagamine, Yatabe, Ibaraki 305, Japan.

Cathia data file, see in Proceedings. Lydie Lavanant, CMS, BP147, 22302 Lannion, France.

An atmospheric correction method fo AVHRR using HIRS 2, Mikio Takagi, Institute of Industrial Science, University of Tokyo.

J.G.R., Vol. 92, pgs. 2859-2874, March 15, 1987 for using also HIRS 2 for atmospheric correction of AVHRR.

Frouin, R., and C. Gautier, "Calibration of the NOAA-7 AVHRR, GOES-5, and GOES-6 VISSR/VAS Solar Channels," Remote Sensing Environment, 22, 73-101.

Smith, G. R., R. H. Levin, P. Abel, and H. Jacobowitz, "Calibration of the solar channels of the NOAA-9 AVHRR using high-altitude aircraft measurements," Accepted for publication in J. Tech. 1988.

Rao, C. R. Nagaraja, "Pre-launch calibration of channels 1 and 2 of the advanced very high resolution radiometer," NOAA Technical Report, NESDIS 36, October 1987.

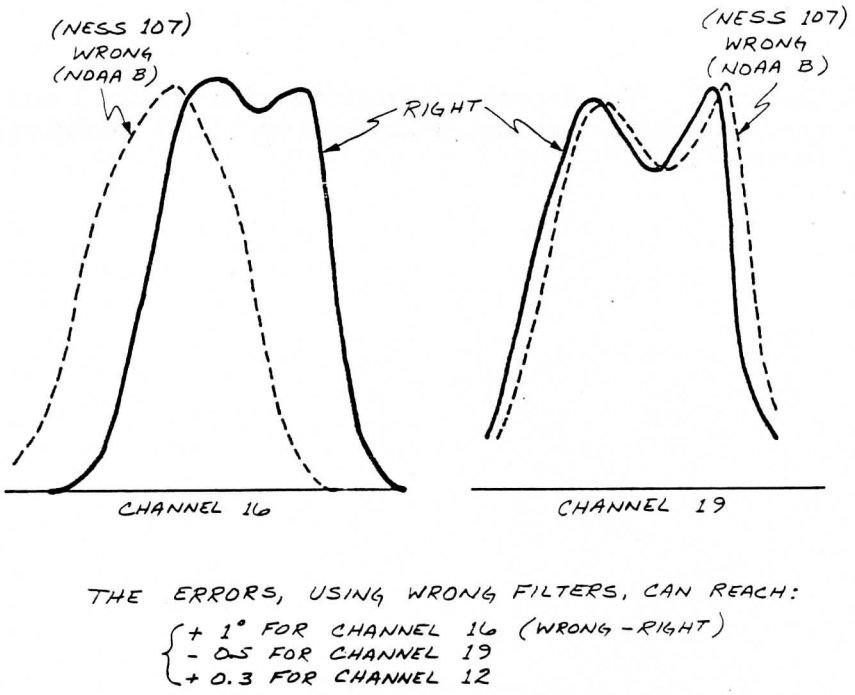

Fig. 1. NOAA-7 HIRS filter errors.

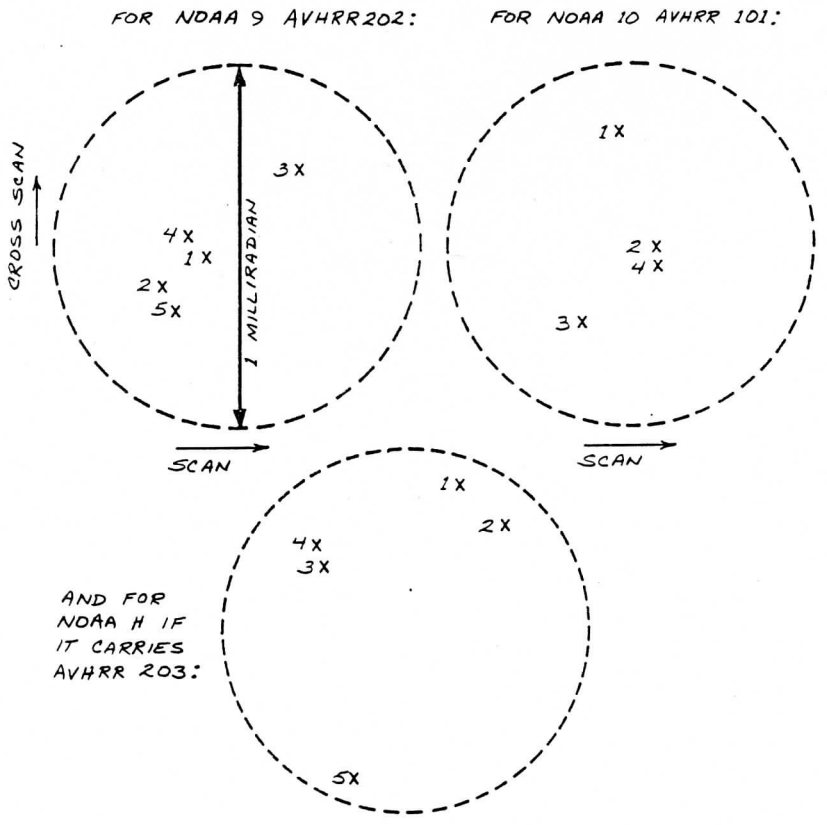

Fig. 2. Multispectral alignment for AVHRR.

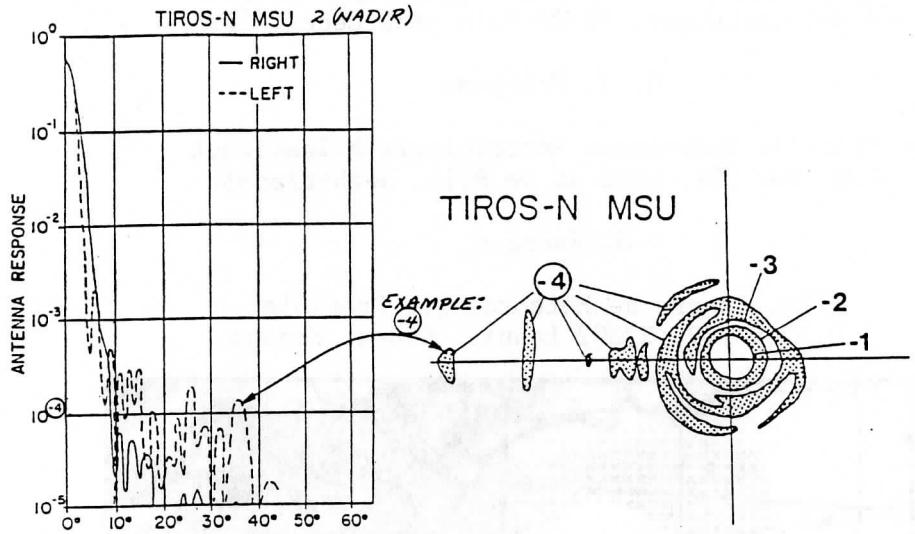

Fig. 3. An illustration of MSU antenna pattern corrections.

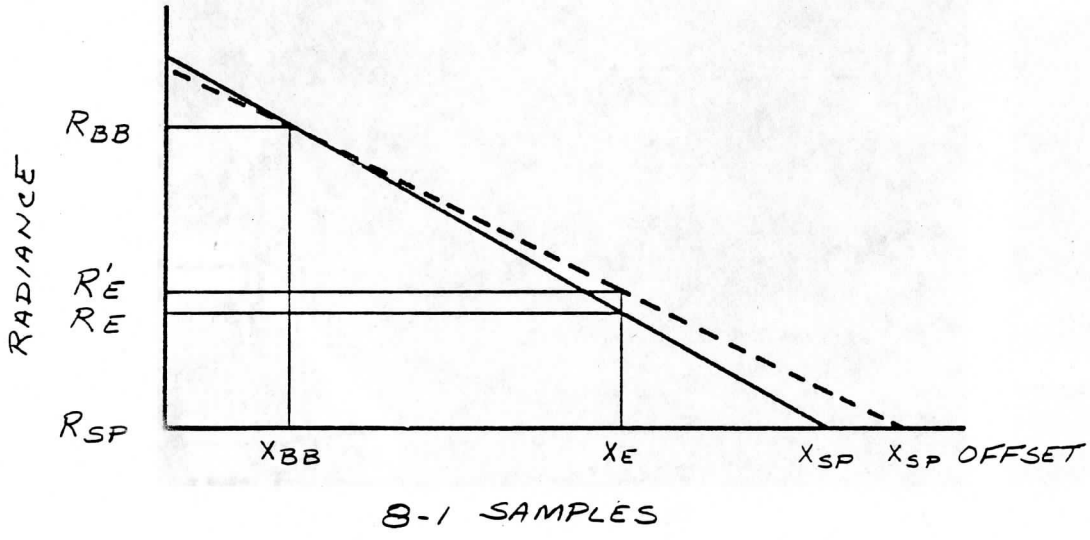

Fig. 4. Effect of spaceview counts on calibration.

RECENT ADVANCES IN THE RETRIEVAL OF METEOROLOGICAL PARAMETERS THROUGH THE "3I" SYSTEM

N. A. Scott, A. Chedin, F. M. Breon, C. Claud,
J. F. Flobert, N. Husson, C. Levy, and Y. Tahani

Laboratoire de Meteorologie Dynamique du CNRS
Ecole Polytechnique, 91128 Palaiseau Cedex, France

G. J. Prangsma

Koninklijk Nederlands Meteorologisch Instituut
P.O. Box 201, 3730 AE De Bilt, Netherlands

G. Rochard

EERM, Centre de Meteorologie Spatiale
P.O. Box 147, 22302 Lannion Cedex, France

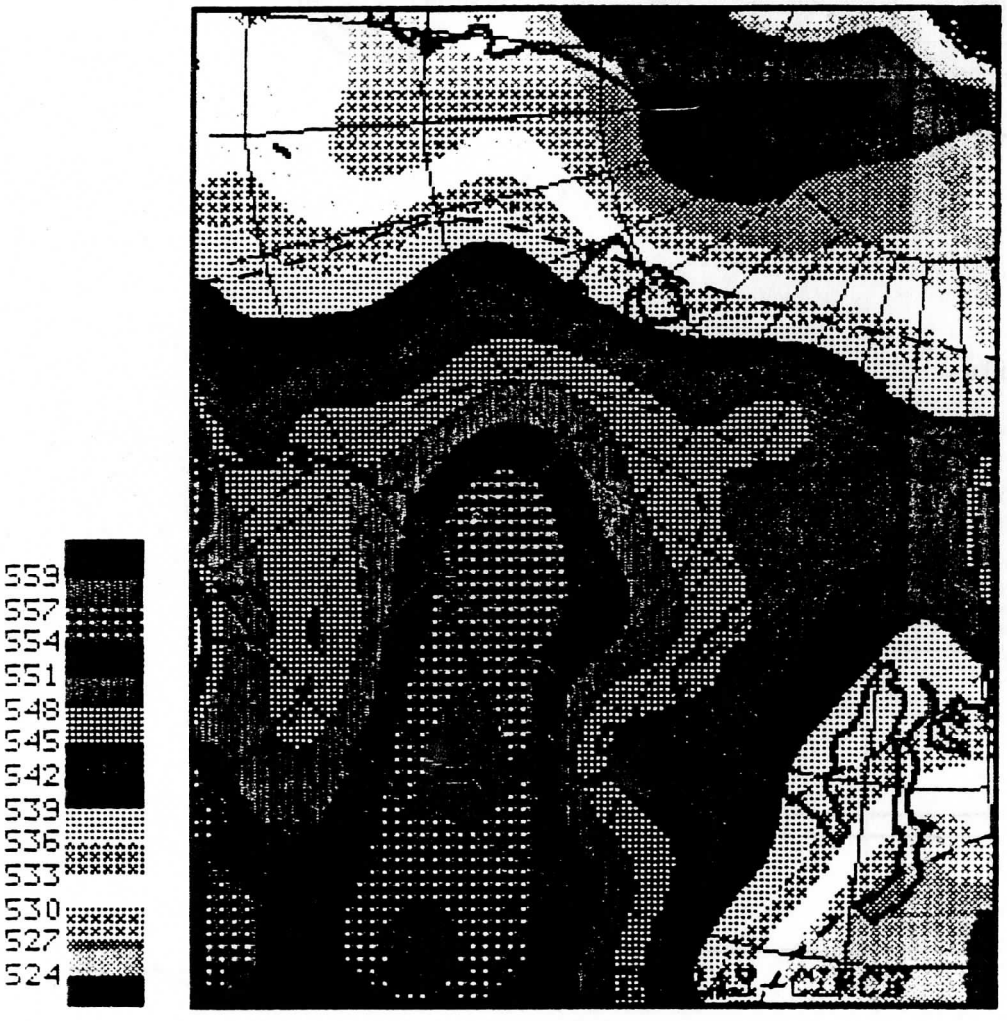

March 1988

Cover Figure: 3I retrieved geopotential thicknesses for the layer 1000-500 hPa, NOAA-9, 5 June 1986 at 9.57Z. ARCTEMIZ CAMPAIGN. Superimposed: ECMWF analysis for the same day at 12.00Z. Values range from 524 dam (blue) to 559 dam (red).

1. INTRODUCTION

Aiming at the three-dimensional analysis of the Earth's atmosphere structure from observations of the operational meteorological satellites of the TIROS-N/NOAA series, algorithm "3I", since the last meeting of the International TOVS working group, has been developed and refined following three main directions :

- improvement of the physics involved for a better handling of a priori information on the medium observed in the pattern recognition approach to initialization of the inversion process leading to a better accuracy of the retrieved products. In particular, the role of the surface, the detection and impact of snow and ice, the role of the clouds in the water vapor inversion, have been the subject of detailed studies ;

- through numerous applications to special situations, 3I has progressively been extended and now produces retrievals at global scale. These applications were conducted either within international programmes : MIZEX and ARCTEMIZ for polar latitudes, FASINEX and GALE for west Atlantic at low latitudes, or through cooperations with meteorological offices : France (CMS, Lannion), Netherlands (KNMI, De Bilt), China (CMS, Beijing), Europe (ECMWF, Reading), etc... ;

- improvement and simplification of the code itself for a more rational use in routine or in operation and for an easier transfer to other centers. In particular, the "educated" data set "TIGR" (TOVS Initial Guess Retrieval) has been made unique, whatever the number of satellites to be processed is. Its validation, from one satellite to a new one has been greatly simplified and can now be easily done by any center.

2. DETERMINATION OF MESOSCALE METEOROLOGICAL PARAMETERS FOR POLAR LATITUDES

2.1 Introduction

Observations from the satellites of the TIROS-N series on polar regions, where in-situ data are very scarce are helpful for the study of the interactions between ocean, ice and atmosphere through the retrieval of atmospheric and surface parameters. The "3I" - Improved Initialization Inversion - method (Chedin et al., 1985 ; Chedin and Scott, 1986), developed in the past few years at LMD, has shown ability to retrieve with a good accuracy temperature profiles through inversion of the Radiative Transfer Equation (Le Marshall, 1985). The MIZEX (Marginal Ice Zone EXperiment) and ARCTEMIZ (MIZ of the European ARCTic) campaigns, conducted respectively during the summer 1984 in the Fram Strait and since 1986 north and south of Fram Strait, have given the opportunity of applying this retrieval algorithm to high latitude observations. Associated to numerous in situ data, these campaigns have also allowed for comparisons with the retrieved products.

Satellite data have been provided by the Tromso Telemetry Station (Norway). TOVS data were on HRPT format tapes associated with corresponding images from AVHRR channel 2 ; the TOVS data have been navigated and calibrated at the Centre de Météorologie Spatiale in Lannion (France). MSU data are corrected for limb effects, liquid water attenuation and surface effects with the exception of MSU1 which is not corrected for surface effects.

In situ data include radiosoundings acquired during the campaigns and coming either from ships or from the synoptic network. For MIZEX, they have been obtained from the World Data Center for Glaciology, Boulder, USA. In addition, synoptic maps, ice charts and sea surface temperature analyses for the period of the campaign are also available (Lindsay, 1985). For the ARCTEMIZ campaign, surface analyses and thicknesses charts have been obtained from the SMHI and the ECMWF.

Five days for MIZEX (5th and 19th of June 1984, 1st and 2nd of July 1984, 5th of August 1984) and 17 consecutive days for ARCTEMIZ (from 5th to 21st of June 1986) have been processed through the inversion algorithm "3I" and results have been compared with conventional data.

2.2 Detection of sea ice. Incidence on the cloud detection procedure

Discriminating between the elements of a system comprising open water, sea ice and cloud from space observations is a well identified problem : for a clear situation and day time observations, distinction between sea ice and open water is a relatively easy task since their albedo (obtained from the visible channel) is very different. Obviously, this approach cannot be used for cloudy conditions or night time observations. Microwave observations due to their low sensitivity to clouds may help the solution to the problem in most cases. Moreover, microwave observations display an interesting property related to the variation of emissivity (ϵ) at 50 GHz with the type of the surface : sea ice, from young (ϵ = 0.95) to multiyear (ϵ = 0.7) and open water (ϵ = 0.6).

Two different methods for determining surface emissivities directly from satellite observations have been developed and are briefly described below.

Direct statistical method

This method relies upon the fact that channel MSU1 is sensitive to surface emissivity and to temperature in the lower atmosphere and down to the surface whereas channel MSU2 is mostly a function of the temperature of the low atmosphere and relatively not sensitive to the surface because of its low overall transmission (close to 0.1). It is thus possible to extract the surface emissivity from a combination of these 2 channels. Such a particularity has already been used by Grody (1983).

A relation between the surface emissivity ϵ, the brightness temperature of MSU channel 1, TBMSU1, and MSU channel 2, TBMSU2, has been established under a form similar to the one found by Grody :

$$\epsilon = a + b\ TBMSU1 + c\ TBMSU2$$

In Grody's approach, the coefficients have been obtained from a sample of data restricted in space (United States) and in time (April 1979).

In our study, the coefficients a, b, c have been regressed independently for the polar situations and for the mid-latitude situations archived in TIGR. There are 525 polar type situations and 545 mid-latitude situations in TIGR (cf. Table 1).

Latitude class	Number of situations	a	b	c	Standard deviation on ϵ
Polar	525	0.797	0.0082	-0.0083	0.040
Midlatitude	545	1.080	0.0074	-0.0083	0.032

Table 1 Values of the different constants a, b, c, for the two latitude zones concerned.

Direct physical method

Microwave surface emissivity may also be extracted by considering the Radiative Transfer Equation itself. The measured radiance can be written as follows :

$$I = \epsilon\ [\tau B_s - \tau \int^{\downarrow} B d\tau] + [\int^{\uparrow} B d\tau + \tau \int^{\downarrow} B d\tau]$$

For a given class (polar or mid latitude), it has been found that the quantities τ, $\int\uparrow B d\tau$ and $\int\downarrow B d\tau$ may be considered as constant to within a good approximation, at least with the purpose of determining ϵ to the

required accuracy. Standard deviations of each of these quantities and their means are given in Table 2.

As a consequence and using the Rayleigh Jeans approximation (radiance is a linear function of temperature), the preceding equation may be written as :

$$TBMSU1 = \epsilon \, [\tau \, T_s - \alpha] + \beta$$

This relation indicates that emissivity may be obtained when MSU1 brightness temperature and surface temperature are known.

Transmittance values are calculated using the fast line-by-line model"4A" (N.A. Scott, A. Chedin, 1981) and the surface temperature can be estimated from HIRS-2 channel 8 brightness temperature corrected for water vapour and surface emissivity effects (Wahiche, 1984).

	Midlatitude		Polar latitude	
	Mean value	Standard deviation	Mean value	Standard deviation
τ	0.679	0.012	0.664	0.012
$\int\uparrow B d\tau$	$1.89\ 10^{-3}$	$0.02\ 10^{-3}$	$1.90\ 10^{-3}$	$0.02\ 10^{-3}$
$\int\downarrow B d\tau$	$1.97\ 10^{-3}$	$0.03\ 10^{-3}$	$1.97\ 10^{-3}$	$0.03\ 10^{-3}$

Table 2 Mean values and standard deviations for the quantities τ, $\int\uparrow B d\tau$ and $\int\downarrow B d\tau$ for the 545 midlatitude situations and the 525 polar situations archived in TIGR. $\int\uparrow B d\tau$ and $\int\downarrow B d\tau$ are expressed in $mw.cm^{-2}.sr^{-1}$.

Using results of Table 2, we may write TBMSU1 as follows :

$TBMSU1 = \epsilon \, (0.664 \, T_s - 56.24) + 137.9$ Polar zone

$TBMSU1 = \epsilon \, (0.679 \, T_s - 57.42) + 138.8$ Midlatitude zone

In the recent past, another attempt has been made to detect and delimit sea ice using MSU data (Yamamouchi, Seo, 1984). Instead of using a threshold value for the emissivity, their method is based on a threshold value on the MSU1 brightness temperature. We have applied their method to the satellite observations considered in this study. The results are not always satisfactory. This is apparently due to T_s which is considered as a constant whereas it shows an important variability.

Results and discussion

For each of the selected orbits, surface microwave emissivities have been calculated by the two direct methods described above. Results are very similar apart from a systematic bias of about 0.1 (larger values for the physical method). However, such a bias does not prevent either method from identifying sea ice covered areas. The mean of the values given by these two methods is very close to the value obtained through the full physical inversion method (Wahiche, 1984). Results are illustrated on Figure 1 for a NOAA-9 pass on June 11, 1986. Sea ice is displayed in red and pink. Results too close to coast lines should be discarded due to the low resolution of the MSU sounder.

Impact of this information on cloud detection

Two tests, which are also part of the operational NOAA/NESDIS retrieval algorithm (McMillin et al., 1982) may benefit from an a priori knowledge of the presence of sea ice : the so-called "frozen sea" test and the albedo test. Details on the modifications introduced as well as more details on the methods reported here are given in Claud et al. (1988). Results are illustrated on Figure 2 for the same pass as above.

2.3 Geopotential thicknesses

As an example of the results obtained for the domain observed, the cover plate shows for a particular pass (5 June 1986, 9:57Z) retrieved geopotential thicknesses for the layer 1000-500 mb (in dam).

Figure 1

Microwave surface emissivity. NOAA-9. 11 June 1986. ARCTEMIZ campaign. Sea ice is in red and pink. Results close to coast lines should be discarded as contaminated by the continent.

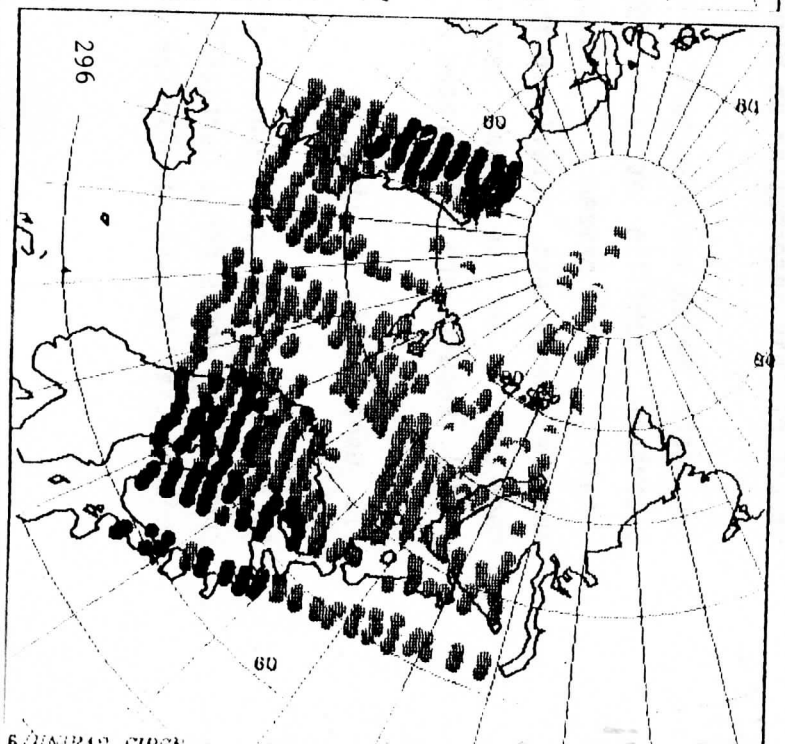

Figure 2

Results of the revised cloud detection algorithm. In blue (over sea) and green (over land) are the clear areas. The cloud system between Svalbard and Norway was not detected previously.

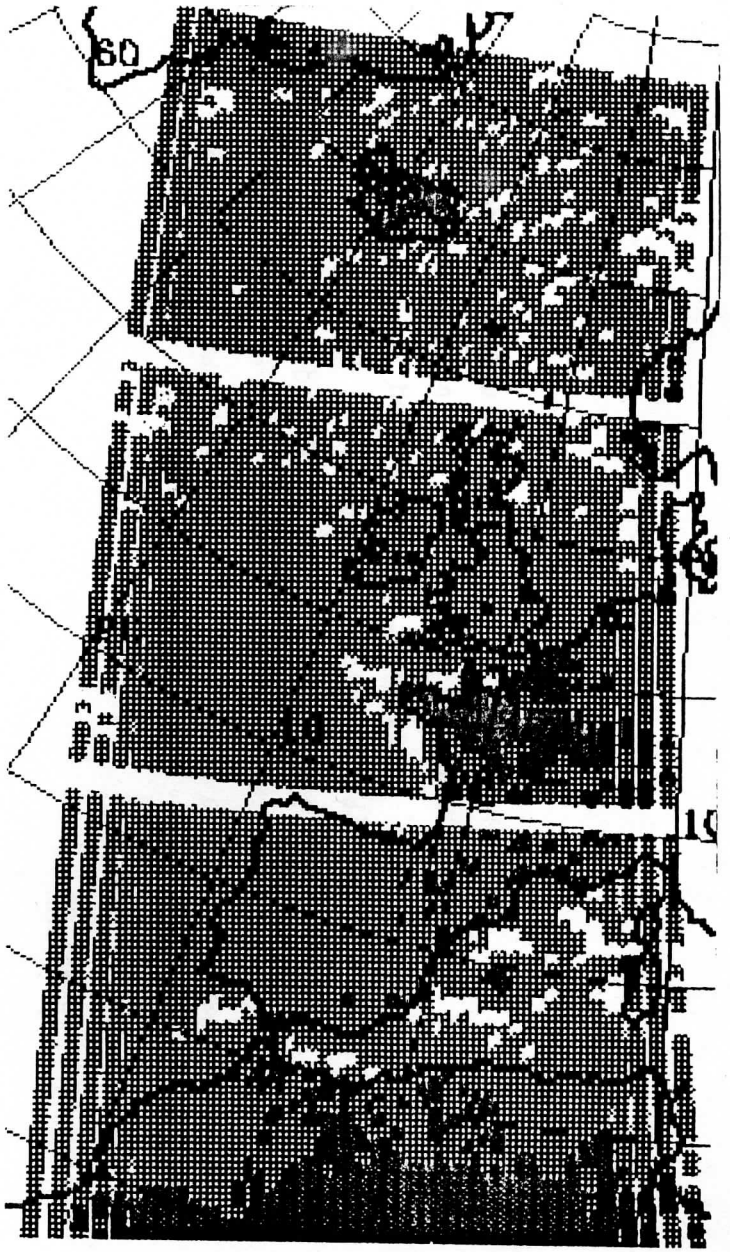

Figure 3 Snow detection from HIRS-2. Snow : yellow. Clear areas : blue (sea) or green (land). NOAA-9. Orbit 6209.

Comparisons with analyses coming from either the ECMWF or the SMHI for the same day at 12:00Z, show good agreement. "3I" retrieved maps display more details : see for example the warm air coming from the Scandinavian continent and going in two directions (towards Greenland and towards Franz Joseph Land). Analyses indicate only one axe (towards Franz Joseph Land).

This work is developing towards analysis of situations characterized by "polar lows", in cooperation with DNMI (Norvegian Meteorological Institute).

3. DETECTION OF SNOW FROM HIRS-2

Because of its high albedo, snow cover is often seen as cloud by cloud detection algorithms during day time. Moreover, snow and low cloud top temperatures may be similar. It has already been reported in the literature (see for example : S.Q. Kiddder et al., Mon. Wea. Rev., 112, 2345) that comparisons between channels at 11μm and 3.7 μm could help discriminating between snow and clouds. Computation of the ratio :

$$\{ T_B \text{ (HIRS,19)} - T_B \text{ (HIRS,8)} \} / \cos \theta_s ,$$

where T_B(HIRS,n) is the brightness temperature of channel n of HIRS-2 and θ_s the solar zenith angle, has resulted in high values for the clouds and in much lower values for snow covered areas. This is due to the low albedo of snow at 3.7 μm as compared to clouds and to the fact that the ratio given above isolates (and normalizes) the solar contribution to the brightness temperature of channel 19.

The following test has consequently been implemented in the cloud detection algorithm : if, simultaneously, the albedo is greater than 20%, and an estimate of the surface temperature (regression based upon channel 8) smaller than 273 K and the ratio

$$\{ T_B \text{ (19)} - T_B \text{ (8)} \} / \cos \theta_s$$

smaller than 14 K, the field of view considered is supposed to be clear, with snow covering it. Several NOAA-9 passes have been processed, for which manual nephanalyses had clearly identified snow covered areas. Figure 3 illustrates one example. Snow in in yellow and the areas concerned are in perfect agreement with manual analysis.

4. ANALYSIS OF SATELLITE OBSERVATIONS OVER WEST ATLANTIC : FASINEX AND GALE EXPERIMENTS

4.1 Introduction

During February 1986, the FASINEX experiment was in its intensive phase. It was designed to study the response of the upper ocean to atmospheric forcing, the response of the atmosphere in the vicinity to an oceanic front, and the associated two way interaction between ocean and atmosphere. For this experiment, there was one research ship on each side of a very sharp oceanic front, launching radiosondes every 6 hours and studying the ocean in the vicinity of the front (SST, fluxes, velocity profiles). Data from satellites, aircrafts and buoys were also collected (Stage and Weller, Bull. Amer. Meteor. Soc., 67, 1986).

During the same period of February 1986, the GALE experiment (Genesis of Atlantic Lows Experiment) went on over the same area, on a somewhat larger scale. This experiment intended to study the atmospheric cyclogenesis over the American East coast. February 24th was seen as the biggest cyclogenesis day.

The California Space Institute (CSI) is deeply involved in the FASINEX experiment and has archived the corresponding data. The interest of studying, for both FASINEX and GALE, the atmospheric signal shown by satellite data using 3I retrieval method, has led CSI and our group to start cooperating (Drs. C. Gautier and J. Bates).

4.2 Implementation of the 3I system on CSI VAX computer

The 3I system has been implemented on a micro-VAX I at CSI, starting from the version installed at CIRCE (Centre Inter-Régional de Calcul Electronique), France (IBM-3090 and Siemens VP200 computers). Table 3 shows the computer resources needed for this method (retrieval procedure from calibrated, navigated satellite data, to atmospheric parameters). These results and especially the 1h15mn elapsed time for a one orbit retrieval (about 130 HIRS scan lines), shows that the 3I system can be used easily on an operational daily basis with a micro-VAX computer connected to an HRPT receiving station.

Charged CPU	1 h 00 mn
Central Memory	3 MBytes
Elapsed Time	1 h 15 mn
TIGR Size	35 MBytes
Topography File (global)	16 MBytes

Table 3 Computer needs for the "3I" retrieval method running on a Micro-VAX

4.3 The results

At CSI, TOVS data have been analysed using 3I for 16 NOAA-9 passes from February to mid-March. The physical parameters retrieved by 3I over the area covered by the satellite passes are : air mass types (polar, temperate or tropical), temperature profiles, geopotential thicknesses, thermal winds, cloud heights, cloud amounts (equivalent of black clouds), surface emissivity, total water-vapor content and three layers relative humidities. About 150 radiosoundings have been collocated with retrievals. AT LMD, 5 passes (out of the 16) have been processed and 3 of them, around the period of the most active cyclogenesis (February 24th and 25th) in great detail. Figures 4 and 5 present, for seven

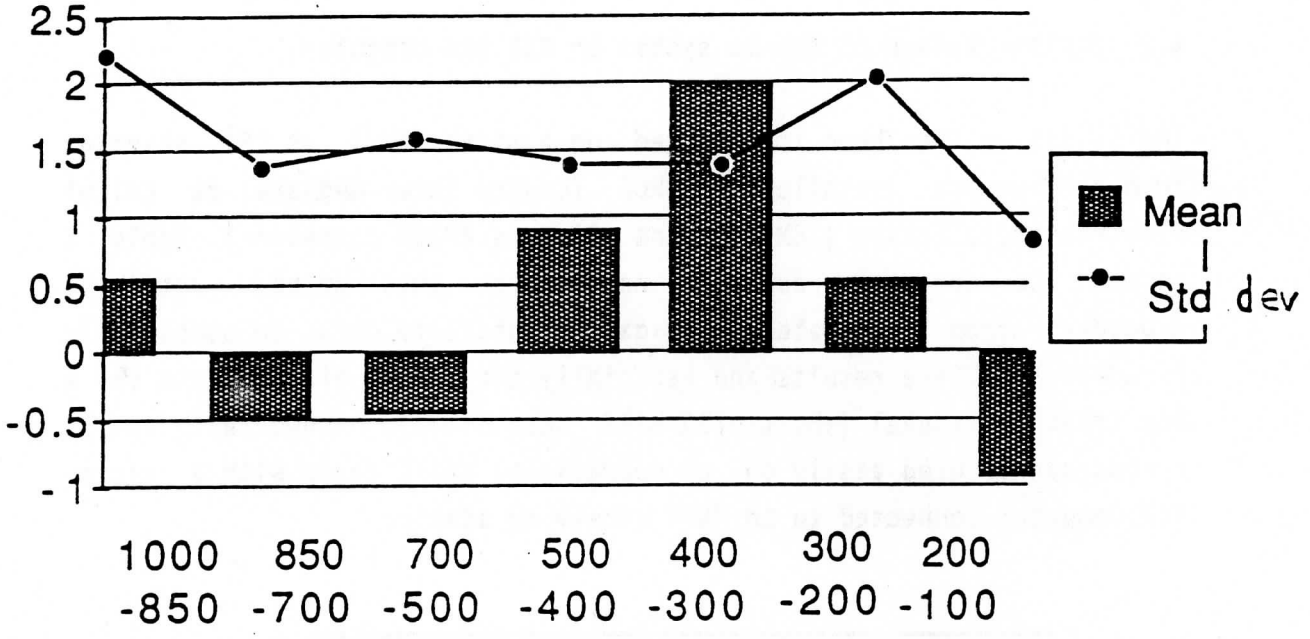

Figure 4 Mean and standard deviation of the differences between 3I retrieved layer temperatures and collocated radiosoundings (about 25 items). NOAA-9 passes 6191. 24 February 1986 at 8.15Z. Radiosoundings at 12.00Z.

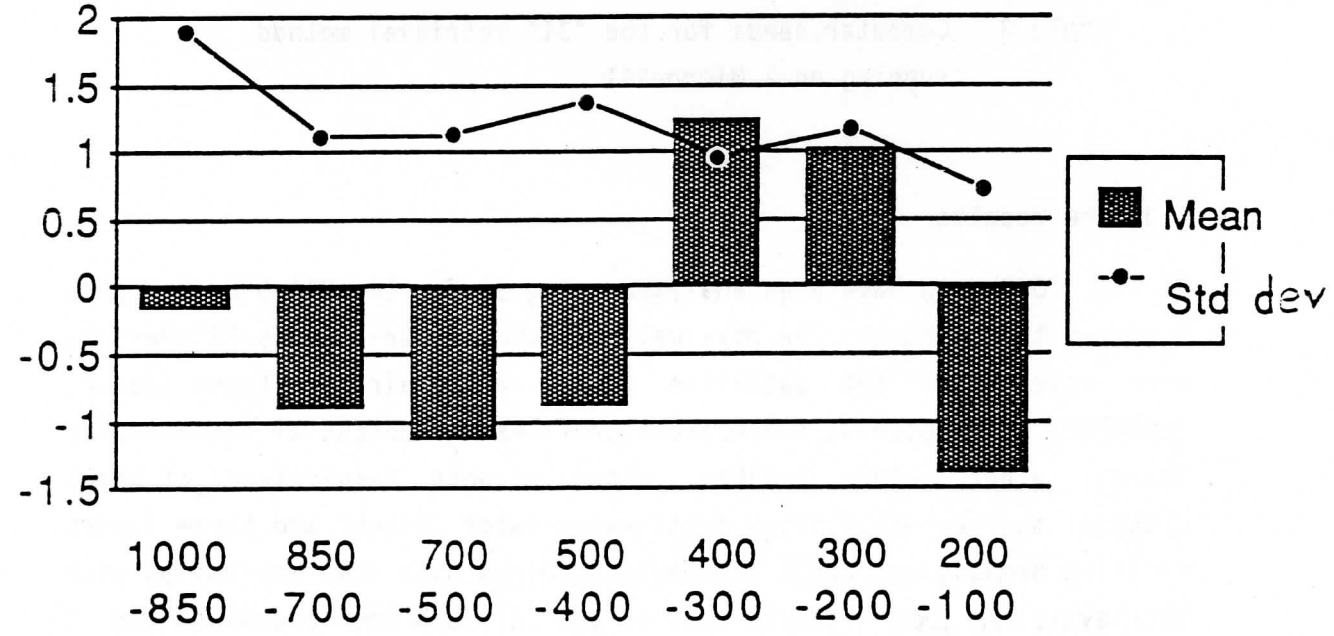

Figure 5 Same as for Figure 4. NOAA-9 pass 6198. 24 February 1986 at 19.32Z. Radiosoundings at 18.00Z.

layers between 1000 hPa and 100 hPa, the results of statistics for the deviations between 3I and radiosoundings for two consecutive passes of NOAA-9 on February 24th, 1986.

Although satisfactory in the two cases, results are significantly better for orbit nb. 6198. This is probably due to the good time coincidence of the collocations since the radiosoundings were launched approximately at 18.00Z. Figures 6 and 7 show the results of similar comparisons for water vapor retrievals. Four layers are considered, the last one, 1000-500 HPa, including approximately the total precipitable water vapor. Once more, the results, relatively satisfactory in both cases, are better for orbit nb. 6198 for the same reason as above.

This work has demonstrated that the 3I system is easily "exportable" and that its use in operational mode is possible, even with limited computer facilities.

5. WATER VAPOR RETRIEVALS FROM NOAA-7 AND NOAA-9 OBSERVATIONS OVER EUROPE

5.1 Presentations of the situations adopted

The NOAA-7 "situations"

Six "situations" were selected, corresponding either to a single satellite pass (giving a more restricted geographic zone of coverage), or to two successive satellite passes. They are generally related to complex atmospheric situations, often characterized by a very rapid evolution and have resulted in substantial errors in forecasting either by the European Center in Reading (ECMWF) or by the French Met. Office, or both. The dates range from September to December 1983 (see Chedin et al, 1987). For a few of them, the analysis is also in error. In such cases, the differences between retrievals and operational analyses must be interpreted having in mind these errors.

A total of nine passes has been studied.

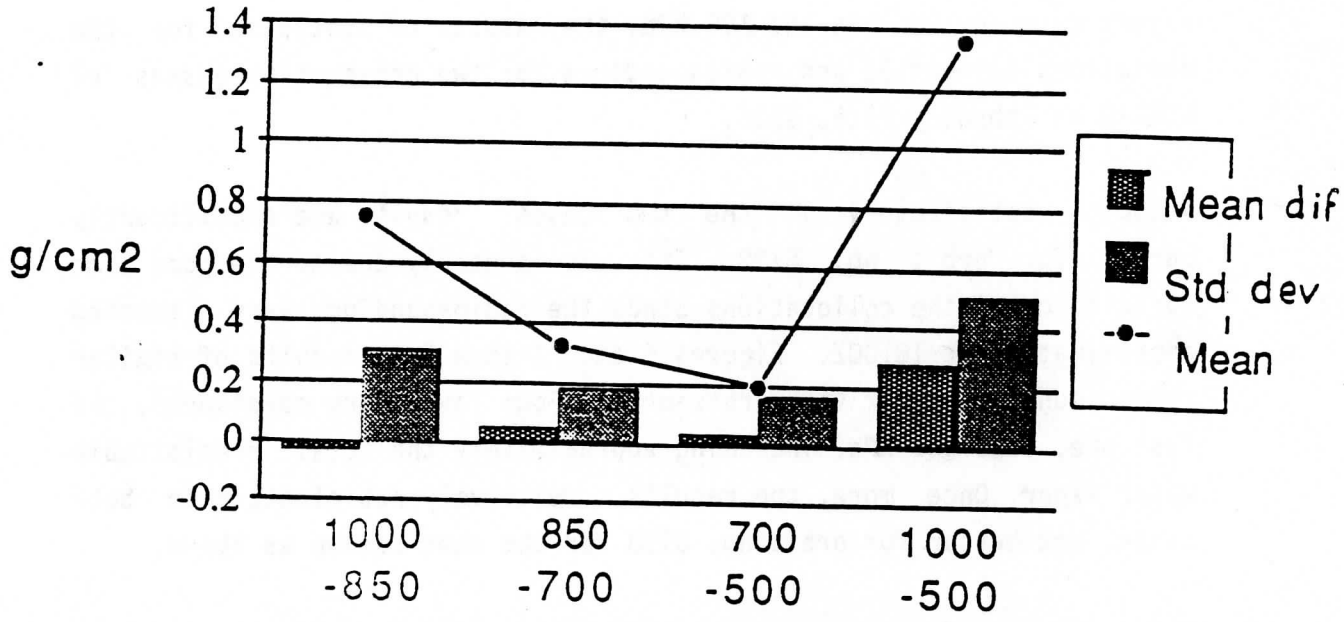

Figure 6 Mean and standard deviations of the differences between 3I retrieved layer precipitable water vapor and collocated radiosoundings (about 15 items). NOAA-9 pass nb. 6191. 24 February 1986 at 8.15Z. Radiosoundings at 12.00Z. Solid line : mean value of the sample.

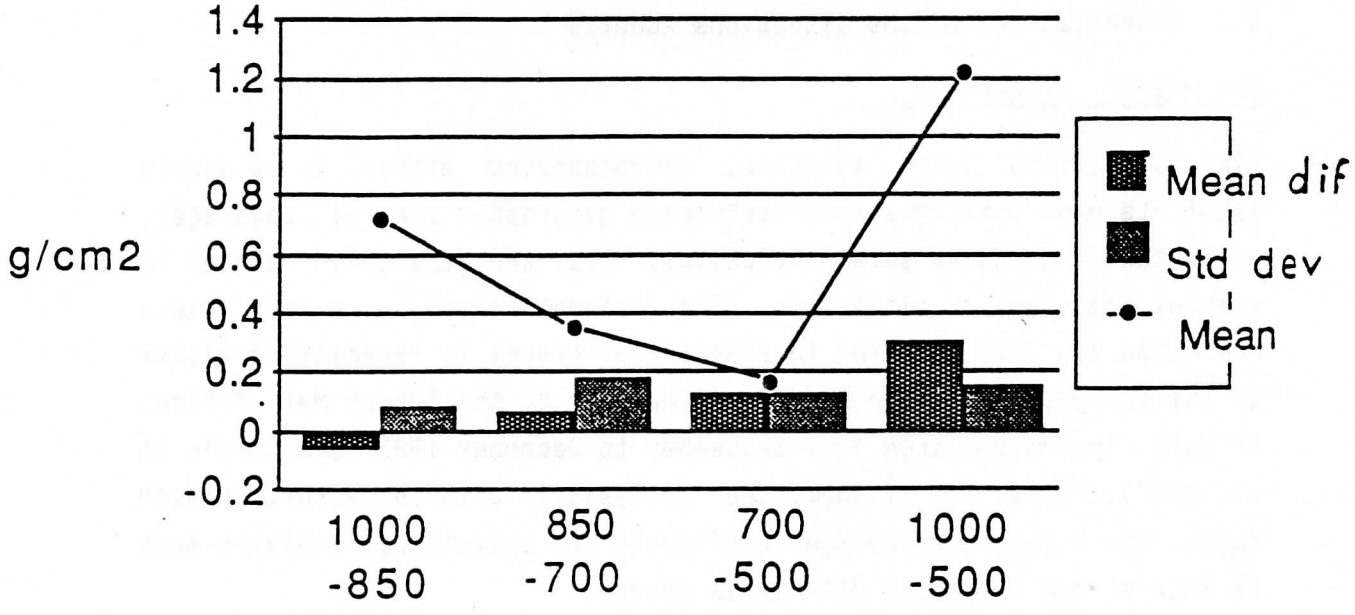

Figure 7 Same as Figure 6. NOAA-9 pass nb. 6198, 24 February 1986 at 19.32Z. Radiosoundings at 18.00Z.

The NOAA-9 situations

Observations from NOAA-9 were chosen, for two satellite passes, over the "HAPEX-MOBILHY" ("Hydrology - Atmospheric Pilot Experiment" - "Modélisation du Bilan Hydrique") experiment site (André et al., Bull. Amer. Meteor. Soc., 1987) corresponding to June 9, 1987, orbit nb. 7676, and to June 19, 1987, orbit nb. 7817 (C. Ottlé, private communication).

5.2 Results of comparisons between conventional analysis and 3I algorithm results for the NOAA-7 and NOAA-9 cases

The quality of retrieved products, thermal structure as well as water vapor related quantities, has been estimated, for the NOAA-7 and NOAA-9 situations mentioned above, through comparisons with ECMWF conventional analyses. Visual comparisons have also been made on the basis of geopotential thickness fields.

A quantitative assessment of the accuracy of the retrieved products has been approached by a statistical analysis of the deviations between the 3I retrievals and the ECMWF thickness fields. The results of this statistical evaluation are reported on Figures 8 and 9 for two representative passes of NOAA-7 and Figures 10 and 11 for two passes of NOAA-9. The parameter considered in these comparisons is the virtual temperature obtained from retrieved layer thicknesses (standard levels). The agreement is basically satisfactory.

Statistics on total water vapor contents ($g.cm^{-2}$) are given on Figure 12 for the two NOAA-9 passes and for 7 NOAA-7 passes. For most of them, rms errors are in the range 25% to 35%. The largest values are for those situations rather poorly analysed (NOAA-7). In one case (not presented in Figure 12), NOAA-7 orbit 11664, the difference between 3I and ECMWF becomes exceptional reaching an rms value of 46 %. Going deeper into the analysis of this result has led us to point out an area for which discrepancies between 3I retrieved and ECMWF analysed total water vapor contents are very large.

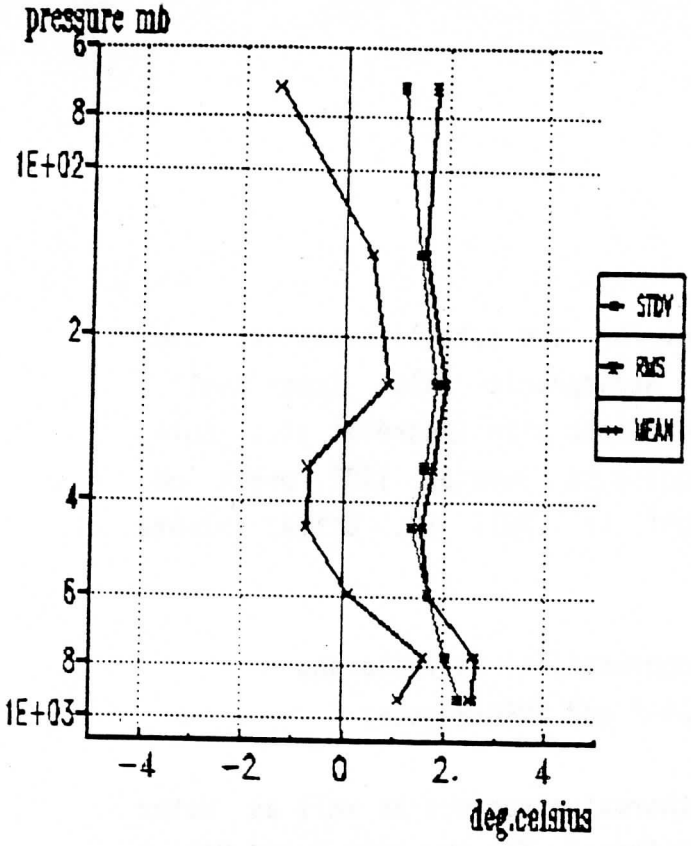

Figure 8 3I retrieval minus ECMWF analysed virtual temperature statistics for NOAA-7, orbit nb. 11664 (27 sept. 1983), 14.35Z).

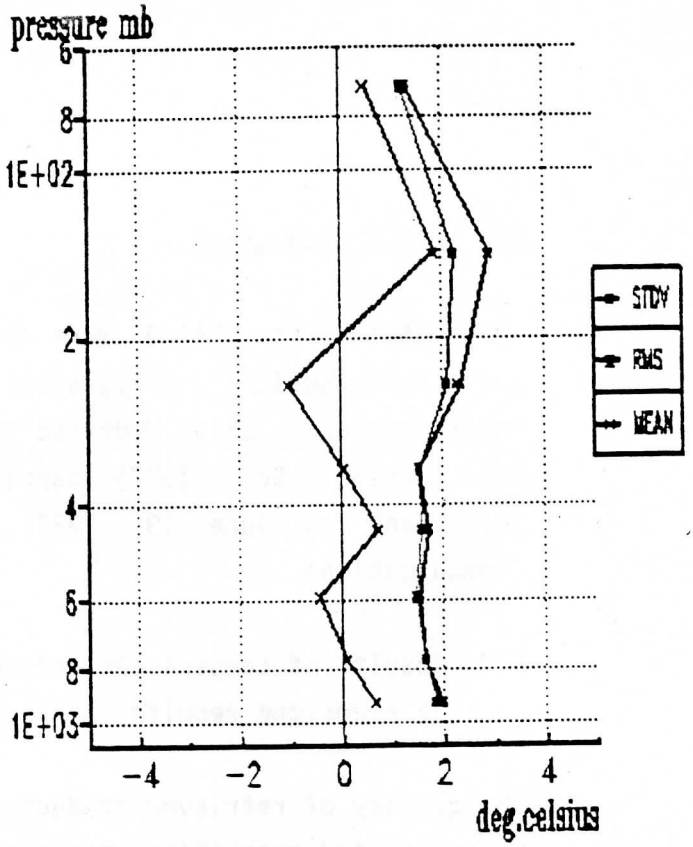

Figure 9 See Figure 8. NOAA-7, orbit nb. 12963 (28 Déc. 1983, 14.17Z).

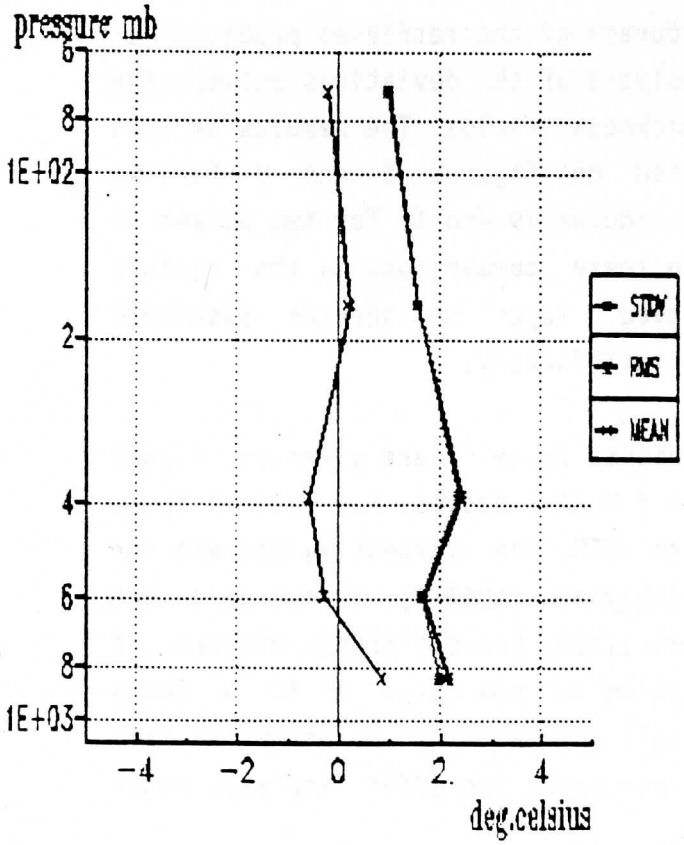

Figure 10 See Figure 8. NOAA-9, orbit nb. 7676 (9 June 1987, 14.02Z).

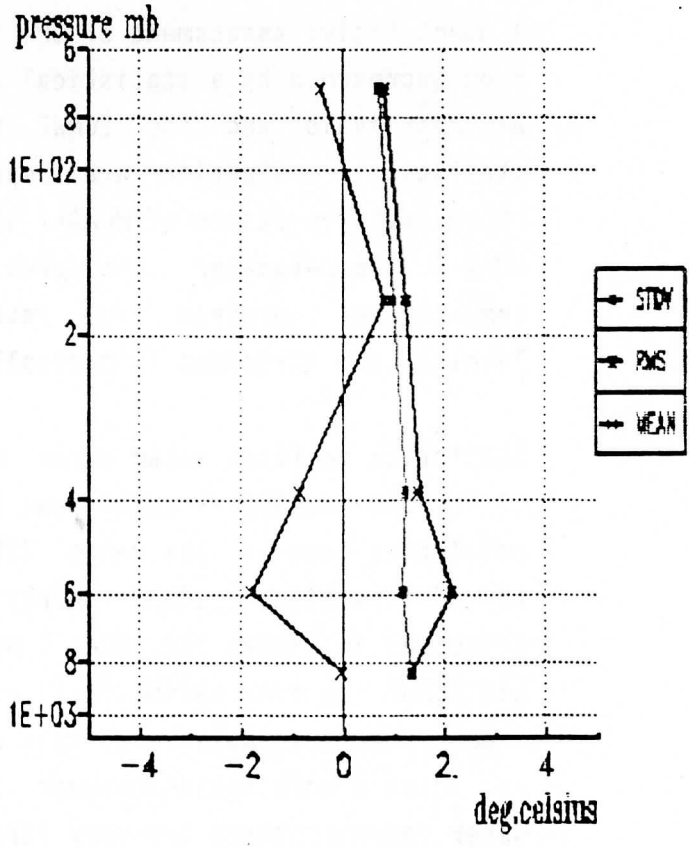

Figure 11 See Figure 8. NOAA-9, orbit nb. 7817 (19 June 1987, 14.39Z).

This is shown on Figure 13 : over Spain, values of the order of 4 $g.cm^{-2}$ are given by ECMWF whereas 3I retrieves values of the order of 1.5 $g.cm^{-2}$. As a preliminary attempt to elucidate this question, comparisons have been made between radiosonde data, 3I retrievals and ECMWF values. They are shown on Figure 14, which concludes in favor of 3I. Such differences are quite exceptional and significant improvements have been made, since 1983, in the analysis of water vapor related quantities at ECMWF (J. Pailleux, private communication).

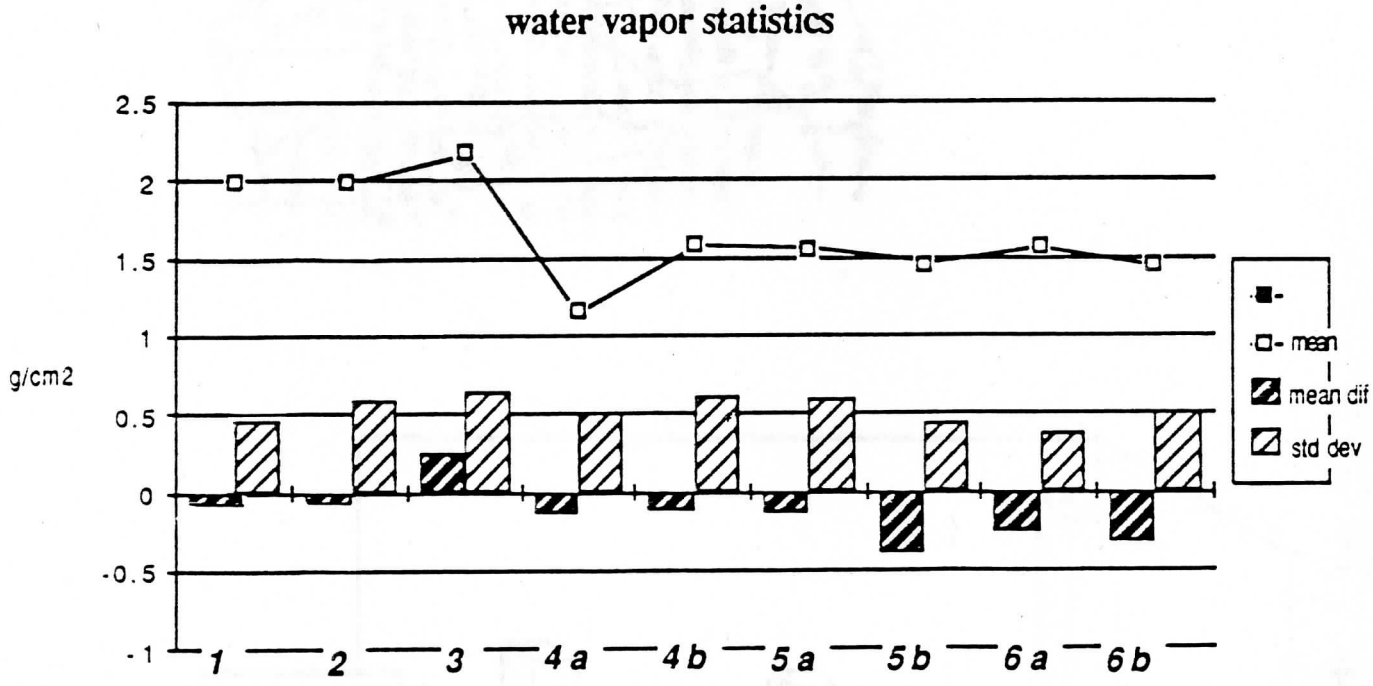

Figure 12 3I retrieved minus ECMWF analysed total water vapor contents for 2 NOAA-9 passes (1 = 7676 ; 2 = 7817), 7 NOAA-7 passes (3 = 12512 ; 4a = 12681 ; 4b = 12682 ; 5a = 12949 ; 5b = 12950 ; 6a = 12963 ; 6b = 12964).

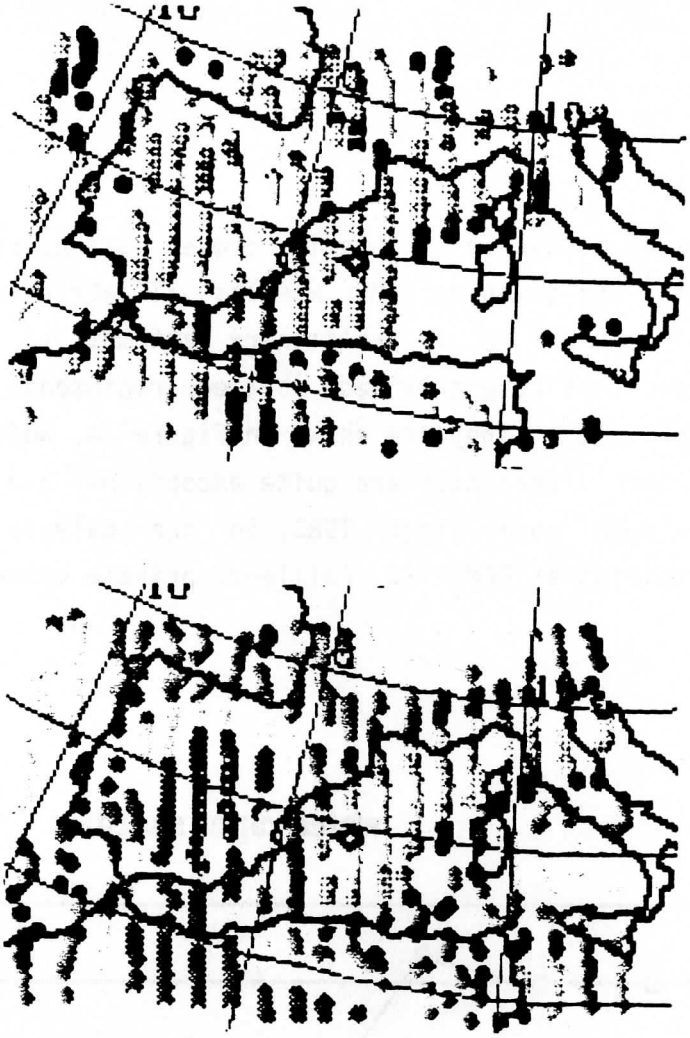

Figure 13

Illustration of an exceptional difference between 3I retrieved (up) and ECMWF analyses (down) of total water vapor content. NOAA-7, 27 sept. 1983, 14.35Z. Radio-soundings for Madrid, La Coruna and Gibraltar favour 3I results.

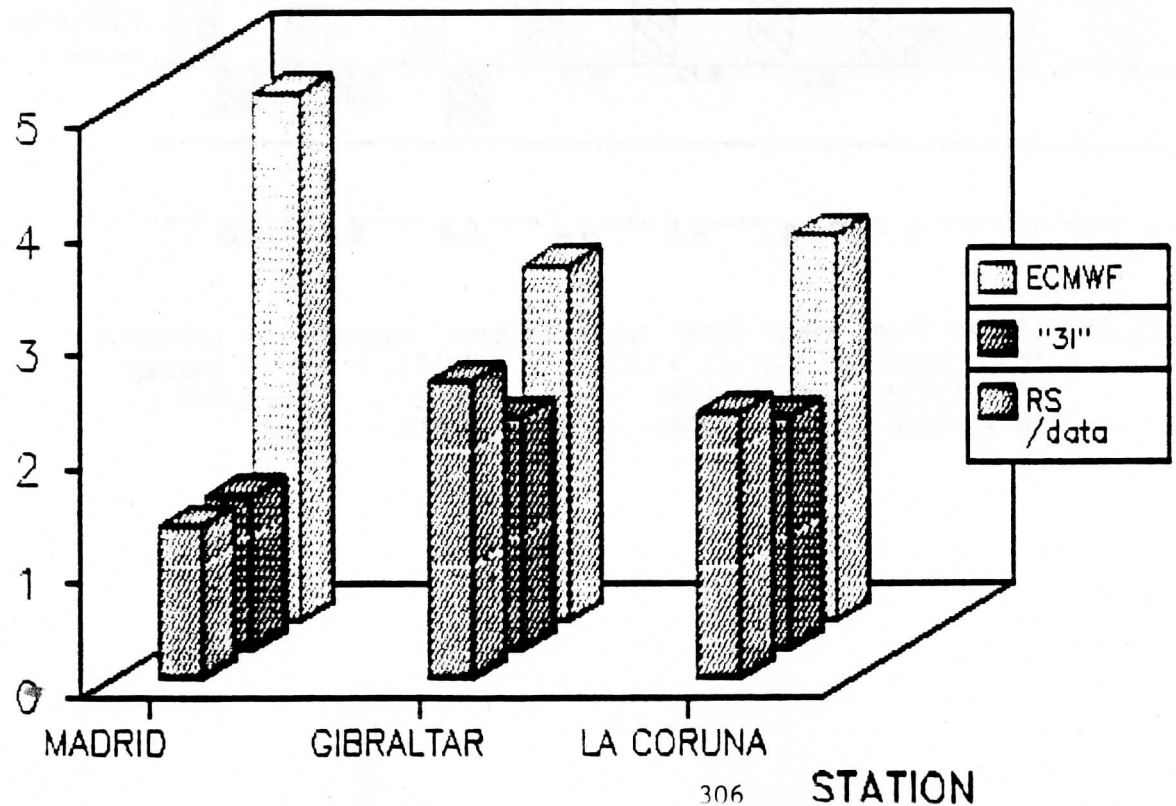

Figure 14

See Fig. 13. Comparison between radiosonde data, 3I retrievals and ECMWF analysis for total water vapor content (g/cm^2).

6. THE NOAA-10 TOVS RETRIEVALS FOR JUNE 7, 1987. The Whit-Sunday severe weather events in SW France

6.1 Introduction

During the afternoon hours of Whit-Sunday, June 7, 1987, the passage of a very active squall line over Southwestern France with extremely gusty winds caused the loss of several lives and considerable material damage.

The suddenness of the events, which developed out of the meteorological situation over the poorly observed Bay of Biscay, put forward the question, to what extent satellite observations (both imagery and soundings) could have added to help forecast the experienced weather events.

In order to assess this question - admittedly in hindsight and free from operational time constraints - some of the available satellite and synoptic data are discussed in relation to each other.

6.2 Synoptic situation

In the W-SW flow observed at 0.00 UT on the 7th June 1987, over the Gulf of Biscay and the western part of Europe (Figs. 15a,b), the polar air mass is bounded on the south by a W-E frontal line along the northern coast of Spain. The upper-air trough associated with this frontal system extends from Ireland in south-westerly direction to the Azores area.

The synoptic situation in this area has dramatically changed by 12.00 UT on the same day, when a well-developed frontal wave is present over Brittany (Figs. 16a,b), with the upper-air trough well-advanced, just west off Cape Finisterre. Over South-Western France a southerly to south-easterly wind in combination with the Föhn-effect over the Pyrenees causes marked warming-up of the surface layers which heating effect - in the early afternoon - is reinforced by a spell of clearing skies.

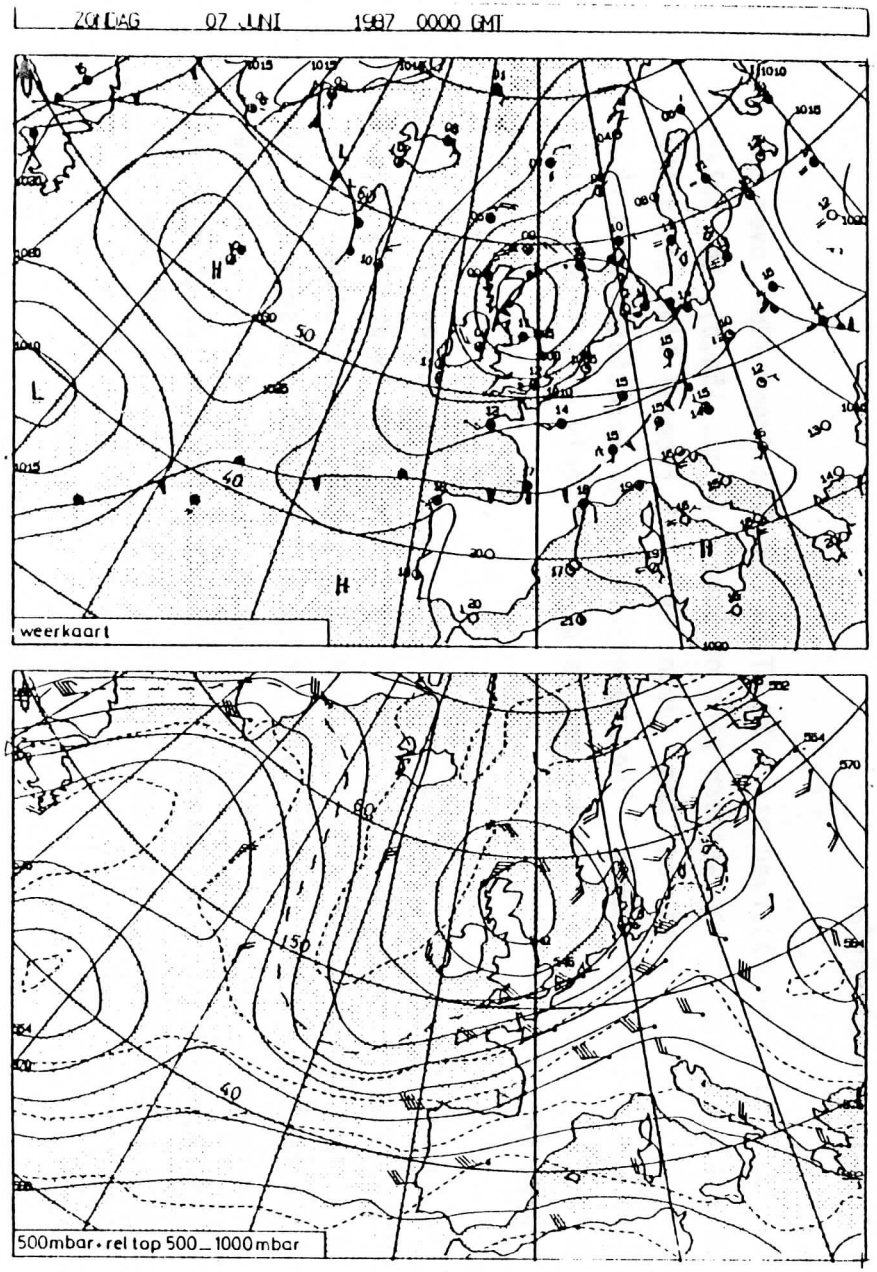

Figure 15 Synoptic analyses for June 7, 1987 at 0.00 UT. (a) : surface map ; (b) : 500 HPa height (full lines) and 1000-500 HPa thicknesses (dashed lines)

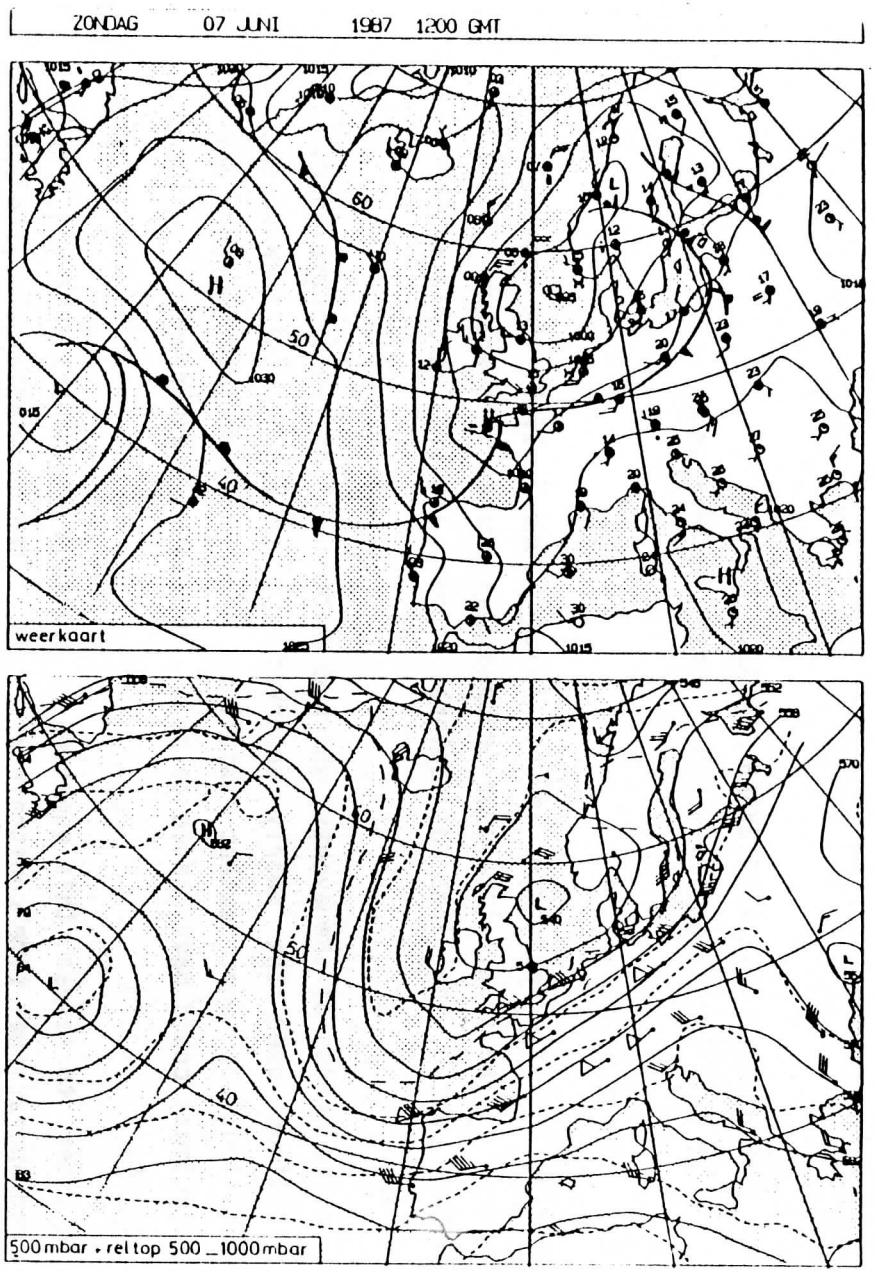

Figure 16 As Fig. 15, for June 7, 1987, at 12.00 UT

Thus the maximum temperatures observed in the area were quite high (26°C at Bordeaux) preconditioning the air column for strong convection.

The upper-air flow with velocities of 50 knots (and even 80 knots at Cape Finisterre) at the 500 hPa level rapidly advects colder air. Moreover, the differences in wind speed, indicated above, suggest already the presence of a pronounced convergence zone at the 500 hPa level also over the Gulf of Biscay. In the northerly flow west of the front and of the convergence zone, cold air (temperature of -25°C are reported) is advected into the region.

All these synoptic data point to a zone of baroclinic instability being present just upstream of the area of interest ; a baroclinic instability capable of causing rapid and very active developments in the 6-hour period to come.

6.3 Satellite data

The available satellite data consist of images of two orbits : from NOAA-9 at 04.40 UT (orbit 12791, see Fig. 17) and from NOAA-10 at 08.55 UT (orbit 3735, Fig. 18), along with TOVS data for the latter orbit, processed using the 3I-system (shown in Figs. 19a-d).

From Fig. 17, it is immediately evident that in the developing wave west of Brittany, the vertical movements are very strong and locally driven by strong convection, resulting in marked variations in the cloud top temperatures.

Further west convective clouds in the cold air behind the front are evidently being organized in a vertical structure (Fig. 17). As can be taken from Fig. 18, where the same vertical cloud structure is barely separated from the frontal wave clouds, this vortex centre is rapidly progressing towards the south-southeast and coming closer to the southern edges of the frontal wave.

From the thermal wind fields (Figs. 19c,d), we conclude that this vortex centre has a complex vertical structure, in that the 1000-850 hPa layer (Fig. 19d) clearly shows two separate cells, whereas the higher layers (850-700 and 700-500 hPa, not shown) display the presence of one cell (near 50N, 13W) only, resulting in a single structure for the whole of the 1000-500 HPa layer (Fig. 19c).

In Fig. 19a, the strong thermal gradient from Brittany to Cape Finisterre and then westward delineates the cold front in the 1000-500 hPa layer, with a marked cold tongue oriented mainly N-S along 13W, with a warmer wedge over the British Iles, indicative of the developing wave.

In the spirit of earlier findings (see Sutcliffe, Q.J.R.M.S., 73, 370-383, 1947 ; Prangsma et al., 1987, and Prangsma, 1988), we have also derived the thermal vorticities for the layers of interest (Figs. 20a-c). From these plots it is readily seen that strong, alternating vorticity gradients exist over a few hundreds of kilometers only, just upstream of our area of interest.

Preliminary estimates - to be followed on by more rigorous analyses - following Sutcliffe's development model suggest strong, alternating cyclonic-anticyclonic-cyclonic developments to have landfall between 4-8 hours after the satellite overpass in the Aquitania coastal region.

6.4 Discussion

As already expressed in the introduction, the following remarks and analyses have been arrived at in hindsight and away from operational time constraints.

The scenario for the weather events in South-West France during the afternoon of June 7, 1987, can - on the basis of the data and analyses presented above - be considered of a rare coincidence of several mutually reinforcing factors :

Figure 17 NOAA-9 AVHRR channel 4, orbit 12791 at 04.40, June 7, 1987.

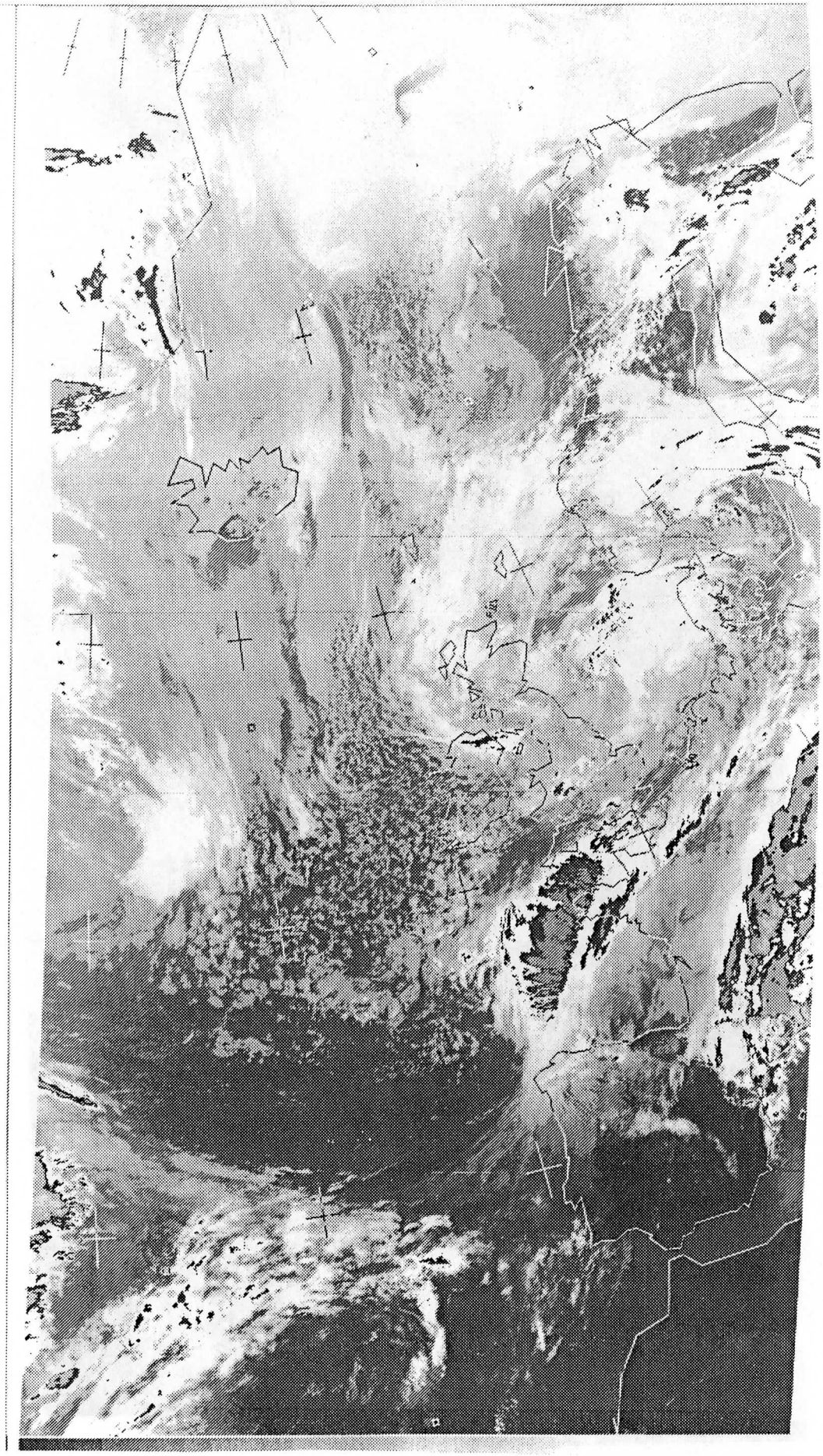

Figure 18 NOAA-10 AVHRR channel 4 for orbit 3735, June 7, 1987 at 8.55 UT. Enhanced for cloud top temperature.

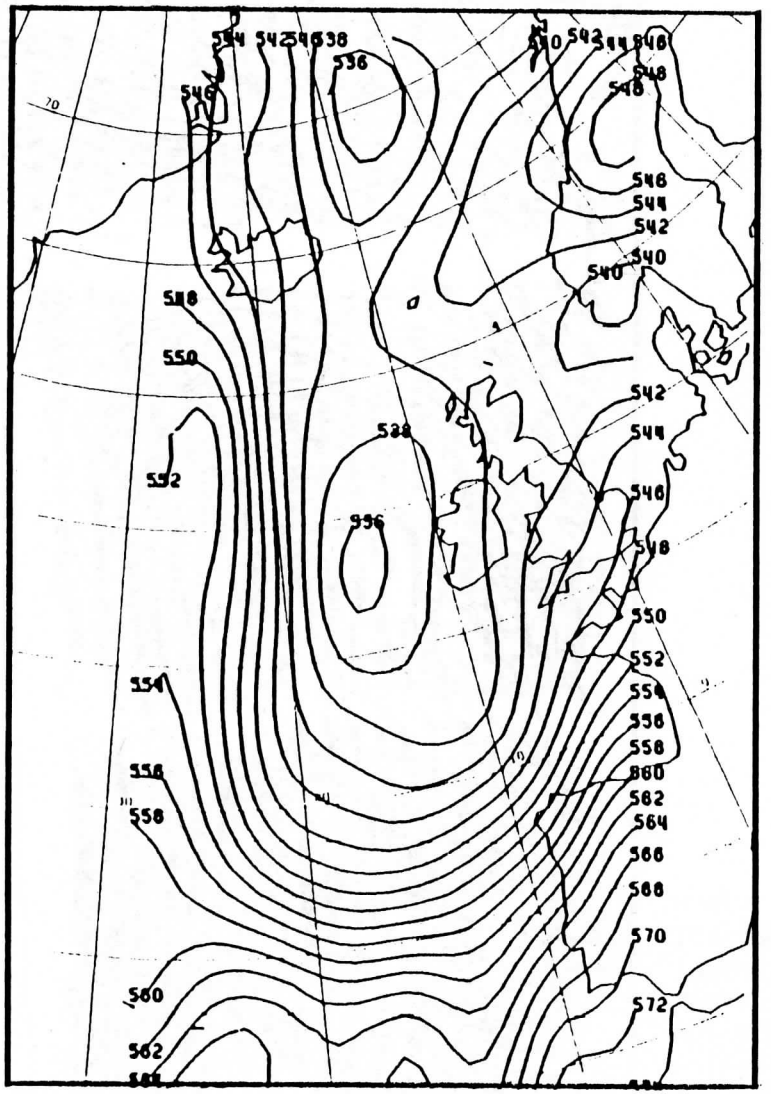

Figure 19a TOVS retrievals for NOAA-10 orbit 3735. 1000-500 HPa thickness.

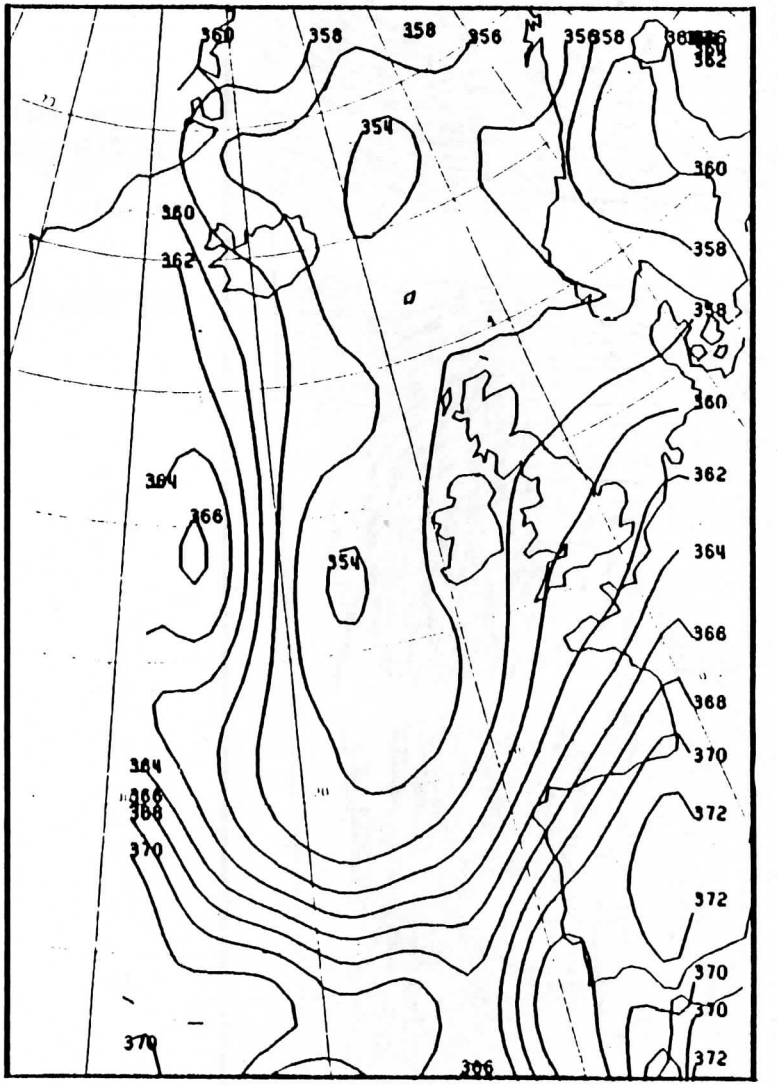

Figure 19b Same as Fig. 19a. 500-300 thickness.

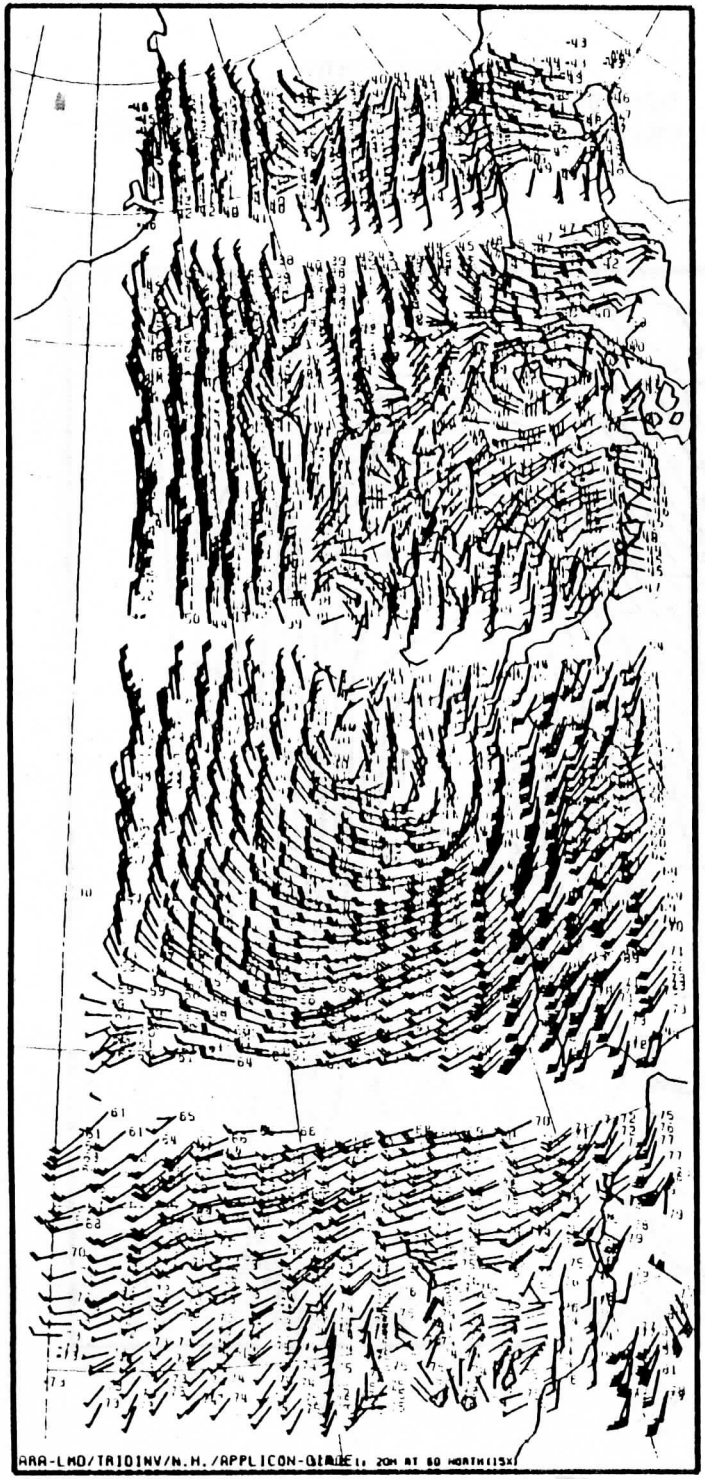

Figure 19c

TOVS retrievals for NOAA-10 orbit 3735, 1000-500 HPa thermal winds.

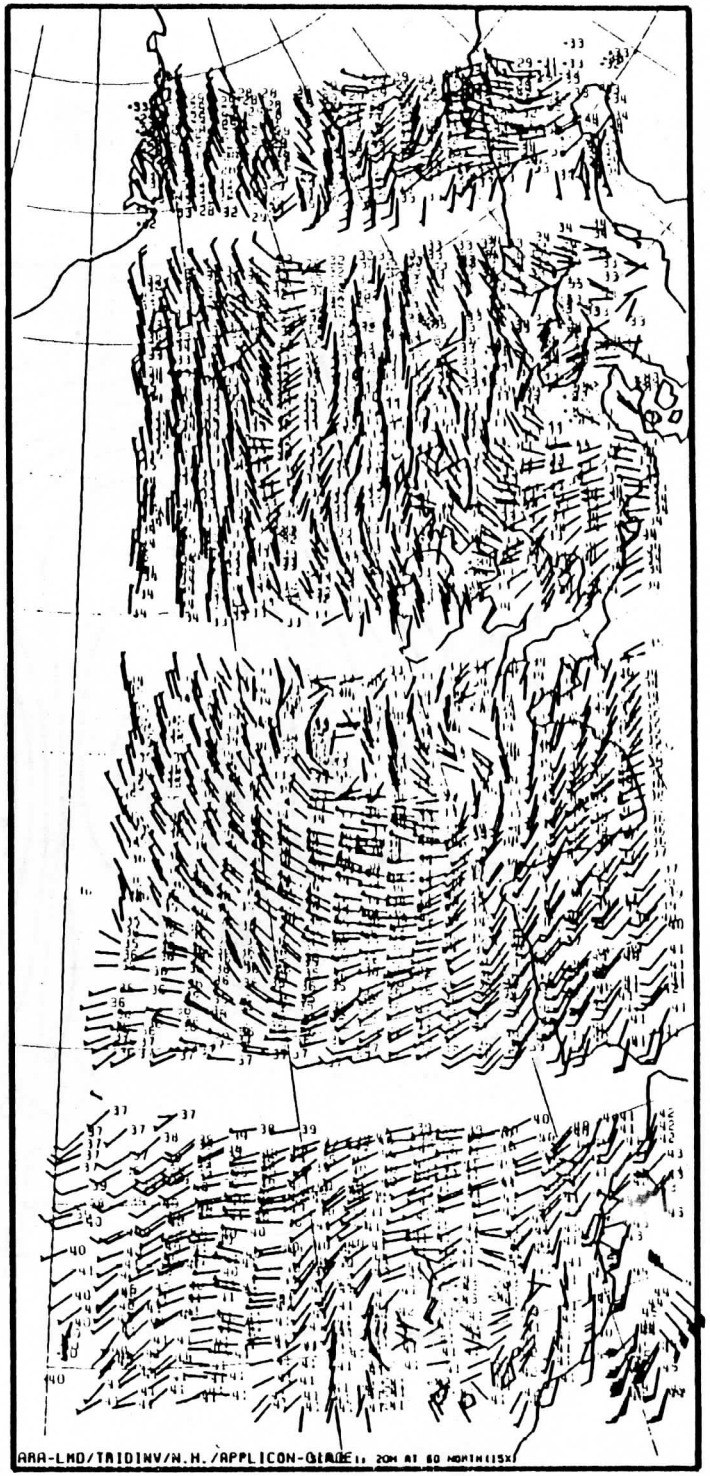

Figure 19d

Same as Fig. 19c, 1000-850 HPa thermal winds.

- the Föhn-effect in the lee of the Pyrenees after an earlier front passing, caused the land surface being strongly heated around noon and the early afternoon ;

- the advection of cold air over the ocean amplified the thermal contrast across the undulating cold front with active wave development over the entrance of the Channel ;

- advection of strong and alternating thermal vorticity gradients over a 400-500 km stretch on the southern flank of the forming frontal wave.

Each of these elements would on its own have led to the formation of thunderstorms in the whole of the coastal region of SW France. It is the combination of the pre-conditioning by the Föhn-effect and the active cold front which led to the formation of a narrow squall line ahead of the cold front, the squall line being rapidly and strongly reinforced by the vorticity advection.

The question could be asked whether or not such developments could have been forecast and by what means.

The detailed imagery (orbit 12791, at 04.40 UT, Fig. 17, and orbit 3735 at 08.55 UT, Fig. 18) combines to delineate the rapid progression of a small, but clearly discernible vortex in the cold air ; the cloud top temperatures at 04.40 UT (Fig. 17) indicate strong convective motions in the vicinity of the developing wave. The two pictures could - in combination - provide a warning signal : a strong squall line is - almost certain - developing. This signal could be available to a forecaster around 09.15 UT, providing a reasonable delay for the transmission of such high-detail pictures. Assuming a one-hour production time for the thermal vorticity map (Fig. 20a), the hypothetical forecast for extremely strong cyclonic (after some alternating) development could be assessed around 10.15 UT, issuing a subsequent warning around 10.30 UT, some 3-4 hours before the - registered - advent of the devastating winds in the squall line.

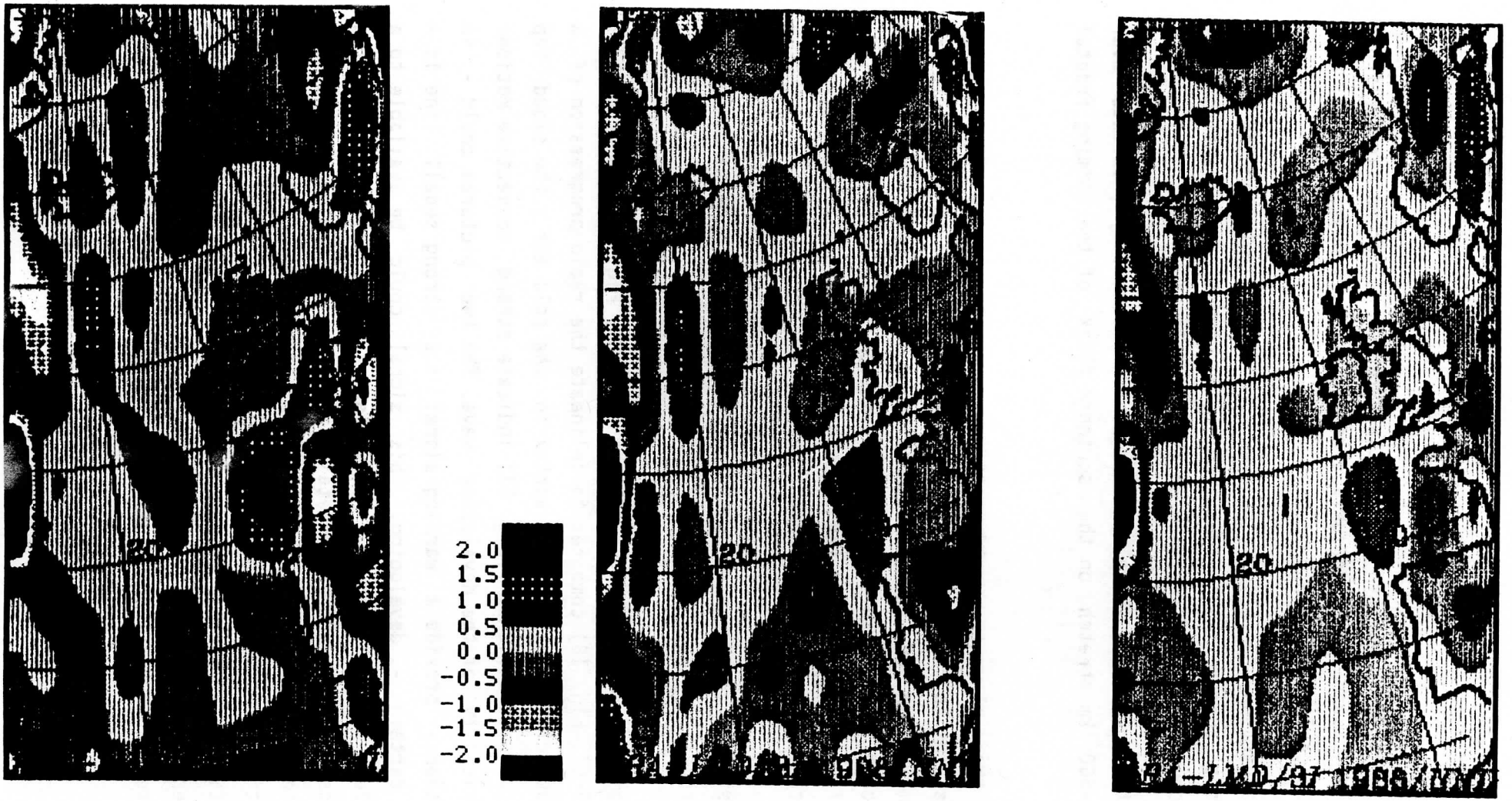

Figure 20 TOVS derived thermal vorticities for NOAA-10. Orbit 3735. (a) : 1000-500 HPa ; (b) : 500-300 HPa ; (c) : 700-500 HPa. (in 10^{-4} s^{-1}).

A suitable limited area model run, assuming a three-hourly update cycle with 2 hours delivery delay, could have confirmed the warning around one hour later (11.15-11.30 UT).

It should be noted that, for such a scenario, a highly sophisticated data - and model - infra-structure is needed. This could however be realized with present day technology.

The scenario also shows the combined importance of both high-detail imagery and TOVS products being timely available to forecaster and model. It moreover shows the essential role to be played by a robust TOVS retrieval method in the implied model scenario.

7. IMPACT OF SATELLITE DATA ON MIDDLE RANGE GLOBAL WEATHER FORECASTING

Since December 1986, the ARA/LMD group participates, in cooperation with ECMWF, in a programme aiming at evaluating the impact of physically retrieved meteorological parameters on the forecast. A one month demonstration period has been chosen from 15 January to 15 February 1987 covered by the two satellites NOAA-9 and NOAA-10. The up-to-date version of the assimilation and forecast system (T106 model, 19 levels in the vertical) is used. First retrieval experiments have been made globally for a period of 5 days within this period using the 3I system. Now implemented on the CRAY-1 XMP48 of the Center, and using only one processor, it takes 23 minutes (CPU time) for a period of 6 h and 2 satellites. Very recently, preliminary testing in assimilation have been performed successfully.

The use of 3I at the ECMWF involves the replacement of the present operational "Satems" (produced by the NOAA-NESDIS in Washington) used in the data assimilation by the corresponding 3I products : thicknesses and relative humidity for the standard layers.

The operational "Satems" received at the ECMWF have a resolution of 250 km, whereas the 3I products have a resolution of about 100 km.

The first assimilation runs have started, over a short period of 18 hours (3 cycles of data assimilation). It has highlighted the spatial coverage of the retrievals, and also the need for a screening aiming at reducing, through quality control, the number of retrievals (about 30,000 per analysis cycle) to a maximum of 15,000 to 20,000 acceptable by the analysis.

Preliminary results show a satisfactory quality, at least as good as the operational NOAA/NESDIS "satems". 3I results seem to be a little less noisy (better standard deviations) and a little more biased, a problem that should be at least partly solved by a better validation of the forward model used.

However, final conclusions have to be drawn on the basis of the impact on the forecast and not on the basis of statistics against radiosondes which cumulate in-situ observation errors and colocation problems.

8. IMPLEMENTATION OF 3I ON VARIOUS COMPUTING SYSTEMS. RECENT DEVELOPMENTS AND SIMPLIFICATIONS

The 3I system is now in use at several places raising the question of an easy maintenance with respect to satellite evolution or replacement.

8.1 The TIGR data set

The 3I system relies upon the TIGR (TOVS Initial Guess Retrieval) data set for both the initialization (pattern recognition) and the inversion (precomputation of brightness temperatures and partial derivatives) process. The validation procedure in use up to recently, was based on the so-called γ-δ procedure : radiances computed from a forward model are adjusted to observations through :

$$I_{obs} = I_{calc} (\tau^{\gamma}) + \delta$$

where γ, in principle close to 1, modifies the computed transmittances and δ represents the instrumental bias. This procedure, quite empirical, has been simplifed due to the good quality of the forward model used resulting in γ values very close to 1 : $|1-\gamma|$ is almost never larger than 0.05 and usually smaller. Since $d\tau$, and not τ, is the quantity governing the retrieval process, the error made by using it, instead of $d(\tau\gamma)$ becomes negligible. Moreover, transparent channels (windows), for which τ itself is used for surface temperature determination, always correspond to γ values equal to 1 as not being affected by this parameter. This is due to the compensation between the surface contribution and the atmospheric contribution to the total radiance.

The interesting consequence is that only δ factors are needed to adjust brightness temperatures to the observation. This correction is made on line within the initialization or inversion routines. A single TIGR data set may then be used whatever the number of platforms to be processed is. The δ values take account of both the γ factors and the slight shifts between the filters from one satellite to the other. The present TIGR data set was computed using NOAA-8 filters. Adaptation to NOAA-10 observations gives rise to reasonably small δ values : the mean of $|\delta|$ for all the channels is close to 0.7 with a standard deviation of 0.6. δ factors are determined, and regularly updated, from satellite and radiosonde matched data using the fast "3R" (Rapid Radiance Recognition) forward model (Flobert et al., 1986). Implemented on the CRAY-1 XMP48 of ECMWF, it takes, as an example, about 2 minutes to compute the brightness temperatures of all the TOVS channels for all the grid points of the forecast model. Its accuracy is equivalent to that of the line-by-line model "4A" (Scott and Chedin, 1981).

The TIGR data set will be soon recreated on the basis of the new NOAA-11 filters, with revised values of CO_2 and N_2O amounts.

8.2 Rejection tests

The 3I system includes tests designed for identifying and rejecting retrievals suspected to be of bad quality. They are based upon comparisons between the observations and the corresponding initialization obtained from TIGR. They have been fully automatized and expressed as functions of channel brightness temperatures standard deviations. These values are obtained from TIGR and take into account the conditions of observation (angle, surface elevation, ...).

A new rejection test has been added, based upon comparisons between initialization and final retrieval and separating the upper and the lower parts of the profiles. A retrieval is rejected if between the two profiles, the distance for the upper part is too different from that for the lower part.

8.3 Exportation of 3I : present status

The 3I system is presently implemented :

- at CMS Lannion (French Met. Office). Bull SPS-9 and IBM-3090,
- at KNMI (Netherlands Met. Office). Micro-Vax II,
- at California Space Institute (Scripps Institution of Oceanography), Micro-Vax I,
- at the European Center for Medium Range Weather Forecasting, CRAY-1 XMP48,
- at Strasbourg University (Scientific Spatial Remote Sensing Group), IBM 4341.

It will be soon implemented at Satellite Meteorologial Center, in Beijing. IBM 4381.

At CNRS-LMD, the 3I system runs on IBM 3090, SIEMENS, VP-200 and CRAY-2. In the latter case, TIGR and associated files are in central memory.

References

Chedin, A., Scott, N.A., Flobert, J.F., Husson, N., Levy, C., Rochard, G., Quere, J., Bellec, B., Siméon, J., "Analyse des champs d'épaisseurs obtenus par la méthode "3I" d'inversion des observations satellitaires de la série Tiros-N". *La Météorologie*, 16, 24-34 (1987).

Chedin, A., Scott, N.A., Wahiche, C. and Moulinier, P., "The improved initialization inversion method : a high resolution physical method for temperature retrievals from the Tiros-N series", *J. Clim. Appl. Meteor.*, 24, 124-143 (1985).

Chedin, A. and Scott, N.A., "Initialization of the radiative transfer equation inversion problem from a pattern recognition type approach", *Advances in Remote Sensing Retrieval Methods*. Academic Press, A. Deepak Ed., 495-515 (1986).

Claud, C., Chedin, A., Scott, N.A. and Gascard, J.C., "Retrieval of meso-scale meteorological parameters for polar latitudes (MIZEX and ARCTEMIZ campaigns). To be submitted to Annales Geophysicae.

FLOBERT, J.F., SCOTT, N.A., CHEDIN, A, 1986, "A fast model for TOVS (Tiros-N Operational Vertical Sounder) radiances computations". 6th Conference on Atmospheric Radiation, May 13-16, 1986, Williamsburg, Va.

Grody, N.C., "Severe storm observations using the Microwave Sounding Unit", *J. Clim. Appl. Meteor.*, 22, 609-625 (1983).

Le Marshall, J.F., 1985, "An intercomparison of temperature and moisture fields from Tiros Operational Vertical Sounder data". The Technical Proceedings of the 2nd International TOVS Study Conference, Igls, Austria. Ed. W.P. Menzel, p. 106-161.

Lindsay, R.W., "MIZEX-84 meteorological atlas and surface data set", Polar Science Center, Univ. of Washington, Seattle, USA (1985).

McMillin, L.M., and Dean, C., "Evaluation of a new operational technique for producing clear radiances", *J. Appl. Meteor.*, 21, 1005-1014 (1982).

Prangsma, G.J., Chedin, A., Scott, N.A., Husson, N., Quere, J., Rochard, G., "Observations of the development of mesoscale systems by operational meteorological satellites". Proc. Symp. Mesoscale Analysis and Forecasting, Vancouver, Canada, ESA SP-282, 117-122 (1987).

Prangsma, G.J., "Mesoscale analysis and the use of TOVS. A case study using 3I results". This volume.

Scott, N.A. and Chedin, A., "A fast line-by-line method for atmospheric absorption computations : the Automatized Atmospheric Absorption Atlas", *J. Appl. Meteor.*, 20, 802-812 (1981).

Wahiche, C., "Contribution au problème de la détermination de paramètres météorologiques et climatologiques à partir des données fournies par les satellites de la série TIROS-N. Impact de la couverture nuageuse", Thèse de 3e Cycle (1984).

Yamamouchi, T. and Seo, Y. "Discrimination of sea ice in the Antarctic, from NOAA-MSU", Proc. 6th Symp. on Polar Meteorology and Glaciology, National Inst. of Polar Research, Tokyo, Japan (1984).

DEVELOPMENT OF RETRIEVAL OF ATMOSPHERIC TEMPERATURE PROFILES IN HUNGARY

Gy. Sipos
Central Institute for Weather Forecasting
Numerical Modellling Branch
H-1675 Budapest, POB 32.

1. INTRODUCTION

In Hungary temperature and water vapour retrieval were started in the 1970-s. G. Major (1978), F. Miskolci (1973) and Gy. Molnár (1976) investigated several methods for retrieving profiles and for accurate calculation of the transmission function. Unfortunately, at that time there was not any satellite receiving station, so they had difficulties getting satellite data. They could use the NIMBUS SCR data in their studies. A few methods were developed for solving the radiation transfer equation - physical, statistical and combined methods.

Comparing the obtained profiles and the radiosonde observations, the average RMS error was about 3K. The largest errors were found at the tropopause level. The accuracy was insufficient over cloud covered areas.

In the near future new satellite reciving station for AVHRR, TOVS and METEOSAT data is going to be

operational in Hungary. Studies have also been restarted again. In these works our first step was adapting of TOVS Export Package, developed by Space Science and Engineering Center of University of Wisconsin in Madison (UW/SSEC), (Smith et al., 1983).

2. ADAPTING THE EXPORT PACKAGE

This work was started on a TPA-1148 minicomputer. This is an old type and not enough fast PDP-like computer, made in Hungary. A real-time, multiuser, multitasking operating system was installed on it. The computer is supplied with 2 MByte RAM, and more than 300 MByte disk storage capacity. To display the results, images, etc., the TPA is connected with a PERICOLOR-2000 colour image processing system.

First the statistical version of the ITPP (International TOVS Processing Package) software was installed. Originally this software was written for VAX computers, in FORTRAN-77. F77 uses the FPP (Floating Point Procesor), but it is not included in our computer. If the compiler generates a floating instruction code for FPP, it causes a trap in the operating system, and a software floating point emulator makes the processing,

which is slightly slow. Since the programs compiled with FORTRAN-IV compiler in our computer is faster, we have to use this one, but the its use is inconvenient. (The FORTRAN-IV uses the built-in Floating Instruction Set).

In order to use enough RAM of the TPA, we have to use the ODL, the Overlay Descriptor Language, too. For the time consuming parts of ITPP (I/O, bit operations, etc.), it is better to substitute the FORTRAN programs with assembly language (MACRO-11) programs.

3. PRELIMINARY RESULTS

As we have not yet AVHRR-TOVS receiving station, we had difficulties to get data for our experiments and investigations.

The first retrieved profiles were derived from an experimental DSB receiving in 1982. Though these data were in very bad quality (without bit and frame synchronizing, with errors), we could start our works.

In the beginning of 1988 we obtained preprocessed TOVS data from the USSR, for the purpose of experiments

and comparing methods. We obtained synchron radiosonde data on a magtape, too.

With these TOVS measurements we shall retrieving meteorological data. At first we will compare the different methods (statistical, physical), then make a detailed statistical investigations in order to determine the errors of these methods, compared with radiosonde data. The results of some retrievals can be seen in Fig. 1. Our experiences also show, that the errors arise at the tropopause, and in the cloudy atmosphere.

4. FUTURE PLANS

If our receiving station starts to receive TOVS data in an operational manner we intend to process them regularly, in order to help forecasting works, for example nowcasting, and assimilate them in the national LAM NWP model.

We intend to use the advantage of the connection between the PERICOLOR -2000 and TPA-1148 that gives a possibility for interactive processing. We plan install the ITPP software on a stand-alone PC system (for the DSB

broadcast) having the main advantages of the PC systems, portability and simplicity.

We continue our statistical investigations about the nature of errors of retrieved temperature and moisture profiles, and would like to develop methods for cloudy cases.

REFERENCES

Major,G., Miskolci,F., Molnár,Gy.:Studies carried out in Hungary on remote sounding of the atmospheric temperature. Proceeedings of the Met. Ser. of Hungary, 1978.

Miskolci,F.: Optimal utilization of Smith's method for temperature sounding. Reports on Scientific Researches Carried out in 1973. Budapest

Molnár,Gy.: Simplified method for determining atmospheric vertical profiles using satellite inrared radiance data. D. Phil. thesis, Institute for Atmospheric Physics, Budapest, 1976.

Smith, W. L., H. M. Woolf, C. M. Hayden, A. J. Schreiner, and J. M. Le Marshall: The physical retrieval TOVS Export package.Presented at the First International TOVS Study Conference, Igls, Austria, 29 August - 2 September 1983.

retrieved • radiosonde +

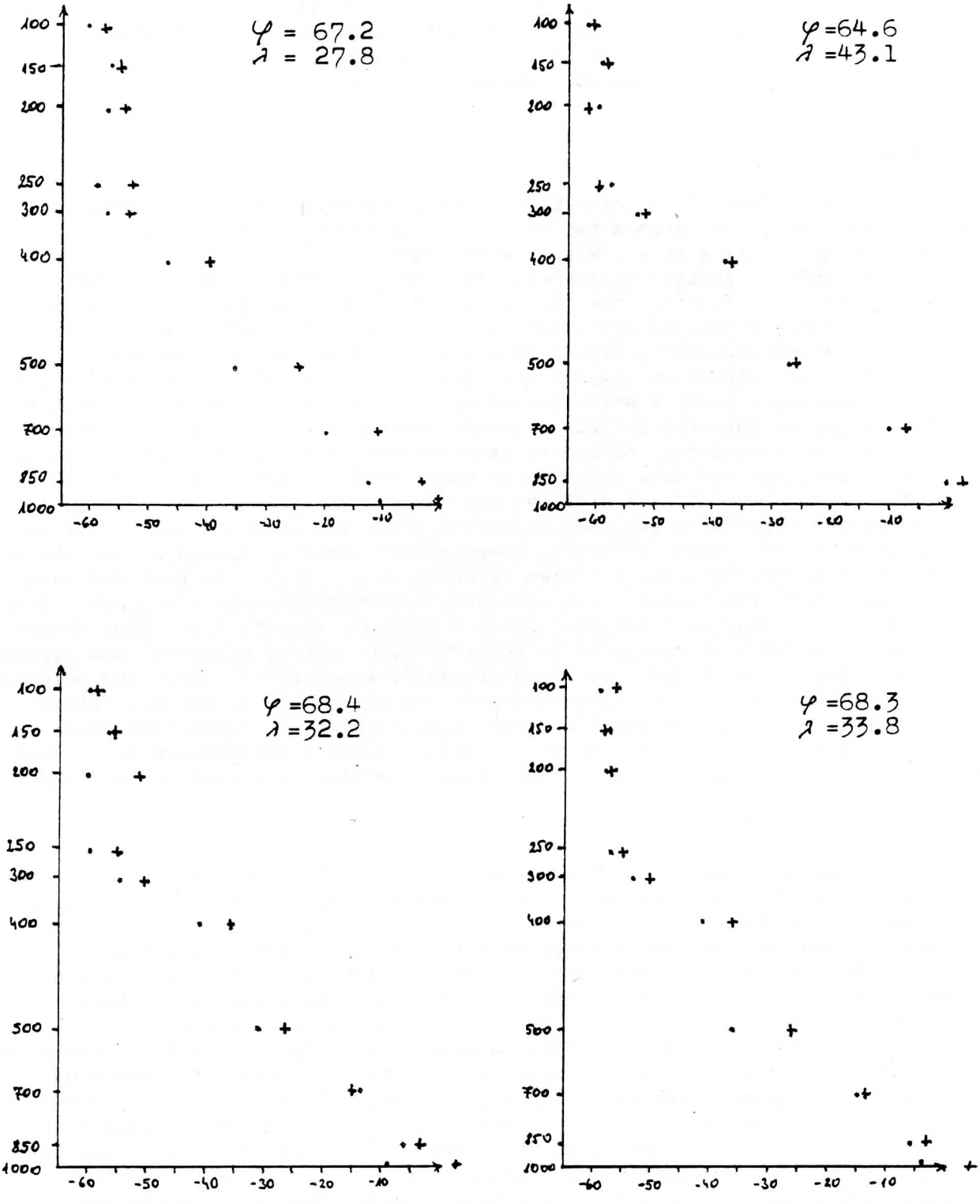

Fig.1. Examples of retrieved profils /26.10.87 0600 UTC/

A LINEAR SIMULTANEOUS SOLUTION FOR TEMPERATURE AND ABSORBING CONSTITUENT PROFILES FROM RADIANCE SPECTRA

W. L. Smith and H. M. Woolf
Cooperative Institute for Meteorological Satellite Studies
University of Wisconsin
Madison, Wisconsin 53706 USA

ABSTRACT

A linear form of the radiative transfer equation (RTE) is formulated for the direct and simultaneous estimation of temperature and absorbing constituent profiles (e.g., water vapor, ozone, methane, etc.) from observations of spectral radiances. This unique linear form of the RTE results from a definition for the deviation of the true gas concentration profiles from an initial specification in terms of the deviation of their "effective temperature" profiles from the true atmospheric temperature profile. The "effective temperature" profile for any absorbing constituent is that temperature profile which satisfies the observed radiance spectra under the assumption that the initial absorber concentration profile is correct. Differences between the "effective temperature", derived for each absorbing constituent, and the true atmospheric temperature is proportional to the error of the initial specification of the gas concentration profiles. The gas concentration profiles are thus specified after inversion of the linearized RTE from the retrieved "effective temperature" profiles assuming that one of the assumed concentration profiles is known (e.g., CO_2). Because the solution is linear and simultaneous, the solution is computationally efficient. This efficiency is important for dealing with radiance spectra containing several thousand radiance observations as achieved from current airborne[1] and planned future spaceborne interferometer spectrometer sounders[2,3]. Here the solution is applied to spectral radiance observations simulated for current filter radiometers and planned interferometer spectrometers to demonstrate the anticipated improvement in future satellite sounding performance as a result of improved instrumentation and associated sounding retrieval methodology.

1. INTRODUCTION

It has been shown from simulation studies[4,5,6] and airborne experiments[7,8] that atmospheric temperature and water vapor profiles can be achieved with drastically improved vertical resolution and accuracy from remotely sensed infrared radiance observations which have a spectral resolution and spectral observation density which is one to two orders of magnitude better than current satellite systems. As a result of these studies, future polar orbiting and geostationary satellite sounding instrumentation is being specified to possess the high spectral resolution and spectral observation density properties required to achieve the sounding quality improvement. However, a practical application of this new instrument technology to the real-time operational production of soundings from their data requires the utilization of an extremely efficient profile retrieval algorithm. Such an algorithm is defined here and tested using spectral radiances simulated for both the currently operational High-resolution Infrared Sounder (HIRS) filter radiometer on the TIROS-N series of polar

orbiting satellites and the planned Advanced Infrared Radiation Sounder (AIRS) interferometer spectrometer planned for the polar platform.

2. ANALYTICAL DEVELOPMENT

In this section, we develop a linearized form of the radiative transfer equation (RTE) and formulate its inverse solution for the temperature and absorbing gas profiles from spectral radiance observations. In the equations which follow:

R_ν = spectral radiance with subscript ν denoting spectral frequency

$B_\nu(p)$ = Planck radiance at pressure level p

p = pressure with subscript s denoting the surface

$\tau_\nu(p)$ = the total transmittance of the atmosphere above atmospheric pressure level p

$\delta()$ = the difference between the true quantity and the initial value denoted by a superscript o

$\Pi()_i$ = the product of i quantities

$\Sigma()_i$ = the summation of i quantities

τ_i = the transmittance of the atmosphere for the ith absorbing constituent

k_{ν_i} = absorption coefficient for the ith absorbing constituent

U_i = concentration of the ith absorbing constituent

T(p) = the true atmospheric temperature profile

$T_i(p)$ = the "effective temperature" of the ith absorbing constituent where the "effective temperature" profile is that atmospheric temperature profile which would give rise to the radiance observed in spectral regions where the ith absorbing constituent dominates the absorption/emission process assuming that the initial gas concentration profile is correct.

T_{B_ν} = the brightness temperature at spectral frequency ν

The true spectrum of monochromatic radiance exiting the earth-atmosphere system is

$$R_\nu = B_\nu(P_s)\tau_\nu(P_s) - \int_o^{P_s} B_\nu(P)d\tau_\nu(P) \ .$$

The radiance spectrum corresponding to an assumed initial temperature and absorbing gas distribution is

$$R_\nu^o = B_\nu^o(P_s)\tau_\nu^o(P_s) - \int_o^{P_s} B_\nu^o(P)d\tau_\nu^o(P) \ .$$

Thus, the difference between the true and initial radiance spectrum is

$$(1) \quad \delta R_\nu = R_\nu - R_\nu^o = B_\nu(P_s)\tau_\nu(P_s) - B_\nu^o(P_s)\tau_\nu^o(P_s) - \int_o^{P_s} B_\nu(P)d\tau_\nu(P) + \int_o^{P_s} B_\nu^o(P)d\tau_\nu^o(P) \ .$$

Employing the linear perturbation definition:

$$\delta B_\nu(P) = B_\nu(P) - B_\nu^o(P)$$

$$\delta\tau_\nu(P) = \tau_\nu(P) - \tau_\nu^o(P)$$

(1) becomes

$$(2) \quad \delta R_\nu = B_\nu^o(P_s)\delta\tau_\nu(P_s) + \delta B_\nu(P)\tau_\nu(P_s) - \int_o^{P_s} B_\nu^o(P)d[\delta\tau_\nu(P)] - \int_o^{P_s} \delta B_\nu(P)d\tau_\nu(P) \ .$$

Since

$$\int_o^{P_s} B_\nu^o(P)d[\delta\tau_\nu(p)] = B_\nu^o(P_s)\delta\tau_\nu(P_s) - \int_o^{P_s} \delta\tau_\nu(P)dB_\nu^o(P)$$

as a result of integration by parts,

it follows that

$$(3)\quad \delta R_\nu = \delta B_\nu(P_s)\tau_\nu(P_s) - \int_o^{P_s} \delta B_\nu(P)d\tau_\nu(P) + \int_o^{P_s} \delta\tau_\nu(P)dB_\nu^o(P) \ .$$

Also, since

$$\tau_\nu = \tau_\nu^o + \delta\tau_\nu$$

then

$$\delta R_\nu = \delta B_\nu(P_s)\tau_\nu(P_s) - \int_o^{P_s} \delta B_v(P)d\tau_\nu^o(P) - \int_o^{P_s} \delta B_\nu(P)d[\delta\tau_\nu(P)]$$

$$+ \int_o^{P_s}\delta\tau_\nu(P)dB_\nu^o(P)$$

Using the integration by parts

$$\int_o^{P_s}\delta B_\nu(P)d[\delta\tau_\nu(P)] = \delta B_\nu(P_s)\delta\tau_\nu(P_s) - \int_o^{P_s}\delta\tau_\nu(P)d[\delta B_\nu(P)] \ ,$$

so that

$$(4)\quad \delta R_\nu = \tau_\nu^o(P_s)\delta B_\nu(P_s) - \int_o^{P_s} \delta B_\nu(P)d\tau_\nu^o(P) + \int_o^{P_s} \delta\tau_\nu(P)dB_\nu(P)$$

Using the chain rule; $dB_\nu(P) = \beta_\nu^o(P)dT(P)$, and the Taylor approximation; $\delta B_\nu(P) = \beta_\nu^o(P)\delta T(P)$, where $\beta_\nu^o = \partial B_\nu(T^o)/\partial T$, then

$$(5)\quad \delta R_\nu = \beta_\nu^o(P_s)\tau_\nu^o(P_s)\delta T_s - \int_o^{P_s}\beta_\nu^o(P)\delta T(P)d\tau_\nu^o(P) + \int_o^{P_s}\beta_\nu^o(P)\delta\tau_\nu(P)dT(P)$$

Now for monochromatic radiation, the total atmospheric transmittance can be defined as the product of the transmittance of all the individual absorbing gases; thus,

$$\tau^o = \Pi \tau_i^o$$

and

$$(6) \quad d\tau^o = \tau^o \sum_{i=1}^{N} d\ln\tau_i^o, \text{ where N = number of absorbing constituents}$$

Relation (6) leads to the finite difference approximation

$$(7) \quad \delta\tau = \tau^o \sum_{i=1}^{N} \delta\ln\tau_i$$

Also, for monochromatic radiation it can be shown that

$$\ln\tau_{\nu i} \sim U_i$$

for a constant temperature profile condition.

Thus, the Taylor Expansion

$$(8) \quad \delta \ln \tau_{\nu i} = \frac{d\ln\tau^o_{\nu_i}}{d\, U^o_i} \delta U_i = \frac{d\ln\tau^o_{\nu_i}}{dT} \frac{dT}{dU^o_i} \delta U_i$$

is an excellent linear approximation. It is noted, however, that (8) ignores the transmitted function dependence upon temperature which is second order compared to the transmittance dependence on absorber concentration U.

Finally, to completely linearize the radiative transfer equation, we employ the definition

$$T_i(P) \equiv T(P) - \frac{dT(P)}{dU_i^o(P)} \delta U_i$$

or

$$(9) \quad \delta U_i(P) \equiv \frac{dU_i^o(P)}{dT(P)} [T(P) - T_i(P)]$$

where $T_i(P)$ is the true temperature as a function of the initial gas concentration profile, $U_i^o(P)$. We note that if the initial gas concentration profile is correct, then $T_i(P) = T(P)$.

Substituting (9) into (8) and the result into (7) yields

$$(10)\quad \delta\tau_\nu(P) = \tau_\nu^o(P) \sum_{i=1}^{N} \frac{d\ln\tau_{\nu i}^o}{dT(P)} [T(P) - T_i(P)]$$

Finally, substituting (6) and (10) into (5) yields

$$\delta R_{\nu_i} = \beta_\nu^o(P_s)\tau_\nu^o(P_s)\delta T_s - \sum_{i=1}^{N} \int_o^{P_s} \beta_\nu^o(P)\{[T(P)-T^o(P)]-[T(P)-T_i(P)]\}\tau_\nu^o d\ln\tau_{\nu_i}^o$$

or

$$(11)\quad \delta R_\nu = \beta_\nu^o(P_s)\tau_\nu^o(P_s)\delta T_s - \sum_{i=1}^{N} \int_o^{P_s} \beta_\nu^o(P)\delta T_i(P)\tau_\nu^o(P) d\ln\tau_{\nu_i}^o(P)$$

which is a general and fully linearized perturbation form of the radiative transfer equation.

In (11), N is the number of optically active atmospheric constituents,

$$\beta_\nu^o(P) = \partial B_\nu(T^o)/\partial T \quad ,$$

and

$$\delta T_i(P) = T_i(P) - T^o(P) \quad .$$

3. INVERSE SOLUTION

The general strategy for solving (11) for atmospheric temperature and absorbing constituent profiles from a satellite observed spectral radiance distribution involves the following steps:

(1) solve for $\delta T_i(P)$ for all constituents using a direct linear simultaneous matrix inverse solution of (11), given a spectrum of radiance, R_ν

(2) let $T(P) = T^o(P) + \delta T_k(P)$ where k denotes a consituent whose concentration, and therefore atmospheric transmittance profile (i.e., $\tau_i(P)$) is known a priori (e.g., CO_2)

(3) use (9) to solve for the concentration of all remaining constituents, i.e.,

$$U_i(P) = U_i^o(P) + \frac{dU_i^o(P)}{dT(P)} [T(P) - T_i(P)]$$

A. Statistical Matrix Inverse Solution of (11)

It is convenient to write (11) in terms of brightness temperature by assuming

$$\delta R_\nu = \frac{\partial B_\nu(T_B{}^o)}{\partial T} \delta T_{B\nu}$$

or

$$\delta T_{B\nu} = \tilde{\beta}_\nu^o(P_s)\tau_\nu^o(P_s)\delta T_s - \sum_{i=1}^{N} \int_o^{P_s} \tilde{\beta}_\nu^o(P)\delta T_i(P)\tau_\nu^o(P) d \ln \tau_{\nu i}^o(P)$$

where

$$\tilde{\beta}_\nu^o(P) = (\partial B_\nu(T^o)/\partial T)/(\partial B_\nu(T_B{}^o)/\partial T)$$

In matrix form

$$(12)\quad t_b = At$$

The elements of A are

$$A_{\nu,o} = \tilde{\beta}_\nu^o(P_s)\tau_\nu^o(P_s)$$

$$A_{\nu,j} = -\tilde{\beta}^{o}_{\nu}(P_{i,j})\tau^{o}_{\nu}(P_{i,j})d \ln \tau^{o}_{\nu i}(P_{i,j})$$

$$j = 1, 2, ,,, N*M_i$$

where N is the number of constituents and M_i is the number of quadrature pressure levels devoted to each constituent.

The generalized statistical/physical solution of (12) is given by the Maximum Likelihood Retrieval[4,5]

$$(13)\quad t = S_d A^T (A S_d A^T + E_b)^{-1} t_b$$

S_d is a dependent sample statistical covariance matrix and E_b is the covariance of the brightness temperature error covariance matrix

$$S_{i,j} = \frac{1}{N_s} \sum_{n=1}^{N_s} [T_{i(Pj)} - T^{o}_{i(Pj)}] [T_{j(Pi)} - T^{o}_{j(Pi)}]$$

where $T_{i(P_i)}$ and $T_{j(P_i)}$ is the temperature of a given constituent at a given constituent pressure level and N_s is the number of atmospheric profiles in the statistical sample.

Here,

$$(14)\quad T_i(P_j) = T(P_j) - \frac{dT(P_j)}{dU^{o}_{i}(P_j)} [U_i(P_j) - U^{o}_{i}(P_j)]$$

The linear dimension of the matrix to be inverted in (13) is the number of spectral channels which in our case is the largest of the dimensions considered. In order to reduce the dimensionality of the matrix inverse, we can use the matrix identity[6]

$$S_d A^T (A\, S_d A^T + E_b)^{-1} = (A^T E_b^{-1} A + S_d^{-1})^{-1} A^T E_b^{-1}$$

to achieve

$$(15)\quad t = (A^T E_b^{-1} A + S_d^{-1})^{-1} A^T E_b^{-1} t_b = C\, t_b$$

Now the linear dimension of the matrix to be inverted is $(N*M_i + 1)$. In (14), the elements of N are

$$E_{b(i,j)} = E_{b(i,j)} = \sigma_\varepsilon^2 (T_b) \ (\nu_i) \quad i=j$$

$$E_{b(i,j)} = 0 \quad i \neq j$$

where σ_ε = expected brightness temperature noise for a given spectral wave number, and it is assumed that the errors are totally random.

It is noted that C is a constant matrix if the temperature dependence of the atmospheric transmittance is small. In principle, the C matrix is dependent only on the temperature and absorbing constituent profile statistics utilized (i.e., their means and covariances) and not on the actual profiles to be retrieved.

B. Error Analysis

The derivation below follows closely the work of Fleming[6] for efficiently estimating the profile errors to be expected from the application of (15) to actual radiance observations.

1. Temperature Errors

Consider an independent sample of soundings for which we wish to apply (15) and evaluate the errors in retrieval of T_i and U_i. If we let D denote the difference between the actual soundings and the retrieved soundings (i.e., $D = T - T_r$), then it follows from (15) and (12) that

$$(16)\ D = T - (A^T E_b^{-1} A + S_d^{-1})^{-1} A^T E_b^{-1} AT - (A^T E_b^{-1} A + S_d^{-1})^{-1} A^T E_b^{-1} \tilde{E}_b$$

where T is the matrix of constituent temperatures and $\tilde{E}_b$ is a matrix of radiant brightness temperature errors for the independent statistical sample and the superscript -1 indicates the matrix inverse.

It follows that

$$D = (I-CA)T - C\tilde{E}_b$$

where I is the identity matrix and $C = (A^T E_b^{-1} A + S_d^{-1})^{-1} A^T E_b^{-1}$. Thus, the retrieval error covariance matrix, D*, is

$$D^* = DD^T = (I-CA)TT^T(I-A^TC^T) + CE_bC^T = (I-CA)S_I(I-A^TC^T) + CE_bC^T$$

where $S_I = TT^T$ of the independent sample set and the covariances between temperature and random measurement errors are assumed to be zero.

Thus,

$$D^* = [I-(A^TE_b^{-1}A+S_d^{-1})^{-1}A^TE_b^{-1}A]\ S_I\ [I-A^TE_b^{-1}A(A^TE_b^{-1}A+S_d^{-1})^{-1}] + CE_bC^T$$

Using the matrix identity

$$[I - (x+y)^{-1}\ x] = (x+y)^{-1}\ y$$

and assuming the same radiance error covariance characteristics for the independent and dependent same sets, then

$$(17)\ D^* = (A^TE_b^{-1}A + S_d^{-1})^{-1}\ (A^TE_b^{-1}A + S_d^{-1}S_IS_d^{-1})(A^TE_b^{-1}A + S_d^{-1})^{-1}$$

It is interesting to note that if $S_I = S_d$, then

$$D^* = (A^TE_b^{-1}A+S_d^{-1})^{-1}$$

which is the form originally derived by Fleming.[6]

The RMS retrieval error is simply the square root of the diagonal of D*.

2. Constituent Concentration Errors

It follows from (9) that

$$(18)\ U = \alpha[T_a-T]$$

where U is the vector of gas concentrations for each constituent and pressure level, α is a vector of the vertical derivative of the mean gas concentration with respect to atmospheric temperature, and T_a is the atmospheric temperature (i.e., that portion of t for which the gas concentration profile is known).

In matrix form, it follows that the retrieval error of $U(E_u)$ is

$$E_u = U-\hat{U} = \alpha[E_{T_a} - E_{T_j}]$$

or

$$(19)\quad E^* = E_u{}^T E_u = \alpha^2 [D^*_{T_a} - 2D^*_{T_a,T_u} + D^*_{T_j,T_u}]$$

where D* is given by (17); $D^*_{T_a}$ is that portion of the matrix referring to the covariance of the error of temperature for the "known" constituent, $D^*_{T_a,T_u}$ is that portion of the matrix referring to the covariance of the error of Ta with the error of the temperature of the "unknown" constituent (T_u), and $D^*_{T_j,T_u}$ is that portion of the matrix referring to error covariance for the unknown constituent.

The RMS retrieval error is simply the square root of the diagonal of E^*_u.

4. RESULTS OF RETRIEVAL ERROR ANALYSIS

An error analysis was performed for the Advanced Infrared Radiation Sounder (AIRS) which will be a facility instrument on the Polar Platform. The AIRS will provide a continuous spectral measurement of the earth-atmosphere upwelling radiance from 590 cm^{-1} to 2940 cm^{-1} with a spectral resolution ($\nu/\Delta\nu$) of 1200/1. The AIRS radiometer accuracy will be equivalent to a brightness temperature performance of better than 0.25°C for a scene temperature of 260°K. The AIRS instrument performance specification[9] is based on the airborne High resolution Interferometer Sounder (HIS)[10] which has demonstrated high vertical sounding resolution and sounding accuracy from NASA high altitude aircraft.[3,8]

The error analysis was performed by a numerical solution of equations (17) and (19) using a global climatological data set[11] to define the independent and dependent sample covariance matrices (S_I and S_D) and FASCODE[11] to calculate the spectrum of atmospheric transmittance profiles for the instruments considered. The absorbing constituents considered were water vapor, ozone, and the uniformly mixed constituents (CO_2, N_2O, CH_4, SO_2 CO). The uniformly mixed constituents were treated as a unit so that the number of atmospheric transmittance components was three. Forty pressure levels ranging between 0.1 mb and 1000 mb were considered for each of the three constituents so that the linear dimension of the matrix inverse was 121. The error matrix, E_b, was constructed assuming that the errors were random (i.e., uncorrelated from wavelength to wavelength) and equivalent to a brightness temperature error of 0.25°C for a scene temperature of 260°K. Retrieval errors were estimated for five cases: (I) full AIRS spectral resolution and coverage (590-2940 cm^{-1} with 1200/1 spectral resolution, (II) partial AIRS spectral coverage (590-1930 cm^{-1}), (III) limited AIRS spectral coverage (590-1100 cm^{-1}), (IV) the 19 low spectral resolution (15 cm^{-1}) channels of the HIRS (High resolution Infrared Radiation Sounder) now flying on operational polar orbiting satellites,[12] and (V) a selection of 115 AIRS spectral channels listed in the AIRS Basic Information Package (BIP) distributed by NASA.[9]

Figures 1a and 1b show the anticipated AIRS retrieval performance when using all or portions of the specified spectral coverage. It is shown that most of the atmospheric temperature and lower level moisture information is contained in the 590-1100 cm^{-1} region of the spectrum. This results from the temperature profile sensitive 15μm CO_2 radiance spectrum and the lower tropospheric water vapor radiance producing rotational water vapor lines in

this spectral region. The inclusion of the 1100-1930 cm^{-1} region does not induce a significant improvement in temperature profiling accuracy, but does provide a very significant improvement in middle and upper tropospheric water vapor profiling accuracy due to the inclusion of radiance from the moderately strong vibrational water vapor lines in this spectral region. Inclusion of the 2160-2940 cm^{-1} region produces further significant improvements in the temperature and water vapor profiling accuracy in the lower troposphere ($p > 750$ mb) due to the water vapor lines and mixed N_2O and CO_2 emission lines coupled with the strong Planck radiance dependence upon temperature in this short wavelength region. The lower tropospheric temperature accuracy improvement of 0.5°C due to the inclusion of 4.3μm region N_2O/CO_2 radiances is particularly noteworthy for accurate profiling of the meteorologically important thermal structure of the boundary layer.

Figure 2 shows the expected accuracy of the AIRS temperature and water vapor retrievals relative to that estimated for the currently operational HIRS radiometer (curve IV). It is noteworthy that the HIRS estimate achieved here is very consistent with that shown from comparisons of actual HIRS statistical retrievals with collocated radiosonde observations.[12,13,14,15] This result gives credibility to the expected errors calculated for the future AIRS instrument. As can be seen from Fig. 2, the AIRS represents a major improvement over the HIRS in terms of sounding capability with the temperature and moisture profiling accuracy being improved by a factor of two or better at all levels between the surface and ten millibars. It is also noteworthy that although the majority of this improvement can be achieved with the minimum set of 115 channels given in the AIRS "BIP", significant added accuracy improvement ($\simeq$0.5°C and 5-10% for temperature and moisture, respectively) is achieved by using the entire spectrum for the sounding retrieval.

The reason one might want to limit the number of spectral channels sent to the ground for profile retrievals, is to minimize the telemetry band width requirements. However, it follows from equation (15) that a more efficient means of limiting the data rate without sacrificing profiling accuracy could be achieved by computing the term $(A^T E_b^{-1}) t_b$ on board the spacecraft and transmitting the elements of this vector which is of the dimension the number of atmospheric retrieval levels (e.g., 40 as used here) times the number of profile constituents (e.g., three; water vapor, ozone, and the uniformly mixed gases) plus one (for surface temperature). Since $(A^T E_b^{-1})$ is a constant matrix, it can be stored on-board and updated when necessary. The data volume for transmission could then be reduced to about 200 data words from the otherwise required 4000. The 200 data words could also include many specific channel radiances for "windows" and in minor constituent absorbing regions which are useful for purposes other than profiling temperature, water vapor and ozone.

Finally, Fig. 3 shows the ozone profile retrieval accuracy estimated from a solution of equation (19). Shown is the accuracy of the "effective ozone temperature" retrieval (obtained from equation (17)) and the accuracy of the integrated ozone concentration. It can be seen that the accuracy of the vertically integrated ozone concentration is nearly constant at about 2.5%, but this is due to the fact that most of the ozone is in the stratosphere where the effective ozone temperature retrieval accuracy is better than 2.0°C. As can be seen, the effective ozone temperature retrieval in the troposphere is very poor indicating that there is little tropospheric ozone mixing ratio

profile information in the AIRS data. However, the 1-3% accuracy shown for the stratospheric concentration profile is very good.

5. SUMMARY

An efficient linear sounding retrieval methodology has been formulated to deal with large volume radiance spectra to be achieved with future advanced infrared sounding instruments. The sounding solutions were used to estimate profile retrieval errors associated with the future Polar Platform AIRS facility instrument and the currently operational HIRS sounding radiometer. The results show that the AIRS will improve our currently achievable temperature and water vapor profiling accuracy by at least a factor of two and enable us to observe the concentration profile of stratospheric ozone with an accuracy of 3% or better.

The linear algorithm also enables the satellite radiance spectral data to be condensed through simple on-board processing by at least an order of magnitude, prior to telemetry to the ground, without the loss of any of the profile information content of the spectrum. This feature is important if data transmission bandwidth becomes a limitation of high spectral resolution, large spectral coverage approaches.

In conclusion, it is noted that the algorithm developed here has been successfully applied to both airborne and surface-based radiance spectra achieved with the HIS instrument.[1] The results of these real data applications of the "linear simultaneous solution" will be reported in a forthcoming publications.

REFERENCES

[1]Revercomb, H. E., H. Buijs, H. B. Howell, R. O. Knuteson, D. D. LaPorte, W. L. Smith, L. A. Sromovsky, and H. M. Woolf, 1987: Radiometric calibration of IR interferometers: experience from the High-resolution Interferometer Sounder (HIS) aircraft instrument. Proceedings of the International Workshop on Remote Sensing Retrieval Methods, Williamsburg, VA.

[2]Smith, W. L., H. B. Howell, and H. M. Woolf, 1979: The use of interferometric radiance measurements for sounding the atmosphere. J. Atmos. Sci., 36, 566-575.

[3]Smith, W. L., H. E. Revercomb, H. M. Woolf, H. B. Howell, D. LaPorte, and K. Kageyama, 1987: Improved geostationary satellite soundings for the mesoscale weather analysis/forecast operation. Proc. Symp. Mesoscale Analysis and Forecasting, Vancouver, Canada, August 17-19, ESA SP-282, 79-83.

[4]Smith, W. L., H. E. Revercomb, H. B. Howell, and H. M. Woolf, 1983: HIS - a satellite instrument to observe temperature and moisture profiles with

high vertical resolution. Fifth Conference on Atmospheric Radiation, Baltimore, MD, October 31-November 4.

[5]Spankuch, D., J. Guldner, and W. Dohler, 1986: Investigations on temperature soundings using partial interferograms. Beitr. Phys. Atmos., 60, 103-122.

[6]Fleming, H. E., and Lillian L. Barnes, 1988: Satellite tomographic remote sensing retrieval methods. A. Deepak Publishing.

[7]Smith, W. L., H. M. Woolf, H. B. Howell, H.-L. Huang, and H. E. Revercomb, 1987: The simultaneous retrieval of atmospheric temperature and water vapor profiles - applications to measurements with the High spectral resolution Interferometer Sounder (HIS). Proceedings of the International Workshop on Remote Sensing Retrieval Methods, Williamsburg, VA.

[8]Smith, W. L., H. M. Woolf, H. B. Howell, H.-L. Huang, and H. E. Revercomb, 1988: High resolution interferometer sounder - the retrieval of atmospheric temperature and water vapor profiles. Proceedings of the Third Conference on Satellite Meteorology and Oceanography, American Meteorological Society, Boston, MA.

[9]Basic information package for the polar platform AIRS. NASA Headquarters, 1988.

[10]Revercomb, H. E., H. Buijs, H. B. Howell, D. D. LaPorte, W. L. Smith, and L. A. Sromovsky, 1987: Radiometric calibration of IR Fourier transform spectrometers: solution to a problem with the High-resolution Interferometer Sounder (HIS). Submitted to Applied Optics, December 11.

[11]Smith, W. L., H. M. Woolf, P. G. Abel, C. M. Hayden, M. Chalfant, N. Grody, 1974: NIMBUS-5 sounder data processing system, Part I: measurement characteristics and data reduction procedures. NOAA Technical Memorandum NESS 57, Washington, DC, June.

[12]Smith, W. L., H. M. Woolf, C. M. Hayden, D. Wark, and L. McMillin, 1979: The TIROS-N Operation Vertical Sounder. Bull. Amer. Meteor. Soc., 60, 1177-1187.

[13]Phillips, N. A., L. M. McMillin, D. Wark, and A. Gruber, 1979: An evaluation of early operational temperature soundings from TIROS-N. Bull. Amer. Meteor. Soc., 60, 1188-1197.

[14]LeMarshall, J. F., 1985: An intercomparison of temperature and moisture fields retrieved from TIROS operational vertical sounder data. Technical Proceedings of the Second International TOVS Study Conference, Igls, Austria, February 18-22, W. P. Menzel (editor), CIMSS Report.

[15]Phillips, N., J. Susskind, and L. McMillin, 1988: Results of a joint NOAA/NASA sounder simulation study. J. Atmos. Ocean. Tech., 5, 44-56.

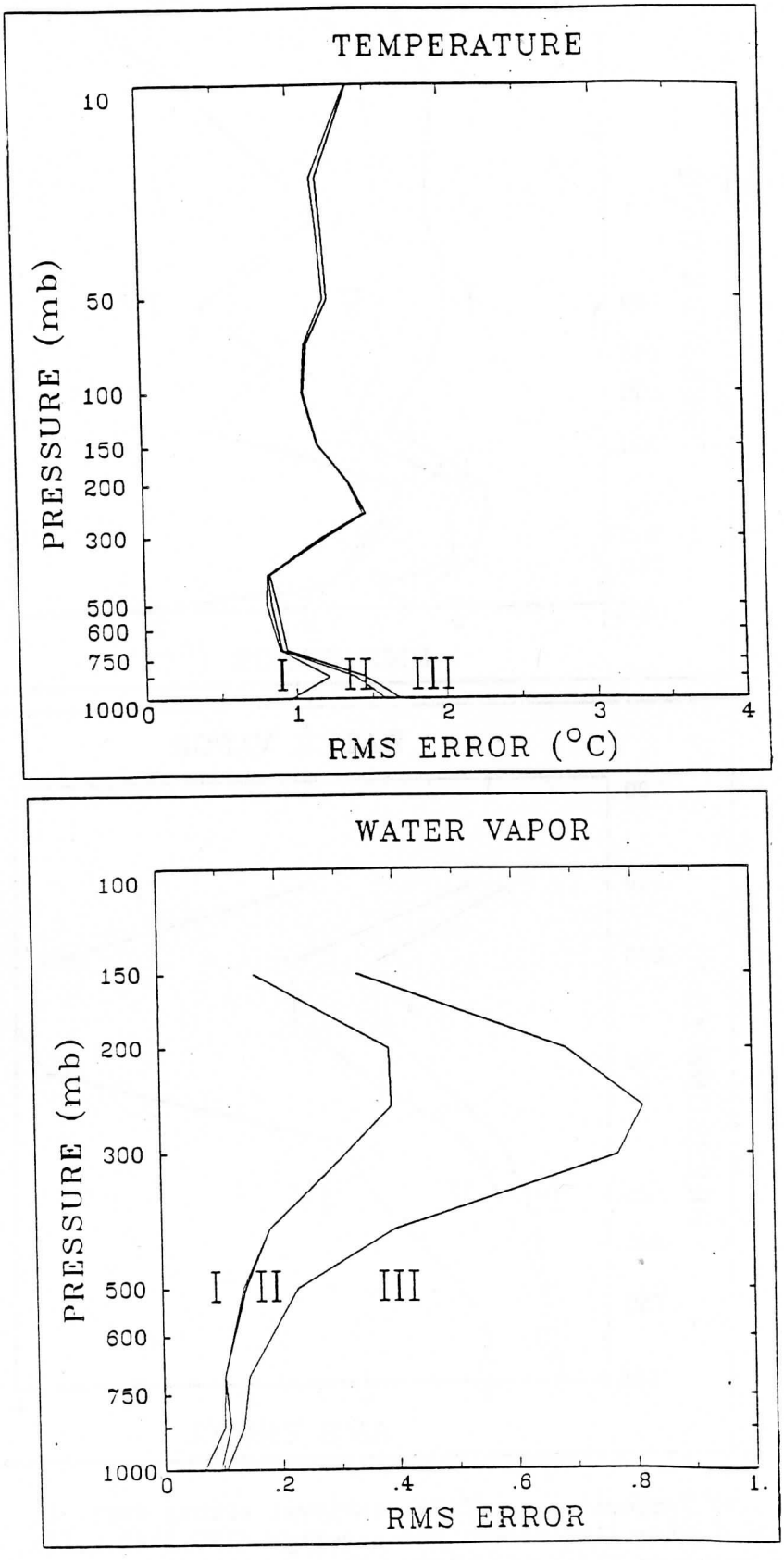

Figure 1: (a) Temperature profile retrieval errors for: I. Full AIRS spectral resolution ($\lambda/\Delta\lambda$=1200) and coverage (590-2940 cm^{-1}), II. Partial AIRS spectral coverage (590-1930 cm^{-1}), and III. Limited AIRS spectral coverage (590-1100 cm_{-1}). (b) Water vapor profile retrieval errors for I, II, III spectral coverages listed above.

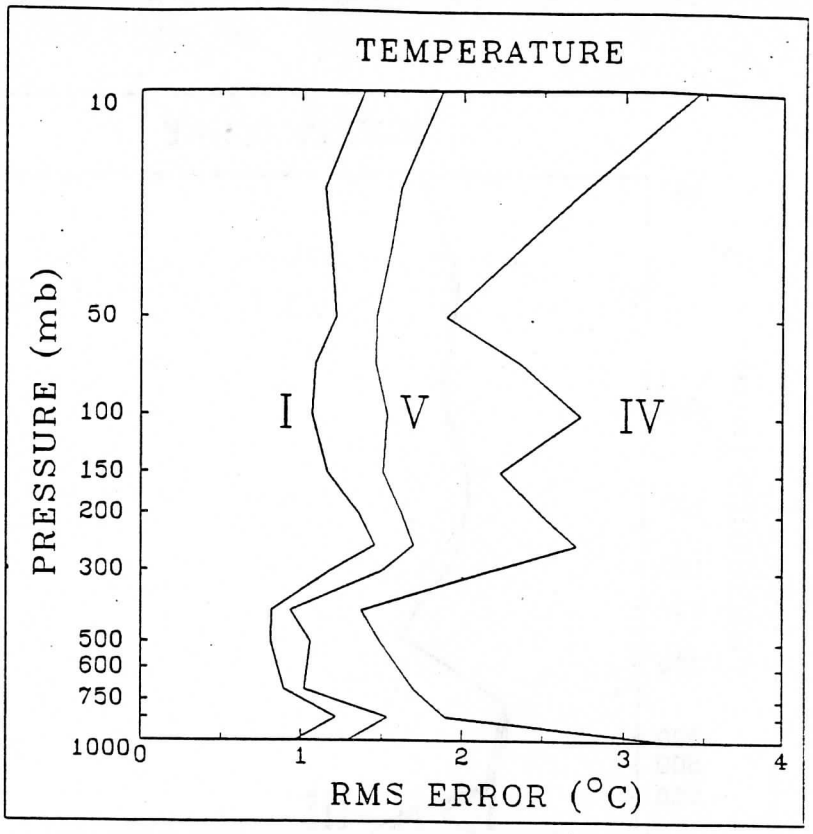

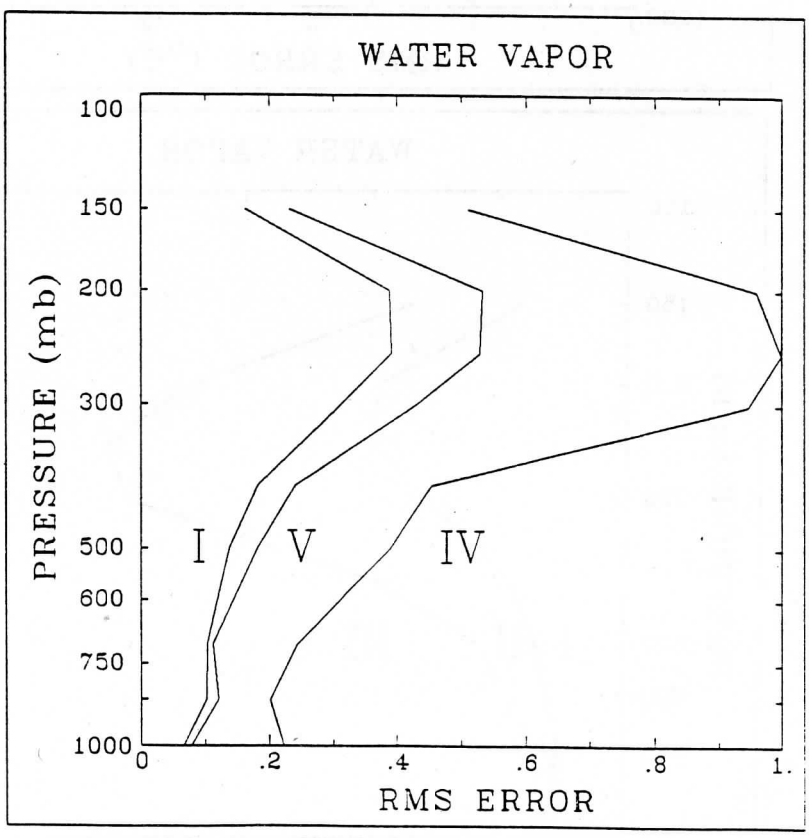

Figure 2: (a) Temperature profile retrieval errors for: I. Full AIRS spectral resolution ($\lambda/\Delta\lambda$=1200) and coverage (590-2940 cm^{-1}), IV. The 19 low spectral resooution ($\lambda/\Delta\lambda$=50) HIRS infrared channels, V. A selection of 115 AIRS spectral channels listed in the NASA Basic Information Package (BIP). (b) Water vapor profile retrieval errors for the I, IV, and V spectral characteristics listed above.

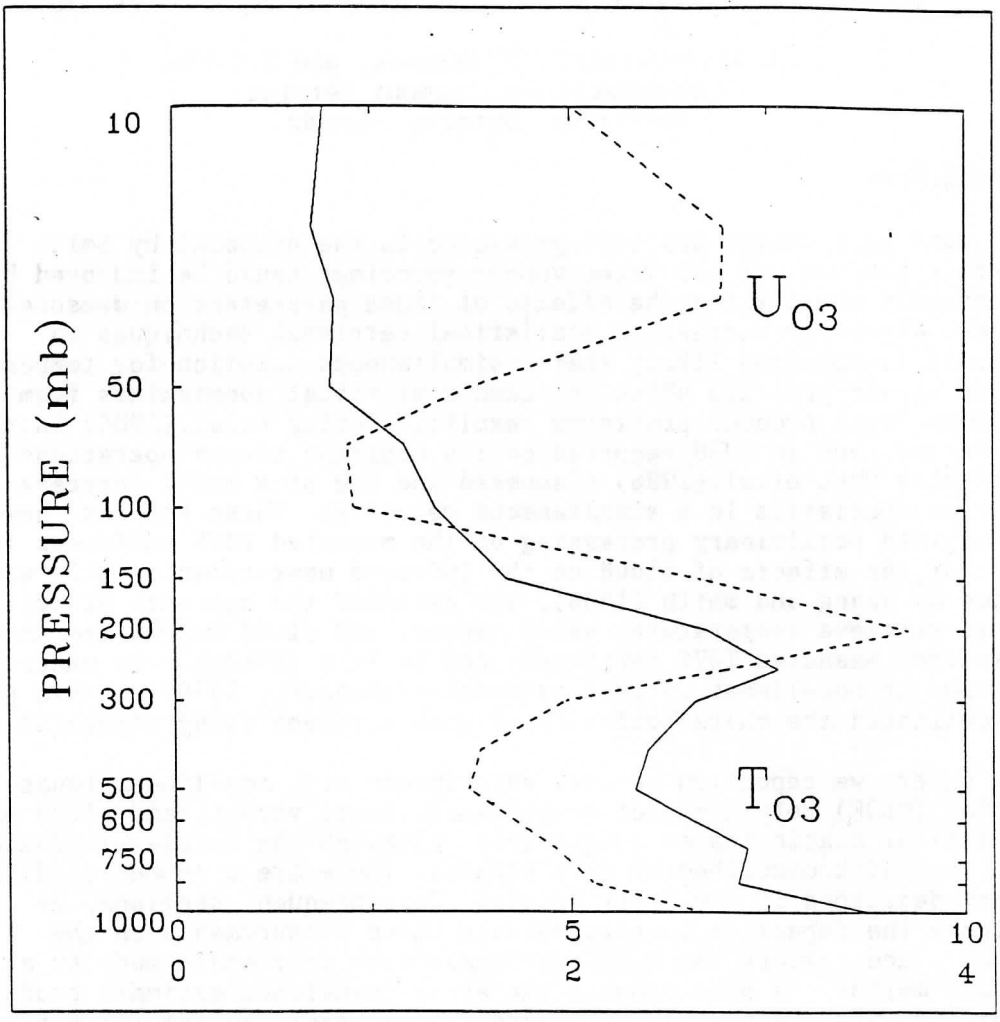

Figure 3: Retrieval error of "effective ozone temperature" and vertically integrated ozone concentration. The temperature scale ranges from 0 to 10°K whereas the relative concentration scale ranges from 0 to 4%.

SOME EXPERIMENTS WITH NON-LINEAR OPTIMAL ESTIMATION RETRIEVALS FROM RAW TOVS RADIANCES USING CLIMATOLOGICAL CONSTRAINTS

J.D.Steenbergen, B.T.Greaves, and T.C.Yip
Atmospheric Environment Service
Downsview, Ontario, Canada

1. INTRODUCTION

A great deal of interest has been generated in the proposal by Smith et.al. (1985) that temperature and water vapour soundings could be improved by simultaneously considering the effects of these parameters on measured TOVS radiances. Given the success of statistical retrieval techniques in operations, it appeared likely that a simultaneous solution for temperature and water vapour profiles which included statistical constraints from climatology would produce promising results. Fleming et.al.(1986) introduced such a method, and in 1988 reported on its progress toward operations in NESDIS; while Eyre et.al.(1986) discussed the use of a model forecast and model error statistics in a simultaneous retrieval. These schemes, however, still required preliminary processing of the measured TOVS radiances to correct for the effects of cloud on the infrared measurements. This was addressed by Huang and Smith (1986), who extended the approach of Smith et.al. (1985) to retrieve temperature, water vapour, and cloud height and amount directly from measured TOVS radiances; and by Eyre (1987a), who described the application of non-linear optimal estimation (Rodgers, 1976) to this problem and investigated the characteristics of such a scheme using simulated data.

In this paper, we report on several experiments with non-linear (quasi)optimal estimation (NLOE) retrievals of temperature, water vapour, and cloud using climatological statistics as constraints. Although the retrievals follow the overall framework described by Eyre (1987a), there are a number of differences which are described in the first section. In subsequent sections, we investigate the impact of in-situ surface-based measurements on the retrievals, and compare the NLOE retrievals with retrievals made by a regression method. We also compare the error covariance estimate produced by the retrieval with retrieval-radiosonde differences; compare the results of retrievals done using slant-path radiances to retrievals using limb-corrected measurements, and report on a preliminary attempt to include information on relative humidity derived from cloud parameters in the retrievals.

2. METHOD

After ITSC-3 we attempted to extend Huang and Smith's approach to include statistical information by using eigenfunctions of temperature and relative humidity covariance matrices as basis functions. The method was essentially the same as we used for clear conditions only (Steenbergen et. al. 1986), except that the profile vector **b** was extended to include the cloud top pressure, cloud amount, microwave emissivity, and the difference between the surface skin temperature and the surface air temperature. (More precisely, **b** included the differences of these quantities from their a priori values.) As before, the eigenfunctions of the vertical covariance matrix of temperature corresponding to the six largest eigenvalues were used to describe the temperature profile, and three eigenfunctions were used to describe the relative humidity profile.

The inverse solution we used was an application of the constrained linear inversion technique using empirical orthogonal functions described by Twomey (1977). The solution is given by

$$\mathbf{b} = (\mathbf{A}^t\mathbf{A} + \gamma\Lambda^{-1})^{-1}\,\mathbf{A}^t\mathbf{g} \qquad (1)$$

The diagonal elements of the constraint matrix Λ were the eigenvalues corresponding to the temperature and relative humidity eigenfunctions, and estimates of the variance of the other profile vector elements. All the off-diagonal elements of Λ were zero. γ was a Lagrangian multipier which was determined by trial and error. (We obtained a value of 1.0 although the results were not very sensitive to this value.) The measurement vector $\mathbf{g}$ contained the differences between the observed brightness temperatures and the brightness temperatures calculated from the first guess, normalized by the standard deviations of differences between observed brightness temperatures and forward calculations from collocated radiosondes. In-situ measurements of surface air temperature and surface relative humidity could also be optionally added to $\mathbf{g}$. The elements of $\mathbf{A}$ ($A_{ij}=\partial g_i/\partial b_j$) were calculated by perturbing the profile vector.

When the measurements are normalized by their expected error and γ=1, Twomey's solution can be written

$$\mathbf{b} = \Lambda\,\mathbf{K}^t(\mathbf{K}\Lambda\,\mathbf{K}^t + \mathbf{S}_m)^{-1}\,\mathbf{y} \qquad (2)$$

where $K_{ij} = \partial y_i/\partial b_j$, $\mathbf{y}$ contains the differences between observed and calculated brightness temperatures, and $\mathbf{S}_m$ contains the "error" variances of the measurements on the diagonal. This is equivalent to the linear maximum-likelihood approach described by Rodgers (1976) except for the truncation of the eigenfunctions of the covariance matrices.

The retrievals were carried out in three steps in a manner similar to that used by Huang and Smith (1986). In the first step, only the microwave channels were used to obtain an updated temperature profile, and the relative humidity was held fixed. In the second step, cloud detection tests were applied and the CO_2 slicing method (Smith and Platt, 1978) was used to obtain an initial estimate of the cloud height and amount. In the third step, both the HIRS and MSU channels were used and all the elements of the profile vector were solved for by applying equation (1) to the changes from the previous step.

Although we were able to produce retrievals in this way (Steenbergen et. al., 1987) the approach was not statistically optimal because the constraint was applied incorrectly on iterations after the first. When the linear maximum-likelihood method is applied iteratively, the solution is constrained to the output of the previous guess rather than the a priori mean (Rodgers,1976). Rodgers described a Newtonian iteration method which applies the statistical constraints correctly in problems with non-linear physics, which has been applied to TOVS retrievals from cloudy radiances by Eyre (1987a). (We would like to thank Dr. John Eyre for a very helpful discussion on this topic and for providing a copy of his work in draft form.)

Following Eyre's approach, we modified equation (2) to

$$\mathbf{b}_{n+1} = \mathbf{b}_n - \mathbf{I}^r\mathbf{b}_n + \Lambda^r\mathbf{K}_n{}^t(\mathbf{K}_n\Lambda^r\mathbf{K}_n{}^t + \mathbf{S}_m)^{-1}\,(\mathbf{y} - \mathbf{y}_n + \mathbf{K}_n\mathbf{I}^r\mathbf{b}_n) \qquad (3)$$

where Λ^r contained reduced values of variance for the cloud top pressure and cloud amount[1] (as used by Eyre to control oscillation in the retrieved cloud parameters) and I^r was a unit matrix except for the elements corresponding to the cloud parameters, which were $\Lambda^r_{ii}/\Lambda_{ii}$.

3. DATA

The results shown here are based on 551 collocated rawinsonde and NOAA-8 satellite measurements during May and June 1984. For purposes of analysis, the collocated measurements were sorted according to an independent estimate of the cloud amount obtained by subjective analysis of the AVHRR imagery. In order to minimize sampling differences, we used only cases in which the satellite and rawinsonde observation times differed by one hour or less. The satellite radiances were centred at the closest scan spot to the location of the rawinsonde station according to orbit model calculations. The time constraint combined with our use of direct readout satellite data limited the suitable radiosonde observations to 00Z ascents in eastern North America.

4. RESULTS

4.1 Effect of adding surface observations to the retrievals

RMS layer mean temperature differences between radiosondes and NL0E retrievals with and without surface air temperature and relative humidity added to the measurement vector are shown in figure 1a. The RMS differences increased with increasing cloud throughout the profile whether surface data were used in the retrieval or not, with the largest increases (other than below 850 mb) occurring between 300 and 500 mb. When ancillary surface data were not used in the retrievals, the 850-1000 mb RMS difference increased markedly with increasing cloud. The increase in the 850-1000 mb RMS difference was presumably caused by the loss of surface skin temperature information from the HIRS as the cloud amount increased. This information could not be provided by the MSU due to the uncertainty in the surface emissivity.

We assumed the a priori distribution of microwave surface emissivity was quite wide, with a mean of 0.80 and a standard deviation of 0.20 (as in Eyre (1987a)). The variation of retrieved emissivity values when surface air temperature measurements were used in the retrievals provides an indication of the actual variations in the emissivity. 67% of the retrieved emissivities fell between 0.83 and 0.96, in a nearly Gaussian distribution around the mode of 0.90. The other 1/3 of the retrieved emissivities were in a long tail extending from 0.83 down to 0.52. The retrievals in this tail were collocated with island or coastal radiosonde stations, so that a substantial part of the

---

[1]The variances of the cloud top pressure and cloud amount which had been used in our non-optimal retrievals were close to the "reduced" values used by Eyre. Λ was changed to increase the background variances of the cloud parameters to the values used by Eyre. No terms involving the background value of $\mathbf{b}$ appear above since this value is zero. It was expedient to continue to use truncated sets of eigenvectors as bases for the temperature and relative humidity profiles. Because the full a priori covariance matrix of temperature and relative humidity is not used, this solution is not quite optimal. However, as long as the neglected eigenfunctions explain very little variance and their effect on the radiances is small, the difference should be small.

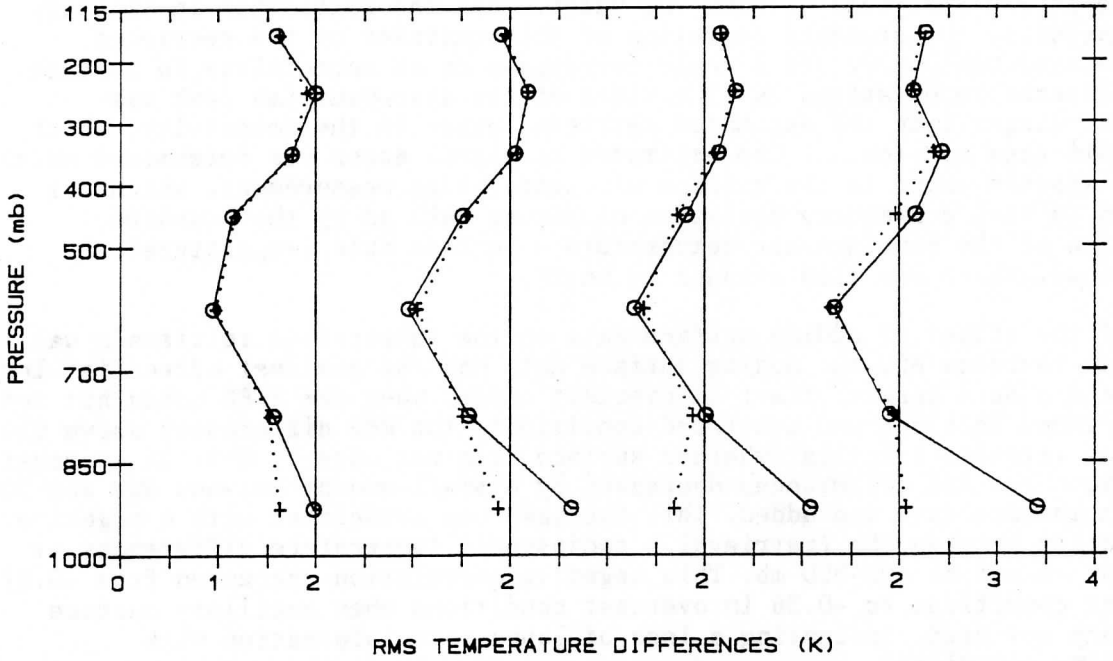

Figure 1a. RMS layer mean temperature differences between radiosondes and: NLOE retrievals with ancillary surface data (dotted lines); NLOE retrievals without ancillary surface data (solid lines). From left to right, 99 clear cases, 106 scattered cloud cases, 127 broken cases, 151 overcast cases.

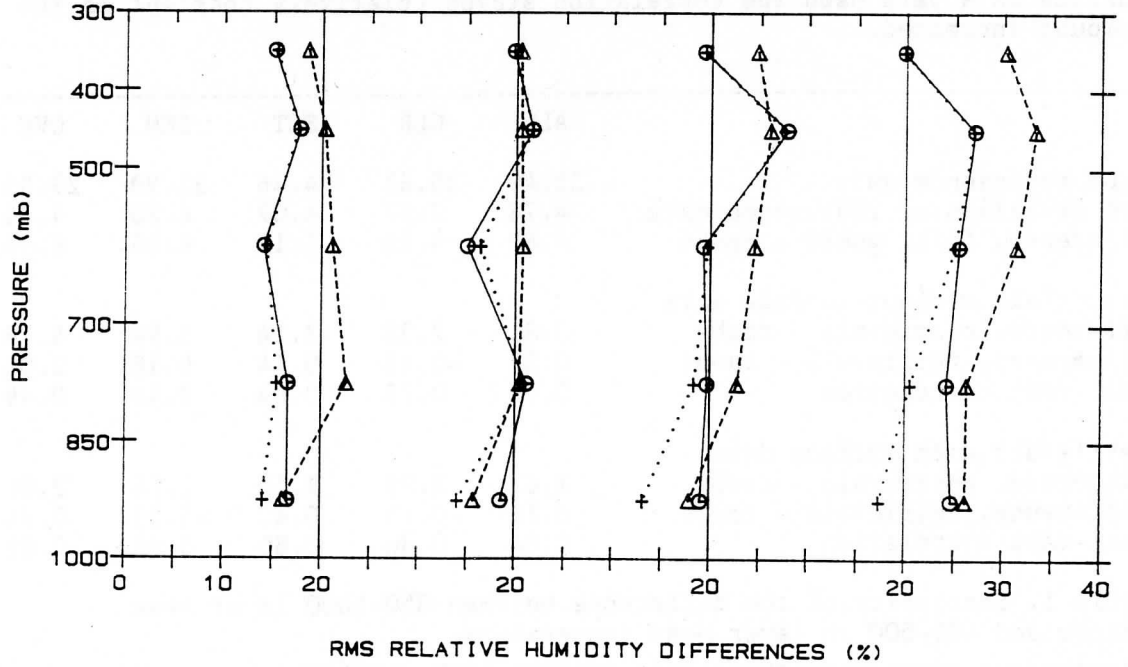

Figure 1b. As in figure 1a for layer mean relative humidities, plus RMS difference between first guess relative humidity profile and radiosondes (dashed lines).

surface in the MSU field of view was water. When the retrievals in the tail were excluded, the standard deviation of the remainder of the retrieved emissivities was 0.027, which would correspond to an uncertainty in surface skin temperature of around 7K. The width of the near-Gaussian peak was somewhat larger than the estimated retrieval error in the emissivity, which was 0.016 (see section 5). The estimated retrieval error was determined mainly by the assumed error in the surface air temperature measurement, which was assumed to have a standard deviation of 2K; as well as by the standard deviation of the (surface air temperature - surface skin temperature) difference, which was also assumed to be 2K.

Most of the effect of adding surface data on the temperature retrievals was confined to below 850 mb. Adding surface data had the smallest effect in clear cases and a much larger effect in overcast cases, when the HIRS could not see the surface. In clear and scattered conditions, the RMS differences above 850 mb were virtually identical whether surface data was used or not. In overcast conditions the RMS differences decreased by a small amount between 300 and 500 mb when surface data was added. This decrease was associated with a negative correlation between the (retrieval - radiosonde) temperature differences at 850-1000 mb and at 400-500 mb. This negative correlation increased from -0.07 in clear conditions to -0.36 in overcast conditions when ancillary surface data were not used, indicating a loss of lapse rate information with increasing cloudiness.

The loss of lapse rate information can be seen in statistics of the vertical temperature difference between the 850-1000 mb layer and the 400-500 mb layer. The correlation between this vertical temperature difference from the retrieved profiles and from the radiosonde data (table 1) decreased sharply as the cloud amount increased when no surface data were used in the retrievals. When surface data were used the correlation stayed relatively constant as the cloud amount increased.

	ALL	CLR	SCT	BKN	OVC
Mean from radiosonde data	33.40	35.61	34.46	33.99	29.93
Standard deviation of radiosonde data	4.78	3.67	4.07	4.26	4.65
RMS difference, first guess - raobs	4.82	4.10	4.15	4.26	6.05
NLOE retrievals without surface data					
RMS difference, retrievals - raobs	3.81	2.35	3.14	3.98	4.78
Mean difference, retrievals - raobs	0.59	-0.13	0.44	0.18	2.08
Retrieval-raob correlation	0.62	0.77	0.64	0.49	0.49
NLOE retrievals with surface data					
RMS difference, retrievals - raobs	2.61	2.19	2.50	2.58	2.80
Mean difference, retrievals - raobs	0.11	-0.15	0.42	-0.23	0.34
Retrieval-raob correlation	0.84	0.80	0.80	0.81	0.81

Table 1. Statistics of the difference between 850-1000 layer mean temperature and 400-500 mb layer mean temperature.

The RMS differences between the relative humidity retrievals and radiosondes (figure 1b) also increased with increasing cloud, as one would expect. The

effect of the surface relative humidity measurement (assumed to have an uncertainty of 15%) increased as the cloud amount increased and the sensitivity of the HIRS radiances to relative humidity changes went down.[2]

4.2 Comparison with statistical retrievals

Comparisons were made between the NLOE retrievals (without ancillary surface data) and statistical retrievals using regression coefficients generated locally from synthetic data. The retrievals were sorted according to whether the cloud detection/correction routine in the statistical scheme (which generally followed the approach of McMillin and Dean (1982)) was able to produce clear radiances; as well as according to the cloud cover estimated by AVHRR. The results are presented in figure 2.

When the statistical cloud-clearing scheme succeeded, two temperature retrievals were available from the statistical scheme (one from MSU data only and the other from HIRS aided by MSU). In these conditions, the NLOE retrievals improved over the statistical retrievals below 400 mb (figure 2a). The statistical cloud-clearing scheme was unable to produce clear radiances in 25 of 99 clear cases identified by AVHRR, 14 of 106 scattered cases, 27 of 127 broken cases, and 78 of 151 overcast cases. (In overcast conditions clear radiances should not have been produced.) When the cloud-clearing failed, the MSU-only statistical retrievals (which were the only product available from the statistical scheme) performed noticeably worse than they did when the cloud-clearing succeeded. The NLOE retrievals were also degraded in these conditions but not by as large a margin (figure 2b). The association between the performance of the MSU-only retrievals and the cloud-clearing scheme is not surprising because of the heavy dependence of the cloud-clearing on statistical relationships between the HIRS and MSU channels.

RMS differences between retrieved layer mean relative humidities and radiosonde values for the NLOE and statistical retrievals are shown in figures 2c and 2d. Also shown are the RMS differences between the radiosonde measurements and the first guess relative humidity profile. In clear conditions, the NLOE retrievals improved substantially over the first guess. The improvement was smaller (and absent or negative for some layers) in scattered and broken conditions. In overcast conditions, there was an improvement over the first guess in the higher troposphere, although the RMS differences were still large. In general, the NLOE retrievals improved over the first guess in conditions when a moisture retrieval was unavailable from the statistical scheme due to failure of the cloud correction scheme (figure 2d). The statistical scheme failed to improve over the first guess even in clear conditions. In overcast conditions when the statistical scheme produced clear radiances (and probably should not have) the statistical scheme was noticeably worse than the first guess in the 500-700 mb layer.

Examination of the AVHRR imagery and mean radiosonde profiles showed that the overcast cases in which clear radiances were produced generally had lower

---

[2]The impact of the surface measurements in these retrievals may be overestimated because the surface measurements were obtained from the radiosonde reports against which the retrievals were subsequently compared. However, in assigning errors to these measurements we tried to keep the variability of surface temperature and relative humidity in mind.

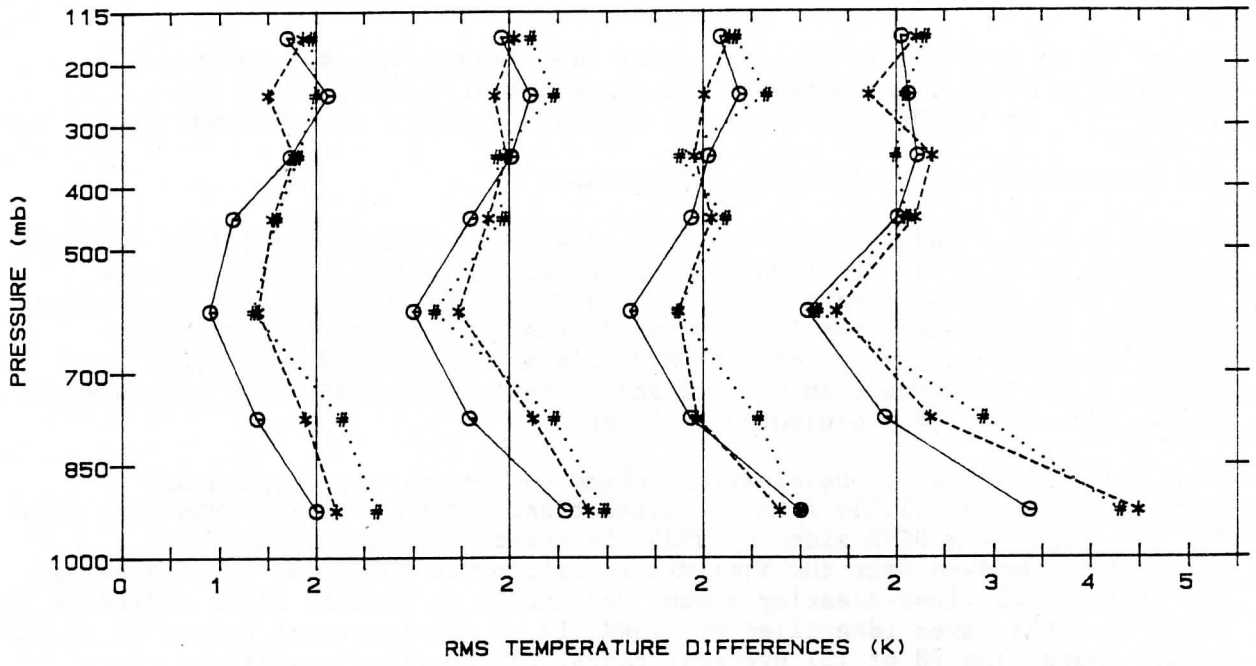

Figure 2a. RMS layer mean temperature differences between radiosondes and: NLOE retrievals (solid lines); HIRS statistical retrievals (dotted lines); MSU-only statistical retrievals (dashed lines); when statistical cloud-clearing succeeded. From left to right, 74 clear cases, 92 scattered cases, 99 broken cases, 73 overcast cases.

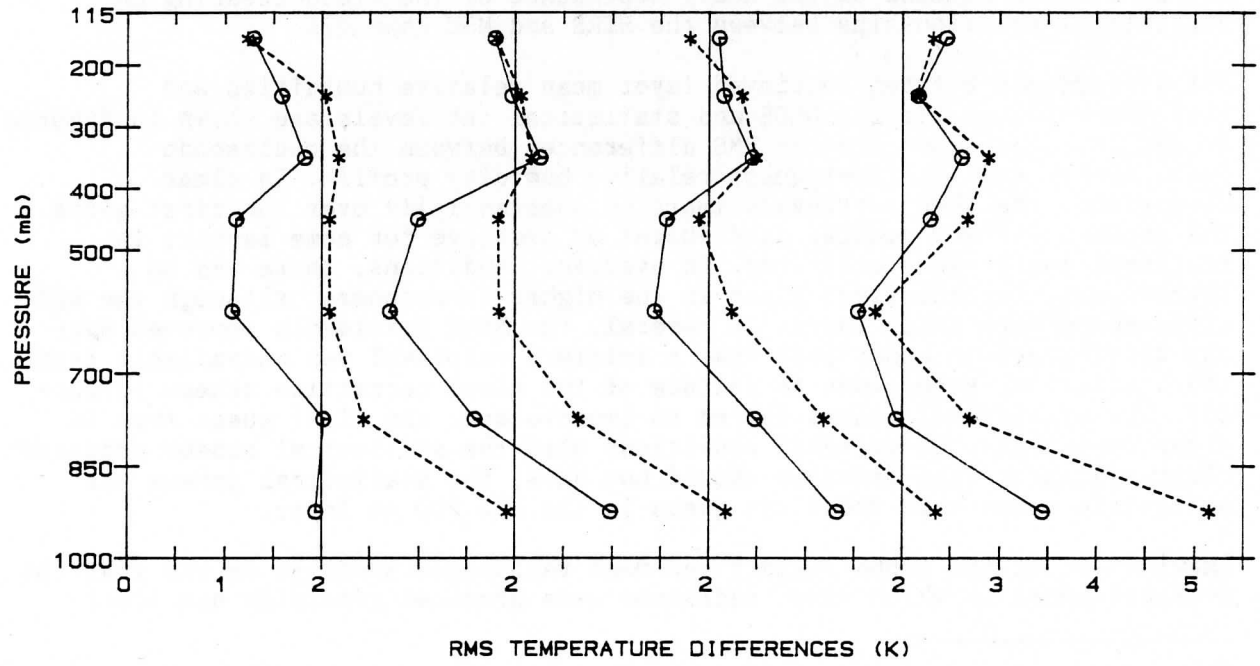

Figure 2b. RMS layer mean temperature differences between radiosondes and: NLOE retrievals (solid lines); MSU-only retrievals (dashed lines); when statistical cloud-clearing failed. From left to right, 25 clear cases, 14 scattered cases, 28 broken cases, 78 overcast cases.

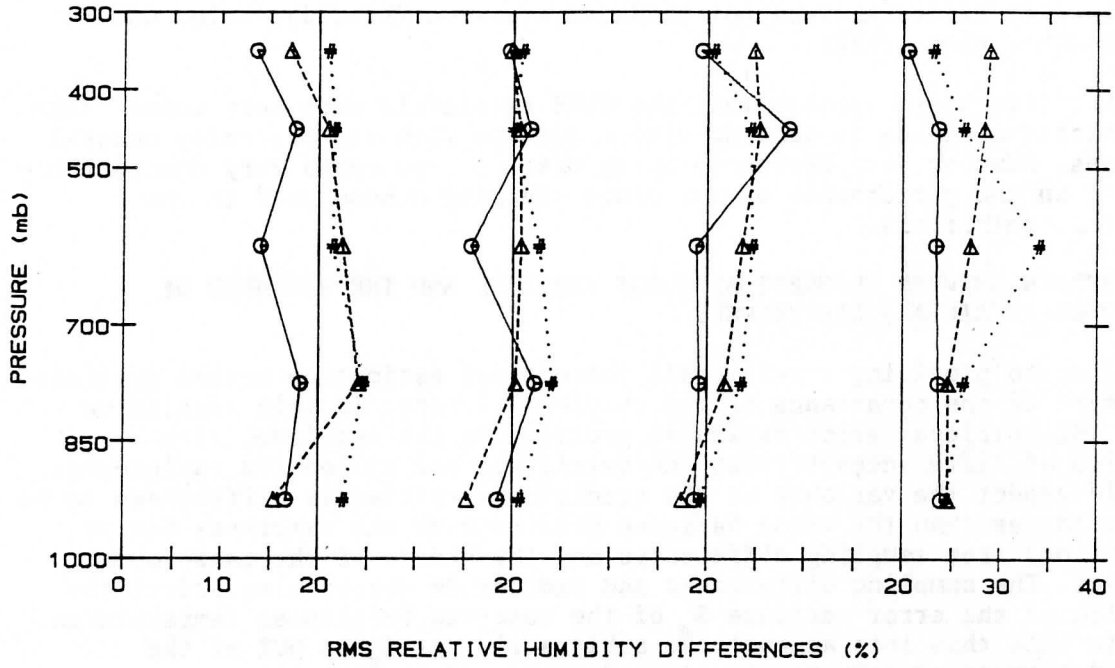

Figure 2c. RMS layer mean relative humidity differences between radiosondes and: NL0E retrievals (solid lines); HIRS statistical retrievals (dotted lines); first-guess relative humidity profile (dashed lines); when statistical cloud-clearing succeeded. From left to right, 74 clear cases, 92 scattered cases, 99 broken cases, 73 overcast cases.

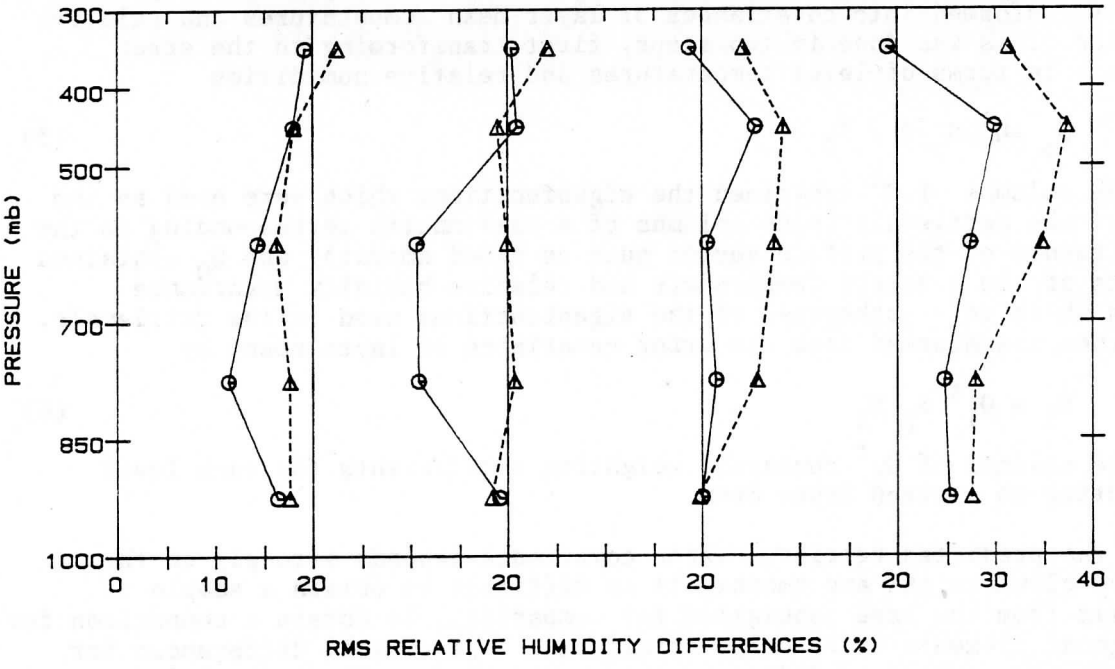

Figure 2d. RMS layer mean relative humidity differences between radiosondes and: NL0E retrievals (solid lines); first-guess relative humidity profile (dashed lines); when statistical cloud-clearing failed. From left to right, 25 clear cases, 14 scattered cases, 28 broken cases, 78 overcast cases.

cloud than those in which clear radiances were not produced. The clear cases in which clear radiances were not produced averaged 9K colder below 400 mb than the other clear cases.

It appears from these results that the NLOE retrievals were more robust than the statistical scheme in dealing with cloud and with statistically unusual situations. However, the degree to which this is true could vary considerably depending on the performance of the cloud-clearing scheme used in the statistical retrievals.

5. COMPARISON BETWEEN THEORETICAL ERROR VARIANCE AND THE VARIANCE OF (RADIOSONDE-RETRIEVAL) DIFFERENCES

In addition to providing a retrieval, the optimal estimation method provides an estimate of the covariance of the retrieval errors. In this section we compare the retrieval error estimates provided by the retrieval with statistics of differences between the retrievals and collocated rawinsondes. One would expect the variance of the (radiosonde-retrieval) differences to be somewhat larger than the error variance predicted by the retrieval due to contributions from sampling differences and the errors of the radiosondes themselves. The sampling differences and radiosonde errors also affect the estimation of the error variance S_m of the observed brightness temperatures. To try to take this into account, we arbitrarily set S_m to 50% of the (observed brightness temperature minus forward model) variance.

The error covariance of b was calculated (following Rodgers(1976)) by

$$S_b = (\Lambda^{-1} + K_n{}^t S_m{}^{-1} K_n)^{-1} \qquad (4)$$

For purposes of comparison, the temperature and moisture profile components of S_b were transformed into covariances of layer mean temperatures and relative humidities. This was done in two steps, first transforming to the error covariance in terms of level temperatures and relative humidities

$$S_p = Q^t S_b Q + S_0 \qquad (5)$$

where the columns of Q^t contained the eigenfunctions which were used as the basis for the retrievals (plus columns of a unit matrix corresponding to the other elements of the profile vector such as cloud amount), and S_0 contained the parts of the a priori temperature and relative humidity covariance matrices which were orthogonal to the eigenfunctions used in the retrievals. S_p was then transformed into the error covariance of layer means by

$$S_1 = Q_1{}^t S_p Q_1 \qquad (6)$$

where the columns of $Q_1{}^t$ contained weighting coefficients for each level contributing to a given layer mean.

Because the predicted retrieval error covariance depends strongly on the retrieved cloud height and amount, it is difficult to obtain a sample of retrievals from the same population for comparison. To obtain a comparison for the diagonal elements of S_1 only, (radiosonde - retrieval) differences for each layer were sorted according to the predicted error variance for that layer; and then sliced into six equal groups, each of which contained a relatively narrow range of predicted error variance. The variance of the

(radiosonde - retrieval) difference and the mean predicted variance were calculated for each group and plotted against each other (figures 3a - 3f). The error bars on the observed variances are 95% confidence limits assuming the samples are drawn from a normal population.

The observed 500-700 layer mean temperature variances fit the predicted values quite reasonably (figure 3b). For the two levels above 500 mb (of which one is shown in fig 3a), the observed layer mean temperature variances increased more rapidly than predicted. When the predicted 850-1000 mb temperature variance was small, it was systematically much smaller than the observed (radiosonde - retrieval) variance (figure 3c). Above 700 mb, the observed variances of (radiosonde - retrieval) layer mean relative humidity were consistently higher than the predicted ones (figures 3d,3e).

It seems likely that the differences between the error variances predicted by the retrievals and the observed (radiosonde - retrieval) variances for relative humidity and 850-1000 mb temperature are due to sampling differences, since one would expect radiosonde measurements of these quantities to be less representative than measurements of temperature above 850 mb. However, the predicted 850-1000 mb temperature variance might also be quite sensitive to the size of the correlation assumed between the surface skin temperature and the surface air temperature. Systematic errors in the retrieved cloud amount or cloud top pressure would also cause biases in the predicted error variance.

6. USE OF CLOUD INFORMATION IN RELATIVE HUMIDITY RETRIEVALS

Examination of the radiosonde data for the 1984 collocated set showed that, not surprisingly, the mean relative humidity profile in clear conditions (as determined by AVHRR) was much drier than the overall mean, while in overcast cases the reverse was true (figure 4). If one used the same a priori constraints in all cloud conditions, the a priori relative humidity profile would be systematically too wet in clear conditions and too dry in overcast conditions. Consequently, one would expect (based on the conclusions of Eyre (1987b)) a corresponding bias in the relative humidity retrievals, particularly in the lower atmosphere where the radiance measurements contain less relative humidity information. We wondered if it might be possible to improve the relative humidity retrievals by using a background relative humidity profile which depended on the cloud conditions. Although the subjective classification into four categories based on AVHRR data which was used above provides very crude cloud information, we felt that it would be adequate for a preliminary test of this idea.

The 1984 radiosonde observations were used to generate overall mean temperature and relative humidity profiles and covariance matrices, as well as separate ones for each cloud amount class obtained by sorting the data according to the AVHRR cloud estimates. A set of NOAA-10 TOVS measurements (chosen to coincide with radiosonde locations) from the same season in 1987 were sorted into the same four cloud categories based on the AVHRR imagery. Two sets of retrievals were carried out from the 1987 radiances. The first set used the overall statistics from the 1984 data as the constraint, and the second set of retrievals used different constraints for each cloud class, again calculated from the 1984 data.

When the overall 1984 statistics were used as the constraint, the clear 1987 retrievals were more than 10 % too wet (compared to the radiosondes) below 700

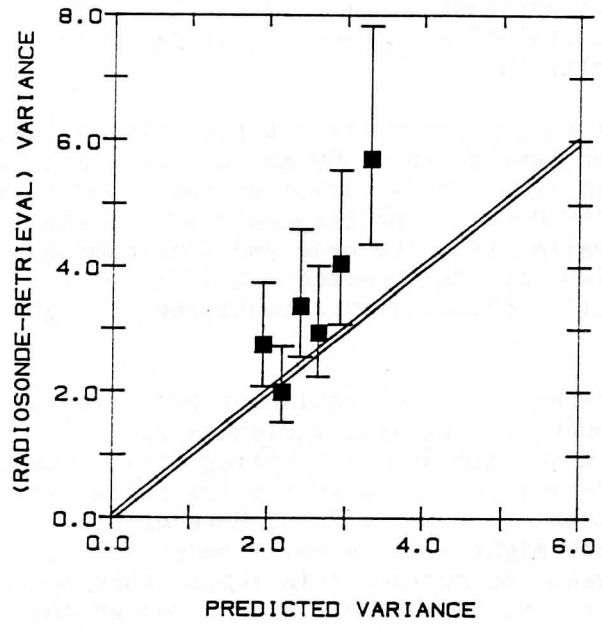

Figure 3a. Variance of (retrieved minus radiosonde) 300-400 mb layer mean temperatures vs. error variance predicted by NLOE retrievals. The x=y line is shown for reference.

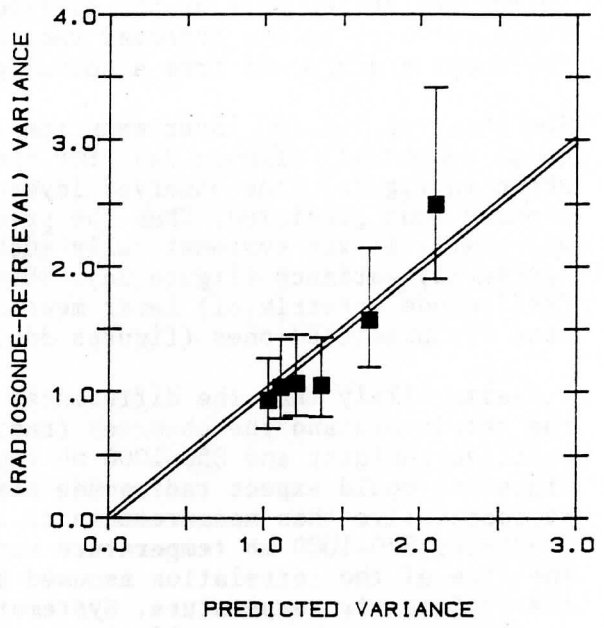

Figure 3b. As in figure 3a for 500-700 mb layer mean temperature.

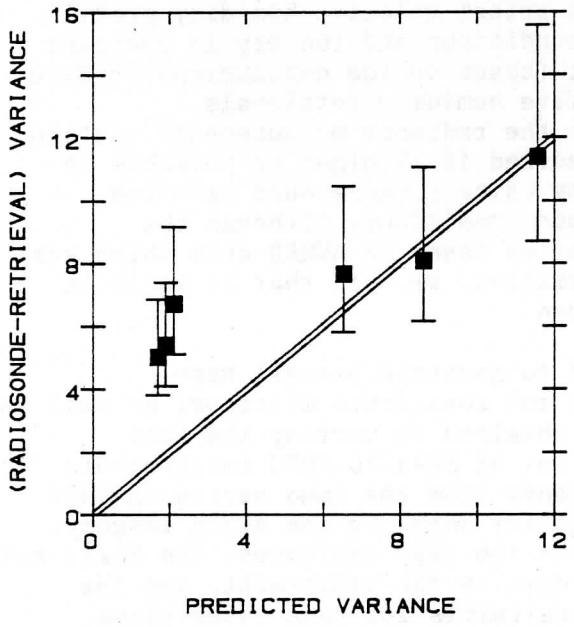

Figure 3c. As in figure 3a for 850-1000 mb layer mean temperature.

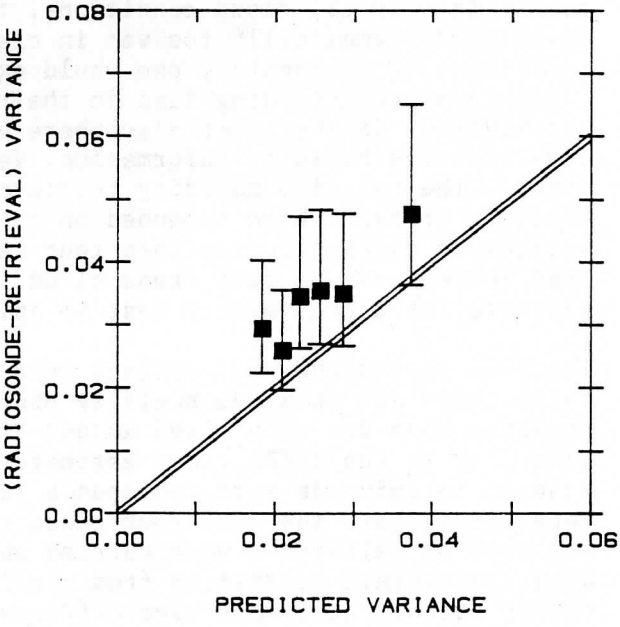

Figure 3d. As in figure 3a for 300-400 mb layer mean relative humidity.

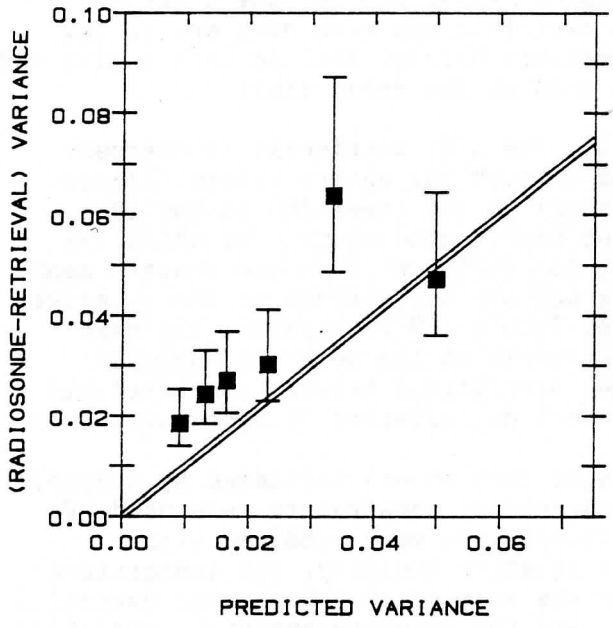

Figure 3e. As in figure 3d for 500-700 mb layer mean relative humidity.

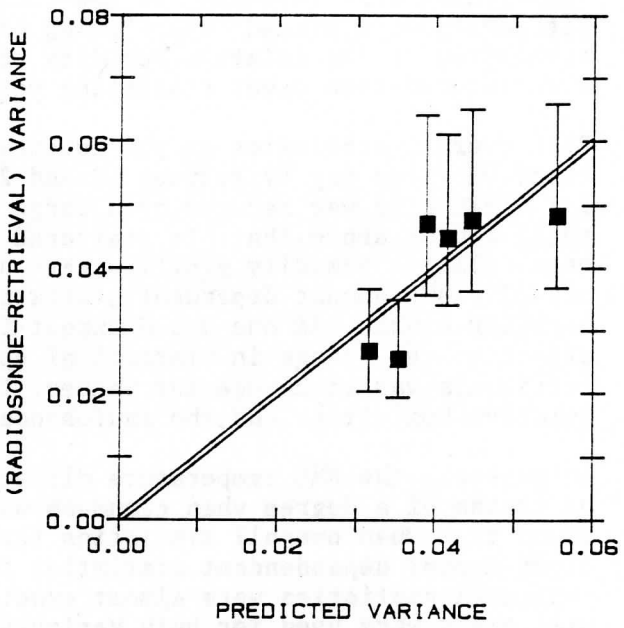

Figure 3f. As in figure 3d for 850-1000 mb layer mean relative humidity.

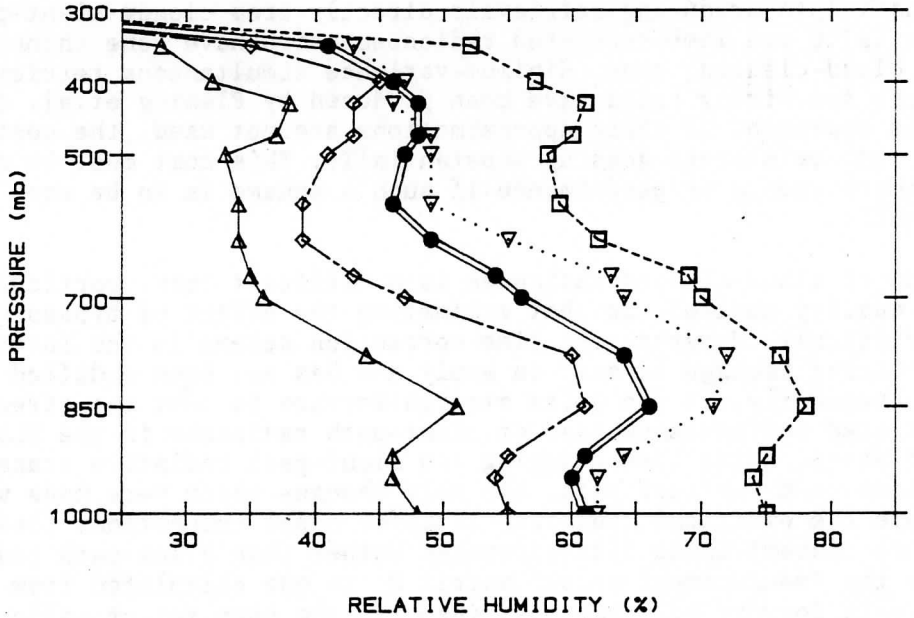

Figure 4. Mean relative humidity profiles from May-June 1984 radiosondes over eastern North America. From left to right: clear cases, scattered cloud, overall mean (double solid line),broken cloud, overcast cloud.

mb (figure 5). This bias was reduced by two-thirds when 1984 statistics from clear cases only were used as the constraint. Above 600 mb, the clear retrievals were biased toward being too dry. This may have been due to the truncation of the relative humidity covariance matrix. Bias in this region was also reduced when clear statistics were used as the constraint.

With overall statistics as the constraint, the 1987 retrievals in overcast cases were too dry by between 10 and 20% through the entire column (figure 5d). This bias was reduced by a large amount in the lower 300 mb and by a small amount above that. In scattered and broken conditions (for which the mean relative humidity profiles were not too different from the overall mean) use of cloud-amount dependent statistics had smaller effects on the relative humidity biases. As one would expect from Eyre's (1987) results, the main effect of the change in statistical constraints on the relative humidity retrievals was to change the biases. The correlations between the retrieved relative humidities and the radiosondes were not affected in most cases.

In general, the RMS temperature differences (not shown) increased by a couple of tenths of a degree when cloud-amount-dependent constraints were used. We found that when overall statistics for temperature were combined with cloud-amount dependendent statistics for relative humidity, the temperature retrieval statistics were almost exactly the same as they were when overall statistics were used for both variables, and the relative humidity statistics were essentially the same as they were when cloud-amount-dependent statistics were used for both variables. It seems reasonable that the relationship between the temperature profile and cloud amount should be much less stable (and hence less valuable as a predictor) than the relationship between relative humidity and cloud amount.

7. COMPARISON OF RETRIEVALS WITH/WITHOUT LIMB CORRECTION

An alternative to producing retrievals directly from cloudy slant-path radiances is to use limb-corrected radiances which have gone through a previous cloud-clearing step. Minimum-variance simultaneous retrievals of temperature and mixing ratio have been produced by Fleming et.al. (1986,1988) using this approach. If these approximations are not used, the cost in computer time or storage goes up substantially. This cost must be offset against improvements in performance if such a scheme is to be used operationally.

Estimation of cloud-cleared radiances is a difficult task, particularly in terms of quality control, so that estimating the effect of bypassing this step is also difficult. However, the limb-correction scheme in the International TOVS Processing Package is easy to apply and has not been modified in some years. Consequently, it was quite straightforward to test the effect of using limb-corrected radiances instead of slant-path radiances in the NLOE scheme described above. Aside from changing the slant-path radiative transfer calculations to a vertical path, the only changes which were made were to recalculate the empirical radiative transfer model corrections (brightness temperature biases) using limb-corrected rather than slant-path radiances, and to change the "measurement error" matrix S_m to one calculated from vertical-path forward calculations. (Exactly the same set of collocated measurements was used to calculate S_m for limb-corrected and non-limb-corrected observations. There was a slight increase in (observed minus forward model) variance for lower peaking HIRS channels and for MSU

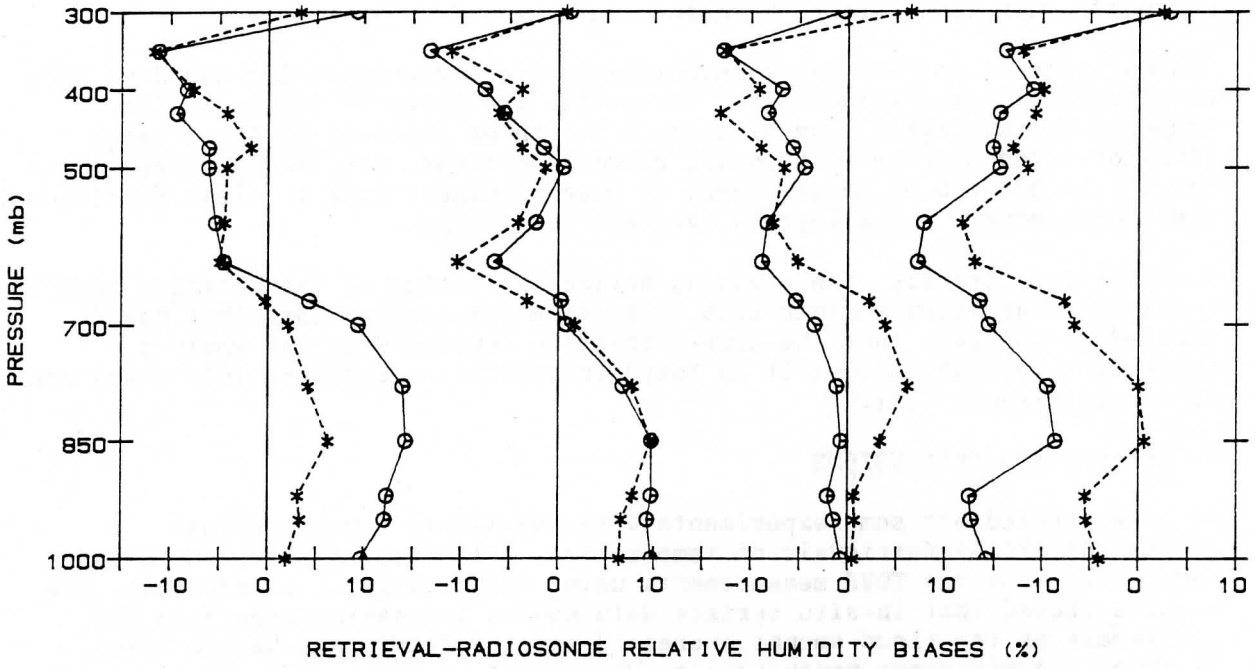

Figure 5. Biases in relative humidity retrievals using constant statistical constraints (solid lines) and using cloud-amount-dependent constraints (dashed lines). From left to right: 97 clear cases, 118 scattered cloud cases, 154 broken cases, 115 overcast cases.

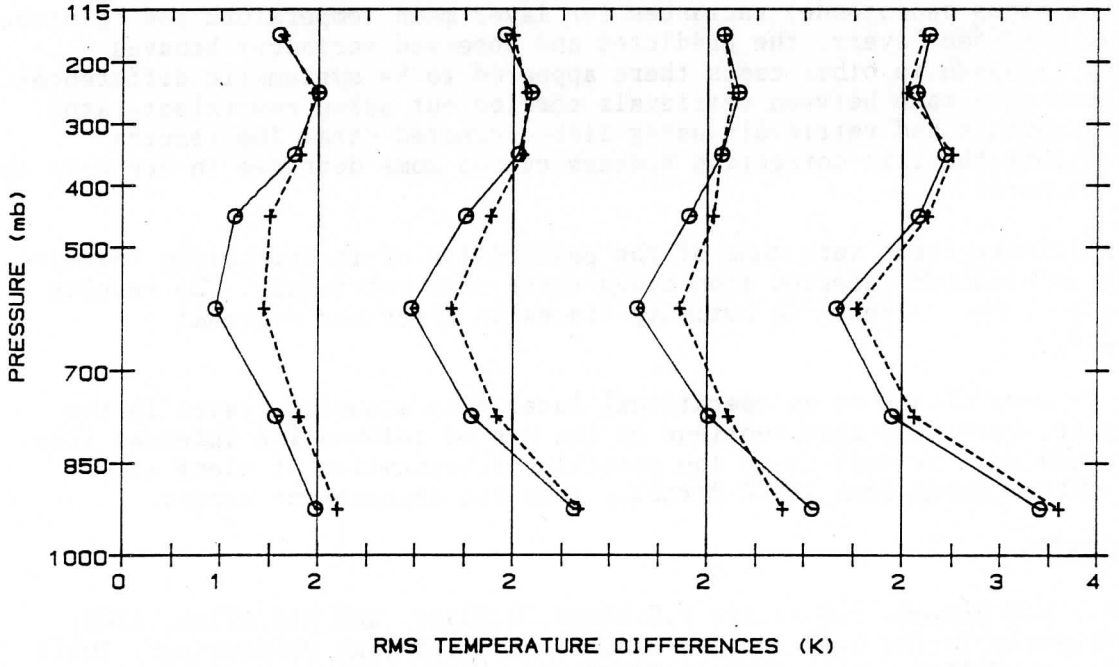

Figure 6. RMS temperature differences between radiosondes and: NLOE retrievals from slant-path radiances (solid lines); NLOE retrievals from limb-corrected radiances (dashed lines). From left to right, 99 clear cases, 106 scattered cloud cases, 127 broken cases, 151 overcast cases.

channel 2 when limb-corrected measurements were used.)

Comparisons of the RMS layer mean temperature differences for May-June 1984 retrievals with and without limb correction are shown in figure 6. The temperature retrievals from slant-path radiances improved on those using limb-corrected measurements in all cloud conditions. The largest improvement was in the 500-700 mb layer, where it reached almost 0.5K in clear conditions. The improvement was smallest in overcast conditions.

Somewhat surprisingly, there was no noticeable change in the relative humidity retrieval statistics whether limb correction was used or not. This may be related to the fact that the limb-correction routine does not apply a correction to HIRS channel 11 in "dry" conditions, a category into which many of our retrievals fell.

8. SUMMARY AND CONCLUSIONS

We have carried out some experiments with non-linear (quasi)optimal estimation (NLOE) retrievals of temperature, relative humidity, and cloud parameters from raw TOVS measurements using climatological constraints. The results showed that in-situ surface data had an increasing impact on the retrievals as the cloud amount increased and the retrievals became more dependent on microwave measurements. The amount of lapse rate information in the retrievals dropped off sharply with increasing cloud when surface data was not used. Comparisons with statistical retrievals using locally generated regression coefficients indicated that the NLOE retrievals were more robust in cloudy and unusual situations. However, this result may depend strongly on the quality of the cloud-clearing scheme used in the statistical retrievals. The retrieval error variance predicted by the NLOE method was compared with (retrieval minus radiosonde) variances for layer mean temperature and relative humidity. For some layers, the predicted and observed variances behaved similarly although in other cases there appeared to be systematic differences. Comparisons were made between retrievals carried out using raw (slant-path) TOVS measurements and retrievals using limb-corrected data. The results indicated that the limb correction process caused some decrease in accuracy in the troposphere.

Some preliminary tests were made of the possibility of incorporating relative humidity information inferred from cloud cover into retrievals. The results showed a decrease in relative humidity biases in clear and overcast conditions.

We hope to move closer to an operational local area sounding system in the coming year. Work will also continue on the use of information inferred from cloud parameters, as well as on the possible incorporation of cloud and surface measurements from AVHRR directly into the measurement vector.

9. REFERENCES

Eyre,J.R., R.W.Pescod, P.D.Watts, P.E.Lloyd, W.Adams, and R.J.Allam, 1986: TOVS retrievals in the U.K.: Progess and Plans. Technical Proceedings, Third International TOVS Study Conference (ITSC-3), Madison, Wisconsin, 13-19 August 1986, pp. 60-91. CIMSS,1986.

Eyre,J.R., 1987a: Inversion of cloudy TOVS radiances by non-linear optimal

estimation. Draft version, U.K. Met. Office 19 Branch Memo.

_____,1987b: On systematic errors in satellite sounding products and their climatological mean values. Q.J.R.Meteorol.Soc. **113**, pp.279-292.

Fleming,H.E., M.D.Goldberg, and D.S.Crosby, 1986: Minimum variance simultaneous retrieval of temperature and water vapor from satellite radiance methods. Preprint Volume, Second Conference on Satellite Meteorology/Remote Sensing and Applications, Williamsburg, Virginia, 13-16 May 1986, pp.20-23. American Meteorological Society.

_____,1988: Operational implementation of the minimum-variance simultaneous retrieval method. Preprint Volume, Third Conference on Satellite Meteorology and Oceanography, Anaheim, California, 1-5 February 1988, pp.16-19. American Meteorological Society.

Huang,H.-L.A.,and W.L.Smith, 1986: An extension of the simultaneous TOVS retrieval algorithm - The inclusion of cloud parameters. ITSC-3, pp.118-130.

McMillin,L.M., and C.Dean, 1982: Evaluation of a new operational technique for producing clear radiances. J. Appl. Meteor. **21**, pp.1005-1014.

Rodgers,C.D., 1976: Retrieval of atmospheric temperature and composition from remote measurements of thermal radiation. Rev. Geophys. Space Phys. **14**, pp.609-624.

Smith,W.L. and C.M.R.Platt, 1978: Comparison of satellite-deduced cloud heights with indications from radiosonde and ground-based laser measurements. J.Appl. Meteor. **17**, pp.1796-1802.

Smith,W.L., H.M.Woolf, C.M.Hayden, and A.J.Schreiner, 1985: The simultaneous retrieval TOVS export package. ITSC-2, Igls, Austria, 18-22 February 1985, pp.224-253. CIMSS,1985.

Steenbergen,J.D., B.T.Greaves, and T.-C. Yip, 1986: Simultaneous retrieval of temperature and relative humidity using empirical orthogonal functions. ITSC-3, pp.259-275.

_____,1987: Simultaneous physical retrieval of temperature, relative humidity, and cloud from TOVS measurements using statistical constraints. Preprint Volume, Second Workshop on Operational Meteorology, Halifax, Nova Scotia, 14-16 October 1987. Atmospheric Environment Service/Canadian Meteorological and Oceanographic Society.

Twomey,S., 1977: Introduction to the mathematics of inversion in remote sensing and indirect measurements. Elsevier Scientific, pp.139-144.

Processing of TOVS-data at SMHI

Jan Svensson
Swedish Meteorological and Hydrological Institute (SMHI)
Norrköping, Sweden

1. BACKGROUND

The work with TOVS-data at SMHI started in 1983 with the implemntation of the International TOVS Processing Package, version 2 (ITPP2). ITPP2 was used during the ONSAM Experiment ,see [1], where satellite soundings were compared to radiosondes, see [5]. A new nonlinear, physical inversion method THAP was developed at SMHI and included in our version of ITPP2. Due to the cloud-clearing algorithm in ITPP2, we were only able to test THAP for clear retrievals, see [6],[7] and [8]. The cloud-clearing algorithm in ITPP3 was more suitable for us, and we incorporated THAP in our version of ITPP3, see [9] and [10]. Until now we have used climate as first guess, with the possibility to include analyzed tropopause height.

In 1985 a coordinated Nordic research project, the HIRLAM-project [1], was started. An improved utilization of TOVS data was given high priority within the HIRLAM-project. A data assimilation experiment with TOVS-data, using THAP, was carried out, see [4]. This data assimilation experiment was using historical data from May, 1983. The purchase of a satellite data receiving and processing station PROSAT [2], giving us TOVS-data in real-time, started some years ago. Due to problems with subcontractors, it was delayed but now it has been installed at SMHI. PROSAT is described in [2] and [3]. A description of the computer system of SMHI, including the interconnection to PROSAT, is shown in Figure 1.

[1]HIRLAM= HIgh Resolution Limited Area Model

[2]PROSAT=PROcessing system for meteorological SATtellite data

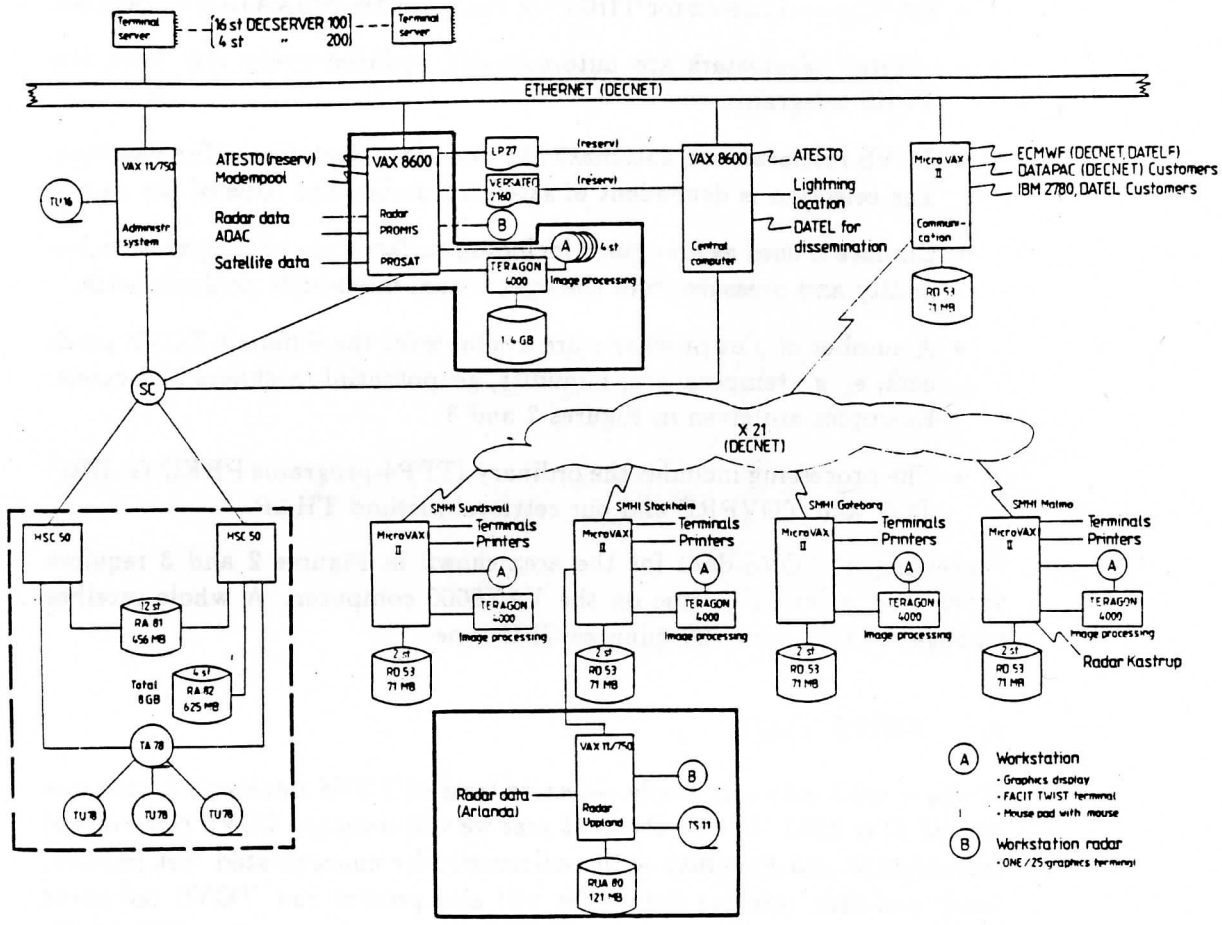

Figure 1: The computer system at SMHI

2. REAL-TIME PROCESSING OF TOVS DATA

The satellite data receiving and processing system PROSAT is located at SMHI in Norrköping ($58°N$,$16°E$). PROSAT includes receivers for the polar NOAA-satellites and the geostationary METEOSAT. The host computer for PROSAT is a VAX8600. For each NOAA passage, PROSAT automatically extracts TIP-data from the HRPT Minor Frames (see [11]). The TOVS processing system includes the following facilities:

- Satellite coefficients for TIROS-N and NOAA6–NOAA10 are available.
- Orbital parameters are automatically updated every day from the TBUS telegrams.
- TOVS retrievals are automatically done for selected satellite passages. The selection is dependent of satellite number and time of the day.
- Climate is used as first guess including surface data of temperature,humidity and pressure from the operational meso-scale analysis fields.
- A number of plot programs are available for the different TOVS products, e. g. temperature, humidity, geopotential thickness and ozone. Examples are given in Figures 2 and 3.
- The processing includes the ordinary ITPP4-programs PREING, INGTOV and TOVPRE and our retrieval method THAP.

Processing of TOVS-data for the area shown in Figures 2 and 3 requires appr. 8 minutes CPU-time on the VAX8600 computer. A whole satellite passage requires appr. 20 minutes CPU-time.

3. FUTURE PLANS

We have until now only made objective tests of TOVS retrievals during one period; May 1983. During the next year we will compare TOVS retrievals of temperature and humidity with radiosondes for concentrated test periods, using real-time satellite data. We will also present raw TOVS radiances and processed TOVS products on the image processing system of PROSAT. With this image processing system, we are able to combine TOVS data with e. g. forecast fields and AVHRR pictures. These images will be used by the operational forecasters. The usefullness of TOVS images for the operational forecaster will be evaluated.

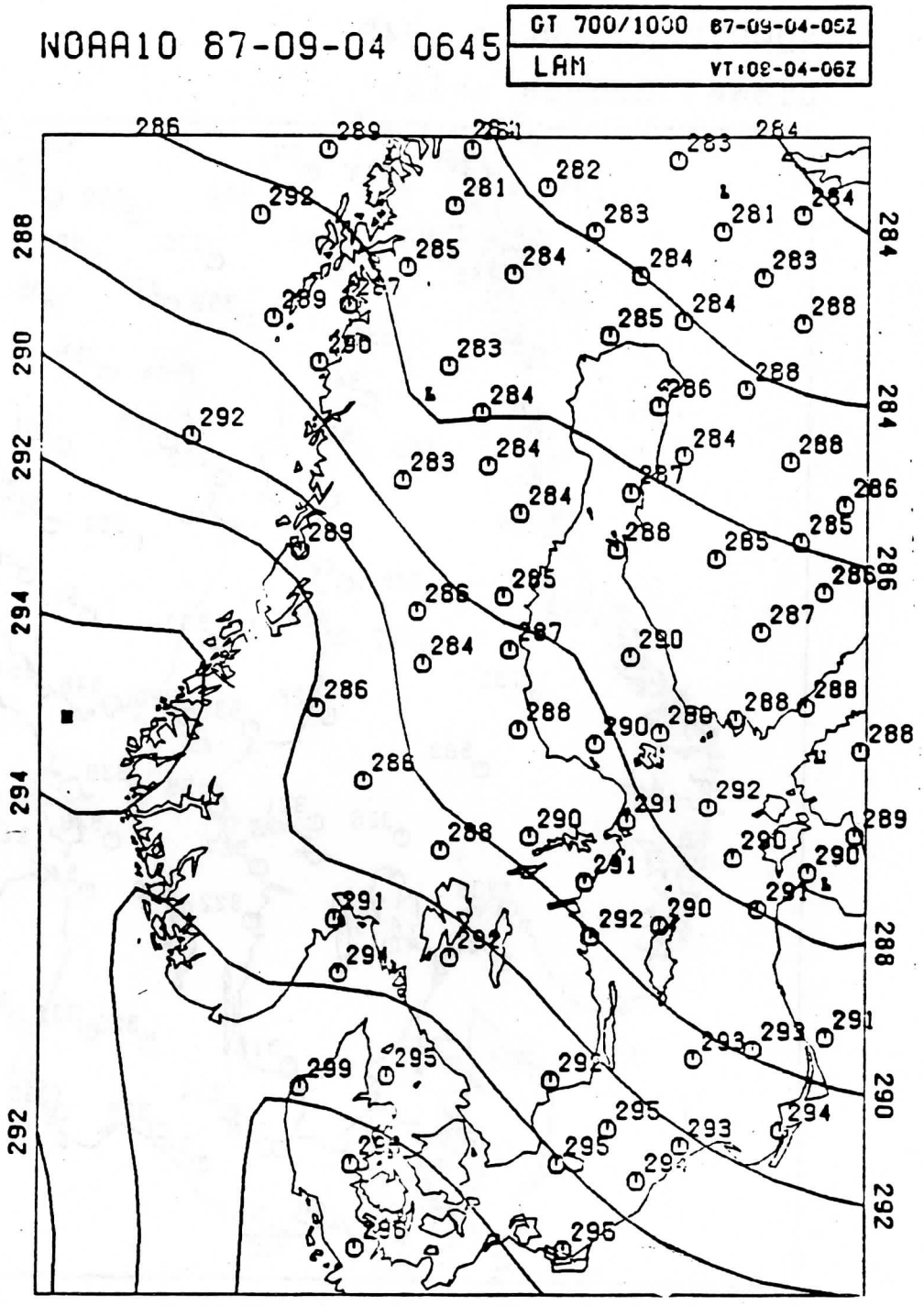

Figure 2: Geopotential thickness 700–1000 hPa. TOVS retrievals compared to the operational LAM-analysis.

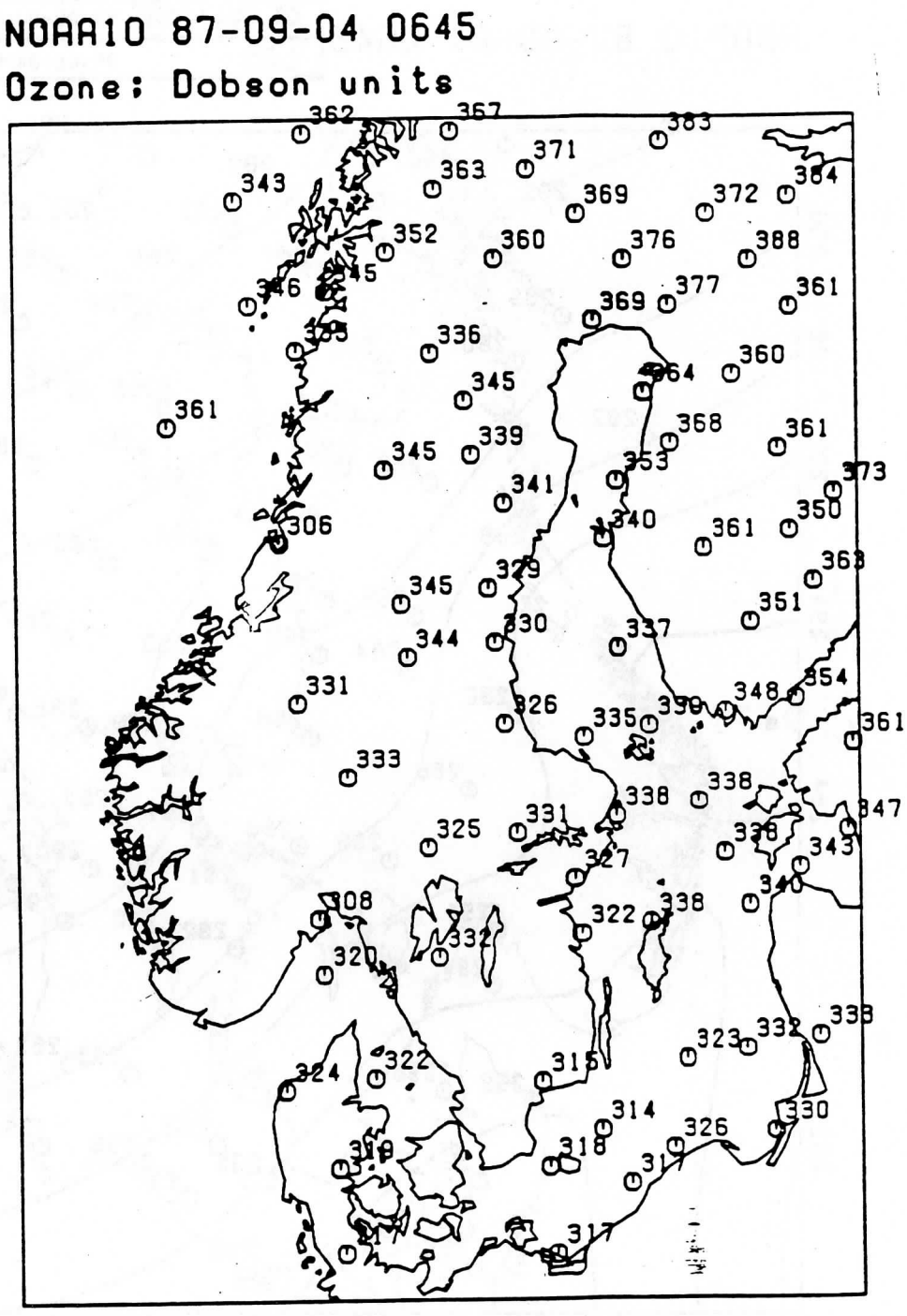

Figure 3: Ozone retrievals from TOVS-data

The work with the integration of TOVS retrievals and HIRLAM data assimilation will continue. The aim is to use TOVS-data operationally in HIRLAM starting in 1989/90.

In June, 1988, NABAS [3] will arrange a symposium in Norrköping on the processing of TOVS-data in Northern latitudes.

REFERENCES

[1] Askne, J. , G.Elgered, H.Nordius, G.Skoog, E.Winberg, A.Hågård, E.Andersson, N.Gustafsson, J.Svensson and I.Carlsson,1987: The ONSAM Experiment: Remote Sensing Techniques for Vertical Sounding of the Atmosphere.*Journal of Atmospheric and Oceanic Technology* , 4, 180–190.

[2] Dahlström, B.(ed),1988: Annual Report 1986–87. *PROMIS Reports 7,* SMHI, Norrköping, Sweden, 25 pp.

[3] Karlsson, K-G.,1988: Development of an operational cloud classification model.*International Journal of Remote Sensing*, (special issue from the Third AVHRR Data User's Meeting in Oxford, December 16–18,1987, to appear)

[4] Gustafsson, N. and J.Svensson,1988: A data assimilation experiment with high resolution TOVS data. *HIRLAM Technical Report 9*, SMHI, Norrköping,Sweden,37 pp.

[5] Svensson, J.,1984: Temperature profile retrievals from TIROS Operational Vertical Sounder during the ONSAM-experiment. *R&D notes 33*, SMHI, Norrköping, Sweden, 13 pp.

[6] Svensson, J.,1985: Remote sensing of atmospheric temperature profiles by TIROS Operational Vertical Sounder.*RMK 45*, SMHI, Norrköping, Sweden, 61 pp.

[7] Svensson, J.,1985: Numerical treatment of an ill-posed problem in remote sensing of atmospheric temperature profiles. *Report LiU-TEK-LIC-1985:23*, Dept of Mathematics, Linköping University, 69 pp.

[3] NABAS=working group for the utilization of satellite data with participation from the meteorological institutes in Denmark, Finland, Norway and Sweden.

[8] Svensson, J.,1985: A nonlinear Inversion Method for Derivation of Temperature Profiles from TOVS-data. *Technical Proceedings of The Second International TOVS Study Conference,Igls,Austria,February 18–22, 1985*, 292–307.

[9] Svensson, J.,1986: Estimating the Correct Degree of Smoothing in the Simultaneous Retrieval Method. *Technical Proceedings of The Third International TOVS Study Conference, Madison, Wisconsin, August 13–19, 1986*, 276–282.

[10] Svensson, J.,E. Andersson and N. Gustafsson,1987: Towards an operational TOVS processing package. *R&D notes 50*, SMHI, Norrköping, Sweden, 18 pp.

[11] Werbowetzki, A. (ed.), 1981: Atmospheric Sounding User's Guide. *NOAA Technical Report NESS 83*, U.S.Department of Commerce, National Oceanic and Atmospheric Administration, National Earth Satellite Service, Washington D.C., 82 pp.

The Effect of Collocation Radiosonde Errors on the Assessment of the Performance of a Physical Retrieval Estimator

MICHAEL J. UDDSTROM

New Zealand Meteorological Service
PO Box 722, Wellington, New Zealand

10 March 1988

1. INTRODUCTION

A necessary prerequisite to the development of a physical retrieval estimator is the requirement that, for a given atmosphere and observing radiometer, radiative transfer in the atmosphere can be modelled to "sufficient" accuracy and precision. Defining what accuracy is "sufficient" is to some degree dependent upon the way a particular retrieval algorithm uses the satellite observations, but the precision of the radiative transfer model should ideally be no worse than the radiometer instrumental measurement errors. If this prerequisite is satisfied then it is expected that physical retrieval schemes will outperform standard regression estimation, if only for the reason that more a priori information can be incorporated into a physical algorithm.

The problem of the indeterminacy of "errors" in the NESDIS fast transmittance model, and the resulting effects on a particular type of physical retrieval estimator will be demonstrated. The retrieval algorithm employed for the analysis is the Typical shape function Maximum a posteriori Simultaneous (TMS) sequential physical algorithm developed in Uddstrom (1988). This estimator utilizes pattern recognition to determine a first guess profile, and the simultaneous retrieval equations are solved using statistical constraints pertinent to the class of atmosphere described by the chosen first guess profile.

2. EXPERIMENT DESIGN

Two kinds of data were employed in this experiment. As the TMS algorithm requires very large samples of a priori data, the retrieval constraints were developed using the radiosonde data archive of the New Zealand Meteorological Service. For each month of the year more than 5000 solar radiation error corrected profiles, from all southern latitudes can be utilised to determine Typical Shape Function (TSF) (Uddstrom and Wark, 1984) a priori first guess profile estimates and retrieval constraints. From the resulting TSF samples, TMS radiance discrimination equations and radiance dependent retrieval constraints were developed using the NESDIS fast parameterised model for the radiative transfer equation (rte). The coefficients and γ values employed were those supplied in the VAX release of the International TOVS Processing Package (ITPP).

The second data set, provided by Dr L. McMillin of NOAA/NESDIS, consists of a global sample of NOAA 7 and 8 satellite observations collocated with solar corrected radiosonde data. The satellite data have been corrected to clear radiance temperatures, and reduced to equivalent nadir measurements. The associated NESDIS (operational) regression retrievals are also given. The collocated data were collected over a period of one year (1983/84) and consist of

some 6000 profiles. Both the TSF, and collocation sample radiosonde temperature profiles were extrapolated to 0.1 hPa using the zonal regression method supplied in the ITPP.

Given the TMS TSF classes for a particular month (in this case, July) and a specific satellite, these same classes can be duplicated in the collocation data set for the same month, by the method given in Uddstrom (1988). However, because of the smallish size of the monthly samples, data from adjacent months had to be included, and northern hemisphere observations were shifted in time by 6 months. Fifteen percent of the collocated sample data, chosen at random, were then set aside as independent data.

For an example month, the collocation (duplicated) TSF sample means are given in fig 1. Using these samples, airmass dependent corrections for the rte modelled radiance temperatures may be computed, and applied to satellite observations used by the TMS retrieval algorithm.

Consequently, three types of retrieval error statistics can be considered: those arising when the TMS algorithm is applied to the rte radiances (suitably perturbed by measurement noise), and those calculated from retrievals by either the TMS or the NESDIS estimators using the satellite observations.

3. ESTIMATION OF RTE MODEL ERRORS

a. *Delta estimation*

The usual method employed to determine rte model errors relies on computing differences between satellite observed radiances and those generated by an rte model from the associated collocated radiosonde observations. Hence, for a given atmosphere and rte model, equivalent satellite observations are estimated according to (1).

$$\hat{\mathbf{T}}^{sat} = \mathbf{T}^{rte} + \boldsymbol{\delta} \tag{1}$$

Where $\hat{\mathbf{T}}^{sat}$ is an estimate of the vector of radiance temperatures the satellite radiometers would measure if the atmosphere in question had been observed, $\mathbf{T}^{rte}$ is the rte model radiance temperature vector generated for that atmosphere, and $\boldsymbol{\delta}$ is a vector of empirically defined corrections for the rte model. Further, the standard deviations of the δ_i (i=1,2...n, for n channels) estimates indicate the precision with which $\hat{\mathbf{T}}^{sat}$ can be computed and therefore the effective "measurement" noise to be used in any optimal physical retrieval algorithm.

Here, the $\boldsymbol{\delta}$ vectors may be calculated as a function of TSF identified airmasses. Accordingly (1) can be recast to reflect this additional refinement, in which case;

$$\hat{\mathbf{T}}^{sat}_{TSF} = \mathbf{T}^{rte} + \boldsymbol{\delta}_{TSF} \tag{2}$$

If the individual TSF class $\boldsymbol{\delta}_{TSF}$ vectors are not significantly different, then (1) will suffice, otherwise airmass dependent $\boldsymbol{\delta}$ corrections should be employed in the retrieval algorithm. In the case of the TMS retrieval estimator, where all retrieval constraints are computed in terms of model radiance temperatures [$\boldsymbol{\delta}_{TSF} = \mathbf{0}$], the satellite radiance temperatures are in fact converted to equivalent model radiance temperatures.

The mean values, standard deviations and standard errors of a selection of individual channel δ_{TSF} estimates are plotted in fig 2. Both day and night results are shown, for each of the TSF classes (as identified in fig 1). Considering the general characteristics of these results first, it is evident that whilst the HIRS δ values are similar for TSF classes having similar mean profiles,

there are significant differences for some of the airmass types, for example, classes 21 and 22. Interestingly though, the MSU δ corrections are in all cases rather small, as are the associated class standard deviations. The between class differences are significant in a number of cases, but the δ estimates are, by and large, well defined having small sample standard deviations relative to the expected (0.3 K per IFOV) channel measurement noise. However, apart from these channels, the expected noise in the δ estimates is disappointingly large, relative to both the measurement noise characteristics of the HIRS and the within TSF class radiance temperature variances.

There are clear and systematic differences between the day and night statistics for some of the classes and channels, e.g., class 311. However the most noticable features in the day and night $\boldsymbol{\delta}_{TSF}$ vector differences relate to the surface and near surface channels. For daylight observations these channels show a positive bias relative to the computed radiances whilst the night values show a bias of the opposite sign (see, e.g., channel 8). There are a large number of continental soundings in the collocation sample so this sign change is presumably due to the skin effect. The night soundings often have substantial surface inversions.

Those channels which have an important upper stratospheric component (i.e. channels; 1, 2 and 17) are susceptible to radiosonde extrapolation errors, as demonstrated by the results for channel 1 in fig 2. It would seem that profiles having warm stratopauses are not well extrapolated by the ITPP equations (i.e., classes 12, 22, 32, 41, 42 and 43). This is surprising, since these atmospheres tend to be more tropical in origin, where the atmospheric temperature variance in the middle stratosphere is smaller than that of mid-latitudes and polar atmospheres.

Two further contributing factors to noise in the $\boldsymbol{\delta}_{TSF}$ vectors can be identified, even assuming perfect cloud clearance, correction to nadir and collocation data interpolation. The first is the absence of surface information in the collocation data set (apart from surface height) and the second is the inherent limitation in the standard NESDIS transmittance algorithm, where pressures greater than 1000 hPa are not permitted. The first problem was resolved through estimating the surface pressures, temperatures and mixing ratios from a mean sea level pressure climatology and the radiosonde profiles and surface height information. Although this approach doesn't solve the problem, it should remove some of the noise variance arising from this source. The second problem requires further research, although a simple approach is to employ an extrapolation technique (e.g. piecewise continuous cubic splines) to infer the transmittance at the surface pressure and hence compute appropriate radiance temperature corrections.

However, inherent to the delta approach for determining "errors" in an rte model is the implicit assumption that the sample of collocated radiosondes suffers only from random, zero mean, measurement errors. This would be a satisfactory assumption if the collocation sample used only one kind of radiosonde, or all radiosondes in the sample had been adjusted in some uniform way so as to effectively reduce them to some "standard" radiosonde type. However, results from the WMO International Radiosonde Intercomparison (Nash and Schmidlin, 1987) indicate that significant between sonde biases exist, in part because radiosondes are affected by short and long wave radiation in different ways. Since these errors tend to be correlated in the vertical, they may contribute as much as 1 degree of more to the $\boldsymbol{\delta}_{TSF}$ estimate variances for night time observations alone (see Nash and Schmidlin, Table 11.1), in addition to causing erroneous estimates of the $\boldsymbol{\delta}_{TSF}$ vectors. The radiosonde bias errors are not limited to the stratosphere either; significant differences exist at all standard levels. Obviously, the day time differences will be even larger because of the rather more variable solar radiation effects. Uddstrom (1988b) has found between sonde temperature biases as large as 1.5 degrees (see fig 3.), from a comparison of Väisälä RS80 DIGICORA data with Philips RS4 (similar to the VIZ sonde) data, corrected to effective night time values.

b. *An alternative correction method*

If the radiosonde data in collocation samples cannot be corrected to yield measurements equivalent to some standard radiosonde, because either the particular radiosondes employed are unknown, or consistency corrections do not exist for all of the sondes utilized, then the δ method determination of "errors" in the rte model radiance temperatures is untenable. This is for two reasons. Firstly, the δ corrections will always be erroneous, leading to what appear to be incorrect retrievals, when compared with the collocated radiosondes, and secondly the "apparent" measurement noise, the sum of both instrumental and δ estimation noise, will be so large that all retrievals will lie close to the first guess estimates.

An alternative approach to this problem is to estimate equivalent rte model radiance temperatures from the observed radiances (as required by the TMS estimator) in such a way that the errors to which the δ estimation procedure is susceptible are minimised. This is easily arranged, in principle, by rewriting the correction equation as:-

$$\hat{\mathbf{T}}^{rte}_{TSF} = \mathbf{D}_{TSF}\mathbf{T}^{sat} + \mathbf{C}_{TSF} \tag{3}$$

where $\mathbf{D}_{TSF}$ and $\mathbf{C}_{TSF}$ are respectively the regression coefficient and constant matrices derived from the dependent TSF class samples. In the following discussion, this will be called the **D** method.

For a regression on all channels except 9, 20 and 21—implying therefore, perfect cloud clearance of the satellite observed radiances—the resulting rms error (and bias) statistics for (3) applied to the independent collocation data, are given in fig 4a. The same error statistics for the δ_{TSF} method of (2) applied to the independent data are plotted in fig 4b. With only a few exceptions, the rte radiance temperature estimates derived from (3) are superior to those derived from (2).

This result is perhaps a little surprising, given the generally small samples used to derive the **D** equations, and the gross cloud clearance assumption. However, the **D** method of computing rte model "errors" does have a number of advantages when it is known a priori that the "truth" radiosonde profiles are, in reality, variably biased estimates of the true state of the atmosphere. Because a component of radiosonde error is vertically correlated, using more than one channel's information to fit the rte model "error" should yield better error correction equations, when the results are validated against the biased data. Therefore, this method may only be useful for collocation samples where the radiosonde data have not been reduced to some common standard. In practice a combination of the δ and **D** methods could be employed in order to reduce the impact of possible undesirable side effects resulting from the **D** method, such as the propagation of cloud contamination errors into channels not previously affected.

4. RETRIEVAL RESULTS

a. *NESDIS method*

Plotted in fig 5 are error statistics for the operational NOAA/NESDIS retrieval scheme and the independent data. As expected, the sample standard deviation statistics indicate that the regression retrievals, in general, display less sample variance than that in the "true" sample.

In considering the rms error results, it is important to keep in mind the problem of radiosonde errors discussed in the previous sections. Since the regression retrieval coefficients are derived from the NESDIS collocation archive, the resulting equations will also have the property

that they minimise the effect of errors arising from radiosonde data bias problems. Regression retrievals, although in error, because they faithfully reproduce a proportion of the radiosonde bias errors, will appear to be accurate when compared with the collocated (biased) radiosondes!

b. TMS retrieval results

Three kinds of TMS retrieval results can be constructed from the collocation data; in the first, retrievals are computed from rte radiances, suitably perturbed by Gaussian noise, commensurate with the expected measurement noise values of the radiometers. The second kind utilizes satellite radiances, adjusted by the TSF dependent δ_{TSF} correction method, while the third uses satellite radiances adjusted by the $\mathbf{D}_{TSF}$ correction scheme described by (3).

Results from the first approach define the inherent accuracy of the retrieval algorithm and remove any effects due to radiosonde biases, because in this case the radiosonde does define the "truth". With the second approach, errors in the ground truth are propagated into the retrieval error statistics in a number of ways. Contributions arise from incorrect estimates of the δ rte correction vectors, degradation of the information in the satellite observations through the necessity of using large "measurement" noise estimates relative to those fundamental to the measurement process, and comparison of the retrieved profiles with a biased estimate of the true state of the atmosphere. The third method produces retrievals which are not so severely affected by collocation sample radiosonde biases, in so far as they affect the problem of estimating rte and collocation radiosonde bias errors. Also the "apparent" between channel error covariances are reduced.

Results for the first method, using the TMS estimator and two different sets of TOVS radiance observations are given in fig 6. In both examples the a priori information used to constrain the solution is determined from Bayesian discrimination equations defined on channels 24, 2, 3, 4, 5, 23 and 12. In fig 6a, the retrieval estimator made use of only channels 8, 24, 23, 22, 2, 4, 5 and 6, and the solution was iterated twice. Fig 6b demonstrates the results for a more complex four pass estimator where in the first pass a log(pcw) representation (Uddstrom, 1988) of the simultaneous retrieval equations is applied for channels 18, 12, 11 and 10, then a simple non log(pcw) representation of the equations is employed for channels 18, 12, 10, 1, 2, 24, 3, 23, 4, 5, 6, 7, 8, 16, 15, 14 and 13, and this latter selection is iterated twice more. Clearly, the rms error statistics for the second TMS estimator are superior to those of the first, as would be expected. In particular the water vapour retrievals are substantially improved as are the temperature errors in the lower troposphere. Of course, because there is no error due to skin effect problems in these results, the retrieval of the surface information is good.

When δ_{TSF} corrected satellite observed radiances are employed in the TMS algorithm, and the same channels as the estimator of fig 6a are used, the accuracy of the results, as defined by the differences between the collocated radiosondes and the TMS retrievals is substantially reduced (fig 7). A component of this error is however fictitious, since the TMS satellite retrievals do not produce profiles which include the radiosonde bias effects. Even allowing for this fact, the temperature and thickness errors of the NESDIS and TMS algorithms are not too dissimilar, except near the surface where the NESDIS results are superior (see fig 5). The NESDIS water vapour retrievals are better than the TMS results. The variance in the retrieved samples (not shown) is significantly less than that in the "true" sample.

Additional experiments were attempted in order to improve upon the TMS estimator results given in fig 7. For example, more and different selections of channels were used, and the δ_{TSF} corrections were modified so as to combine day and night estimates for channels where solar radiation was not expected to have an important effect (i.e., excluding channels 7, 8, 13, 17, 18

and 19). However, no major improvements in the error statistics occurred. These experiments only underlined the fact that the physical estimator is, not unexpectedly, sensitive to the choice of the δ_{TSF} vectors.

However, using radiances corrected by the **D** method of (3), and a TMS estimator identical to that used to derive the fig 7 statistics, results in important improvements in the rms error statistics at nearly all levels. The improvement in the lower troposphere is especially pronounced, as demonstrated in fig 8.

In fig 9 some example retrievals are displayed for NESDIS, TMS from satellite observations (both δ_{TSF} and $\mathbf{D}_{TSF}$ corrected) and TMS from noise contaminated rte radiance temperatures. The most noticable difference between the TMS (δ_{TSF} corrected) and NESDIS retrievals, is that the regression algorithm appears to make better use of the near surface channels. However the situation is reversed for the TMS retrievals computed from the **D** method corrected satellite observation, even though the TMS retrieval estimators were identical in both cases.

The retrieval at 35°S 58°W, computed from one of the outermost (NESDIS) retrieval boxes, is included to demonstrate the kind of errors that result when the observed radiances simply do not agree with those computed from the rte model. For this example, there is a simple linear shift between the retrieved temperature profiles and the radiosonde measurements. Whether this is due to bias errors in the radiosonde data, or perhaps the nadir correction algorithm, is unclear.

In other regards, the TMS and NESDIS retrievals, for these examples, show striking similarities except perhaps for the retrieval at 66°S 14°E, where the TMS algorithm has more faithfully reproduced the structure of the tropopause. The TMS retrievals computed from the synthetic radiances do however demonstrate that, in principal,there is sufficient information in TOVS radiances to compute accurate temperature and water vapour profiles.

5. DISCUSSION AND CONCLUSIONS

If errors due to undetected or incorrectly identified clouds, nadir correction methods and collocation data interpolation are excluded, two important sources of error remain for physical retrieval estimator algorithms. The first of these arises because rte models are unable to accurately and precisely simulate infrared satellite observations. Consequently, in order to bring the modelled and measured observations into agreement—a prerequisite of all physical retrieval algorithms—some adjustment scheme must be developed so that effective rte radiance temperatures can be estimated from the satellite observed measurements (or vice versa). As a further complication to this problem, it is apparent that these corrections are airmass dependent. The second, and associated problem relates to what is regarded as the "truth" when determining corrections for rte models. Empirically derived δ radiance temperature adjustments will always yield bad estimates of rte model errors if the collocation sample from which the correction vectors are derived is not homogeneous. Any inhomogeneities in the collocation sample will additionally decrease the precision of the δ estimates, forcing the retrieval algorithm to reduce the weight attached to the observed radiances and so degrade the value of the direct measurements. As a consequence, the variance in retrieved profile samples will be reduced because the retrieval solutions are always forced to lie close to the first guess profiles. Therefore, airmass dependent δ correction terms (and their variances) can, properly, only be calculated from samples of collocated radiosondes which have systematically been reduced to some effective "common radiosonde", because the channel measurement and modelling errors are assumed to be independent. Unfortunately there is no space in the present WMO Upper Temps code for radiosonde make, model and processing information, and the WMO catalogue of "Radiosondes

in use by members" (see e.g. WMO, 1982) is invariably out of date and sometimes inaccurate. For these reasons it may be impossible to make consistency corrections to the standard NESDIS collocation archive.

Accordingly, regression retrieval algorithms, which minimise the effects of errors introduced by radiosonde dependent measurement biases, will have an apparent advantage over physical retrieval schemes utilizing δ type rte model corrections, when their respective outputs are compared with collocated radiosondes.

The **D** correction method, in effect a generalisation of the δ scheme, is, in principle a better estimator of rte "errors", since the corrections are derived from all the available information. However, this regression estimator may also produce undesirable side effects if the observed data do not satisfy the assumptions implied in the development of the **D** equations.

To further underline the importance of the radiosonde bias problem, it has been possible to demonstrate that these errors have a measurable effect on the performance of a a primitive equation NWP model. When all radiosonde data used in the New Zealand Meteorological Service optimal interpolation analysis scheme were adjusted to make them "look like Väisälä RS80" radiosondes (by the method given in Uddstrom, 1988b), the NWP 6 hour verification statistics (against observed data) showed improvements at most levels. The bias error statistics for heights improved by as much as 50% at 200 hPa and above. Even at the surface, the model showed a 0.2 hPa performance improvement (Purnell and Revell (1988) pers. comm.).

Therefore, perhaps proper assessment of the relative merits of both physical and regression retrieval algorithms must await the arrival of a quality controlled set of collocation data, where the coincident radiosonde data have been reduced to some equivalent "standard". It is to be hoped that the Base line Upper Air Network will provide a data set having these properties.

REFERENCES

Nash J. and F.J. Schmidlin, 1987: WMO International radiosonde comparison (U.K. 1984, U.S.A. 1985) Final Report, *Instruments and Observing Methods Rep No. 30*, 103pp

Richner, H. and P.D. Phillips, 1982: The radiosonde intercomparison SONDEX Spring 1981, Payerne. *Pure and Appl. Geophys.***120**, p852-1198

Uddstrom M.J., 1988: Retrieval of atmospheric profiles from satellite radiance data by typical shape function maximum a posteriori simultaneous retrieval estimators. In press *J. Appl. Meteor.*

Uddstrom M.J., 1988b: A comparison of Philips RS4 and Väisälä RS80 Radiosonde Data. Submitted as a Note to *J. Atmos. Oceanic Tech.*

WMO, 1982: WMO catalogue of radiosondes in use by members. *Instruments and Observing Methods, Rept No 11, Upper-Air data compatibility* 19pp

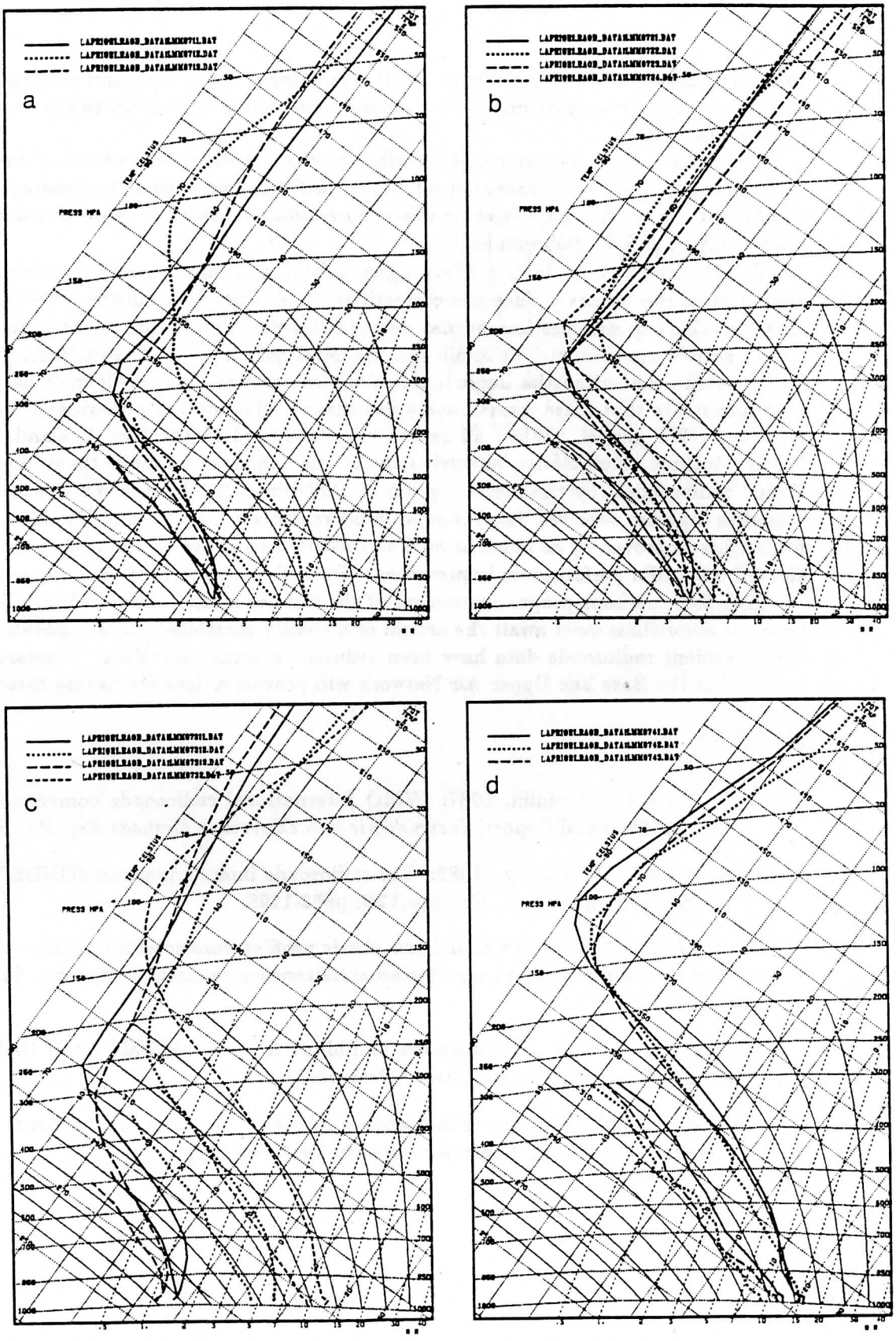

Fig.1. Mean profiles for winter, TMS duplicated, TSF samples of collocation radiosonde data. Panel (a) is classes 11, 12 and 13; panel (b) is classes 21, 22, 23 and 24; panel (c) is classes 311, 312, 313 and 32; and panel (d) is classes 41, 42 and 43.

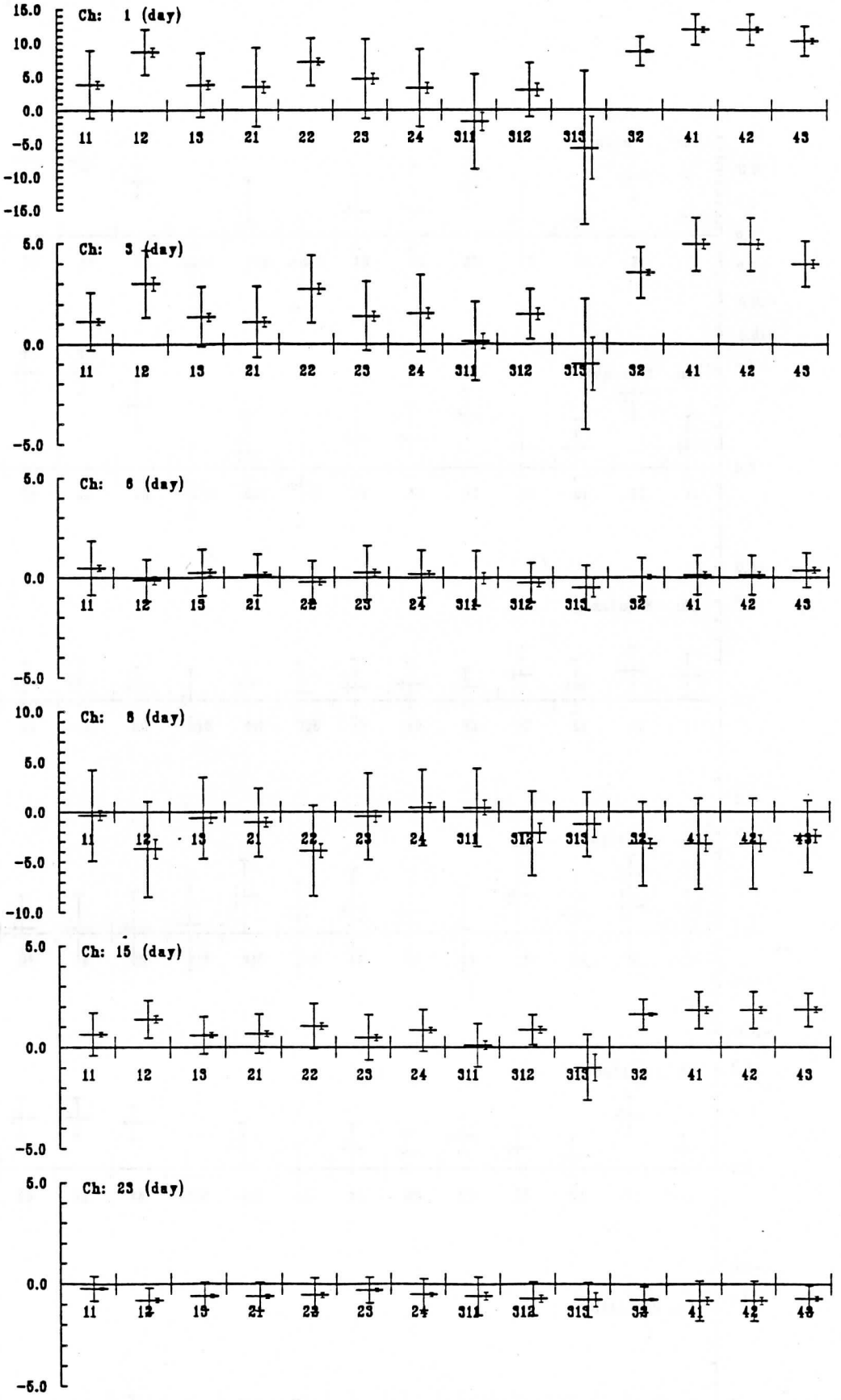

Fig.2. Mean, standard deviation and standard error statistics for a selection of NOAA-7 rte δ channel correction estimates (dependent sample), as a function of TSF class, and the time of day of the collocation observations.

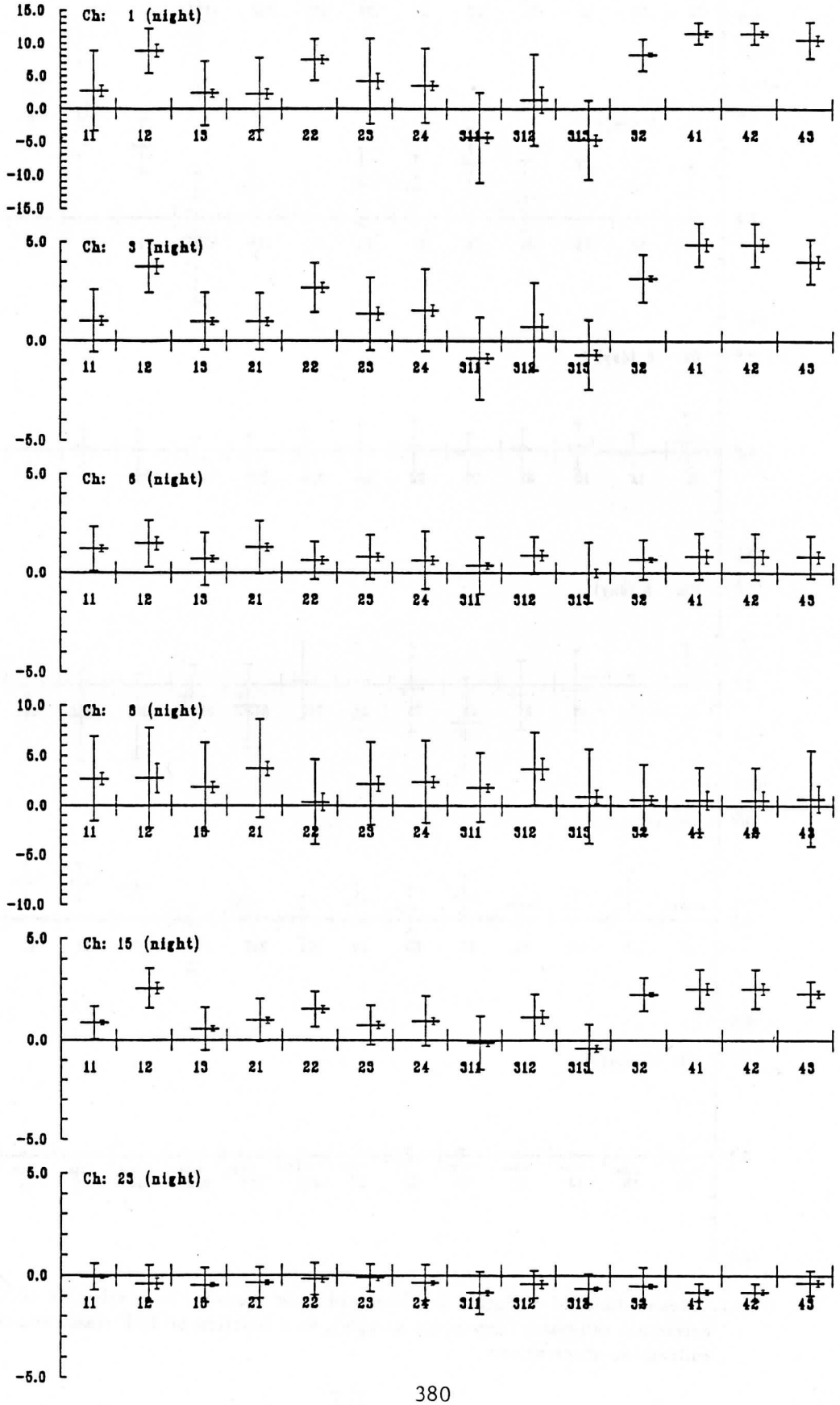
Ch: 1 (night)
15.0
10.0
5.0
0.0
-5.0
-10.0
-15.0
11 12 13 21 22 23 24 311 312 313 32 41 42 43
Ch: 3 (night)
5.0
0.0
-5.0
11 12 13 21 22 23 24 311 312 313 32 41 42 43
Ch: 6 (night)
5.0
0.0
-5.0
11 12 13 21 22 23 24 311 312 313 32 41 42 43
Ch: 8 (night)
10.0
5.0
0.0
-5.0
-10.0
11 12 13 21 22 23 24 311 312 313 32 41 42 43
Ch: 15 (night)
5.0
0.0
-5.0
11 12 13 21 22 23 24 311 312 313 32 41 42 43
Ch: 23 (night)
5.0
0.0
-5.0
11 12 13 21 22 23 24 311 312 313 32 41 42 43

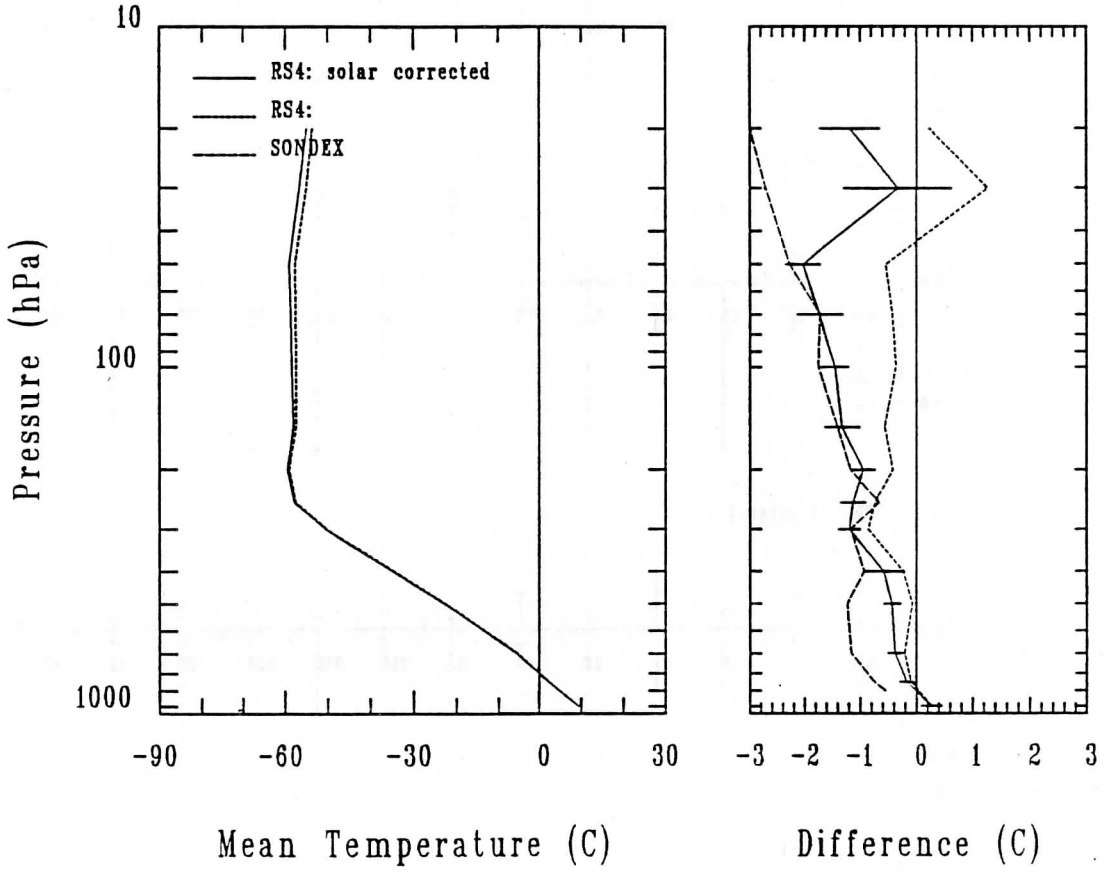

Fig.3. Mean (Philips RS4) and difference (RS4 minus Väisälä RS80) profiles for temperature profiles, for both solar and non solar corrected RS4 data and a sample of eighteen 0000 UTC soundings at Christchurch (44S 173E), New Zealand. The error bars indicate the standard errors of the solar corrected RS4 difference profile. Equivalent difference (VIZ minus RS80) profiles from SONDEX are also given (after Richner and Phillips, 1982).

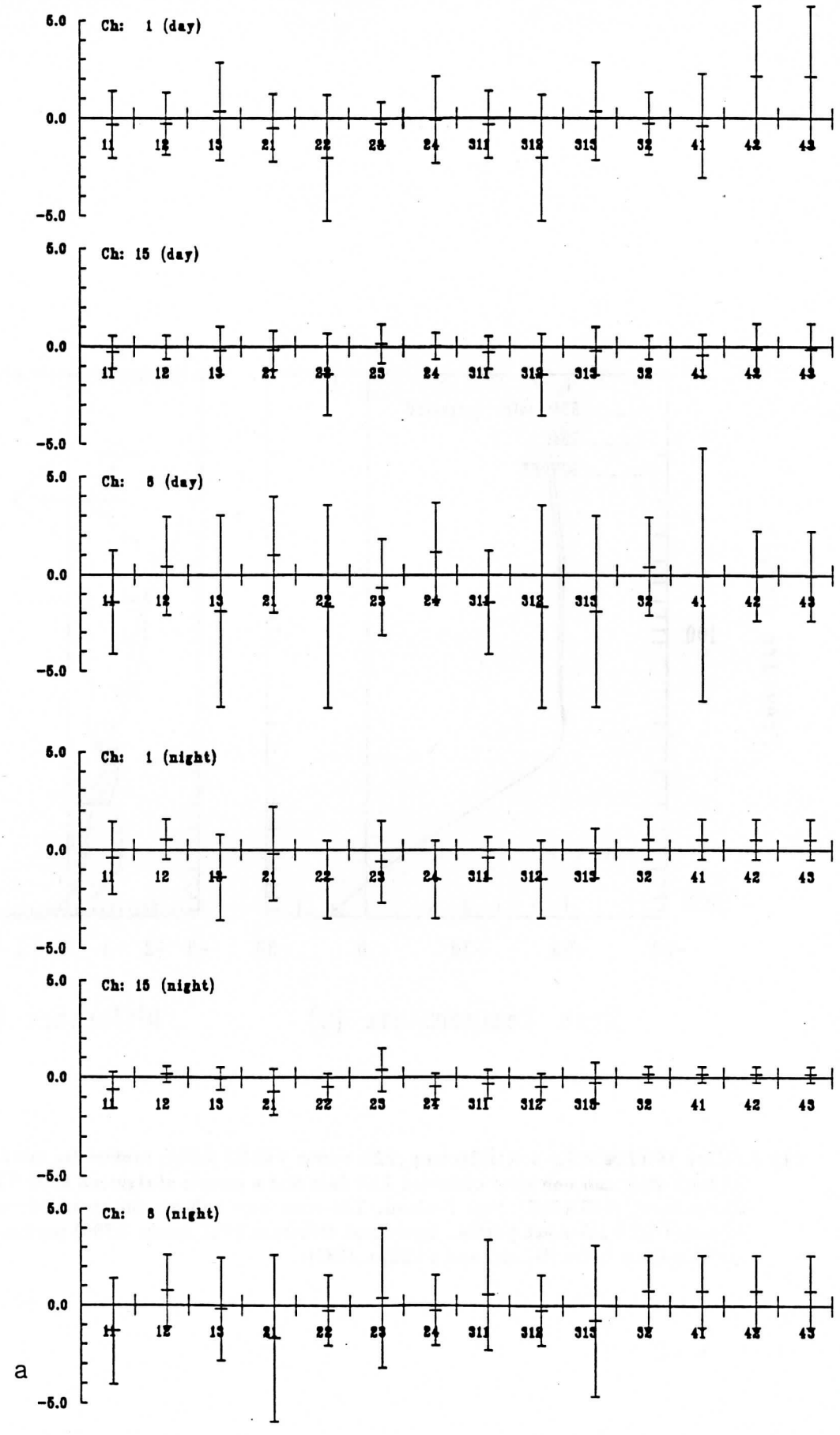

a

Fig.4. (a) Rms and bias errors for NOAA-7 satellite observations corrected to equivalent rte model values by the **D** method (independent sample), as a function of TSF class, and time of day of the collocation observations. (b) Rms and bias errors for the same data as (a), but corrected to equivalent rte model values by the δ_{TSF} method.

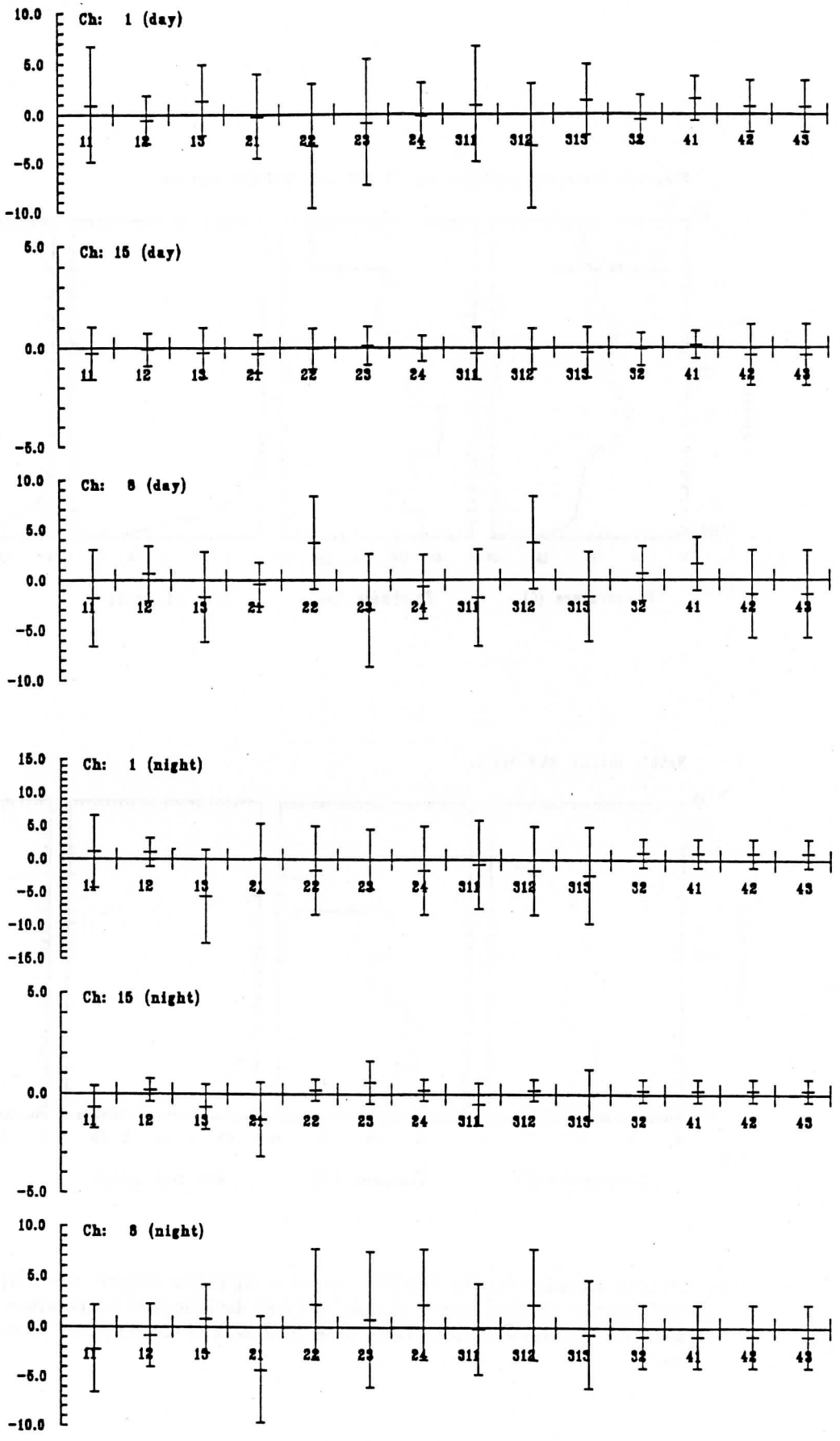
Ch: 1 (day)
Ch: 15 (day)
Ch: 8 (day)
Ch: 1 (night)
Ch: 15 (night)
Ch: 8 (night)
11
12
13
21
22
23
24
311
312
313
32
41
42
43

b

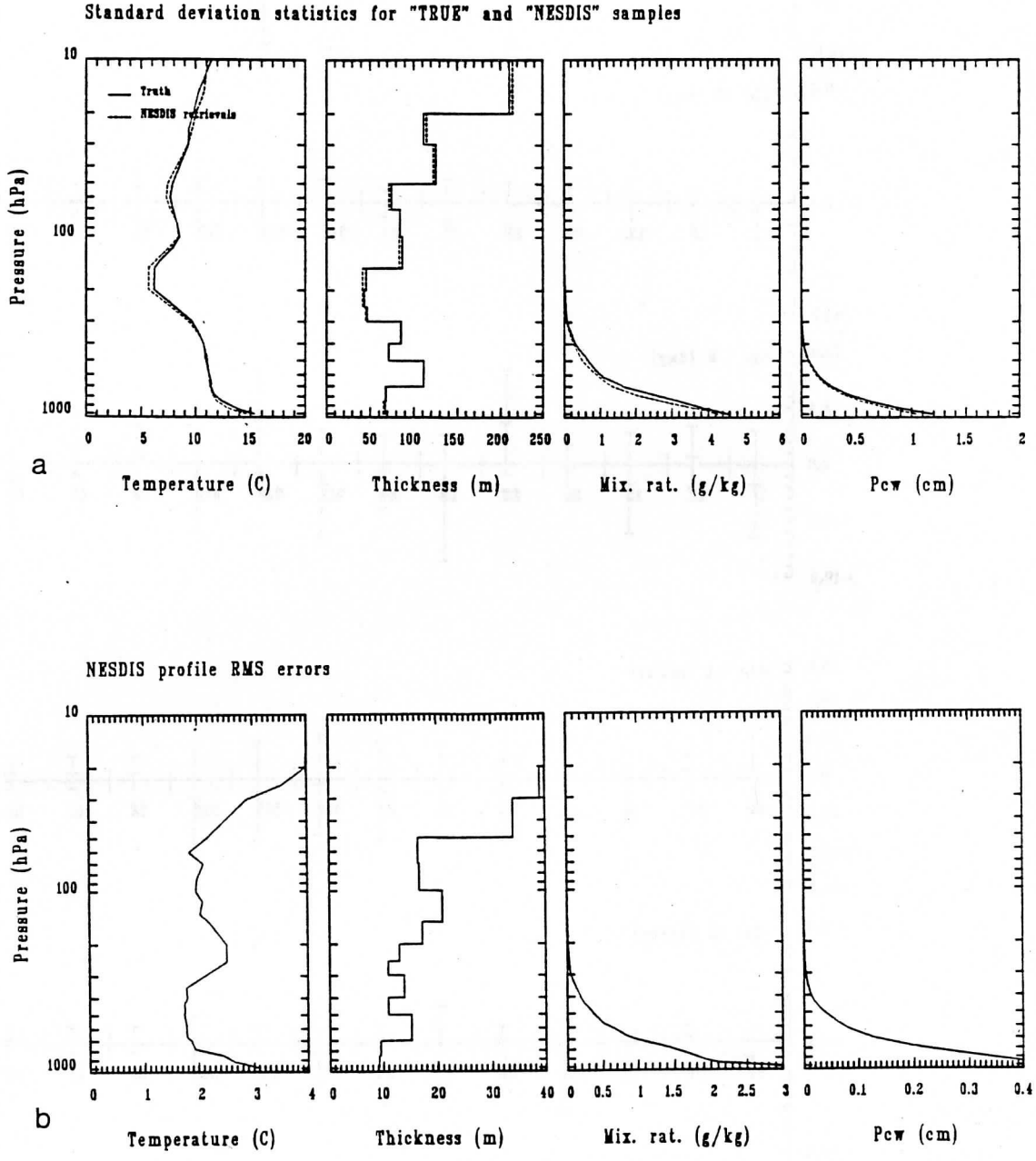

Fig.5. Retrieval statistics for the NESDIS regression algorithm (sample size 192). (a) Retrieved (solid curve) and true (broken curve), sample standard deviations of temperature, standard layer thicknesses, mixing ratio and precipitable water profiles, and (b) rms error profiles for the same quantities.

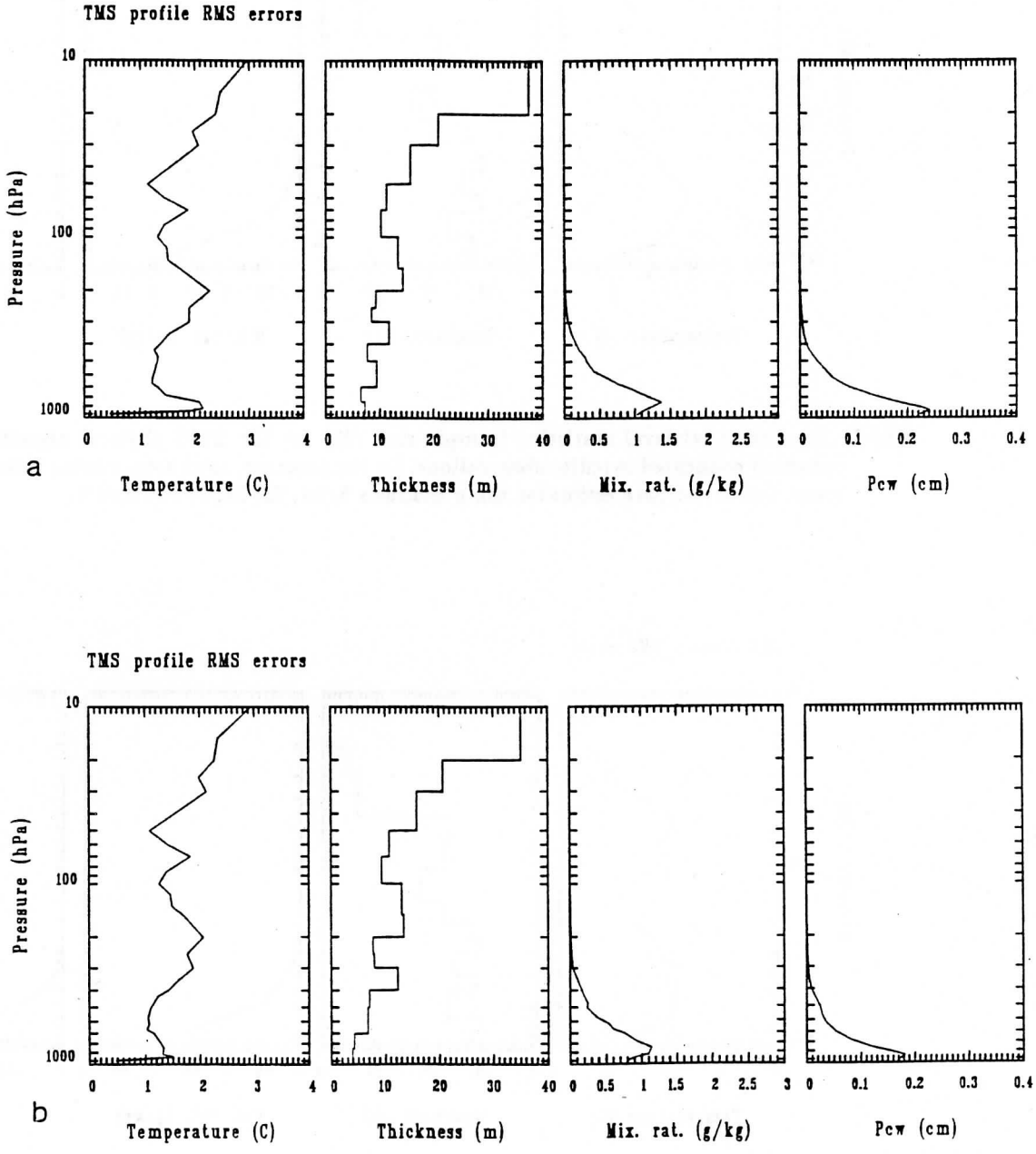

Fig.6. Rms error retrieval statistics (sample size 192) for the TMS physical algorithm applied to noise perturbed rte radiance temperatures, for temperature, thickness, mixing ratio and precipitable water for (a) a two pass estimator using channels 8, 24, 23, 22, 2, 4, 5 and 6, and (b) a 4 pass estimator (see text).

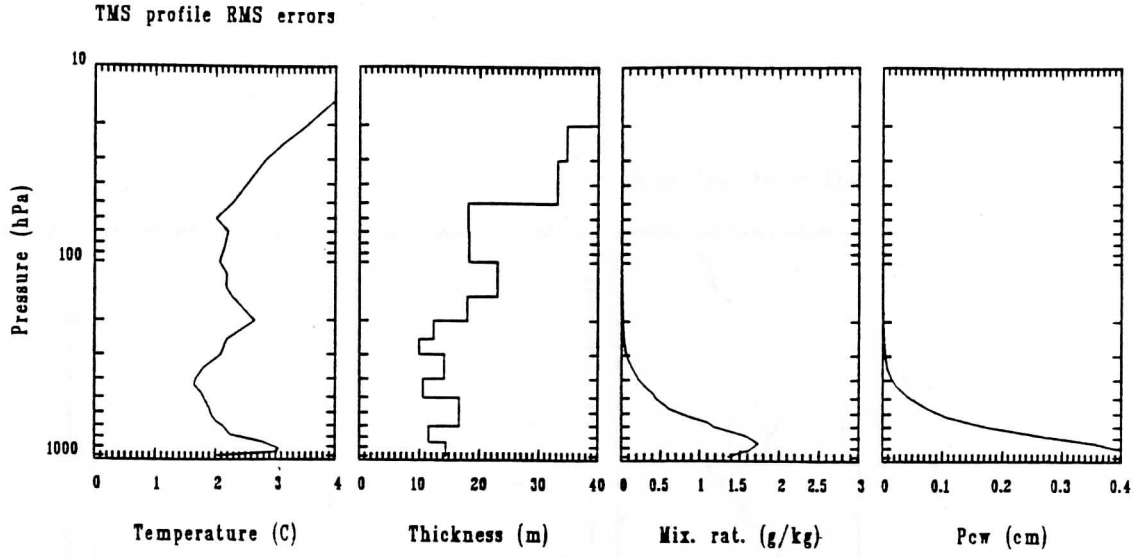

Fig.7. Rms error retrieval statistics (sample size 192) for the TMS physical algorithm applied to δ corrected collocated satellite observations, for temperature, thickness, mixing ratio and precipitable water and a two pass estimator using channels 8, 24, 23, 22, 2, 4, 5 and 6.

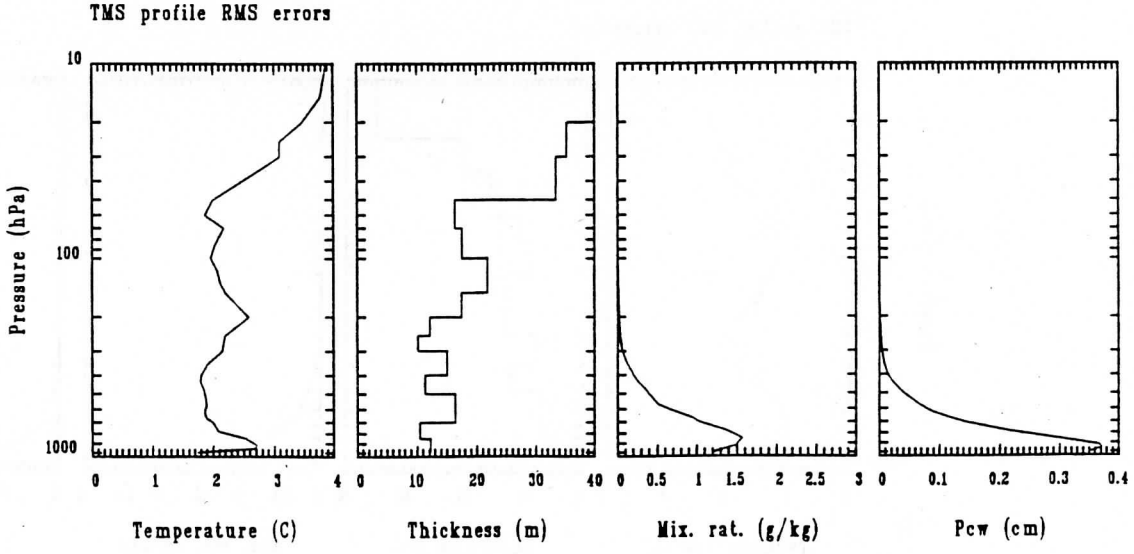

Fig.8. Rms error retrieval statistics (sample size 192) for the TMS physical algorithm applied to D corrected collocated satellite observations, for temperature, thickness, mixing ratio and precipitable water and a two pass estimator using channels 8, 24, 23, 22, 2, 4, 5 and 6.

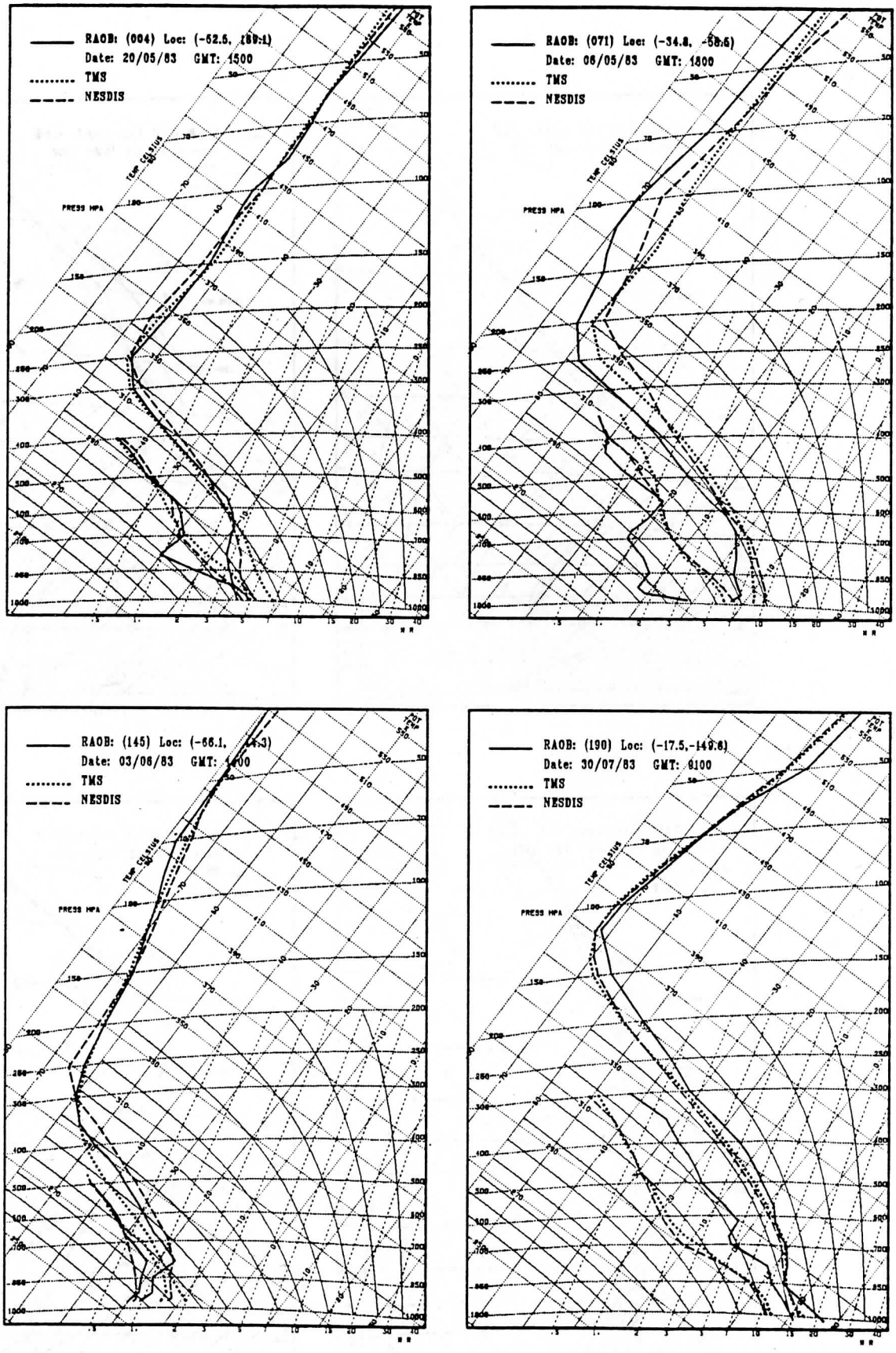

a

Fig.9. Example retrievals for, (a) NESDIS and TMS δ_{TSF} corrected satellite measurements, (b) NESDIS and TMS $\mathbf{D}_{TSF}$ corrected satellite measurements, and (c) TMS from noise perturbed rte radiance temperatures.

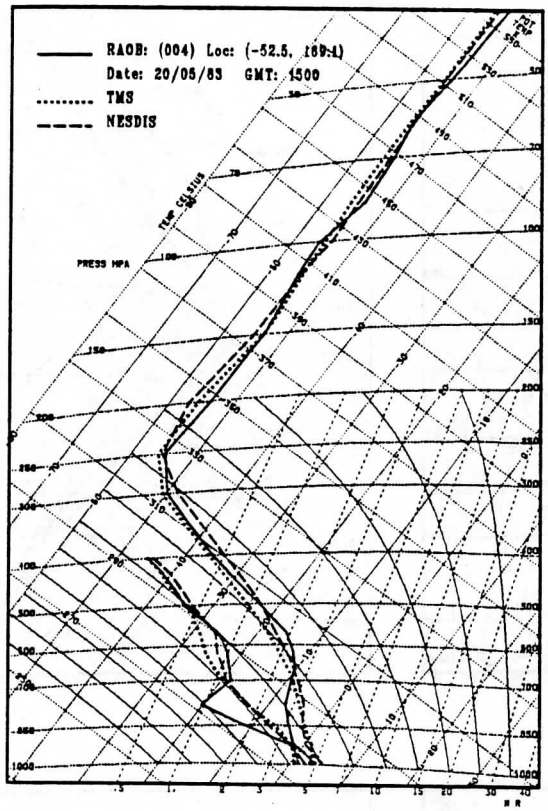
RAOB: (004) Loc: (-52.5, 169.1)
Date: 20/05/83 GMT: 1500
TMS
NESDIS
TEMP CELSIUS
PRESS HPA

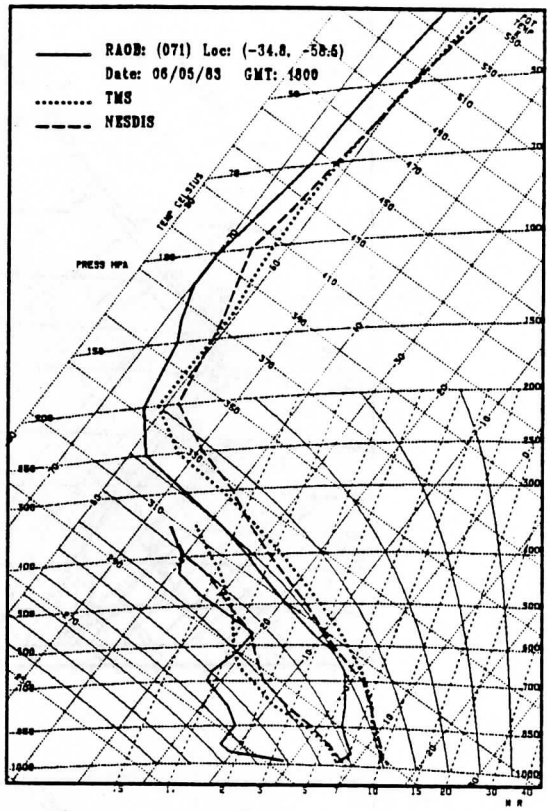
RAOB: (071) Loc: (-34.8, -58.5)
Date: 06/05/83 GMT: 1800
TMS
NESDIS
TEMP CELSIUS
PRESS HPA

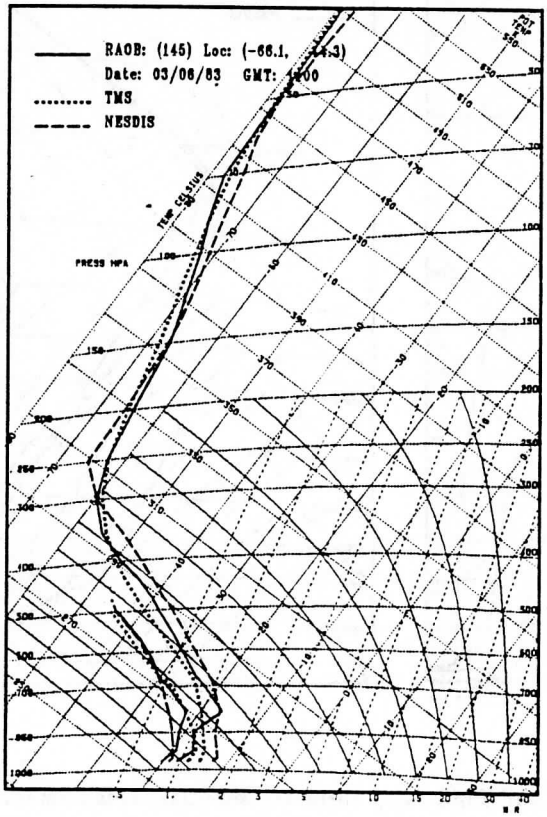
RAOB: (145) Loc: (-66.1, -[illegible])
Date: 03/06/83 GMT: [illegible]
TMS
NESDIS
TEMP CELSIUS
PRESS HPA

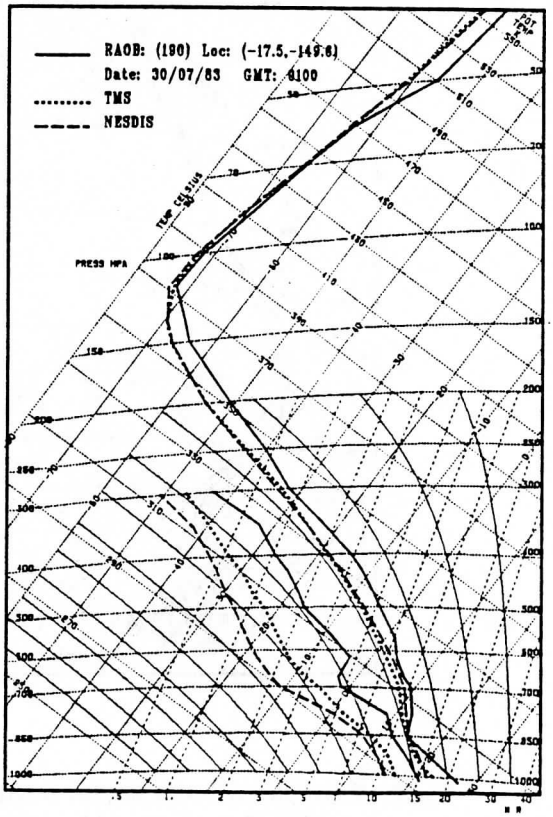
RAOB: (190) Loc: (-17.5,-149.6)
Date: 30/07/83 GMT: 0100
TMS
NESDIS
TEMP CELSIUS
PRESS HPA

b

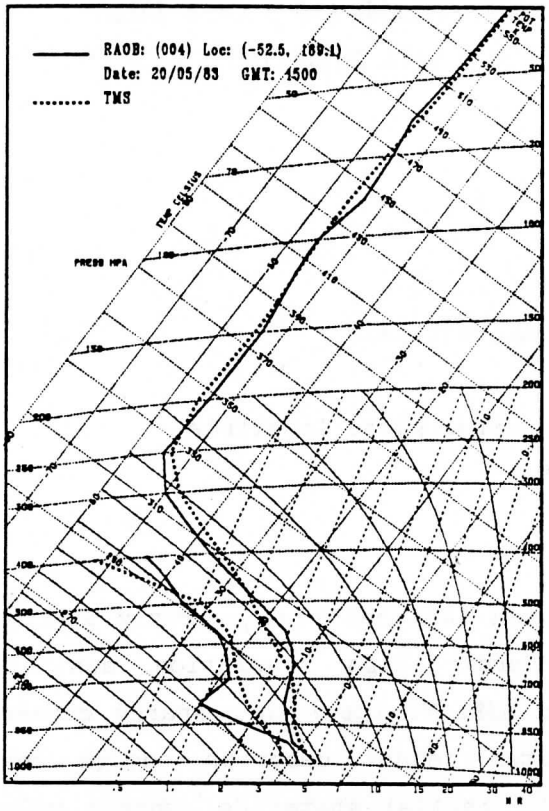
RAOB: (004) Loc: (-52.5, 169.1)
Date: 20/05/83 GMT: 1500
TMS
TEMP CELSIUS
PRESS HPA

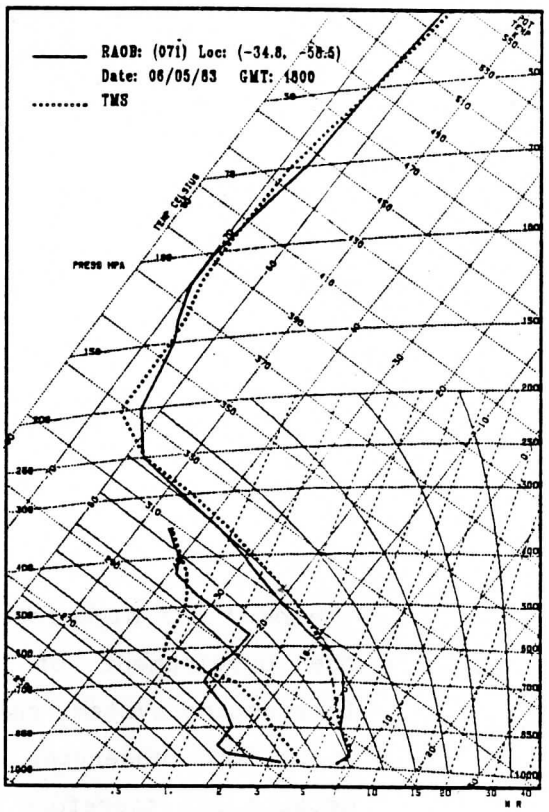
RAOB: (071) Loc: (-34.8, -58.5)
Date: 06/05/83 GMT: 1800
TMS
TEMP CELSIUS
PRESS HPA

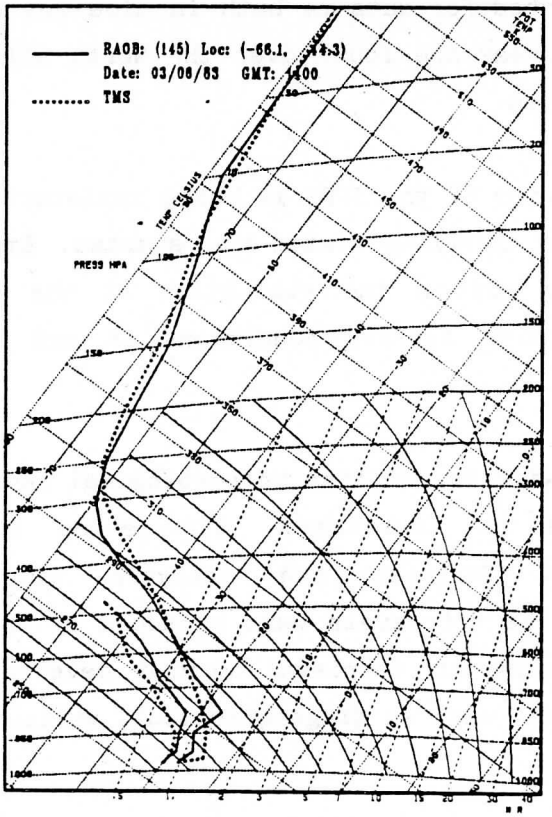
RAOB: (145) Loc: (-66.1,
Date: 03/06/83 GMT: 1400
TMS
TEMP CELSIUS
PRESS HPA

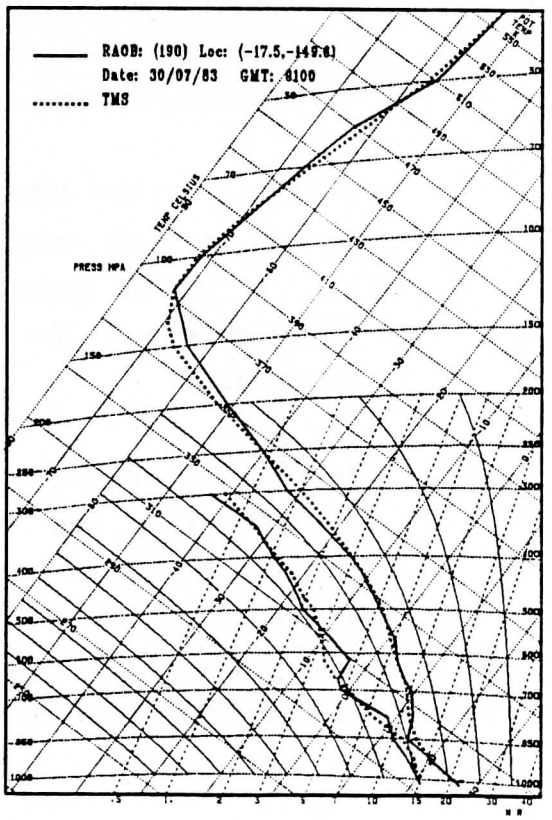
RAOB: (190) Loc: (-17.5,-149.6)
Date: 30/07/83 GMT: 0100
TMS
TEMP CELSIUS
PRESS HPA

C

TOVS PROCESSING IN FINLAND AND A CASE STUDY ON TOVS QUALITY IN A DATA ASSIMILATION CYCLE

Sakari Uppala

Finnish Meteorological Institute

The need for high resolution data has been recently increased by the development of a Nordic high resolution analysis and forecasting system, called HIRLAM. The rather sparse conventional upper air observing system cannot describe enough mesoscale details and therefore model initial states do contain relatively large errors, which then probagate and amplify through the subsequent forecast. The need for data is both in time and space, but most urgent datavoid areas are found over the North Atlantic, the North Sea and the Baltic.

At the moment the VAX-version of the ITPP is being implemented and testing of local retrieval sounding system has started. Emphasis will be in the beginning put on the evaluation of the system performance over the complex surface conditions in and around Scandinavia.

In a cooperation project with the British Meteorological Institute a case study was made to investigate differences between retrievals, first quess forecast and analysis within a data-assimilation cycle. The retrievals were produced by the BMO LASS system using the physical retrieval method developed by J.Eyre. These data were only used as diagnostic tool, while the

coarse resolution soundings from NOAA/NESDIS, available from GTS, were used in the data assimilation in addition to all conventional data.

A case on the 13th Oct 1987 12GMT, a southbound NOAA-10 pass over Atlantic was selected. The retrieved, first guess and the analyzed temperatures were averaged line by line on all levels. Cross-sections are shown of the differences between mean retrieval and mean analyses (Fig. 1) and between mean retrieval and mean forecast (Fig. 2).

Above tropopause and in the middle troposphere the LASS retrievals seem to be colder than the analysis. Immediately under the tropopause they however are significantly warmer than the analysis. Explanation for this could be, that the NESDIS coarse resolution soundings have too smooth tropopause and analysis follows this or that the analysis does the smoothing. The difference to the forecast shows a fairly large scale structure, the small scales being absorbed to LASS retrievals from the forecast. The difference also seems to be less dependent on the tropopause level than was the case with the difference to the analysis. Here the difference can partly be explained by the systematic error of the model and partly by the systematic retrieval error. In short we can say that there is a large inconsistency in the way tropause is described by analysis, by the retrieval scheme and by forecast model. In order to improve the forecast skill effort should be made to have higher resolution data and more levels in forecast models around tropopause.

$\overline{T}_{Retrieval} - \overline{T}_{First\ guess}$

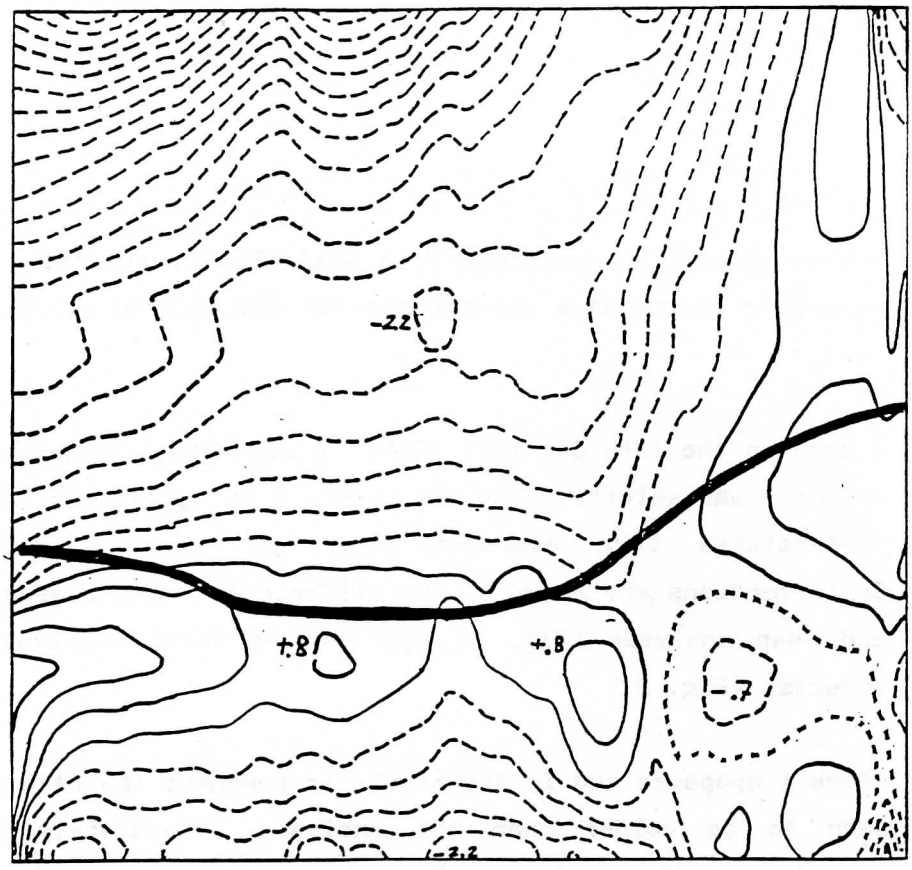

Mean analyzed tropopause level

Fig. 2

$\overline{T}_{Retrieval} - \overline{T}_{Analysis}$

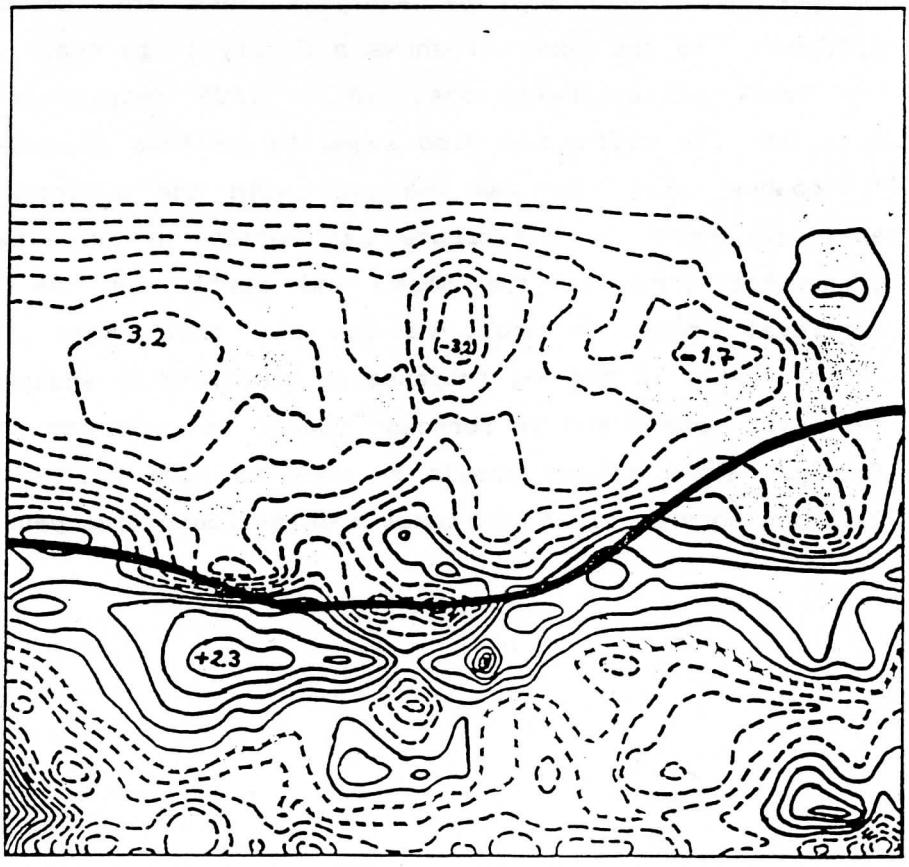

Mean analyzed tropopause level

Fig.1

RECEPTION AND USE OF TIROS OPERATIONAL VERTICAL SOUNDER DATA IN THE ANTARCTIC

David Warren
British Antarctic Survey
Natural Environment Research Council
High Cross, Madingley Road
Cambridge CB3 OET, UK

ABSTRACT

This paper describes the increasing use being made of TOVS data for meteorological research in the British Antarctic Survey.

During the 1988/89 season we intend to install a VHF receiver at Halley (75.5°S, 26.9°W) to receive TOVS data from the operational NOAA satellites. The data acquired with this system will be used in the study of the occurrence, structure and development of meso-scale meteorological systems in the Weddell Sea.

A brief description is included of the interim results of a case study of a small, vigourous depression which developed, matured and declined in the south east corner of the Weddell Sea over seven days in January 1986. This system is being examined using surface and upper-air observations made at Halley, processed TOVS data and analyses provided by the British Meteorological Office.

1. ANTARCTICA

There are only eleven upper-air stations in the Antarctic, a continent which covers an area one and a half times that of Europe (see Figure 1). As a result detailed studies of the structure of atmospheric systems in the region, even on synoptic scales, have not been possible using only data from the routine observational network.

The British Antarctic Survey (BAS) has three permanent bases in the Antarctic, two, Rothera (67.6°S, 68.1°W) and Faraday (65.5°S, 64.9°W), sited on the west side of the Antarctic Peninsula and one, Halley (75.5°S, 26.9°W), on the Brunt Ice Shelf. At each of these bases a programme of three hourly surface meteorological observations is carried out, and daily 12 GMT radio-sonde flights are launched from Halley.

2. DSB

Early last year (1987) it was decided to install equipment at Halley which would receive the Direct Sounder Broadcast (DSB) from the NOAA satellites, extract the TOVS data and pass it through the processing package we have obtained from the UK Meteorological Office to provide temperature profiles and thickness fields over Coats Land, the Weddell Sea and the Antarctic Peninsula (see Figure 1).

The receiver is being purchased from Mariner Radar Ltd. of Lowestoft, and is of a relatively inexpensive, simple and robust design which was originally developed to collect data from the ARGOS Data Collection System which is also contained in the DSB transmissions.

We estimate that, using an omni-directional whip antenna, the system's effective horizon will be at an elevation of 30 degrees which will mean that a satellite will be 'visible' over an area with a radius of approximately 1200 km. This means that data will be available from roughly a quarter of the Antarctic continent (see Figure 1).

3. THE RETRIEVAL SCHEME

Recently a MicroVAX II has been installed at Halley to handle communications with BAS HQ at Cambridge and to act as a general purpose computer for the base. This computer will be used to retrieve the temperature and humidity profiles from the raw TOVS information.

The retrieval package was obtained from the UK Meteorological Office and is identical to the scheme used operationally there (Eyre, 1984). However we will be restricted to using a climatological first guess, not having timely access to a forecast field. We have recently received a new cloud clearing scheme (Eyre & Watts, 1987), which we are now using in preference to the older N* version, as well as a physical retrieval system which has not been installed yet.

In operational use, data from each satellite pass will be passed from the receiver to an IBM PC and stored on a 20 Mbyte Winchester disk. Once or twice a day all the collected sounder data will be transferred from the PC to the MicroVAX and passed through the retrieval package. The soundings or thickness fields will be plotted for use by the base meteorologists or, in instances of particular interest it will be possible to transfer either the original data or the products to Cambridge via a DECnet link over Inmarsat.

4. OPERATIONAL USE

We anticipate that some of the other data contained in the DSB will be useful. At the moment a group within BAS, in collaboration with the Scott Polar Research Institute, is investigating sea-ice dynamics in the Weddell Sea using several drifting buoys. It would be possible to compute the buoy

positions from the ARGOS system messages which are also contained in the TIP data-stream and to have them available in near real time.

5. RESEARCH USE: AN EXAMPLE

Our first priority is research rather than operational meteorology. We have been studying the structure of meso-scale systems over the Weddell Sea using TOVS and AVHRR 4 km resolution data purchased from NOAA/NESDIS.

There are particular, well-known problems associated with temperature sounding over the Antarctic continent. The surface lies at an average altitude of about 2000 m, for the most part it is permanently covered with ice or snow, and there are frequently strong temperature inversions in the lowest few hundred metres of the atmosphere. Despite these difficulties it is possible to obtain useful information from TOVS, largely by only using retrievals from over the sea or low lying coastal areas.

A good example of the value of TOVS soundings is provided by the study of a meso-scale depression which developed, matured and decayed between 1 - 8 January 1986, off the coast of Coats Land close to Halley. The surface observations and daily radio-sonde ascents from the base together with TOVS derived 1000 - 500 hPa thickness fields have lead to a self-consistent, qualitative understanding of the development of the system.

Figure 2 shows a sequence of TOVS derived 1000-500 hPa thickness fields from two days during the development of the system, whose position is indicated in the centre of the charts. The presence of a pool of warm air over the Ronne Ice sheet to the south and advection of cold air along the coast of Coats Land, to the north east, lead to the creation of a region of strong temperature gradients on the 3rd and 4th. The development took place towards the warmer side of this region, apparently as a result of the approach of a mid-level trough from the north east.

The retrievals were derived using a climatological first guess field and there are large differences between co-located TOVS and radio-sonde derived temperature profiles from Halley. However, as might be expected, the discrepancies between the height-integrated fields derived from the two systems are much smaller, and furthermore, warming or cooling trends at particular levels are well represented, qualitatively at least, by the TOVS retrievals. This gives us some confidence that the structure of larger scale features and their development can be reliably inferred from the TOVS data.

REFERENCES

Eyre, J. R., 1984, "High Resolution Temperature Retrievals at the UK Meteorological Office", Tech Proc 1st International TOVS Study Conference, Igls, Austria.

Eyre, J. R., & Watts, P. D., 1987, A Sequential Estimation Approach to Cloud Clearing for Satellite Temperature Soundings. *Q. J. R. Meteorol. Soc.*, 113, 1369-1376

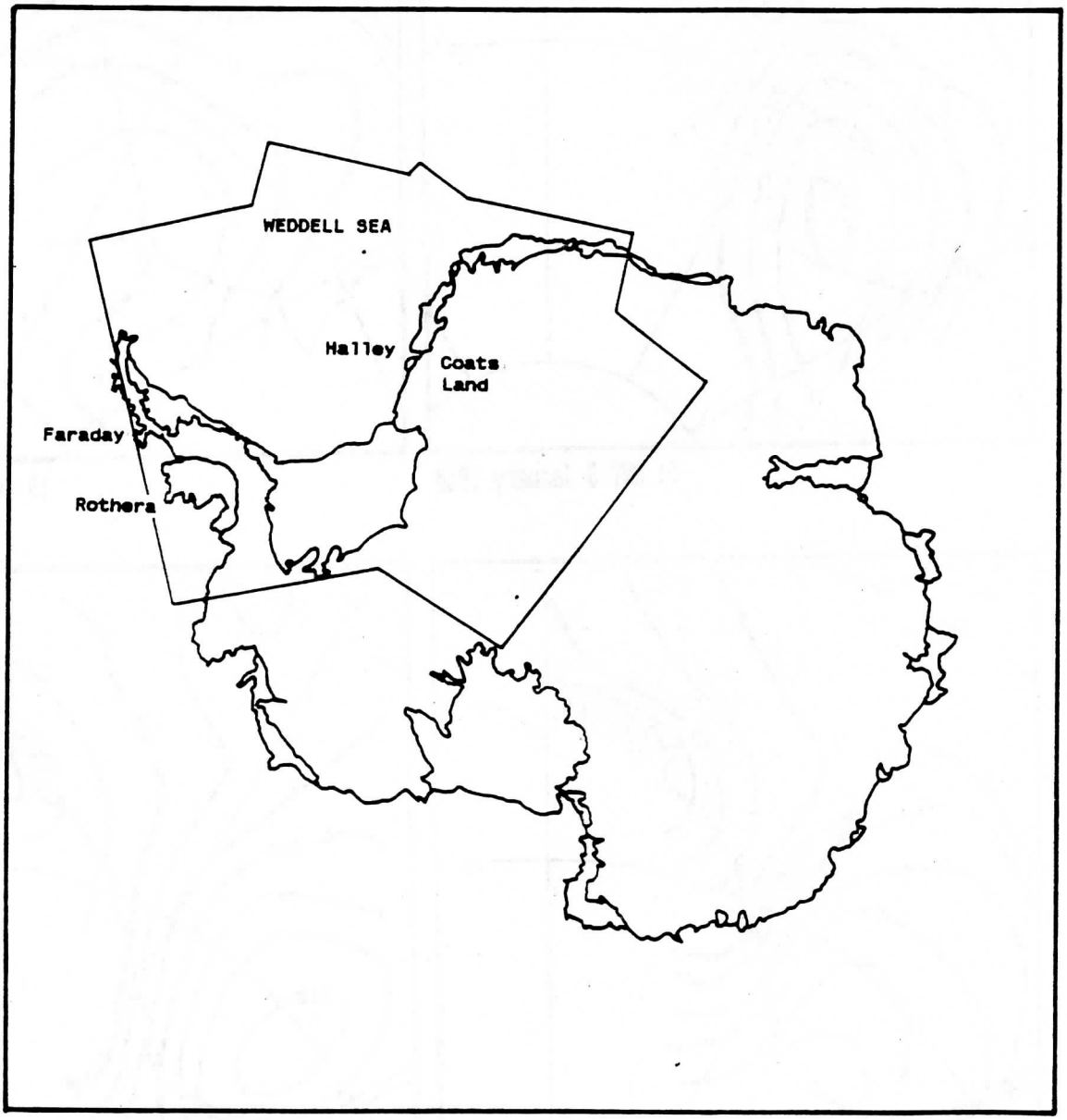

Figure 1. The Antarctic, showing expected coverage of TOVS data acquired from three consecutive satellite passes by a VHF receiver sited at Halley.

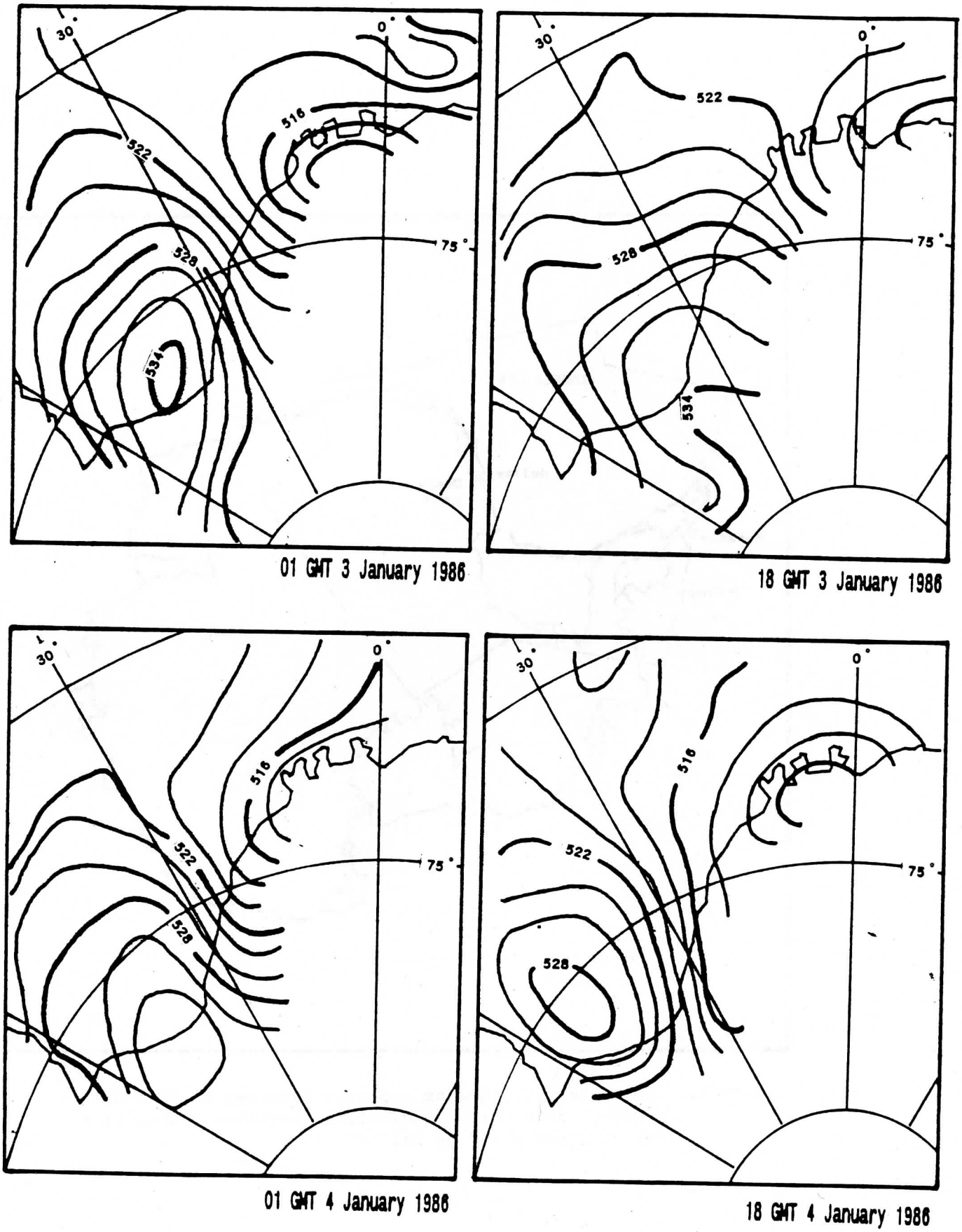

Figure 2. 1000-500 hPa thickness field derived from TOVS data from four passes on 3 January and 4 January 1986. Contours are drawn at intervals of 2 gpdm.

THE SENSITIVITY OF A MINIMUM VARIANCE RETRIEVAL SCHEME TO THE VALUES OF ITS PRINCIPAL PARAMETERS

P D Watts[1] and A P McNally[2]

Robert Hooke Institute for Cooperative Atmospheric Research,
Clarendon Laboratory, Oxford, U.K.

[1] Meteorological Office Unit
[2] Department of Atmospheric, Oceanic and Planetary Physics

1. INTRODUCTION

The U.K. Met Office has recently implemented a TOVS retrieval scheme which uses a forecast profile as a first guess in a minimum variance retrieval of temperature and humidity (Eyre et al, 1986). An initial estimate of the profile with known error covariance and satellite measurements with known error covariance are combined with weights that minimise the expected error in the retrieved profile at all levels. Preliminary results with the scheme (as gauged by comparisons with collocated radiosondes) show that we now have retrievals of significantly higher accuracy than those from a previously used regression scheme (which effectively used a climatological first guess). However, comparison of the forecast with the radiosonde shows that the first guess and the retrieval are of comparable accuracy, suggesting that the retrieval is providing no additional information. Admittedly this validation is principally over N.W. Europe where the 6-12 hour forecast may be expected to be very good and any improvement difficult to make. Nevertheless, if we are modelling the problem correctly the minimum variance solution should be an improvement over the first guess. The purpose of this work was to find our sensitivity to errors in the 'model' thereby establishing why the theoretical improvement over the guess profile is not realised and also to obtain a better 'model'.

2. THEORY AND METHOD

The minimum variance solution is a linear one and assumes a linear forward problem:

$$\mathbf{Y} - \mathbf{Y_o} = \mathbf{K}.(\mathbf{X_t} - \mathbf{X_o}) \qquad (1)$$

where $\mathbf{Y}$ and $\mathbf{X_t}$ are the brightness temperature measurements and true atmospheric temperature profile and $\mathbf{Y_o}$ and $\mathbf{X_o}$ are the forecast values. $\mathbf{K}$ are brightness temperature derivatives $\mathbf{dY/dX}$ ('incremental weighting functions') and are

assumed, for now, to be independent of $\mathbf{X}$. Note that $\mathbf{X}$ includes both temperature and humidity profiles which are to be retrieved simultaneously. If the measurements $\mathbf{Y}$ and forecast $\mathbf{X}$ have error covariances $\mathbf{E}$ and $\mathbf{C}$ respectively, then the minimum variance solution, $\hat{\mathbf{X}}$, is

$$\hat{\mathbf{X}} = \mathbf{X_o} + (\mathbf{K.C})^{\mathbf{T}}(\mathbf{K.C.K^T} + \mathbf{E})^{-1}.(\mathbf{Y} - \mathbf{Y_o}) \tag{2}$$

$$\text{or} \qquad \hat{\mathbf{X}} = \mathbf{X_o} + \mathbf{W}.(\mathbf{Y} - \mathbf{Y_o})$$

(See Rodgers, 1976). The expected value $\mathbf{S}$ of $(\hat{\mathbf{X}} - \mathbf{X_t}).(\hat{\mathbf{X}} - \mathbf{X_t})^{\mathbf{T}}$, may be written,

$$\mathbf{S} = \mathbf{C} - \mathbf{W.K.C} \tag{3}$$

The diagonals S_{jj} are the expected error variances of the retrieval at the profile levels and the ratio S_{jj}/C_{jj} gives the reduction in variance expected (this ratio is called the fractional unexplained variance, FUV). The matrices $\mathbf{C}$, $\mathbf{K}$ and $\mathbf{E}$ constitute the 'model' discussed in the introduction and it is the sensitivity of the retrieval to these parameters with which we are concerned. This sensitivity is gauged by calculating the error covariance $\mathbf{S'}$ expected when the true conditions are $\mathbf{C'}$,$\mathbf{E'}$ and $\mathbf{K'}$ but $\mathbf{C}$,$\mathbf{E}$ and $\mathbf{K}$ have been used to derive $\mathbf{W}$. $\mathbf{S'}$ may be shown to be:

$$\mathbf{S'} = \mathbf{C'} - \mathbf{W.K'.C'} - (\mathbf{W.K'.C'})^{\mathbf{T}} + \mathbf{W}.(\mathbf{K'.C'.K'^{T}} + \mathbf{E'}).\mathbf{W^T} \tag{4}$$

which reduces to equation 3 when $\mathbf{C'} \rightarrow \mathbf{C}$, $\mathbf{E'} \rightarrow \mathbf{E}$ and $\mathbf{K'} \rightarrow \mathbf{K}$. This equation can be used to study the theoretical sensitivity of the scheme to incorrect assumptions about the principal parameters, mainly by examining the diagonals S'_{jj}.

New estimates of $\mathbf{C}$, $\mathbf{K}$ and $\mathbf{E}$ were obtained and used both in the simulation described above and to perform retrievals on real data. The source of the new estimates was a data set collected over three months of collocated forecast, measurement and radiosonde data. These data were split into two sets for the study, independent data being (arbitrarily) the even days of the month and the dependent data being the odd days. The dependent data were used to calculate the matrices and the retrievals were performed on the independent data. To ease description of the results the following convention is adopted. A result described as P1$\diamond$W(P2) indicates an estimator W derived using a matrix **P2** was used where the

true conditions were actually described by **P1**. For example, Ep$\diamond$W(E) describes the result of using a **W** derived using **E** with measurements that actually have an error covariance **Ep**. Normally there will be three simulations:

- $P \diamond W(P)$—the expected result with the original parameter,
- $P' \diamond W(P)$—how we may expect to 'suffer' given the wrong parameter in the operator,
- $P' \diamond W(P')$—how well we can expect to do with 'correct' parameters. (We expect P' to be nearer the truth than P)

The following three sections deal with each matrix parameter in turn, firstly describing how the new estimate was obtained, secondly giving the results of the simulation experiments and finally the results using real data.

3. C - FORECAST ERROR COVARIANCE

3.1 C: Derivation

The original forecast error covariance matrix, denoted hereafter by C1, was obtained from the Meteorological Office Forecasting Research Branch and was calculated by comparing 12–hour forecasts with the next verifying analysis. A single matrix was supplied to describe all conditions. Certainly one problem with this method is that it will tend to underestimate forecast errors, especially in data–sparse areas, because the analysis uses the forecast as a background field. An attempt was made to allow for this with a simple multiplier. We may also suppose that the error characteristics of the forecast model will at least be a function of location, and that this approach may not assess correctly the inter–level correlations of error.

The new **C** matrix, denoted by C2, was estimated by comparing the forecast profile with the 'true' collocated radiosonde profile from the dependent data. The behaviour of **C** derived in this way when the collocation distance is reduced is not strong so we can be reasonably sure that forecast errors are not being seriously overestimated. Three **C** matrices were obtained; C2 from all the dependent collocation data, CW from collocations West of 14 Deg W representing an area of relatively high forecast error and CE from collocations East of 14 Deg W, an area of low forecast error. CE resembled the original C1 in size whereas the elements were much larger in CW. However, the correlation of forecast errors implied by CE, CW and C2 were very similar and generally higher than those in C1.

3.2 C: Simulations

The result C2◇ W(C1), is shown in figure 1. Compared with C1◇W(C1) it is apparent that even with the wrong operator, guess errors as described by C2 are easier to correct in the retrieval (at most levels) than those described by C1. Using the correct estimator, C2◇W(C2), the result is still better but only markedly so near the surface and above 400 mb. The C2 guess is easier to improve upon than C1 because the errors are more strongly correlated between levels. Measurements are able to 'see' errors that are highly correlated over a vertical range comparable to, or greater than, the weighting function width.

A second experiment was done with matrices CW and CE and the simulation suggested there is no advantage in such a stratification. Again the reason appears to be the similarity of the error correlations in the two areas. If there are areas or times where the forecast has significantly different error *correlations* then there may be scope for further improvement.

3.3 C: Real data

The result with real data equivalent to the first simulation is given in figure 2 showing, following the notation, Ind◇W(C1) and Ind◇W(C2) i.e. the result of using Ws calculated from the matrices C1 and C2 both applied to the independent data. As in the simulation there is some gain around 1000mb and above 300mb, though the latter is not significant below 150mb. There appears to be an increased error near the surface (1.5m T_s) which may be caused by the lack of a skin temperature measurement in the sonde report. Notice that at all levels with C1 the FUV is close to or greater than unity. The use of C2 at least reduces this to make it a useful retrieval around 1000mb. The effects on humidity retrieval is, in accordance with the simulation, negligible.

In summary, the C matrix derived from collocated radiosonde data appears to be a better description of the guess error than C1 and improves the retrieval accuracy. That this method of deriving C is subject to unwanted collocation errors appears not to be a serious objection as the behaviour of C with decreasing collocation distance is not strong. As expected from simulation, simple stratification by areas of high and low forecast error is not an advantage.

4.1 E: Derivation

The error covariance of the measurements is poorly known although we have reasonable bounds on the diagonal elements (see Watts, 1984). Errors in different channels are almost certainly correlated (by preprocessing, cloud–clearing procedures etc.). The measurement error is taken to refer to the term $(\mathbf{Y} - \mathbf{Y_o})$ and consequently should include any random error in the radiative transfer calculations. The original **E** matrix used in the scheme was diagonal implying no correlations between errors in any of the channels. The values for the diagonals were chosen to lie between two limits, a minimum defined by the radiometric noise (very low in HIRS channels) and a maximum determined by routine comparisons of measured brightness temperatures and brightness temperatures calculated from collocated radiosondes.

Essentially the same procedure was used for the new **E** matrix using the radiosonde profiles from the dependent collocation data but the full covariance of errors was derived rather than just the variances in each channel. Three **E** matrices were derived because the 'clear' radiances are obtained through three distinct routes namely: clear FOVs where no cloud is detected, FOVs where an adjacent FOV has been used to estimate the clear radiances (N^* method), and FOVs where cloud conditions preclude the N^* method and the HIRS brightness temperatures are obtained by regression on MSU data (for details see Eyre and Watts 1987). The **E** matrices thus derived have different characteristics both in the size of the elements and the correlations. The clear **E** is most like the diagonal **E** originally used with low off–diagonal values. The N^* **E** has larger off–diagonals with some strong negative correlations. Strongest correlations (up to 0.5) are found for **E** in the HIRS estimated from MSU.

4.2 E: Simulations

A sample simulation result, that for the E_{msu} (HIRS–MSU regression), is shown in figure 3. The three results shown are,

- solid line; $E_{diag} \diamond W(E_{diag})$ i.e. our originally assumed expected error,
- dashed line; $E_{msu} \diamond W(E_{diag})$ i.e. what we may expect when the diagonal **E** is used on real data and
- dotted line; $E_{msu} \diamond W(E_{msu})$ representing the best we may expect given our best estimate of the measurement error characteristics.

The detrimental effect of using E_{diag} on MSU–regression data is substantial throughout the profile, and affects both temperature and humidity. A smaller effect is found for 'clear' and N^* cases. In most cases the accuracy of the profile is mostly restored when the correct **E** is used though there is always some loss because the non–zero correlations in the new **E** matrices imply less information. Interestingly, the size of effect is much larger than found with the **C** matrix simulations and is actually capable of pushing the FUV up to and over 1.0 which is what is found with the original routine scheme. Use of the correct **E** reduces this to ≈ 0.8 or less representing a useful retrieval.

4.3 E: Real data

Results analogous to the simulations just described but using the real independent data were obtained and the sample MSU–regression shown in figure 4. Here the three lines are,

- solid; $Ind \diamond W(E_{diag}, C1)$,
- dashed; $Ind \diamond W(E_{diag}, C2)$ and
- dotted; $Ind \diamond W(E_{msu}, C2)$.

In this case the using the new **E** much reduces the retrieval error in temperature and significantly reduces it in humidity. In temperature the FUV reduction is $\approx$ 0.25 at maximum decreasing to 0.05 at the tropopause. More importantly, the FUV is reduced to less than 1.0 and, considering the large proportion of soundings that this route provides ($\approx 80\%$), this represents a considerable improvement.

In the clear cases for temperature retrieval any change was small (0.1 or 0.2 FUV) but positive. In the humidity the gain was larger though still not close to the simulated effect. With N^*, more gain was made at most levels in temperature though far less than the simulations suggested. The effect on humidity was as in the clear case.

In summary, the new **E** matrices are substantially different from the original diagonal **E** and differ also according to the cloud–clearing route used. The simulated effect of these **E** matrices is large and, at least in the case of MSU–regression FOVs, borne out in real retrievals. This case, because of the large proportion of soundings it constitutes, is the most important. For clears and N^*s the effect is smaller than simulated though still positive and useful. The relatively small numbers of these cases available when generating the **E** matrices may mean the estimates are not close to the best possible and we feel that a larger impact, in line with that made on the MSU–regression FOVs, should be possible.

5. K - INCREMENTAL WEIGHTING FUNCTIONS

5.1 K: Derivation

The original **K** matrix was the mean of the incremental weighting functions calculated for 100 randomly selected mid–latitude profiles. The standard deviation about this mean is found to be fairly high (5–10% of the mean value), i.e. there is a significant dependency on the profile – the problem is non–linear. In order that our model be correct, **K** should be evaluated at the true profile or, this being impossible, at the guess profile, $\mathbf{K_o}$. **W** would then be calculated using $\mathbf{K_o}$. This procedure would be computationally expensive and would only be justified if the retrieval were found to be relatively sensitive to the exact value of **K**.

The new **K** was obtained by randomly extracting a profile from the mid–latitude set. This is not an improved **K** of course but it allows us to gauge the sensitivity to this part of the model.

5.2 K: Simulations

Equation 4 is derived on the basis that the retrieval can be written;

$$(\hat{\mathbf{X}} - \mathbf{X_o}) = \mathbf{W}.(\mathbf{Y} - \mathbf{Y_o}) = \mathbf{W}.\mathbf{K}'.(\mathbf{X_t} - \mathbf{X_o}) + \mathbf{W}.\epsilon \qquad (5)$$

Where $\mathbf{X_t}$ is the true profile and ϵ is a measurement noise vector. In practise the guess brightness temperatures are calculated with a full radiative transfer routine using approximately the correct physics, the measurements by definition use the correct physics. We may use $\mathbf{K}'$ to simulate the difference between the true atmosphere and the linearised model, **K**, used in **W**.

The usual third simulation $K'\diamond W(K')$ was not done because of the symmetry of the problem; the result of $K'\diamond W(K')$ should be approximately $K\diamond W(K)$. Five cases were tried but since the results were very similar only one is shown here in figure 5. The temperature retrieval is moderately affected in both cases with 0.05–0.1 K increase in error or 0.05 FUV throughout the profile. The dramatic effect is in the humidity retrieval which is degraded typically by 5-10% relative humidity or up to 0.4 FUV. It demonstrates the non-linearity of constituent retrieval; **K** is strongly dependent on the humidity part of the profile for water vapour channels.

5.3 K: Real data

It appears necessary to calculate **K** and therefore **W** at the true profile if the humidity retrieval is to be anywhere near the optimum result. This is clearly

impossible in practise and the best that can be done is to evaluate $\mathbf{K}$ at $\mathbf{X}_o$. This approach, however, is tending towards a fully non–linear scheme which is planned for the next generation of retrieval schemes and beyond the scope of this study. More in keeping with the approach adopted here is to see if there is some simple *ad hoc* stratification that provides a $\mathbf{K}$ closer to the true value than the climatological one used currently. Most of the non–linearity of the problem arises from humidity profile and, because a high temperature indicates a high absolute humidity, we stratified $\mathbf{K}$ according to temperature. The effect of using this stratification on the independent real data set is not shown but was almost totally negligible. It is possible that the collocated radiosonde humidity is not a good ground truth for testing retrievals against but a substantial effect was seen with the $\mathbf{E}$ changes. It therefore appears that a simple stratification is not adequate and a full on–line calculation of $\mathbf{K}$ may be required.

6. CONCLUSIONS

Significant improvements can be made to the performance of the retrieval scheme by using error covariances that are estimated from real data. A guess error covariance was calculated from forecast profiles and collocated radiosondes and was found to give results broadly in agreement with simulations; improvements around 1000 mb and above 300 mb. Also in agreement with simulations, stratification into high and low error forecast areas proved not to be profitable. The effect of more realistic measurement error covariances was more marked, probably because the original (diagonal) estimate was so crude. Stratification into cloud–clearing routes was found to be necessary. The gain for clear and partly cloudy FOVs did not match the simulated effect and we feel there is perhaps some statistical problem remaining here. Attempts at simple stratification of the $\mathbf{K}$ matrix proved useless, and improvement here awaits further investigation in fully non–linear retrieval schemes.

The new $\mathbf{C}$ and $\mathbf{E}$ matrices have been adopted by the routine scheme and work will continue on their refinement, especially the estimation of $\mathbf{C}$ since it is probable that the forecast guess will remain central to routine processing of sounding data in the Met Office for the foreseeable future.

REFERENCES

EYRE, J.R., PESCOD, R.W., WATTS, P.D., LLOYD, P.E., ADAMS, W. AND ALLAM, R.J.(1986), TOVS retrievals in the U.K.: progress and plans. *Tech. Proc. 3rd Int. TOVS study conf.; Madison, Wisconsin, USA; 13–19 Au-*

gust 1986; pp 60-91. Report of CIMSS, University of Wisconsin, Madison. Editor: W. P. Menzel.

EYRE, J.R. AND WATTS, P.D. (1987), A sequential approach to cloud-clearing for satellite temperature sounding. *Q.J.R.Meteorol.Soc.* **113**, *1949-1976*

RODGERS, C.D. (1976), Retrieval of atmospheric temperature and composition from remote measurements of thermal radiation. *Reviews of Geophysics and Space Physics,***14**, *609-624*

WATTS, P.D. (1984), A study of local area synthetic coefficients for use in the LASS system. *Met O 19 Branch Memorandum No. 76, Meteorological Office, Bracknell, U.K.*

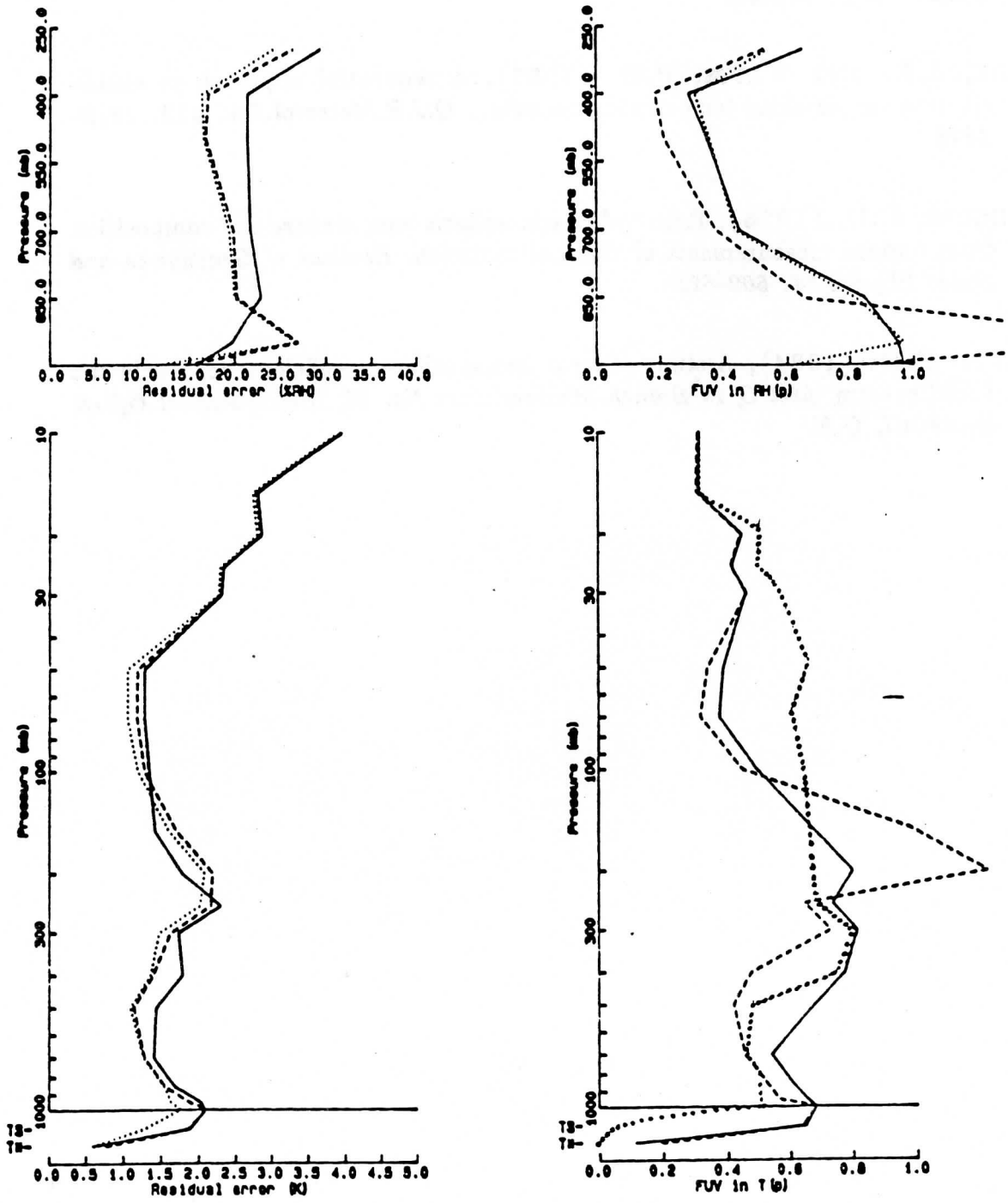

Figure 1. C-matrix Simulation

C1◇W(C1) ——————

C2◇W(C1) - - - - - - -

C2◇W(C2) .....

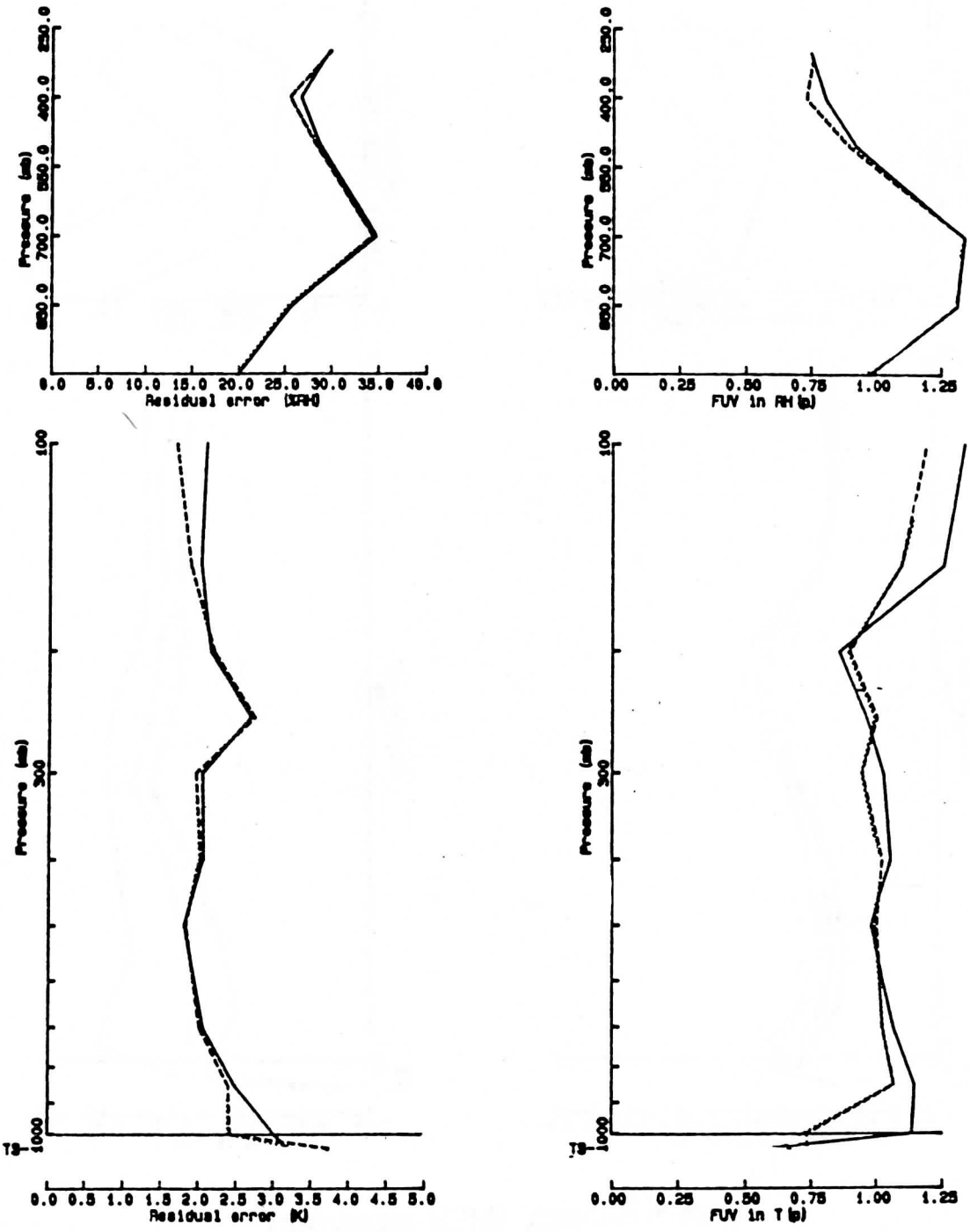

Figure 2. C-matrix Real data

Ind<>W(C1) ——————

Ind<>W(C2) - - - - - - -

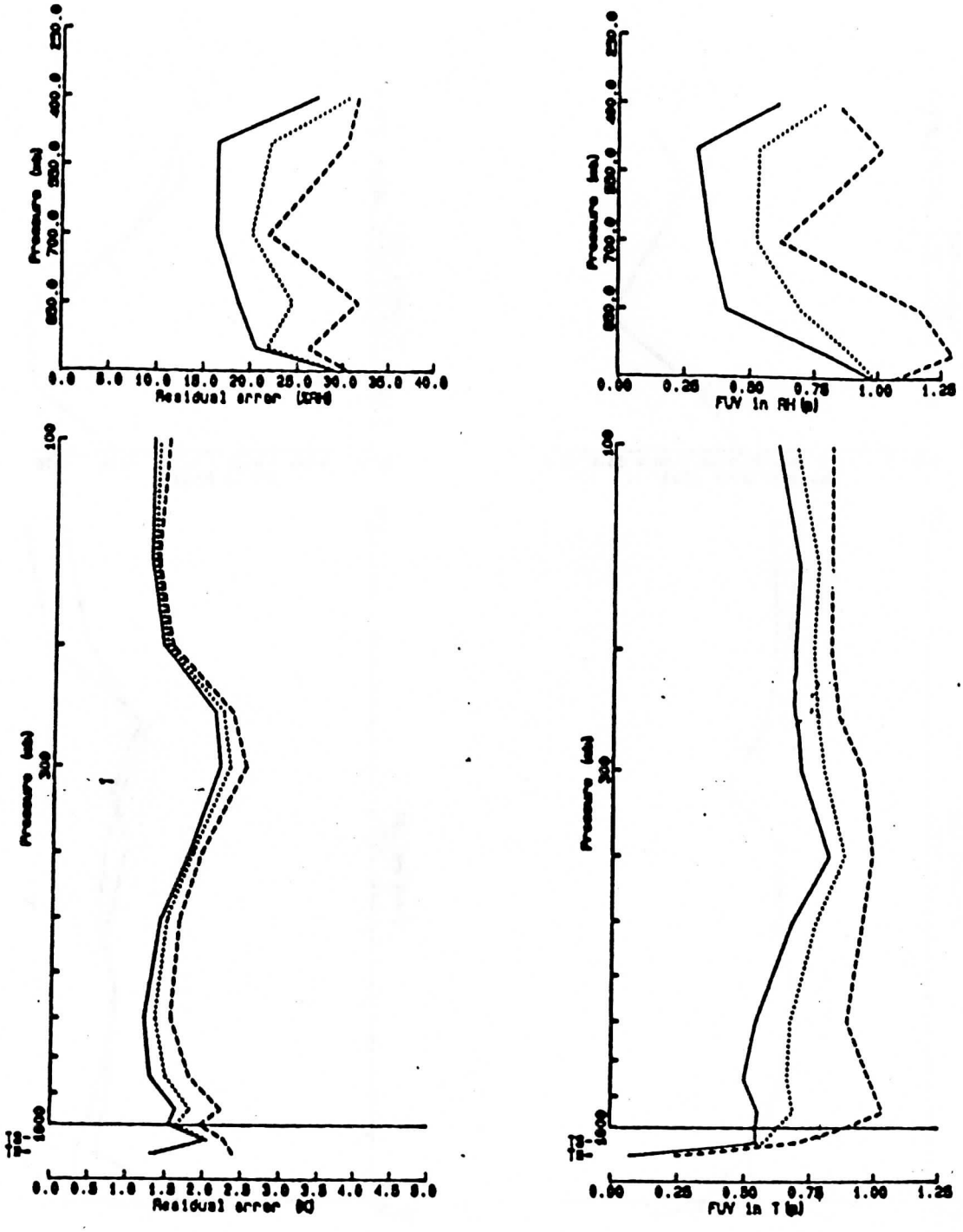

Figure 3. E-matrix (MSU-regression)

Simulation

$E_{diag} \diamond W(E_{diag})$ ——————

$E_{msu} \diamond W(E_{diag})$ - - - - - - -

$E_{msu} \diamond W(E_{msu})$ .....

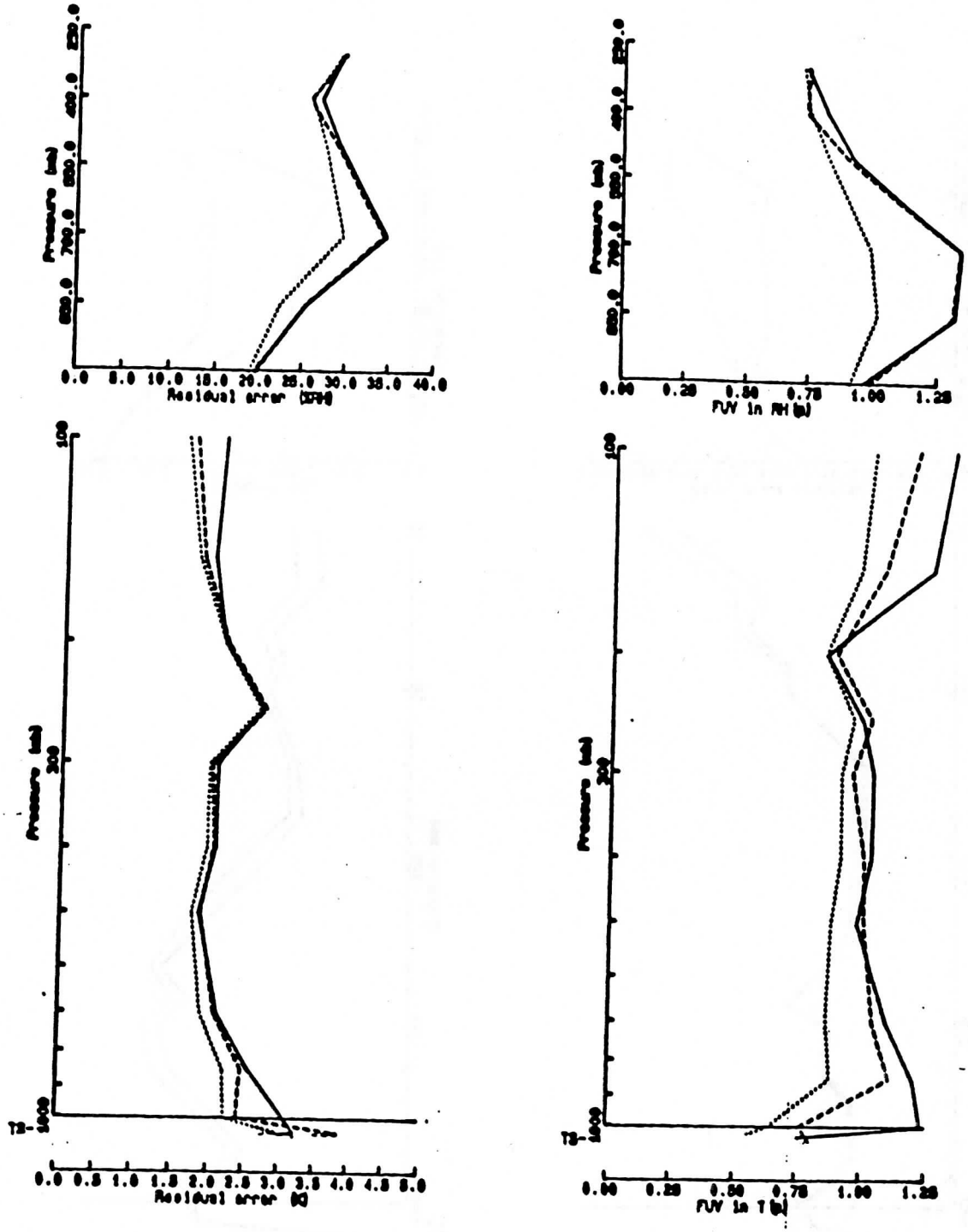

Figure 4. E-matrix (MSU-regression)

Real data

$Ind\Diamond W(E_{diag}, C1)$ ——————

$Ind\Diamond W(E_{diag}, C2)$ - - - - - - -

$Ind\Diamond W(E_{msu}, C2)$ ·····

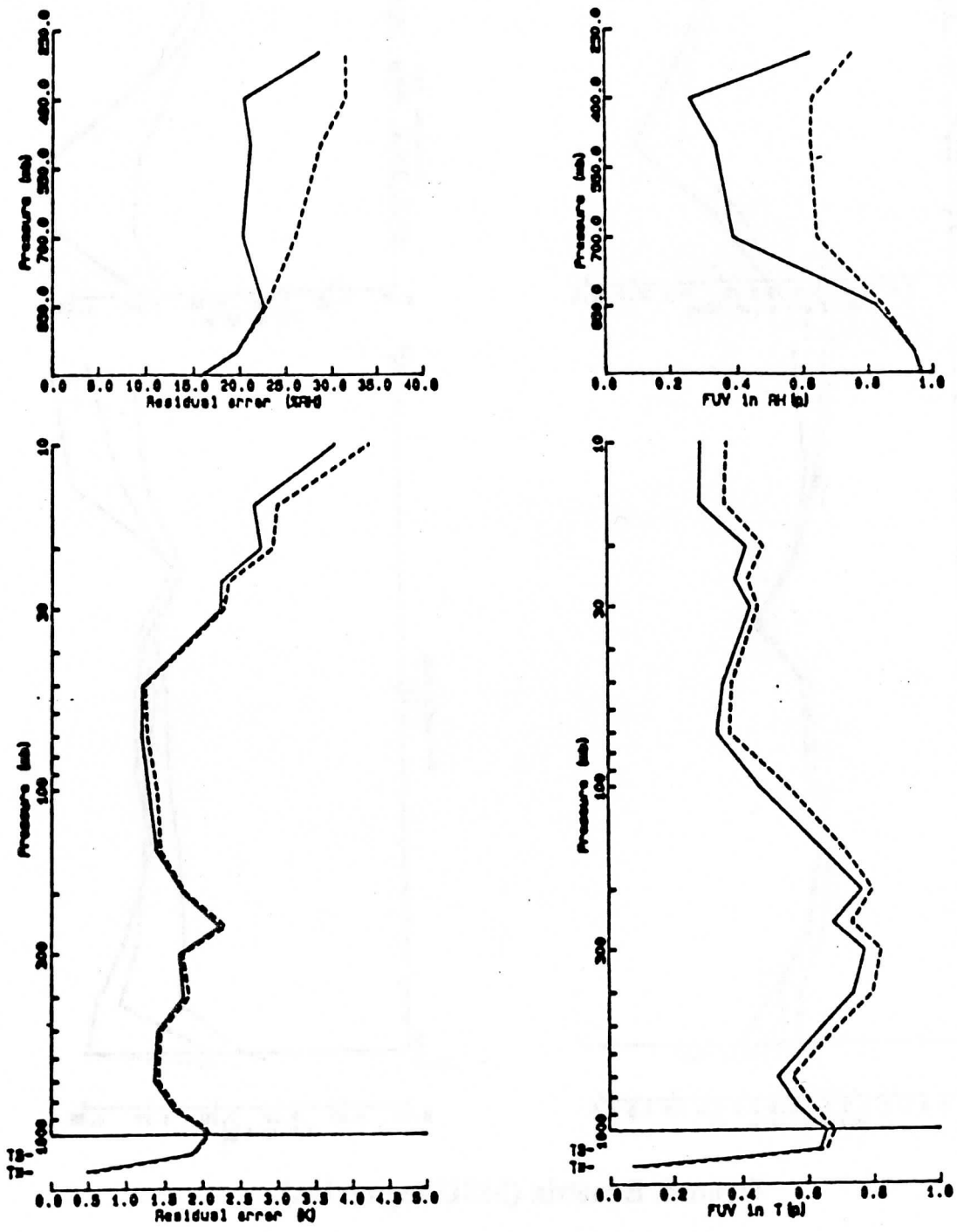

Figure 5. K-matrix Simulation

K◇W(K) ——————

K'◇W(K) - - - - - - -